University of Southampton

Faculty of Environmental and Life Sciences

School of Biological Sciences

The Effect of Systemic Inflammation on the Accumulation and Spread of Tau Pathology

by

Sarah Elizabeth Howard

Thesis for the degree of Doctor of Philosophy

October 2021

University of Southampton

Abstract

Faculty of Environmental and Life Sciences

School of Biological Sciences

Doctor of Philosophy

The Effect of Systemic Inflammation on the Accumulation and Spread of Tau Pathology

by

Sarah Elizabeth Howard

Alzheimer's disease (AD) is a secondary tauopathy categorised by the presence of insoluble amyloid plaques and neurofibrillary tangles. Neurofibrillary tangles consist of hyperphosphorylated and misfolded tau protein. The pathological form of tau spreads through the limbic circuit and to the wider neocortex as the disease progresses. The spreading of aggregated tau throughout the brain in AD has long been associated with cognitive decline. These observations in AD patients have prompted further investigation behind this mechanism. It is hypothesised that the primary immune cell within the brain, microglia may be facilitating the spread of tau. In AD patients, systemic inflammatory episodes have been shown to correlate with an increase in cognitive decline. Therefore, peripheral inflammation may induce an inflammatory response within the brain and in turn promote the spread of tau pathology. This thesis aims to mimic the spreading of tau and observe the effect of systemic infection *in vivo*.

In this thesis, a tau spreading model was generated using C57BL/6 mice and H1*Mapt-/-* mice, a mouse which expresses all six isoforms of human tau with no disease-associated mutation. Mice received a unilateral injection of lysate enriched for Sarkosyl-insoluble tau derived from AD post-mortem tissue. Two months post-injection, mice received an intraperitoneal injection of either saline or *Salmonella enterica* serovar Typhimurium. *S. typhimurium* is a gram-negative bacterial strain which induces prolonged upregulation of pro-inflammatory cytokines, changes in microglial markers and splenomegaly, all of which are observed up to four weeks post-infection. Extensive histology was carried out in C57BL/6 and H1*Mapt-/-* mice to observe AT8-positive tau in distinct brain regions and examine the effect of systemic infection on tau burden. This infection was first established in the C57BL/6 and H1*Mapt-/-* mice without the spreading model to assess the baseline response to infection.

This thesis demonstrates propagation of tau pathology to regions within the limbic circuit connected synaptically. It was observed that systemic infection increases the rate of spread of AT8-positive tau through the brain. In regions within the limbic circuit, such as the mammillary nuclei, a significant increase in AT8-positive tau was observed after systemic infection. Markers of cellular and microglial activation MHCII and FcγRI, demonstrate a potential effect of 'priming' whereby the presence of tau pathology induces an exaggerated microglial response following systemic infection. MHCII also highlights a potential role of the vasculature. Differences were observed between the C57BL/6 and H1*Mapt-/-* mice both in tau burden and microglial response, supporting the role of systemic infection in the spatiotemporal spread of tau. The work described in this thesis demonstrates that systemic infection increases the spreading of tau pathology and prompts further study to investigate this mechanism further.

Table of Contents

Table of Tables

Table of Figures

Research Thesis: Declaration of Authorship

Print name: Sarah Howard

Title of thesis: The Effect of Systemic Inflammation on the Accumulation and Spread of Tau Pathology

I declare that this thesis and the work presented in it are my own and has been generated by me as the result of my own original research.

I confirm that:

1. This work was done wholly or mainly while in candidature for a research degree at this University;
2. Where any part of this thesis has previously been submitted for a degree or any other qualification at this University or any other institution, this has been clearly stated;
3. Where I have consulted the published work of others, this is always clearly attributed;
4. Where I have quoted from the work of others, the source is always given. With the exception of such quotations, this thesis is entirely my own work;
5. I have acknowledged all main sources of help;
6. Where the thesis is based on work done by myself jointly with others, I have made clear exactly what was done by others and what I have contributed myself;
7. None of this work has been published before submission
8. Signature: ..... Date: 12/07/2021

Presentation of the work in this thesis

Oral presentations

2016-2020 SoNG seminars, Southampton

2016-2020 Eli Lilly CASE Day, Surrey

2019 Postgraduate Symposium, School of Biological Sciences, Southampton

2019 ARUK Conference: Early Careers Day, Harrogate

2018 SoNG Conference: Immune to Brain Axis, Southampton

2017 ARUK South Coast network Early Career Researcher (ECR) meeting, Brighton

Poster presentations

2021 121st Meeting of the British Neuropathological Society, virtual

2019 ARUK Conference, Harrogate

2018- 2019 Wessex Immunology Group symposia, Southampton

2018 Keystone symposia, Colorado, USA

2018 School of Biological Sciences Postgraduate symposium, Southampton

2018 Doctoral Research College Showcase, Southampton

Grants and awards

2021 British Neuropathological Society– Small grant award

2019 British Neuropathological Society– Small grant award

2019 ARUK South Coast network – Equipment grant

2018 Guarantors of Brain - Travel grant awarded

2018 ARUK South Coast network - Travel grant awarded

2018 Wessex Immunology Group meeting - Poster presentation prize

2018 Southampton Neuroscience Group (SoNG) Symposium - Oral presentation prize

Acknowledgements

I would first like to thank my supervisors, Professor Jessica Teeling, Dr Katrin Deinhardt and Dr Zeshan Ahmed for all their help and support over these many years. Their help and guidance with this project has been invaluable and I appreciate all the time and advice they have given me. A specific thank you to Jessica who has been a constant support throughout my thesis and was always encouraging of my work. I would also like to thank Dr Mariana Vargas-Caballero for allowing me to use her lab and for genotyping and being so generous with her time and advice.

I would like to thank all members of the Teeling lab who I worked with. In particular I need to thank Dr Alex Collcutt and Dr Mike Hurley who contributed to this thesis. Thank you to Alex for help with the *in vivo* work for the P301S mice and Mike for the α-Synuclein histology. Thank you to Joe Chouhan for your help with burrowing behaviour. Thank you to Dr Sarmi Sri for help learning the genotyping. I would also like to mention Dr Daniel Cohn and everyone else in the JT and DGN labs who were so helpful both in and out of the lab. I was lucky enough to spend time at Eli Lilly and many people gave me their time and support. Thank you to Jane Cooper, Dr Annalisa Cavallini, Emma Dyke and Dr Tracey Murray for your help with training and answering all of my many questions. I would also like to thank Laurie Lau, Richard Jewell and Grielof Koster at SGH for their technical help and knowledge. The BRF staff were always so helpful and I am forever grateful for the support. I would like to thank Leslie Lawes and Russell Soper who were always available despite how busy they were.

I would like to acknowledge the British Neuropathological Society (BNS) and Alzheimer's Research UK (ARUK) for their help funding this project and allowing me to present my work. We would like to thank the South West Dementia Brain Bank (SWDBB) for providing brain tissue for this study. The SWDBB is part of the Brains for Dementia Research programme, jointly funded by Alzheimer's Research UK and Alzheimer's Society and is supported by BRACE (Bristol Research into Alzheimer's and Care of the Elderly) and the Medical Research Council.

A massive thank you to Joe Chouhan and Georgie Dawes for their support over the years. Work would have been significantly more stressful and less enjoyable without them and I will definitely miss our chats in the office the most. A huge thank you to Katie Askew for giving me your desk and also being a constant friend whether you are at an adjacent desk or in Edinburgh. I would like to thank Issy and Emma for being the best people and amazing friends throughout this.

Finally, I would like to thank my family and Bob. To Mum and Dad, thank you for always being so supportive even when my phone calls are just me being stressed. You are always positive and

helpful, hopefully we can see each other more now that this is finished. To Pebs, I miss you. And to Bob, this would not have been possible without you and your support over the last 8 years has been the best thing. Thank you for always being there for me no matter how stressed I got. We can go cycling now!

xx

Definitions and Abbreviations

3R tau	Three-repeat tau
4R tau	Four-repeat tau
α-SMA	alpha-smooth muscle actin
aa	Amino acids
AD	Alzheimer's Disease
ADAS-Cog	Assessment Scale-Cognitive subscale
ANOVA	Analysis of Variance
APC	Antigen presenting cell
APOE	Apolipoprotein E
APP	Amyloid precursor protein
APS	Aminopropylsilane
ASC	Apoptosis-associated speck-like protein containing a caspase recruitment domain
ATP	Adenosine triphosphate
Aβ	Amyloid-beta
BBB	Blood brain barrier
Bp	Base pairs
BSA	Bovine serum albumin
C1q	Complement 1q
C3	Complement 3
C3aR	Complement 3a Receptor
C(t)	Threshold cycle
CAA	Cerebral amyloid angiopathy
CA	*Cornu Ammonis*
Ca2+	Calcium
CaMKIIα	Ca^{2+}/calmodulin-dependent protein kinase II alpha
CBD	Corticobasal degeneration
CCR7	CC chemokine receptor type 7
CD	Cluster of differentiation
Cdc42	Cell division control protein 42
Cdk5	Cyclin dependent kinase 5
cDNA	Complementary DNA
CL2	Containment level 2

CNS	Central nervous system
CSF	Cerebrospinal fluid
CVD	Cardiovascular disease
DAB	3,3 Di-aminobenzidine
DAM	Disease-associated microglia
DAPI	4',6-Diamidino-2-Phenylindole
DCs	Dendritic cells
DLB	Dementia with Lewy Bodies
DM	Diabetes mellitus
DPBS	Dulbecco's phosphate buffered saline
DTI	Diffusion tensor imaging
E14	Embryonic day 14
EOAD	Early-onset Alzheimer's Disease
EOFAD	Early-onset familial Alzheimer's Disease
ERK	Extracellular signal-regulated kinase
FDA	Food and Drug Administration
FRET	fluorescence resonance energy transfer
fFTD	Familial Frontotemporal Dementia
FTD	Frontotemporal Dementia
FTDP-17	Frontotemporal Dementia with Parkinsonism-17
G3BP	ras GAP-binding protein
GAPDH	Glyceraldehyde 3-phosphate dehydrogenase
GFAP	Glial fibrillary acidic protein
GOI	Gene of interest
GSK3β	Glycogen-synthase kinase-3 beta
HCB	Hippocampal cingulate bundle
HIV-1	Human immunodeficiency virus-1
HMW	Heavy molecular weight tau
HSPGs	Heparan sulfate proteoglycans
HTRF	Homogenous Time Resolved Fluorescence
i.c.	Intracerebral
i.p.	intraperitoneal
i.v.	intravenous
IFN-γ	Interferon gamma
IHC	Immunohistochemistry
IL	Interleukin

IMS	Industrial methylated spirits
ITAM	Immunoreceptor Tyrosine-based Activation Motif
ITIM	Immunoreceptor Tyrosine-based Inhibitory Motif
JNK	c-Jun N-terminal kinase
KC/GRO	Keratinocyte chemoattractant/human growth-regulated oncogene
kD	kilodaltons
LBD	Lewy Body Dementia
LMW	Low molecular weight tau
LMN	Lateral mammillary nuclei
LOAD	Late-onset Alzheimer's Disease
LPS	Lipopolysaccharide
M cells	Microfold cells
MAP	Microtubule associated protein
MAPK	Mitogen-activated protein kinase
MAPT	Microtubule associated protein tau
MARK	Microtubule-associated regulatory kinase
MCI	Mild cognitive impairment
MCP-1	Monocyte chemoattractant protein-1
MHC	Major histocompatibility complex
MMSE	Mini-Mental State Examinations
mRNA	Messenger RNA
MWM	Morris Water Maze
NFTs	Neurofibrillary tangles
NF-κB	Nuclear factor kappa-light-chain-enhancer of activated B cells
NLRC4	NLR family caspase recruitment domain-containing protein 4
NLRP3	Nucleotide-binding oligomerization domain (NOD)-like receptor protein 3
Nm	Nanometre
NO	Nitric oxide
Nramp1	Natural resistance-associated macrophage protein 1
OCT	Optimal cutting temperature
P. gingivalis	*Porphyromonas gingivalis*
PAC	P1 bacteriophage-derived artificial chromosome
PAMPs	Pathogen-associated molecular patterns
PBS-T	Phosphate buffered saline with 0.01% Triton
PCR	Polymerase chain reaction
PET	positron emission tomography

PFA	Paraformaldehyde
PFU	Plaque forming units
PHF	Paired helical filaments
PiD	Pick's Disease
PPs	Peyer's patches
PrP^{C}	Native prion protein
PrP^{Sc}	Pathological prion protein
PRRs	Pattern recognition receptors
PSEN1	Presenilin 1
PSEN2	Presenilin 2
PSP	Progressive supranuclear palsy
PVDF	Polyvinylidene difluoride
qPCR	Quantitative polymerase chain reaction
RA	Rheumatoid arthritis
Rcf	Relative centrifugal force
REF	Reference gene
RhoG	Ras homology Growth-related
ROS	Reactive oxygen species
Rpm	Revolutions per minute
RT	Room temperature
S. Typhi	*Salmonella enterica* serovar Typhi
S. typhimurium	*Salmonella enterica* serovar Typhimurium
SCV	*Salmonella*-containing vacuole
SPI	*Salmonella* pathogenicity island
SuMN	Supramammillary nuclei
SWDBB	South West Dementia Brain Bank
T3SS	Type III secretory systems
TAE	Tris Acetate-EDTA buffer
TauKO	Tau knockout
TBE	Tris/Borate/EDTA buffer
TBI	Traumatic Brain Injury
TBS	Tris buffered saline
TDP-43	TAR DNA-binding protein 43
TEMED	Tetramethylethylenediamine
TLRs	Toll-like receptors
TNF-α	Tumour Necrosis Factor alpha

TRE	Tetracycline response element
TREM2	Triggering Receptor Expressed On Myeloid Cells 2
tTA	Tetracycline transactivator
UPS	Ubiquitin-proteasome system
VaD	Vascular dementia
WT	Wild type

Chapter 1 Introduction

1.1 Pathogenesis of tauopathies

Tauopathies are neurodegenerative diseases categorized by the accumulation of aggregated tau protein within the brain to the detriment of cognitive function and eventual neuronal loss. Primary tauopathies include but are not limited to frontotemporal dementia with Parkinsonism linked to chromosome 17 (FTDP-17), progressive supranuclear palsy (PSP), corticobasal degeneration (CBD) and Pick's disease (PiD). Alzheimer's disease (AD) is the predominant tauopathy diagnosed in patients and therefore one of the most heavily researched (Mroczek, Annesley and Fisher, 2020). AD is a form of dementia categorized as a secondary tauopathy due to a second pathological hallmark, extracellular amyloid plaques. Tauopathies can only be confirmed in post-mortem study and with symptoms often overlapping and patient variance in onset and progression it can be difficult to achieve an accurate diagnosis. Tauopathies are differentially diagnosed through changes in cognition or movement. These clinical symptoms are proposed to be dependent on where pathology develops, and the region-specific functions altered by such changes. For example, FTDP-17 is diagnosed through the presence of motor symptoms such as bradykinesia and altered personality such as loss of inhibition (Wszolek *et al.*, 2006). Post-mortem analysis of FTDP-17 brain tissue suggests pathology largely resides in the cerebral cortex, brainstem and the dentate nucleus of the cerebellum, concurrent with patient symptoms (Bugiani *et al.*, 1999; Lossos *et al.*, 2003). It has long been hypothesised that tau pathology plays a significant role in neuronal death and cognitive decline in tauopathies. Tau spread in AD was initially characterised through Braak staging (Braak *et al.*, 2006), more recently positron emission tomography (PET) in AD patients has shown that tau burden correlated with atrophy in the cortex in a longitudinal study (Joie *et al.*, 2020). Therefore, in theory slowing or preventing the spread of tau pathology through the brain should ameliorate cognitive decline.

1.2 Alzheimer's disease; a secondary tauopathy

AD is the most prevalent form of dementia, with approximately three quarters of dementia cases diagnosed as AD (Qiu, Kivipelto and Von Strauss, 2009). Anterograde episodic memory dysfunction is one of the first reported symptoms; however as AD progresses, wider cognitive function including speech becomes gradually altered (Potkins *et al.*, 2003), and non-cognitive symptoms such as gait or vision problems develop (Chang *et al.*, 2014; Lim, Mamun and Lim, 2014). AD symptoms are clinically observed predominantly after 65 years of age, making age a major risk factor. The prevalence of AD in ages 45-64 years is approximately 1 in every 14 people, yet once over the age of 80 the prevalence increases to 1 in every 6 people (Prince *et al.*, 2014).

AD is a devastating disease to both patients and their families; with increasingly expensive care and an aging population, research into prevention of this neurodegenerative disease is crucial.

One key issue for clinicians and in selecting patient groups for clinical trials is that a diagnosis of AD can only be confirmed post-mortem by the presence of two pathological hallmarks. These pathological hallmarks consist of extracellular amyloid beta (Aβ) plaques from Amyloid Precursor Protein (APP), and intracellular tau protein which aggregates into neurofibrillary tangles (NFTs) (Kametani and Hasegawa, 2018). AD is predominantly sporadic with <1% of total cases reported to have familial mutations in genes associated with amyloid protein processing; the only known mutations are found in either the *APP* gene, Presenilin 1 gene (*PSEN1*) or Presenilin 2 gene (*PSEN2*) (Cruts, Theuns and Van Broeckhoven, 2012; Guerreiro, Gustafson and Hardy, 2012). APP is cleaved by the enzyme β-secretase and subsequently γ-secretase; this leads to the production of the amyloid-beta peptide, consisting of either 40 or 42 amino acids ($A\beta_{40/42}$ respectively) (Zhang *et al.*, 2011). $A\beta_{42}$ monomers aggregate to form toxic oligomers which then undergo further aggregation, leading to the formation of extracellular senile plaques (Benilova, Karran and De Strooper, 2012). Presenilins regulate APP cleavage through γ-secretase therefore it is possible to observe how these mutations promote accumulation of toxic aggregated amyloid protein. Notably there are no known mutations in the microtubule-associated protein tau (*MAPT*) gene which encodes tau protein with a causative link to AD. This highlights a key issue when studying AD in mouse models as the lack of tau mutations related to familial AD.

Most familial forms of AD are classified as an early onset form of AD. Early onset AD (EOAD) cases present with disease symptoms at <65 years of age, representing approximately 10% of all AD cases. Within EOAD cases, nearly 10% are due to a familial mutation and referred to as early onset familial AD (EOFAD) (Mendez, 2019). EOFAD often presents clinically at 40 years of age, whilst sporadic EOAD is more likely to be diagnosed between 50 and 60 years of age (Miyoshi, 2009). There is evidence based on cognition tests, mini-mental state examinations (MMSE) and Assessment Scale-cognitive subscale (ADAS-Cog), that EOAD patients show significantly faster cognitive decline than late onset AD (LOAD) patients (Panegyres and Chen, 2013). EOAD patients also show earlier deficits in visual and language functions (Smits *et al.*, 2015). The differences between EOAD, EOFAD and LOAD and even population variability within these groups serves to highlight the innate heterogeneity in both the progression of AD and the symptoms associated. Familial AD and EOAD patients have a different age of onset, prognosis and symptoms, yet it is primarily these three aforementioned gene mutations that are the crux of AD mouse models. One of the key issues in AD research is the extrapolation of familial AD mouse models to LOAD in humans; to what extent can a genetic mutation inform clinical routes in a largely idiopathic disease?

When examining the sporadic form of AD, genetic risk factors are considered rather than causative mutations. One important note in regard to this thesis is that over half of gene variants identified as risk factors in AD play a role in the innate immune system (Shi and Holtzman, 2018). The apolipoprotein E (*APOE*) gene is the main risk factor for sporadic AD. APOE mediates transportation of lipids including cholesterol throughout the brain (Husain, Laurent and Plourde, 2021). AD cases with APOE-ε4 reported disease onset years prior to cases without (van der Flier *et al.*, 2011). However, APOE-ε4 is not expressed ubiquitously in sporadic AD cases. There is great disparity in the genetic epidemiology of the more common sporadic late-onset form of the disease (Reitz, Brayne and Mayeux, 2011). Therefore, AD is largely idiopathic, despite decades of research into multiple overlapping theories of causality.

The two prevailing theories of causality in AD research are the amyloid hypothesis and the tau hypothesis. These two theories hypothesise that each hallmark protein is the pathological root of the disease respectively. The discovery of causative mutations in APP processing genes and APOE as a risk factor is one of the primary reasons that the amyloid hypothesis was, and still is considered such a promising therapeutic avenue. Research into the amyloid cascade hypothesis has largely focused on how changes in APP processing leading to aggregation may be the cause of neuronal death and cognitive decline in AD. Furthermore, as observed in **Figure 1.1**, the two major downstream effects are an increase in inflammation and changes in tau protein to form the second pathological hallmark. Despite increased understanding of how Aβ deposition is theorised to advance neurodegeneration in AD cases, the amyloid hypothesis shows relatively little correlation with pathology spread and clinical progression compared to tau pathology (Ingelsson *et al.*, 2004; Cho *et al.*, 2016). Furthermore, whilst antibody therapies such as bapineuzumab or immunisation against $A\beta_{42}$ in human patients does decrease amyloid load, there is no alteration in cognitive decline observed (Holmes *et al.*, 2008; Roher *et al.*, 2013). A recent decision to approve aducanumab by the Food and Drug Administration (FDA) has heralded the first approved treatment for AD that reduces amyloid pathology (Cavazzoni, 2021). Despite this recent update, aducanumab is the only drug in almost a decade which slows the rate of cognitive decline by focusing on the removal of plaques.

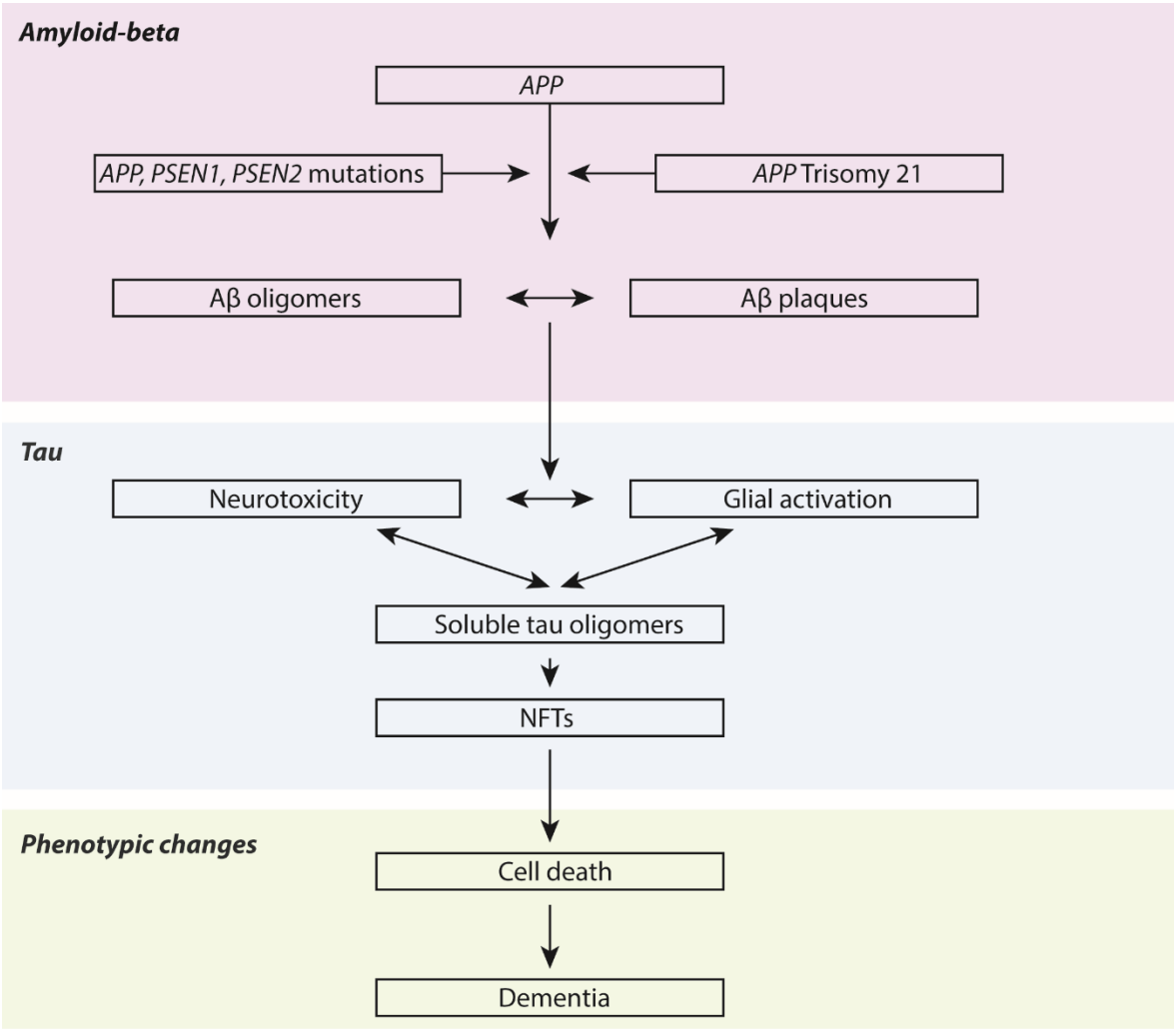

Figure 1-1: The intersection of the amyloid and tau hypothesis

The amyloid hypothesis highlights the processing of APP as a potential therapeutic avenue. The amyloid hypothesis proposes that genetic mutations lead to amyloid plaques and with this, activation of glial cells within the brain. This in turn leads to a neurotoxic environment where tau becomes misfolded and dissociates from the microtubules. Build-up of these two aggregated proteins leads to an increasingly pro-inflammatory response within the brain. Subsequent neuronal toxicity from immune cell dysfunction and accumulation of tau is hypothesised to be the cause of cell death and memory dysfunction in AD patients. Diagram adapted from Giacobini & Gold, 2013.

As a result, this has led to greater exploration in wider fields of interest, such as the tau hypothesis, as seen in **Figure 1-1** (Giacobini and Gold, 2013). Given the research in AD patients, clinical trials are turning increasingly to therapeutics which target tau. There are multiple clinical trials targeting tau such as the antibody semorinemab which attempts to remove extracellular tau (Zilkova *et al.*, 2020). However, with the exception of aducanumab no clinical trial success has been reported. The amyloid cascade hypothesis and tau hypothesis both have merits, and it is

widely demonstrated that both pathologies cause deleterious effects within the AD brain. To what extent one pathological hallmark can be removed without the other and expect cognitive recovery is unclear. Despite this, the clear effect of tau pathology on cognitive function as it progresses through regions highlights the importance of understanding the mechanism behind tau spread.

1.2.1 Propagation of pathological tau through the human brain in AD

Tau pathology spreads through the brain as AD progresses. This spread was first characterised by Heiko Braak, subsequently termed Braak stages I-VI with VI demonstrating the highest tau burden. The transentorhinal cortex and locus coeruleus first show signs of tau pathology, termed as Braak stage I. Following this tau pathology is observed in the entorhinal cortex (Braak stage II) (Braak and Braak, 1991). The following Braak stage is marked by mild pathology spread to the CA1 region of the hippocampus (Braak stage III). Braak stage IV is marked by ghost tangles in the entorhinal cortex and increasing NFT presence in the CA1 of the hippocampus. Eventually the hippocampal formation and wider regions of the neocortex display tau burden (Braak stage IV-VI) (Braak *et al.*, 2006). This spreading has since been confirmed in PET imaging, where tau is visible in AD patients and does not rely on post-mortem tissue (Vogel *et al.*, 2020).4

The hippocampus is a medial temporal lobe structure found within the human and mouse brain. The hippocampus proper consists of the *Cornu ammonis* 1 (CA1) which becomes the CA2, CA3 and CA4, with the full hippocampal formation including the dentate gyrus, subiculum and entorhinal cortex (Anand and Dhikav, 2012). The hippocampus is conserved in mammals and plays an indispensable role in episodic and spatial memory. The entorhinal cortex and the hippocampus are both key structures within the limbic circuit, also referred to as the Papez circuit, described in **Figure 1-2** (Bubb, Kinnavane and Aggleton, 2017; Nelson, Perry and Vann, 2018). The hippocampus projects to the mammillary nuclei through the fornix, the mammillothalamic tract then connects the anterior thalamus. The cingulate gyrus then connects to the entorhinal cortex which projects to the hippocampal formation through the perforant pathway. The limbic circuit has been shown to be involved in memory function (Rolls, 2015), with the entorhinal cortex crucial for spatial memory. People with amnestic mild cognitive impairment (MCI) or AD show clear functional deficits in spatial memory tasks (Serino *et al.*, 2015; Coughlan *et al.*, 2018). People with MCI may not go on to develop AD (Griffith *et al.*, 2006), however this highlights the very early changes to cognitive function in the regions where initial tau pathology builds. PET imaging studies have since confirmed correlation between tau burden and cognitive decline (Brier *et al.*, 2016).

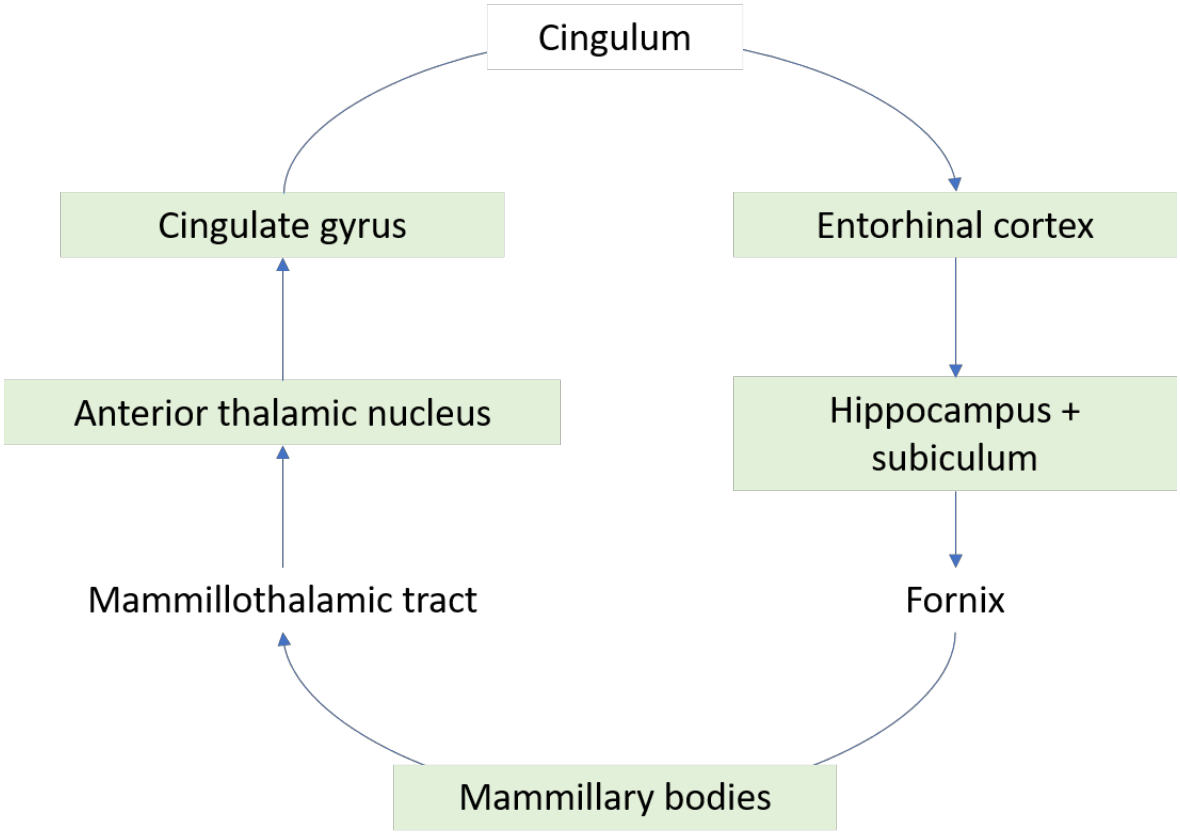

Figure 1-2: Overview of the limbic circuit

The limbic circuit is a group of structures within the brain, synaptically connected to process memory function. The structures included are the hippocampus, cingulate gyrus, anterior thalamic nucleus, entorhinal cortex, subiculum and mammillary nuclei. These regions are connected by the cingulum, fornix and mammillothalamic tract. This figure is a brief overview and does not include wider regions such as the retrosplenial cortex, amygdala and the full parahippocampal region which all play a role in memory processing. Figure adapted from Bubb *et al*. (2017) and Nelson *et al.* (2018)

1.2.2 Structure of tau

The *MAPT* gene located on chromosome 17q21.31 in humans and chromosome 11 in mice encodes microtubule-associated protein (MAP) tau. Tau is one of many neuronal microtubule associated proteins (including MAP1, MAP2 and MAP4) which enable microtubule stability within the healthy brain through binding (Chen *et al.*, 1992; Dixit *et al.*, 2008). As a result, tau promotes and mediates axonal transport through its binding to microtubules. Human tau is expressed within the adult brain in six isoforms through alternative splicing of messenger RNA (mRNA) (Goedert *et al.*, 1989), consisting of between 352 to 441 amino acids and 16 exons total. Exons 1-5 encode the N-terminal; the splicing of exons 2 and 3 determines the presence of N-terminal

inserts (Martin, Latypova and Terro, 2011). Exons 9-12 encode four microtubule-binding repeat domains, with splicing of exon 10 determining the absence or presence of the second repeat domain. These isoforms are referred to as three repeat (3R) or four repeat (4R) tau respectively. Therefore, the nomenclature of these six tau isoforms is dependent on exons 2, 3 and 10 (Wang and Mandelkow, 2016). Hence, the isoform 4R/2N contains four microtubule binding domains and two N-terminal inserts; all six isoforms are displayed in **Figure 1-3**.

Tau protein in the healthy brain is demonstrated to have an equal ratio of 3R:4R tau. It has been demonstrated that 3R and 4R tau mediate axonal transport. However, *in vitro* these isoforms appear to encourage anterograde (towards the synapse) and retrograde (towards the cell body) transport respectively (Lacovich *et al.*, 2017). An increase in 4R tau has been reported in tauopathies such as PSP (Chambers *et al.*, 1999; Ingelsson *et al.*, 2007) where only 4R tau makes up the aggregate pathology (Rösler *et al.*, 2019). AD by contrast has been shown to contain both 3R and 4R tau in the tangles. One study has reported a small increase in 4R tau in AD patients (Ginsberg *et al.*, 2006), however this has not been observed in similar studies (Ingelsson *et al.*, 2007). Three-repeat tau has been shown to supress the aggregation of four-repeat tau *in vitro* whilst four-repeats in the microtubule domain confers stronger binding to microtubules; it also confers a propensity to greater aggregation (Adams *et al.*, 2010). Whilst splicing of mRNA may alter the tau isoforms, modifications at the post-translational stage also play a significant role in tau function.

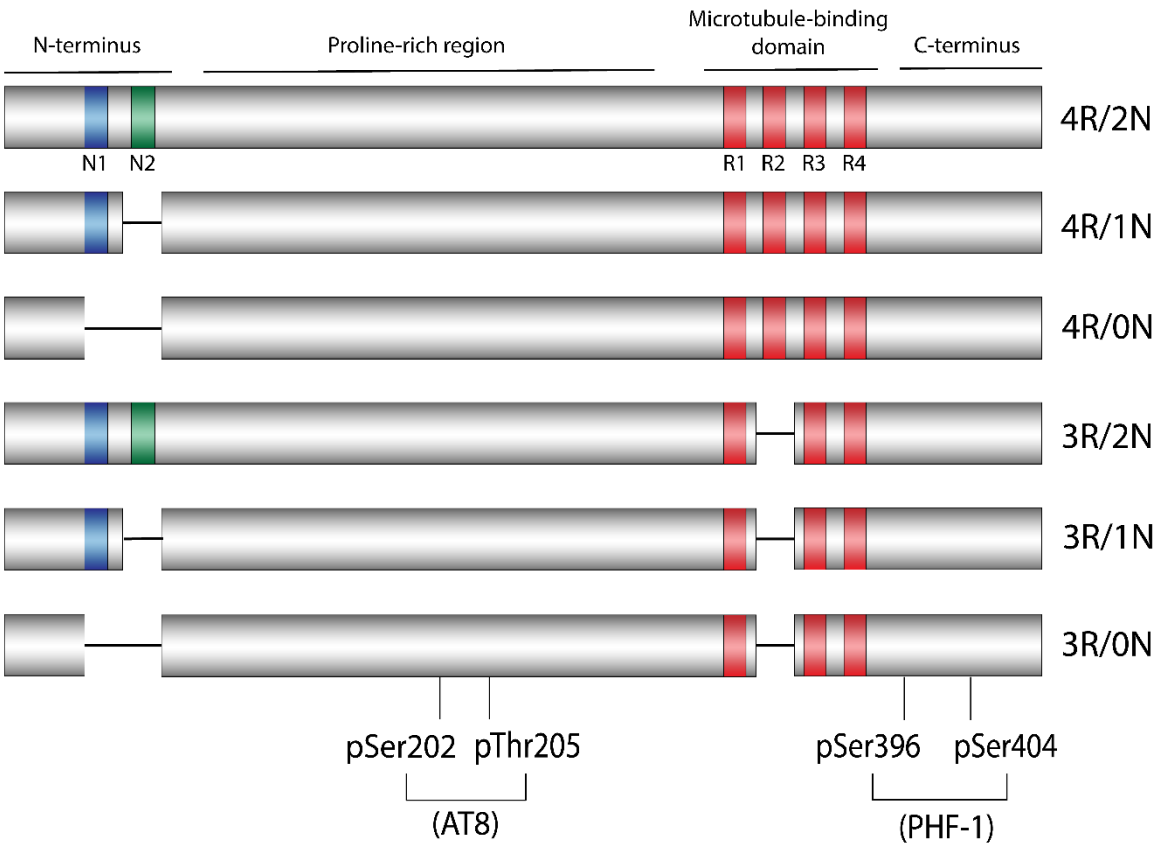

Figure 1-3: Tau isoforms and phosphorylation epitopes of interest

In the human brain there are six isoforms of tau (shown above: 4R/2N, 4R/1N, 4R/0N, 3R/2N, 3R/1N and 3R/0N). In mouse adult brains, only four-repeat tau is expressed. Phosphorylation epitopes are associated with AD pathology and the associated antibody which is commonly used to detect these epitopes are shown. Diagram based on Wang & Mandelkow, 2016.

1.2.3 Post-translational modifications of tau

Tau plays an important physiological role within the healthy brain by regulating axonal transport and neurite outgrowth (Rodríguez-Martín *et al.*, 2013). Tau is natively unfolded in the naïve brain, yet becomes misfolded and hyperphosphorylated in both AD and primary tauopathies, such as PSP and CBD (Mroczko, Groblewska and Litman-Zawadzka, 2019). Hyperphosphorylated tau dissociates from the microtubule, causing instability. This release of dissociated tau leads to the formation of soluble toxic tau oligomers through dimerization and subsequent nucleation (Friedhoff *et al.*, 1998). This will in turn form paired helical filaments (PHFs) and sequential aggregation into NFTs (Eidenmüller *et al.*, 2000). NFTs accumulate within the neuron and following neuronal death remain as a ghost tangle within the brain parenchyma.

Post-translational modifications of soluble and insoluble tau, such as phosphorylation, ubiquitination and truncation are understood to alter tau function (Martin, Latypova and Terro, 2011). Phosphorylation of tau is the most common modification; it must be noted that not all phosphorylation of tau is pathological and only select epitopes are commonly associated with the development of tauopathies. There are 83 tau phosphorylation sites, however those known to be associated with both the dissociation from microtubules and subsequent aggregation, are primarily threonine and serine phosphorylation epitopes as seen in **Figure 1-3** (Gong and Iqbal, 2008). Hyperphosphorylation of tau leads to conformational changes and a shift to a β-pleated sheet structure.

In the naïve brain, one function of phosphorylation of tau is the regulation of neurite outgrowth through kinase glycogen-synthase kinase-3 beta (GSK3β) (Stoothoff and Johnson, 2005). Tau in AD however becomes hyperphosphorylated through dysregulation of kinase activity. Another kinase regulating tau phosphorylation is cyclin dependent kinase 5 (cdk5); cdk5 is expressed in all cell types, with the highest expression and kinase activity in neurons (Dhavan and Tsai, 2001). Cdk5 phosphorylates serine or threonine amino acids that are followed by a proline residue. Cdk5 is activated either by its regulatory subunit p35, or hyperactivated by the truncated p25 following excitotoxicity or oxidative stress (Kimura, Ishiguro and Hisanaga, 2014). p25 expression is significantly increased in post-mortem AD brains, and cdk5 is understood to phosphorylate tau epitopes associated with AD pathology (pSer202, pThr205, pSer235 and pSer404) (**Figure 1-3**) (Kimura et al. 2014; Patrick et al. 1999). A developmental study looked at murine embryonic day 14 (E14) and determined that *cdk5*-/- mice show no difference in total tau, but the cerebellum, spinal cord and brain stem show a significant decrease in pSer202 and pThr205 (Takahashi *et al.*, 2003). Studies focus on hyperphosphorylation of certain epitopes such as pSer396 to generate specific tau antibodies (Chukwu *et al.*, 2018). However, the exact trigger of tau hyperphosphorylation is unclear or even which epitopes are linked to AD-specific conformational changes in tau protein.

In post-mortem studies of AD patients, antibodies for specific phosphorylation epitopes of tau are used to observe the pathology burden in the brain. The development of different tau antibodies has advanced understanding of how specific phosphorylation sites on tau contribute to disease onset and progression (Petry *et al.*, 2014). AT8 is a mouse monoclonal antibody commonly used to examine tau hyperphosphorylation in post-mortem AD brains, transgenic AD mouse models and cell culture. This antibody detects the phosphorylation sites pSer202 and pThr205 (Goedert, Jakes and Vanmechelen, 1995). Another antibody of interest is PHF-1, a mouse monoclonal antibody used in the detection of PHF tau, recognising the pSer396 and pSer404 epitopes. It is clear that specific epitopes of tau are commonly associated with different stages of

tau fibrilization. AT8 and PHF-1-positive tau is associated with intracellular and extracellular NFTs (Augustinack *et al.*, 2002). This is crucial to understand when looking at the spatiotemporal development of pathology.

Modifications to tau protein, such as the truncation of the N-terminus have been shown to correlate with decline in episodic memory in AD patients (Ghoshal *et al.*, 2002). In post-mortem AD tissue, western blots showed a clear enrichment of truncated tau in the heavy molecular weight (HMW) fraction. HMW tau was not detected in control brains and was specific to AD tissue (Zhou *et al.*, 2018). Tau truncated at the C-terminal was also found in the AD cases, yet not within the HMW tau. Truncation and hyperphosphorylation of tau in turn leads to the release of tau from the presynaptic neuron and so contribute to the spread of pathology (Amadoro *et al.*, 2020).

Ubiquitination, the binding of ubiquitin to soluble proteins to designate for degradation by the cytosolic ubiquitin-proteasome system (UPS), was found to be significantly upregulated in cerebrospinal fluid (CSF) levels of tau of AD patients (Iqbal *et al.*, 1998). Disturbance of homeostatic protein degradation through the UPS has been highlighted in a multitude of neurodegenerative diseases including AD (Jansen, Reits and Hol, 2014; Zheng *et al.*, 2016). Furthermore, tau has been suggested to accumulate within the cytosol as a direct result of dysfunction in this system (Bertolotti, 2018). In AD post-mortem tissue, synapses were enriched for hyperphosphorylated tau compared to control tissue; this finding was linked to deficits in the UPS (Tai *et al.*, 2012). Dementia progression is associated with synapse loss and tau accumulation (Ingelsson *et al.*, 2004; Spires-Jones and Hyman, 2014). The loss of physiological function of tau has far reaching consequences, including but not limited to protein degradation. This highlights how truncation and hyperphosphorylation of tau which results in aggregation and accumulation within the cell has further downstream consequences such as neurotoxicity.

1.2.4 The validity of murine models of tauopathies

In order to examine the spread of tau pathology, mouse models are often utilised. These models provide the capacity to carry out studies not possible in AD patients, providing a greater wealth of information prior to therapeutic research. However, mouse models are not without flaws, particularly when gene editing is necessary. For a successful mouse model, three categories of validity must be considered; construct validity, face validity and predictive validity (Chesselet and Richter, 2011). For construct validity, the gene mutations associated with the disease must also be present within the mouse model. If the mouse subsequently exhibits the outward behaviour associated with the disease that constitutes face validity. Finally, predictive validity is dependent on similarity in drug response between human patients and the mouse model.

Therefore, the overarching aim of mouse model research is to develop mouse models that resemble the human disease as closely as possible. As a result, the majority of AD mouse models are based around the three APP processing gene mutations (Oakley *et al.*, 2006; Saito *et al.*, 2011). This provides a very narrow view of the heterogeneity in pathology; this model does not consider the role of tau and does not mimic the progression of LOAD. Subsequent models have been crossed with mice expressing human tau mutations, yet there are limitations to these mouse models.

The mouse models used to examine the function of tau fall largely into three categories:

1) A model which expresses a human tau mutation, mainly either the P301S or P301L mutation found in FTDP-17

2) A model which expresses either one or multiple isoforms of human tau with no disease-associated mutation

3) A tau knockout (TauKO) mouse, which expresses no endogenous mouse tau.

FTDP-17 is one of the few tauopathies where a mutation in the *MAPT* gene has been shown to cause the disease. Whilst this is very rare, FTDP-17 mutations form the basis of generating mouse models of tauopathy. P301S and P301L are key mutations used in mouse models of tauopathy which both correspond to a mutation found in FTDP-17 patients. (Allen *et al.*, 2002; SantaCruz *et al.*, 2005; Yoshiyama *et al.*, 2007). FTDP-17 is a pre-senile dementia and has autosomal dominant inheritance that largely presents with bradykinesia and deficits in executive function. This is one of the few mutations in the tau gene known to be linked to a neurodegenerative disease, hence the P301S mouse model of tauopathy was bred to examine the aetiology of tau pathology (Allen *et al.*, 2002). P301S human tau mutation is expressed in the mouse with the 4R/0N isoform downstream of the murine *Thy1* promoter, a cell-surface glycoprotein expressed on thymocytes and neurons (Allen et al. 2002; Campsall et al. 2002). The P301S mouse model develops insoluble AT8-positive tau pathology within the brainstem and spinal cord at 5 months (Allen *et al.*, 2002) (**Table 1-1**). However changes in the plasticity of cortical dendritic spines are reported a month prior to pathology (Hoffmann *et al.*, 2014). P301S mice show signs of motor and balancing deficits in the rotarod test at 3-4 months, progressing to severe paraparesis at 6-7 months (Scattoni *et al.*, 2010; Xu *et al.*, 2014). Therefore it is possible to see that by using a mutation known to exist in human disease, the mouse exhibits similar symptoms such as motor deficits.

Table 1-1: Tauopathy and AD mouse models

Name	Primary paper	Gene	Genetic background	Mutation	Promoter	Genotype (3R/4R tau)	Hyperphosphorylation of tau epitopes	Inflammation	Neuronal/synapse loss	Cognitive changes
hTau.P301S	Allen *et al.* 2002	MAPT	CBA;C57BL/6	MAPT P301S	Thy-1	Four-repeat tau (4R0N) + murine tau	AT8-positive tau in the frontal cortex, brainstem and SC at 5 months (Allen *et al. 2002)*	↑ *Clec7a* and ↑ *Itgax* (SC) (Torvell *et al*. 2019)	Motor neurons loss in the SC at 3 months (Allen *et al.* 2002); cortical neuron loss at 5 months (Hampton *et al.* 2010)	↓ Morris Water Maze (MWM) at 2 months (Xu *et al.* 2014); ↓ rotarod at 3 months and severe paraparesis at 6 months (Scattoni et al. 2010)
PS19	Yoshiyama *et al.* 2007	MAPT	C57BL/6;C3H	MAPT P301S	Prnp	Four-repeat tau (4R0N) + murine tau	PHF-1 positive tau in the hippocampus, amygdala and spinal cord at 6 months (Yoshiyama *et al.* 2007); AT8-positive tau in the	↑ GFAP (HPC, EC and SC) at 6 months, ↑ MHCII and CD11b (HPC) at 4 months	Synaptophysin decreases at 3 months; reduced fEPSPs at 6 months followed by	↓MWM at 6 months (Takeuchi *et al.* 2011)

							hippocampus at 4 months (Takeuchi *et al.*, 2011)	(Yoshiyama et al. 2007)	neuronal loss at 8 months (Yoshiyama *et al.* 2007)	
3xTg-AD	Oddo *et al.* 2003	APP, PSEN1, MAPT	C57BL/6;129X1/SvJ;129S1/Sv	APP KM670/671NL (Swedish), MAPT P301L, PSEN1 M146V	Thy-1	Four-repeat tau (4R0N) + murine tau	MC1 & AT8-positive tau at 12 months; PHF-1-positive tau at 18 months (Oddo *et al.*, 2003)	↑ *TNfα* and *MCP-1* mRNA (EC) at 6 months (Janelsins *et al.*, 2005)	LTP reduced at 6 months (Oddo *et al*. 2003)	↓Barnes test at 6.5 months (Stover *et al.*, 2015)
rTg4510	SantaCruz *et al.* 2005	MAPT	129S6;FVB	MAPT P301L	CaMKIIα	Four-repeat tau (4R0N) + murine tau	MC1-positive tau at 1 month, PG5-positive tau at 2.5 months, argryophilic tau at 4 months in the cortex and 5 months in the HPC	↑ *Gfap*, *Clec7a*, *CD68* and *Itgax* mRNA (EC) from 4 months (Castanho *et al.*, 2020)	CA1 hippocampal neuronal loss at 5.5 months (SantaCruz *et al.* 2005)	↓ MWM at 4 months (SantaCruz *et al.* 2005); ↓Y-maze at 4 months (Blackmore *et al.*, 2017)

							(SantaCruz *et al.* 2005)			
htau	Andorfer *et al.* 2003	MAPT	Swiss Webster;129/SvJae;C57BL/6	No disease-associated mutation	PAC cloning vector driven by MAPT promoter	All six human tau isoforms, higher 3R tau ratio (8c mice have 4R mouse tau)	Minimal PHF-1 neuronal staining in HPC at 4 months (Polydoro *et al.*, 2009); MC1- and PHF-1-positive tau in the cortex and HPC at 9 months (Andorfer *et al.* 2003)	Microglia are reported to maintain the homeostatic profile up to 22 months of age (Zhu *et al.*, 2020)	LTP induced by high frequncy stimulation is impaired at 12 months (Polydoro *et al.* 2009)	↓ Object recognition and MWM at 12 months (Polydoro *et al.* 2009); ↓food burrowing at four months (Geiszler, Barron and Pardon, 2016)
H1*Mapt*-/-	Wobst *et al.* 2017	MAPT	C57BL/6	No disease-associated mutation	PAC cloning vector driven by MAPT promoter	All six human tau isoforms, higher 3R tau ratio. No endogenous mouse tau.	No HT7-positive pathology in the cortex or HPC at 21 months (Wobst *et al.* 2017)	Not reported	Normal LTP function reported (Vargas-Caballero *et al.* 2017)	Potential increase in anxiety-like behaviour in elevated plus maze (Wobst *et al.* 2017)

Tg2576	Hsiao *et al.*, 1996	APP	C57BL/6; SJL	APP KM670/671 NL (Swedish)	Prnp	Murine tau	N/A	Reduction in *Trem2* mRNA expression at 5 months in the HPC and cortex (Porrini *et al.*, 2015)	Loss of spine density and impaired LTP at 4 months (Jacobsen *et al.*, 2006)	↓T maze performance at 16 months (Chapman *et al.*, 1999); ↓MWM at 12-18 months (Westerman *et al.*, 2002)
5xFAD	Oakley *et al.* 2006	APP	C57BL/6; SJL	APP K670N/M671L (Swedish); APP I716V (Florida); APP V717I (London); PS1 M146L/L286V	Thy-1	Murine tau	AT8-positive tau in the HPC and cortex at 5 months (female) and 7 months (male) (Shin *et al.*, 2021)	↑ GFAP and F4/80 staining (HPC) from 2 months (Oakley *et al*. 2006)	PSD-95 declines at 9 months; neuronal loss in cortical layer V at 6 months (Oakley *et al.* 2006)	↓MWM at 2 months (Tang *et al.*, 2016)

Tau22	Schindowski *et al.* 2006	MAPT	C57BL6;CBA	Transgene of human 4R tau with G272V and P301S mutations	Thy-1	4R	AT8 at 3 months and PHF-1 at 6 months in the HPC (Schindowski *et al.*, 2006)	↑GFAP at 3 months (Schindowski *et al.* 2006)	↓ CA1 neuronal loss, ↓fEPSP at 14 months (Schindowski *et al.* 2006)	↓memory in MWM at 10 months (Schindowski *et al.* 2006)
T44mTau KO	He *et al.* 2020	MAPT	C57BL/6	No disease-associated mutation	Prnp	3N0R	PHF-1 tau reported at 6 months in the cortex (Ishihara *et al.*, 1999)	N/A	N/A	↓ tail suspension test at 9-12 months (Zhang *et al.*, 2005)
Abbreviations: SC= spinal cord, HPC= hippocampus, EC= entorhinal cortex MWM= Morris Water Maze, fEPSP= field excitatory postsynaptic potentials										

The rTg4510 mouse model is an alternate model, examining the spread of tau within the forebrain. The rTg4510 mouse model possesses a P301L human tau mutation found in familial frontotemporal dementia (fFTD) (Alberici *et al.*, 2004). The human P301L tau mutation (4R0N) is expressed under the calcium (Ca^{2+})/calmodulin-dependent protein kinase II α (*CaMKIIα*) promoter, and thus expressed predominantly in neurons in the forebrain (Colbran, 2004). The rTg4510 mice are a conditional mouse model with a Tet-Off system, where the use of a tetracycline transactivator (tTA) binds to a Tetracycline Response Element (TRE) upstream of the gene of interest. Following the administration of doxycycline, doxycycline binds to the tTA and prevents the expression of the gene of interest (Mizuguchi and Hayakawa, 2002). It has been shown that rTg4510 mice express pathological tau in the hippocampus and frontal cortex at 5.5 months, as shown with the aforementioned PG-5 antibody although pre-tangles are observed at 2.5 months (**Table 1-1**) (Jicha *et al.*, 1999; SantaCruz *et al.*, 2005). These mice also exhibit cognitive deficits in the Morris Water Maze (MWM) at 4 months (Jul *et al.*, 2016). However, the rTg4510 mice do exhibit hyperactivity at 5 months of age in correlation with tau pathology (Wang *et al.*, 2018).

Pathology simply from overexpression of human tau has been observed in *Drosophila melanogaster* (Jackson *et al.*, 2002) and the P301S and rTg4510 mice both significantly overexpress mutant tau and develop pathology without intervention. However, these P301S and P301L tau mutations linked to FTDP-17 are not found in AD. It highlights a crucial problem when examining tau pathology; how can the aetiology of tau pathology in FTDP-17 mouse models, be extrapolated to our understanding of AD? When there is only one isoform of overexpressed human tau, there is a loss of context as to how different tau isoforms may interact. In the P301S and rTg4510 mouse there is still mouse tau expressed in the brain, which has significant differences to human tau. Primarily, mice solely express four-repeat tau (Götz *et al.*, 1995; Andorfer *et al.*, 2003). This is crucial as there is evidence that whilst in the healthy human brain the 3R/4R tau ratio is approximately equal, four-repeat tau shows greater aggregation *in vitro* (Adams *et al.*, 2010). As a result, studies are increasingly turning to 'humanised' mouse models, in an attempt to mimic the conformational changes to tau in AD.

There have been several human tau mouse models, commonly referred to as hTau mice. These mice were primarily developed to combat the need for overexpression of mutant isoforms and attempt to develop tau pathology in a mouse which expresses all six isoforms of human tau. One of the initial models, the 8c model, expressed all six isoforms of human tau in addition to normal mouse tau. The predominant isoforms were three-repeat tau, and the expression of four-repeat tau was mostly murine (Duff *et al.*, 2000). To combat this, the hTau mouse was developed

by crossing the 8c mouse with TauKO mice (Andorfer *et al.*, 2003). They report MC1- and PHF-1 positive hyperphosphorylated tau by 6 months and significant PHF-1 tau burden in the cortex and hippocampus by 9 months (**Table 1-1**). Crucially pathology was predominantly observed in the cortex and hippocampus. This suggests that the expression of all six isoforms, despite an altered ratio in favour of three-repeat tau, induces tau aggregation in accordance with AD pathology.

The mouse model utilised in this thesis is a more recently developed human tau mouse model. The H1*Mapt-/-* mouse model does not exhibit tau pathology, even at 21 months of age (Wobst *et al.*, 2017). The H1 refers to the H1 haplotype, a haplotype significantly associated with an increased risk of LOAD (Pastor *et al.*, 2016). These hemizygous mice expressed significantly less total tau than wild type (WT) mice. The H1 transgene was generated by sub-cloning the 143kb WT H1 locus into a pCYPAC2 P1 bacteriophage-derived artificial chromosome (PAC) vector (Peruzzi *et al.*, 2009). The human *MAPT* locus vector (pPAC-*MAPT-H1*) was used to generate transgenic mice through pronuclear injection (Ittner and Götz, 2007). The transgenic mice which express the entire human *MAPT* locus (Wobst *et al.*, 2017), were backcrossed for 9 generations with the C57BL/6 *Mapt-/-* mice (Dawson *et al.*, 2001). This mouse therefore has a pure C57BL/6 background and expresses the H1 haplotype on chromosome 6. The H1*Mapt-/-* mouse does show higher expression of three-repeat tau than in human brains, yet not as high as in the 8c mouse model. As a result there is greater exon 10 splicing within this model (Vargas-Caballero *et al.*, 2017). This model is useful to look at the spreading of tau; by experimentally inducing tau pathology in mice which otherwise would not develop pathology, it allows greater control and understanding of the mechanisms which may be involved. This thesis aims to address how once tau propagates through the brain, what factor determine the rate of spread.

1.2.5 Seeding and spreading of tau pathology in Alzheimer's Disease

There is a wealth of evidence suggesting that tau propagates both in an antero- and retrograde manner along axons leading from the entorhinal cortex to the larger limbic circuit including the hippocampus (Hyman *et al.*, 1984). From there pathology is observed in the wider neocortex at Braak stages V and VI (Schultz, Del Tredici and Braak, 2010). In post-mortem AD brains the spreading of tau pathology correlates with both neurodegeneration and cognitive loss (Gomez-Isla *et al.*, 1997; Ingelsson *et al.*, 2004). Subsequent PET imaging of tau confirmed that it is tau pathology which correlates to cognitive decline in AD patients (Zhou and Bai, 2017). Yet how does tau pathology spread through the diseased brain? There have been a multitude of studies in mice attempting to recapitulate the spreading of tau observed in AD. Theoretically mimicking and investigating the propagation mechanism leads to understanding of how tau spread may be

interrupted, slowed or stopped entirely. If tau spread correlates with cognitive decline, finding a mechanism to slow this spread in humans may slow cognitive decline observed in AD patients.

Mechanisms of tau spreading was initially hypothesised to occur primarily through neuron-to –neuron interaction (**Figure 1-4**). It has been suggested that the majority of extracellular tau is membrane-free (Yamada, 2017); it has been shown that tau is released through its association with extracellular vesicles (Lee *et al.*, 2012), regulated by excitation of primary cortical neurons *in vitro* (Pooler *et al.*, 2013). In order to be taken up by the 'recipient' neuron, tau uptake is also mediated by receptors *in vitro* such as APP and heparan sulfate proteoglycans (HSPGs) using macropinocytosis (Holmes *et al.*, 2013). Exosomes facilitate both the release and uptake of tau by recipient neurons; tau has been shown to associate with exosomes both in the blood of AD patients and the CSF of patients with mild AD (Saman *et al.*, 2012; Fiandaca *et al.*, 2015). Isolating exosomes from the rTg4510 mouse model of tauopathy (**Table 1-1**) were shown to both contain tau and possess the capacity to spread tau *in vitro* (Polanco *et al.*, 2016). Therefore, there are a multitude of mechanisms, primarily studied *in vitro*, which facilitate the spreading of tau between neuronal pathways.

Using AD post-mortem tissue, several mechanisms of tau spread were initially proposed by Heiko Braak; it was hypothesised that tau may spread across the brain regardless of region, or that pathology spreads dependent on synaptic networks (Schultz, Del Tredici and Braak, 2010). To study this mechanism *in vivo*, murine 'spreading models' were established. The premise of the spreading model is that by injecting pathological forms of tau into the brain parenchyma of a mouse it is possible to observe how the tau protein spreads and to which region it propagates. Initial studies utilised mouse models of tauopathy, such as the P301S mouse model which quickly develops significant tau pathology over a period of months. P301S brain lysate from late-stage mice was injected unilaterally into the hippocampus of young P301S mice prior to pathology development; this was also carried out in the P301L mouse model. Both models showed spreading of pathological tau into the contralateral hemisphere and clear spread to regions connected by synaptic pathways rather than proximity (Ahmed *et al.*, 2014; Peeraer *et al.*, 2015). In the P301S mouse, pathological tau was shown to spread to the contralateral hemisphere as early as 1 month post-injection (Ahmed *et al.*, 2014). It must be considered that the P301S mouse does not develop pathology in the hippocampus at this time point without the injection. This demonstrated the clear capacity of tau pathology to spread through the limbic circuit in an antero- and retrograde path (Ahmed *et al.*, 2014). Key areas highlighted were the fornix (a white matter tract), the mammillary nuclei and the retrosplenial cortex, all regions of the wider limbic circuit (**Figure 1-2**).

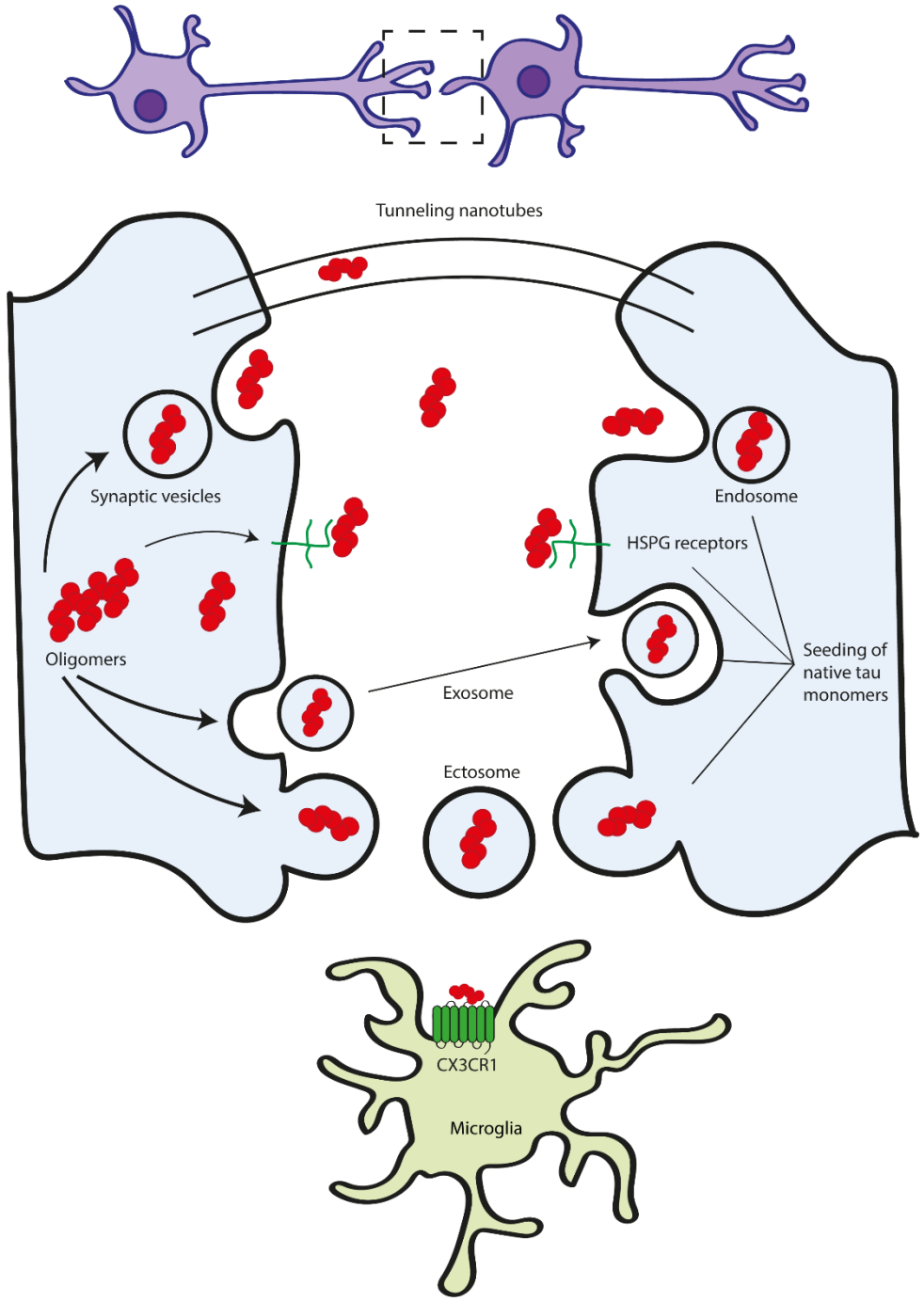

Figure 1-4: The mechanism by which tau propagates through neurons

Tau seeds are proposed to be released through the formation of exosomes, synaptic vesicles, tunnelling nanotubes and the binding of free tau to HSPG receptors. Uptake mechanisms of tau include macropinocytosis and endocytosis, by which toxic soluble oligomers are taken up by actin cytoskeleton rearrangement and invagination of the membrane respectively. This leads to the formation of an endosome and release of the oligomers. Furthermore, the exosome is thought to fuse with the recipient neuron. Microglia are then able to uptake tau seed through fractalkine receptor binding. Diagram based on Šimić *et al.* 2016, Gibbons *et al*. 2019 and Perea *et al.* 2020

Pathological tau propagates along synaptic pathways yet is also proposed to recruit native unfolded tau to a pathological form. This is termed seeding and is a crucial hypothesis of neurodegenerative disease progression (Walker *et al.*, 2013). The tau hypothesis states that it is the accumulative seeding of physiological tau by its pathological counterpart and subsequent aggregation that is the principal cause of AD (Iqbal *et al.*, 2010). First described in 1982, prion aggregation was proposed to be the pathogenic cause behind the central nervous system (CNS) disease scrapie found in sheep (Prusiner, 1982). Pathological prion protein (PrP^{Sc}) recruits native prion protein (PrP^{C}) to undergo conformational changes, including a significant shift towards β-sheet structure (Pan *et al.*, 1993). Furthermore, prion diseases require existing prion protein for the pathological form to 'seed' and recruit, thereby accumulating and spreading the pathology. Due to the mechanism by which tau has been observed to spread through the brain and recruit native protein, pathological tau is often referred to as 'prion-like' in nature.

It is not currently defined at which stage in aggregation tau is at its highest seeding capacity. It is hypothesised that tau oligomers are neurotoxic, however its seeding capacity is debated (Gerson *et al.*, 2016; Shafiei, Guerrero-Muñoz and Castillo-Carranza, 2017). One study examined at which stage of tau pathology the greatest seeding was occurring. A common method of extracting tau at various stages of aggregation (and therefore molecular weight) is to separate them along sucrose gradient fractions. Jackson *et al.* (2016) determined that within the tau mouse model P301S, Sarkosyl-soluble oligomeric tau was detected within the 10-20% fraction, whilst HMW Sarkosyl-insoluble tau was detected in the 40% fraction (Jackson *et al.*, 2016). Jackson *et al.* (2016) unilaterally injected 10% and 40% fractions of lysate from P301S brains at late-stage pathology into the parenchyma of young P301S mice. Ten weeks later the 40% fraction of tau had spread to the contralateral hemisphere; by contrast, the group injected with the 10% tau fraction observed no pathology (Jackson *et al.*, 2016). This suggests that it is the fibrillar hyperphosphorylated structures of tau which have the highest seeding capacity; specifically, this pathological form of tau was highly AT8-positive.

Investigation into the concept of seeding inevitably highlighted a need for development of the spreading models. The P301S study aforementioned (Ahmed *et al.*, 2014) showed clear spreading of tau through synaptic pathways. However, spreading models in mice such as the P301S or Tg4510 mouse have several limitations. For example, these mouse models of tauopathy express a single isoform of human tau which also contains a mutation for FTDP-17. Seeding, as observed in prion studies, requires native protein. Whilst ideal for understanding the initial mechanism of tau spreading, it must be considered that this spreading model may not explain the spreading of tau observed in AD. Therefore, studies examining tau spreading have shifted towards a 'humanised' version of tauopathy. Post-mortem tissue is homogenised and enriched for

insoluble fractions of tau. This aggregated pathological form of tau is then injected into the brain parenchyma of WT or hTau mice. One recent study carried out this spreading model and reported tau pathology similar to Ahmed *et al.* (2014) in synaptically connected regions such as the hippocampus, mammillary nuclei and the entorhinal cortex (Henderson *et al.*, 2020). These studies highlights the importance of the limbic circuit as a pathway for the spreading of tau. The areas synaptically connected where pathology was observed is demonstrated in **Figure 1-5**. The importance of the white matter fimbria fornix in spreading pathology to these ventral brain regions is clear to observe.

Previous studies in mice have shown that intracerebral (i.c.) injection of pathological tau from AD, CBD and PSP post-mortem tissue does not result in identical pathology. Distinct pathology from each tauopathy was recapitulated in WT mice (Narasimhan *et al.*, 2017) and prior to this, in mice which express WT human tau (line ALZ17) (Clavaguera *et al.*, 2013). When human brain lysate enriched for insoluble tau from each disease is injected into WT mice, there are differences both in how aggressively the pathology spreads and also whether the pathology is found exclusively in neurons (AD) or in glial cells such as oligodendrocytes (CBD) (Narasimhan *et al.*, 2017). This suggests that the differences in pathology observed in human tauopathies can be mimicked in mouse models. This has since been confirmed by the same group that conformation of the tau protein imparts differences in seeding through the mouse brain (He *et al.*, 2020). In WT mice (4R tau) and a mouse which only expressed 3R tau (T44mTauKO), lysate enriched for AD tau demonstrated pathology spread in both brains, by contrast lysate enriched for PSP-tau showed pathology spread only in the WT mice. This demonstrates clearly how the interaction between native protein expressed in the mouse brain and the conformation of tau within the AD-lysate will determine the seeding capacity and subsequent pathology burden observed. Therefore, to study the mechanism behind propagation of AD-tau, it is imperative to utilise tau derived from AD post-mortem tissue.

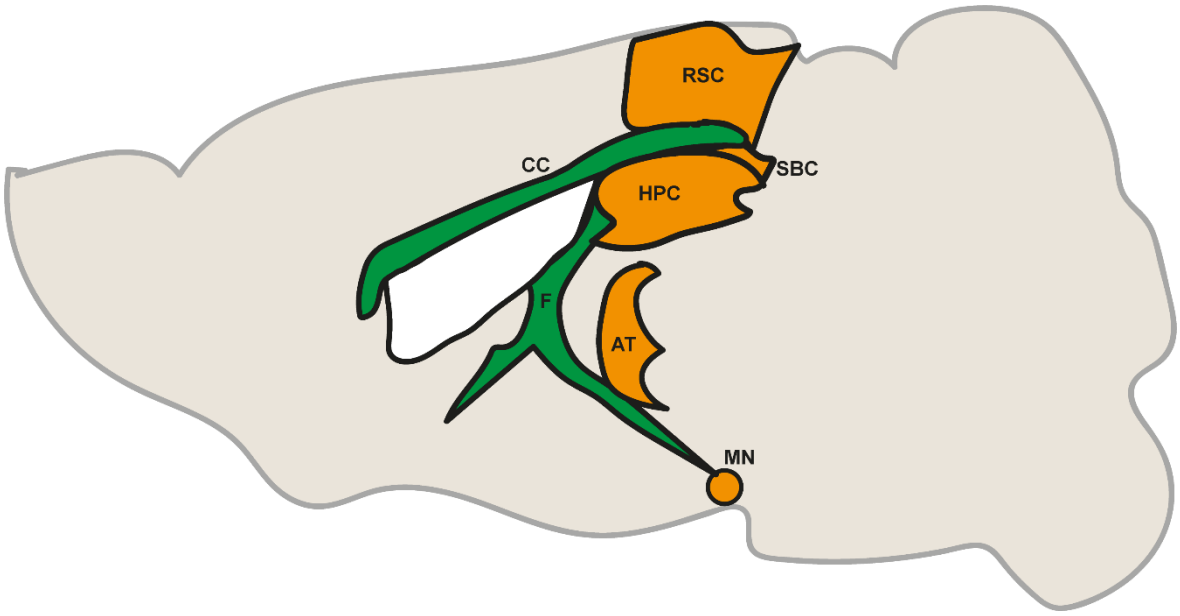

Figure 1-5: Tau propagates through synaptically connected regions of the brain

Regions which showed immunoreactivity against antibodies for hyperphosphorylated tau in Ahmed *et al.* (2014). The retrosplenial cortex (RSC), subiculum (SBC), hippocampus (HPC), anterior thalamus (AT) and mammillary nuclei (MN) all show clear propagation of tau pathology in the P301S mouse model at 2.5 months post-injection. The corpus callosum (CC) and fornix (F) are two of the main white matter tracts in the brain, the connection of these regions along these white matter tracts is clear to observe in the sagittal cross-section. Grey matter regions of interest shown in orange, white matter tracts shown in green. Figure adapted from Ahmed *et al.* (2014).

1.2.6 The role of microglia in the uptake and release of tau

In more recent years, it has been proposed that microglia may alter tau spreading. Microglia (described further in sections 1.2.3 and 1.3.1), reside within the brain parenchyma and are the primary immune cell within the brain. Microglia in the healthy brain play a role in synaptic pruning and maintain contact with synapses. There is evidence in mouse models that microglia engulf synapses in AD (Xie *et al.*, 2017). Intracerebral injection of tau tagged with Cy5 in C57BL/6 mice demonstrated that microglia are capable of tau uptake *in vivo* (Bolós *et al.*, 2015); this same study demonstrated an overlap of NFTs and pan-microglial marker Iba1 in AD post-mortem tissue. A separate study examined tau propagation *in vivo* in microglia of the P301S tau mouse model (Asai *et al.*, 2015). Synthesis inhibition of microglial exosomes was carried out using GW4869, a neutral sphingomyelinase inhibitor which prevents release of mature exosomes from multivesicular bodies. Notably this inhibitor is not specific to microglial exosomes. Daily intraperitoneal (i.p.) injection of GW4869 over 4 weeks reduced tau spread to the dentate gyrus

from the entorhinal cortex (Asai *et al.*, 2015). Based on established Braak stages, tau pathology propagates from the entorhinal cortex to the dentate gyrus in AD patients, highlighting the importance of this synaptic pathway (Schultz, Del Tredici and Braak, 2010). This suggests that disruption of microglial exosome function alters the spreading of tau.

It is proposed that tau uptake by microglia is in part facilitated through the fractalkine receptor (CX3CR1) (**Figure 1-4**). A transmembrane glycoprotein expressed on myeloid cells, CX3CR1 has been purported to be involved in recruitment of circulating monocytes in the periphery (Geissmann, Jung and Littman, 2003). CX3CR1 expressed on microglia interacts with the neuronal ligand CX3CL1, demonstrated to maintain the homeostatic role of microglia and supress release of pro-inflammatory cytokines. *In vitro* data shows that *Cx3cr1*$^{-/-}$ primary microglia have decreased uptake of 2N4R tau compared to WT primary microglia (Bolós *et al.*, 2017). Maphis *et al.* (2015) utilised mice expressing human tau and a knockout of fractalkine receptor (hTau*Cx3cr1*$^{-/-}$ mice) to compare development of pathology in hTau mice over time; hTau*Cx3cr1*$^{-/-}$ mice exhibited an increase in AT8-positive tau in the hippocampus up to two years of age (Maphis et al. 2015). It must be considered in these studies that CX3CR1 is a marker for all myeloid cells not simply microglia. However, *in vitro* studies suggest the fractalkine receptor allows uptake of tau by microglia through competitive binding which may facilitate spread (Chidambaram, Das and Chinnathambi, 2020). Whilst the mechanism behind this requires greater elucidation, it suggests that microglia and the central immune system may play a crucial role in the spreading of tau. it is possible that the mislocalisation of tau to the synapse due to post-translational modifications leads to greater uptake of tau and so wider spread of pathology. How the release and uptake of the tau 'seed' between neurons occurs is still unclear and the role of alternative cells in the brain such as immune cells such as microglia must not be ignored (**Figure 1-4**) (Šimić *et al.*, 2016).

If it is proposed that the rate of tau spread may be altered, by what mechanism is this occurring? The spreading of tau in the brain has been linked to immune cells such as microglia (Bolós *et al.*, 2017) yet how does the immune system within the brain link to this pathology? The rTg4510 mouse model shows significant upregulation of the complement system in aging, which is involved in phagocytosis and prompting inflammation (Wes *et al.*, 2014). The complement pathway forms one of the initial and most important responses to removal of pathogens through lysis of bacteria and recruitment of immune cells (Davies and Spires-Jones, 2018). Upregulation of the complement system has been found in human AD post-mortem brains (Yasojima *et al.*, 1999); peripheral readouts in AD patients show increased pro-inflammatory cytokines such as interleukin-6 (IL-6), interferon gamma (IFNγ) and IL-1β (Lai *et al.*, 2017). Furthermore, IL-6 expression showed an inverse correlation with cognition scores. The role of microglia in the

spread of tau suggests that inflammation and the spread of pathology may overlap. This suggests that in addition to tau pathogenesis, the immune system is disrupted within AD.

1.3 Homeostasis and dysregulation of neuroinflammation

One of the major shifts in the brain during aging and neurodegenerative disease is found in the regulation of the immune system. It has been hypothesised that during aging there is an imbalance between the regulations of pro- and anti-inflammatory cascades, crucial for neurological function. It is postulated that a decrease in adaptive immunity induces compensation in the innate immune system, hence elderly people lack the ability to quickly resolve viral or bacterial infections (Weng, 2006). It appears that inflammation, which in development and adulthood is regulated to our benefit for the removal of pathogens, becomes dysregulated in aging and may contribute to the development of neurodegeneration.

Aging increases susceptibility to systemic inflammation, a whole-body inflammatory response, commonly due to an infection. Many studies have examined the role of chronic systemic inflammatory diseases in the development of neurodegenerative diseases, and specifically in AD. Diseases such as type 2 diabetes mellitus (DM) are hypothesised to be a risk factor for AD development (Huang *et al.*, 2014); it is proposed that the heightened presence of oxidative stress within the brain due to chronic inflammation leads to increased occurrence of AD diagnosis (Butterfield, Di Domenico and Barone, 2015). However, studies comparing different patient cohorts often reach variable conclusions; studies examining correlation between rheumatoid arthritis (RA) and AD often present opposing hypotheses (Chou et al. 2016; Kao et al. 2016). This is most likely because some RA patients take anti-inflammatory drugs at different ages and for different lengths of time during their life. Variation between populations offers conflicting evidence, even without considering the variation in their AD presentation.

The initial notion was that the CNS possessed complete immune privilege, separated entirely from the peripheral inflammatory response by the blood brain barrier (BBB). This hypothesis has been rejected now for several years, although there is tight regulation by the BBB to maintain the homeostasis within the CNS (Carson *et al.*, 2006). However, peripheral inflammation caused by systemic infection can lead to changes in BBB integrity, potentially inducing an inflammatory response within the parenchyma (Varatharaj and Galea, 2017). Studies in AD patients highlight the link between inflammation in the brain and progression of AD (Holmes *et al.*, 2009; Newcombe *et al.*, 2018). This thesis attempts to answer whether these changes in the periphery and subsequently the brain, lead to greater tau pathology.

1.3.1 Interaction of the peripheral and central immune system

The parenchyma is protected from infection and injury by both the meninges and the BBB. The meninges consist of the superficial dura mater, and the arachnoid and pia mater which together form the leptomeninges. The subarachnoid space sits between the arachnoid and pia mater and has increasingly been highlighted as a key area for immune cell regulation (Weller *et al.*, 2018). This space is important for maintaining homeostasis as the arteries which vascularise the brain are a potential entry point to the CSF for immune cells. Leptomeningeal cells and vascular endothelial cells act as a barrier for the artery at the entry point to the parenchyma, whilst the glia limitans made of astrocytic end feet acts as a barrier between the meningeal environment and the parenchyma (Engelhardt *et al.*, 2016). The meninges are crucial both in protecting the parenchyma from injury and infection. Without these barriers even small infections could be damaging to the CNS due to the restricted window within which neuroinflammation is regulated.

The central immune system is highly regulated by the BBB, which separates the parenchyma from the peripheral blood by regulating infiltration of molecules through tightly packed endothelial cells. The BBB is a mesh of vascular endothelial cells and basement membrane surrounded by astrocytes, pericytes and perivascular macrophages, these cells make up the 'neurovascular unit' (Sharif *et al.*, 2018). There are multiple ways with which to cross the BBB, water-soluble molecules diffuse through tight junctions between endothelial cells. Molecules with high lipid solubility pass through endothelial cells by passive diffusion, and there are also transport proteins for molecules such as glucose which require greater regulation. There is also absorptive- and receptor-mediated transcytosis of crucial molecules for brain function such as plasma protein albumin and insulin respectively (Fu and Wright, 2018). Water moves freely through the BBB, yet countless regulatory systems control the movement of proteins and peptides to maintain homeostasis both for baseline immune cell function, but also for neuronal and vascular function (Serlin *et al.*, 2015). Alterations to the blood brain barrier can be as minimal as increased signalling of cytokines; or as severe as impairment to the endothelial cells and tight junctions which make up the BBB itself (Varatharaj and Galea, 2017). There is evidence that disruption of the hippocampal BBB, denoted by build-up of proteins such as fibrin, occurs in aging and deteriorated further in individuals with mild cognitive impairment (Montagne *et al.*, 2015).

In a cohort of 4,629 AD patients, 80% presented with vascular pathology (Toledo *et al.*, 2013). One form of vascular pathology is cerebral amyloid angiopathy (CAA), whereby amyloid is deposited in blood vessels of the brain leading to breakdown of both the vasculature and the BBB (Toledo *et al.*, 2013). Whilst CAA involves the deposition of amyloid within the vasculature,

changes in the leptomeninges of AD post-mortem tissue with markers such as collagen are reported with increased Braak staging (Merlini, Wanner and Nitsch, 2016). Furthermore, in AD post-mortem tissue insoluble phosphorylated tau was inversely correlated with tight junction proteins occludin and claudin-5 expression (Liu *et al.*, 2020).

There is evidence in post-mortem AD brains and in the CSF of preclinical AD that blood-derived proteins such as fibrinogen and albumin are increasingly present, suggestive of progressive BBB breakdown (Cullen, Kócsi and Stone, 2005; Montagne *et al.*, 2015; Sweeney, Sagare and Zlokovic, 2015). Vascular damage has also been observed in mouse models of AD along with blood-derived fibrin deposits (Paul, Strickland and Melchor, 2007). The deposition of plasma proteins such as fibrinogen and albumin within the parenchyma is indicative of infection or injury; microglial cells within the brain become activated in response, potentially leading to greater neuronal damage (Ralay Ranaivo and Wainwright, 2010; Davalos *et al.*, 2012). AD causes the build-up of aggregated protein which in itself is neurotoxic (Wegmann *et al.*, 2015). Therefore, the combination of pathology and breakdown of the BBB may serve to create a more pro-inflammatory and neurotoxic environment within the brain (Sweeney, Sagare and Zlokovic, 2018). This may highlight why an episode of systemic infection in AD patients correlates with an exaggerated pro-inflammatory cytokine response and increased cognitive decline (Holmes *et al.*, 2009) (discussed further in 1.2.3 and 1.3).

1.3.2 The immune response to infection

Humans possess both an innate and adaptive immune response. The innate immune response is highly conserved across species; encoded within an individual's germline it allows for detection of molecules identified as 'non-self' (Sankowski, Mader and Valdés-Ferrer, 2015). By contrast, the adaptive immune system is found in vertebrates alone, this response is experience-dependent and cooperates with the innate immune system to identify initial pathogens (Cooper and Alder, 2006).

Following infection or inflammation, pathogen-associated molecular patterns (PAMPs) are recognised by the innate immune system. PAMPs are motifs such as lipopolysaccharide (LPS), the endotoxin on gram-negative bacterial cell membranes. These PAMPs are identified by toll-like receptors (TLRs) or pattern recognition receptors (PRRs) of neutrophils, macrophages and dendritic cells (DCs) (Lehnardt *et al.*, 2003). This detection of pathogenic motifs initiates a signalling cascade and an inflammatory response (Kumar, Kawai and Akira, 2011) through the subsequent release of pro-inflammatory cytokines such as Tumour Necrosis Factor alpha (TNF-α), IL-1β and IL-6 by macrophages and neutrophils.

This initiates a cascade which can induce a great many changes, such as neuronal damage. For example, primary neurons exposed *in vitro* to IL-1β and TNF-α showed upregulation of glutaminase isoform kidney type glutaminase. Glutaminase converts glutamine to glutamate, disproportionate glutamate production leads to neurotoxicity and neuronal death (Ye *et al.*, 2013). This has previously been reported in AD through excessive glutamatergic N-methyl-d-aspartate receptor (NMDAR) activity (Wang and Reddy, 2017). Furthermore, cortical endothelial cells in microvessels of post-mortem AD brain have significantly upregulated expression of IL-1β, TNF-α and IL-6 (Grammas and Ovase, 2001). This suggests that in the AD brain there is a significant increase in pro-inflammatory cytokines, which appear to mediate neurotoxicity. There is also potential for development of sickness behaviour such as lethargy and anhedonia in response to cytokine production (Perry, 2004); a cohort of 300 patients with AD showed correlation with sickness behaviour and elevated TNF-α and IL-6 in the serum (Holmes *et al.*, 2011).

The immune response to infection or injury is primarily carried out by macrophages, DCs and lymphocytes, although all cells expressing TLRs can be involved. Macrophages and DCs are both derived from hematopoietic stem cells and are from the myeloid lineage from common precursors in the yolk sac, foetal liver and bone marrow, dependent on the different adult populations (Fogg *et al.*, 2006; Epelman, Lavine and Randolph, 2014). Macrophages are resident within the tissue and display both pro- and anti- inflammatory roles through phagocytosis and production of cytokines (Lavin *et al.*, 2015). These populations were shown to be maintained by monocytes derived from adult bone marrow progenitor cells. In the periphery, monocytes circulate within the blood stream with the capability of differentiation to DCs or tissue-resident macrophages, although the exact role of these cells and their peripheral population dynamics are still debated (Lavin *et al.*, 2015).

The innate immune response propagated by macrophage and DCs results in the activation of the adaptive immune response primarily in the form of B-cell and T-cell activation. DCs are the primary initiator of the adaptive immune response through antigen presenting (Steinman, 1983). DCs are professional antigen presenting cells (APCs); following an infection these cells will internalise antigens and present the associated peptides to T cells through upregulation of major histocompatibility complexes (MHC) (den Haan, Arens and van Zelm, 2014). The T-cell and B-cell lymphocytes are the crux of the adaptive immune response, derived from the thymus and bone marrow respectively. $CD4^+$ and $CD8^+$ cells both express T cell receptors, although they only recognise MHC class II and I respectively (Bonilla and Oettgen, 2010). MHCI class I (MHCI) is generally found endogenously due to either viral infection or bacteria which replicate within the cell. By contrast, MHC class II (MHCII) is commonly expressed on antigen presenting cells. MHCII

upregulation induces T-cell expansion and the release of cytokines. $CD8^+$ cytotoxic T-cells become activated and phagocytic in nature to remove the pathogen by cell-mediated immunity. By contrast, $CD4^+$ helper T-cells will promote B-cells, neutrophils and cytotoxic T-cells to the site of infection (Dempsey, Vaidya and Cheng, 2003). From this B-cells are able to produce antibodies from plasma cells in order to combat the pathogen through humoral immunity; phagocytosis and lysis of the pathogen can also occur by cytotoxic T-cells. There are then memory B-cells, helper T-cells and cytotoxic T-cells which remain. It is evidenced that memory $CD8^+$ and $CD4^+$ T-cells are stored in the bone marrow in survival niches (Becker *et al.*, 2005; Tokoyoda *et al.*, 2009; Chu and Berek, 2013).

This research refers to the periphery. By contrast the brain is far less understood, with different populations and stem cell niches. The peripheral immune system should be separate from the central immune system, yet there is evidence that by dysregulation through aging and neurodegenerative disease, these barriers are disrupted. Therefore, the peripheral infection can induce a response within the brain due to changes in the BBB, ranging from minimally to highly disruptive.

1.3.3 Resident immune cells of the central nervous system

In the brain there are populations of immune cells distinct from the periphery. The prominent immune cell in the parenchyma is the microglial cell, derived from erythro-myeloid progenitors in the yolk sac (Hashimoto *et al.*, 2013; Mass *et al.*, 2016). However, due to the isolated location of microglial cells within the brain they are ontogenically different to peripheral mononuclear phagocytes. Contribution from circulating monocytes is only found at postnatal day 3 with no further renewal by peripheral progenitors from the bone marrow observed, and microglia self-renew through proliferation (Ginhoux *et al.*, 2010; Askew and Gomez-Nicola, 2018). There are also border associated macrophages and DCs within the meninges and choroid plexus; they are now thought to be distinct populations yet do show similarity to the macrophages residing in the parenchyma (Goldmann *et al.*, 2016). Leukocytes such as monocytes, B-cells, T-cells and eosinophils are reported in the CNS of a healthy 2-month old C57BL/6 mouse (Mrdjen *et al.*, 2018). The majority of these were found to be resident within the tissue as opposed to within the vasculature. The technical difficulties behind studying resident and infiltrating immune cell populations within the brain should be highlighted; these populations shift both in the healthy brain and in the presence of infection or disease, as a result there still remains uncertainty in this field.

Microglia are the most prominent immune cell in the CNS, although only between 5 and 12% of the glial population are microglia (Lawson *et al.*, 1990). In the healthy brain, each microglia surveys its own 'microenvironment' with long processes to detect potential pathogens. Microglia are proposed to be crucial for the control of neurogenesis during development, synaptic pruning and removal of cell debris (Paolicelli *et al.*, 2011; Tremblay *et al.*, 2011; Cunningham, Martinez-Cerdeno and Noctor, 2013). However, there is a homeostatic regulation of microglia whereby in the steady-state, microglia exhibit different functions and a different phenotype than under the influence of infection or injury. Following neuronal cell death, there is release of nitric oxide (NO) and adenosine triphosphate (ATP). This evokes an initial response by microglia referred to as 'directed motility' (Madry and Attwell, 2015), whereby microglia become polarised and extend their processes towards the source of ATP through the use of purinergic receptors such as P2Y12 (Haynes *et al.*, 2006). This denotes the progression of microglia from a ramified phenotype to an activated phenotype, the microglial processes shorten and microglia both proliferate and migrate towards the site of infection and/or injury. The resting and activated microglia were previously viewed to be separate M1 and M2 phenotypes (Cherry *et al.*, 2014), however this is now considered to be a spectrum with most microglia exhibiting a mixed profile (Morganti, Riparip and Rosi, 2016).

The primary function of microglia following an insult is to initiate the innate immune response. Similar to peripheral macrophages, microglia release pro-inflammatory cytokines such as IL-1β (Hartlage-Rübsamen, Lemke and Schliebs, 1999), TNF-α (Guadagno *et al.*, 2013), IL-6 (Burton, Sparkman and Johnson, 2011) and monocyte chemoattractant protein-1 (MCP-1) (Babcock *et al.*, 2003) as chemoattractants to the source of injury or infection. $CD11c^+$ microglia (transmembrane protein expressed on monocytes and macrophages) also have the capacity to recruit $CD4^+$ T-cells (Wlodarczyk *et al.*, 2014). Following infection microglia upregulate expression of CD11b, an integrin which is a subunit of complement receptor 3 involved in phagocytosis (Jurga, Paleczna and Kuter, 2020). Expression of high-affinity IgG-binding Fc receptors, such as FcγRI (also referred to as cluster of differentiation 64 (CD64)) are upregulated on microglia following infection or injury, this receptor plays a role in phagocytosis, antigen presentation and the release of cytokines (Nimmerjahn and Ravetch, 2007). Microglia begin to express activation markers such as MHCII (Mrdjen *et al.*, 2018). Upregulated expression of MHCII following *in vivo* infection is mediated by the release of pro-inflammatory cytokine interferon gamma (IFNγ) (Zhou *et al.*, 2007), allowing microglia to act as APCs. This cascade results in a population of activated microglia and the release of pro-inflammatory cytokines aforementioned. As a result, the BBB becomes increasingly permeable to infiltration from the periphery. Therefore, the microglial cells

play a crucial role both in the maintenance of the steady-state and following infection. However, the homeostatic regulation of microglia may become altered in AD.

Microglia release both pro-inflammatory and anti-inflammatory cytokines, hence the multitude of roles they have been assigned within the brain. Infection or injury within the CNS requires pro-inflammatory cascades to be activated; it is crucial that these pathways are dampened following resolution to prevent excessive damage. One of the major differences between pro- and anti-inflammatory actions by microglia is their cytokine secretion; microglial G-protein coupled chemokine receptors have two major groups, CC and CXC receptors, to which CC chemokines and CXC chemokines bind respectively (Biber, Vinet and Boddeke, 2008). Through downstream mitogen-activated protein kinase (MAPK) pathways such as the extracellular signal-regulated kinase (ERK) and c-Jun N-terminal kinase (JNK) pathway, chemokines are able to activate many microglial functions including chemotaxis (Fan, Xie and Chung, 2017).

In aging, changes in microglial populations have been observed both in humans and animals, with significant increase in the microglial population of rhesus monkeys aged 25-35 compared to monkeys aged 5 years (Peters, Josephson and Vincent, 1991). Regarding their function, the microglial cells in aging human populations are hypothesised to become increasingly senescent with loss or fragmentation of processes (Streit *et al.*, 2004; Davies *et al.*, 2017). It has been suggested using RNA-seq that in aging, there is an upregulation of interferon signalling and antigen processing in microglia, leading to an increasingly pro-inflammatory state and association with pathology (Olah *et al.*, 2018).

It has been proposed that microglia become 'primed' in AD, due to the presence of misfolded protein and changes in neuronal function. This suggests that microglia have a lowered threshold for secondary activation, meaning that an additional stimulus such as infection results in an aggravated response (**Figure 1-6**) (Perry and Holmes, 2014). Mrdjen *et al.* (2018) showed a shift in microglial signature in both the APP/PS1 mouse model (**Table 1-1**) and aged mice of increased markers of activation CD11c and CD14 (Mrdjen *et al.*, 2018). Notably, homeostatic markers such as fractalkine receptor CX3CR1 were decreased and markers of activation MHCII increased (Mrdjen *et al.*, 2018). When considering the reported loss in BBB integrity in AD post-mortem tissue by plasma proteins such as fibrin in the parenchyma (Halliday *et al.*, 2016), this suggests why there is such a significant shift in microglial profiles.

More recently, disease-associated microglia (DAM) have been reported in models of neurodegeneration; these microglia show significant decrease in expression of 'homeostatic' markers and increase in phagocytic markers. DAM were first categorised in 5xFAD mice by increased expression of *Itgax*, *Clec7a* and *Trem2* and a decrease in homeostatic *Cx3cr1* and

P2ry12 (Keren-Shaul *et al.*, 2017). These DAM have since been shown in APP/PS1 mice to co-localise with amyloid plaques (Mrdjen *et al.*, 2018) and express markers of senescence such as beta-galactosidase (Hu *et al.*, 2021). This implies that immune cells within the brain respond to the aggregation of misfolded protein and permanent changes to microglia likely occur over time in AD. However, in human tissue, one study reported increase in markers such as *APOE*, *Trem2* and MHCII genes (Mathys *et al.*, 2019), yet an alternative paper reported microglia populations distinct from the DAM profile observed in mouse models (Srinivasan *et al.*, 2020). This again highlights the distinction between AD and the mouse models replicating pathology through gene mutations.

This research suggests that both in aging and in AD, the microglia shift towards this pro-inflammatory profile and homeostatic regulation is altered (Koellhoffer, McCullough and Ritzel, 2017; S. Rangaraju *et al.*, 2018). Increasingly senescent and dystrophic microglia may lead to disruption in both homeostatic and phagocytotic function (**Figure 1-6**). In the aging population, hospitalised AD patients often present with co-morbidities such as pneumonia and are more susceptible to infections than elderly patients without AD (Heun *et al.*, 2013). Systemic infections are known to alter microglia within the brain; post-mortem tissue in patients who had sepsis showed significant upregulation of microglial markers MHCII and CD68 (Lemstra *et al.*, 2007). To what extent systemic inflammation further alters the microglial population and so promotes greater disruption in the AD brain is not fully defined.

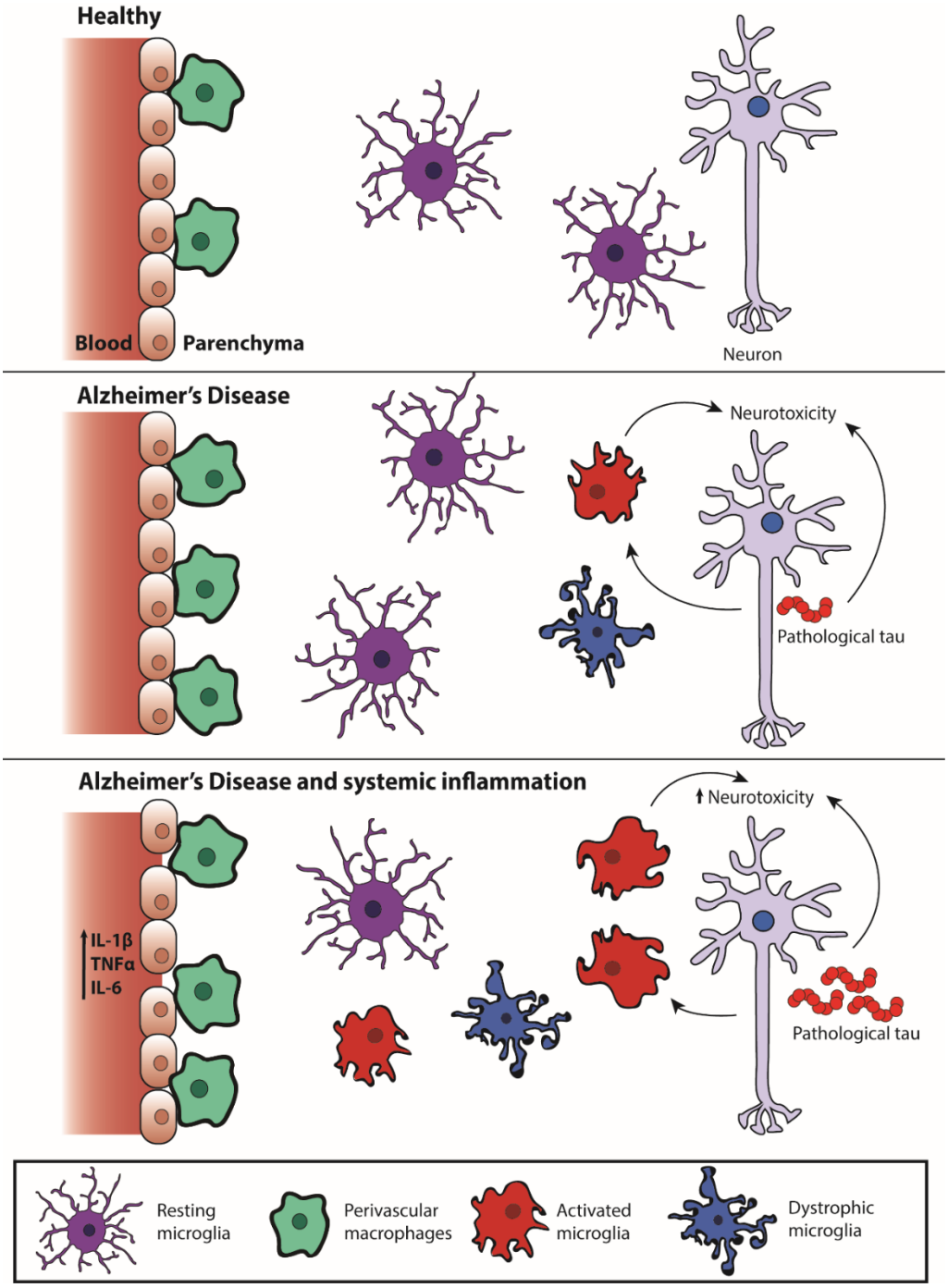

Figure 1-6: Microglial priming in neurodegenerative disease

Microglia in the naïve brain play a crucial role both in synaptic pruning, clearing debris and responding to infection or injury. However, in aging and neurodegenerative disease there is evidence that microglia become increasingly pro-inflammatory, creating a neurotoxic environment. Therefore, whilst it is clear there is a change in microglial homeostasis, the exact expression profile and morphology of these cells in AD is unclear. Whether referring to 'primed', 'dystrophic' or 'disease-associated' microglia, further clarification is required regarding how microglia are altered in AD and in response to tau pathology. Diagram based on Perry & Holmes, 2014.

1.3.4 The role of microglia in tau pathology

It has been suggested that in chronic inflammatory diseases and AD there is an exaggerated increase in pro-inflammatory microglia. In the presence of neurodegenerative pathology, it is possible that a greater number of the microglia population become increasingly disrupted and increasingly neurotoxic (Luo, Ding and Chen, 2010). Inflammation and the release of pro-inflammatory cytokines by microglia are shown to precede neuropil breakdown and tau pathology (Eikelenboom *et al.*, 2012).

One review found that activation markers MHCII, CD68 and CD11c were all increased in histology of AD post-mortem tissue compared to control, with inconsistent findings for CD11b (Hopperton *et al.*, 2018). One study compared $Iba1^+$ microglia and $AT8^+$ tau and observed dystrophic microglia co-localised with NFTs and even prior to NFT detection in the middle temporal gyrus (Braak stage III) (Streit *et al.*, 2009). Notably dystrophic microglia were not observed around amyloid plaques. Microglia positive for MHCII are localised around NFTs in post-mortem AD brain (Perlmutter *et al.*, 1992), suggesting that pathology may elicit a change in microglia function creating a vicious cycle. It was shown in a later study that post-mortem MHCII protein level inversely correlates with cognition in mild and moderate AD brain (Parachikova *et al.*, 2007). There is an increased number of $CD4^+$ T cells in post-mortem AD tissue (Togo *et al.*, 2002), suggesting that antigen presentation may be upregulated in AD brains to the detriment of microglial function.

There have been a multitude of studies examining the role of microglia in Aβ accumulation and clearance alike. One hypothesis frequently investigated is that of the role of Triggering Receptor Expressed on Myeloid Cells 2 (TREM2). TREM2 is expressed on myeloid cells and proposed to play a role in microglia senescence and Aβ clearance (Wang *et al.*, 2015). *In vivo* studies show that hTau;Trem2−/− mice exhibit both increased levels of AT8 and PHF-1 phosphorylated tau, in the hippocampus and the cortex at 3 months of age (Bemiller *et al.*, 2017). There is also a significant upregulation of phospho- GSK3β expression in both regions. In human AD patients, TREM2 has been proposed as a potential biomarker for AD associated with APOE-ε4; peripheral levels of TREM2 are significant upregulated in MCI patients (Casati *et al.*, 2018). Therefore, microglia respond to the initial stages of the disease, however to what extent microglia may alter disease progression through interaction with tau is not fully understood.

Studies suggest that microglia are capable of internalising tau through the fractalkine receptor. It has previously been observed that the fractalkine receptor is neuroprotective in its function (Cardona *et al.*, 2006; Lauro *et al.*, 2015); *Cx3cr1−/−* mice show significantly greater neuronal death in the dentate gyrus following repeated i.p. injection of LPS (100µl at 0.2mg/ml)

(Cardona et al., 2006). LPS, an endotoxin, is utilised as a bacterial mimetic which induces an acute inflammatory response (discussed further in section 1.4.1). In hTauCx3cr1-/- mice, an i.p. injection of LPS (10mg/kg) induced significantly higher levels of AT8-positive tau in the hippocampus (Bhaskar *et al.*, 2010). The microglial fractalkine receptor interacts with the CX3CL1 ligand on neurons, this is shown to contribute to a suppressed immune phenotype through Immunoreceptor Tyrosine-based Inhibitory Motif (ITIM) signalling (Perry and Teeling, 2013). ITIM signalling works in opposition to Immunoreceptor Tyrosine-based Activation Motif (ITAM) signalling, a pathway which utilises IgG Fc receptors to induce a downstream pro-inflammatory response. ITIM and ITAM signalling pathways work through but are not limited to fractalkine and IgG Fc receptors respectively (Perry and Teeling, 2013). These two pathways maintain homeostasis, enabling the immune response to infection or injury without detriment to the self. Therefore, loss of the CX3CR1-CX3CL1 interaction leads to increased neurotoxicity and increased expression of active p38 MAPK in neurons *in vitro* , resulting in aberrant phosphorylation of tau (Bhaskar *et al.*, 2010). This highlights how the loss of ITIM signalling may lead to an imbalance in microglia favouring activation.

The role of microglia in the spread and phosphorylation of tau protein is not yet fully understood. Deletion of CX3CR1 will alter more than microglial function, given steady-state immune cell populations in the brain (Mrdjen *et al.*, 2018). Furthermore, an abundance of research has been carried out examining the clearance of amyloid by microglia, yet the role of microglia on tau spread and clearance is relatively novel. Microglia uptake tau, yet in AD neuronal death and neurotoxicity lead to dysfunction in neuronal-microglial interactions. As a result, regulation of microglial function appears disrupted in AD. If microglia lose anti-inflammatory signalling, to what extent will this propagate phosphorylation of tau? Microglia have a homeostasis between neuroinflammatory and neuroprotective roles within the brain, yet it appears this is altered in the aging brain, and potentially in response to neurodegeneration (**Figure 1-5**). To what extent systemic inflammation may further alter the function of microglia is a question crucial to the understanding of tau pathology in AD.

1.4 Systemic Inflammation and its role in AD

Bacterial infections have long been hypothesised to correlate with AD risk. *Treponema pallidum* spirochetes which cause syphilis and general paresis are proposed to replicate the pathology of AD in the human brain (Miklossy, 2015). *Borrelia burgdorferi* spirochetes have also been suggested *in vitro* to promote tau hyperphosphorylation in rat brain organotypic cultures (Miklossy *et al.*, 2006). Bacteria produce amyloid, yet there is very little subsequent evidence that these bacteria have an effect on tau pathology. The initial amyloid hypothesis centred around the

idea that the presence of amyloid promotes microglial-mediated neurotoxicity and oxidative stress, prompting tau aggregation within these neurons (Hardy and Selkoe, 2002). To what extent this could be aggravated by amyloid-producing bacteria or systemic infection is unclear.

The role of infections in AD development has also been highly examined through the role of *Porphyromonas gingivalis* (*P. gingivalis*), a bacterium which induces periodontal infection (Singhrao *et al.*, 2015). A small case study of 38 healthy elderly people suggested that those presenting with periodontal disease had increased amyloid load within the brain (Kamer *et al.*, 2015). Furthermore, it has also been shown in a study with a small cohort from New York that AD patients tested for antibodies against *P. gingivalis* presented with significantly higher levels than the healthy controls, in addition to increased TNFα expression in the plasma (Kamer *et al.*, 2009). A longitudinal study over six months did suggest that periodontitis is associated with greater cognitive decline in AD patients (Ide *et al.*, 2016). These are a select few of the studies examining the role of *P. gingivalis*, *in vivo* models consistently point to activation of complement and release of pro-inflammatory cytokines as the potential mechanism behind clinical findings (Costa *et al.*, 2021).

How the process of aging, chronic inflammatory diseases and systemic inflammation incidents alter the course of neurodegeneration development is not yet fully defined. It has been shown that peripheral plasma levels of IL-6 and IL-1β are elevated in AD patients compared to healthy controls (Licastro *et al.*, 2000). A later paper examined cytokine expression in post-mortem tissue from AD patients with systemic infection and showed significant upregulation of IL-6, IL-1β and TNFα compared to AD patients without systemic infection reported (Asby *et al.*, 2021). Furthermore, patients that underwent systemic inflammatory events over a 6-month period showed a trend of greater cognitive decline than AD patients without reported infection (Holmes *et al.*, 2009). This highlights that cognitive decline may be accelerated in the presence of chronic low-grade inflammation.

The role of neuroinflammation in AD has been closely examined concerning amyloid-beta pathology (Cai, Hussain and Yan, 2014). However, the role of inflammation, including systemic inflammation in the development and spread of tau pathology is still relatively undetermined. Neuronal death is evidenced to be partially regulated by microglia through production of reactive oxygen species (ROS) and downstream cytokine production; microglial-induced neurotoxicity through oxidative stress is found increasingly in neurodegenerative disease (Lull and Block, 2010; Haslund-Vinding *et al.*, 2017). This suggests that the activation of microglia may trigger toxicity in neurons promoting tau hyperphosphorylation; and vice versa the accumulation of pathological tau in turn induces microglial activation. This may be accelerated by the presence of systemic

infection, which would only serve to further activate these 'primed' microglia and so increase the burden of tau pathology.

Research has examined mouse models of tauopathy to see if there is a similar increase in inflammation observed in these mice as in human patients. rTg4510 mice exhibit significant changes in markers of inflammatory signalling and neurotoxicity with age; there is a significant upregulation in the expression levels of genes such as the recognition of bacteria by PRRs and complement (Wes *et al.*, 2014). Proteins of the complement pathway have been reported upregulated in the AD brains (Tenner, 2020). This suggests that the mouse models of tauopathy mimic to some extent this facet of the neurodegenerative disease observed in human patients.

Systemic inflammation may alter phosphorylation of tau through microglial activation and kinase upregulation. However, which are the crucial pathways that regulate this? One area of increasing interest is the nucleotide-binding oligomerization domain (NOD)-like receptor protein 3 (NLRP3) inflammasome. Inflammasome complexes are a crucial part of the innate immune response, regulating expression of active IL-1β and IL-18 (Liu and Chan, 2014). The inflammasome consists of three key parts: the NLR that acts as a PRR, the adaptor protein and finally the enzyme that cleaves the precursor of cytokines IL-1β and IL-18. Activation of the inflammasome is primarily triggered by activation of the TLR4 pathway by the bacterial endotoxin LPS. This induces downstream activation of nuclear factor kappa-light-chain-enhancer of activated B cells (NF-κB), which in turn promotes *Nlrp3*, pro-IL-1β and pro-IL-18 production (Guo, Callaway and Ting, 2015). NLRP3 forms a complex with adaptor ASC (apoptosis-associated speck-like protein containing a caspase recruitment domain) and pro-caspase-1. Pro-caspase-1 then undergoes oligomerization to its activated form and cleaves pro-IL-1β and pro-IL-18 to active cytokines (Denes, Lopez-Castejon and Brough, 2012).

AD post-mortem tissue showed significantly higher protein expression of the active caspase-1 compared to healthy age-matched controls (Heneka *et al.*, 2013). It has previously been shown that IL-18 protein expression is significantly upregulated in CSF of MCI patients (Ojala *et al.*, 2009). No difference in IL-1β was found in this study, however significant increase in IL-1 expression in temporal lobe AD post-mortem tissue was described in an alternate cohort (Griffin *et al.*, 1989). The interaction of tau and the inflammasome in the context of AD has only recently been studied. Kitazawa *et al.* (2011) used 9 month-old 3xTg-AD mouse (which express APP, PS1 and P301L mutations, **Table 1-1**) and gave an i.p. injection of IL-1 receptor antibody every week for 6 months (Kitazawa *et al.*, 2011). These mice showed improved spatial memory function in the MWM, and decreased AT8, PHF-1 and AT100 expression whilst total tau expression remained constant. However, this may only isolate the role of alternate IL-1 signalling. Tau22 mice crossed

with *Asc* and *Nlrp3* knockout mice showed a reduction in AT8-positive hippocampal pathology and improved spatial memory in the MWM (Ising *et al.*, 2019). Therefore, there does appear to be a link between activation of these pathways and the modulation of tau phosphorylation; activation of the inflammasome may prompt greater tau aggregation and pathology though activation of the IL-1β and IL-18 inflammatory pathways.

Therefore, it is understood that in aging there is a shift towards pro-inflammatory markers in immune cells, and peripheral cytokine production is further heightened if these elderly patients also suffer from AD. It appears there is a loss of homeostasis within the mediation of inflammatory pathways; is this due to increased cellular stress from the development of AD pathology? Does alteration in inflammatory pathway signalling alter tau phosphorylation and its spread? Aging and neurodegeneration promote increased inflammation, therefore systemic infection may further aggravate pathology through primed microglia and an already disrupted BBB.

1.4.1 Models of systemic infection

A multitude of studies have examined the effect of bacterial infections on AD risk and cognitive decline. These include systemic inflammatory episodes (Holmes *et al.*, 2009) or gum disease caused by the presence of bacteria *P. gingivalis* (Ide *et al.*, 2016). It is consistently observed that low-grade systemic infections are correlated with cognitive decline in AD patients. However, inducing systemic infections that mimic the human response in mice has many obstacles both biologically and technically. Therefore, the majority of *in vivo* studies use mimics of bacterial (LPS) or viral (Poly(I:C)) infections to induce reproducible inflammation, which may elicit a different immune response than an actual infection.

In terms of modelling systemic inflammation, lipopolysaccharide (LPS) has been one of the most frequent model used. As the endotoxin on gram-negative bacteria, this infection model activates the innate immune system through TLR4 (Nemzek, Hugunin and Opp, 2008). Lee *et al.* (2010) also examined the pathology of tau seven days after intracerebral LPS challenge in the rTg4510 mouse model at 4.5 months of age (Lee *et al.*, 2010). The rTg4510 mouse showed a significant increase in the staining for phosphorylated tau epitopes pSer396 and pSer199/202 in the hippocampus and wider limbic circuit including entorhinal cortex. Intraperitoneal injections of LPS in the 3xTgAD mouse have been reported to show a significant increase in AT8-positive tau phosphorylation, however this required repeated injections at 0.5mg/kg twice a week for 6 weeks (Kitazawa, 2005); they suggest that cdk5 activation mediated tau phosphorylation in response to

LPS. LPS repeatedly administered to 3xTg-AD mice (**Table 1-1**), caused an increase in phosphorylated tau including AT8, purportedly through increased GSK3β activity (Sy *et al.*, 2011).

If kinase activation is modulated by neuroinflammation this may provide a link between systemic inflammation and aberrant tau phosphorylation. LPS was administered by i.p. injection twice a week for 6 weeks to 4-month old 3xTgAD mice (Kitazawa, 2005). This induced increased AT8-positive tau phosphorylation in the hippocampus. This was inhibited by roscovitine, a selective cdk5 inhibitor. A previously discussed *in vitro* study examining fractalkine receptor function, showed increased phosphorylation at epitopes AT8 and AT180 in the hippocampus following LPS injection in hTau*Cx3cr1-/-* mice (Bhaskar *et al.*, 2010). These studies highlight how tau phosphorylation is induced by LPS administration, making it an obvious choice for use in such studies.

However, the LPS model is not without disadvantages. For example it has been shown that repeated LPS injections show tolerance in pro-inflammatory cytokine expression in the serum, spleen and brain (Püntener *et al.*, 2012). Furthermore, the chosen dose regimen and specific endotoxin utilised will vastly affect the observations *in vivo* (Neher and Cunningham, 2019). Furthermore, and essential to this experiment, the inflammatory response to LPS is only mediated through binding to TLR4 and its downstream pathways (Lu, Yeh and Ohashi, 2008). If the aim of this thesis is to establish a model of human systemic infection, establishing sustained low-grade inflammation *in vivo* is essential.

There are a select few studies which use viral or parasitic infections such as the mouse hepatitis virus or *Leishmania amazonensis* respectively. 3xTg-AD and non-transgenic mice were given an intracerebral injection of 500 plaque forming units (PFUs) of the mouse hepatitis virus. These mice showed increased PHF-1-positive tau at 2 and 4 weeks-post injection in the hippocampus (Sy *et al.*, 2011). By contrast, another study looked at the parasitic infection *Leishmania amazonensis*. The parasite was injected subcutaneously with 10^5 amastigotes in BALB/c mice at 6 weeks of age and tau phosphorylation examined four months later (Gasparotto *et al.*, 2015). The mice treated with the parasite showed a significant increase in expression of pSer396, a site associated with PHF-1. Human immunodeficiency virus 1 (HIV-1) in rats is observed to induce increased hyperphosphorylation of tau again at pSer396 (Cho, Lee and Song, 2017), and as aforementioned there is a large amount of research looking at the role of spirochetes and *P. gingivalis* in AD risk (Miklossy, 2015; Ide *et al.*, 2016). However, these aforementioned studies contribute the majority of our understanding to the role of real infection on tau pathology as discussed in Barron *et al.*, (2017). Therefore, it is clear to see that there are few studies examining the role of real infections in mouse models of tauopathy and there is a necessity for novel study.

1.4.2 *Salmonella enterica* serovar Typhimurium as a model of infection

S. typhimurium is a gram-negative intracellular enteric bacterium. This is a murine model of *Salmonella enterica* serotype *typhi* (*S. Typhi*), which causes typhoid fever in humans. Spread through food or contaminated water, as of 2010 there are estimated between 9.9 and 26.9 million cases a year (Buckle, Walker and Black, 2012; Mogasale *et al.*, 2014). This disease is both widespread and with a high morbidity, presenting with fever, malaise, gastrointestinal complications and even perforation of the intestinal wall (Neil *et al.*, 2012). *S. typhimurium* is largely considered to be a representative murine model for *S. typhi* in humans, although reports suggest that the mice develop enteritis as opposed to typhoid fever due to presentation of the systemic disease (Santos *et al.*, 2001). Whilst this may not be ideal for studying *S. Typhi*, the model has ideal overlap for our studies as mice injected i.p. with *S. typhimurium* develop sustained low-grade systemic inflammation (Püntener *et al.*, 2012).

S. typhimurium belongs to the *Enterobacteriaceae* genus and is gram-negative. The majority of studies have examined *S. typhimurium* infection through oral administration. *S. typhimurium* is an intracellular pathogen, therefore once in the intestinal lumen, the bacteria invades the mucosal lining (Broz, Ohlson and Monack, 2012). The primary function of the intestinal wall is to act as a barrier to exogenous pathogens. The intestinal wall consists of an initial layer of simple columnar epithelial cells, secured by tight junctions, and separates the vascularised lamina propria, which contains lymphatic tissue, from the contents of the gut (Broz, Ohlson and Monack, 2012). The primary method of invasion by *S. typhimurium* is through the microfold (M) cells of Peyer's patches (PPs) in the intestinal wall (Jones, Ghori and Falkow, 1994), although invasion thorough normal epithelial cells has also been observed. PPs are lymphatic follicles present throughout the ileum to the jejunum (Gebert, Rothkötter and Pabst, 1996). M cells allow antigen transportation, which the bacteria exploit during invasion of host cells, as seen in **Figure 1-7**.

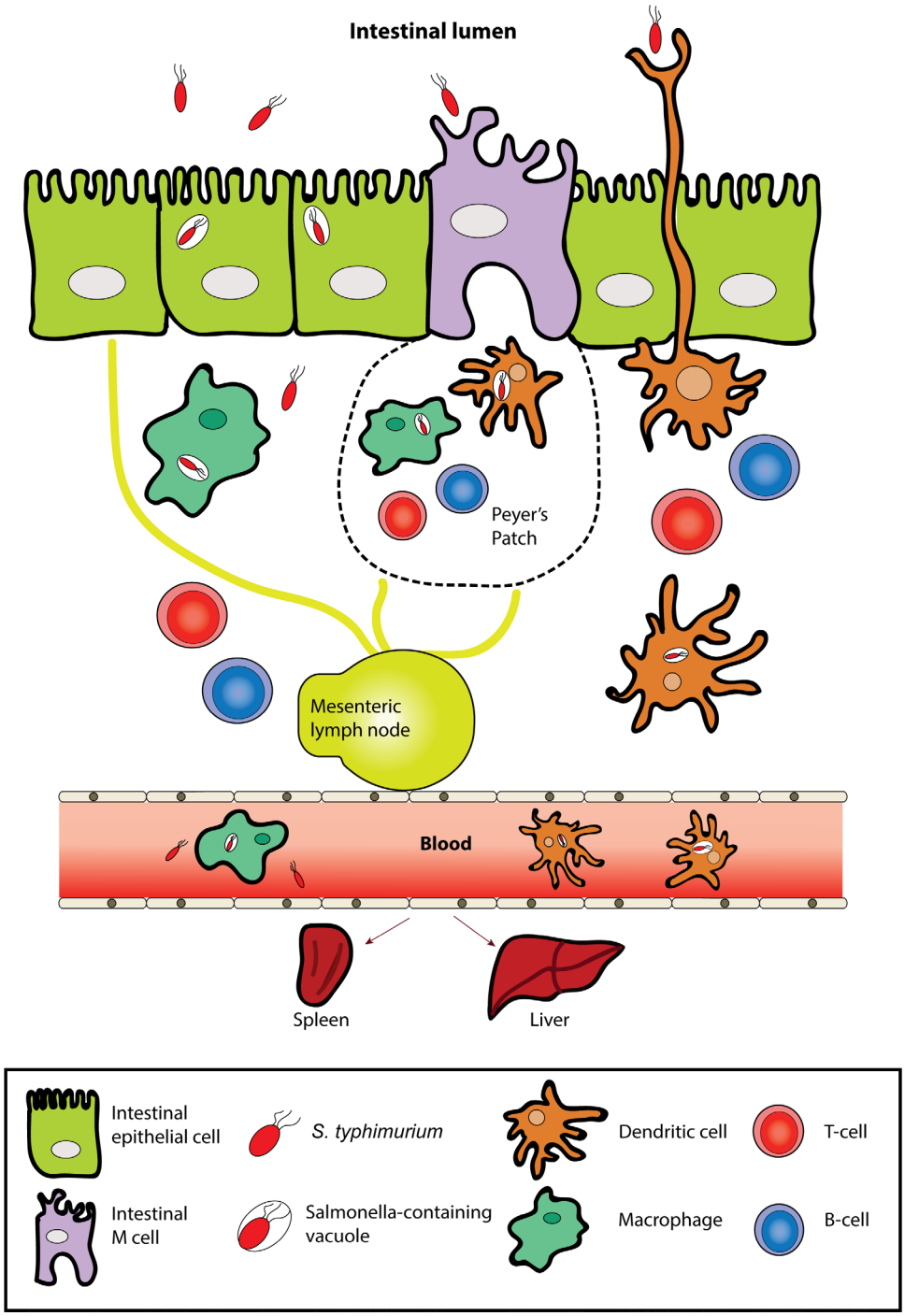

Figure 1-7: The invasion of *S. typhimurium* from the intestinal lumen

The bacterial invasion of the intestinal epithelia by *S. typhimurium* and the subsequent peripheral immune cells is largely dependent on the bacteria's ability to survive and replicate within host cells. The above diagram depicts how *S. typhimurium* passes from the intestinal lumen into the mesenteric lymph nodes and peripheral organs such as the spleen and liver. This movement through intestinal epithelial and M cells, along with dendritic cells and macrophages stimulates an immune response through detection of PAMPs. This results in the recruitment of T-cells and B-cells for the adaptive immune response and resolution of the infection. Adapted from Broz *et al.*, 2012.

In order for *S. typhimurium* to invade host cells, the bacterium adheres to the host cell using fimbrial adhesins, although the exact adhesin varies with serotype (Wagner and Hensel, 2011). The bacteria is able to invade M cells by passive transcytosis (Jones, Ghori and Falkow, 1994; Jepson and Clark, 2001). The bacteria are also able to invade epithelial cells, which are not phagocytic in nature. In addition to invasion of M cells and enterocytes, there is also evidence that *S. typhimurium* can be taken up by $CX3CR1^{+}$ DCs which span the epithelial layer (Niess *et al.*, 2005). The main mechanism which underpins invasion of epithelial cells are *Salmonella* pathogenicity islands 1 and 2 (SPI1/2) (Hansen-Wester and Hensel, 2001). SPI1 and SPI2 both encode type III secretory systems (T3SS); T3SS form a needle-like structure which injects effector proteins into the epithelial cell (Marlovits *et al.*, 2004).

SPI1 has a key role in the invasion of epithelial cells and subsequent colonisation of the gut by *S. typhimurium*. By contrast, the function of SPI2 is involved in colonisation of peripheral organs and survival in cells such as macrophages and DCs (Hansen-Wester and Hensel, 2001). Two key effector proteins are SopB and SopE2 (which both disrupt tight junctions) (Haraga, Ohlson and Miller, 2008). These proteins induce significant cytoskeletal reorganisation through activation of Cell division control protein 42 (Cdc42) and Ras homology Growth-related (RhoG), which are involved in actin regulation; the bacteria is then able to become internalised through macropinocytosis (Friebel *et al.*, 2001; Zhou *et al.*, 2001). From this, the bacteria reside within *Salmonella*-containing vacuoles (SCVs) which allows intracellular replication and survival through expression of the T3SS encoded by SPI2. Once the bacteria have moved through the epithelial cell wall, *S. typhimurium* is phagocytosed by macrophages and DCs. The bacteria again uses the SPI2 T3SS to survive within these cells in a SCV, as the associated effector proteins inhibit the production of ROS (Gart *et al.*, 2016). This also prevents degradation by the endogenous endolysosomal system. The bacteria are capable of leaving macrophages to colonise additional cells. Once within $CD11c^{+}$ DCs, migration occurs to the mesenteric lymph nodes in a CC chemokine receptor type 7 (CCR7)-dependent manner (Voedisch *et al.*, 2009). From here *S. typhimurium* enters the blood through efferent lymphatic vessels and the bacterium largely invades the bone marrow, liver and spleen. In mouse models, *S. typhimurium* is also administered through i.p. injection. From the intraperitoneal cavity, the bacteria has been shown to move through the portal vein to the liver, whereby it colonises peripheral organs such as the spleen (Lukas, Brindle and Greengard, 1971).

From initial invasion, the innate immune response is triggered. The membrane ruffling and actin remodelling within enterocytes induces detection of PAMPs (Broz, Ohlson and Monack, 2012). The purpose of the innate immune response is to recruit neutrophils, activate macrophages for phagocytosis, and recruit T cells. For example, IFNγ production is proposed to be

essential for bactericide by phagocytes (Monack, Bouley and Falkow, 2004). Within the spleen, IFNγ has been shown to be initially produced by neutrophils and macrophages to restrict the *S. typhimurium* population whilst the adaptive immune response develops to fully resolve the infection (Kirby, Yrlid and Wick, 2002). If there is no eventual recruitment of $CD4^+$ T-cells producing IFNγ then mice succumb to the bacterial infection (Ravindran *et al.*, 2005).

For the recruitment of the adaptive immune response, extracellular bacteria and the act of cell invasion allows detection of the PAMPs flagellin and LPS, initiating the immune response by the host. MAPK activation and downstream activation of NF-κB leads to IL-8 production. This in turn causes polymorphonuclear leukocyte migration and a pro-inflammatory response which should initiate T-cell recruitment (Haraga, Ohlson and Miller, 2008). Several TLR pathways are also activated within macrophages by detection of LPS (TLR4), CpG- rich bacterial DNA domains (TLR9) and lipoproteins (TLR1/2/6). This prompts production of inflammatory cytokines such as IL-23, IL-10, pro-IL-1β and pro-IL-18 (Broz, Ohlson and Monack, 2012). Neutrophil recruitment by CXC chemokines then results in phagocytosis of the extracellular *S. typhimurium* (Aujla, Dubin and Kolls, 2007).

However the innate immune system must recruit the adaptive immune system to overcome the infection; macrophages become antigen presenting in an attempt to recruit T cells (Moon and McSorley, 2009). DCs also detect both PAMPs and cytokine production, acting as APCs (Tam *et al.*, 2008). DCs recruit *S. typhimurium*-specific T-cell populations, although this initial response is not adequate to overcome the infection; this is meant to regulate bacterial replication whilst a full adaptive immune response must be generated (Salazar-Gonzalez *et al.*, 2006). Furthermore, the activation of NLR family CARD domain-containing protein 4 (NLRC4) and NLRP3 inflammasomes in macrophages leads to the production of IL-1β and IL-18 (Broz *et al.*, 2010; Qu *et al.*, 2016). IL-18 prompts IFNγ production by T cells (Srinivasan *et al.*, 2007), which serves to clear the bacteria. However, SPI2 can supress the APC action of DCs, and so the virulence of the bacteria increases and the infection cannot be quickly resolved (Swart and Hensel, 2012).

Salmonella primarily invades the liver, bone marrow and spleen; this has been reported to occur via $CD18^+$ phagocytes (Vazquez-Terres *et al.*, 1999), and DCs (Swart and Hensel, 2012). Intraperitoneal injection of *S. typhimurium* in BALB/c mice shows colonisation of the spleen and liver within 4 hours of infection, although severity of infection was significantly reduced in the strain expressing a mutation in SPI2 T3SS function (Shea *et al.*, 1999). There is debate as to the additional involvement of recruited monocytes, macrophages, natural killer cells and T-cells (Conlan and North, 1992; Moon and McSorley, 2009). Following *S. typhimurium* infection, renal

tissue becomes hypoxic, primarily by TLR signalling; this induces erythropoiesis both in the bone marrow and subsequently in the spleen (Jackson *et al.*, 2011).

In the spleen, *S. typhimurium* has been shown to colonise both macrophages and splenic cells with very little bacteria residing outside of a host cell (Jackson *et al.*, 2011). As a result of colonisation within the spleen and the ensuing hypoxia, a significant expansion of immature erythroid reticulocytes occurs; furthermore, $F4/80^{+}$ macrophage population in the red pulp expands and these two cell populations grow past the red pulp, invading the lymphatic white pulp (Rosche *et al.*, 2015). This is proposed to be the primary cause of splenomegaly due to *S. typhimurium*.

One way in which the virulence of *S. typhimurium* can be altered is by the use of different attenuated strains, often for vaccine development; mutations in effector proteins such as SifA which maintain the SCV, will significantly dampen the virulence of the infection (Haraga, Ohlson and Miller, 2008). The attenuated strain used previously by our lab and in this thesis (*S. typhimurium* SL3261) does not express the *aroA* gene. *aroA* knockout results in an auxotrophic strain which cannot synthesise aromatic amino acids, which are not readily available in host cells; however, *aroA* mutants have been reported to show increased virulence in BALB/c mice (Hoiseth and Stocker, 1981; Felgner *et al.*, 2016).

The strain used will significantly alter the virulence, which it is crucial to consider when comparing studies. Sickness behaviours are observed in *S. Typhi* infections along with (in rare cases) abscesses within the brain (Hanel *et al.*, 2000); this highlights that the CNS is affected by this bacterial infection. A study which used oral infection of *S. typhimurium* in multiple inbred strains including BALB/c and C57BL/6, showed meningitis and bacteria within the brain (primarily BALB/c mice displayed infection) (Wickham *et al.*, 2007). The strain used is strain SL1344, an experimental model in calves which was reported to sometimes be lethal (Wray and Sojka, 1978). However, the strain used by our lab is a non-neurotrophic *aroA* mutant, and similar studies showed no bacteria reached the brain after 72 hours (Yang *et al.*, 2011). This suggests that in this thesis it will be the peripheral immune response or tau pathology causes potential changes in the microglial cells.

Another factor which alters the virulence of the infection is different genetic backgrounds in inbred strains. One of the primary factors is the expression of the Natural resistance-associated macrophage protein 1 (Nramp1), encoded by the Solute Carrier Family 11 Member 1 (*Slc11a1*) gene. Lysosomal compartments of immune cells such as macrophages, neutrophils and DCs express Nramp1, and this protein is hypothesised to determine susceptibility to *S. typhimurium* infection (Brown *et al.*, 2013). One of the methods by which Nramp1 alters *S. typhimurium*

susceptibility is through iron availability within the SCV, as iron uptake is crucial for *S. typhimurium* growth (Fritsche *et al.*, 2012). Different genetic backgrounds in mouse models alters the response of the mice to *S. typhimurium* infection.

To what extent the peripheral immune response to *S. typhimurium* infection alters AD progression is unclear. It has been shown in 5XFAD mice that intracerebral injection of *S. typhimurium* (strain SL1344) prompts increased Aβ deposition and bacterium was observed around plaques (Kumar *et al.*, 2016). Despite this, the majority of work has been carried out using the bacterial mimic LPS, which only activates the TLR4 pathways and explores one facet of the acute immune response to an infection. Because *S. typhimurium* is a real, non-neurotrophic bacterial infection, this will allow us to reproduce both the innate and adaptive immune response seen in humans. *S. typhimurium* infection takes much longer to resolve than in LPS; S*. typhimurium* is resolved after approximately three to four weeks whereas LPS immune response is commonly resolved in several days (Püntener *et al.*, 2012).

It is also understood that repeated injections of LPS induces tolerance, and there is a gradual reduction in the systemic cytokine production. By contrast, following *S. typhimurium* injection there is a gradual increase in cytokines such as IFN-γ, IL-12 and IL-1β over three weeks post-injection primarily in the spleen, yet also partially in the brain and serum (Püntener *et al.*, 2012). Furthermore, MHCII expression was observed in cerebral endothelial cells, suggesting that *S. typhimurium* SL3261 infection induces cellular activation within the CNS. The length of systemic inflammation is a crucial consideration, especially to examine the effect of systemic infection on tau pathology spread. The nature of this study requires a sustained low-grade systemic inflammation in order to best establish whether the rate of tau spread is altered, and if so by what mechanisms.

1.5 Summary of literature and aims of thesis

There is significant clinical evidence that the spread of tau pathology correlates with cognition in AD (Gomez-Isla *et al.*, 1997; Ghoshal *et al.*, 2002). Spreading models which initially injected preformed fibrils into the brain, are shifting to the use of lysate enriched with insoluble human AD tau (Narasimhan *et al.*, 2017; He *et al.*, 2020). These studies highlight how the conformation of tau plays a crucial role in the spreading observed. Understandably, these studies are primarily concerned with the mechanism of tau seeding itself and rarely look wider to the effect of the immune response. This thesis aims to induce tau spreading in the C57BL/6 and the H1*Mapt-/-* mice and then prompt a systemic infection. This is to examine the primary question; to what extent to low-grade systemic inflammation promote greater spread of tau pathology?

There is now greater understanding that bacterial infections may in some way be linked to AD pathogenesis (Miklossy, 2015). However, there is still a large degree of heterogeneity in both mouse models and patient groups, resulting in a significant lack of clarity. Systemic inflammation shows a clear link with increased cognitive decline in patients (Giridharan *et al.*, 2019). In mouse models, studies are predominantly restricted to LPS. The use of LPS is adequate to induce a pro-inflammatory response, as the response is strictly limited to TLR4 expression. The effects of chronic low-grade inflammation have not yet been fully studied in the context of tau spreading in AD. Whilst studies have utilised LPS to show changes in tau phosphorylation (Lee *et al.*, 2010), the limitations of using LPS as a mimic leave unanswered questions.

Therefore, the ability to use a real bacterial infection would provide greater insight into how systemic inflammation may alter tau spread (**Figure 1-8**). *S. typhimurium* induces sustained low-grade systemic inflammation with both peripheral and central response. Therefore, this model of systemic inflammation may allow us to examine how prolonged inflammation alters spreading of existing tau pathology. By injecting tau isolated from AD post-mortem cases into the mouse brain, this should allow examination of tau spread and the subsequent effect of systemic infection. Utilising the H1*Mapt-/-* and C57BL/6 mice also allows us to observe whether the native protein within the mouse changes the spatiotemporal spread of tau pathology.

Hypothesis

It is hypothesised that systemic infection and the subsequent inflammatory response within the brain will increase the spatiotemporal spread of tau pathology.

Aims for Chapter 3

- To establish a mouse model which is susceptible to *S. typhimurium*

- To determine which immune markers within the brain will be used throughout this thesis to establish the degree of response to the infection

Aims for Chapter 4

- To establish whether there is an immune response to LPS intracerebral injection
- To establish whether an acute inflammatory response in the brain is adequate to induce microglial priming

Aims for Chapter 5

- To generate a lysate from human post-mortem AD tissue
- To confirm that the AD-tau lysate is enriched for AT8-positive HMW tau

Aims for Chapter 6

- To examine tau propagation through the brain in the *H1Mapt-/-* and C57BL/6 mice at three months post-injection
- To confirm regional spread of tau both dorsal and ventral to the injection site
- To determine whether systemic infection increases the pathology burden and the rate of spread

Aims for Chapter 7

- To determine if tau pathology induces an inflammatory response
- To determine if *S. typhimurium* infection exaggerates microglial activation in the presence of tau pathology
- To compare the inflammatory response in *H1Mapt-/-* mice and C57BL/6 mice

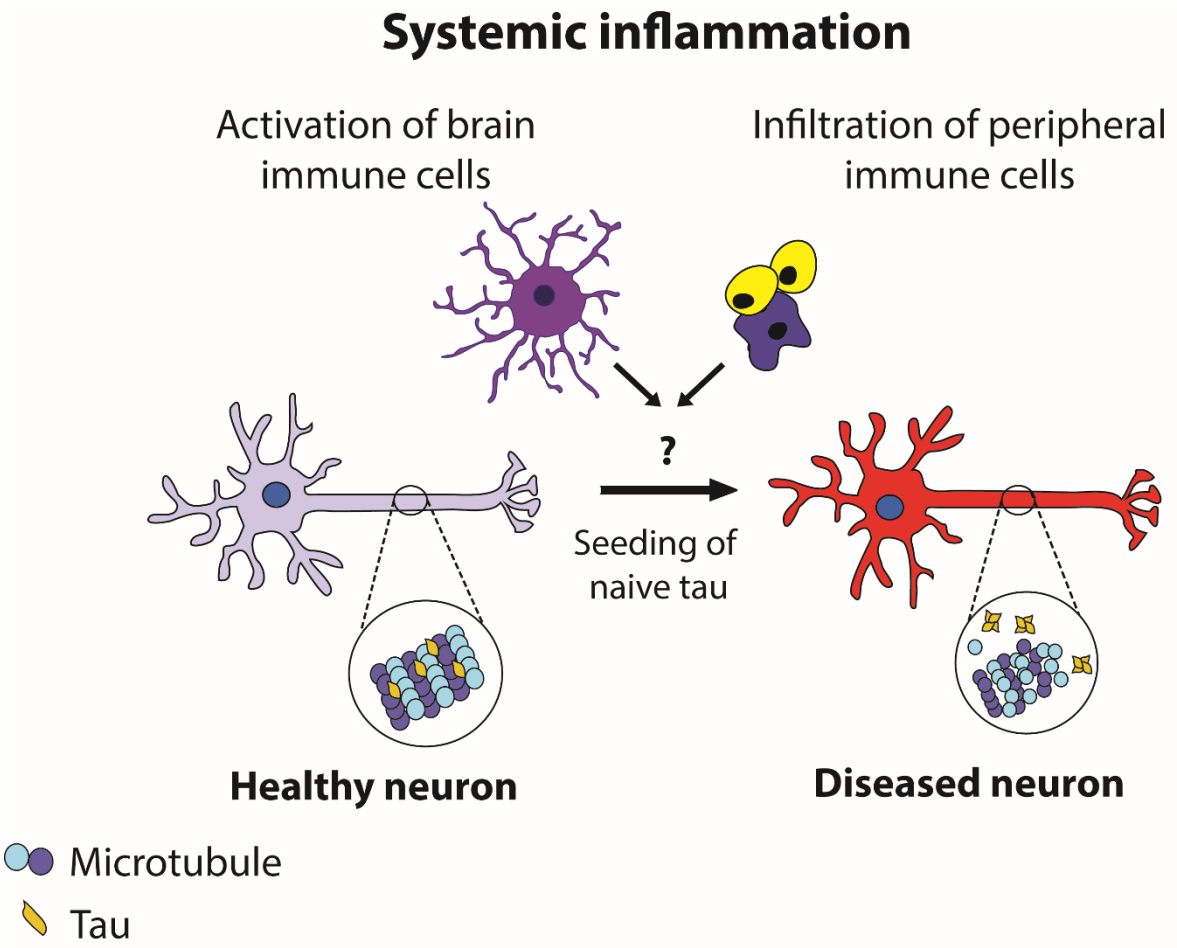

Figure 1-8: How systemic inflammation may alter the rate of tau spread

The literature discussed above highlights how tau spreads between neurons, a facet of AD pathology thought to correlate with cognitive decline. It is now understood that tau interacts with immune cells of the brain and that this may propagate tau pathology further. Furthermore, systemic inflammation is linked to the development and progression of AD. By inducing systemic inflammation in a mouse model of tau spread, this may lead to elucidation of the mechanisms by which the spatiotemporal propagation of pathology is mediated.

Chapter 2 Materials and Methods

2.1 *In vivo* methods

2.1.1 Experimental animals

All mice were housed with water and food (standard chow, RM1, SDS, UK) *ad libitum* in a twelve-hour light cycle that begins at 7am (12h light: 12h dark) in a temperature-controlled room (19-23^{o}C). All procedures were carried out according to the UK Home Office Licensing regulations and requirements under the UK Animals (Scientific Procedures) Act (1986), under project licences 30/3056, 30/3057 and subsequently project licence P4155EEE0. C57BL/6J mice were bred and maintained at the Biomedical Research Facility (BRF), Southampton UK. A final cohort from Chapter 6 were brought in from Charles River (Margate, UK) and remained in house for two weeks prior to the beginning of the experiment. This was due to Covid-19 restrictions and subsequent changes to breeding within the BRF.

In Chapter 3, female P301S and control C57BL/6 mice were used at 2-3 months-old (Allen *et al.*, 2002). In Chapter 3, C57BL/6, H1*Mapt-/-* and *Mapt-/-* (Wobst *et al.*, 2017) were all 2-3 months-old. All C57BL/6 mice were female, yet H1*Mapt-/-* and *Mapt-/-* were male and female. In Chapter 4, female C57BL/6 mice which were culled at 24 hours post- i.c. injection were 4-5 months old. In Chapter 4, female C57BL/6 which then went on to receive *S. typhimurium* i.p. injection were 3 months old at the time of the initial i.c. injection. In Chapters 6 and 7, female C57BL/6 mice were 3-4 months old whilst H1*Mapt-/-* mice (male and female) were 2-4 months old at the time of the initial i.c. injection. For Tg4510 mice (8 months old) (SantaCruz *et al.*, 2005) used as positive controls in western blots, the Tg4510 brains were obtained from Eli Lilly (Windlesham, UK) and shipped on dry ice as snap frozen cortex samples. Tracey Murray carried out the perfusions and collection of Tg4510 tissue only.

2.1.2 Intracerebral stereotaxic injection of LPS or saline

Mice received a stereotaxic injection of 1µl of LPS (0.5mg/ml in sterile saline) from *Salmonella abortus equi* (Sigma). Mice (3 months old female C57BL/6 mice) were given an i.p. injection of ketamine/rompun (10ml/kg), pre-surgical weights were recorded both for clinical welfare and to calculate anaesthesia. After mice reached surgical plane, the skull was shaved (Wella), lacri-lube (Allergan) was applied to the eyes and lidocaine (5% m/m, Teva) to the ears. After this the mouse was fitted to a stereotaxic frame (Kopf) with ear bars (45° atraumatic ear bars, Kopf) to affix the skull. The surgical area was sterilised with Hydrex (Ecolab) before an incision in the skin along the midline of the skull was made. From this exposed region, Bregma was located and the coordinates recorded. From Bregma, the injection site was calculated (AP= -

2.50, ML= -2.0, DV= -1.80). A burr hole was drilled into the skull using a dental drill with a drill bit. A 5µl Hamilton syringe (Model 75 RN, Hamilton) with a 33-gauge needle (Hamilton) affixed was then lowered into the parenchyma and the needle was then left for one minute. After this, 1µl of saline or LPS was slowly injected over a minute. Following this the needle was left for two minutes before being slowly removed from the brain. The incision was sutured (Mersilk 5-0 17mm, Ethicon) and superglue applied to the sutures to prevent premature tearing (RS Pro). Mice were kept in a heated recovery chamber (Datesand) and allowed to recover whilst closely observed. Once mice were fully recovered they were returned to their home cage. Mice were observed for clinical welfare twice a day for the first two days post-i.c. injection. Weights were recorded daily for the first week and then weekly afterwards.

An additional group of female C57BL/6 mice (4-5 months old) also underwent this procedure, however a bilateral i.c. injection of saline or LPS was carried out (Injection site 1: AP= -2.50, ML= -2.0, DV= -1.80; injection site 2: AP= -2.50, ML= +2.0, DV= -1.80). These mice were culled 24 hours post-i.c. injection.

2.1.3 Intracerebral stereotaxic injection of AD-tau seed prep or vehicle

C57BL/6 (3-4 months old) and H1*Mapt-/-* (2- 4 months old) mice were placed in an anaesthesia induction chamber (VetTech) and anaesthetised using isofluorane (IsoFlo, Zoetis). Once surgical plane is reached, the skull was shaved (Wella), lacri-lube (Allergan) was applied to the eyes and lidocaine (5% m/m, Teva) to the ears. Buprenorphine was also administered (10ml/kg) through an i.p. injection. Using ear bars (45° atraumatic ear bars, Kopf) the mouse is fitted into the stereotaxic frame (Kopf) and a nose cone placed over the nose to provide consistent isofluorane (VetTech) and oxygen. The surgical area was sterilised with Hydrex (Ecolab) and an incision made in the skin along the midline of the skull. The skull was exposed using sterile surgical spears (Fine Science Tools) and Bregma located. Using Bregma the injection coordinates were calculated, and the site located (Bregma: AP= -2.50, ML= -2.0, DV= -1.80 and -0.8). A drill hole was made and a 10µl Hamilton syringe (Model 701, Hamilton) with 26s-gauge needle (Hamilton) was inserted into the brain. The syringe either contained AD-tau seed prep (described in 1.5) or 50mM Tris buffer. At the first injection site in the hippocampus (Bregma DV= -1.80) the needle was left in place for 1 minute. After this 2.5µl of the lysate was injected over 2 minutes and then the needle was left in place for 3 minutes. This was then repeated at the second injection site (Bregma DV= -0.80); 2.5µl was also injected into the cortex. After the final 3 minutes, the syringe was slowly drawn out of the brain. The incision was sutured (Mersilk 5-0 17mm, Ethicon) and superglue was applied to the sutures (RS Pro). Mice were kept in a heated recovery chamber (Datesand) and once fully recovered they were returned to their home cage.

Mice were observed for clinical welfare twice a day for the first two days post-i.c. injection and then daily afterwards. Weights were recorded daily for the first week and then weekly afterwards.

There was an initial cohort of C57BL/6 mice which received a tau i.c. injection. There were three C57BL/6 mice in each group (tau i.c./saline i.p. and tau i.c./*S. typhimurium* i.p.). These six mice received intracerebral injections using ketamine-rompun as the surgical anaesthetic. These mice are a separate group in the post-intracerebral injection weight change (Appendix A- Figure S3). These six mice also underwent perfusion with paraformaldehyde (PFA) fixation, however technical issues meant that the hippocampal neurons were destroyed likely due to the osmolarity of the fixative. Therefore, they are excluded from the tau histology in Chapter 6. In Chapter 7, they are included as the parenchyma was intact for staining of inflammatory markers.

2.1.4 Intraperitoneal Injections of Saline and *S. typhimurium*

Prior to *S. typhimurium* i.p. injection, mice were moved to the CL2 facility a week before. Male and female P301S, *H1Mapt-/-, Mapt-/-* and C57BL/6 mice were injected with either the aroA attenuated *Salmonella enterica* serovar Typhimurium strain (SL3261) (generously provided by Dr H. Atkins, DSTL, Salisbury, UK) (Püntener *et al.*, 2012) or saline (Fannin, UK) and culled four weeks post-infection. *S. typhimurium* was injected via i.p. injection to induce systemic inflammation, 10^6 colony-forming units (CFUs)/200µl were injected per mice (Püntener *et al.*, 2012). 200µl of saline was injected i.p. into the control groups of mice. Once the mice have been injected, great care must be taken to ensure that the mice retain a healthy level of weight; any loss greater than 15% is deemed the threshold at which the mouse must be culled. Prior to injection, baseline body weights were recorded. Following i.p. injection, weight was recorded daily for 7 days post infection and then recorded weekly until 4 weeks post infection. C57BL/6 mice in Chapter 4 were culled one-week post-i.p. injection. Alex Collcutt carried out the i.p. injections in the 2-month-old P301S and associated C57BL/6 mice and subsequent weight recording (Chapter 3).

2.1.5 Burrowing tests

Burrowing tests were performed as described previously (Deacon, 2009). Burrowing is measured by the total amount of RM1 standard chow displaced overnight from a plastic cylinder (20cm length x 6.8cm diameter). Each plastic cylinder initially contains 190g of RM1 standard chow and is placed in one corner of the burrowing cage. The corner is alternated throughout the cohort to account for darker and light areas within the cage. For training, all mice from a single home cage are placed within a burrowing cage together for five hours during the day and the group burrowing recorded. Subsequently, each mouse is placed in its own separate burrowing

cage for five hours during the day and then another final training session occurs overnight. These burrowing training sessions are spaced out over two weeks to prevent weight loss or undue stress due to single housing.

Burrowing was carried out on C57BL/6 and H1*Mapt-/-* mice prior to the *S. typhimurium* i.p. injection as described above. Following *S. typhimurium* i.p. injection, burrowing was carried out 6 days post-injection, subsequently burrowing was carried out weekly until the end of the experiment. Due to Covid-19 restrictions and limited access to the CL2 facility, Joe Chouhan assisted with several burrowing sessions.

2.1.6 Nesting behaviour

In Chapter 3, Alex Collcutt carried out nesting behaviour for the P301S mice and associated C57BL/6 mice following *S. typhimurium* injection. One day prior to perfusion, P301S mice and C57BL/6 mice were provided with 8-10g of nesting material and the quality of the nest was scored 24 hours later from 1-5, as reported previously (Gaskill and Pritchett-Corning, 2016). These C57BL/6 mice are separate to the C57BL/6 mice used as WT controls for the H1*Mapt-/-* study in Chapter 3.

2.2 Tissue Collection

All mice received terminal overdose of anaesthetic rat Avertin (2, 2, 2-tribromoethanol) at 10ml/kg. Once anaesthesia is reached, an incision along the midline and across the diaphragm exposes the thoracic cavity. Prior to perfusion, an incision was made in the right atrium and blood collected from the thoracic cavity with a syringe. Transcardial perfusion with ice-cold 0.9% saline was then carried out through the left ventricle. The brain was dissected immediately following complete perfusion. In Chapters 3 and 4, the right hemisphere was mounted in OCT (optimal cutting temperature medium, Cell Path, UK) and frozen on isopentane (Fisher Scientific, UK). The left hemisphere was divided into frontal cortex, coronal section (enriched for the hippocampus) and cerebellar sections and snap frozen in liquid nitrogen. Alex Collcutt carried out the perfusions only for the P301S mice and the associated C57BL/6 mice following *S. typhimurium* infection in Chapter 3.

In Chapter 6 and 7, saline perfusion was followed with 4% PFA and the whole brain was kept in 4% PFA for 24 hours at 4^{o}C. Following 24-hour fixation, all brain tissue was placed in 30% sucrose (Fisher Scientific, UK) at 4^{o}C; once the tissue sinks to the bottom of the sucrose solution it was embedded in OCT and frozen on isopentane (Fisher Scientific, UK).

The spleens of mice from all cohorts were collected and weighed (On Balance CT-250 Carat Scale, OurWeigh, UK); half of the spleen was mounted in OCT and the other half snap frozen. For Chapters 6 and 7 the whole spleen was kept in 4% PFA for 24 hours at 4^{o}C, due to whole body perfusion with 4% PFA prior. Following this, spleens were also kept in 30% sucrose until the tissue sank and subsequently mounted in OCT for use on the cryostat. Immediately after tissue collection, the blood samples were spun at 4000 relative centrifugal force (rcf) for ten minutes in a centrifuge (5417R Eppendorf centrifuge) and the serum collected and frozen at -80^{o}C.

2.3 Genotyping

The P301S mice were homozygous for the P301S mutation, therefore no genotyping was required. The H1*Mapt-/-* mice were genotyped for the expression of the H1 haplotype. However, the mice initially available for breeding expressed the Line102 construct, which was a transgenic APP mouse model, discussed in Chapter 1. This construct was selectively bred out whilst choosing mice with high expression of the H1 haplotype, and therefore likely to have homozygous expression. The mice have previously been confirmed to express no endogenous mouse *Mapt* expression. However, the first litter of a new breeding pair was tested for *Mapt* expression to ensure the mice remain *Mapt-/-*.

Genomic DNA was extracted from ear clippings taken at 3 weeks of age. Ear clippings were initially lysed in lysis buffer (Appendix B- Table 1) by heating at 54°C for 30 minutes (Grant QBD2, UK). Once the tissue had been completely lysed, the samples were centrifuged for 10 minutes at 13,000 revolutions per minute (rpm) at room temperature (RT) (SciSpin Micro, UK). The supernatant was aliquoted into RNase-free Eppendorfs and an equal amount of isopropanol (Sigma, UK) added to precipitate the DNA. The samples were then centrifuged for 5 minutes at 10,000rpm and the supernatants discarded. 100µl of 70% ethanol was added to the pellet and centrifuged for 5 minutes at 10,000rpm. The ethanol was discarded and the Eppendorfs were stood upside down to dry for 30 minutes. Following this, 25µl or DNase-free water was added to re-suspend the pellet.

Genomic DNA was then quantified (ng/µl) by nucleic acid absorption at 260nm using a Nanodrop (ND-1000 Spectrophotometer, Fisher Scientific, UK) and protein and ethanol contamination ratios recorded. The absorbance ratios at 260/280 nanometres (nm) and 260/230nm were recorded to examine potential contamination of proteins or alcohols respectively. Ratio values equal or greater than 1.8 suggested the genomic DNA was of suitably high purity.

Samples were diluted to 50ng/µl with DNase-free water for quantitative polymerase chain reaction (qPCR). Samples were not diluted for polymerase chain reaction (PCR) experiments. Once the samples were diluted for qPCR, the master mix referenced in Appendix B (Table 7) containing SYBR green (Applied Biosystems) and the associated primers, was loaded on ice to the MicroAmp Fast 96-well reaction plate (Applied Biosystems). The corresponding primer sequences for analysis of the H1 haplotype and Glyceraldehyde 3-phosphate dehydrogenase *(Gapdh)* respectively are listed in **Table 2-1** (all primers ordered from Eurofins Genomics). The RNase-free water blanks, samples and standards (standards were diluted from a known hemizygous sample; listed in Appendix B, Table 6) were loaded to the 96-well reaction plate. Positive controls for known homozygous and known hemizygous samples were included in all experiments. The qPCR cycle for *H1* and *Gapdh* genes were run separately, the different reaction conditions for each were detailed in Appendix B (Table 8 and 9) (StepOnePlus, Applied Biosystems). Following this, average threshold cycle (C(t)) values for the standards were plotted into a base-10 logarithmic graph. From this the average C(t) values from unknown samples were extrapolated using the equation from the line of best fit (see equation below; GOI= gene of interest, REF= reference gene). This was carried out both for the gene of interest and the housekeeping gene, the H1 expression was then normalised to GAPDH. Looking at the known samples, this provides a scale of expression whereby the known homozygous sample has significantly higher expression than the known hemizygous samples. The unknown samples can then be sorted based on expression as to whether they likely have hemizygous or homozygous expression of the H1 haplotype. Further confirmation may be required, a western blot looking a total tau can be used to determine if the mouse had homozygous or hemizygous H1 haplotype expression (**Figure 2-1**).

$$Power\ (normalised\ to\ housekeeping\ gene) = \frac{\left[10\text{^}\left(\frac{(Mean\ GOI\ C(t) - y\ intercept)}{gradient}\right)\right]}{\left[10\text{^}\left(\frac{(Mean\ REF\ C(t) - y\ intercept)}{gradient}\right)\right]}$$

For PCR there was no dilution of the DNA and the sample was loaded immediately into the plate with the master mix and then spun for 3 minutes at 3,000rpm at 4°C (Sorvall Legend RT). 96-well certified thin wall plates (Starlab, UK) were loaded with the master mixes for Line 102 and endogenous *Mapt*, the master mixes contain REDTaq Master Mix (Sigma) and GoTaq Green Master Mix (Promega) respectively (Appendix B- Table 2 and 3). PCR reaction conditions are listed in Appendix B (Table 4 and 5) (GeneAmp PCR System 9700). Following the PCR reaction, the PCR products were analysed on a 1% agarose gel. One gram of agarose (Sigma) was dissolved in 100ml of 1X TBE (Tris/Borate/EDTA; see Appendix B). 10µl of GelRed (Cambridge Bioscience) was added to the solution (1:10,000), the solution was then poured into the gel casting mould and left to set for 30 minutes. The gel was placed into the electrophoresis tank (FisherBrand) and the tank was

filled with 1X TBE. The comb was removed from the gel and the wells were flushed with TBE to ensure no air bubbles. 6µl of DNA ladder (Both Hyperladder, Bioline and Quick-Load 1kb Plus DNA ladder, New England BioLabs were used) was added, followed by 10µl of PCR product into successive wells. The gel was then run at 120V using a power pack for 50 minutes (PowerPac Basic, Bio-Rad, UK). Once the gel had run it was imaged by a G:Box UV Transilluminator (SynGene, UK). Using the product sizes listed in **Table 2-2**, both the *Mapt* and Line102 genotype can be determined as seen in **Figure 2-1**; the western blot used to confirm H1 haplotype expression is also shown. C57BL/6 mice exclusively express four-repeat tau. By contrast, the H1*Mapt-/-* mouse model expresses all six isoforms of human tau. When establishing the model, it was demonstrated that the hemizygous H1*Mapt-/-* mouse model showed almost a quarter of total tau expression compared to WT mice (Wobst *et al.*, 2017). The genotyping demonstrated that homozygous mice had almost twice the amount of total tau expression compared to the hemizygous mouse, although this was not significant (**Figure 2-1**).

Table 2-1: Primers for the Line 102, H1*Mapt-/-* and *Mapt-/-* genotyping

Primers (all from Eurofins Genomics)	**Oligonucleotide sequence (5'-3')**
PrP-S-J	GGGACTATGTGGACTGATGTCGG
PrP-As-J	AGCCTAGACCACGAGAATGC
Tn10	CGCTGTGGGGCATTTTACTTTAG
VP16	CATGTCCAGATCGAAATCGTC
S36	CCGAGATCTCTGAAGTGAAGATGGATG
PAC-MAPT up	Forward: ATGGCTCATAACACCCCTTG Reverse: GGTATGGGGGTCATTTTTCC
PAC-MAPT down	Forward: ACTGACCCCACCAAACCTC Reverse: CAATGACCTGACCATTTGATG
***Mapt* WT**	Forward: TTGAATCTCTCCCTGGACATGG Reverse: TTGTGTCAAACTCCTGGCGAG
***Mapt* KO**	Forward: TTGAATCTCTCCCTGGACATGG Reverse: CTTCTATCGCCTTCTTGA
Gapdh	Forward: TGAACGGGAAGCTCACTG Reverse: TCCACCACCCTGTTGCTG

Table 2-2: Genotyping primer products

Primers for the Line 102, H1*Mapt-/-* and *Mapt-/-* genotyping		
	Gene	**Product size (bp)**
Line 102	PrP	750
	tTA	480
	APP	400
Endogenous murine *Mapt*	*Mapt* WT	700
	Mapt KO	500
H1 haplotype	H1 PAC upstream	397
	H1 PAC downstream	306
	Gapdh	307

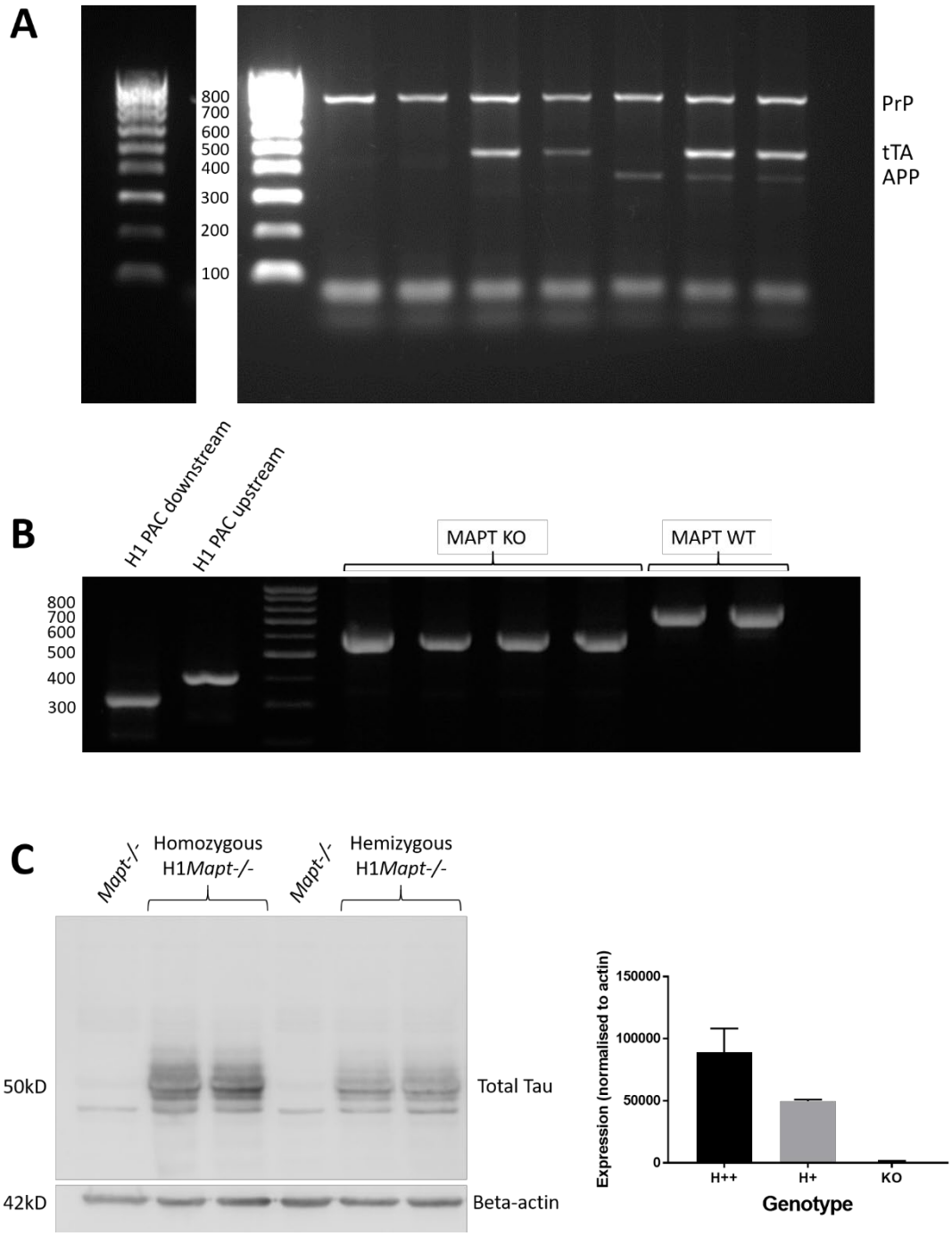

Figure 2-1: Genotyping of H1*Mapt-/-* mice

A) Agarose gel showing the expression of PrP in all samples and then the selective expression of the APP and tTA gene at 400 and 480bp respectively. **B)** Agarose gel showing the expression of the H1 PAC both upstream and downstream sections with the *Mapt* KO and WT gene. **C)** Western blot showing confirmation of H1 haplotype expression; 15µl of lysate was loaded at 1µg/µl. Tau was stained for by Total Tau. Beta actin was used as the housekeeping gene. Quantification of expression of total tau normalised to actin (n=4 for homozygous, n=2 for hemizygous and *Mapt-/-* mice). *Gapdh* product shown in Figure 2-2.

2.4 PCR for Nramp1

Ear clippings were used to determine S*lc11a1* expression (Primers from Sigma-Aldrich; **Table 2-3**), with housekeeping gene *Gapdh* as a control. Primers were designed using Primer-BLAST NCBI, to generate primers with a high GC percentage (60%) and a melting temperature of 60°C. Initially, each ear clippings from C57BL/6 and P301S mice were heated at 56°C (Grant QBD2, UK) in 50ml of lysis buffer Type 1 and 10µl of proteinase K for an hour using the Illustra tissue mini kit (GE Healthcare, UK). The elution buffer Type 5 (GE Healthcare) was then pre-heated to 70°C. 500µl of lysis buffer Type 4 (GE Healthcare) was added and the samples were vortexed for 15 seconds. Each sample was added to a mini column within a collection tube and spun at 11,000rcf for one minute (Eppendorf Centrifuge 5415 R). This was then repeated with the flow-through discarded each time. Wash buffer Type 6 was subsequently added to the mini column, the samples were then spun at 11,000rcf for three minutes. The mini spin column was added to a new 1.5ml Eppendorf. Pre-warmed elution buffer (GE Healthcare) was then added to the mini column, incubated for 1 minute at room temperature; the samples were spun at 11,000rcf for 1 minute, collecting the isolated genomic DNA within a new Eppendorf tube. Genomic DNA samples were stored at -20°C.

The master mix was then added to PCR beads in a multi-well plate (illustra™ PuReTaq Ready-To-Go™ PCR Beads, UK), containing both primers for the gene of interest (*Slc11a1*) and the reference gene (*Gapdh*) listed in **Table 2-3** (Appendix B, Table 10 for master mix dilutions). Each sample was added to the corresponding well and the plate was centrifuged at 3,000rpm for 3 minutes at 4°C (Eppendorf Centrifuge 5810 R). The samples then undergo PCR reaction within a PTC20 Tetrad 2 Peltier thermal cycler (MJ Research, Canada) (full PCR cycle listed in Table 11). To visualise the samples on a gel, 1.6g agarose (Fisher Scientific) was dissolved in 100ml of 1X Tris Acetate-EDTA (TAE) buffer with 3µl GelRed (Biotium, USA). The solution was poured into a gel case and set for 30 minutes. Once set, the gel was placed in the electrophoresis tank (Fisher Brand, UK) and the tank was filled with 1X TAE buffer. 5µl of GeneRuler 1kb Plus DNA ladder (Thermo Scientific, UK) was added to the initial well. 5µl of 6X DNA loading dye (Thermo Scientific) was added to each PCR product, 15µl of each sample was then added to each subsequent well. The tank was connected to a power pack (PowerPac Basic, Bio-Rad, UK) and run at 100V for 1 hour. The gel was then imaged in a UV Transilluminator (UVP, UK) PCR product size shown in **Table 2-3** and **Figure 2-2**.

Table 2-3: Primer sequences for *Slc11a1* PCR

Gene	NCBI Gene ID	Product length (bp)	Oligonucleotide sequence (5'-3')
Slc11a1	18173	451	Forward: CGTGATGGAGGTGGGTATCG Reverse: CATGGGGCTCACCAGTAGAC
Gapdh	14433	307	Forward: TGAACGGGAAGCTCACTGG Reverse: TCCACCACCCTGTTGCTGTA

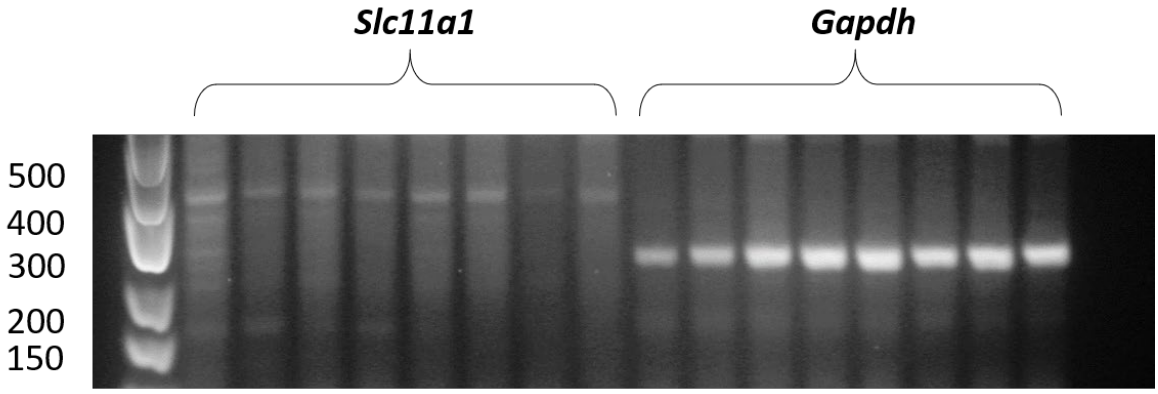

Figure 2-2: *Slc11a1* and *Gapdh* primer products
A) Agarose gel showing the expression of *Slc11a1* and *Gapdh* primer products at 451 and 307 respectively.

2.5 AD seed prep

2.5.1 Post-mortem human brain samples

Ten post-mortem human brain samples were obtained from the South West Dementia Brain Bank (SWDBB, Bristol, UK) under ethics approval from London-City and East NRES committee (08/H0704/128+5). All cases had a primary diagnosis of AD and cases were chosen dependent on a confirmed Braak staging of V-VI for tau pathology. Approximately 10g of frozen tissue from the frontal cortex was requested for each case and the frozen tissue was stored at -80°C. **Table 2-4** details both the age, post-mortem delay and comorbidities of each patient.

Table 2-4: AD post-mortem tissue from SWDBB

Case No.	MRC ID	Age	Sex	Post-mortem delay (h)	Primary diagnosis	Secondary diagnosis	Tertiary diagnosis
859	BBN_4238	85	F	14	AD	CVD	CAA
903	BBN_10252	89	F	22	AD	VaD	TDP43 pathology
912	BBN_14405	82	F	22	AD	Hippocampal sclerosis	TDP43 pathology
935	BBN_19632	91	M	43	AD	Hippocampal sclerosis	TDP43 pathology, CVD
959	BBN_24327	74	M	16	AD	CVD	LBD (amygdala only)
962	BBN_24330	80	F	14.5	AD	CAA	VaD
966	BBN_24334	82	M	61	AD	CAA, CVD	LBD and TDP43 pathology (amygdala only)
982	BBN_24898	76	M	47.5	AD	CAA	DLB
1027	BBN006.28978	72	M	81.5	AD	DLB	CAA, TDP43 pathology
1033	BBN006.29162	81	M	7.5	AD	DLB	CAA, TDP43 pathology
AD= Alzheimer's disease, CVD= Cardiovascular disease, VaD= Vascular dementia, CAA= Cerebral amyloid angiopathy, DLB= Dementia with Lewy bodies							

2.5.2 Seed prep method

The three cases with the highest AT8-positive tau expression were to be identified by western blot. There were three stages to generating the seed prep. First, only 0.5g from each case was used to screen for the expression of AT8-positive tau and select the three cases with the

greatest tau burden. The following protocol was carried out for all 10 cases with 0.5g utilised from each sample. The western blot was run using S1 (**Figure 2-3**) to establish the three cases of interest. The second requirement was then to establish the protocol was feasible using a larger volume of tissue and that the high-speed centrifugation and sonication worked to enrich the lysate. To determine this 10g of tissue was chosen from a case which showed low AT8 expression, and the entire protocol was carried out (**Figure 2-3**). Finally, 30g of frozen tissue from the three cases with the highest AT8/total tau ratio was processed to produce the final AD seed, this AD tau lysate was then used in intracerebral injections to induce the tau spreading model.

Once the three cases with the highest AT8/total tau ratio had been identified in Southampton, diagnostic images from the SWDBB were requested. These diagnostic images were from the cerebral cortex in the dorsolateral prefrontal region. At both 10x and 40x magnification, the slices were stained for AT8 showing high molecular weight pathological tau. These images were used to confirm the presence of high levels of tau burden. All processing of the fixed tissue, subsequent histology and images taken were carried out by the SWDBB.

2.5.3 Homogenisation

Prior to homogenisation, the exterior blood vessels were excised from the tissue. The tissue was weighed on a fine scale to calculate the volume of homogenisation buffer required. Tissue was homogenised at 20% weight by volume in ice cold, sterile Dulbecco's PBS (DPBS) (Gibco, UK) supplemented with cOmplete Protease Inhibitor Cocktail (Roche, UK) using an SM1 polytron homogeniser (Stuart, UK) for 10 minutes. The SM1 polytron homogeniser has a maximum motor speed of 35,000rpm, the tissue was homogenised at this speed until there was no visible tissue remaining. An aliquot was taken of the homogenate for biochemical analysis. For the initial homogenisation of 0.5g of tissue from each case, the lysis buffer was also supplemented with Phosphatase Inhibitor Cocktails 2 and 3 (Sigma). The homogeniser probe was cleaned with dH_20 and 70% ethanol (Fisher Scientific, UK) twice between samples.

The homogenate was centrifuged at 10,000rcf for 10 minutes at 4°C (Eppendorf, centrifuge 5417R). The supernatant (referred to as S1) was filtered using a fine tissue (Scott, UK) and decanted into a glass beaker. The remaining pellet was homogenised at 40% weight by volume in ice cold, sterile Dulbecco's PBS and the lysate centrifuged at 10,000 rcf for 10 minutes at 4°C. The second supernatant (S2) was filtered through a fine tissue (Scott) and pooled with S1. The homogenisation of the pellet at 40% weight by volume in PBS and subsequent centrifugation was repeated to produce the third supernatant (S3). All three supernatants (S1-S3) were pooled.

Aliquots of all supernatant (S1-3) and homogenate (P1-2) individually and pooled were taken for biochemical analysis.

Approximately 10% of total volume is lost through filtration, leaving an approximate final volume of 270ml. The pooled supernatant was then incubated in N-Lauroylsarcosine sodium salt

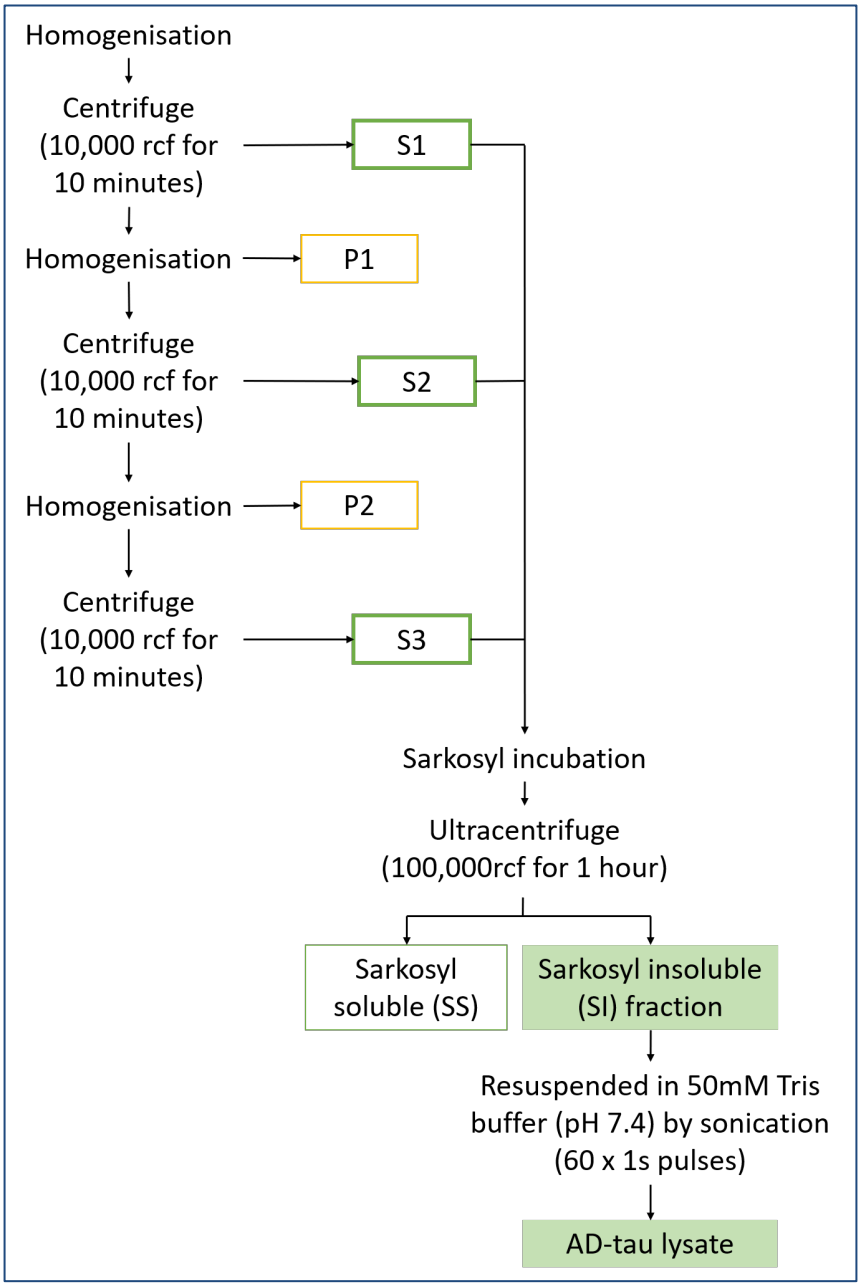

Figure 2-3: Protocol to establish seed prep

This protocol demonstrates how sequential homogenisation and centrifugation of post-mortem tissue generates three supernatants from low-speed centrifugation (S1-3). These supernatants are then pooled and incubated in Sarkosyl. Following high-speed centrifugation, the insoluble fraction can be resuspended and sonicated to resuspend the pellet and finish the seed prep.

(Sarkosyl 20% solution, Sigma). The 20% Sarkosyl solution was added to the supernatant to give a final concentration of 1%. The supernatant was incubated in 1% Sarkosyl on a flat orbital shaker (Luckham R100) for one hour at room temperature.

2.5.4 Ultracentrifuge and sonication

Following Sarkosyl incubation, the pooled supernatant was centrifuged for 1 hour at 100,000 rcf in an ultracentrifuge (Beckman Optima LE-80K Ultracentrifuge). The supernatant was aliquoted into polyallomer centrifuge tubes (Beckman Coulter, Catalogue No. 331374) and placed within the six swing bucket rotor tubes (SW40 TI, Beckman Coulter). The ultracentrifuge was balanced to within 0.1g and the rotor tubes were cooled to 4°C overnight prior to use.

After centrifugation, the Sarkosyl-soluble supernatant was removed from the centrifuge tube and aliquoted. The Sarkosyl-insoluble pellet was washed gently in DPBS with cOmplete Protease Inhibitor Cocktail, the DPBS was then removed using a pipette. The Sarkosyl-insoluble pellet was resuspended in 50mM Tris (pH7.4) containing cOmplete Protease Inhibitor Cocktail. The final pooled sample was then sonicated (MSE Soniprep 150) for 10x 1-second pulses until pellet is in suspension. An aliquot of both Sarkosyl-soluble and Sarkosyl-insoluble fractions were collected for biochemical analysis. Prior to stereotaxic injection and biochemical analysis, the Sarkosyl insoluble lysate was sonicated for 60x 1-second pulses and the centrifuged at 5,000rcf for 10 minutes.

2.6 Western Blot

2.6.1 Homogenisation of mouse tissue

For western blot, frozen murine tissue must first be homogenised. The frozen frontal cortex tissue collected was weighed and the lysis buffer listed in Appendix B (Table 12) added to make a 20% weight per volume solution. The lysis buffer for mouse tissue in Chapter 5 (Tg4510 and *Mapt-/-* controls) contained PhosSTOP phosphatase inhibitor (Roche) and cOmplete Protease Inhibitor (Roche). However, mouse tissue homogenised in Chapter 6 following the tau propagation study used lysis buffer which contained Phosphatase Inhibitor Cocktails 2 and 3 (Sigma) and cOmplete Protease Inhibitor Cocktail (Roche).

The tissue was then homogenised using a SHM1 polytron homogeniser and 5x75mm flat head probe (Stuart, UK); the homogeniser probe was cleaned with dH_20 and 70% ethanol (Fisher Scientific, UK) twice between samples. The samples were homogenised and left on wet ice for 15 minutes. The samples were then centrifuged at 4°C at 20,000 rcf for 30 minutes (Eppendorf,

centrifuge 5417R). The supernatant was aliquoted and the pellet stored at -80°C. The Pierce bicinchoninic acid assay (BCA) protein assay (Thermo Scientific, UK) was then used to determine the total protein concentration (µg/ml) of each sample. 90µl of buffer listed in Appendix B (Table 12) was used to dilute 10µl of lysate. Protein standards were made using bovine serum albumin (BSA) included in the kit and lysis buffer listed in Appendix B (Table 12). 25µl of standard and unknown samples were added to a Greiner 96-well flat-bottomed plate (Sigma, UK). 200µl of the working reagent (50:1 dilution of reagent A: reagent B) (Thermo Scientific, UK) was then added to each sample. The plate was then mixed gently for 30 seconds and incubated at 37°C for 30 minutes (INCU-line, VWR, UK). The total protein concentration was then read at 570nm using the Infinite F200 Pro plate reader and the i-control software (TECAN, Switzerland).

In Chapter 6, the western blot was run with four mice for each group and frozen lysate from the rTg4510 mouse model used as a positive control. Tissue from the *Mapt-/-* mouse hippocampus was used as a negative control when staining for tau. For the western blot, 20µl total volume was to be added to each well, with a total protein load of 50µg in each well. This was calculated using BCA results for each individual sample to reach a total concentration of 2.5µg/µl.

2.6.2 Homogenisation of post-mortem AD tissue

The method of homogenisation for human tissue is described in section 2.5.3. Tg4510 and *Mapt-/-* samples were included as positive and negative controls and homogenised as described in section 2.6.1.

2.6.3 SDS-PAGE

To prepare the samples for SDS-PAGE, protein concentration was normalised across samples using the BCA assay results. For each sample, 4x loading buffer was added at a consistent volume to reach a final 1x concentration. dH_20 was added to normalise protein concentration and make a total volume of 25µl (this volume was used to account for subsequent boiling and ensure a final volume of 20µl). However, in Chapter 5 (except where specified in the figure legend) lysate from human tissue was not diluted with dH_20 and only 4x loading buffer was added. After the addition of loading buffer and dH_20, samples were then pulse centrifuged and heated at 95°C for five minutes (QBT1 Grant, UK). The samples were quickly moved to wet ice before being pulse centrifuged again and kept on wet ice until ready to load into the well.

Migration (10%) and stacking (2.5%) gels were made for a gel of 1.5 millimetre (mm) as seen in Appendix B (Table 13). Tetramethylethylenediamine (TEMED) was only added to the migration gel and gently mixed; the migration gel was poured into the mini-PROTEAN short plate

and 1.5mm spacer plate set in the casting frame (Mini-PROTEAN, Bio-Rad, UK). Isopropanol (Sigma, UK) was pipetted on top of the migration gel to level the surface and set for 30 minutes. The isopropanol was poured off once the gel had set and the gel was washed three times with dH20. TEMED was then added to the stacking gel, mixed and pipetted on top of the migration gel in the casting frame. The 10 or 15-well 1.5mm comb was then placed into the casting frame and the stacking gel allowed to set for 30 minutes. Once set the gel was removed from the casting frame and placed in the Mini-PROTEAN tetra electrode module (Bio-Rad, UK). The module was placed in the buffer tank (Bio-Rad, UK) and filled with ~800ml 1X Laemmli buffer (listed in Appendix B). The comb was removed and the wells flushed out to ensure the removal of air bubbles. 5µl of Precision Plus Protein Kaleidoscope standard (Bio-Rad, UK) was added to the first well to compare kilodaltons (kD) through blot. Following this, 20µl of the samples were added to each subsequent well. The gel was run at 100 volts (V) using a power pack (PowerPac Basic, Bio-Rad, UK) until the line of loading buffer reaches the bottom of the gel.

Following this the transfer buffer was prepared (1X Laemmli with 20% methanol; listed in Appendix B) and the sponges and grade 0.34mm cellulose chromatography paper (GE Healthcare, UK) pre-soaked in the transfer buffer. The 0.45µm pore size PVDF transfer membrane (Polyvinylidene difluoride, Merck, Germany) was charged in methanol (Fisher Scientific, UK) for 2 minutes. Once the gel had been run, half the pre-soaked sponges and chromatography paper were loaded into the mini gel holder cassette (Bio-Rad, UK). The charged PVDF membrane was then added and the gel removed from the glass plates and placed onto the PVDF membrane. The second half of the pre-soaked sponges and chromatography paper were then assembled on top of the gel. The mini gel holder cassette was then placed into the mini trans-blot central core in the mini trans-blot cell (Bio-Rad, UK) and filled with ~1L transfer buffer. The tank was then attached to a power pack (PowerPac Basic, Bio-Rad, UK) and run at 100V at 4°C for 90 minutes.

After transfer of the blot, the PVDF membrane was removed and placed into TBS (listed in Appendix B). The membrane was then blocked in 5% BSA (Fisher Scientific, UK) for an hour and subsequently incubated in primary antibodies overnight as listed in **Table 2-5**, on a rotator (Stuart SRT6B, UK). The next day, the membrane was washed in TBS and then washed with TBS-T (0.05% Tween, Fisher Scientific) three times for 5 minutes each. The membrane was then washed in TBS and incubated in secondary antibodies listed in **Table 2-6** for 2 hours on a rotator (Stuart SRT6B, UK). The membrane was subsequently washed with TBS and then TBS-T three times for five minutes; after this, the membrane was then placed in TBS for a final time. Following this the membrane was either imaged on a ChemiDoc MP Imaging System (Bio-Rad, UK), Odyssey 9210 Gel Imaging System or Odyssey Fc Imaging System (Both Odyssey Imaging Systems are LI-COR

Biosciences, USA). Images were taken with Image Lab software (Bio-Rad, UK) or Image Studio Lite (LI-COR Biosciences, USA).

Analysis of the images was carried out using Image Studio Lite (LI-COR Biosciences, USA). The images were set to a global threshold and the signal for each sample recorded. The signal for both the protein of interest and the reference protein were recorded. All beta actin signals were standardised to the largest beta actin signal, forming a ratio. From this all values for the protein of interest were normalised to beta actin expression. The values for the protein of interest were then normalised to the mean of the C57BL/6 saline group. Western blots in Chapter 5 did not include beta actin and therefore analysis was carried out simply by examining the AT8/total tau ratio.

Table 2-5: Primary antibodies used in western blot

Primary Antibody	Host species	Class	Company	Clone number	Dilution
AT8	Mouse	Monoclonal	Invitrogen	MN1020	1:1,000
PHF-1	Mouse	Monoclonal	Kind gift from Peter Davies	-	1:5,000
Total Tau	Rabbit	Polyclonal	DAKO	A0024	1:10,000
Beta-Actin	Mouse	Monoclonal	Sigma	A2228	1:4,000

2.6.4 Dot blot

A dry 0.45µm nitrocellulose membrane (Bio-Rad, UK) was placed flat on a surface cleaned with 70% ethanol. For each sample 1µl is pipetted onto the membrane and left to dry for 1 hour. The membrane is then blocked in 2% BSA (Fisher Scientific) in TBS-Tween (0.1%) for 1 hour at room temperature on a flat orbital shaker. The blot was then incubated in primary antibodies diluted in 2% BSA (see **Table 2-5** for dilutions). The membrane was washed in TBS followed by three washes in TBS-T. The membrane was subsequently incubated in secondary antibodies diluted in 2% BSA (see **Table 2-6** for dilutions) for 1 hour at room temperature. The blot was then imaged with the Odyssey 9210 Gel Imaging System (Li-Cor, USA). Analysis of the images was carried out using Image Studio Lite (LI-COR Biosciences, USA). The images were set to a global threshold and the signal for each sample recorded. The signal from the *Mapt-/-* sample was considered background and so each sample of interest had this background signal subtracted to determine the genuine signal.

Table 2-6: Secondary antibodies used in western blot

Host species	Target species	Class	Conjugate	Company	Reference number	Dilution
Goat	Rabbit	Polyclonal	IRDye® 680RD	Li-Cor	926-68071	1:2000
Goat	Rabbit	Polyclonal	IRDye® 800CW	Li-Cor	926-32211	1:2000
Goat	Mouse	Polyclonal	IRDye® 680RD	Li-Cor	926-68070	1:2000
Goat	Mouse	Polyclonal	IRDye® 800CW	Li-Cor	926-32210	1:2000
Goat	Rabbit	Polyclonal	Alexa Fluor® 568	Invitrogen	A-11011	1:500
Goat	Rabbit	Polyclonal	Alexa Fluor® 488	Invitrogen	A-11008	1:500
Goat	Mouse	Polyclonal	Alexa Fluor® 488	Invitrogen	A-11029	1:500
Donkey	Mouse	Polyclonal	NorthernLights™ 557	R&D Technologies	NL007	1:500

2.7 Homogenous Time Resolved Fluorescence assay

Homogenous Time Resolved Fluorescence (HTRF) assay was used to support the findings in the western blot regarding the seed prep; HTRF uses the mechanism of fluorescence resonance energy transfer (FRET) technology. The HTRF assay detects the presence of Ser202 and Thr205 phosphorylation epitopes of tau (Cisbio). The assay consists of diluent, anti-human tau-d2 conjugate (acceptor) and anti-human tau-Tb^{3+} Cryptate conjugate (donor) to detect signal within the sample. Control wells within the 384-well microplate (Greiner) were included to test signal from the diluent and the cryptate conjugate individually. A negative control was also included which consisted of diluent and both conjugates but no sample. For all remaining sample readouts, the two conjugates were mixed and a 10µl conjugate mix added to each well. The sample itself underwent five three-fold dilutions (beginning 1:4000) and 10µl of each dilution was added in duplicate to the microplate. The microplate was sealed and incubated at room temperature for 2 hours and 20 hours. After each time point the microplate was read on a Varioskan Flash (Thermo Scientific), with fluorescence emission recorded at both 665nm and 620nm.

To calculate the HTRF ratio the following equation was applied:

$$Ratio = \frac{Signal\ 665nm}{Signal\ 620nm}\ x\ 10^4$$

From this delta ratio (ΔR) is calculated to determine the signal without the background recorded from the negative control (diluent and both conjugates but no sample):

$$\Delta \mathrm{R} = Ratio_{sample} - Ratio_{background}$$

This ΔR is then plotted against log dilution to observe the presence of phosphorylated tau epitopes within the sample.

2.8 Histology

Tissue mounted in OCT was cut into 10µm sections using the cryostat (Leica CM3050 S). Fresh-frozen tissue sections were mounted onto aminopropylsilane (APS)-coated slides and subsequently stored at -20°C. PFA-fixed tissue sections were mounted on gelatin-coated slides and subsequently stored at -20°C. Recipes for the slide coatings are listed in Appendix B.

2.8.1 Immunohistochemistry

To being immunohistochemistry (IHC), tissue was dried at 37°C for thirty minutes (INCU-line, VWR, UK). If tissue was fresh frozen, then it was subsequently fixed in 100% ethanol (Fisher Scientific, UK) for ten minutes at 4°C. All slides were then washed in phosphate buffer saline (PBS) with 0.01% Triton (PBS-T) three times for 5 minutes each. In Chapter 6 and 7, Tris buffered saline (TBS) was used in place of PBS, including using 0.01% Triton in the washes (TBS-T). All protocol steps remained the same, the buffer was replaced throughout.

Using a wax pen (Vector, UK) the sections were traced around to create a hydrophobic barrier. Slides were then quenched in 1% hydrogen peroxide (Sigma, UK) in PBS for 10 minutes, and washed in PBS-T three times for 5 minutes each. Slides were incubated in blocking buffer containing 10% Normal Animal Serum (Sigma, UK) and 2% BSA (Fisher Scientific, UK) diluted in PBS-T for 1 hour at room temperature. The slides were then incubated in primary antibodies (diluted in 1:5 diluted blocking buffer) (**Table 2-7**) overnight at 4°C.

The brain sections were then washed in PBS-T and incubated in the secondary antibodies (**Table 2-8**) (made in a 1:5 diluted blocking buffer) for 1 hour at room temperature. Slides were washed in PBS-T again three times for 5 minutes each. Avidin Biotin Complex (ABC Vectastain, Vector, UK) was prepared by adding 50µl of both Reagent A and Reagent B to 5ml of PBS-T. The ABC complex was then left for 30 minutes at 4°C. ABC was then added to the slides for 30 minutes at room temperature. After a final PBS-T wash, slides were then exposed to DAB (3,3 Di-aminobenzidine) solution and removed to PBS once sufficiently exposed (DAB substrate solution is listed in Appendix B). The slides were then placed in haematoxylin (Sigma, UK) for 3 seconds

and washed in tap water for 15 minutes. The slides were then placed in acid alcohol for 20 seconds and washed in tap water for 15 minutes. The slides were dehydrated by the following steps:

1. 70% Industrial methylated spirits (IMS) for 20 seconds.
2. 80% IMS for 20 seconds.
3. 90% IMS for 20 seconds
4. Absolute alcohol for 1 minute
5. Absolute alcohol for 1 minute
6. Xylene (Fisher Scientific, UK) for 1 minute
7. Xylene for 5 minutes

Once dehydrated the slides were covered in DPX mounting media (Merck, Germany) and a cover glass slip (VWR, UK) placed on top. The slides were then kept at 4°C. Mike Hurley carried out the immunohistochemistry for the phosphorylated alpha-synuclein (pSer129) stain only (**Table 2-7**).

Table 2-7: Primary antibodies for IHC and IF

Primary Antibody	Host species	Class	Company	Clone number	Dilution
PHF-1	Mouse	Monoclonal	Kind gift from Peter Davies	-	1:500
Ser396	Rabbit	Polyclonal	Biolegend	807401	1:500
Thr205	Rabbit	Polyclonal	Biolegend	806901	1:500
Biotinylated AT8	Mouse	Monoclonal	Kind gift from Eli Lilly	-	1:2000
FcγRI (CD64)	Rat	Monoclonal	BioRad	MCA5997	1:500
MHC II	Rat	Monoclonal	eBioscience	M5/114.15.2	1:500
CD11b	Rat	Monoclonal	ThermoFisher	MA5-16527	1:500
Laminin	Rabbit	Polyclonal	Sigma	L9393	1:1000
Alpha-synuclein (pSer129)	Mouse	Monoclonal	Biolegend	825701	1:3500
3D6	Mouse	Monoclonal	Produced in-house by James Fuller	-	1:500

Table 2-8: Secondary antibodies for IHC and IF

Host species	Target species	Class	Conjugate	Company	Reference number	Dilution
Goat	Mouse	Polyclonal	Biotinylated	Vector	BA-9200	1:200
Rabbit	Rat	Polyclonal	Biotinylated	Vector	BA-4001	1:200
Goat	Human	Polyclonal	Biotinylated	Vector	BA-3000	1:200
Goat	Rabbit	Polyclonal	Alexa Fluor® 568	Invitrogen	A-11011	1:500
Donkey	Rat	Polyclonal	Alexa Fluor® 488	Invitrogen	A-21208	1:500
-	-	-	Streptavidin, Alexa Fluor™ 488	Invitrogen	S32354	1:1000

2.8.2 Immunofluorescence

The protocol for immunofluorescence initially follows the same methods as with DAB IHC. Slides were dried at 37^{o}C for 30 minutes and only fresh frozen slides were then fixed in 100% ethanol for 10 minutes. Both fresh and fixed slides were subsequently washed in PBS-T for 5 minutes three times. The slides were then drawn around with a wax pen, blocked in blocking buffer (10% Normal Animal Serum (Sigma, UK) and 2% bovine serum albumin (Fisher Scientific, UK) diluted in PBS-T) as aforementioned for 1 hour at room temperature. The primary antibodies were incubated on the slides overnight (**Table 2-7**). The next day, the slides were washed in PBS-T, and incubated in the secondary antibodies (**Table 2-8**) at room temperature for sixty minutes. The slides were then incubated in 1:2000 dilution of DAPI (4',6-Diamidino-2-Phenylindole, Dihydrochloride) (d9542, Sigma, UK) nuclear stain at room temperature for three minutes. Slides were then washed in PBS-T, covered in Mowiol mountant and a glass clover slip (VWR, UK) placed on the slide. Slides were stored at 4°C.

2.8.3 Thioflavin S staining

Thioflavin S (Sigma) was diluted 1:500 in PBS and filtered 5 times. In order to carry out Thioflavin S staining, slides were dried at 37^{o}C for 30 minutes. Following this the slides were washed three times in TBS-T for 5 minutes each. The slides were then incubated in 1:2000 dilution of DAPI (d9542, Sigma, UK) nuclear stain at room temperature for three minutes. Following this, slides were placed in Thioflavin S for 2 minutes and then immediately into 80% IMS for a further 2 minutes. The slides were then dehydrated as follows:

1. 80% IMS for 2 minutes
2. 95% IMS for 2 minutes
3. 100% IMS for 2 minutes
4. Xylene for 3 minutes
5. Xylene for 2 minutes

Slides were then mounted with cover slips as before using DPX mounting media.

2.8.4 Imaging and quantification

Immunohistochemistry and immunofluorescence images were captured using the Leica DM4B microscope (Leica Microsystems) with a sCMOS camera. Immunofluorescent images for Chapter 3 were captured using the Leica DM5000 microscope (Leica Microsystems). Images were captured with the use of Leica LAS-X and LAS-AF image acquisition software respectively. Images were scaled using ImageJ software, objective used was stated in corresponding figure legend. All subsequent analysis was carried out using ImageJ software.

Analysis of immunohistochemical staining was carried out in different brain regions (**Figure 2-4**). In Chapters 3 and 4, a minimum of three images of the hippocampal fissure from each mouse brain were taken for analysis. In Chapter 6, four images per region of interest (ROI) were taken in most brains, although 1-2 brains had fewer images per ROI. In Chapter 7, three images were taken per ROI for each brain. However, due to small brain regions in the ventral hippocampus (Bregma AP= -3.00) only two images from each brain were taken in these ROIs for MHCII and FcγRI (ventral hippocampus, perirhinal cortex and mammillary nuclei).

For quantification, 20x objective images were de-convoluted using HDAB RGB values to produce a separate haematoxylin and DAB channel. HDAB RGB is an ImageJ plugin which separates a DAB immunohistochemistry image into three channels through colour deconvolution. This generates three distinct images based on colour, including one image with only the blue haematoxylin stain and one image with only the brown DAB staining. The image which isolated the DAB staining was converted to an 8-bit binary image and percentage area measured above a set threshold. The threshold for each ROI was determined by examining the histogram of two random images and establishing a threshold representative for all images within said ROI. All positive staining above the set threshold was measured as a percentage of the area. Quantification of DAB immunohistochemistry was carried out using an automated macro. All ROIs for the chapters are demonstrated below (**Figure 2-4**).

A small initial subset of images in Chapter 7 were analysed manually whereby images were assigned randomised titles by ImageJ to allow blinded analysis. The same threshold was set both

in the manual thresholding and in the macro for all images. In Chapter 6, due to the low levels of tau pathology any result below 0.02% mean percentage area was deemed to be background. A small percentage (~4% for most regions) of some images either had to be cropped due to folds in the tissue or the threshold changed due to significant background. This was specific only to the quantification in Chapter 6 for tau pathology. Cohort distribution for histology in Chapter 6 and Chapter 7 is described in **Table 2-9**. Tissue from Cohort 3 was stained for tau pathology but there was insufficient time to stain for microglial markers in this cohort, due to Covid-19 restrictions.

	Group size	**Chapter 6**	**Chapter 7**
Cohort 1	n= 3 for tau i.c./saline i.p. n= 3 for tau i.c./*S. typhimurium* i.p.		✓
Cohort 2	n= 3 for tau i.c./saline i.p. n= 3 for tau i.c./*S. typhimurium* i.p. n= 5 for vehicle i.c./saline i.p. n= 6 for vehicle i.c./*S. typhimurium* i.p.	✓	✓
Cohort 3	n= 3 for tau i.c./saline i.p. n= 5 for tau i.c./*S. typhimurium* i.p.	✓	

Table 2-9: Cohort distribution for histology in Chapter 6 and Chapter 7

Microglial cell count was also carried out on the same images from Chapter 7 which were stained for MHCII. Images were assigned randomised titles. For cell count analysis, the original image was measured for area (µm^2). The results were then normalised to the area with the following equation:

$$Cell\ count\ (mm^2) = \frac{Initial\ cell\ count}{\left(\frac{Area\ (\mu m^2)}{1x10^6}\right)}$$

For quantification of fluorescent images, again images were randomised to allow blinded analysis. Images were converted into 8-bit files and a specific threshold was set for each marker. Again, three images of the hippocampal fissure from each brain were used for quantification (except for one WT brain in Chapter 4 for CD11b quantification where two images were taken). Mean % area was calculated as the signal above the set threshold.

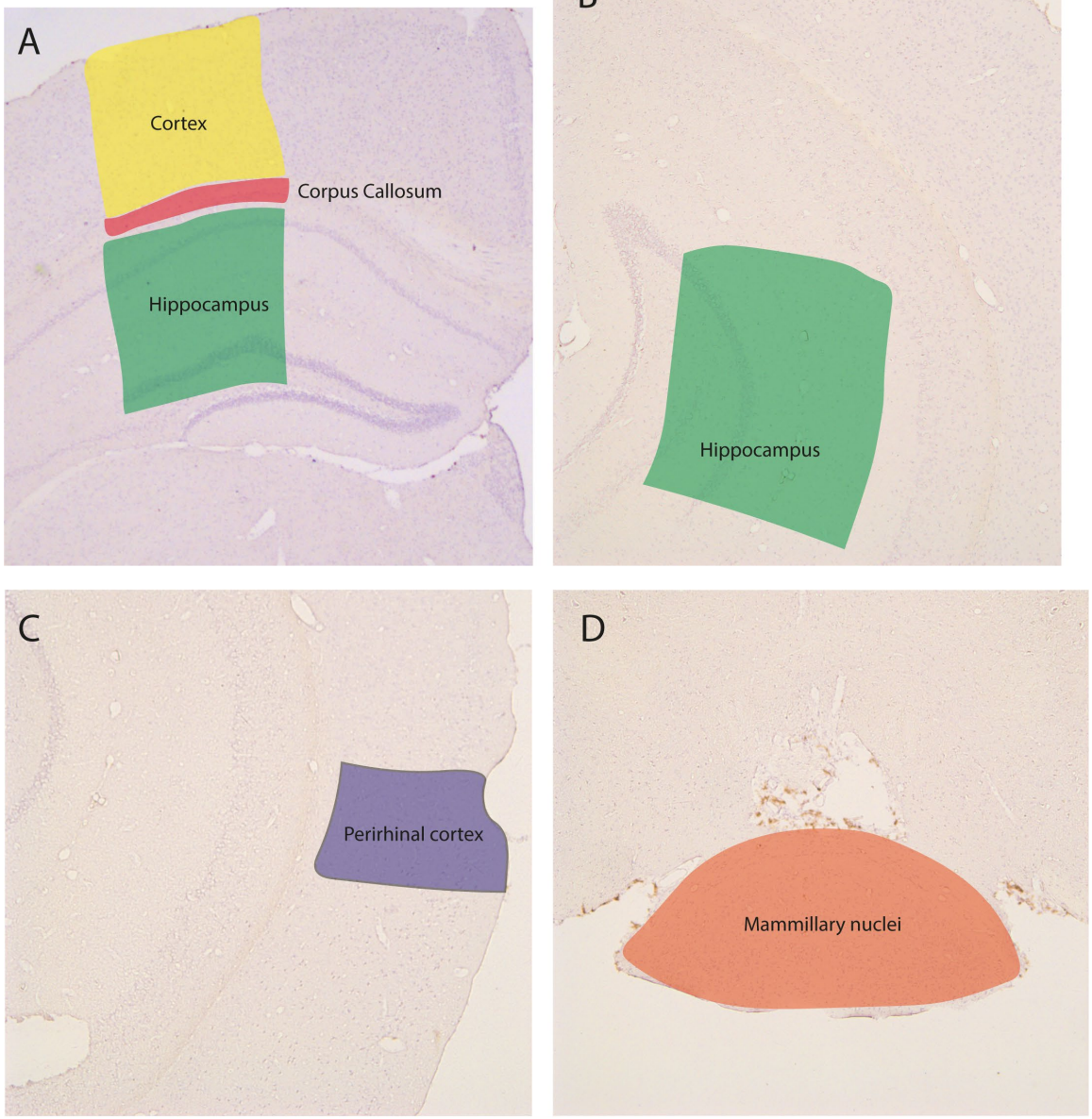
A
Cortex
Corpus Callosum
Hippocampus
B
Hippocampus
C
Perirhinal cortex
D
Mammillary nuclei
E
Corpus callosum
Dorsal fornix

Figure 2-4: Regions of interest for IHC and IF quantification

A) The cortex (yellow), corpus callosum (red) and hippocampus (green) were all key areas in Chapters 6 and 7. In Chapters 3 and 4, only the hippocampus area was the ROI as this area focused on the hippocampal fissure. **B)** The hippocampus ROI in the ventral hippocampus at Bregma AP= -3.00, this ROI is only analysed in Chapters 6 and 7. **C)** The perirhinal cortex ROI in the ventral hippocampus at Bregma AP= -3.00, this ROI is only analysed in Chapters 6 and 7. **D)** The mammillary nuclei ROI in the ventral hippocampus at Bregma AP= -3.00, this ROI is only analysed in Chapters 6 and 7. **E)** The corpus callosum (red) and dorsal fornix (blue) at the Bregma AP= -1.00, this ROI is only analysed in Chapter 6

2.9 Statistical analysis

Statistical analysis was carried out using GraphPad Prism 8 (GraphPad Software, USA). If normality assumptions were met, statistical analysis was carried out using repeated measures Analysis of Variance (ANOVA), three-way ANOVA, two-way ANOVA, one-way ANOVA, Student's t-test and mixed-effects analysis. For repeated measures ANOVA with Tukey's post-hoc test, the F values were reported and the Greenhouse-Geisser correction was used if the Mauchly's Test of Sphericity was significant. For three-way ANOVA, two-way ANOVA and one-way ANOVA the Tukey's post-hoc test was used. Two-way ANOVAs in Chapter 6 and 7 had one between-subject effect and one within-subject effect, therefore in this analysis the Sidak's post-hoc test was used. In the case of missing data values, mixed-effects analysis with Sidak's post-hoc test was carried out. In Student's t-test, Welch's correction was used if standard deviations were unequal. If normality assumptions were not met, either the Mann-Whitney U test or the Kruskal Wallis test with Dunn's multiple comparisons was carried out. All data is presented as Mean ± standard deviation (SD), except for quantification of histology where data is presented as Mean ± S.E.M. Statistical significance is denoted as follows; *p≤0.05, **p≤0.01 and ***p≤0.001.

Chapter 3 *S. typhimurium* infection in the P301S and H1*Mapt-/-* mouse model of tauopathy

3.1 Introduction and objectives

Systemic infection has been shown to correlate with cognitive decline in AD patients (Holmes *et al.*, 2009). To investigate the potential mechanism behind this finding, this thesis hypothesises that systemic infection may increase the spread of tau through the mouse brain. Prior to inducing tau spread, it must first be confirmed that the mouse strain used is susceptible to *S. typhimurium. S. typhimurium* (SL3261) is an attenuated bacterial strain; when administered orally or through an intraperitoneal (i.p.) injection, there is low-grade inflammation induced which resolves within four weeks. Mice were injected i.p. with 10^6 cfu of *S. typhimurium* as this has been established in our lab prior to induce an immune response within the brain without inducing excessive weight loss (Püntener *et al.*, 2012).

The response to systemic infection in two distinct mouse strains is described in this chapter, the P301S mouse model of tauopathy and the H1*Mapt-/-* mouse. The P301S transgenic mouse was first described as a murine model of FTDP-17 (Allen *et al.*, 2002). The P301S mouse model was included given the quick development of pathology and the use of the P301S mouse in previous propagation studies (Ahmed *et al.*, 2014). There has been no research thus far establishing the immune response to *S. typhimurium* bacterial infection in the P301S mouse model. Previous studies utilised LPS (Qin *et al.*, 2016), however the endotoxin will only induce an inflammatory response through activation of the TLR4 pathway. Therefore, LPS only induces an acute inflammatory response, and so *S. typhimurium* was used to induce a low-grade sustained infection.

The H1*Mapt-/-* mouse also received a *S. typhimurium* injection in this chapter. The H1*Mapt-/-* mouse expresses all six isoforms of human tau with no disease-associated mutation and is bred on a pure C57BL/6 background (Wobst *et al.*, 2017). In this chapter, I discuss the immune response of C57BL/6, P301S and H1*Mapt-/-* mice to an *S. typhimurium* infection. *Mapt-/-* mice are included to provide a control for the knockout of the *Mapt* gene but will not be used in the tau spreading model, as they express neither endogenous tau nor the H1 haplotype. The *Mapt-/-* mice may highlight potential confounding factors caused by the knockout of the *Mapt* gene. No current research demonstrates the immune response to *S. typhimurium* infection in tauopathy mouse models. Hence, prior to induction of the seeding model, a response akin to WT must be confirmed in these models.

Aims addressed in this chapter are as follows:

- *To establish if P301S or H1Mapt-/- mice are susceptible to the attenuated Salmonella enterica serovar Typhimurium vaccine strain SL3261 through changes in body weight and spleen size*

- *To establish if there are inflammatory changes in immune markers in the brains of H1Mapt-/- and P301S mice following S. typhimurium infection*

3.2 Methods

3.2.1 *S. typhimurium* intraperitoneal injections

2-3-month-old C57BL/6, P301S and H1*Mapt-/-* mice were moved to the containment level 2 area (CL2) a week prior to the experiment. Mice were given an i.p. injection of 1 x 10^6 colony-forming units (CFUs) of *S. typhimurium* (SL3261) or 0.9% saline i.p. as previously described in Püntener et al. (2012). Alex Collcutt carried out all *in vivo* work for the P301S mice. Mice were weighed daily and observed for clinical signs of stress or pain in the first week. After this, weight was recorded once a week for three weeks.

Table 3.1: P301S Group sizes

	Saline i.p.	***S. typhimurium* i.p.**
C57BL/6	8	8
P301S	10	10

Table 3.2: H1*Mapt-/-* Group sizes

	Saline i.p.	***S. typhimurium* i.p.**
C57BL/6	10	10
H1*Mapt-/-*	10	10
Mapt-/-	6	6

3.2.2 Perfusion and collection of tissue

Four weeks after i.p. injection the mice were transcardially perfused with ice-cold 0.9% saline. One brain hemisphere was embedded in OCT (Cell Path, UK). Punches from the hippocampal area and remaining cortical tissue were taken from the alternate hemisphere and snap frozen in liquid nitrogen. The spleen weight was recorded; half of the spleen was mounted in OCT and half of the spleen snap frozen for biochemical analysis.

3.2.3 Quantification of DAB immunohistochemistry

The hippocampal fissure (**Figure 3-1**) was imaged using a 20x objective for CD11b and FcγRI, and imaged using a 10x objective for MHCII expression levels. Analysis of mean percentage was carried out as described in Chapter 2.

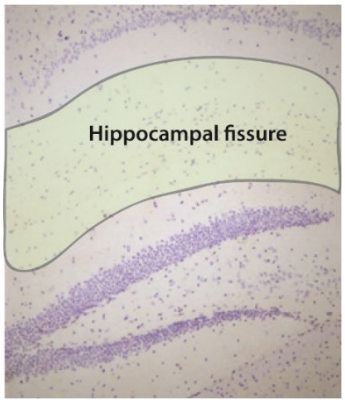

Figure 3-1: Area of interest for DAB quantification

The hippocampal fissure is highlighted; this area was used to analyse the relative expression of MHCII, CD11b and FcγRI at four weeks-post saline or *S. typhimurium* treatment.

3.3 Results

3.3.1 Weight changes following *S. typhimurium* infection in the P301S mouse model of tauopathy

Weight loss is measured in most murine models of infection to confirm a physiological response to the infection and the potential severity (Püntener *et al.*, 2012; Linkenhoker and Linton, 2013). Therefore, weight change following *S. typhimurium* infection was examined to establish the response to infection in both C57BL/6 and P301S mice.

One day post-injection both C57BL/6 and P301S mice lost on average 8% body weight following injection with *S. typhimurium* compared to the saline i.p. control group (C57BL/6 saline i.p.= 1.09% ± 1.50; C57BL/6 *S. typhimurium* i.p.= -8.88% ± 2.82, p<0.001; P301S saline i.p.= 1.48% ± 1.29; P301S *S. typhimurium* i.p.= -7.95% ± 0.73, p<0.001) (**Figure 3-2**). When examining the P301S and C57BL/6 mice weight change, there was an overall significant main effect over time in weight change ($F(2.12, 65.75) = 87.72$, $p < 0.001$), a significant main effect of *S. typhimurium* i.p. injection ($F(1, 31) = 94.73$, $p < 0.01$) and a significant main effect of genotype ($F(1, 31)= 11.5$, $p<0.01$). Subsequently there was a significant interaction between i.p. injection and time ($F(10, 310) = 10.12$, $p<0.001$). Furthermore, there was a significant interaction of time and genotype ($F(10, 310)= 2.4$, $p<0.001$). Eight days post-injection, P301S mice infected with *S. typhimurium* had returned to baseline weight and this was no longer significant to the saline i.p. group (saline i.p. injection= 6% ± 3.17; *S. typhimurium* i.p.= 5.44% ± 3.57, p>0.99). This, along with the significant main effect of genotype, suggests variability in the physiological response to *S. typhimurium* infection between C57BL/6 and P301S mice. Further confirmation using immune markers within the brain will be required to establish whether P301S mice undergo a systemic response to *S. typhimurium* akin to C57BL/6 mice.

Starting weight can often highlight variations in weight change and acts as a method of control for significant weight loss. There was no significant difference in starting weight between the C57BL/6 and P301S mice (C57BL/6 = 24.78 ± 0.65; P301S = 24.99 ± 0.78) ($t(33.90)= 0.2$, $p= 0.84$) (**Figure 3-2**). Therefore, it is unlikely the starting weight confounded the weight change results. Nesting has been used prior to document sickness behaviour or cognitive function in mice. Nesting did not change following infection (**Figure 3-2**) with *S. typhimurium* in either C57BL/6 or P301S mice, hence there is no significant main effect of infection observed ($F (1, 31) = 3.498e-005$, $p = 0.99$). However, there is a significant main effect between genotypes ($F (1, 31) = 93.96$, $p < 0.001$), with the P301S mice exhibiting a significantly lower score of nesting than the C57BL/6 mice both in the saline (C57BL/6 = 4.5 ± 0.53; P301S = 2.6 ± 0.97) and *S. typhimurium* groups

(C57BL/6 = 4.875 ± 0.35; P301S = 2.22 ± 0.67). Therefore, it is possible to conclude that whilst *S. typhimurium* has no significant effect on nesting, P301S mice do exhibit a significantly lower baseline of nesting activity. The implications of this observation in relation to pathology in the P301S mice are considered in the chapter discussion.

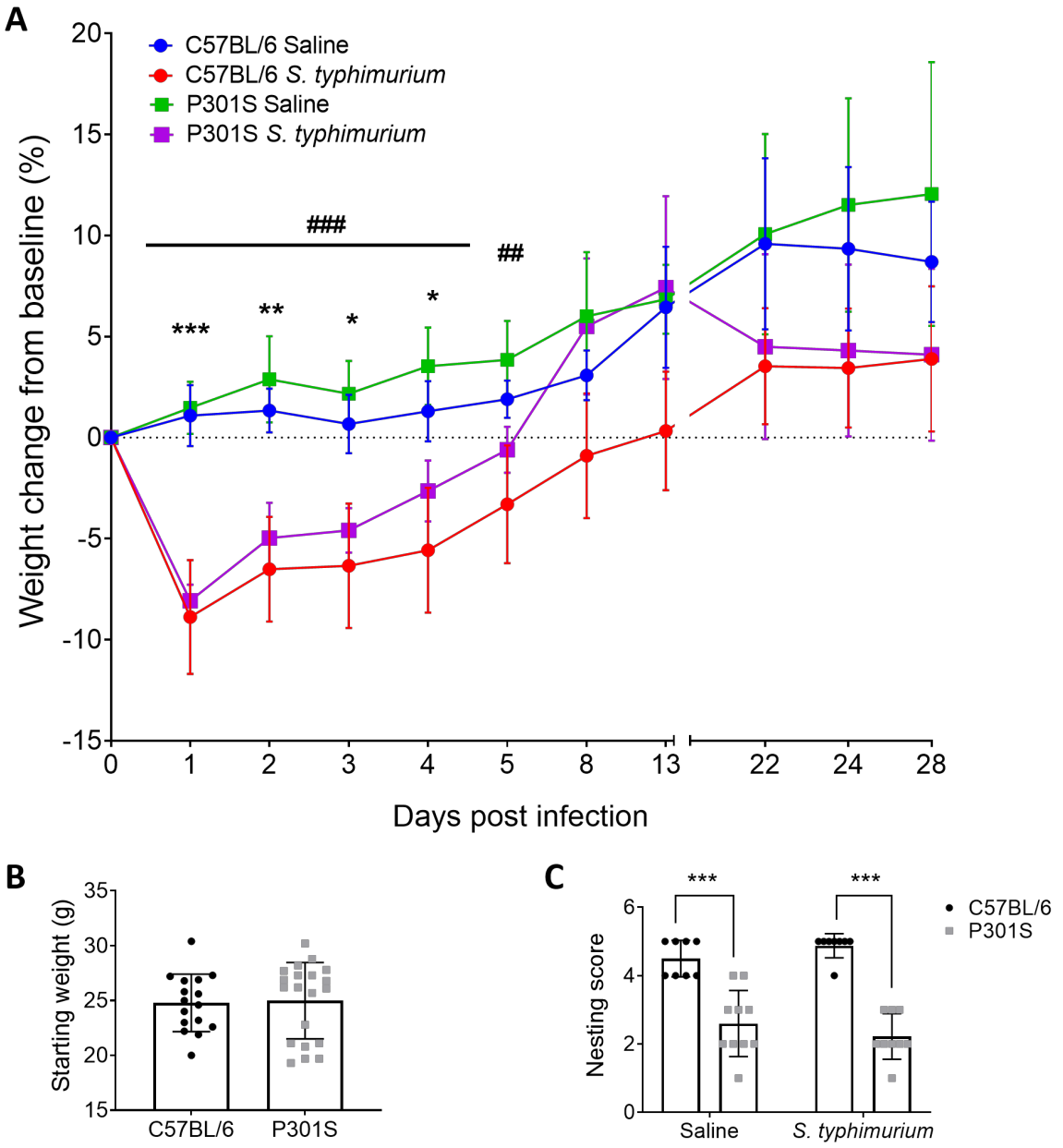

Figure 3-2: Weight change in C57BL/6 and P301S mice following *S. typhimurium* infection

A) Weight change in C57BL/6 and P301S mice as a percentage of baseline weight following i.p. injection of saline or *S. typhimurium*. n= 8 for both C57BL/6 i.p. groups, n=10 for P301S for both i.p. groups. *= significance between C57BL/6 mice injected with saline or *S. typhimurium* i.p. #= significance between P301S saline i.p. and *S. typhimurium* i.p. injection (*p<0.05, **p<0.01. ***p<0.001); repeated measures ANOVA with Greenhouse-Geisser correction and Tukey's post-hoc test was carried out for C57BL/6 and P301S weight change. **B)** Starting weight prior to i.p. injection of saline or *S. typhimurium*; unpaired Student's t-test with Welch's correction. **C)** Nesting score in C57BL6 and P301S mice after saline or *S. typhimurium* i.p. injection; two-way ANOVA with Tukey's post-hoc test. All data is presented as mean ± standard deviation (SD). Alex Collcutt carried out all *in vivo* work detailed here; data analysis was carried out by the author.

3.3.2 MHC II expression in the hippocampus following *S. typhimurium* infection

MHCII are cell surface proteins undetectable in the naïve brain, yet expressed on vascular endothelial cells following systemic infection with *S. typhimurium* (Püntener *et al.*, 2012). To identify whether there was an immune response within the brain to *S. typhimurium*, MHCII expression levels were assessed in the hippocampal fissure between the dentate gyrus and CA1 by histology. No positive staining for MHCII is observed in either C57BL/6 or P301S mice following saline injection (**Figure 3-3**). However, following *S. typhimurium* infection, MHCII is detectable in the C57BL/6 group but undetectable in P301S mice (**Figure 3-3**). The positive MHCII staining in the C57BL/6 mice overlaps with laminin, an extracellular matrix glycoprotein and a marker of basement membranes. Laminin is highly expressed in the endothelial cells surrounding blood vessels and is used as a marker to detect vasculature. Staining in the vasculature with laminin suggests that at 4 weeks post-infection, MHCII is expressed in association with the vascular endothelial cells. Imaging at a higher magnification allows for closer qualitative analysis of this staining overlap. Only the C57BL/6 mice that have been injected with *S. typhimurium* show positive MHCII staining. P301S mice do not exhibit MHCII expression in the hippocampal fissure following either saline or *S. typhimurium*. This data suggests that P301S mice do not undergo upregulation in MHCII expressions within the brain following *S. typhimurium* injection.

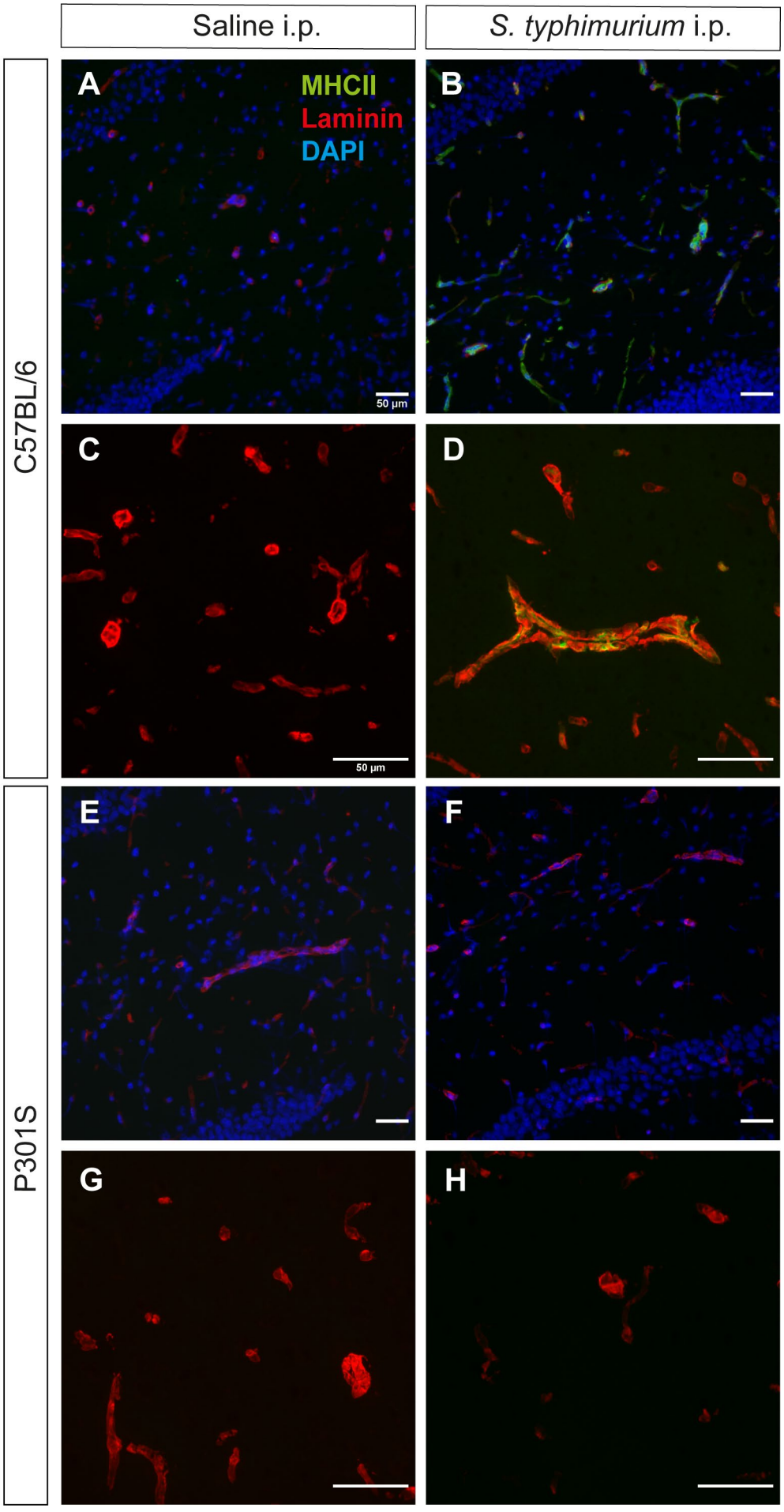
Saline i.p.
S. typhimurium i.p.
C57BL/6
P301S
A
MHCII
Laminin
DAPI
50 µm
B
C
50 µm
D
E
F
G
H

Figure 3-3: MHCII expression in the hippocampus following *S. typhimurium* infection

A, E) C57BL/6 and P301S mice injected i.p. with saline. Slide is stained for MHCII to show non-classical antigen presentation and laminin to stain for basement membrane; images taken with 20x objective. **C, G)** Images taken with 40x objective. **B, F)** C57BL/6 and P301S mice following *S. typhimurium* injection. Slide is stained for MHCII and laminin; images taken with 20x objective. **D, H)** Images taken with 40x objective; scale bar= 50μm for all images. n= 1 for all groups expect P301S *S. typhimurium* i.p. where n= 2.

3.3.3 CD11b expression in the hippocampus following *S. typhimurium* infection

CD11b expression was also examined in the hippocampus. CD11b forms a receptor with CD18 referred to as integrin alpha M or CR3. CD11b is found largely on the myeloid cell surface, and its expression is upregulated following LPS *in vitro* (Roy *et al.*, 2006). This makes it an ideal activation marker to examine the expression of microglia cells following *S. typhimurium* infection. Following *S. typhimurium* infection in C57BL/6 mice there is no observable increase in fluorescence intensity (**Figure 3-4**). Both saline and *S. typhimurium* injected C57BL/6 and P301S mice show similar levels of expression (**Figure 3-4**). CD11b expression in C57BL/6 mice following infection shows macrophages in close proximity with the laminin staining. This is only clearly observable in this group. Both groups of saline injected mice show low-level staining of CD11b, and CD11b expression in P301S mice injected with *S. typhimurium* also shows no qualitative association with laminin staining.

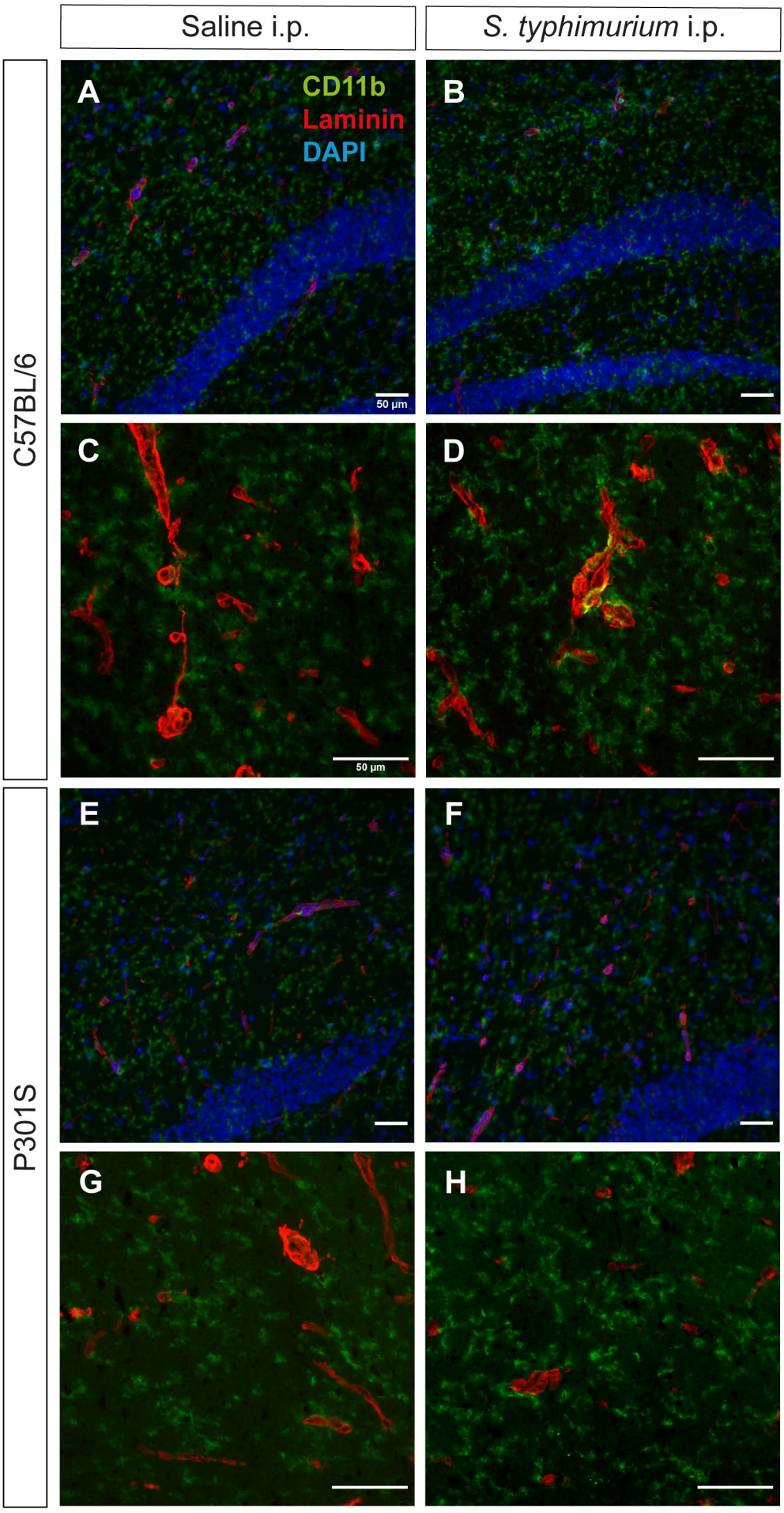
Saline i.p.
S. typhimurium i.p.
C57BL/6
P301S
A
B
C
D
E
F
G
H
CD11b
Laminin
DAPI
50 µm
50 µm

Figure 3-4: CD11b and laminin expression in the hippocampus following *S. typhimurium* infection

A) C57BL/6 and (**E)** P301S mice injected i.p. with saline. Slide is stained for CD11b as a microglia marker and laminin for basement membrane; Images taken with 20x objective. **C, G)** 40x objective images of these groups. **B, F)** C57BL/6 and P301S mice following *S. typhimurium* injection, showing expression of CD11b and laminin. Images taken with 20x objective. **D, H)** 40x objective images of these groups. All scale bars= 50μm. n= 1 for all groups expect P301S *S. typhimurium* i.p. where n= 2.

Qualitative changes are also observable with DAB immunohistochemistry (**Figure 3-5**). CD11b expression levels appear comparable in the brain of C57BL/6 mice and P301S mice following *S. typhimurium*. Microglia in all groups appear ramified with processes extended and no signs of clustering. Whilst no significant conclusion can be made without statistical analysis, this suggests that there is no observable change in CD11b expression at four weeks post-infection.

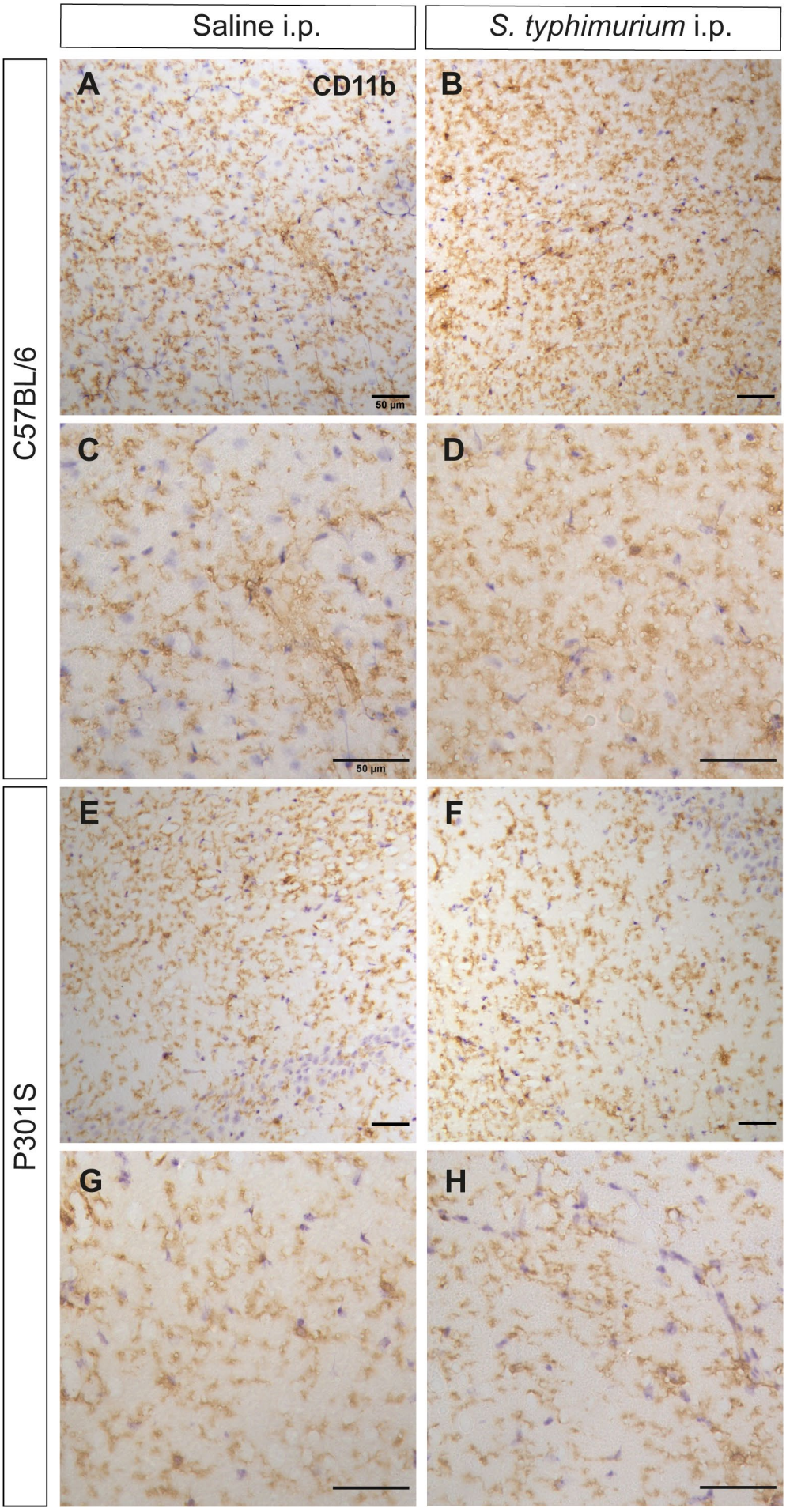
Saline i.p.
S. typhimurium i.p.
C57BL/6
P301S
A
CD11b
B
C
D
E
F
G
H
50 µm
50 µm

Figure 3-5: CD11b DAB immunohistochemistry after systemic infection in P301S and C57BL6 mice

A, C) CD11b expression in C57BL/6 mice and **(E, G)** P301S mice after saline i.p. injection. **B, D)** CD11b expression in C57BL/6 mice and **(F, H)** P301S mice after *S. typhimurium* i.p. injection. **A, B, E, F)** Images taken with 20x objective. **C, D, G, H)** Images taken with 40x objective. Scale bar for all images= 50µm. n= 1 for all groups expect P301S *S. typhimurium* i.p. where n= 2.

3.3.4 FcγRI expression in the hippocampal fissure

FcγRI, also referred to as CD64 is a receptor which strongly binds monomeric IgG. FcγRI is constitutively expressed on macrophages and microglia and is upregulated following LPS i.p. injection (Hart *et al.*, 2012). Furthermore, FcγRI has been shown to mediate *S. typhimurium* internalization in murine bone marrow-derived macrophages *in vitro* (Uppington *et al.*, 2006). FcγRI is expressed in microglia within the hippocampal fissure in both P301S and C57BL/6 mice injected with saline i.p. (**Figure 3-6**). The microglia appear largely ramified in morphology, and there are no large clusters indicative of proliferation visible at the larger magnifications. The P301S mice injected with *S. typhimurium* i.p. also appear to exhibit FcγRI expression akin to the saline controls (**Figure 3-6**). The microglia appear ramified and there is no clear indication of an inflammatory response. By contrast, in C57BL/6 mice injected with *S. typhimurium* i.p. microglia appear to be located around blood vessels. Microglia appear to have clustered and show signs of activation. This staining suggests that FcγRI is upregulated in response to *S. typhimurium* i.p., and so P301S mice do not appear to undergo this same inflammatory response following infection.

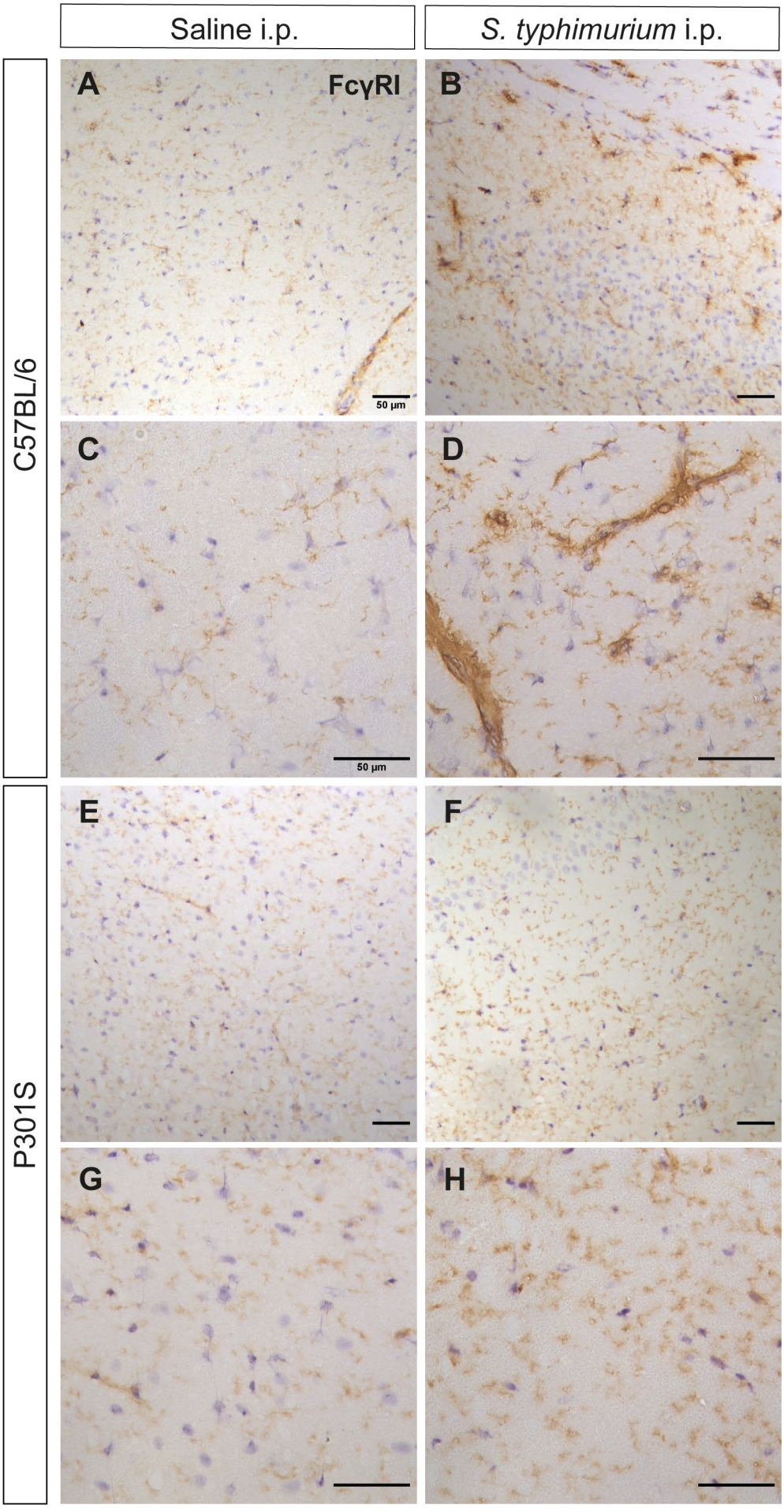
Saline i.p.
S. typhimurium i.p.
C57BL/6
P301S
A
FcγRI
B
C
D
E
F
G
H
50 µm
50 µm

Figure 3-6: FcγRI in the hippocampus following *S. typhimurium* infection

The hippocampus of (**A, C)** C57BL/6 and (**E, G)** P301S mice four weeks post-saline injection. Slide is stained for FcγRI to show Fc receptor expression with DAB immunohistochemistry. **B, D)** C57BL/6 and (**F, H)** P301S mice following *S. typhimurium* injection, stained as above. **A, B, E, F)** Images taken with 20x objective. **C, D, G, H)** Images are taken with 40x objective. Scale bar for all images= 50μm. n= 1 for all groups expect P301S *S. typhimurium* i.p. where n= 2.

3.3.5 *Slc11a1* polymorphism in P301S mouse model of tauopathy

Nramp1 expression has been shown to play a crucial role in susceptibility to intracellular pathogens (Valdez *et al.*, 2008). A loss-of-function allele present in the C57BL/6 mice confers susceptibility to *S. typhimurium* (Brown *et al.*, 2013). However, CBA mice express functional *Slc11a1* gene and so are not susceptible to *S. typhimurium*; the P301S mouse has both a partial CBA and C57BL/6 background. Given that there are significant variations in weight change between P301S and C57BL/6 mice (Fig. 4.6) this highlights a potential disparity in their susceptibility to *S. typhimurium*. As the P301S mice show initial weight loss, this suggests there is a response to the infection, but this is resolved. Furthermore, the absence of MHCII expression in the infected P301S group and variation in CD11b expression highlights a lack of neuroinflammatory response in the P301S mouse.

Subsequently, a PCR looking at the presence of *Slc11a1* was conducted to examine any potential differences between the genotypes. A polymorphism at 169aa in the gene has been reported to indicate susceptibility to *S. typhimurium* infection (Brown *et al.*, 2013). The PCR was run with primers for *Slc11a1* with a product size of 451 bp along with housekeeping gene *Gapdh* (**Figure 3-7**). It is possible to see that whilst both P301S and C57BL/6 mice express *Slc11a1* (band at 451 bp) there are polymorphisms present in only the C57BL/6 samples (band at 169 bp), suggesting that the partial CBA background of the P301S is altering the Nramp1 expression.

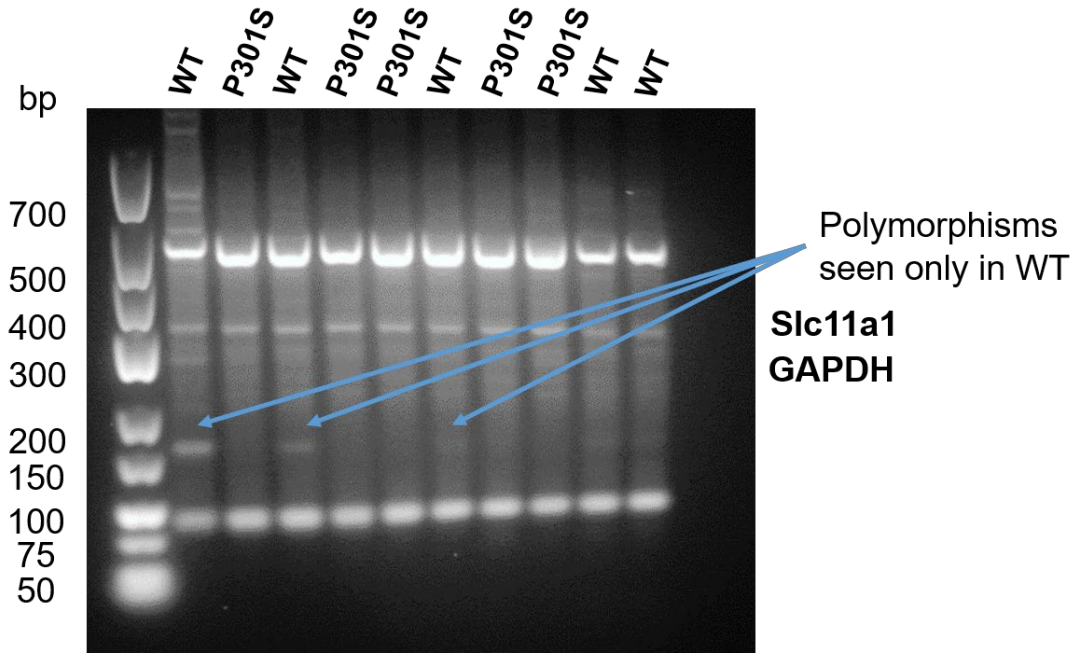

Figure 3-7: *Slc11a1* in the P301S and C57BL/6 mice

The DNA samples were run on a 3% agarose gel whereby it is possible to see the polymorphisms present only in the C57BL/6 samples. N= 5 for both C57BL/6 and P301S samples. The *Gapdh* and *Slc11a1* products are consistent throughout the samples at approximately 307 bp and 451 bp respectively.

3.3.6 Weight change following *S. typhimurium* infection in the H1*Mapt-/-* mouse model

Following from evaluation of the infection response in P301S mice, H1*Mapt-/-*, *Mapt-/-* and C57BL/6 control mice were injected with *S. typhimurium* and tissue collected four weeks later. In order to establish whether C57BL/6, H1*Mapt-/-* and *Mapt-/-* mice all undergo a response to *S. typhimurium* injection compared to saline injection, weight change as a percent of baseline was plotted (**Figure 3-8**).

Weight loss at one day post-injected was observed in all *S. typhimurium* i.p. groups regardless of genotype (C57BL/6= -9.42% ± 1.59; H1*Mapt-/-*= -5.43% ± 2.13; *Mapt-/-*= -7.48% ± 2.98). In order to establish whether there were genotypic differences, a three-way repeated-measures ANOVA was carried out. This analysis established there was no significant main effect of genotype on weight change ($F(2, 46)= 1.63$, $p= 0.21$). Subsequent statistical analysis was carried out using repeated-measure ANOVAs for each genotype. C57BL/6 mice were all female whilst the H1*Mapt-/-* and *Mapt-/-* mice were both male and female. There was no significant effect of sex on weight change found in H1*Mapt-/-* mice (Appendix A, Figure S1); due to cohort size no analysis was carried out on the *Mapt-/-* cohort. In C57BL/6 mice, there was a significant main effect of

time (F(3.3, 59.86) = 52.24, p < 0.001) and infection (F(1, 18) = 40.84, p < 0.001). There was also a significant interaction of time and infection (F(10, 180) = 9.59), p < 0.001). H1*Mapt-/-* mice showed a significant main effect of time (F(3.84, 69.19)= 46.94, p<0.001), a significant main effect of i.p. injection (F(1, 18)= 5.50, p<0.05) and a significant interaction (F(10, 180)= 14.31, p<0.001). Notably, the main effect of *S. typhimurium* is to a lesser degree in H1*Mapt-/-* mice compared to C57BL/6 mice. Finally, *Mapt-/-* mice also show a significant main effect of time (F(1.66, 18.30)= 15.75, p<0.001), a significant main effect of *S. typhimurium* (F(1, 11)= 32.99, p<0.001) and a significant interaction (F(10, 110)= 8.92, p<0.001). From these results it is possible to conclude that C57BL/6, H1*Mapt-/-* and *Mapt-/-* mice all show metabolic changes as a result of *S. typhimurium* i.p. injection.

It is possible to observe that there are differences in the rate of recovery to baseline between genotypes after *S. typhimurium* i.p. injection (**Figure 3-8**). Within the first 24 hours post-injection C57BL/6 mice lost more weight on average as a percent of baseline than H1*Mapt-/-* mice infected with *S. typhimurium* (C56BL/6 = -9.42% ± 1.59; H1*Mapt-/-* = -5.43% ± 2.13). Weight loss is observed until a week after infection in the C57BL/6 mice, at which point the *S. typhimurium*-injected group return to their baseline weight (**Figure 3-8**). By contrast, H1*Mapt-/-* mice recover much faster than C57BL/6 mice, no significant difference is observed between the H1*Mapt-/-* saline and *S. typhimurium* i.p. groups from day 5 post-infection (**Figure 3-8**). This highlights potential strain differences in the response to systemic infection.

Mapt-/- mice infected with *S. typhimurium* exhibit significant weight loss compared to the saline *Mapt-/-* controls and do not exhibit weight recovery until the end of the experiment four weeks later (**Figure 3-8**). *Mapt-/-* mice return to baseline weight in a delayed manner compared to C57BL/6 mice; significance between *Mapt-/-* mice injected with saline or *S. typhimurium* is still detected at day 14 post-infection. This suggests that whilst all mice regardless of genotype respond to infection, H1*Mapt-/-* mice recover sooner than C57BL/6 mice, whilst the *Mapt-/-* mice do not recover within the study period. This suggests that all genotypes are susceptible to *S. typhimurium* infection despite variability. Given the P301S data, further readouts both from the periphery and within the brain parenchyma are required to confirm this.

3.3.7 Starting weight and spleen weight following four-week *S. typhimurium* infection

Starting weights were recorded (**Figure 3-9**) and it was observed that although C57BL/6 and H1*Mapt-/-* show similar starting weights, *Mapt-/-* mice have significantly higher starting weights. There was a significant weight difference when comparing *Mapt-/-* mice to both C57BL/6 and H1*Mapt-/-* (*Mapt-/-* = 26.14g ± 4.17; versus C57BL/6 = 20.96g ± 1.13, p<0.01; versus H1*Mapt-*

/- = 20.73g ± 1.68, p<0.001;). A Kruskal-Wallis test determined that there was a significant difference between starting weights (H(2)= 23.63, p<0.001). However, there was no significant difference in starting weight between the C57BL/6 and H1*Mapt-/-* mice.

Following the four-week infection, spleen weights were recorded as a sign of splenomegaly and further confirmation of infection (**Figure 3-9**). All three genotypes show a significant increase in spleen weight following *S. typhimurium* infection, however there are significant differences in spleen weight between genotypes in the infected groups. There was a significant effect of genotype on spleen weight (F(2, 47) = 12.28, p<0.001) and a significant effect of infection on spleen weight (F(1, 47) = 180.8, p<0.001). As a result, there is a significant interaction of genotype and infection on spleen weight (F(2, 47) = 8.69, p<0.001). C57BL/6 mice that underwent *S. typhimurium* infection exhibit splenomegaly to a larger degree than both the H1*Mapt-/-* and *Mapt-/-* mice (C57BL/6 = 553.5mg ± 161.6; H1*Mapt-/-* = 305.7mg ± 87.5, p<0.001; *Mapt-/-* = 391.4 ± 87, p<0.01). These results highlight a potentially dampened response in the H1*Mapt-/-* and *Mapt-/-* mice to the bacterial infection.

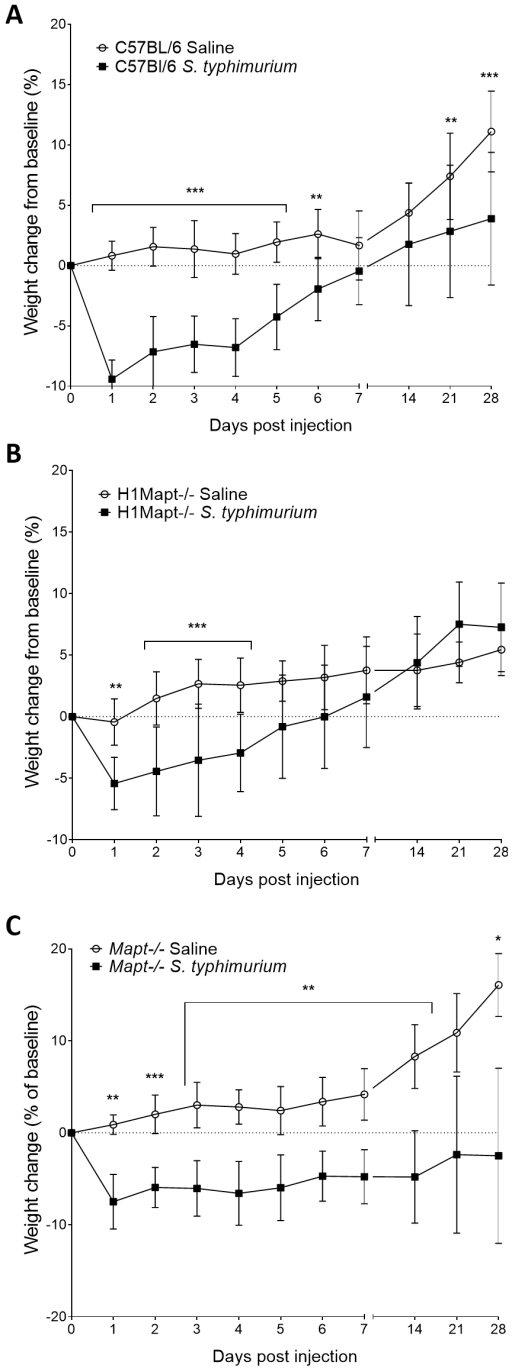

Figure 3-8: Weight change following *S. typhimurium* infection in C57BL/6 and H1*Mapt-/-* mice.

A) C57BL/6 mice weight change is displayed as a percentage of baseline weight subsequent to i.p. injection of saline or *S. typhimurium*. n=10 for saline-injected, n=10 for *S. typhimurium*-injected. **B)** Weight change from baseline of H1*Mapt-/-* mice following i.p. injection of saline or *S. typhimurium*. n=10 for saline-injected, n=10 for *S. typhimurium*-injected. **C)** *Mapt-/-* mice weight change is displayed as a percentage of baseline weight prior to IP injection of saline or *S. typhimurium*. n=6 for saline-injected, n=7 for *S. typhimurium*-injected. **A-C)** Repeated measures ANOVA with Greenhouse-Geisser correction and Tukey's multiple comparisons test; (*p<0.05, **p<0.01, ***p<0.001). All data is presented as mean ± standard deviation (SD).

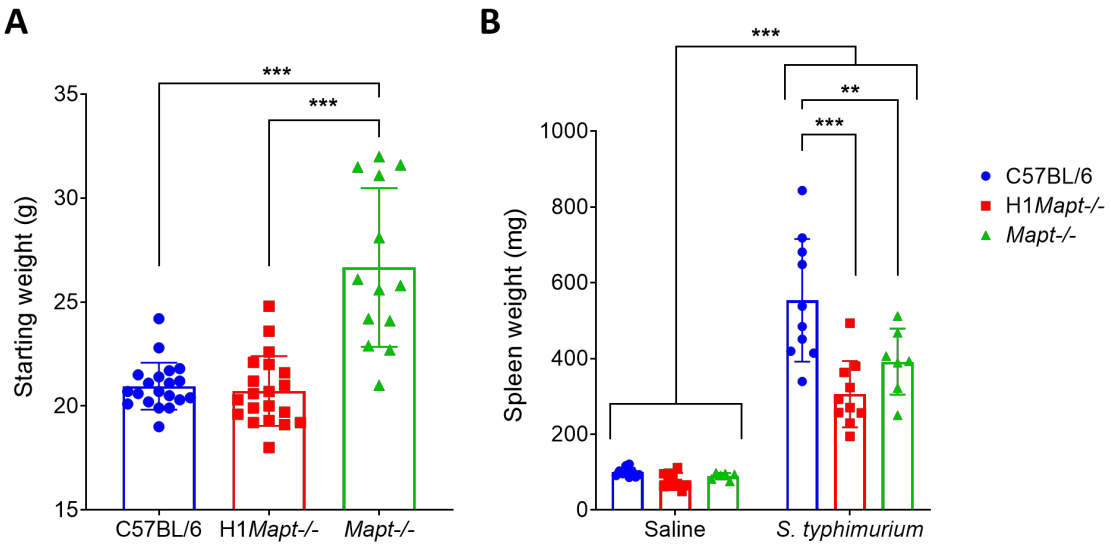

Figure 3-9: Starting weight and spleen weight following four-week *S. typhimurium* infection

A) Starting weight for C57BL/6, H1*Mapt-/-* and *Mapt-/-* mice was recorded prior to i.p. injection of saline or *S. typhimurium.* n=20 for C57BL/6 and H1*Mapt-/-* mice, n=13 for *Mapt-/-* mice. Kruskal Wallis test with Dunn's multiple comparisons test; (***p<0.001). **B)** Spleen is removed after perfusion with saline and weighed using a fine scale to the nearest 10mg. n= 10 for both C57BL/6 groups, n= 10 for both H1*Mapt-/-* groups, n= 6 for *Mapt-/-* saline i.p., n= 7 for *Mapt-/- S. typhimurium* i.p. Two-way ANOVA with Tukey's multiple comparisons test; (**p<0.01, ***p<0.001). All data is presented as mean ± standard deviation (SD).

3.3.8 MHCII expression in the hippocampus following *S. typhimurium* infection

Positive MHCII staining was detected in the hippocampus of C57BL/6, H1*Mapt-/-* and *Mapt-/-* mice infected with *S. typhimurium* (**Figure 3-10**). This suggests that, unlike the P301S mouse model, both H1*Mapt-/-* and *Mapt-/-* mice do show upregulated MHCII expression within the brain following *S. typhimurium* infection. There was a significant main effect of infection ($F(1, 12)= 69.88$, $p<0.001$), yet no significant main effect of genotype ($F(2, 12)= 2.70$, $p = 0.11$) on MHCII expression. There was a significant ten-fold increase in MHCII expression following systemic infection in C57BL/6 mice (C57BL/6 saline i.p.= 0.23% ± 0.07; C57BL/6 *S. typhimurium* i.p.= 2.79% ± 0.20, $p<0.01$). The H1*Mapt-/-* mice showed a seven-fold increase in MHCII expression which was not significant, and no trend was observed (H1*Mapt-/-* saline i.p.= 0.23% ± 0.06; H1*Mapt-/- S. typhimurium* i.p.= 1.63% ± 0.4, $p= 0.10$). Finally, the *Mapt-/-* mice did show a significant eighteen-fold increase in MCHII expression after systemic infection (*Mapt-/-* saline i.p.= 0.18% ± 0.02; *Mapt-/- S. typhimurium* i.p.= 3.19% ± 0.70, $p<0.001$). There is also a trend ($p= 0.06$) that shows MCHII expression in *Mapt-/-* mice after systemic infection is greater than observed in H1*Mapt-/-* mice. Despite this, because MHCII is expressed after systemic infection in all mice it is possible to include there is an immune response within the brain. However, there is a clear dampened immune response in H1*Mapt-/-* mice.

Immunofluorescence was utilised to compare MHCII and laminin staining. As in the C57BL/6 mice prior, it is possible to see that there is no MHCII-positive staining in the saline-injected groups of C57BL/6, H1*Mapt-/-* or *Mapt-/-* (**Figure 3-11**). MHCII-positive staining was confirmed in the *S. typhimurium*-injected C57BL/6, H1*Mapt-/-* and *Mapt-/-* mice (**Figure 3-11**). Furthermore, at higher magnification it is possible to see that the MHCII expression is found in the vasculature with laminin in all three genotypes of *S. typhimurium*-injected mice (**Figure 3-11**). This suggests that H1*Mapt-/-* and *Mapt-/-* mice are susceptible to *S. typhimurium* infection and MHCII is likely associated with cerebral endothelial cells.

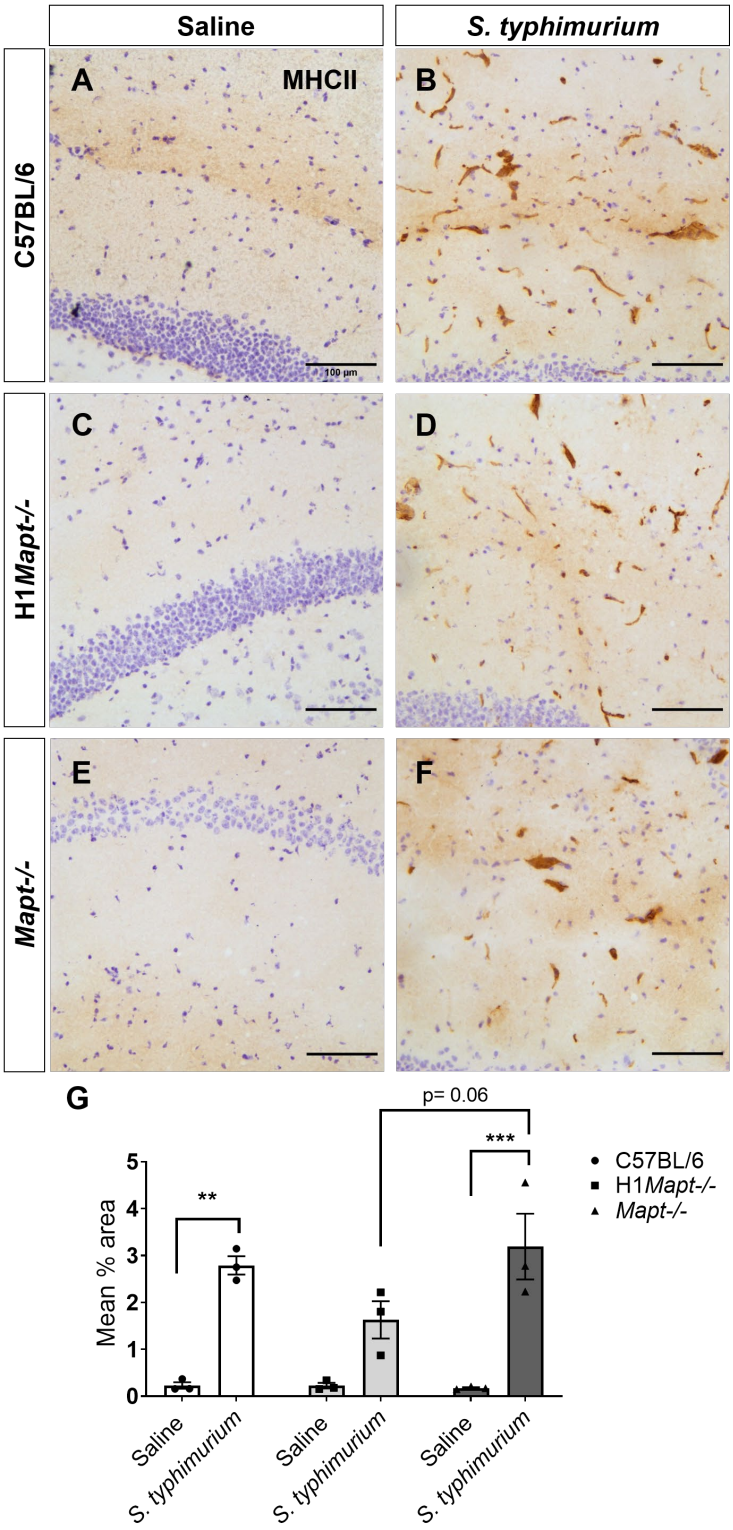

Figure 3-10: MHCII staining following saline and *S. typhimurium* injection

A, C, E) C57BL/6, H1*Mapt-/-* and *Mapt-/-* mice injected i.p. with saline. Slide is stained for MHCII. **B, D, F)** MHCII expression in C57BL/6, H1*Mapt-/-* and *Mapt-/-* mice injected i.p. with *S. typhimurium*. Slide is stained for MHCII. All images taken with 20x objective. Scale bar = 100µm. **G)** Percentage of area stained was calculated at the hippocampal fissure, n= 3 for all groups. Two-way ANOVA with Tukey's post-hoc test; **p<0.01, ***p<0.001. All data is presented as mean ± S.E.M.

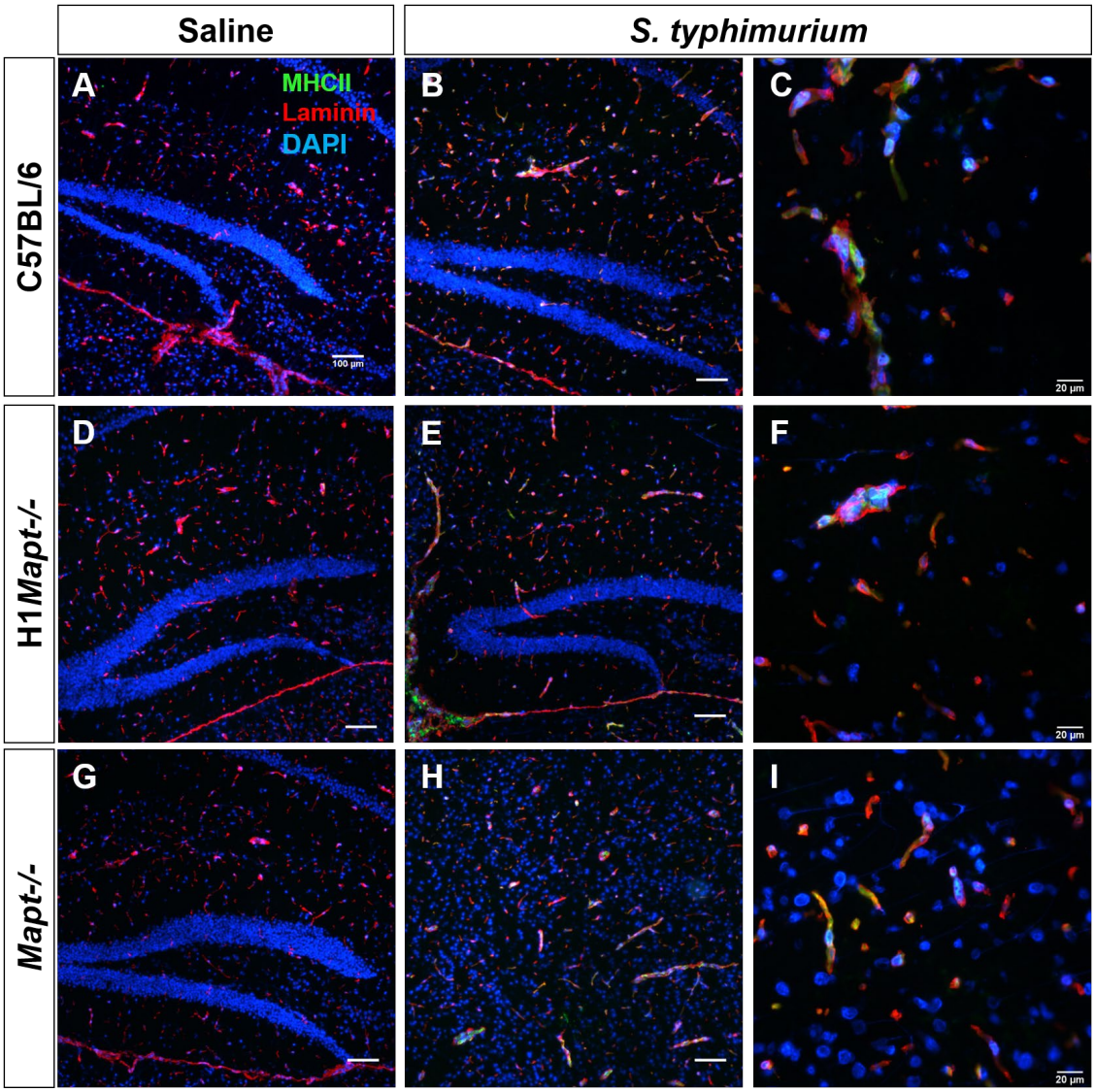

Figure 3-11: MHCII and laminin in the hippocampus following systemic infection

A, D, G) C57BL/6, H1*Mapt-/-* and *Mapt-/-* mice injected with saline i.p. Slide is stained for MHCII and laminin; 10x objective. Scale bar = 100µm. **B, E, H)** C57BL/6, H1*Mapt-/-* and *Mapt-/-* mice injected with *S. typhimurium* i.p.; 10x objective. Scale bar = 100µm. **C, F, I)** C57BL/6, H1*Mapt-/-* and *Mapt-/-* injected i.p. with *S. typhimurium*; 40x objective, scale bar = 20µm.

3.3.9 CD11b expression in the hippocampus following *S. typhimurium* infection

CD11b expression was examined in the hippocampus both in saline-injected and *S. typhimurium*-injected groups (**Figure 3-12**). There is a significant main effect of infection ($F(1, 12)= 7.70$, $p<0.05$) yet no significant main effect of genotype ($F(2, 12)= 0.46$, $p= 0.64$). As a result, no significant interaction was observed ($F(2, 12)= 0.20$, $p= 0.82$). Following post-hoc tests, there was no significant upregulation of expression following *S. typhimurium* infection. In the C57BL/6 mice, CD11b expression is increased 1.4-fold after systemic infection (C57BL/6 saline i.p.= 7.54% ± 0.94; C57BL/6 *S. typhimurium* i.p.= 10.89% ± 3.30, p= 0.81). In H1*Mapt-/-* mice, CD11b expression was increased three-fold after systemic infection (H1*Mapt-/-* saline i.p.= 5.42% ± 1.78; H1*Mapt-/-* *S. typhimurium* i.p.= 9.39% ± 0.97, p= 0.69). The *Mapt-/-* mice showed a two-fold increase in CD11b expression after *S. typhimurium* i.p. injection compared to saline i.p. (*Mapt-/-* saline i.p.= 5.22% ± 0.41; *Mapt-/- S. typhimurium* i.p.= 10.89% ± 2.4, p= 0.35). Therefore, considering the significant main effect of i.p. injection, there is an overall biological effect of systemic infection, but this time point may be too late to observe significant differences.

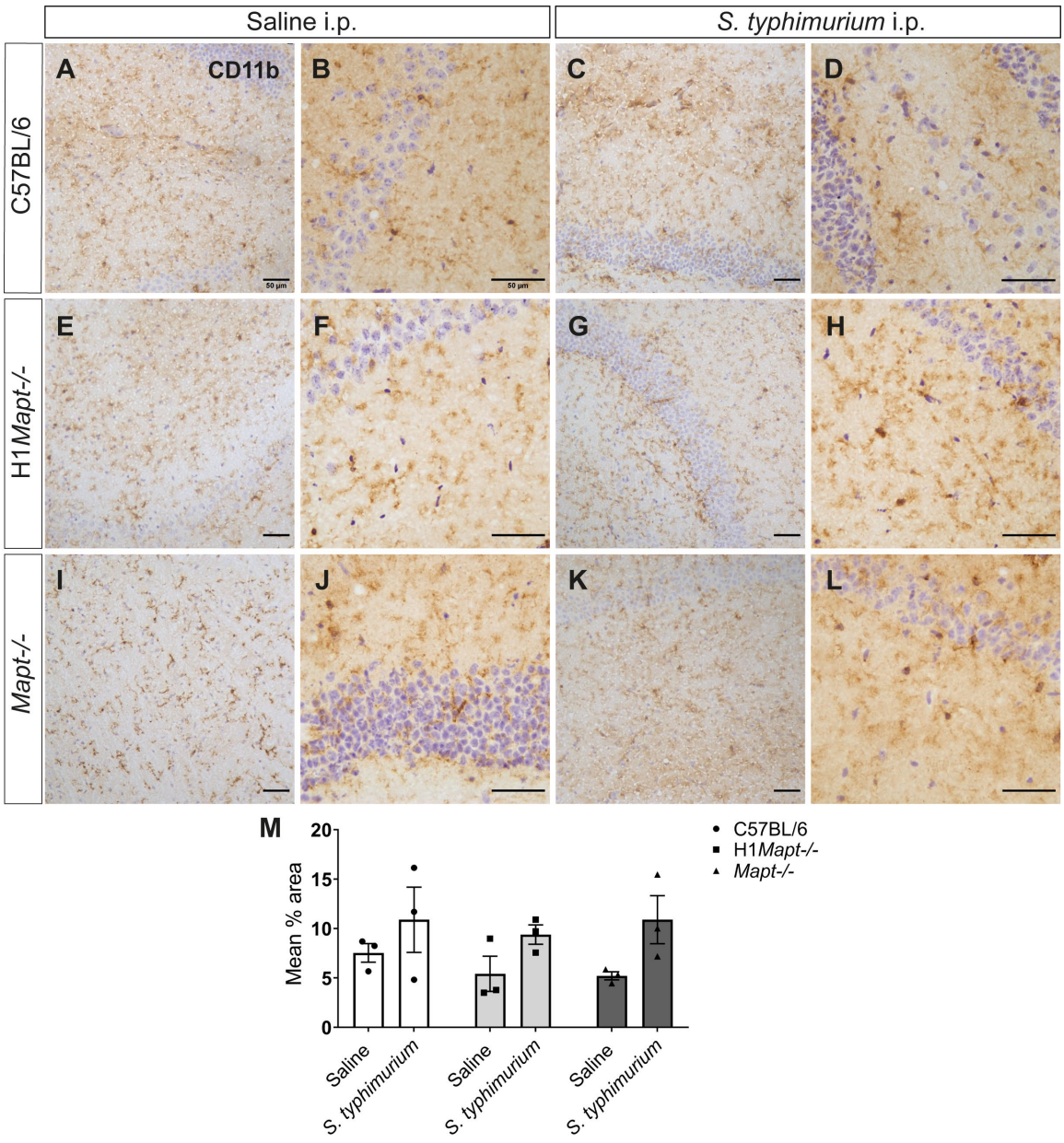

Figure 3-12: CD11b immunohistochemistry following saline and *S. typhimurium* injection

A, E, I) CD11b expression in C57BL/6, H1*Mapt-/-* and *Mapt-/-* mice after saline i.p. injection; 20x objective. **B, F, J)** CD11b expression after saline i.p. injection; 40x objective. **C, J, K)** CD11b expression in C57BL/6, H1*Mapt-/-* and *Mapt-/-* mice after *S. typhimurium* i.p. injection; 20x objective. **D, H, L)** CD11b expression after *S. typhimurium* i.p. injection; 40x objective. **M)** Mean percentage area stained at the hippocampal fissure, n= 3 for all groups. Two-way ANOVA with Tukey's post-hoc test. All data is presented as mean ± S.E.M.

3.3.10 FcγRI expression in the hippocampus following *S. typhimurium* infection

FcγRI expression was examined both in saline and *S. typhimurium*-injected mice. In all saline-injected mice, there is baseline expression of FcγRI in the hippocampus (**Figure 3-13**). There was a significant main effect of infection ($F(1, 12)= 26.33$, $p<0.001$), yet no significant main effect of genotype ($F2, 12)= 1.41$, $p= 0.28$). No significant interaction was observed ($F(2, 12)= 0.88$, $p= 0.44$). Following post-hoc tests, only C57BL/6 mice showed significantly upregulated expression following *S. typhimurium* infection compared to their saline group. In C57BL/6 mice, FcγRI expression was increased five-fold after systemic infection (C57BL/6 saline i.p.= 0.67% ± 0.15; C57BL/6 *S. typhimurium* i.p.= 3.37% ± 0.65, $p<0.05$). The H1*Mapt-/-* and *Mapt-/-* mice showed a three-fold and four-fold increase in FcγRI expression respectively after systemic infection, however neither showed post-hoc significance (H1*Mapt-/-* saline i.p.= 0.59% ± 0.06; H1*Mapt-/- S. typhimurium* i.p.= 2.18% ± 0.59, $p=0.23$) (*Mapt-/-* saline i.p.= 0.48% ± 0.07; *Mapt-/- S. typhimurium* i.p.= 2.11% ± 0.73, $p=0.21$). No significant difference in FcγRI expression was observed between genotypes, in the saline or *S. typhimurium* groups. FcγRI expression shows a clear effect of systemic infection, however these results highlight a potentially dampened response in the H1*Mapt-/-* mouse.

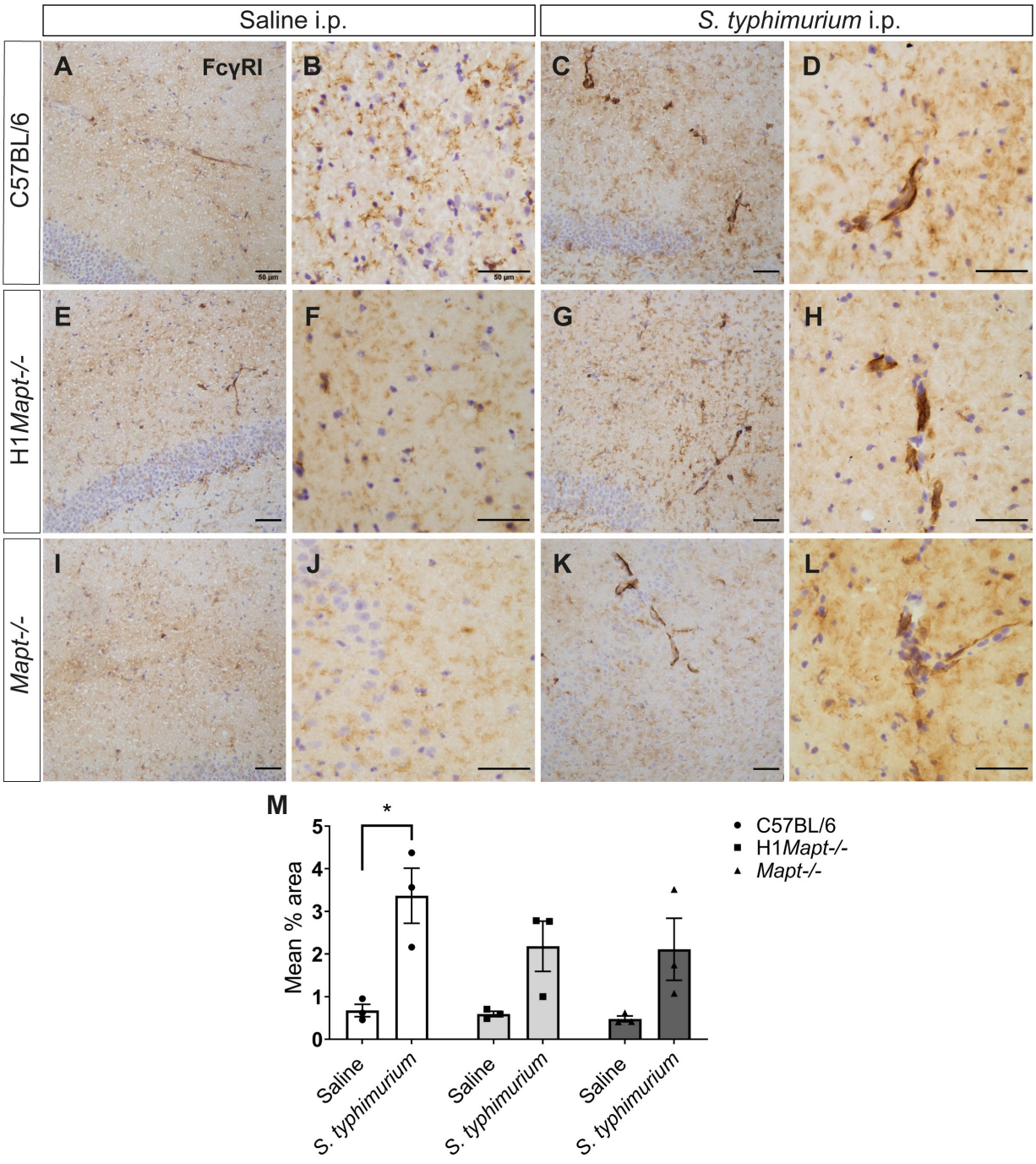

Figure 3-13: FcγRI in the hippocampus following saline and *S. typhimurium* injection

A, E, I) FcγRI expression in C57BL/6, H1*Mapt-/-* and *Mapt-/-* mice after saline i.p. injection; 20x objective. **B, F, J)** FcγRI expression after saline i.p. injection; 40x objective. **C, J, K)** FcγRI expression in C57BL/6, H1*Mapt-/-* and *Mapt-/-* mice after *S. typhimurium* i.p. injection; 20x objective. **D, H, L)** FcγRI expression after *S. typhimurium* i.p. injection; 40x objective. **M)** Mean percentage area stained at the hippocampal fissure, n= 3 for all groups. Two-way ANOVA with Tukey's post-hoc test; (*$p<0.05$). All data is presented as mean ± S.E.M.

3.4 Discussion

3.4.1 Weight change and nesting behaviour following *S. typhimurium* infection

S. typhimurium induces both an innate and adaptive immune response. This begins with recognition of PAMPs on the bacteria through invasion of macrophages and hepatocytes, which is eventually restricted and resolved through expansion of T cells and the acquired response of the adaptive immune system (Mittrücker, Köhler and Kaufmann, 2002; Ravindran and McSorley, 2005). Following *S. typhimurium* infection, recording weight loss is a useful indicator of welfare and an indicator of susceptibility (Ren *et al.*, 2009). Weight change following *S. typhimurium* is understood to be associated both with survival rates and the strength of the infection.

During systemic infection it was found that P301S mice do initially show weight loss akin to what has previously been observed in the C57BL/6 mice (Püntener *et al.*, 2012) (**Figure 3-2**). However, as there was a significant main effect of genotype, this suggested that there was an overall difference in response to the *S. typhimurium* infection. In LPS i.p. injections it is commonly observed that weight returns to baseline at approximately three days post-infection (Lawrence, Brough and Knight, 2012). Therefore, it is possible that P301S mice do lose weight simply through TLR4 activation by LPS; TLR4 activation promotes NF-κB activation and LPS also promotes caspase-1 function which has been shown to regulate weight loss and severity of infection (Boulangé *et al.*, 2016; Lei *et al.*, 2016). There is no significant difference in starting weight (**Figure 3-2**), a measurement which would have highlighted any gross phenotypic differences between the two genotypes. This suggests the differences observed are due to strain or genetic background of the mouse.

Measuring sickness behaviour (such as lack of movement and hunched posture) during infection is well-established and allows correlation with pro-inflammatory cytokine production to determine the severity of infection (Cunningham *et al.*, 2007). Nesting is a behavioural test that can be used to examine depression behaviour in mice (Negus *et al.*, 2015), however it can also be used to observe sickness behaviour such as a reduction in movement (Jirkof, 2014). No significant change in nesting behaviour was observed because of *S. typhimurium* infection, nonetheless the P301S mice do show a significantly lower rate of nesting in both infection groups (**Figure 3-2**).

MC1-positive misfolded tau has been detected in the P301S hippocampus from 2 months of age when behavioural deficits are first reported (Xu *et al.*, 2014). This suggests that a significant decrease in nesting behaviour may correlate with the development of the tau pathology. Two month-old P301S mice show deficits in open field, yet nesting deficits have been first reported as late as 12 months old (Scattoni *et al.*, 2010; Sun *et al.*, 2020). Studies into AD transgenic mice such

as Tg2576 and the 3xTg-AD models both show deficits in nesting behaviour (Wesson and Wilson, 2011; Torres-Lista and Giménez-Llort, 2013). Tg2576 and 3xTg-AD mice both express the P301L mutation, however tau pathology is evident at 3 months and 12 months of age respectively, this coincides with aforementioned deficits observed in nesting behaviour (Lewis *et al.*, 2001; Oddo *et al.*, 2003).

To what extent the early misfolding and hyperphosphorylated stages of tau pathology link to dysfunction in behavioural paradigms is unknown. It is notable that C57BL/6 mice do not begin to show nesting deficits in the presence of systemic infection, suggesting *S. typhimurium* is not sufficient to induce chronic deficits in nesting. It would appear that the pathology in P301S mice is sufficient to induce nesting deficits, however as the infection was not robust enough the effect of *S. typhimurium* must be disregarded for the P301S mice. These findings suggest that examining hippocampal function using behavioural tests such as nesting, and burrowing may be a useful indicator of tau spread within this model.

3.4.2 Immune cell marker expression within the hippocampus following systemic infection

Immune markers are key to understanding how the brain is responding to an immune challenge. Four weeks post-infection, MHCII and CD11b were stained for as markers of cellular and microglial activation. Our lab has already established that MHCII and CD11b are upregulated in the brain following *S. typhimurium*, with the expression peaking at one week post-infection (Püntener *et al.*, 2012). However, it was an aim to establish how the P301S mice responded compared to the C57BL/6 mice.

All saline-injected mice show no MHCII expression due to the lack of infection or injury (Gottfried-Blackmore *et al.*, 2009). There is strong MHCII expression in the *S. typhimurium*-infected C57BL/6 mice and laminin shows that MHCII expression is associated with the vascular endothelium (**Figure 3-3**). It is possible that MHCII may be expressed in perivascular macrophages. However, given the morphology of MHCII staining both in DAB immunohistochemistry and immunofluorescence it appears to reside within the endothelial cells. Furthermore, MHCII expression is reported in the cerebral vasculature weeks after *S. typhimurium* infection utilising the same strain (Püntener *et al.*, 2012). In future experiments, co-staining of MHCII with CD31 as a marker expressed by endothelial cells would elucidate this further. MHCII expression in the brain is considered to be induced by expression of IFNγ and TNFα in the blood (Kim *et al.*, 2002). Notably, there is no MHCII-positive staining in the brain of the infected P301S group. Considering the difference in weight change and MHCII expression to C57BL/6 mice after

systemic infection, this suggests that the infection was resolved prior to development of a neuroinflammatory response.

It is possible that cell turnover will confound the detection of MHCII in the P301S. MHCII expression is observed in the vascular endothelial cells at four weeks post-infection. Vascular endothelial cell turnover in the brain is largely unknown despite research into peripheral endothelial turnover (such as intestinal) however it is widely understood to be slow with the shortest time reported as 47 days (Woywodt *et al.*, 2002). Therefore, it is unlikely that these results are due to endothelial cell turnover in the P301S mice, especially when considering this is not observed in the C57BL/6 hippocampus. This suggests that the difference in MHCII expression observed is due to early resolution of infection by the P301S mouse, and subsequent absence or reduced release of cytokines inducing MHCII expression such as TNFα and IFNγ.

CD11b expression was also examined in the hippocampus. CD11b regulates MyD88-dependent TLR4 signalling of DCs following LPS injection (Ling *et al.*, 2014). It is a useful marker to examine as CD11b-positive cells are shown to persist in peripheral tissue *in vivo* following *S. typhimurium* infection (Tam *et al.*, 2014). Our lab has established that CD11b along with CD68 show an expression peak at 1 week post-infection (Püntener *et al.*, 2012). As the brains are examined at 4 weeks post-infection in this study, it may be too late to identify expression changes. CD11b in infected C57BL/6 and P301S mice does not show observable changes in expression (**Figure 3-5**). Potentially, CD11b expression would have benefitted from quantification, however limited time prevented this.

Brain tissue was also stained for immunoglobulin Fc receptor FcγRI in the hippocampus. Due to its high affinity for IgG (Mkaddem, Benhamou and Monteiro, 2019), FcγRI clearly plays an important role in the processing of an immune response to *S. typhimurium*. Immunohistochemistry qualitative results confirm observations from MHCII. There is a clear upregulation of FcγRI expression in C57BL/6 mice injected with *S. typhimurium* (**Figure 3-6**). The microglia appear to increase both in population size and to be located around blood vessels. By contrast, P301S mice which received either saline or *S. typhimurium* i.p. injection show microglia which are notably similar in morphology to saline-injected mice. This suggests that FcγRI is not upregulated in P301S mice, further confirming that in the brains of P301S mice there is less infiltration of IgG suggesting the bacterial infection is resolved.

By considering FcγRI, MHCII and CD11b expression, it is possible to propose that there has not been a neuroinflammatory response in the P301S mouse at 4 weeks post-infection, it remains to be determined if earlier time point would show evidence of such a response. This is a novel finding in a mouse model of tauopathy and suggests that the P301S mouse is less susceptible to *S.*

typhimurium than the C57BL/6 mouse. A faster resolution in the P301S mouse may explain these findings, however for this study a prolonged systemic inflammatory response is required, meaning the P301S is less suitable for future experiments.

3.4.3 Nramp1 and infection susceptibility

The results in this chapter suggest that the P301S mouse model is able to resolve *S. typhimurium* infection quicker than the C57BL/6 mouse. One protein, which is proposed to alter the host's response to *S. typhimurium*, is Nramp1 (encoded by the *Slc11a1* gene). Nramp1 is a cation transporter expressed on macrophages and other peripheral immune cells (Fritsche *et al.*, 2012). The cation transport removes iron from phagosomes. As a result, there is less iron availability for *S. typhimurium*, the bacteria are subsequently less able to colonise peripheral organs (Loomis *et al.*, 2014).

The resistance to intracellular bacterial infections is conveyed solely in WT Nramp1. By contrast, a mutation at 169aa leads to deficient Nramp1 and an inability to resolve the infection. Studies have examined the *Slc11a1* gene in multiple inbred murine strains and those with *Slc11a1* deficiency include the C57BL/6 mice, meaning the C57BL/6 is susceptible to *S. typhimurium* and would not be able to resolve a lethal dose (Brown *et al.*, 2013)**.** By contrast, the P301S mouse is partially bred on a CBA background, a strain that encodes WT Nramp1 and is subsequently able to resolve *S. typhimurium* infection. *Slc11a1* primers were used in a PCR and observed polymorphisms exclusively in the C57BL/6 DNA samples (**Figure 3-7**).

However, P301S mice do lose a significant amount of weight, therefore the mouse model does initially respond to infection. From this, it can be concluded that it is likely the P301S mouse model is able to resolve intracellular pathogen infections such as *S. typhimurium* due to the expression of WT Nramp1 encoded in the partial CBA background. This puts into question whether the P301S mouse model is appropriate to answer the hypothesis of this thesis.

3.4.4 The suitability of the P301S mouse model

In conclusion, the data presented suggests that the P301S mouse model resolves *S. typhimurium* infection faster than C57BL/6 mice, resulting in a lack of sustained neuroinflammation. As a result, the P301S mouse model of tauopathy is not ideal to test the overall hypothesis as tau spreading in this model occurs over 2 months. If the mouse is able to resolve the established systemic infection model, it will not be possible to assess the effect of sustained low-grade inflammation within the brain. It has been shown that P301S mice do not express MHCII in the brain following systemic infection. It is most likely this is due to the lack of

inflammatory signals responsible for MHCII expression. Furthermore, the background of the P301S mouse, which has a partial CBA strain, confers greater resistance to *S. typhimurium*. If there is an acute immune response within the periphery and subsequently the brain, it is unlikely that it will be possible to examine the effects of systemic infection on tau spreading. Therefore, further investigation into different mouse strains must be carried out, such as the H1*Mapt-/-* mouse. The H1*Mapt-/-* mouse is bred on a C57BL/6 background, therefore following *S. typhimurium* infection a neuroinflammatory response within the brain should be observed.

3.4.5 Weight loss in H1*Mapt-/-* mice following *S. typhimurium* infection

The primary aim following the P301S study was to confirm that H1*Mapt-/-* mice are susceptible to *S. typhimurium* and develop neuroinflammatory changes following infection. The H1*Mapt-/-* mouse has undergone both a knock-out of the murine tau gene, and the knock-in of the H1 human haplotype. The *Mapt-/-* mice, which express no endogenous mouse tau were used as an internal control for the H1*Mapt-/-* mice. As the *S. typhimurium* infection is novel in this mouse model, the *Mapt-/-* mouse allowed us to examine solely the effect of *Mapt* deletion. As the H1*Mapt-/-* mice in this thesis are homozygous as opposed to hemizygous, based on previous studies by Wade-Martins *et al.* (Wobst *et al.*, 2017), these C57BL/6 mice were not littermates. Whilst control littermates would be ideal, H1*Mapt-/-* mice are bred on a solely C57BL/6 background. Therefore, C57BL/6 mice were included to establish a 'wild type' response to systemic infection and so highlight potential differences in the H1*Mapt-/-* mice.

It was noted that all three genotypes injected with *S. typhimurium* lost weight 24 hours post-injection (**Figure 3-8**). There was no significant main effect of genotype. However, it possible to observe that H1*Mapt-/-* mice appear to gain weight at an earlier time point than C57BL/6 mice (**Figure 3-8**). The *Mapt-/-* mice also lost significant weight 24 hours post-infection. However, it was observed that the *Mapt-/-* mice do not return to baseline weight as quickly as either C57BL/6 or H1*Mapt-/-* mice, and still had not fully resolved the weight lost four weeks post-injection. The largest variability is observed between *S. typhimurium*-injected H1*Mapt-/-* and *Mapt-/-* mice which exhibit differences in weight change from five days post-infection (**Figure 3-8**). This suggests that whilst there is significant weight loss following systemic infection, differences between genotypes are observed once again.

There is also notable variability in the starting weights of these three different mouse strains. C57BL/6 and H1*Mapt-/-* mice both have similar starting weights, whilst *Mapt-/-* mice starting weights are significantly higher (**Figure 3-9**). *Mapt-/-* mice have been reported to exhibit hyperactivity and muscle weakness (Ikegami, Harada and Hirokawa, 2000; Wobst *et al.*, 2017). It

has also been reported that these mice display insulin resistance, resulting in increased body weight (Marciniak *et al.*, 2017). This paper suggested that tau may partially mediate peripheral metabolism as glucose intolerance is observed in these mice (Marciniak *et al.*, 2017); glucose is a crucial metabolite used by *S. typhimurium* (Thompson, Fulde and Tedin, 2018). Therefore, it is likely that metabolism deficits in the *Mapt-/-* mice are responsible for the significant increase in starting weight and subsequent weight change following *S. typhimurium*. Glucose intolerance may lead to greater colonisation of host cells by *S. typhimurium* and so delay weight recovery. It is interesting that the H1*Mapt-/-* mice do not show increased starting weight and return to baseline weight after infection on average two weeks faster compared to *Mapt-/-* mice. This suggests that the H1*Mapt-/-* mice may not exhibit glucose intolerance. The findings regarding the *Mapt-/-* mice correlate with previous studies and suggest that the deletion of tau alters metabolism. A previous study examining an alternative hTau mouse model did not show a rescue of this insulin resistant phenotype (Gonçalves *et al.*, 2020). In fact, the hTau mouse was the only strain in which this phenotype was observed. This study highlights how there are distinct differences between hTau models which express all six isoforms. In Chapter 3 it was possible to conclude that the *Mapt-/-* mice do show gross phenotypic differences not observed in the H1*Mapt-/-* mice.

Increased spleen size is widely reported in *S. typhimurium* studies, although the degree of increase varies with duration of infection and dose administered (Jackson *et al.*, 2011; Püntener *et al.*, 2012; Betz *et al.*, 2018). It was observed that all saline-injected mice, regardless of genotype, showed no significant change in spleen size (**Figure 3-9**). Following *S. typhimurium* infection, C57BL/6, H1*Mapt-/-* and *Mapt-/-* mice all exhibit significantly increased spleen size from their respective saline-injected controls. However, it is notable that for the *S. typhimurium*-injected groups of H1*Mapt-/-* and *Mapt-/-* mice, spleen size is significantly smaller than in the C57BL/6 group. When weight change is plotted against spleen weight in the *S. typhimurium*-injected groups, there is a significant linear regression ($F(1,24)= 10.17$, $p<0.01$), however the R square value is very low ($R^2= 0.3$) meaning there is a high level of variance in this data set (Appendix A, Figure S2). However, it is interesting that spleen weight does appear to partially correlate with weight loss and response to infection. Furthermore, the significantly smaller spleen size observed in H1*Mapt-/-* mice compared to C57BL/6 mice highlights a potentially dampened response to *S. typhimurium* infection. Even if the H1*Mapt-/-* mice do show a dampened reaction to *S. typhimurium* compared to C57BL/6 in weight change and spleen size, they are still a suitable model as the above results suggest they are susceptible. However, the response to *S. typhimurium* in the H1*Mapt-/-* brain must be fully characterised and variability from response in C57BL/6 mice highlighted.

3.4.6 Pro-inflammatory marker changes in the hippocampus of the H1*Mapt-/-* mouse model following systemic infection

MHCII expression is increased following exposure of cells to TNFα and IFNγ, two cytokines released after *S. typhimurium* infection (Nauciel and Espinasse-Maes, 1992). MHCII expression induces professional APCs (such as DCs) to process the bacteria and present them to T cells, which mounts an immune response with the aim of eliminating the infection. Following LPS i.p. injection, MHCII expression is commonly reported in microglia; these classical APCs express MHCII as an immediate response to the infection (Henry *et al.*, 2009). However, following sustained inflammation, MHCII expression on non-professional APCs has been reported. Vascular endothelial cell expression of MHCII has been reported on as a result of exposure to IFNγ (Geppert and Lipsky, 1985). Furthermore, *S. typhimurium* infection has been reported to inhibit T cell response through mediating APC function (McLaughlin and van der Velden, 2016).

Our group has established MHCII expression in the brain three weeks-post infection with *S. typhimurium*; by contrast, single or repeated LPS injections did not elicit MHCII expression on vascular endothelial cells (Püntener *et al.*, 2012). Increased expression of VCAM and ICAM was also observed following *S. typhimurium* infection, suggesting that BBB function is altered (Püntener *et al.*, 2012). MHCII-positive staining was noted in both H1*Mapt-/-* and *Mapt-/-* mice following a four-week *S. typhimurium* infection (**Figure 3-10**). By staining for laminin to highlight basement membranes, it was possible to demonstrate that MHCII is associated with blood vessels, possibly on vascular endothelial cells. These results suggest that H1*Mapt-/-* mice are susceptible to *S. typhimurium* and undergo a response in the brain similar to that of the C57BL/6 controls.

The expression of CD11b (**Figure 3-12**) and FcγRI (**Figure 3-13**) were examined. For both markers there was a significant main effect of infection; this suggests that following *S. typhimurium* infection there is upregulated expression of these macrophage and microglial markers. Following post-hoc tests, significance was only observed in C57BL/6 mice for FcγRI expression after systemic infection. It is possible that the sample size for analysis needs to be increased. However, CD11b expression has been reported to peak at 1 week post-*S. typhimurium* infection (Püntener *et al.*, 2012). At 3 weeks post-infection, there is still upregulated expression, yet this is reduced. This is likely due to macrophages and microglia playing a role in the initial immune response, and being able to migrate, self-renew and alter the inflammatory profile. By contrast, MHCII expression observed is likely located in cells which are not transient and so expression remains significantly higher in all mouse strains even four weeks post-infection.

3.4.7 Conclusions and future directions

From this experiment it is possible to conclude that despite variability in the response, both the H1*Mapt-/-* and *Mapt-/-* mice are susceptible to *S. typhimurium*. This is clear both in the spleen weight and the MHCII expression in immunohistochemistry. Examining weight change, starting weight and spleen weight shows there are variabilities between genotypes. These results suggest that H1*Mapt-/-* may exhibit a dampened response to *S. typhimurium*; compared to C57BL/6 mice the H1*Mapt-/-* mice show less weight loss and smaller spleen weight. The *Mapt-/-* mice do also show variability, however a potential rescuing effect of gross phenotypic changes as a result of *Mapt* deletion is observed in the H1*Mapt-/-* mice. Therefore, whilst it is crucial to understand the mechanism behind the observed variability, these mice should respond to systemic infection in further experiments.

Neither C57BL/6 mice nor the H1*Mapt-/-* mouse model express tau with pathological mutations and previous research suggests that *S. typhimurium* alone is not adequate to induce hyperphosphorylation in naïve tau (Alex Collcutt, thesis (2017)). Inducing pathological tau spread through intracerebral injection of AD-tau will allow us to properly assess the effect of systemic infection. Therefore, although there is deviation from the immune response in the C57BL/6 mice, it has been established that *S. typhimurium* does elicit a classical peripheral and central immune response in H1*Mapt-/-* mice. Subsequently, the H1*Mapt-/-* mice is a suitable model to examine tau spreading under the presence of systemic infection.

Future aims:

- *To establish the effect of intracerebral injection on subsequent systemic infection*
- *To isolate AD-tau from post-mortem AD tissue and enrich for HMW tau*
- *To establish a tau spreading model using a mouse model expressing human tau*
- *To determine if systemic infection alters the rate of tau spreading in vivo*

Chapter 4 *S. typhimurium* infection following LPS i.c. injection

4.1 Introduction

Priming is a widely researched phenomenon in microglia dynamics. 'Priming' begins with an initial insult in the parenchyma, either from an infection, injury or the presence of misfolded protein which induces a pro-inflammatory response (Perry and Holmes, 2014). This leaves the microglial 'primed', whereby a secondary insult induces a greater response by the microglia than observed without the prior event (Li *et al.*, 2018). In neurodegenerative diseases, proteins such as tau become aggregated and disrupt protein degradation systems (Ciechanover and Kwon, 2015). It is hypothesised that the build-up of aggregated protein may induce a microglial response, whereby the loss of homeostatic function results in an increasingly activated profile after a secondary insult. Systemic infections are associated with accelerated cognitive decline in dementia, which may be a result of the activation of these 'primed' microglia (Hoeijmakers *et al.*, 2016).

The aim of this thesis is to induce pathology through injection into the mouse brain; the combined effect of tau pathology and systemic infection on the microglial population is unknown. The question addressed in this chapter is whether an acute inflammatory process such as an i.c. injection of LPS results in priming, or if this only occurs if the initial stimulus is sustained such as with aggregated pathology. C57BL/6 mice infected with the bacterial strain *S. typhimurium* show sustained, low-grade neuroinflammation (Püntener *et al.*, 2012). Subsequent LPS challenge through i.c. injection results in exaggerated activation of microglia, suggestive that systemic infection and following changes in the brain resulted in priming. However, repeated LPS injections show induction of tolerance as opposed to priming. This is proposed to be due to TLR4 activation from LPS injection, as endotoxin is a TLR4 agonist (Liu *et al.*, 2019). To model an acute inflammatory response, C57BL/6 mice received an i.c. injection of LPS followed by an i.p. injection of *S. typhimurium*. Control mice also received an i.c. injection of saline which examines to what extent the damage caused by injection alone is adequate to result in reactivation of immune cells. In this study it is investigated whether prior activation of microglia using an acute challenge with LPS, influences microglial response to systemic infection with *S. typhimurium.*

Aims addressed in this chapter are as follows:

- *To establish whether there are changes in microglial marker expression following LPS intracerebral injection*
- *To establish whether an acute inflammatory response in the brain is adequate to induce microglial priming*

4.2 Methods

4.2.1 Lipopolysaccharide intracerebral injection

C57BL/6 female mice (3 months old) underwent stereotaxic injections into the cerebrum as described in Chapter 2.1.2. The Bregma position for injection is as follows: Anterior-Posterior (AP): -2.5, Lateral-Medial (LM): -2.0, Dorsal-Ventral (DV): -1.8. The choice of injection site refers to previous experiments and published data carried out by industrial collaborators (Ahmed *et al.*, 2014). Bregma coordinates place the injection site above the dentate gyrus. A 33-gauge needle with a 7 series Hamilton syringe was used to inject 1µl of either saline or LPS (0.5µg/µl) (*Salmonella enterica* serotype Abortus Equi; L5886 Sigma), unilaterally into the hippocampus. A low dose was chosen considering that these mice would receive a systemic infection one week later. Group sizes are found below in **Table 4-1**. After i.c. injection monitoring and recording was carried out as reported in Chapter 2. Four to five-month-old C57BL/6 mice also underwent the same procedure of an i.c. injection of either LPS or saline (n= 3 for both groups), histology shown in **Figure 4-2** and **Figure 4-3**. However, this injection was bilateral, and the mice were culled 24 hours post-injection.

Table 4-1: Group sizes for i.c. and i.p. injection

	Saline i.p.	***S. typhimurium* i.p.**
Saline i.c.	3	3
LPS i.c.	3	3

4.2.2 *S. typhimurium* intraperitoneal injections and perfusion

One-week post-i.c. injection, mice received a 200µl intraperitoneal injection of either saline or *S. typhimurium* as described in Chapter 2. Mice were weighed daily for seven days. On the seventh day the mice were transcardially perfused with 0.9% saline as described in Chapter 2. The brain tissue was collected, mounted in OCT and frozen on isopentane.

4.2.3 Histology

Images were taken at the hippocampal fissure and with 20x objective for MHCII, CD11b and FcγRI, all analysis was carried out as described in Chapter 2.

4.3 Results

4.3.1 Acute inflammatory marker changes

The first question posed is whether the LPS dose (0.5µg/µl) would induce an acute inflammatory response in the brain. C57BL/6 mice underwent an intracerebral injection of either LPS or saline. Prior to examining the effect of systemic infection following LPS, a cohort of mice were perfused 24 hours post-LPS or saline injection and the brain tissue stained for inflammatory markers.

The tissue was stained for MHCII, CD11b and FcγRI. It is possible to observe that at one day post-injection, there is considerable expression of inflammatory markers. There is MHCII-positive staining in the parenchyma 24 hours post-LPS injection (**Figure 4-1**). There is also MHCII expression in the corpus callosum, showing cross-talk between the two hemispheres. When examining higher magnification images of MHCII expression, the cells appear to be ameboid in morphology in the hippocampus and cortex (**Figure 4-2**). It is unclear whether this MHCII expression is in classical or non-classical APCs. However, the ameboid appearance of the staining suggests a more acute response with activation of classical antigen presenting cells such as microglia.

Expression levels of FcγRI were also investigated and a similar pattern of expression to MHCII was observed. Whilst there is a low level of endogenous FcγRI expression in the naïve murine brain, the injection site displayed observably higher expression (**Figure 4-1**). At a higher magnification, the FcγRI positive macrophages also appear to be ameboid in morphology. FcγRI staining also suggests that 24 hours post-injection of LPS, a localised inflammatory response is induced.

Expression levels of CD11b showed visibly increased expression following LPS i.c. injection (**Figure 4-1**). The CD11b positive macrophages observed in the brain suggest recruitment of immune cells to the injection site as a result of the inflammatory response. At the injection site CD11b-positive macrophages are ameboid in morphology, suggesting a localised inflammatory response which then dissipates as the distance from the injection site increases. This inflammatory response appears localised to the ipsilateral hemisphere (**Figure 4-2**).

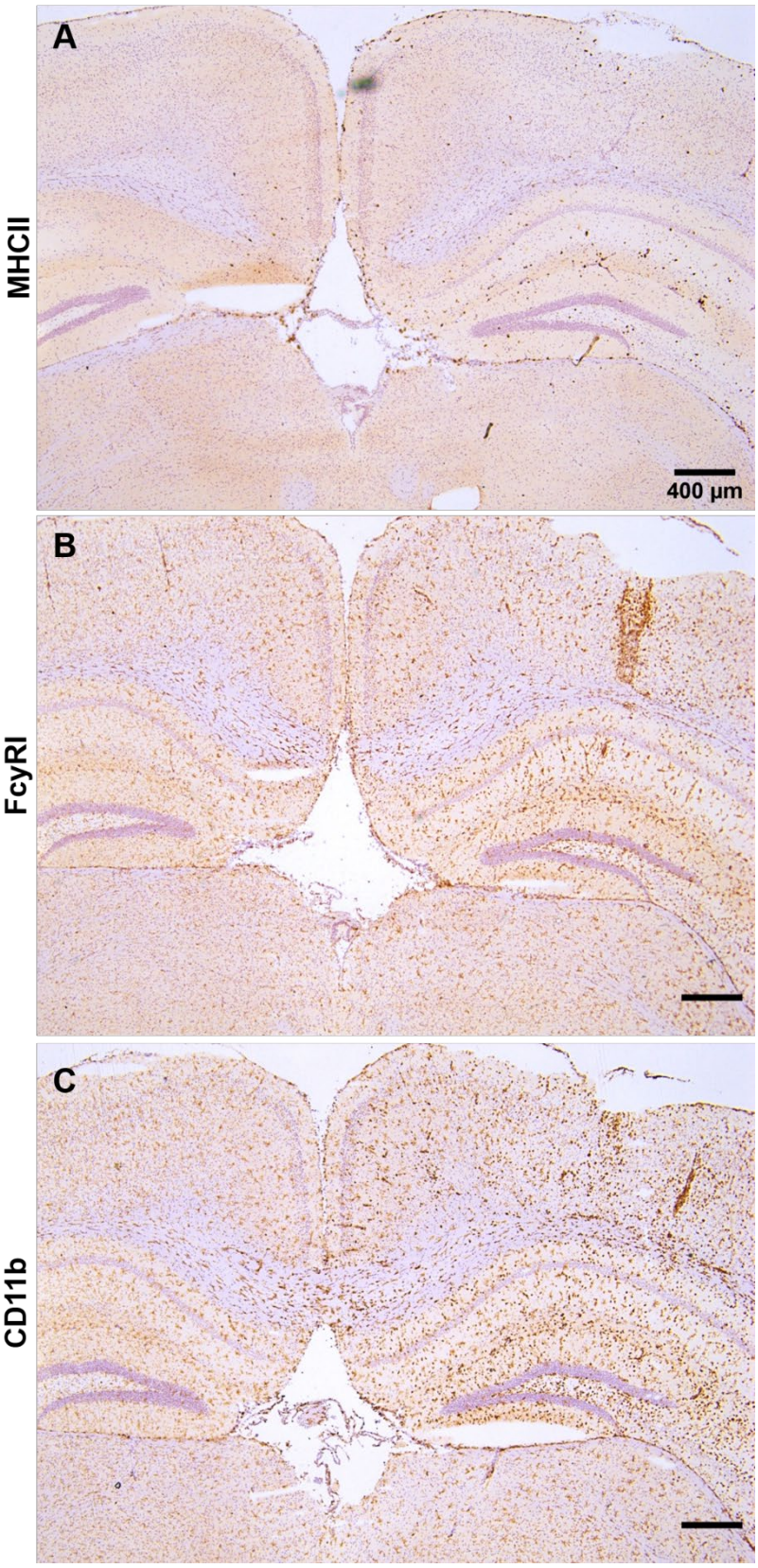

Figure 4-1: 24 hours post-LPS and saline I.C injection

One day post-i.c. injection, the parenchyma was stained for **A)** MHCII expression **B)** FcγRI expression **C)** CD11b expression. All images taken at 2.5x objective; scale bar= 40µm.

Mice which underwent saline intracerebral injection also showed activation of immune markers within the parenchyma at one day post-injection. However, MHCII expression levels at both high and low magnification showed very minimal staining. This suggests that saline injection and the damage caused by the needle does not indue MHCII activation on macrophages to the same degree that LPS i.c. injection does (**Figure 4-3**). CD11b staining showed observable activation of macrophages to ameboid morphology. However, it is notable that this staining is visibly weaker than CD11b staining observed following LPS injection. It is possible to see that the activation of macrophages is more highly localised to the needle path. This would suggest that local microglial populations were activated due to the injury, yet there is no response to the saline. Furthermore, FcγRI showed similar dampened activation compared to LPS injection (**Figure 4-3**). Whilst the main readout is the effect of this i.c. injection on a subsequent systemic infection, it is important to note that LPS i.c. injection does induce a very acute inflammatory response. By then examining metabolic changes and peripheral readouts it will be possible to observe the effects of a bacterial mimic versus a murine bacterial infection.

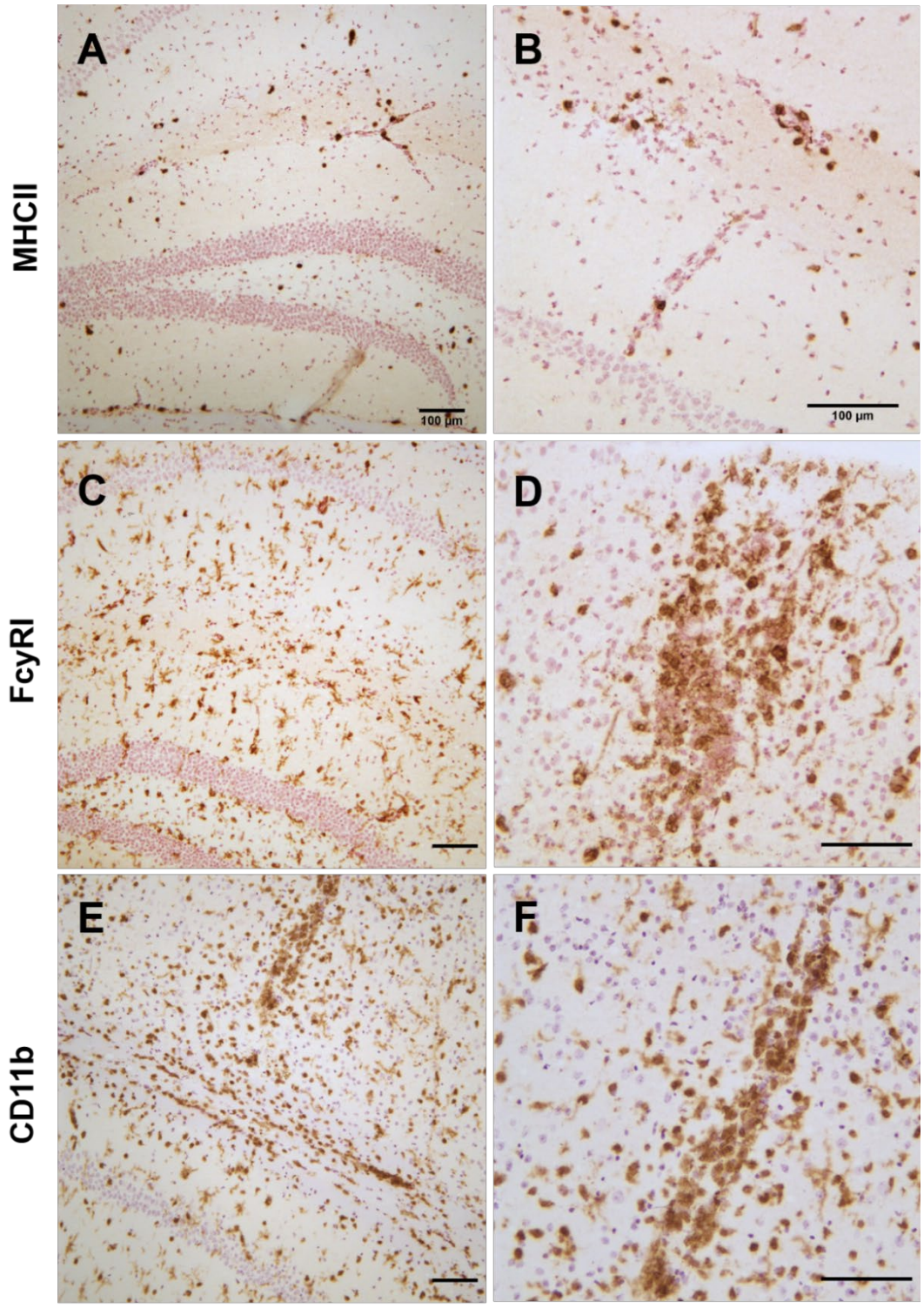

Figure 4-2: Comparison of immune markers 24 hours post-LPS injection

A, B) Representative staining of MHCII at 24 hours post-LPS i.c. injection. The MHCII is primarily focused on the hippocampal fissure. **C, D)** Staining of FcγRI at 24 hours post-LPS i.c. injection in the (**C**) hippocampal fissure and (**D**) cortex. **E, F)** Representative staining of CD11b at 24 hours post-LPS i.c. injection in the (**E)** hippocampal fissure and (**F)** cortex. **A, C, E)** 10x image objective; scale bar= 100µm. **B, D, F)** 20x objective; scale bar= 100µm.

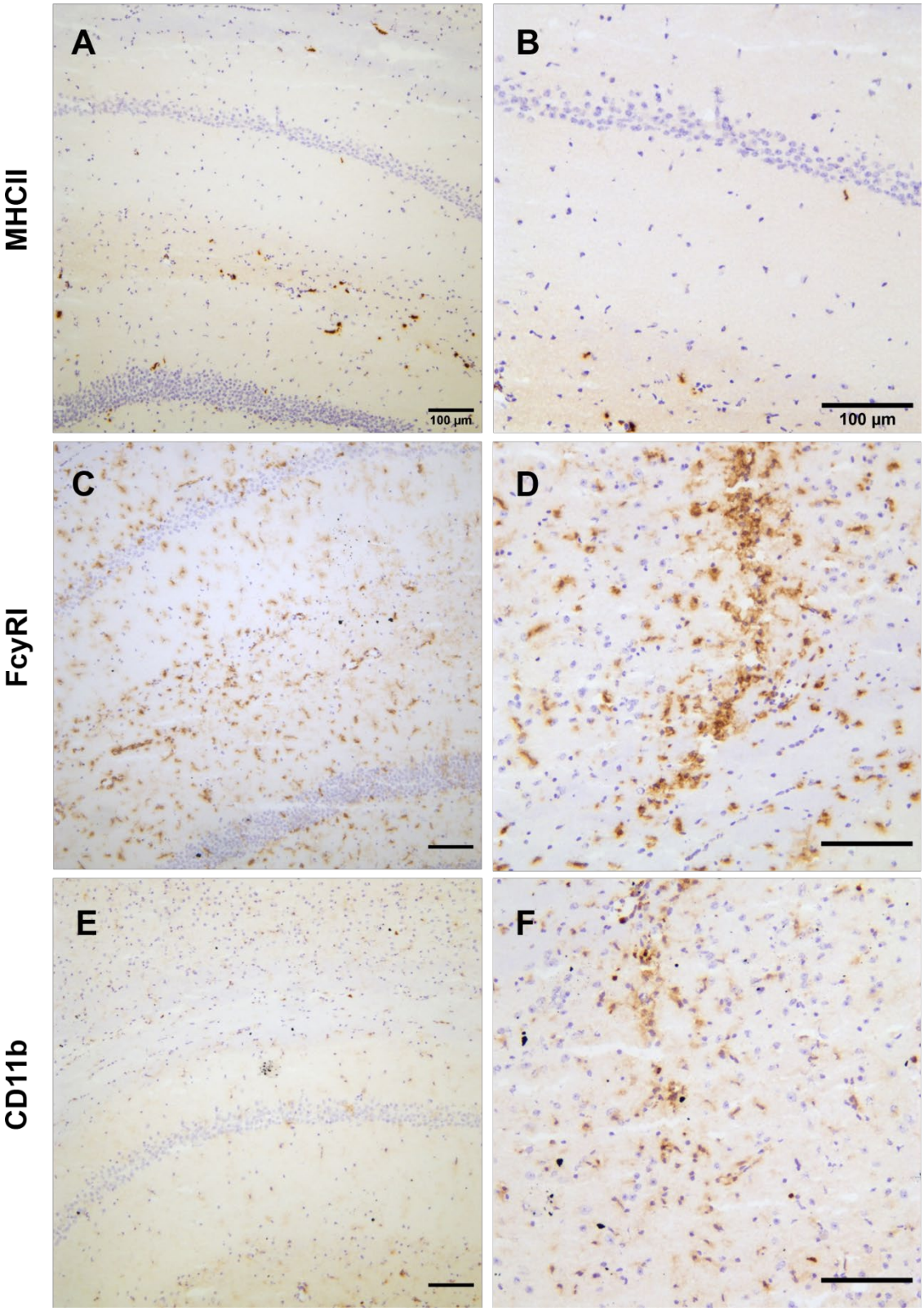

Figure 4-3: Immune markers 24 hours post-saline intracerebral injection

A, B) MHCII, (**C, D)** CD11b and (**E, F)** FcγRI staining in mice which underwent saline i.c. injection 24 hours prior. **A, C, E)** The hippocampal fissure and **(B, D, F)** the injection site are imaged. **A, C, E)** 10x objective used; scale bar= 100µm. **B, D, F)** 20x objective used; scale bar= 100µm.

4.3.2 LPS and *S. typhimurium* induce metabolic changes yet differ in immune activation

Having established that LPS i.c. injection at 0.5µg/µl induces an acute inflammatory response, it was then possible to examine the effects of a subsequent systemic infection. This experimental procedure requires two key steps. Firstly, the intracerebral injection of LPS or saline followed by the intraperitoneal injection of *S. typhimurium* or saline. Firstly, starting weights were recorded; all mice injected were littermate C57BL/6 female mice. There was no significant difference in starting weight between any group ($F(3, 8) = 0.76$, $p= 0.55$).

Injection of saline into the cerebrum causes minimal weight loss, even one day post-saline injection (weight change (% baseline); -2.69% ± 2.2 (Mean ± SD). By contrast, injection of LPS into the cerebrum causes significant weight loss compared to the saline i.c. group one day post-injection (weight change (% baseline); -11.3% ± 1.7, $p<0.001$) (**Figure 4-4**). This weight loss is observed one day post-injection; by three days post-injection the LPS-injected mice have returned to baseline weight comparable to saline-injected mice. There was a significant main effect of time ($F(7, 70)= 22.18$, $p<0.001$), however there was no significant main effect of LPS injection ($F(1, 10)= 2.11$, $p= 0.18$). There was a significant interaction of time and i.c. injection on weight loss ($F(7, 70)= 7.61$, $p<0.0001$), suggesting that the use of LPS or saline significantly altered the degree of weight change in the initial 24 hours, yet the weight change was not significantly different for the remaining six days. This confirms that there was an initial metabolic response to the LPS injection, yet as LPS is a bacterial mimic this was quickly resolved.

By contrast, following the intraperitoneal *S. typhimurium* injections, the weight loss observed is over a greater number of days. There was no significant main effect of previous i.c. injection on the response to *S. typhimurium* ($F(1, 8)= 0.39$, $p= 0.55$). Therefore, the previous intracerebral injection of LPS appears to have no significant effect on weight change during bacterial infection. Mice which previously underwent saline i.c. and then a subsequent saline i.p. injection showed minimal weight loss from baseline at one day post-i.p. injection (0.55% ± 1.86). *S. typhimurium*-injected mice displayed greater weight loss however this was not significant compared to the saline i.c./saline i.p. group (saline i.c./*S. typhimurium* i.p.= -6.79% ± 3.08, $p= 0.43$). This weight loss is observed until seven days post injection at which point both groups reach baseline weight (**Figure 4-4**). There was a significant main effect of time ($F(2.07, 16.53)= 24.04$, $p<0.001$) and there was a significant main effect of *S. typhimurium* ($F(1, 8)= 12.41$, $p<0.01$). There was also a significant interaction of time and systemic infection ($F(7, 56)= 5.63$, $p<0.001$). Notably, there is no significant difference in the weight change between the two groups injected with *S. typhimurium*. The lack of post-hoc significance is likely due to the small sample size within these groups.

One-week post-injection, the mice were perfused, and the spleen weights recorded (**Figure 4-4**). *S. typhimurium* -injected mice show significant splenomegaly, with an approximate four-fold increase in spleen weight regardless of i.c. injection (Saline i.c./saline i.p.= 113.67mg ± 14.57; saline i.c./*S. typhimurium* i.p.= 479.33mg ± 132.68; LPS i.c./saline i.p.= 99.67mg ± 6.66; LPS i.c./ *S. typhimurium* i.p.= 438.67mg ± 103) and there was a significant main effect of bacterial infection ($F(1, 8)= 52.32$, $p<0.0001$). Notably, the prior intracerebral injection did not have a significant main effect on spleen weight ($F(1, 8)= 0.31$, $p= 0.59$) and no interaction was observed ($F(1, 8)= 0.07$, $p= 0.79$).

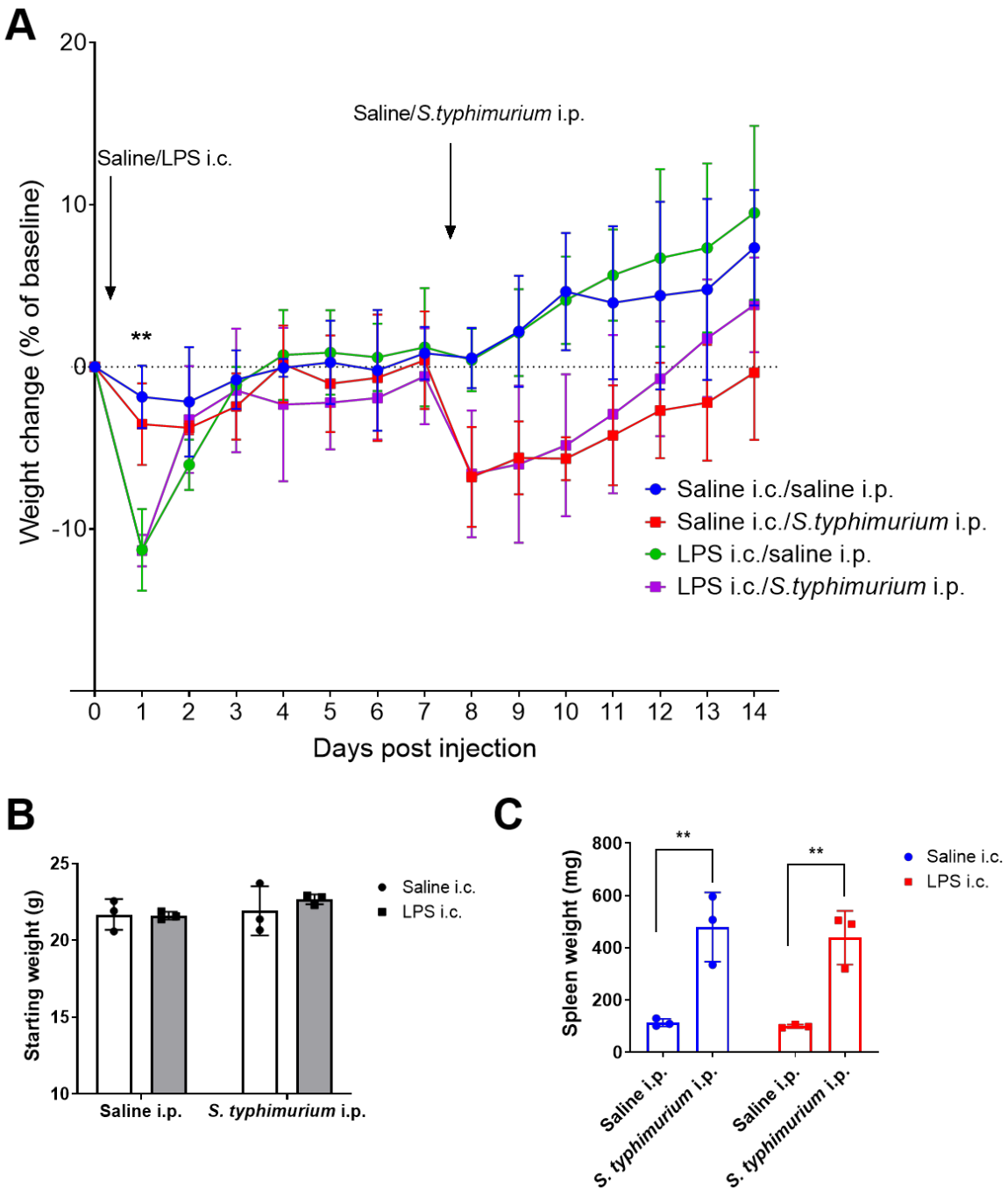

Figure 4-4: Body weight changes and spleen weights following LPS and *S. typhimurium* injections

A) Weight change is shown as a percentage of baseline from weight measured prior to both i.c. and i.p. injection. n=3 for each group. Repeated measures ANOVA with Greenhouse-Geisser correction and Tukey's post-hoc test. *= significance between saline i.c. and LPS i.c. groups (**p<0.05). **B)** Starting weight for C57BL/6 female mice prior to saline or LPS i.c. injection. One-way ANOVA with Tukey's post-hoc test. **C)** Spleen weights one-week post-i.p. injection. Two-way ANOVA with Tukey's post-hoc test; (**p<0.01). All data is presented as mean ± standard deviation.

4.3.3 MHC II expression in the hippocampus following *S. typhimurium* infection

Within 24 hours of intracerebral injection of LPS, MHCII is upregulated at the injection site in the ipsilateral hemisphere (**Figure 4-1**). Yet how does this compare to MHCII expression following a bacterial infection? One-week post-i.c. injection, mice were injected intraperitoneally with either saline or *S. typhimurium*. One-week post-*S. typhimurium* the brains were processed and stained for several inflammatory markers, specifically examining expression in the hippocampal fissure. MHCII was co-stained with laminin to show how MHCII staining overlaps with the vasculature (**Figure 4-5**). There is no positive MHCII staining in the hippocampal fissure of mice which received an i.c. and i.p. injection of saline. Mice which underwent LPS i.c. injection followed by saline i.p., showed MHCII-positive staining, but this was a very low level of staining and was not significant compared to the saline i.c./saline i.p. group. All mice injected with *S. typhimurium* show positive MHCII staining, confirming and inflammatory response to the infection. Due to the proximity with laminin the vasculature can be clearly observed and MHCII expression appears to be located proximal to the basement membrane (**Figure 4-5**). This suggests that by one-week post-injection of *S. typhimurium*, the expression has been restricted predominantly to the basement membrane, as opposed to the resident microglia observed at 24 hours post-LPS injection.

A three-way ANOVA determined that there was no significant main effect of hemisphere ($F(1, 8)= 3.21$, $p= 0.11$), therefore all subsequent analysis was carried out as two-way ANOVAs for each hemisphere. Following analysis of MHCII staining in the ipsilateral hemisphere, there is a significant main effect of *S. typhimurium* ($F(1, 8)= 14.43$, $p<0.01$). By contrast, there was no significant main effect caused by LPS i.c. injection ($F(1, 8)= 1.14$, $p= 0.32$). There was also no significant interaction found between the i.c. and i.p. injections ($F(1, 8)= 2.58$, $p= 0.15$). Following *S. typhimurium* i.p. injection there was a 40-fold significant upregulation in MHCII expression in the saline i.c. group (saline i.c./saline i.p.= 0.06% ± 0.02; saline i.c./*S. typhimurium* i.p.= 2.42% ± 0.84, $p<0.05$) (**Figure 4-5**). There was no significant difference found between the LPS i.c. groups regardless of subsequent i.p. injection (LPS i.c./saline i.p.= 0.30% ± 0.16; LPS i.c./*S. typhimurium* i.p.= 1.26% ± 0.17, $p= 0.45$), despite the MHCII-positive staining in the LPS i.c./*S. typhimurium* i.p. group. This suggests there is reduced MHCII express in the LPS i.c./*S. typhimurium* i.p. group compared to the saline i.c./*S. typhimurium* i.p. group.

There was no significant difference when comparing relative ipsilateral versus contralateral expression in all treatment groups (**Figure 4-5**, **Figure 4-6**). This suggests that the changes in MHCII expression were ubiquitous across both hippocampal fissures, suggesting a more global response to *S. typhimurium* that is not determined by the coordinates of the intracerebral

injection prior. In the contralateral hemisphere there was once again no significant main effect of i.c. injection ($F(1, 8)= 2.41$, $p= 0.16$), and a significant main effect of *S. typhimurium* i.p. injection ($F(1, 8)= 10.50$, $p<0.05$). As observed in the ipsilateral hemisphere, there was no significant interaction ($F(1, 8)= 3.36$, $p= 0.10$). The post-hoc comparisons only showed significance between the saline i.c./*S. typhimurium* i.p. group and both saline i.p. groups, regardless of saline or LPS i.c. injection prior. There is an almost 100-fold increase in MHCII expression after systemic infection in the saline i.c. group (saline i.c./saline i.p.= 0.04% ± 0.01; saline i.c./*S. typhimurium* i.p.= 3.57% ± 1.38, $p<0.05$). When comparing MHCII expression in the LPS i.c./saline i.p. group to the saline i.c./*S. typhimurium* i.p. group, a significant increase is observed after systemic infection (LPS i.c./saline i.p.= 0.23% ± 0.09; saline i.c./*S. typhimurium* i.p.= 3.57% ± 1.38, $p<0.05$). No significant effect of systemic infection is observed in post-hoc between the LPS i.c. groups (LPS i.c./saline i.p.= 0.23% ± 0.09; LPS i.c./*S. typhimurium* i.p.= 1.21% ± 0.16, $p= 0.76$). Overall, this suggests that MHCII expression may be reduced after systemic infection in the LPS i.c. injection group. To what extent there is a significant dampening effect would require further investigation and potentially a higher powered study.

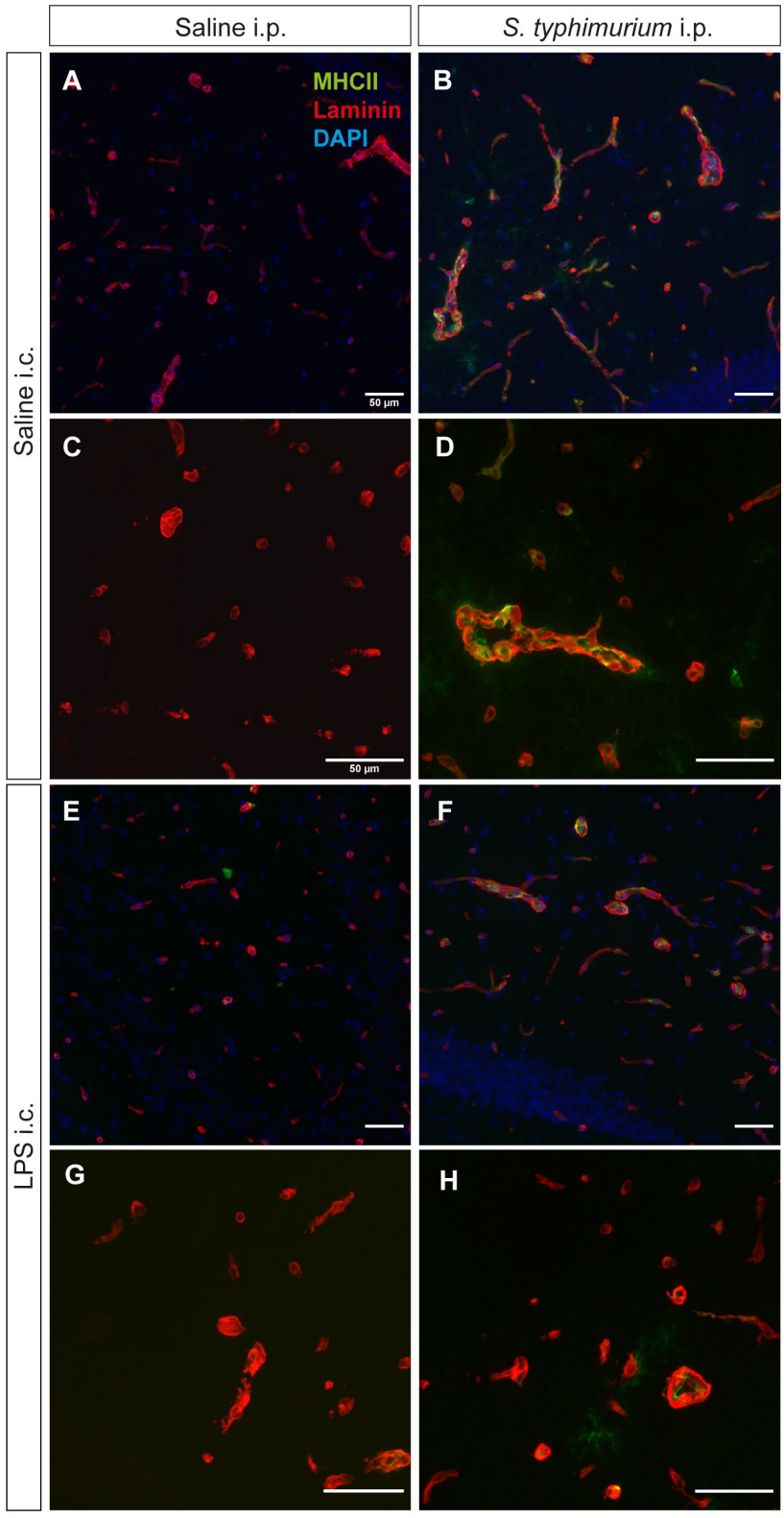
Saline i.p.
S. typhimurium i.p.
Saline i.c.
LPS i.c.
A
MHCII
Laminin
DAPI
B
C
D
E
F
G
H
50 µm
I
Ipsilateral hemisphere
Mean % area
0
1
2
3
4
5
*
*
Saline
LPS
Intracerebral injection
Saline i.p.
S. typhimurium i.p.

Figure 4-5: MHCII expression in the ipsilateral hemisphere following i.c. and i.p. injection
Ipsilateral hemisphere staining of MHCII and laminin. Saline i.c. followed by **(A, C)** saline i.p. or **(B, D)** *S. typhimurium* i.p. injection. LPS i.c. followed by **(E, G)** saline i.p. or **(F, H)** *S. typhimurium* i.p. injection. **A, B, E, F)** Image taken with 20x objective, scale bar= 50µm for all images. **C, D, G, H)** Image taken with 40x objective, scale bar= 50µm for all images. **I)** Two-way ANOVA for the ipsilateral hemisphere with Tukey's post hoc test (*$p<0.05$). n= 3 for all groups. Data is presented as mean ± SEM.

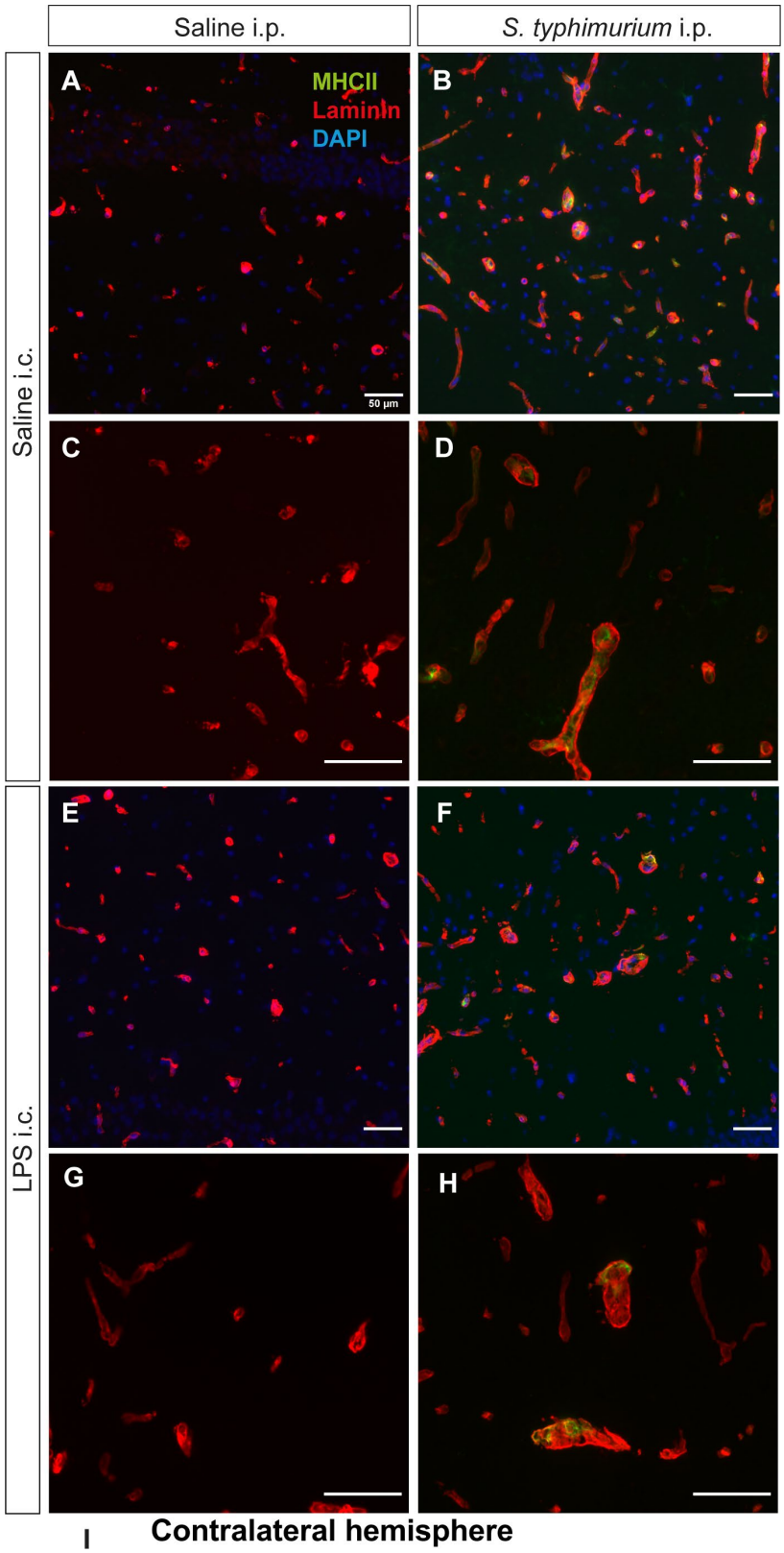
Saline i.p.
S. typhimurium i.p.
Saline i.c.
LPS i.c.
A
MHCII
Laminin
DAPI
50 µm
B
C
D
E
F
G
H

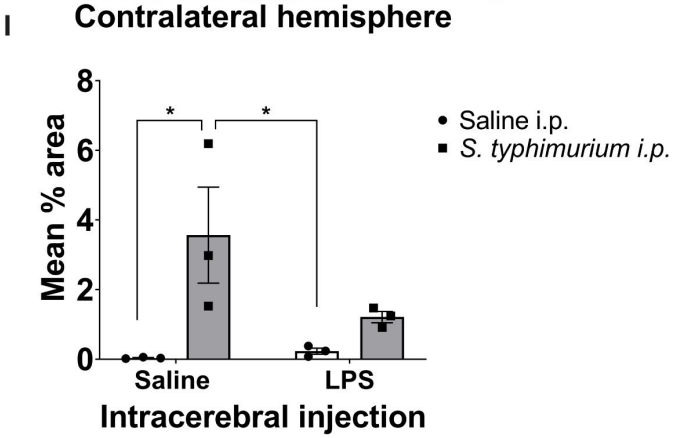
I
Contralateral hemisphere
Mean % area
8
6
4
2
0
*
*
Saline
LPS
Intracerebral injection
Saline i.p.
S. typhimurium i.p.

Figure 4-6 MHCII expression in the contralateral hemisphere following i.c. and i.p. injection
Contralateral hemisphere staining of MHCII and laminin. Saline i.c. followed by **(A, C)** saline i.p. or **(B, D)** *S. typhimurium* i.p. injection. LPS i.c. followed by **(E, G)** saline i.p. or **(F, H)** *S. typhimurium* i.p. injection. **A, B, E, F)** Image taken with 20x objective, scale bar= 50µm for all images. **C, D, G, H)** Image taken with 40x objective, scale bar= 50µm for all images. **I)** Two-way ANOVA for the ipsilateral hemisphere with Tukey's post hoc test (*p<0.05). n= 3 for all groups. Data is presented as mean ± SEM.

4.3.4 Expression of CD11b following acute and systemic inflammation

CD11b staining at 24 hours post-LPS injection was indicative of microglial activation in the ipsilateral hemisphere localised to the injection site (**Figure 4-1**). CD11b expression was then quantified when examining the effect of LPS injection and subsequent systemic infection (**Figure 4-7**). CD11b expression showed a significant difference between hemispheres ($F(1, 8)= 39.77$, $p<0.001$). There was a significant main effect of i.c. injection ($F(1, 8)= 7.98$, $p<0.05$) whilst there is no significant main effect of *S. typhimurium* i.p. injection ($F(1, 8)= 0.04$, $p= 0.84$). There is no significant interaction between i.c. and i.p. injection ($F(1, 8)= 1.97$, $p= 0.20$). There was a significant two-fold upregulation in CD11b expression in the ipsilateral LPS i.c/saline i.p. group compared to the saline i.p./saline i.p. group (saline i.c./saline i.p.= 3.72% ± 0.28; LPS i.c./saline i.p.= 10.73% ± 2.07, $p<0.05$). The ipsilateral LPS i.c./saline i.p. group also showed significant two-fold upregulation of CD11b compared to the ipsilateral saline i.c./*S. typhimurium* i.p. (LPS i.c./saline i.p.= 10.73% ± 2.07; saline i.c./*S. typhimurium* i.p.= 4.59% ± 1.25, $p<0.05$). This highlights how LPS i.c. injection induces upregulation of CD11b. However, there is no significant difference in CD11b expression between the two LPS i.c. groups in the ipsilateral hemisphere despite one group also receiving *S. typhimurium* i.p. injection (LPS i.c./saline i.p.= 10.73% ± 2.07, LPS i.c./*S. typhimurium* i.p.= 8.12% ± 0.43, $p= 0.78$). Notably both LPS i.c. groups showed significant upregulation in the ipsilateral hemisphere compared to the corresponding contralateral hemisphere. These results suggest that LPS is the predominant factor inducing upregulation of CD11b expression and one-week post-i.p. injection may be premature to observe the effect of *S. typhimurium* infection.

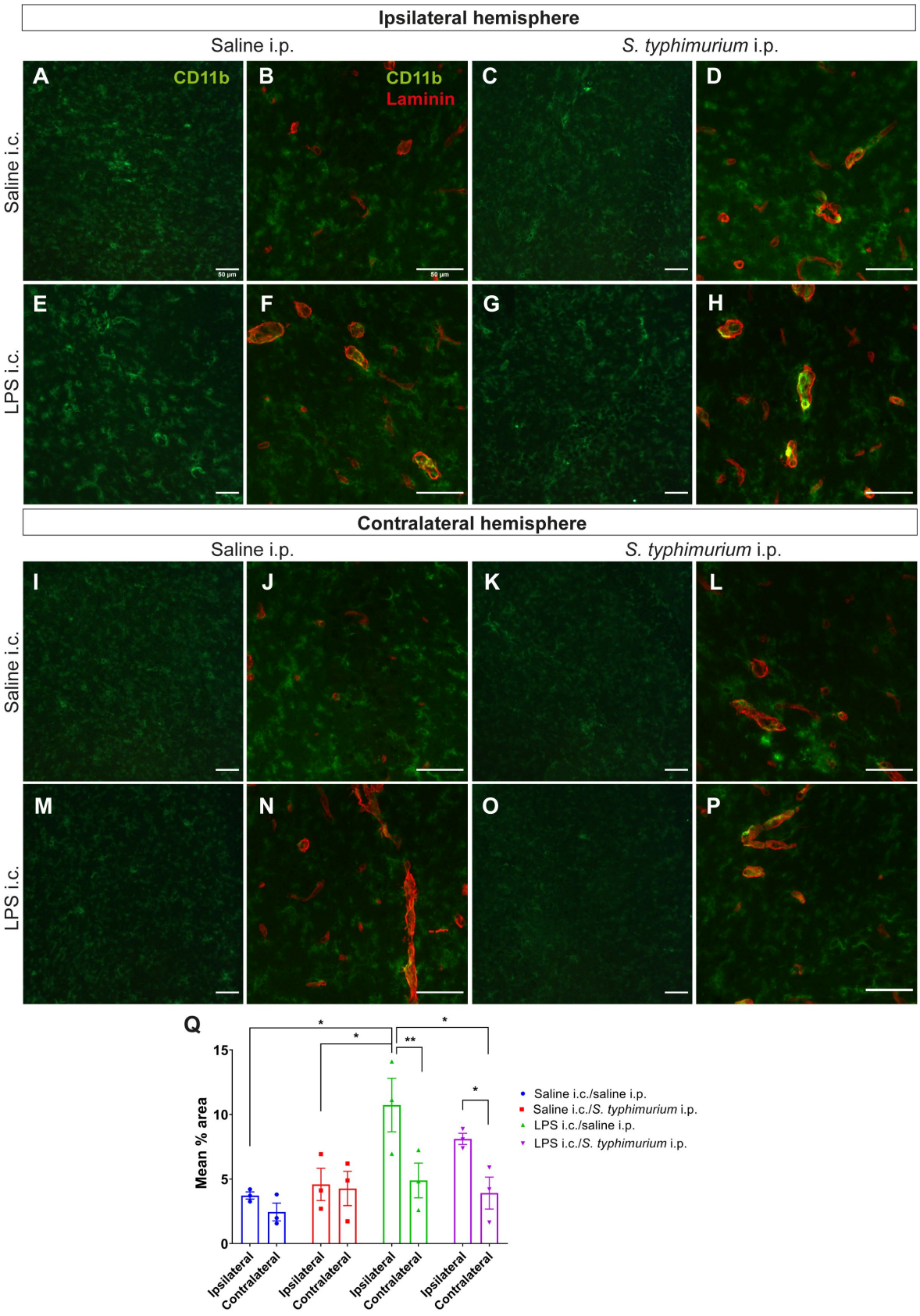
Ipsilateral hemisphere
Saline i.p.
S. typhimurium i.p.
Saline i.c.
LPS i.c.
A
CD11b
B
CD11b
Laminin
C
D
E
F
G
H
50 µm
Contralateral hemisphere
Saline i.p.
S. typhimurium i.p.
Saline i.c.
LPS i.c.
I
J
K
L
M
N
O
P
Q
Mean % area
15
10
5
0
Ipsilateral
Contralateral
Saline i.c./saline i.p.
Saline i.c./S. typhimurium i.p.
LPS i.c./saline i.p.
LPS i.c./S. typhimurium i.p.

Figure 4-7: CD11b expression following LPS i.c. injection and *S. typhimurium* i.p. injection

A-H) CD11b expression in the ipsilateral hemisphere of mice which had received **(A, B)** saline i.c./saline i.p., **(C, D)** saline i.c./*S. typhimurium* i.p. injection, **(E, F)** LPS i.c./saline i.p. or **(G, H)** LPS i.c./*S. typhimurium* i.p. injection groups. **I-P)** Contralateral hemisphere images of CD11b expression in groups which had received **(I, J)** saline i.c./saline i.p. or (**K, L**) saline i.c./*S. typhimurium* i.p. injection. CD11b expression in the contralateral hemisphere of **(M, N)** LPS i.c./saline i.p. or **(O, P)** LPS i.c./*S. typhimurium* i.p. injection groups. **A, C, E, G, I, K, M, O)** Images taken with 20x objective, scale bar= 50µm for all images. **B, D, F, H, J, L, N, P)** Images taken using 40x objective, scale bar= 50µm for all images. **Q)** Mean % area analysis at hippocampal fissure. n= 3 for all groups. Three-way ANOVA with Tukey's post-hoc test (*p<0.05, **p<0.01). All data is presented as mean ±SEM.

4.3.5 FcγRI expression following LPS and *S. typhimurium* treatment

FcγRI expression 24 hours post-LPS injection demonstrated that FcγRI-positive macrophages were predominantly expressed in the ipsilateral hemisphere compared to the contralateral (**Figure 4-2**). The morphology of the macrophages was observably ameboid. By contrast, when observing microglia two weeks post-LPS injection, the morphology of the microglial population is more ramified (**Figure 4-8**). Therefore, it was of interest to examine the effects of LPS injection and systemic infection. There was a significant main effect of hemisphere when examining FcγRI expression ($F(1, 8)= 12.26$, $p<0.01$). There was no significant effect of i.c. injection ($F(1, 8)= 0.04$, $p= 0.84$), and no significant main effect of *S. typhimurium* i.p. injection ($F(1, 8)= 0.48$, $p= 0.51$). There was also no significant interaction of i.c. and i.p. injection ($F(1, 8)= 0.001$, $p= 0.97$). As a result, there is also no post-hoc significance when comparing any of the groups which underwent either saline or LPS i.c. injection initially. This suggests that in this experiment there is no biologically notable change in FcγRI expression either across either i.c. or i.p. injection.

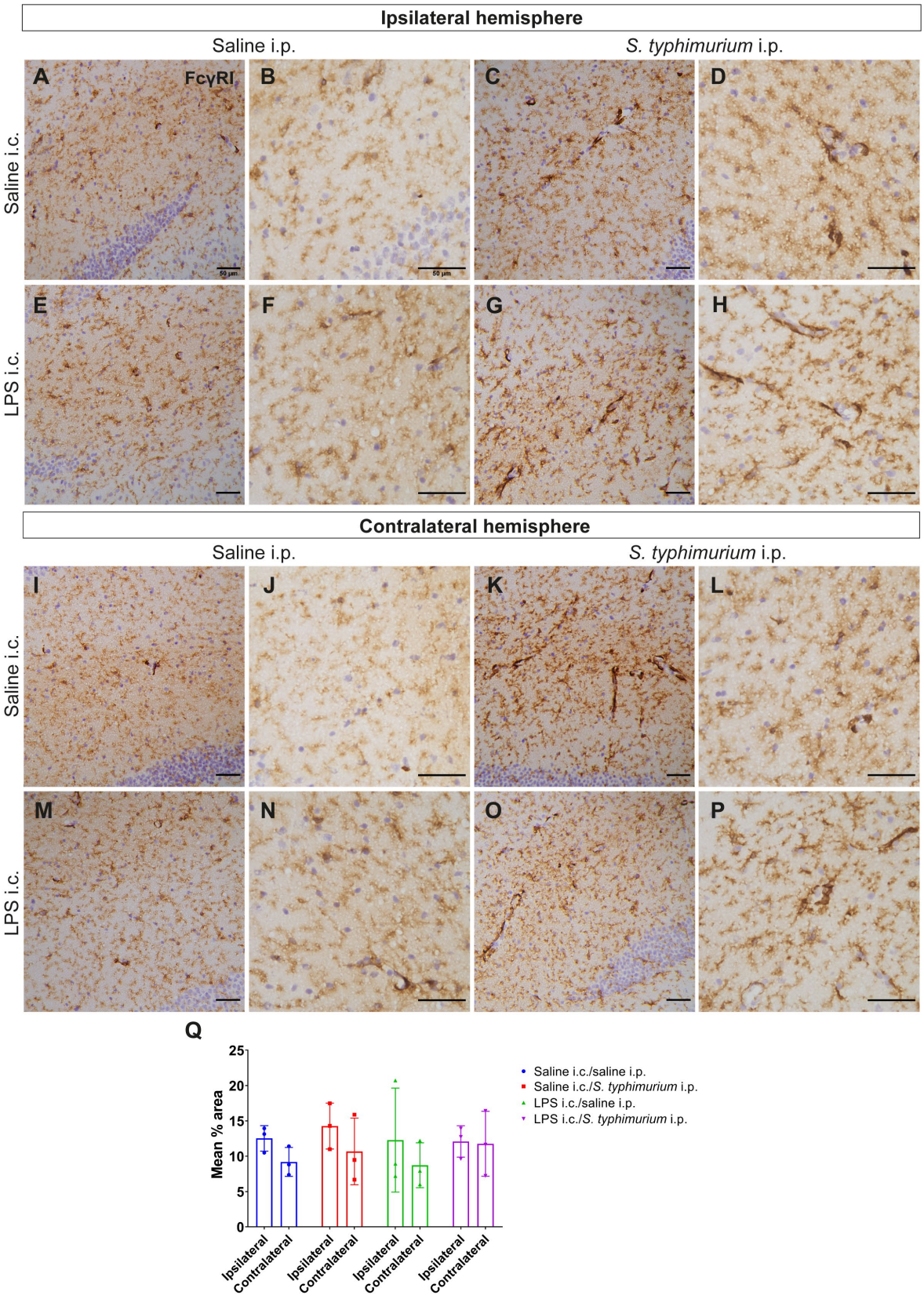
Ipsilateral hemisphere
Saline i.p.
S. typhimurium i.p.
Saline i.c.
LPS i.c.
A
FcγRI
B
C
D
E
F
G
H
Contralateral hemisphere
Saline i.p.
S. typhimurium i.p.
Saline i.c.
LPS i.c.
I
J
K
L
M
N
O
P
Q
Mean % area
25
20
15
10
5
0
Ipsilateral
Contralateral
Saline i.c./saline i.p.
Saline i.c./S. typhimurium i.p.
LPS i.c./saline i.p.
LPS i.c./S. typhimurium i.p.

Figure 4-8: Expression of FcγRI following LPS and *S. typhimurium* injection

A-H) FcγRI expression in the ipsilateral hemisphere of mice which had received **(A, B)** saline i.c./saline i.p. or **(C, D)** saline i.c./*S. typhimurium* i.p. injection. FcγRI expression in the ipsilateral hemisphere of **(E, F)** LPS i.c./saline i.p. or **(G, H)** LPS i.c./*S. typhimurium* i.p. injection groups. **I-P)** Contralateral hemisphere images of the same injection groups which had received **(I, J)** saline i.c./saline i.p. or **(K, L)** saline i.c./*S. typhimurium* i.p. injection. FcγRI expression in the contralateral hemisphere of **(M, N)** LPS i.c./saline i.p. or **(O, P)** LPS i.c./*S. typhimurium* i.p. injection groups. **A, C, E, G, I, K, M, O)** Images taken with 20x objective, scale bar= 50μm for all images. **B, D, F, H, J, L, N, P)** Images taken using 40x objective, scale bar= 50μm for all images. **Q)** Mean % area analysis at hippocampal fissure. n= 3 for all groups. Three-way ANOVA with Tukey's post-hoc test. All data is presented as mean ±SEM.

4.4 Discussion

4.4.1 Variability in peripheral changes following LPS and *S. typhimurium* injection

The primary aim of this experiment was to determine to what extent prior inflammatory insults can alter the central response to a systemic infection. Microglial priming and tolerance can significantly alter the immune cell environment within the brain. Tolerance refers to a reduction in microglial activation due to repeated exposure to endotoxin such as LPS and activation of the TLR4 pathway. This appears highly dependent on the serotype and dosing schedule of LPS injections. Priming refers to microglia which upon secondary insult mount an inflammatory response much greater than observed without the initial insult. (Neher and Cunningham, 2019).

It has been previously reported that even one LPS i.p. injection (1mg/kg) induced deficits in memory through the T maze and reduced IL-1β *in vivo* (Schaafsma *et al.*, 2015). A similar study used APP23 transgenic mice and i.p. injections of LPS (500μg/kg) daily for four days. Mice which received one LPS i.p. injection showed a significantly increased number of plaques, whereas the aforementioned repeated LPS group showed a reduction in plaque number (Wendeln *et al.*, 2018). Both of these papers show changes in histones, highlighting how tolerance is linked to epigenetic changes. By contrast, one i.p. injection of *S. typhimurium* leads to IL-1β and IL-12 cytokine production in the brain which slowly increased over three weeks (Püntener *et al.*, 2012) showing no signs of tolerance.

The initial aim was to examine the effects of saline and LPS through intracerebral injection. Injection of LPS into the cerebrum induced an acute inflammatory response 24 hours later, shown by the localised expression of MHCII, CD11b and FcγRI (**Figure 4-1**). This experiment use *S.*

abortus equi LPS serotype, previously used by our lab in the aforementioned study (Püntener *et al.*, 2012). This study injected mice with 1µl of 100pg/1µl LPS, however these mice had an existing *S. typhimurium* infection. For this chapter, an i.c. injection of 1µl at 0.5mg/ml of the *S. abortus equi* LPS serotype was decided as this should induce an acute inflammatory response resolved within days. If the response to the LPS injection is resolved quickly then the effect of systemic infection one week later could be observed and the effects of these two interventions teased apart. Comparing an acute and resolved inflammatory response versus the slow build-up of cytotoxic aggregated protein is important for future study into the interaction of neurodegeneration and systemic infection.

Following intracerebral injection of LPS, mice lost a significant amount of weight compared to saline mice within the first 24 hours (**Figure 4-4**). However, this significance was lost two days post-injection. By contrast, *S. typhimurium* injection caused a significant main effect of weight loss regardless of previous i.c. injection, with the majority of mice still not returned to baseline weight by the time of perfusion seven days later. Due to the use of a three-way repeated measures ANOVA, significance was not shown in the post-hoc tests and likely underpowered. Based on the weight loss data, a power calculation suggested a sample size of 5 mice per group would be sufficient (α= 0.05, power= 90%). Despite this, the significant main effect of *S. typhimurium* and the significant interaction with time supports the conclusion that the infection was the predominant factor in weight loss observed, with i.c. injection having no effect. This suggests that the mice had recovered from their LPS infection and supports the hypothesis that an acute inflammatory response is resolved. The mice do show a mild dampened response in MHCII expression, possibly due to some degree of tolerance in the microglia.

One previous study has examined the peripheral effects of *S. typhimurium* following prior LPS injection. Lehner *et al.* (2001) injected BALB/c mice with *S. abortus equi* LPS i.p. at 1mg/kg daily for three days prior to systemic infection. Following LPS injection, an i.p. injection (10^7 bacteria/kg body weight) of *S. Typhimurium* LT2 strain was administered. Three hours post-*S. typhimurium* i.p. injection, the mice which had previously undergone LPS i.p. injection showed significant reduction in TNFα and IL-6 in the spleen, plasma and liver compared to mice which had only undergone i.p. injection of *S. typhimurium* (Lehner *et al.*, 2001). This suggests that injection of LPS is sufficient to induce cytokine tolerance in the peripheral organs.

In this chapter no effect of LPS on splenomegaly or weight change was observed after *S. typhimurium* injection. Had a peripheral or repeated dose of LPS been administered, tolerance may have been observed. However, this is unlikely given the mechanism behind splenomegaly and the importance of the adaptive immune system. In this experiment *S. typhimurium* was

injected i.p. one week-post LPS. Due to the observable weight recovery (**Figure 4-4**) in the mice, this suggests that there was enough time provided between interventions for the immune response to LPS, to be predominantly mitigated before *S. typhimurium*. Therefore, administering a single i.c. injection of LPS and waiting to give *S. typhimurium* i.p. suggests that a resolved acute inflammatory response within the brain does not affect the adaptive immune response in the periphery.

4.4.2 LPS induces tolerance of MHCII expression following *S. typhimurium*

Having established the effects of LPS and *S. typhimurium* injection on body weight and spleen weight, inflammatory markers within the brain were subsequently examined. This study demonstrated that MHCII, CD11b and FcγRI-positive staining is clearly visible along the needle tract and so likely upregulated in macrophages 24 hours post-i.c. injection of LPS (**Figure 4-2**). Further reports show that CD11c is significantly upregulated five days post-intracerebral injection of LPS (4µg *E. coli* LPS in 3µl of saline injected) (Roy *et al.*, 2006). This is a much higher dose than administered in this study, however it does suggest that infiltration of circulating monocytes occurs following intracerebral injection of LPS. To what extent this is resolved prior to the *S. typhimurium* injection is unclear. Therefore, it is possible that the infiltration of peripheral immune cells and subsequent activation of classical antigen presenting cells alter immune markers within the brain.

MHCII expression was significantly upregulated after systemic infection, with a significant main effect of *S. typhimurium* i.p. injection observed (**Figure 4-5**). MHCII expression in the saline i.c./*S. typhimurium* ip. group was significantly higher than in both the saline i.c./saline i.p. and LPS i.c./saline i.p. groups. However, the LPS i.c./*S. typhimurium* i.p. group did not show significantly upregulated MHCII expression compared to either saline i.p. group. This data suggests that a single LPS injection may be adequate to induce tolerance in microglial populations during a subsequent systemic infection if sufficiently powered. This was noted in both the ipsilateral hemisphere and contralateral hemisphere, suggesting this effect is not restricted to the injection site. However, there was no significant difference between the groups which received systemic infection and so to make further conclusions would require greater investigation with a more highly powered experiment.

Within the hippocampal fissure, a highly vascularised area of the parenchyma, MHCII expression is localised to the cerebral vasculature in mice injected with *S. typhimurium* regardless of i.c. injection. It is proposed that expression of MHCII is induced by IFNγ and is expressed within the vascular endothelial network to act upon effector memory T cells. However, without the

presence of activation markers such as CD86, it is unlikely that long-term recruitment of $CD4^+$ T-cells is occurring through vascular endothelial cell expression of MHCII (Pober *et al.*, 2017). To what extent MHCII expression in the endothelial cells is capable of activating T-cell recruitment is unclear; it would be necessary to examine whether markers of T cells are expressed within the parenchyma.

4.4.3 CD11b and FcγRI following LPS and *S. typhimurium* injection

Inflammatory markers CD11b and FcγRI were also stained for, due to their role in the immediate microglial response. CD11b expression was previously examined after *S. typhimurium* injection at one day, one week and three weeks post-injection (Püntener *et al.*, 2012). CD11b expression appeared to increase at three weeks post-injection, and it is possible that one-week post-*S. typhimurium* injection is too premature to observe enough difference. In this chapter CD11b expression showed a significant main effect of i.c. injection (**Figure 4-7**). The groups which had received LPS i.c. injection showed significant upregulation of CD11b in the ipsilateral hemisphere both in relation to contralateral hemisphere and compared to the saline i.c. groups (regardless of i.p. injection). Previous studies have shown that the TLR4 pathway increases CD11b expression *in vitro* (Zhou *et al.*, 2005). This suggests that one-week post-injection may be too early to observe the effects of *S. typhimurium* on CD11b.

In AD post-mortem cases, CD11b expression did not correlate with Braak stages (Sanchez-Mejias *et al.*, 2016). Therefore, CD11b may not be the most suitable marker if it is not possible to detect changes following the induction of tau pathology. However, it must be considered that there is a high degree of variability in findings amongst these papers; post-mortem delay, co-morbidities and ongoing systemic infections during the time of death may all significantly alter CD11b expression within the brain.

In this chapter, FcγRI expression showed minimal change after either i.c. or i.p. injection (**Figure 4-8**) with only a significant main effect of hemisphere. This is likely due to only looking at one-week post-infection, especially when considering the results in Chapter 3 concerning FcγRI expression. By comparison to CD11b, FcγRI has been shown to be upregulated in AD post-mortem tissue compared to healthy control tissue (Rakic *et al.*, 2018). In those cases where the patient had died with systemic infection such as bronchopneumonia or urinary tract infection, FcγRI showed further upregulation in histology compared to those cases with AD but no systemic infection (Rakic *et al.*, 2018). Considering the results observed in Chapter 3, this potentially makes it a preferable marker to CD11b for this study. Furthermore, prioritising FcγRI as a marker gives capacity to examine IgG in depth, for investigation into BBB integrity.

4.4.4 Conclusions and future directions

This experiment establishes that there are peripheral changes such as weight loss following LPS i.c. injection but these can be quickly resolved and have no effect on *S. typhimurium*-induced changes. MHCII expression is increased by systemic infection, yet TLR4-activated tolerance of may occur from one LPS intracerebral injection. This is not observed with CD11b whereby the LPS injection is the main determinant of CD11b expression and no tolerance is observed. FcγRI shows no significant change in expression within any group. These results allow us to conclude that one-week post-injection is likely too early, and four weeks is the most suitable time point to observe the effect of *S. typhimurium* infection on inflammatory markers in the brain. The primary limitation of this study is the group size, n= 3 across all groups may prevent biological effects from becoming statistically significant. Therefore, these results are a glimpse into the effects of LPS and *S. typhimurium* and how the two interact.

There are distinct differences between LPS and AD-tau. The injection of tau lysate isolated from AD post-mortem tissue is unlikely to induce tolerance due to the nature of the Sarkosyl-insoluble lysate and the subsequent inflammatory response. Aggregated, HMW tau cannot be resolved as easily as LPS. This instead points to the overarching hypothesis; an increasingly cytotoxic environment where protein cannot be degraded will only be worsened by the presence of systemic infection. If the protein cannot be degraded, then the microglial profile cannot be resolved, and so priming is the natural conclusion. This remains to be determined in subsequent chapters.

Future aims:

- *To isolate AD-tau from post-mortem AD tissue and enrich for HMW tau*
- *To establish a tau spreading model using a mouse model expressing human tau*
- *To determine if systemic infection alters the rate of tau spreading in vivo*

Chapter 5 Generating a lysate enriched for high molecular weight AD-tau

5.1 Introduction

The results from Chapter 3 have established the infection response to *S. typhimurium* in C57BL/6 and H1*Mapt-/-* mice. Subsequently, Chapter 4 has shown that allowing four weeks post-*S. typhimurium* injection before collection of tissue allows establishment of low-grade infection. Furthermore, that dependent upon whether saline or LPS is injected intracerebrally, there may be a variability in response following *S. typhimurium*. A remaining question is whether i.c. injection of tau will cause spread of pathology through the brain, and whether systemic infection will promote the rate of spread. The hypothesis of this thesis states that injection of lysate enriched for AT8-positive tau will induce propagation of tau pathology; this will be exacerbated by *S. typhimurium* injection. Chapter 6 examines the spread of pathology whilst immune markers are examined in Chapter 7, to determine how both the i.c. injection of pathological tau and *S. typhimurium* affect microglial populations.

In order to test the hypothesis, it is essential to generate a 'seed prep'. The 'seed prep' is a lysate enriched for HMW tau which is predominantly AT8-positive. AT8-positive tau has previously been shown to have the highest seeding capacity, through a spreading model which intracerebrally injected different tau lysate fractions separated along a sucrose gradient (Jackson *et al.*, 2016). This study used the P301S mouse model, however recent studies have injected tau from human post-mortem cases of dementia into wild-type mice. For example, one study injected lysate from varying tauopathies such as PSP, CBD and AD into the brains of ALZ17 mice which express wild-type human tau and observed differences in the seeding capacity (Clavaguera *et al.*, 2013). This study concluded that it was possible to echo the tau pathology observed in the human disease within the mouse brain, simply just by injection of lysate enriched for said pathology. This highlighted the importance of tau conformation. Therefore, utilising lysate from AD post-mortem tissue should enable us to recapitulate the spreading observed in AD itself. Validation of the seed prep generation should be confirmed by high levels of AT8-positive HMW tau. As this study will only last three months, in order to induce significant pathology deposition, it would be advantageous to inject tau that possesses high seeding capacity.

Aims addressed in this chapter are as follows:

- *To isolate and compare the tau burden across ten human AD post-mortem cases*
- *To process the three cases with highest tau burden for a 'seed prep' enriched for HMW tau*
- *To confirm that AT8-positive HMW tau can be detected in the seed prep*

5.2 Methods

5.2.1 Processing of post-mortem human AD tissue

In order to generate a lysate enriched for HMW tau, frozen post-mortem AD tissue was homogenised in DPBS. This is detailed fully in Chapter 2.5. **Figure 5-1** provides an overview of the process and how the subsequent supernatant (S), pellets (P) and Sarkosyl fractions are referred to within the chapter.

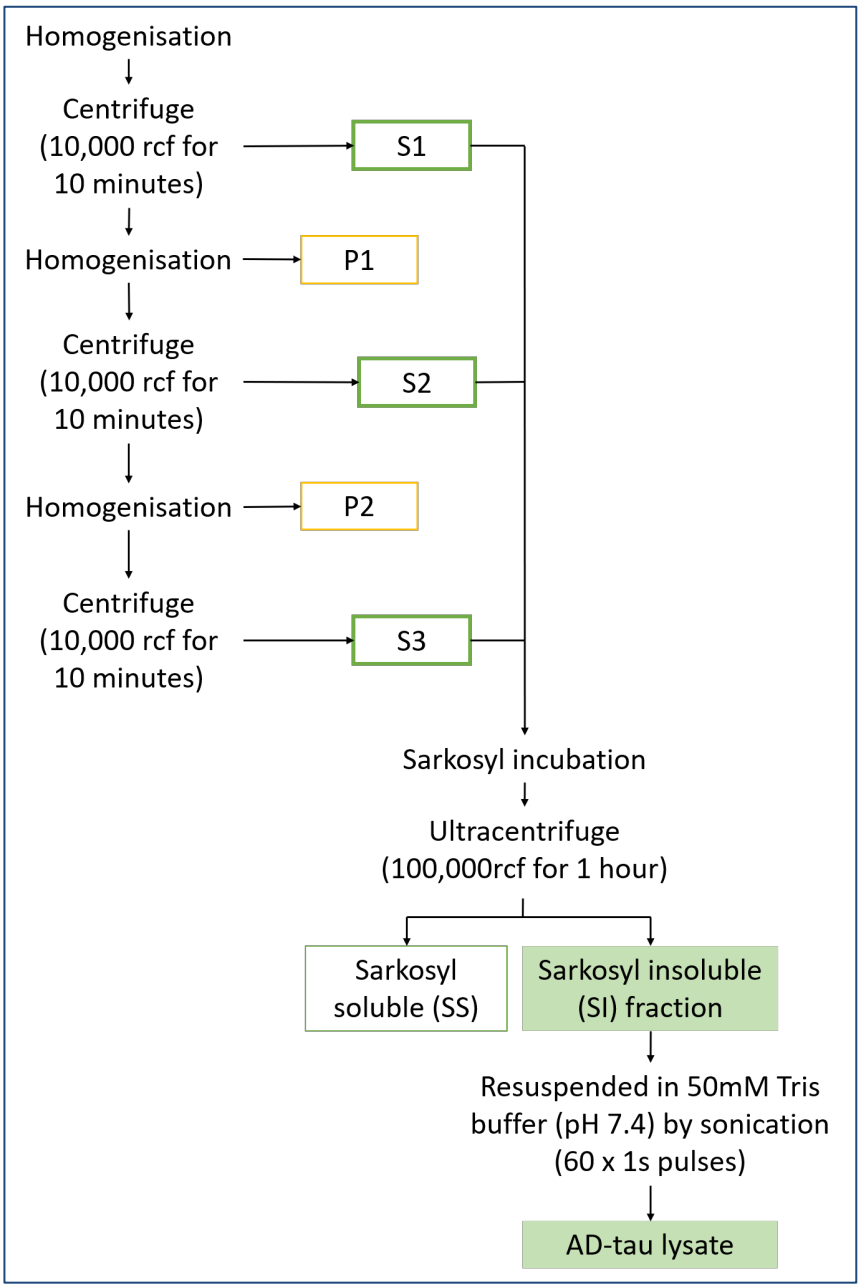

Figure 5-1: Overview of tissue processing to generate Sarkosyl-insoluble fraction

This diagram depicts the sequential homogenisation and centrifugation steps to generate supernatant 1-3 (S1-3) and the associated pellets (P1-P2). The pooled S1-3 then allows for Sarkosyl incubation and subsequent ultracentrifugation.

5.3 Results

5.3.1 Comparison of AT8 positive tau across ten post-mortem AD cases

The initial step in generating the AD 'seed prep' was to determine which case had the highest AT8 signal and AT8 to total tau signal ratio. Ten separate post-mortem cases were selected by the South West Dementia Brain Bank (SWDBB), with 10g of frontal cortex tissue from each case used for detection of tau pathology. All ten cases were confirmed to be Braak stages V-VI in the frontal cortex; with a primary diagnosis of AD for each case observed in **Table 5-1**. Secondary and tertiary diagnoses are included for each case. It is possible to observe there is variability in age, gender and post-mortem delay. The comorbidities of each case were noted yet because the intention is to homogenise the tissue and enrich for aggregated forms of tau, these criteria are not crucial determining factors. Nonetheless, potential of confounding factors are discussed later in this chapter.

Table 5-1: Diagnosis of separate post-mortem AD cases

Chapter No.	Case No.	MRC ID	Age	Sex	Post-mortem delay (h)	Primary diagnosis	Secondary diagnosis	Tertiary diagnosis
1	859	BBN_4238	85	F	14	AD	CVD	CAA
2	903	BBN_10252	89	F	22	AD	VaD	TDP43 pathology
3	912	BBN_14405	82	F	22	AD	Hippocampal sclerosis	TDP43 pathology
4	935	BBN_19632	91	M	43	AD	Hippocampal sclerosis	TDP43 pathology, CVD
5	959	BBN_24327	74	M	16	AD	CVD	LBD (amygdala only)
6	962	BBN_24330	80	F	14.5	AD	CAA	VaD
7	966	BBN_24334	82	M	61	AD	CAA, CVD	LBD and TDP43 pathology (amygdala only)
8	982	BBN_24898	76	M	47.5	AD	CAA	DLB
9	1027	BBN006.28978	72	M	81.5	AD	DLB	CAA, TDP43 pathology
10	1033	BBN006.29162	81	M	7.5	AD	DLB	CAA, TDP43 pathology

AD= Alzheimer's disease, CVD= Cardiovascular disease, VaD= Vascular dementia, CAA= Cerebral amyloid angiopathy, DLB= Dementia with Lewy bodies, LBD= Lewy Body Dementia, TDP43= TAR DNA-binding protein 43

A small-scale homogenisation was used to run a pilot test of this protocol. I utilised 0.5g of tissue from each case and homogenised at 10% weight per volume in DPBS. Complete protease and phosphatase inhibitor cocktails were added to the DPBS to prevent degradation of the protein and phosphorylated tau epitopes respectively. Following the first centrifugation the crude homogenisation (S1) was used to determine the initial tau burden present in each of the 10 cases. An overview of the homogenisation protocol, first detailed in Chapter 2, can be further referred to in **Figure 5-1**.

An initial western blot was carried out to stain for total tau and AT8 to see if phosphorylated tau could be observed in 0.5g of tissue (**Figure 5-2**). The amount of protein loaded for each sample was not normalised; the BCA results can be referred to in Appendix A (Table S1). This was deliberate, to avoid normalisation of high tau burden within the crude homogenisation. Furthermore, total tau detection will allow the generation of an AT8/total tau

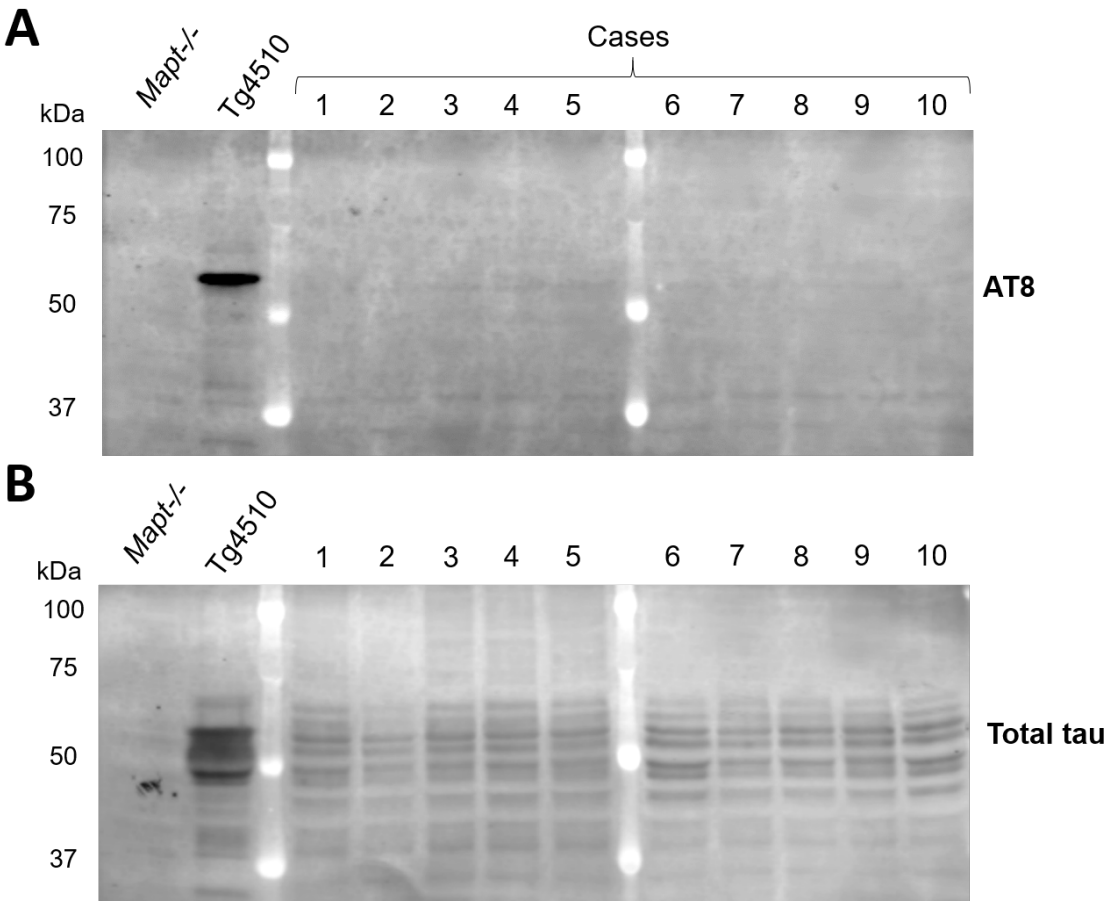

Figure 5-2: Western blot depicting AT8 and total tau in 0.5g tissue crude prep

A) AT8 detection at 50-64kDa and **B)** Total tau where six clear bands are visible. 15µl of lysate and 5µl of 4x sample buffer were loaded per sample into each well. *Mapt-/-* and Tg4510 lysate was included as a negative and positive control respectively. The ladder is shown in white.

ratio, detailing which case has the highest signal of hyperphosphorylated tau as a percentage of total available tau. Total tau is clearly visible with a mix of isoforms in all 10 cases (**Figure 5-2**). However, likely due to the low volume, the western blot was not sensitive enough to detect levels of AT8 only using 0.5g of tissue. The single isoform overexpressed in Tg4510 is visible due to the presence of hyperphosphorylated AT8 epitopes. Due to confirmation of protein within the sample, it was decided a dot blot may allow accommodation for the small levels of AT8 present within the sample.

Subsequently a dot blot was carried out using the same neat samples from the crude homogenisation (S1). From there it was possible to compare the relative presence of AT8-positive tau (**Figure 5-3**). Again, Tg4510 and *Mapt-/-* samples were included as positive and negative controls respectively. **Figure 5-2** confirms that the *Mapt-/-* lysate contains neither total tau nor AT8-positive signal. However, because the protein is stacked within a dot blot, background must be accounted for. Therefore, quantification of dot blot results were carried out by subtracting the *Mapt-/-* signal from all cases.

From the dot blot it was apparent that cases 6, 7 and 8 had the highest AT8 signal, with case 7 showing highest AT8 detection. When examining the total tau signal, case 6 showed low total tau signal, yet cases 7 and 8 were situated within the middle of the group. Therefore case 6 had the highest AT8/total tau ratio, yet all cases 6, 7 and 8 were within the top four of the AT8/Total Tau ratios. Case 10 had the fourth highest AT8 signal, yet a low AT8/total tau ratio due to its very high total tau signal. The total protein concentration for all cases ranged from 1.4-2.6mg/ml and case 10 had a protein concentration of 2.3mg/ml, this was deemed unsuitable as the results are likely due to protein load. Case 9 had a high AT8/total tau ratio, yet due to the very low total tau detection, this case was removed from consideration. Confirmed by the BCA assay, case 9 had the lowest protein concentration at 1.4mg/ml. Therefore, even if there is a high AT8/total tau ratio, with a low protein concentration this may still lead to inadequate enrichment of aggregated tau. Despite the low total tau detection in case 6, this case showed the second highest AT8 signal and therefore is an excellent candidate for the final 'seed prep'. Given the high AT8/total tau ratios and adequate total protein concentration (1.7-1.9mg/ml), these three cases (6, 7 and 8) were deemed the most suitable. Comparison between the total tau detection measured in western blot and dot blot showed a non-significant trend ($F(1, 8)= 5.29$, $p= 0.0505$). The three selected cases are highlighted to show that cases 7 and 8 are consistent to the trendline, although case 6 is further from the trendline. The decision to choose these cases is therefore supported by the initial western blot and dot blot results.

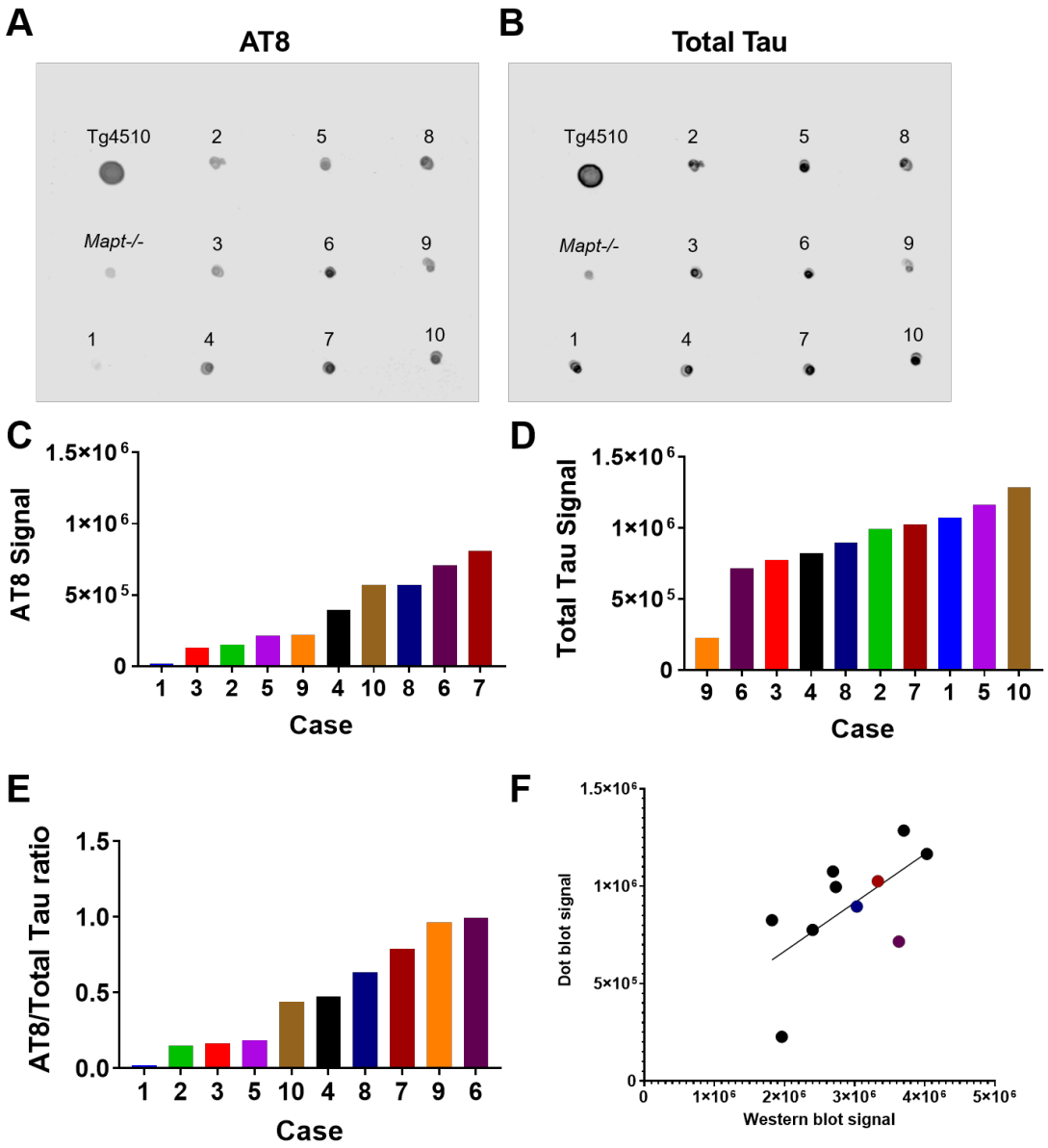

Figure 5-3: Dot blot comparing AT8 signal across ten AD post-mortem cases

A) AT8-positive tau in ten post-mortem cases using dot blot. 1µl of neat lysate added to blot from each sample. **B)** Blot depicting total tau. **C)** Graph comparing relative AT8 signal. **D)** Graph depicting relative total tau signal. **E)** Graph comparing the AT8 to total tau ratio for each post-mortem case. **F)** Linear regression comparing the total tau signal from a western blot and dot blot; R= 0.4.

5.3.2 Confirmation of chosen cases through histology

Pathology images from the SWDBB were then requested from the three cases. The SWDBB had taken slices of the dorsolateral prefrontal cortex and stained for AT8 at both high and low magnification (**Figure 5-4**). Cases 6, 7 and 8 all showed substantial AT8-positive inclusions, confirming the presence of AT8-positive tau pathology within the chosen cases. These images confirm that there is high tau burden in the area selected for homogenisation. Notably, case 7 showed visibly higher expression of AT8 than the other two cases. In the crude prep analysis, case 7 had the highest expression of AT8. This further supports the decision to proceed with cases 6, 7 and 8 for the generation of the final 'seed prep'.

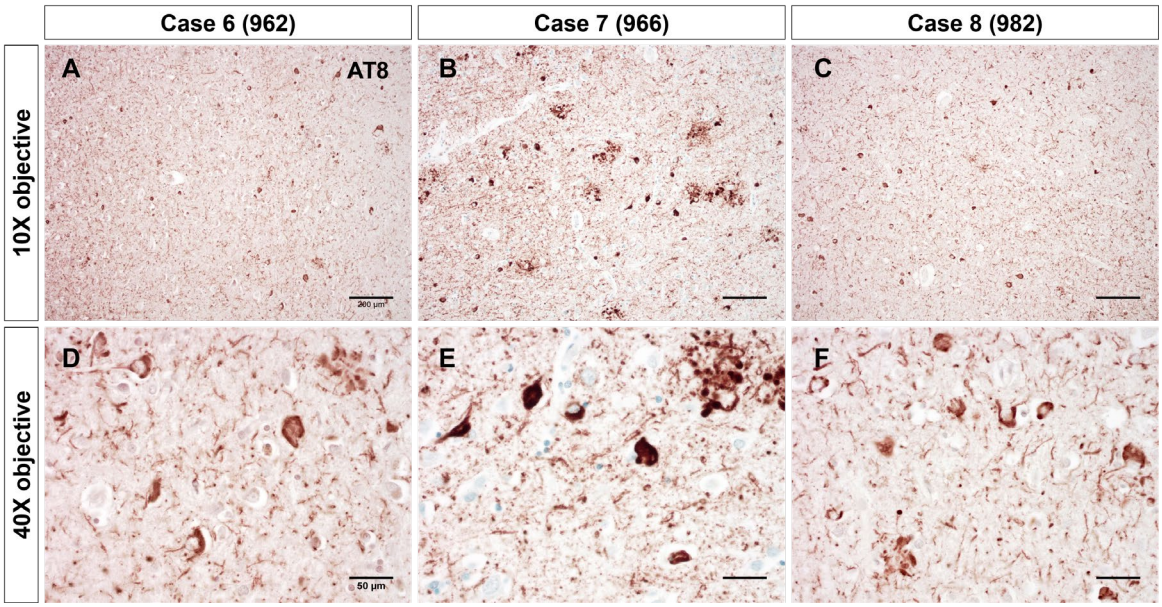

Figure 5-4: Histological confirmation of tau burden

A-C) AT8 (Sigma) positive staining at 10x objective of dorsolateral prefrontal cortex in cases **A)** 6, **B)** 7 and **C)** 8. **A-C)** 10x objective; scale bar= 200µm. **D-F)** AT8 staining at 40x objective in cases **D)** 6, **E)** 7 and **F)** 8. **D-F)** 40x objective; scale bar= 50µm. Tissue processing, histology and images taken by SWDBB. SWDBB case number in brackets.

5.3.3 Generation of the final seed prep

Following on from confirmation of the dot blot, homogenisation of 10g of tissue was carried out to confirm this protocol was successful on a large scale. As case 3 had the lowest signal of AT8, this case was chosen and all 10g of this tissue was processed as a pilot test. This involved homogenising the tissue at 10% weight/volume and subsequent low-speed centrifugation; this method was then repeated twice more. The three supernatants (S1, S2 and S3) were then pooled

and incubated in 1% Sarkosyl for one hour (**Figure 5-1**). Following incubation, the lysate was centrifuged at 100,000rcf for one hour. Afterwards, the Sarkosyl-soluble lysate was removed. The Sarkosyl-insoluble pellet was washed and reconstituted in 50mM Tris using sonication. The Sarkosyl-insoluble fraction was then run in a western blot along with all stages of supernatant and pellet.

Prior to this, the initial 0.5g tissue from case 3 which underwent the crude prep (generation of S1) was also processed through the full protocol in **Figure 5-1**. The 10g Case 3 seed prep was run alongside the 0.5g Case 3 seed prep to allow for comparison. Tg4510 and *Mapt-/-* samples were included again as positive and negative controls (**Figure 5-5**). Both the 0.5g and 10g preps run in a single western blot showed total tau present in the first supernatant and pellet. Total tau signal markedly decreases in the second supernatant and pellet as the homogenate moves through homogenisation and centrifugation steps. Total tau signal is found in both Sarkosyl-soluble and Sarkosyl-insoluble fractions. The Sarkosyl-insoluble fraction showed greater total tau enrichment than the Sarkosyl-soluble fraction. This is to be expected as this lysate will be specifically enriched for aggregated tau, therefore even though the AT8/total tau ratio will be greater in the SI fraction it will still contain greater total tau than the Sarkosyl-soluble fraction.

AT8 (pSer202 and pThr205)-positive tau is denoted by a single isoform in the Tg4510 lysate. No samples of the 0.5g seed prep show AT8-positive tau, this confirms that a western blot is not sensitive enough to detect hyperphosphorylation when a sample this small is used. However, when examining the 10g seed prep, there are clear AT8-positive bands in both repeats of the Sarkosyl-insoluble fraction (the same lysate was loaded twice to account for potential technical issues). PHF-1 epitopes (pSer396-Ser404) show a very similar detection level, also only present in the Sarkosyl-insoluble fractions. This confirms that if 10g of tissue is used, it is possible to visualise the enrichment of the lysate for hyperphosphorylated tau.

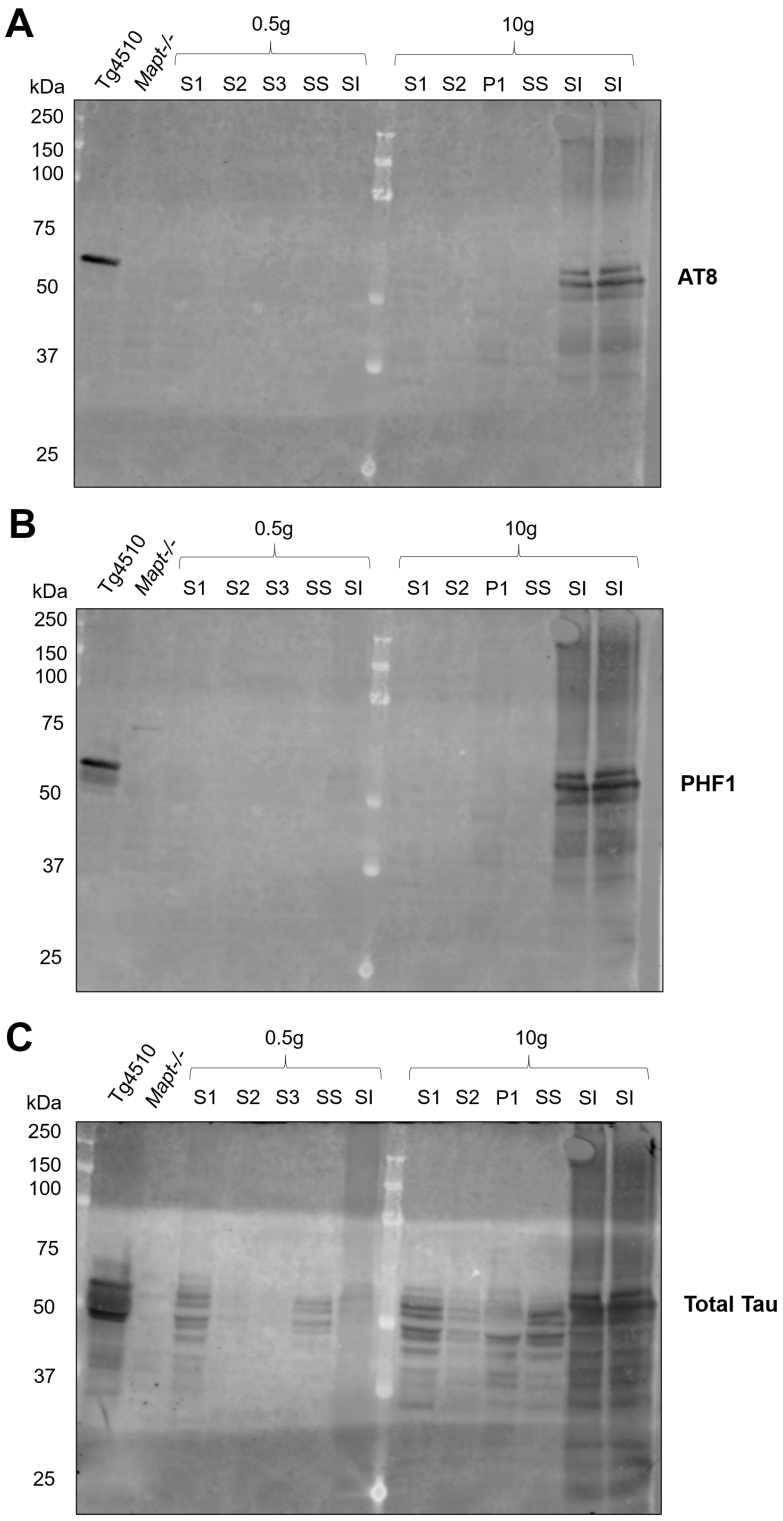

Figure 5-5: Western blot of 0.5g and 10g seed prep

A) Western blot showing staining for AT8 for processing steps both in the 0.5g and 10g preparation of case 3. 15µl of lysate and 5µl of 4x sample buffer were loaded per sample into each well. **B)** PHF1 staining for the seed prep carried out using case 3, both 0.5g and 10g **C)** Western blot showing total tau detection. S1= 1st supernatant, S2= 2nd supernatant, S3= 3rd supernatant, P1= 1st pellet, P2= 2nd pellet, P3= 3rd pellet, SS= Sarkosyl-soluble, SI= Sarkosyl-insoluble.

Following this confirmation, the homogenisation and centrifugation steps were carried out with 30g of tissue for the final 'seed prep'. This consisted of 10g from cases 6, 7 and 8; all three cases were homogenised together with subsequent low-speed centrifugation and all three supernatants (S1-S3) were pooled. This lysate was incubated in 1% Sarkosyl for one hour and then centrifuged at 100,000rcf for one hour. Following reconstitution of the Sarkosyl-insoluble fraction and sonication, the western blot was run to stain for AT8, PHF-1 and total tau as before (**Figure 5-6**).

The 10g seed prep was included as an internal control, along with Tg4150 and *Mapt-/-* samples. Total tau was shown to have a similar result to the 10g seed prep. Total tau signal was strong in the initial supernatant and pellet, with detection slowly decreasing through the processing steps (S2-S3). Total tau was present in the Sarkosyl-soluble fraction and the Sarkosyl-insoluble fraction.

This confirms that the lack of signal in the 0.5g and 10g seed prep was likely due to the tissue sample being too small, as a result the low concentration of AT8-positive tau loaded in the well is undetectable. Notably, PHF-1 epitopes are detectable in the first supernatant of the 30g final seed prep. AT8 was not visible in the first supernatant, however this is likely due to the AT8 antibody being weaker in western blot and more commonly utilised in histology rather than epitope presence, so this is to be expected. However, AT8 is present in the Sarkosyl-insoluble fraction. This confirms that it is possible to enrich lysate for AT8-positive tau. PHF-1 was also present in the Sarkosyl-insoluble fraction. There is the issue of excess protein within the well. However, despite this it is clear to observe there is positive staining for HMW tau.

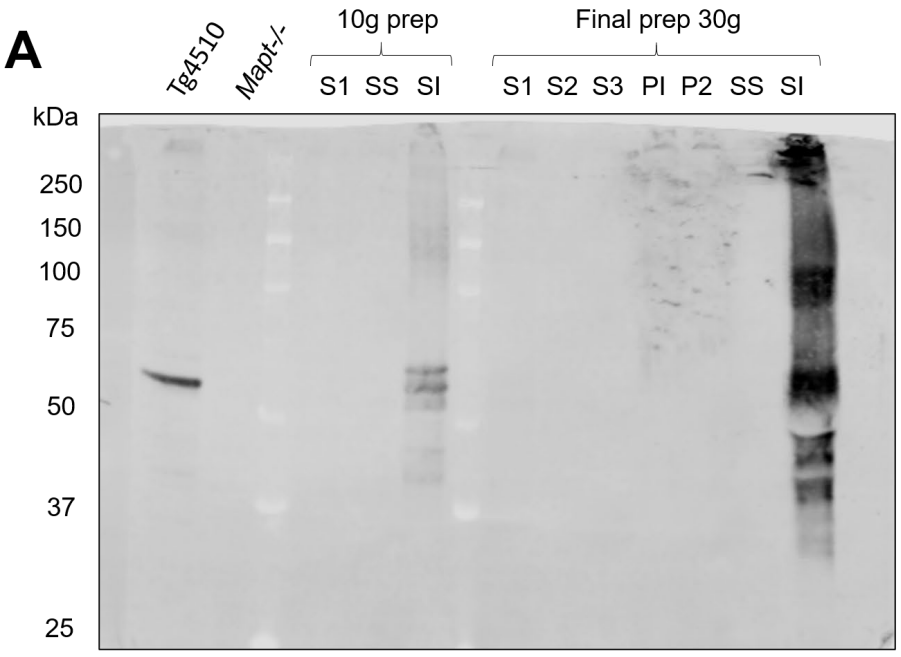
A
Tg4510
Mapt-/-
10g prep
Final prep 30g
S1 SS Sl
S1 S2 S3 Pl P2 SS Sl
kDa
250
150
100
75
50
37
25
AT8

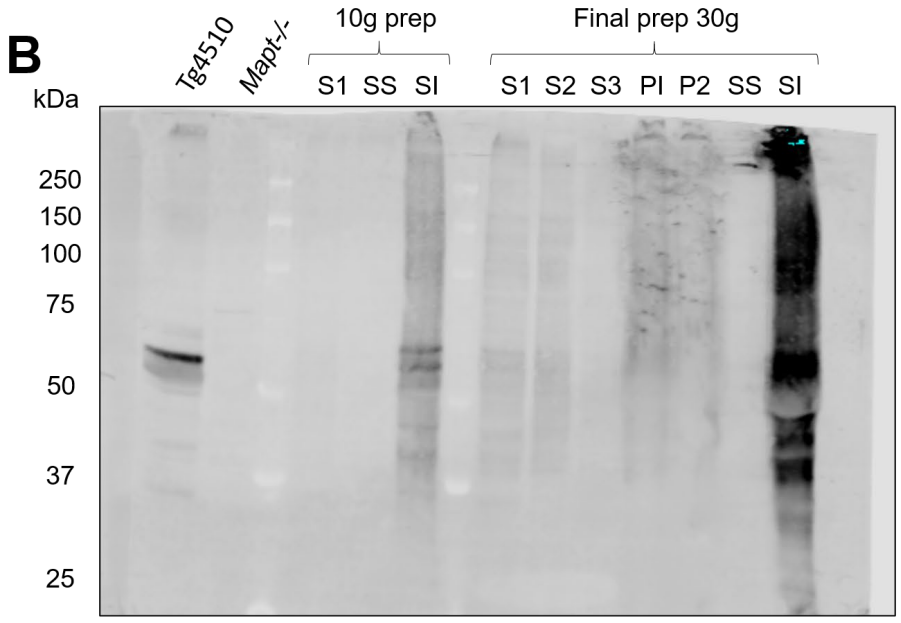
B
Tg4510
Mapt-/-
10g prep
Final prep 30g
S1 SS Sl
S1 S2 S3 Pl P2 SS Sl
kDa
250
150
100
75
50
37
25
PHF1

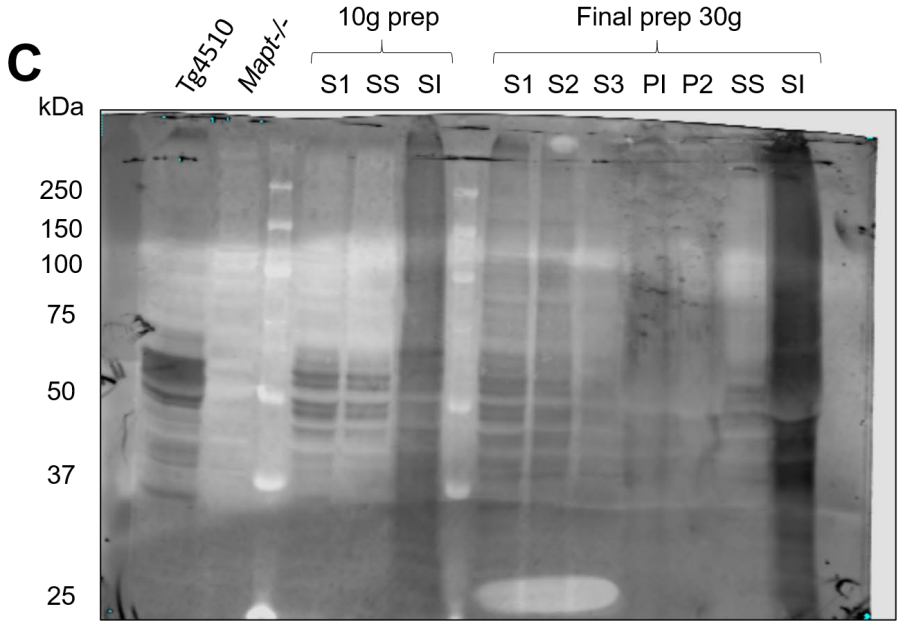
C
Tg4510
Mapt-/-
10g prep
Final prep 30g
S1 SS Sl
S1 S2 S3 Pl P2 SS Sl
kDa
250
150
100
75
50
37
25
Total Tau

Figure 5-6: Western blot of final 30g seed prep

A) Western blot showing AT8-positive tau in both the 10g prep of case 3 and the final 30g seed prep of cases 6, 7 and 8. 15µl of lysate and 5µl of 4x sample buffer were loaded per sample into each well. **B)** Western blot showing PHF1-positive tau in the 10g seed prep of case 3 and the final 30g seed prep of cases 6, 7 and 8. **C)** Total tau in the 10g pilot seed prep using case 3 as a comparison the final 30g seed prep from cases 6, 7 and 8. S1= 1st supernatant, S2= 2nd supernatant, S3= 3rd supernatant, P1= 1st pellet, P2= 2nd pellet, P3= 3rd pellet, SS= Sarkosyl-soluble, SI= Sarkosyl-insoluble.

AT8-positive tau was enriched in the 30g prep, especially compared to the 10g pilot. However, the protein concentration in the SI fraction resulted in staining at all molecular weights. Following this, I diluted the Sarkosyl-insoluble fraction (**Figure 5-7**). This was to determine whether reducing the protein volume would reduce any non-specific binding and reveal the bands associated with AT8-positive staining and the total tau isoforms. Dilutions were carried out and run within the same blot, prior to this all samples (S1-3, P1-2, SS and SI) have all been run neat with 4x sample buffer. Therefore the 75% dilution has the same protein load as all previous figures. Subsequent dilutions are listed in the figure legend.

It is possible to see that at 12.5% dilution AT8-positive bands are clearly visible. PHF-1 and total tau still are unclear at 12.5% dilution. This is likely due to the PHF-1 antibody binding to a much larger range of epitopes, rather than the two epitopes associated with AT8. Furthermore, the method states that for every 10g of initial tissue, the SI fraction is reconstituted in 50µl of Tris buffer (in the final seed prep 30g of tissue is reconstituted to 1,500µl of final lysate). Therefore, this lysate is highly enriched. These results highlight that this lysate contains AT8-positive tau and to detect the bands, dilution of the protein is required.

Following this result, a final western blot was carried out to demonstrate the AT8-positive tau in comparison to the supernatant and pellet samples (**Figure 5-8**). The Sarkosyl-insoluble fractions were diluted, dilutions are denoted in figure legend. The pellets were also diluted, this was due to the pellets being predominantly lipids and DNA with high viscosity which caused technical issues with SDS-PAGE. Whilst faint, it is possible to observe AT8-positive tau in the Sarkosyl-insoluble fraction (once again SI was repeated to ensure optimal running of the gel and avoid technical issues). AT8 is detected from 50 to ~64kDa, where the single Tg4510 isoform is detected. There is also visible AT8-positive tau at 100kDa and ~37kDa as the HMW and low molecular weight (LMW) tau respectively. When staining for total tau, there is a range of unfocused bands. This is likely multiple isoforms overlaid by varying phosphorylation states.

Crucially, it is possible to observe that there is HMW AT8-positive tau within the Sarkosyl-insoluble fraction which is the overarching aim of this chapter.

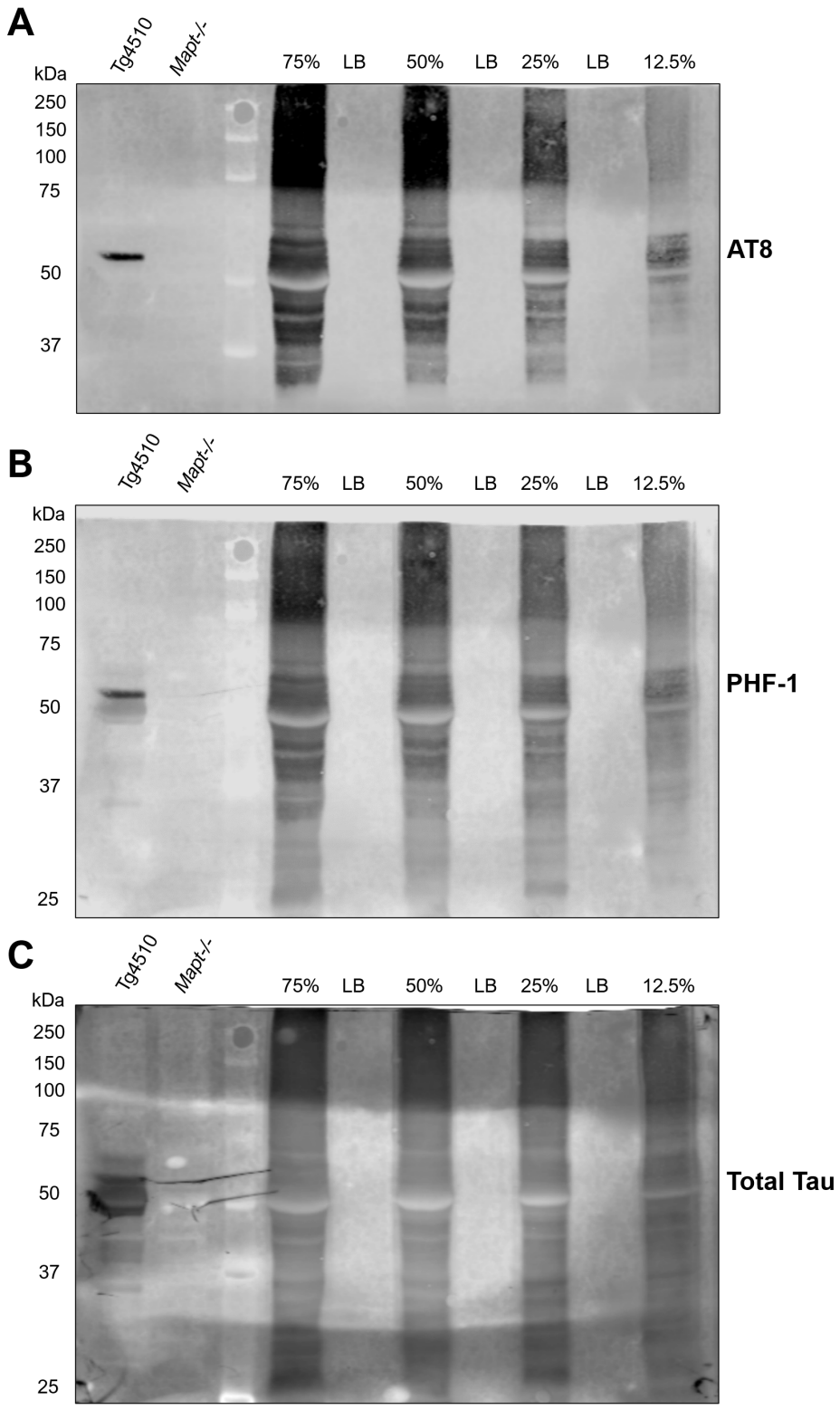

Figure 5-7: Titration of volume loaded for Sarkosyl-insoluble fraction

A) AT8-positive tau in the Sarkosyl-insoluble fraction titrated to observe the individual isoforms **B)** PHF1-positive tau in titrated Sarkosyl-insoluble fraction **C)** Western blot showing total tau and the titrated lanes of Sarkosyl-insoluble tau. The 75% dilution contains 15µl of lysate and 5µl of 4x sample buffer loaded into the well. 50%, 25% and 12.5% dilutions contain 10µl, 5µl and 2.5µl of lysate respectively diluted with dH_2O and 4x loading buffer to a total volume of 20µl per well.

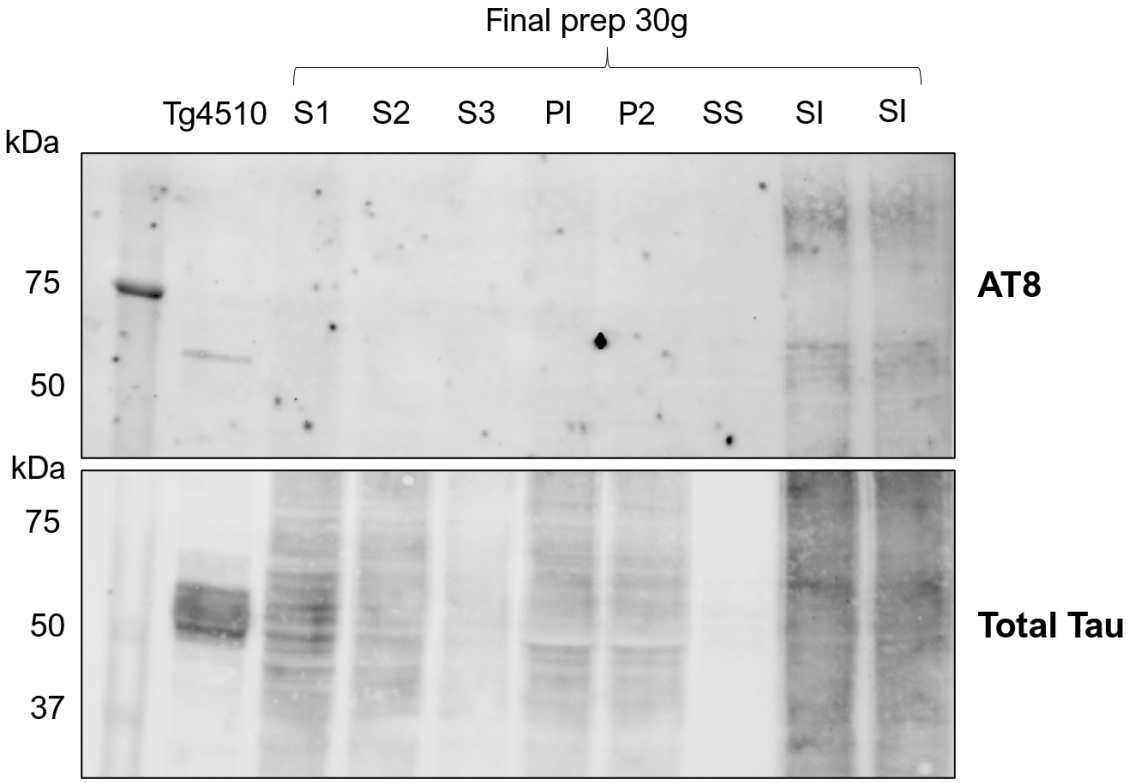

Figure 5-8: Final western blot showing AT8-positive Sarkosyl-insoluble fraction

AT8 and total tau in sequential supernatant and pellet samples. Sarkosyl-soluble and Sarkosyl-insoluble fractions showed detection of total tau and AT8 despite significant protein dilutions. For S1-S3 samples, 15µl of homogenate was used. For P1-P2 samples, 5µl of homogenate was used and for SS and SI fractions, 2µl of homogenate was included in each total 20µl volume. All samples were made up with 4x loading buffer and dH_20 for a total volume of 20µl loaded per well.

5.3.4 HTRF assay to confirm AT8-positive tau in biochemical analysis

Having established AT8-positive tau within the western blot, AT8-positive tau in the final 30g seed prep was quantified. In order to do this, a Homogenous Time Resolved Fluorescence (HTRF) assay was used. The HTRF assay is limited to showing AT8-positive tau within the Sarkosyl-insoluble fraction. This is due to a lack of a standard sample; pre-formed fibrils are normally used to establish a standard for tau concentration. Therefore, due to this experimental limitation the HTRF assay was used to examine the presence of AT8-positive tau. This particular kit detects phosphorylation of tau at the two AT8 epitopes (pSer202 and pThr205) and therefore will detect both soluble and insoluble tau. In this specific experiment the Sarkosyl-insoluble fraction was examined, however the presence of soluble AT8-positive tau cannot be ruled out through this test. The Sarkosyl-insoluble fraction showed clear signal, and despite an outlier there is a response to the serial dilutions (**Figure 5-9**). Neither the diluent control, antibody control or negative control showed any signal. Whilst this method requires further experiments with a

standard to allow quantification, it is possible to observe that there is a signal detected, suggesting that the Sarkosyl-insoluble fraction does have detectable levels of the AT8 epitopes. Therefore, I have been able to generate a lysate which has been enriched for seed-competent tau.

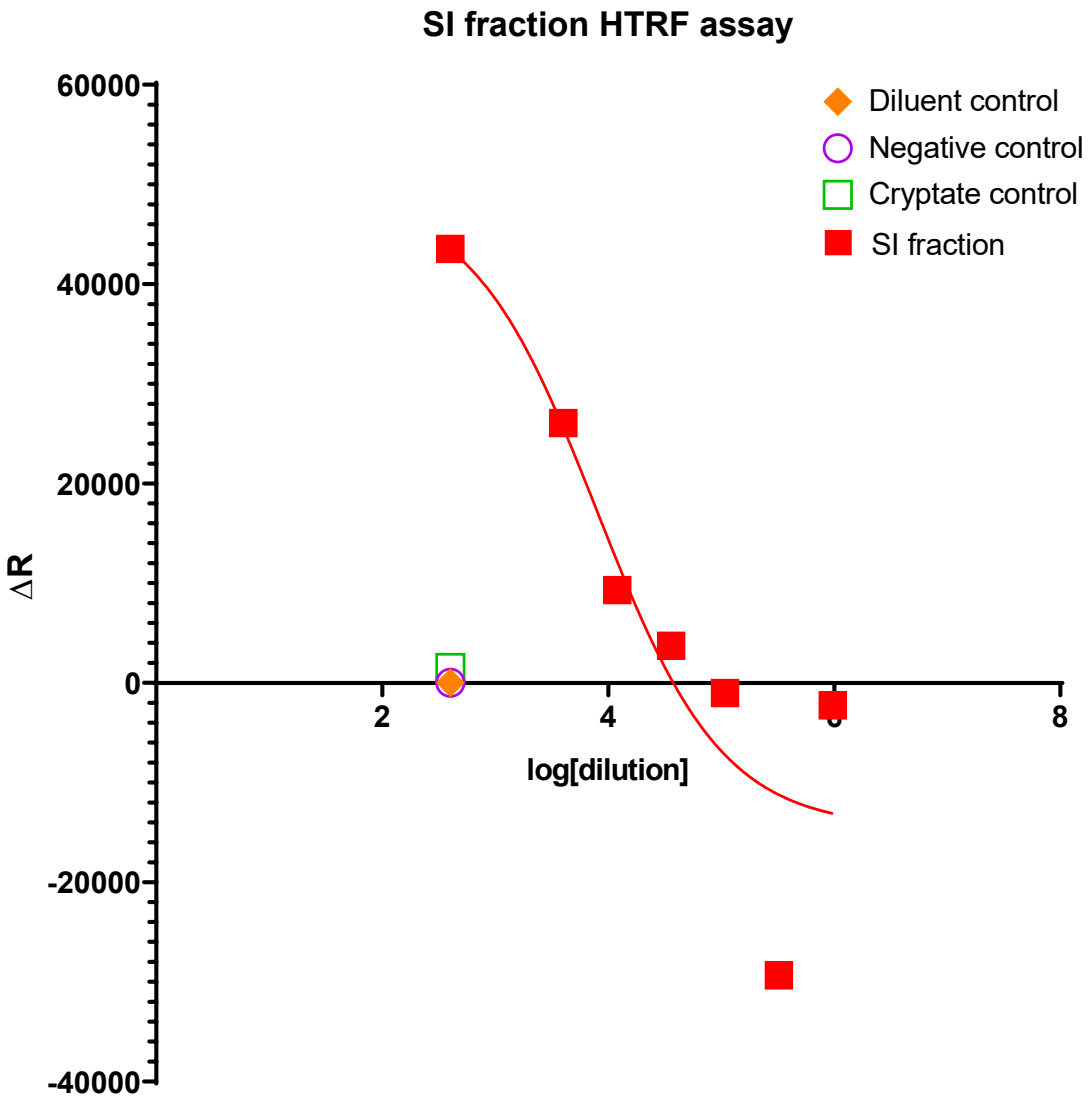

Figure 5-9: HTRF assay to show delta ratio for detection of the HTRF signal

Detection of S202 and T205 tau phosphorylation epitopes. Log dilution plotted against ΔR to show that there is lower detection of the HTRF signal through the serial dilutions. The diluent control, negative control and the control for the cryptate antibody are shown with no signal detected

5.4 Discussion

5.4.1 Selection of post-mortem case

Enrichment for HMW tau has previously been cited for analysis of seeding capacity (Guo *et al.*, 2016) and for the induction of *in vivo* seeding models (Jackson *et al.*, 2016). Using lysate enriched for aggregated tau leads to greater propagation in tauopathy models, and when using lysate isolated from post-mortem tissue. A lysate enriched for AT8-positive human tau from AD post-mortem cases was generated. Injection of tau from AD post-mortem cases has previously been shown to emulate AD pathology in mice (Narasimhan *et al.*, 2017). This paper also utilised AT8 as an antibody to examine the tau burden following AD-tau injection. If it is feasible to examine the relationship between tau propagation and systemic inflammation, mimicking tau propagation in the AD brain makes this study more translational to our understanding of the human disease.

All 10 post-mortem cases from the SWDBB were confirmed to be Braak stages V and VI, with abundant tau pathology in the frontal cortex. The final seed prep consisted of 30g of tissue. At 50µl reconstitution buffer per initial gram of tissue, this would generate 1500µl of lysate. This is to ensure only a single prep is needed for the entire project. Furthermore, as observed in this chapter, a large amount of tissue is required to generate a lysate adequately enriched for aggregated HMW tau (**Figure 5-1**).

As the initial test, a section of tissue weighing 0.5g was homogenised and centrifuged once (**Figure 5-2**). This first supernatant (S1) was then used to determine which of the ten post-mortem cases showed high burden of AT8-positive tau. It must be noted that neither this blot nor subsequent blots were normalised to protein levels generated by the BCA. This was a deliberate decision as one of the most important readouts is the AT8/total tau ratio. By normalising protein levels loss of resolution on total tau burden may occur. Protein extraction was successful in all samples, and the range of total protein concentration was 1.4-2.6mg/ml. The presence of total tau in all samples and AT8-positive tau in the Tg4510 sample suggested that there was protein within these samples. However, despite a clear total tau staining, it was determined that 0.5g was too small a sample for detection of AT8 by western blot.

Therefore, a dot blot protocol was utilised instead. The dot blot allows bypassing of certain issues when using western blots, in this case when there are high levels of protein required for detection. The dot blot showed both AT8 and total tau staining (**Figure 5-3**). Accounting for the background present in a dot blot, the signal produced by the *Mapt-/-* mouse was deducted from all sample signals. The total tau results were then compared to the western blot signals for all ten

cases. Despite a few variable cases, the signal ranking in both dot blot and western blot results aligned. Whilst this was not significant, it must be considered that this is a comparison of two different techniques. This allowed us to confirm the dot blot findings and conclude that cases 6, 7 and 8 were the three cases with the highest AT8-positive tau burden. Notably, cases 6, 7 and 8 each had a protein concentration between 1.7-1.9mg/ml and so this cannot be explained simply by overloading of protein compared to other cases. Cases 6, 7 and 8 all show high AT8/total tau ratios, with every case showing both adequate total tau signal and protein concentration. Therefore, it was decided to progress with these three cases for the final seed prep.

All post-mortem cases had a primary diagnosis of AD, yet the SWDBB also provided secondary and tertiary diagnoses (**Table 5-1**). Cases 6, 7 and 8 did not have secondary diagnosis of Lewy Body Dementia (LBD), although case 7 and 8 did have a tertiary diagnosis of LBD and DLB respectively. It must be noted that case 7 only showed LBD pathology in the amygdala. Interestingly, cases 6, 7 and 8 were the only cases with a secondary diagnosis of CAA (**Table 5-1**). One small study suggested that within CAA patients, those with memory loss show how higher tau burden in PET imaging than those without. They further suggest that cognitive deficits correlated with the PET results (Schoemaker *et al.*, 2020). The additional diagnosis of CAA and LBD may lead to the presence of other amyloidogenic proteins in the lysate. How the presence of other aggregates may impact this study is discussed in Chapter 5.4.2 below.

5.4.2 Generation of seed prep enriched with seed-competent tau

Having established which three cases showed the most AT8 pathology and an AT8/total tau ratio which was indicative of aggregation of tau, histology from these three cases was requested from the SWDBB (**Figure 5-4**). Sections stained for AT8 demonstrated high levels of pathology present in the three cases chosen. As aforementioned, the histology supports the findings in the dot blot experiment. There is clear AT8-positive pathology in all three cases, both filamentous staining and large neuronal inclusions. However, case 7 clearly has greater pathology deposition than the other two cases. This supports the findings which suggests case 7 has the highest level of AT8-positive pathology. From these methods I can progress to optimising the seed prep method.

Prior to the final seed prep, case 3 was processed as a pilot seed prep. Case 3 had the lowest signal of AT8 and a low AT8 to total tau ratio. Case 3 was still classed as Braak stage V-VI and so it was expected that the protocol would be successful, even if there was a low tau load in the final SI fraction. Following Sarkosyl incubation, a western blot proved that in the Sarkosyl-insoluble fraction there was AT8-positive tau, detected at ~64kDa. **Figure 5-5** confirms that the protocol is optimal for enriching lysate for aggregated tau. However, it also highlights that whilst

it is possible to detect protein changes in 0.5g seed prep using a dot blot, this is lost in the western blot. By contrast, the 10g seed prep shows clear AT8-positive tau in the Sarkosyl-insoluble fraction when run through a western blot. Once again, normalisation to protein level was not carried out and all samples loaded neat with 4x sample buffer. This was to avoid skewing the data and to try visualise the distribution of AT8-positive tau as the lysate is homogenised and undergoes sequential processing.

Following this, a final AD seed prep was carried out using 30g of post-mortem tissue with 10g each from cases 6, 7 and 8. A western blot was carried out looking at both the supernatant and pellet steps of the final seed prep. Again, AT8-positive tau was strongly detected in the Sarkosyl-insoluble fraction, confirming the lysate is enriched for seed-capable tau. PHF-1 epitopes are detectable in the first supernatant, suggesting that in this protocol a sample as large as 30g is required to observe phosphorylation epitopes in the first supernatant of human post-mortem tissue. PHF-1 is still a marker heavily associated with aggregated tau pathology in AD and therefore this further supports that the lysate is enriched with seed-competent tau. In addition, the comparison of AT8-positive tau in the 10g vs 30g Sarkosyl-insoluble fraction shows that the degree to which tau can be enriched is dependent upon the volume of tissue used initially. The 30g final 'seed prep' shows much higher levels of AT8-positive tau, which supports the use of this lysate in future *in vivo* work.

Following confirmation of the AT8-positive tau, a titration western blot was carried out. This western blot was used to confirm that the smear observed in **Figure 5-6** was not simply due to non-specific binding. It is possible to observe in **Figure 5-7** that as the Sarkosyl-insoluble fraction undergoes serial dilution, isoforms become visible in bands. However, this blot still showed smear-like staining especially with total tau antibody. Therefore, it was attempted to run a blot with S1-3 and P1-2 with a further dilution for the Sarkosyl-insoluble fraction. In this blot, the Sarkosyl-insoluble fraction shows AT8-positive bands if not as strong as the undiluted blot. A final blot was carried out with all homogenisation steps included with the SI fraction diluted, this blot again confirmed detection of AT8-positive tau both HMW and 50kDa-64kDa (**Figure 5-8**). The HTRF assay also confirmed the presence of AT8 phosphorylation epitopes in the SI fraction (**Figure 5-9**). Therefore, given the successive western blots and HTRF assay it can be confidently stated that this lysate is enriched for AT8-positive tau.

Detecting aggregated forms of tau from human AD brain tissue is often reported as a smear in SDS-PAGE. One study suggested that tau protein was five-fold greater in AD tissue compared to non-AD controls (Zhou *et al.*, 2018). The authors also reported HMW AT8-positive tau at ~100kDa, similar to observations in **Figure 5-6**, **Figure 5-7** and **Figure 5-8**. This was not observed in any of

the control tissue, suggesting that their protocol does not induce this HMW AT8-positive tau and this is an AD-specific observation. The authors also suggest that the HMW tau is predominantly made of N-terminal truncated tau, by comparing tau antibodies which detect a range of epitopes (Zhou *et al.*, 2018). By contrast, LMW tau is detected in control brains, yet is 2.5-fold lower than in AD tissue. Furthermore, they suggest that truncation of tau at the D421 epitope is found predominantly in the LMW tau. This truncation has been shown to correlate with aggregated tau in aging Tg4510 mice using the AlphaScreen assay (Gibson *et al.*, 2013). Both in the 10g and 30g seed prep, it is possible to observe there is LMW tau at ~37kDa. This would correspond to truncated tau and suggests that there is tau present in the lysate prone to aggregation within the HMW tau and potentially even the LMW tau.

It has been shown that amyloid and other proteins such as APOE associated with AD may be found in Sarkosyl-insoluble fragments. One paper suggested that MAPT, APP, APOE and even snRNP70 a small nuclear ribonucleoprotein were present in multi- and single-step fractionation (Diner, Nguyen and Seyfried, 2017). He *et al*. (2020) showed Thioflavin S positive staining was present in 6htau mice three months post-injection of the AD-tau. Yet the authors suggest that this was induced by the injection of tau rather than the presence of amyloid β-sheet structures in the lysate. The authors also reported, with an almost identical protocol to this study, a tau purity of between 20 and 30% (He *et al.*, 2020). Therefore, it is possible to conclude that whilst the lysate generated in this chapter is high in yield for AT8-positive tau, due to time constraints the purity cannot be confirmed.

It must be considered that intracerebral injection of AD-tau is not equivalent to the injection of pre-formed fibrils. It has previously been demonstrated that tau purified from post-mortem tissue propagates through the brain of C57BL/6 mice at a faster rate compared to pre-formed fibrils. The authors reported that without overexpression of native tau observed in transgenic models such as Tg4510, preformed fibrils do not have the same seeding capacity compared to tau lysate derived from AD post-mortem tissue (Guo *et al.*, 2016). Therefore, the conformation of AD-tau must be different and how purity affects this spreading mechanism is as of yet unknown. This paper is from the same group as He *et al*. (2020) and they again reported a tau purity of 10-28%. Following ELISA analysis in both papers the authors also demonstrate low to undetectable concentrations of Aβ and α-Synuclein (Guo *et al.*, 2016; He *et al.*, 2020). Therefore, aggregation of amyloid or α-Synuclein is unlikely yet not impossible. α-Synuclein pathology specifically is deposited primarily in regions other than the dorsolateral prefrontal cortex, with cognitive deficits related to this region only observed later in the disease (Peavy *et al.*, 2013).

In this study, lysate purified from human brain tissue will not have the same properties as preformed fibrils in a laboratory setting. The tau purity is likely to be between 10-30% based on published results using similar protocols to ours (Guo *et al.*, 2016; He *et al.*, 2020). Therefore, the lysate may contain protein which may enhance aggregation of tau or change the pathology. However, these papers cited above are primarily concerned with the mechanism of seeding and how tau conformation alters propagation. These studies seek to determine how different tauopathies can be recapitulated and how the arrangement of tau protein confers this information even when injected into the mouse brain. It must be noted that this is not the aim of this study.

The aim of this thesis is focused on how systemic inflammation alters the propagation of tau. Therefore, the group which will undergo i.c. injection of tau and then i.p. injection of saline form part of the control group. The primary comparison is the effect of systemic infection. Therefore, it may even be beneficial to the research question to generate a lysate which contains mixed aggregates found in real disease.

Given more time and resources, this project would have been best carried out with an additional control group. It would have been ideal to generate the lysate and then from that same lysate, immunodeplete for phospho-tau. This would have formed the basis of a new experimental plan with two intracerebral injection groups, one group would undergo injection of the lysate containing tau whilst the other group would undergo i.c. injection of the immunodepleted lysate. However, this was not possible with the initial seed prep given the low final lysate volume and so further recruitment of cases would have been required. The lysate both with and without tau must be processed at the same time from the same case, with a set amount of volume then set aside for immunodepletion. Otherwise, co-morbidities and even variability in processing could alter the results and the same initial tissue must be used for both the tau and the immunodepleted lysate i.c. injection. Whilst it would be preferable to have the immunodepleted tau group, in this current study the vehicle group will control for the needle injection itself and the buffer the Sarkosyl-insoluble pellet is reconstituted in.

Given further time, analysis of the lysate through Elisa or even characterisation through western blot of other aggregate components such as $A\beta_{40-42}$ or α-Synuclein would be beneficial. If given more time, the use of control brains may provide a suitable alternative. However, it must be considered that once the i.c. injection is administered, mice will then undergo a bacterial infection. Brains which are classed as healthy aged controls may still contain factors which, when purified to a Sarkosyl-insoluble lysate which could be significantly upregulated in the presence of

a bacterial infection. *S. typhimurium* has not been used prior to this and so as a novel study, the effects of bacterial infection on any lysate other than a simple Tris buffer must be considered.

5.4.3 Conclusion

These results confirm that the AD-tau 'seed prep' has produced a lysate highly enriched for tau that is AT8-positive. Despite the HTRF assay having limitations, I have shown through three different methodologies that the final seed prep is highly enriched for AT8-positive tau. This suggests that the tau is seed-competent and if injected into the brain parenchyma should go on to propagate and form inclusions. There was evidence of both HMW and LMW tau in the Sarkosyl-insoluble fraction. This suggests that there is seed-competent tau suitable to induce a spreading model *in vivo*.

Future aims:

- *To establish a tau spreading model using a mouse model expressing human tau*
- *To determine if systemic infection alters the rate of tau spreading in vivo*

Chapter 6 Propagation of tau *in vivo* following systemic inflammation

6.1 Introduction and objectives

The main aim of this chapter is to explore the hypothesis that a systemic, low-grade bacterial infection promotes the rate of tau spreading. Both systemic inflammatory episodes and tau pathology spread have been linked to worsening cognitive decline in AD patients (Holmes *et al.*, 2009; Malpetti *et al.*, 2020). Therefore, mimicking both AD tau pathology and systemic inflammation in AD patients within the mouse was attempted in this chapter. Mice exposed to viral infections such as mouse hepatitis virus and parasitic infections show increased tau phosphorylation at four weeks and four months post-infection respectively (Sy *et al.*, 2011; Gasparotto *et al.*, 2015). However, these models looked at native mouse tau, and not human tau pathology from AD post-mortem tissue. In Chapter 5, AD-brain derived lysate enriched for AT8-positive HMW tau was generated. This lysate provides the ability to observe the effect of systemic infection on AD-tau propagation in the mouse, which should closely mimic the mechanism of spread observed within AD. Understanding the spatiotemporal spreading of tau and which factors alter this rate is essential for translating this research to the human disease.

Studies examining bacterial infections have predominantly utilised LPS, a bacterial mimetic which is an endotoxin found on the surface of real bacteria. Whilst LPS has been reported to induce human tau hyperphosphorylation (Lee *et al.*, 2010), LPS induces an acute inflammatory response and does not induce systemic infection. A real bacterial infection, induced by *S. typhimurium* leads to sustained neuroinflammation in mice (Püntener *et al.*, 2012), but if propagation of tau is affected is not known. This chapter will compare the spreading of human Sarkosyl-insoluble AD tau in wild type C57BL/6 and H1*Mapt-/-* mice expressing human tau. Both C57BL/6 and H1*Mapt-/-* mice underwent intracerebral injection of tau lysate or vehicle, followed by an i.p. injection of saline or *S. typhimurium*. Histology of AT8-positive tau will be the primary readout to determine the effect of systemic infection. By further combining these findings with behavioural readouts, a more complete picture of tau propagation and associated changes in hippocampal function can be formed.

The objectives for this chapter are as follows:

- *To examine tau propagation through the brain in the H1Mapt-/- and C57BL/6 mice at three months post-injection*
- *To confirm regional spread of tau both dorsal and ventral to the injection site*
- *To determine whether systemic infection increases the tau burden and the rate of spread*

6.2 Methods

6.2.1 *In vivo* experimental data

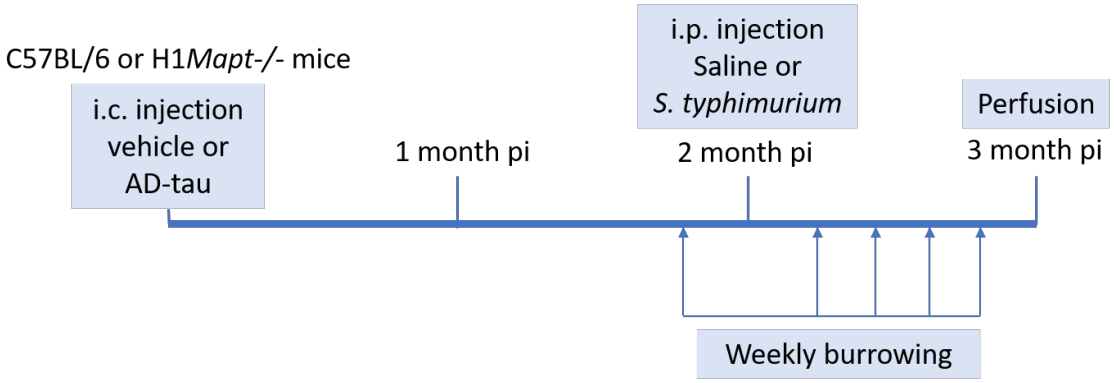

Figure 6-1: Methodology for stereotaxic injections and subsequent i.p. injection

This figure shows the overview of the method for this chapter. C57BL/6 or H1*mapt-/-* mice underwent stereotaxic injection and received either vehicle or AD-tau lysate into the cortex and hippocampus. Two months post-injection the same mice then received an i.p. injection. This figure also denotes the weekly burrowing sessions in relation to the i.p. injection.

C57BL/6 (3-4 months old) and H1*Mapt-/-* (2- 4 months old) received an i.c. injection of either the AD-tau lysate or 50mM Tris buffer as vehicle under anaesthesia using isofluorane (**Figure 6-1**). Initially mice recevied a unilateral intracerebral injection of either tau lysate or vehicle. These were unilateral intracerebral injections, carried out in the ventral hippocampus and the cerebral cortex. Therefore, whilst there were only one set of anterior-posterior and lateral-medial coordinates (AP: -2.50, LM: -2.00) there were two dorsal-ventral coordinates (DV: -1.80 and -0.80) for the hippocampus and cortex respectively (**Figure 6-2**). This reduced damage with only one drill hole in the skull, and one needle tract within the parenchyma.

Two months post-i.c. injection, mice received an i.p. injection of either 200µl of 0.9% saline or *S. typhimurium* (SL3261, 10^6 cfu). The group sizes are listed in **Table 6-1** and **Table 6-2** for C57BL/6 and H1*Mapt-/-* mice respectively. One-month post-i.p. injection, mice were transcardially perfused with 0.9% saline and then the groups for histology were further perfused with 4% PFA. This was to allow for optimal tau phosphorylation epitope fixation. The brains either underwent PFA fixation or were snap frozen in liquid nitrogen for biochemical analysis; the sample sizes are also listed in the subsequent tables. All mice underwent stereotaxic injections using inhalation anaesthetic isoflurane.

Table 6-1: Number of C57BL/6 wild type mice used in behaviour, histology and biochemical studies described in this chapter

	Overall		Burrowing		Histology		Biochemical analysis	
C57BL/6	Vehicle i.c.	Tau i.c.	Vehicle i.c.	Tau i.c.	Vehicle i.c.	Tau i.c.	Vehicle i.c.	Tau i.c.
Saline i.p.	9	13	9	10	5	9	4	4
***S. typhimurium* i.p.**	10	15	10	10	6	11	4	4

Table 6-2: Number of H1*Mapt-/-* mice used in behaviour, histology and biochemical studies described in this chapter

	Overall		Burrowing		Histology		Biochemical analysis	
H1*Mapt-/-*	Vehicle i.c.	Tau i.c.	Vehicle i.c.	Tau i.c.	Vehicle i.c.	Tau i.c.	Vehicle i.c.	Tau i.c.
Saline i.p.	9	10	8	8	4	6	5	4
***S. typhimurium* i.p.**	9	11	8	8	4	5	5	6

6.2.2 Histology regions of interest

Brain regions included for the analysis of AT8-positve tau included the hippocampus (Bregma AP -2.50 and -3.00), the parahippocampal gyrus, the mammillary nuclei (both at Bregma AP -3.00) and the dorsal fornix (Bregma AP -1.00). The corpus callosum (Bregma AP -2.50 and -3.00) was included as area of white matter. ROIs are demonstrated in **Figure 2-4**, and the injection sites highlighted in **Figure 6-2**.

In Chapter 5, AT8 antibody was used to detect HMW AT8-positive tau in the seed prep. Due to the AT8 antibody being anti-mouse, a biotinylated antibody (bAT8) provided by Eli Lilly was utilised in histology. Histological methods were carried out as described in Chapter 2, however the ABC step was omitted for the bAT8 antibody due to the antibody being biotinylated.

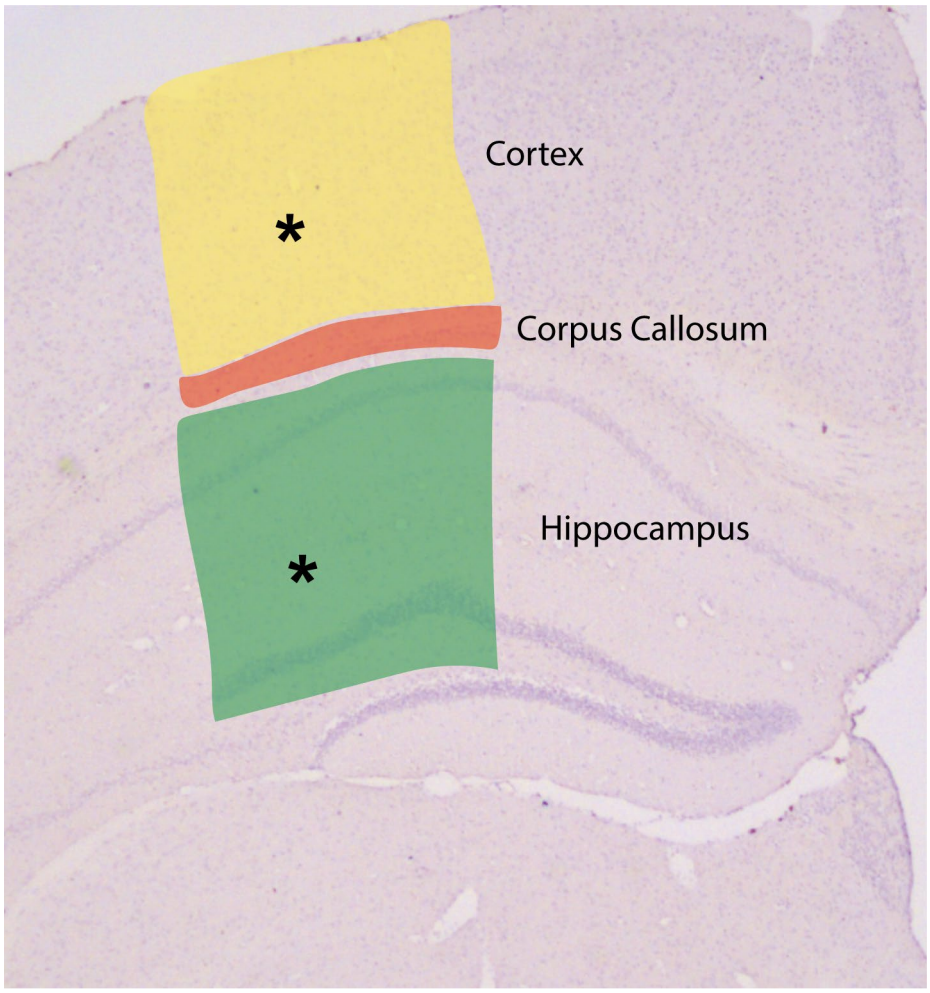

Figure 6-2: Histology ROIs in reference to Bregma coordinates

The injection sites (Bregma AP= -2.50, ML= -2.00, DV= -0.80 and -1.80) are shown by asterisks. The posterior parietal cortex (yellow) and the hippocampus (green) are the two regions where either vehicle or AD-tau lysate was injected. As a result, these regions and the corpus callosum (red) which is sandwiched between, were the initial focus of histology to detect tau pathology.

6.2.3 Statistical analysis

Due to the absence of AT8-positive tau within the vehicle i.c. injection groups, these groups were excluded from statistical analysis. All two-way ANOVAs carried out compare one between subject effect (i.p. injection) and one within subject effect (hemisphere). Within all graphs showing quantification, a dotted line at 0.02% denotes an established mean % area threshold. Individual measurements below this threshold were deemed to be background.

6.3 Results

6.3.1 Physiological changes as a result of *S. typhimurium* infection

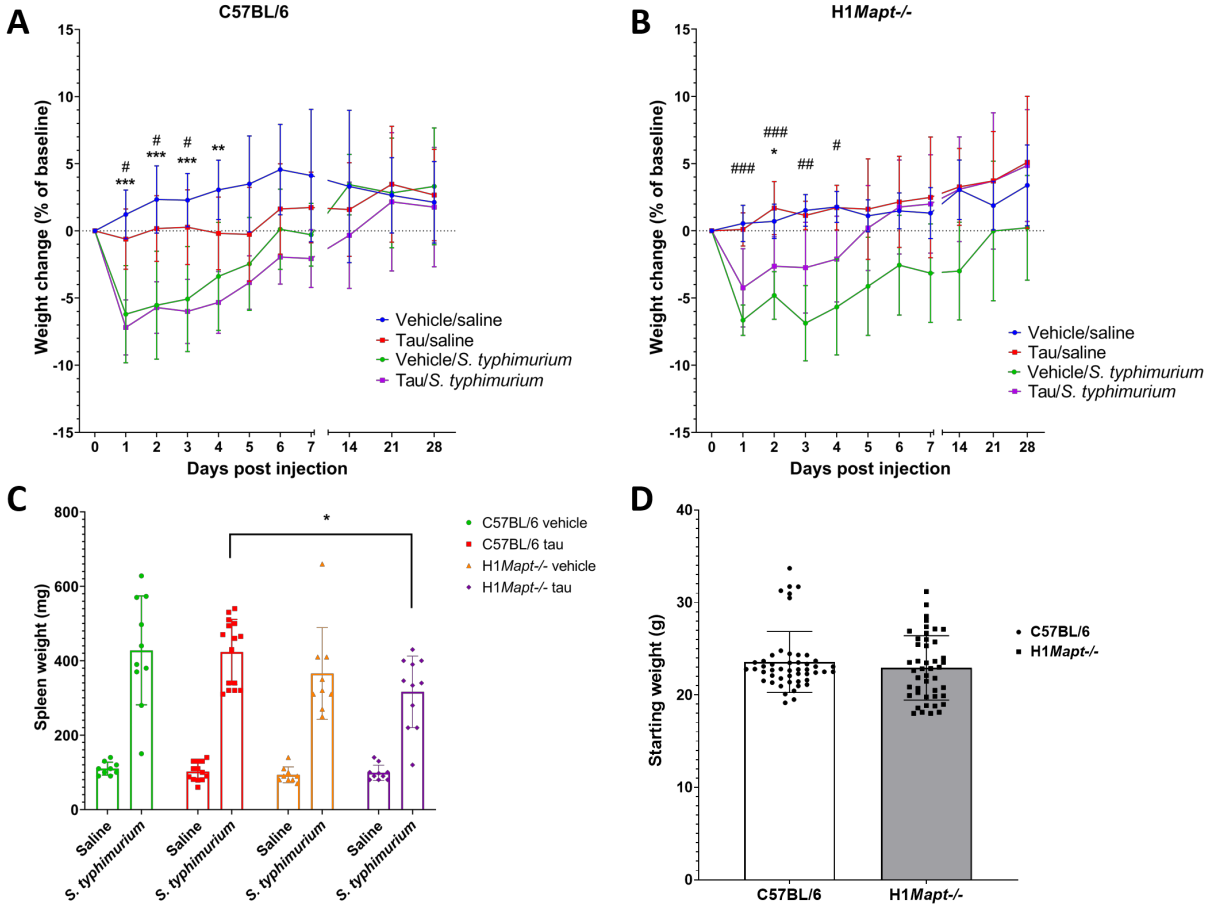

Figure 6-3: Weight change post *S. typhimurium* injection in C57BL/6 mice

A) The body weight change of C57BL/6 mice after saline or *S. typhimurium* i.p. injection, two months post-i.c. injection of the human tau lysate or vehicle control. n= 9 for vehicle i.c./saline i.p; n= 13 for tau i.c./saline i.p; n= 10 for vehicle i.c./*S. typhimurium* i.p.; n= 15 for tau i.c/*S. typhimurium* i.p. Three-way repeated measures ANOVA with Geisser-Greenhouse correction and Tukey's post-hoc test. . *= significance between tau i.c. groups which received saline i.p. or *S. typhimurium* i.p.; #= significance between vehicle i.c. groups which received saline i.p. or *S. typhimurium* i.p. (*p,0.05, **p<0.01, ***p<0.001). **B)** H1*Mapt-/-* mice which received either vehicle or tau i.c. injection show weight loss following *S. typhimurium* i.p. injection. N= 9 for the vehicle groups, n= 10 for tau i.c/saline i.p. and n= 11 for tau i.c./*S. typhimurium* i.p. three-way repeated measures ANOVA with Geisser-Greenhouse correction and Tukey's post-hoc test. *= significance between tau i.c. groups; #= significance between vehicle i.c. groups; (*p,0.05, **p<0.01, ***p<0.001). **C)** Spleen weights of mice which were given saline or *S. typhimurium* i.p. injection, Mann Whitney U test (*p,0.05). **D)** Starting weight of C57BL/6 and H1*Mapt-/-* mice. Unpaired t-test. All data is presented as mean ± SD.

C57BL/6 and H1*Mapt-/-* mice displayed no difference in starting weight (**Figure 6-3**). Intracerebral injections in mice were carried out with isoflurane and as a result, there was small weight change (Appendix A, Figure S3). Two months post-intracerebral injection, mice received an intraperitoneal injection of either saline or *S. typhimurium*. Baseline was established one day prior to i.p. injection, and there was no significant main effect of genotype ($F(1, 78)= 0.19$, $p= 0.67$). Therefore, analysis of weight change was separated by genotype. C57BL/6 mice infected with *S. typhimurium* showed significant weight loss compared to mice receiving the saline injection, with the greatest weight loss observed one day post-injection. This was observed both in the group which underwent vehicle i.c. injection (saline i.p. injection group= 1.22% ± 1.82; *S. typhimurium* i.p.= -6.2% ± 3.62) and the group which underwent tau i.c. injection (saline i.p.= -0.61% ± 2.24; *S. typhimurium* i.p.= -7.19% ± 2.05). There was a significant main effect of time ($F(3.81, 163.7)= 33.64$, $p<0.001$), a significant main effect of i.p. injection ($F(1, 43)= 33.85$, $p<0.001$) and a significant main effect of i.c. injection ($F(1, 43)= 5.88$, $p<0.05$).

The H1*Mapt-/-* mice underwent the same experimental design. **Figure 6-3** shows weight loss in both tau i.c. and vehicle i.c. groups, following infection with *S. typhimurium*. Neither vehicle i.c./saline i.p. or tau i.c./saline i.p. groups lost weight one day post-i.p. injection (vehicle i.c./saline i.p.= 0.54% ± 1.35; tau i.c./saline i.p.= 0.1% ± 1.24). By contrast, both groups which

underwent *S. typhimurium* i.p. injection show significant weight loss at one day post-infection (vehicle i.c./*S. typhimurium* i.p.= -6.65% ± 1.13; tau i.c./*S. typhimurium* i.p.= -4.25% ± 2.91). There is a significant main effect of time ($F(3.02, 105.7) = 28.13$, $p<0001$) and i.p. injection ($F(1, 35) = 22.02$, $p<0.001$). There was also a significant main effect of i.c. injection ($F(1, 35)= 9.16$, $p<0.05$). This is likely due to the recovery in weight of H1*Mapt-/-* mice from the tau i.c*./S. typhimurium* i.p. group. Both C57BL/6 and H1*Mapt-/-* mice show significant weight loss following infection, although H1*Mapt-/-* mice which also received a tau i.c. injection appear to recover quicker. This is likely due to biological variability within the group. However, it must be considered when comparing the tau burden.

6.3.2 Splenomegaly observed after *S. typhimurium* infection

Following perfusion, spleen weights were recorded. All mice infected with *S. typhimurium* infection showed larger spleen weights compared to mice receiving saline (**Figure 6-3**). C57BL/6 mice which underwent *S. typhimurium* infection consistently displayed four-fold enlarged spleen weight compared to saline groups (vehicle i.c./saline i.p.= 110mg ± 17.32; vehicle i.c./*S. typhimurium* i.p.= 427mg ± 146.21; tau i.c./saline i.p.= 102mg ± 24.95; tau i.c./*S. typhimurium* i.p.= 423mg ± 87.62) except for one mouse in the vehicle i.c./*S. typhimurium* i.p. group with a spleen weight of 150mg. H1*Mapt-/-* mice infected with *S. typhimurium* also showed increased spleen size and weight compared to the saline controls, and no difference was seen in mice receiving vehicle or tau i.c. injection. Due to certain groups of spleen data failing to meet normal distribution assumptions, a three-way ANOVA could not be carried out. However, the effect of *S. typhimurium* i.p. injection is clear throughout this data set. One notable result was the comparison between the tau i.c./*S. typhimurium* i.p. group results for the C57BL/6 and H1*Mapt-/-* mice. A Mann-Whitney test determine that there was a significant difference between the spleen weights for these two specific groups, with spleens from C57BL/6 mice significantly larger than the H1*Mapt-/-* mice ($U= 39.50$, $p<0.05$). This demonstrates that H1*Mapt-/-* mice may undergo a weaker adaptive immune response as compared to C57/BL6 wild type mice.

6.3.3 Burrowing behaviour following infection with *S. typhimurium*

Following Covid-19 restrictions, weekly burrowing was reduced to fortnightly burrowing and scheduled burrowing days had to be adjusted. Both of these changes were due to restricted access to the BRF and limitations on animal experiments.

Burrowing was measured to identify potential changes in hippocampal function following both the intracerebral injection of tau, and the intraperitoneal injection of *S. typhimurium* (**Figure 6-4**). Burrowing deficits are often associated with sickness behaviour, such as deficits observed following poly I:C injection. Poly I:C induces innate immune system response and so acts as a viral mimic. However the burrowing deficit is acute and returns to baseline, losing significance 48 hours post injection (Cunningham *et al.*, 2007). Furthermore, following i.p. injection *S. typhimurium* SL3261, mice show acute burrowing deficits with the first three hours of injection; mice return to baseline burrowing activity within 24 hours post-injection (Püntener *et al.*, 2012).

Training had begun three weeks prior to *S. typhimurium* injection to habituate mice to the task and establish a high baseline as close to 100% of pellets removed. One recording was carried out prior to *S. typhimurium* at eight weeks post-i.c. injection, as the baseline by which change in burrowing is calculated. Burrowing in C57BL/6 and H1*Mapt-/-* mice appears to decrease following *S. typhimurium* i.p. injection. As a result of missing cohort data (see Covid-19 restriction statement above), no statistical analysis of the data is carried out on the burrowing data in **Figure 6-4**. However, in order to conclusively determine the effect of i.c. and i.p. injection on burrowing behaviour, future burrowing tests would be required.

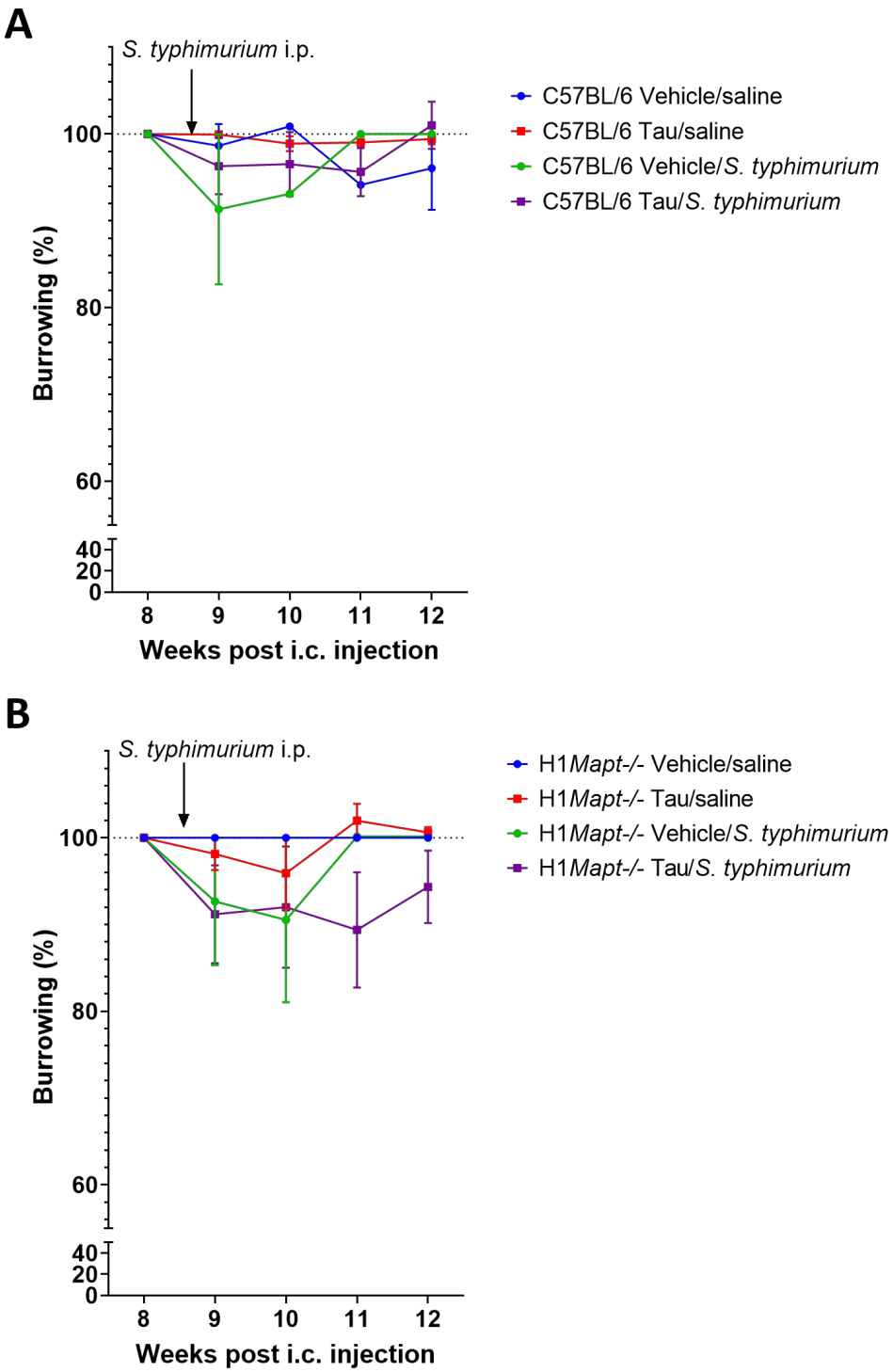

Figure 6-4: Burrowing activity following *S. typhimurium* infection

A) C57BL/6 mice show changes in burrowing as a percent of baseline recorded at 8 weeks post-i.c. injection. After this recording, mice received an i.p. injection of saline or *S. typhimurium*; n= 9 for vehicle i.c./saline i.p. group, n= 10 for vehicle i.c./ *S. typhimurium* i.p., tau i.c./saline i.p. and tau i.c./*S. typhimurium* i.p. groups. **B)** Burrowing activity in H1*Mapt-/-* mice at baseline (8 weeks post-injection) and weekly after i.p. injection of either saline or *S. typhimurium*. n= 8 for all groups. All data is presented as mean ± SEM. Joe Chouhan carried out the set up or recording of several burrowing sessions.

6.3.4 Tau burden in the corpus callosum

Following collection of the brain, tissue was processed to analyse levels of pathological tau using biotinylated AT8 antibody, which detects phosphorylated tau at Ser202 and Thr205 epitopes. At the site of injection, both the corpus callosum and the hippocampus were the primary areas to be analysed. No AT8 immunoreactivity was detected in C57BL/6 mice receiving a i.c. injection of vehicle regardless of subsequent saline or systemic bacterial infection. As a result, vehicle i.c. injection groups were excluded from statistical analysis, however the mean % area results are visible in the respective graphs.

The corpus callosum is the largest commissure which connects the two hemispheres of the brain (Luders, Thompson and Toga, 2010). Tau lysate is injected into the cortex directly above the corpus callosum; therefore, it is to be expected that tau pathology would quickly move into the white matter tract. In C57BL/6 mice, AT8 immunoreactivity was observed in mice receiving a tau i.c. injection (**Figure 6-5**). The AT8 staining morphology was small and dot-like. This staining was not indicative of neuronal inclusions, rather tau protein within synapses or microglia. Mice displayed AT8 immunoreactivity almost exclusively within the ipsilateral hemisphere. Within the ipsilateral hemisphere, mice receiving a systemic bacterial infection show a five-fold increase of bAT8 expression when compared to mice receiving saline (tau i.c./saline i.p.= 0.03% ± 0.01; tau i.c./*S. typhimurium* i.p.= 0.16% ± 0.06). A Student's t-test between the ipsilateral hemispheres of tau i.c./saline i.p. and tau i.c./*S. typhimurium* i.p. groups showed a significant increase in AT8 immunoreactivity following systemic infection ($t(11.56)= 3.63$, $p<0.01$). There is notably no AT8 immunoreactivity in the contralateral hemisphere except for a couple of mice in both tau i.c. groups. However, this is inconsistent even between brain slices from the same mouse. Therefore, AT8 immunoreactivity in the contralateral hemisphere is negligible and similar between the tau i.c. groups (tau i.c./saline i.p.= 0.002 ± 0.001; tau i.c./*S. typhimurium* i.p.= 0.005% ± 0.003). As the corpus callosum is directly located within the needle tract it is to be expected that tau i.c. groups would express tau pathology in this white matter tract, however the effect of systemic infection is clear.

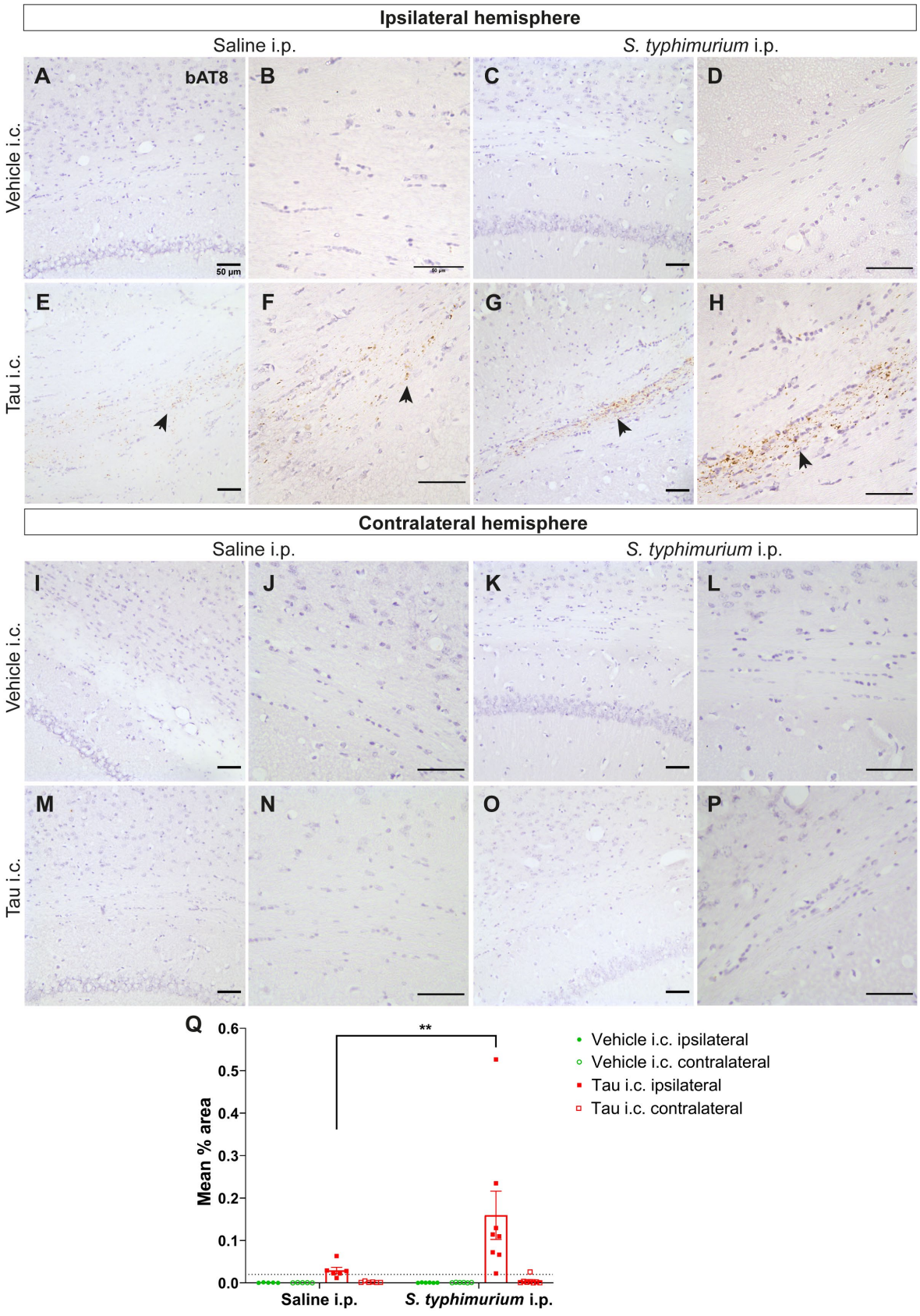
Ipsilateral hemisphere
Saline i.p.
S. typhimurium i.p.
A
bAT8
B
C
D
Vehicle i.c.
50 µm
E
F
G
H
Tau i.c.
Contralateral hemisphere
Saline i.p.
S. typhimurium i.p.
I
J
K
L
Vehicle i.c.
M
N
O
P
Tau i.c.
Q
Mean % area
0.6
0.5
0.4
0.3
0.2
0.1
0.0
**
Saline i.p.
S. typhimurium i.p.
Vehicle i.c. ipsilateral
Vehicle i.c. contralateral
Tau i.c. ipsilateral
Tau i.c. contralateral

Figure 6-5: Tau pathology in the corpus callosum of C57BL/6 mice after saline and *S. typhimurium* infection

Representative analysis images of mice receiving (**A, C, I, K**) vehicle i.c. injection or (**E, G, M, O**) tau i.c. injection; 20x objective, scale bar= 50μm. **B, D, F, H, J, L, N, P**) Images at 40x objective were also shown to observe the tau pathology with greater clarity; scale bar= 50μm. Histology staining for biotinylated AT8 in mice injected with tau i.c./saline i.p. (n= 6), tau i.c./*S. typhimurium* i.p. (n= 8), vehicle i.c./saline i.p. (n= 5), vehicle i.c./*S. typhimurium* i.p. (n= 6). Black arrowheads denote tau pathology. **Q**) Quantification of bAT8 expression levels in the corpus callosum. Unpaired Student's t-test with Welch's correction; (**p<0.01). Data was log transformed for analysis. However, values were <1 so data in the graph is not log transformed to better view the relationship between mean % area. All data is presented as mean ± SEM.

The corpus callosum of H1*Mapt-/-* mice was also analysed (**Figure 6-6**). As with C57BL/6 mice, no pathology was observed in mice receiving vehicle i.c. injection. Mice which received a tau i.c. injection followed by saline i.p. injection did not show any detectable $AT8^+$ tau, while mice receiving tau i.c. injection followed by *S. typhimurium* only showed modest tau pathology (tau i.c./saline i.p.= 0.02% ± 0.01; tau i.c./*S. typhimurium* i.p.= 0.03% ± 0.01). A Mann-Whitney U test demonstrated that within the ipsilateral hemisphere there was no effect of *S. typhimurium* (U= 11, p= 0.54). The contralateral hemisphere showed no AT8 immunoreactivity in either tau i.c. group (tau i.c./saline i.p.= 0.002% ± 0.002; tau i.c./*S. typhimurium* i.p.= 0.003% ± 0.002). This highlights that there appears to be less pathology deposition in the H1*Mapt-/-* mice.

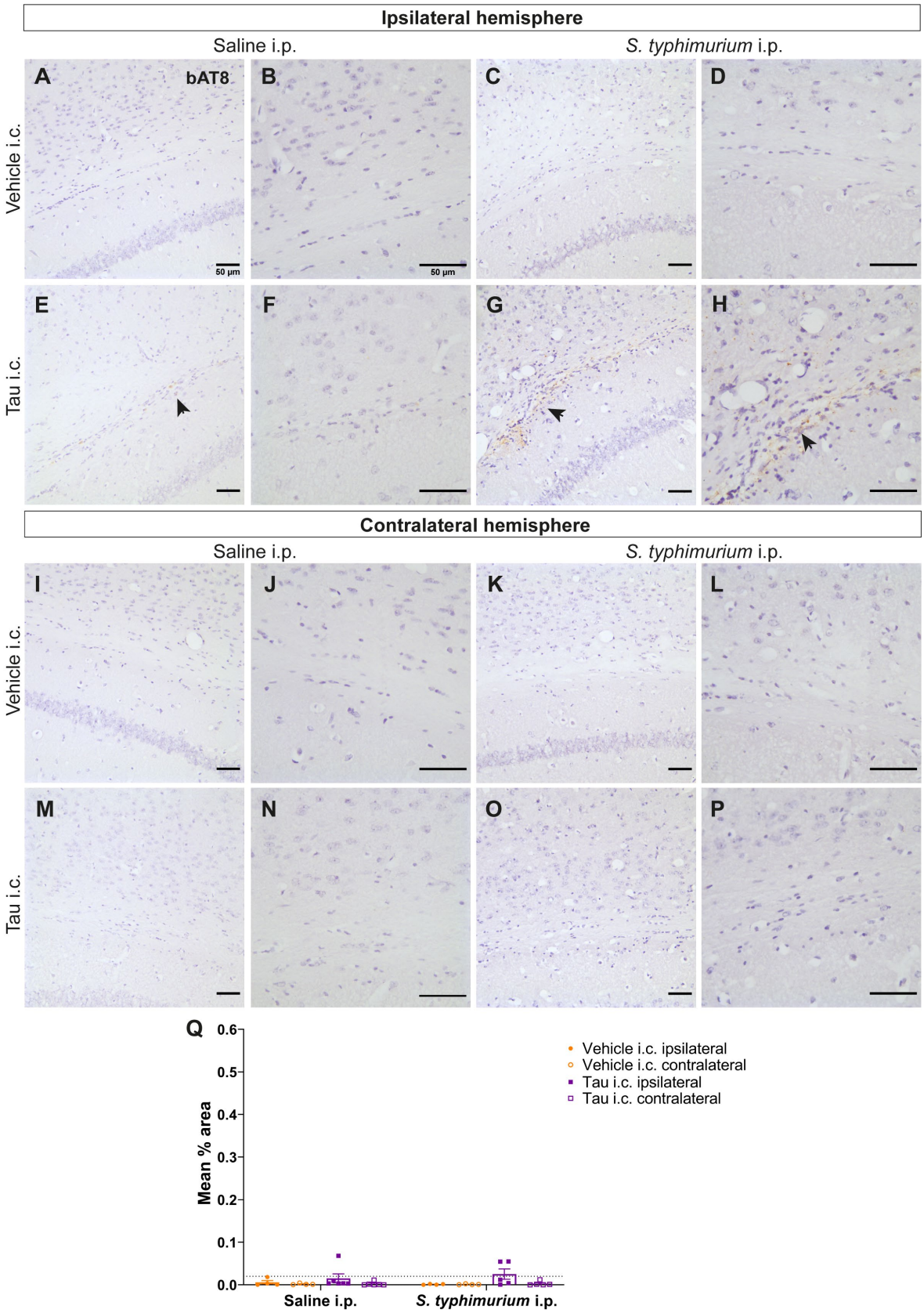
Ipsilateral hemisphere
Saline i.p.
S. typhimurium i.p.
A
bAT8
B
C
D
Vehicle i.c.
50 µm
50 µm
E
F
G
H
Tau i.c.
Contralateral hemisphere
Saline i.p.
S. typhimurium i.p.
I
J
K
L
Vehicle i.c.
M
N
O
P
Tau i.c.
Q
Mean % area
0.6
0.5
0.4
0.3
0.2
0.1
0.0
Vehicle i.c. ipsilateral
Vehicle i.c. contralateral
Tau i.c. ipsilateral
Tau i.c. contralateral
Saline i.p.
S. typhimurium i.p.

Figure 6-6: Tau pathology in the corpus callosum of H1*Mapt-/-* mice

Representative images of histology in the corpus callosum of H1*Mapt-/-* mice received (**A, C, I, K**) vehicle i.c. or (**E, G, M, O**) tau i.c. injection; 20x objective, scale bar= 50μm. **B, D, F, H, J, L, N, P**) Further images at 40x were included for greater observation of tau pathology; scale bar= 50μm. Black arrowheads denote tau pathology. **Q**) Image quantification of bAT8 histology. Mann-Whitney U test; n= 6 for tau i.c./saline i.p., n= 5 for tau i.c./*S. typhimurium* i.p., n= 4 for both vehicle i.c. groups. All data is presented as mean ± SEM.

6.3.5 AT8-positive tau in the hippocampus of C57BL/6 and H1*Mapt-/-* mice

The hippocampus was also a key area for analysis. The specific region of interest included the hippocampal fissure and the dentate gyrus. This region has been shown in previous studies to be an initial area of deposition for tau pathology (Ahmed *et al.*, 2014). Tau pathology is initially deposited in these propagation studies within the CA4 and the granule cell layer of the dentate gyrus. Within the hippocampus there was less consistent AT8 immunoreactivity observed than in the corpus callosum.

AT8-positive immunoreactivity in the hippocampus was observed in C57BL/6 mice which received tau i.c. injection followed by *S. typhimurium* i.p. injection (**Figure 6-7**). Even within the tau i.c./*S. typhimurium* i.p. group half of the mice showed no tau pathology in the hippocampus. Only one mouse in the tau i.c./saline i.p. group showed AT8-positive tau. AT8 immunoreactivity was increased eighteen-fold in the tau i.c./*S. typhimurium* i.p. group compared to the tau i.c./saline i.p. group in the ipsilateral hemisphere (tau i.c./saline i.p.= 0.006% ± 0.003; tau i.c./*S. typhimurium* i.p.= 0.11% ± 0.06, p= 0.51). There is no AT8 immunoreactivity observed in either tau i.c. group within the contralateral hippocampus (tau i.c./saline i.p.= 0.003% ± 0.001; tau i.c./*S. typhimurium* i.p.= 0.01% ± 0.004). Whilst there is pathology present within the tau i.c./*S. typhimurium* i.p. group compared to the absence of AT8-positive tau in the majority of the saline i.p. group, there is a wide distribution of results (**Figure 6-7**). There is no significant main effect of i.p. injection ($F(1, 12)= 1.54$, $p= 0.24$) or hemisphere ($F(1, 12)= 3.10$, $p= 0.10$). This suggests that whilst *S. typhimurium* i.p. injection does increase deposition of tau in the hippocampus, this timepoint is too early to observe consistent pathology in all mice within the group and as a result statistical significance is not reached.

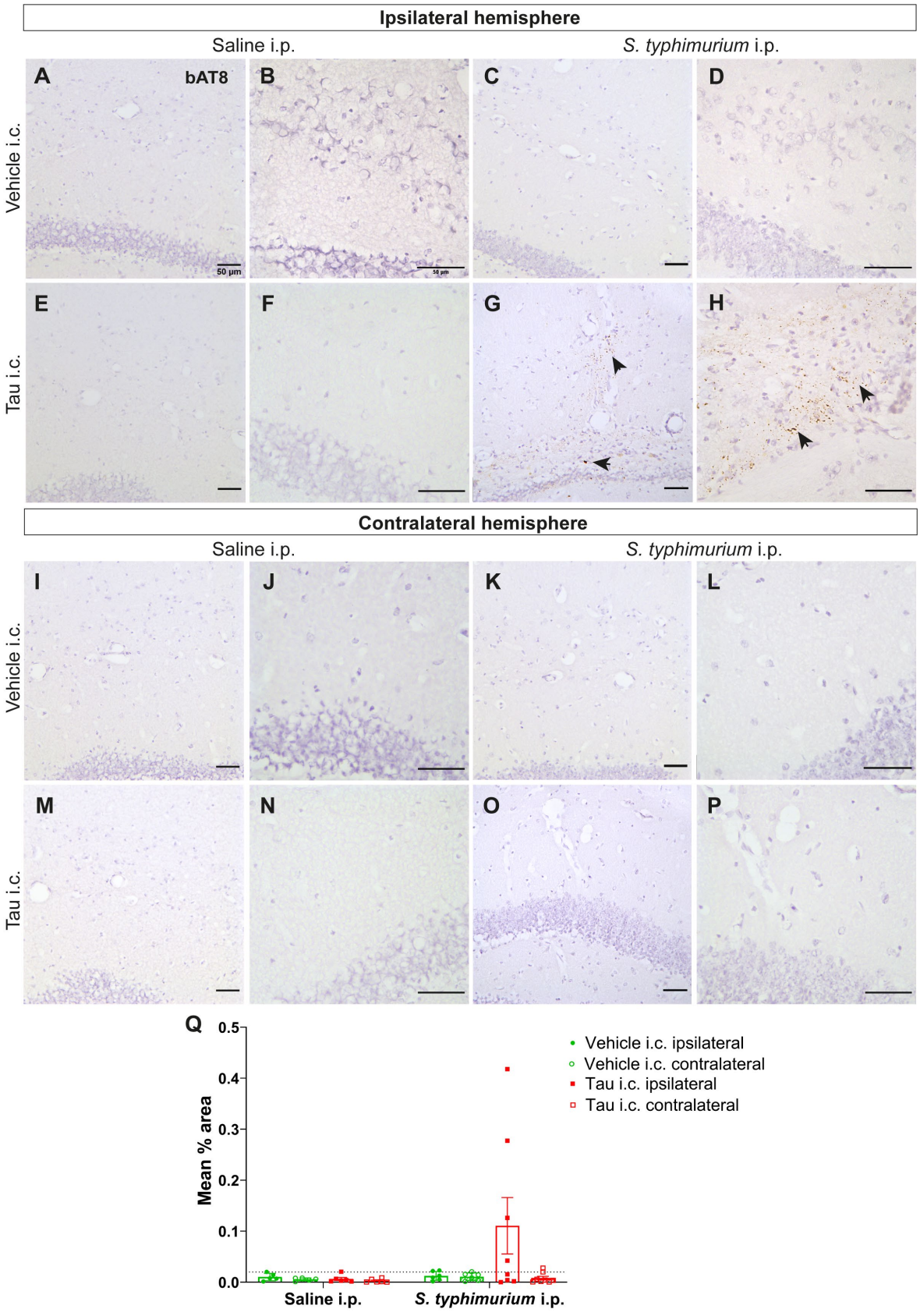
Ipsilateral hemisphere
Saline i.p.
S. typhimurium i.p.
A
bAT8
B
C
D
Vehicle i.c.
E
F
G
H
Tau i.c.
50 µm
Contralateral hemisphere
Saline i.p.
S. typhimurium i.p.
I
J
K
L
Vehicle i.c.
M
N
O
P
Tau i.c.
Q
Mean % area
0.5
0.4
0.3
0.2
0.1
0.0
Saline i.p.
S. typhimurium i.p.
Vehicle i.c. ipsilateral
Vehicle i.c. contralateral
Tau i.c. ipsilateral
Tau i.c. contralateral

Figure 6-7: Tau pathology in the hippocampus of C57BL/6 mice

A, C, I, K) Representative images of vehicle i.c. injection both following saline i.p. and *S. typhimurium* i.p. injection in the ipsilateral and contralateral hemisphere. **E, G, M, O**) Representative images of tau i.c. injection in the ipsilateral and contralateral hemispheres; 20x objective, scale bar= 50µm. Representative images at a higher magnification are included for greater detail of tau pathology following (**B, D, J, L**) vehicle or (**F, H, N, P**) tau i.c. injection; 40x objective, scale bar= 50µm. Black arrowheads denote tau pathology. **Q**) Two-way ANOVA with Sidak's post-hoc test. n= 6 for tau i.c./saline i.p., n= 8 for tau i.c./*S. typhimurium* i.p., n= 5 for vehicle i.c./saline i.p., n= 6 vehicle i.c./*S. typhimurium* i.p. injection group. Data is log transformed for analysis. However, most values are <1 therefore the original mean % area is displayed. All data

The dentate gyrus in the H1*Mapt-/-* mice showed minimal tau pathology (**Figure 6-8**), AT8-positive tau was only observed in the tau i.c./*S. typhimurium* i.p. group. Systemic infection had no notable effect on AT8 immunoreactivity in the ipsilateral hemisphere (tau i.c./saline i.p.= 0.01% ± 0.004; tau i.c./*S. typhimurium* i.p.= 0.02% ± 0.01). There was a significant main effect of *S. typhimurium* i.p. injection ($F(1, 8)= 7.84$, $p<0.05$) and a significant main effect of hemisphere ($F(1, 8)= 7.70$, $p<0.05$). There was no pathology reported in the contralateral hemisphere. As a result, when comparing the hemispheres of the tau i.c./*S. typhimurium* i.p. mean % area values are distinctly close in value (tau i.c./*S. typhimurium* i.p. ipsilateral = 0.02% ± 0.01; contralateral= 0.01% ± 0.002). Therefore, whilst there is pathology in the ipsilateral hemisphere of the tau i.c. groups and a significant main effect, this pathology is minimal and again inconsistent within the group.

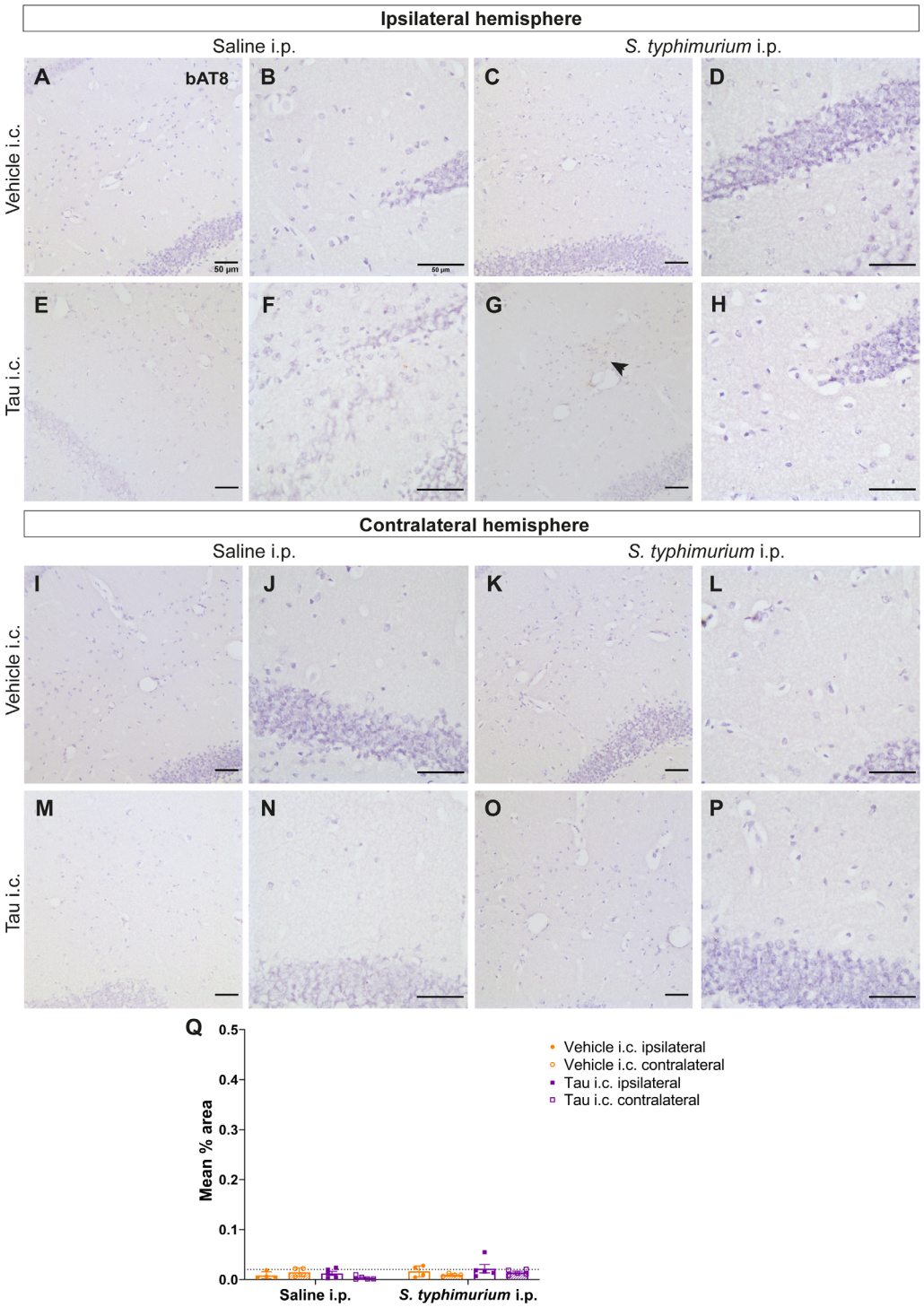

Figure 6-8: Tau pathology in the hippocampus of H1Mapt-/- mice

Representative images of the (**A, B**) vehicle i.c./saline i.p., (**C, D**) vehicle i.c./*S. typhimurium* i.p., (**E, F**) tau i.c./saline i.p. and (**G, H**) tau i.c./*S. typhimurium* i.p. group in the ipsilateral hemisphere. **I-P**) Representative images were included for the contralateral hemisphere. **A, C, E, G, I, K, M, O**) 20x objective, scale bar= 50µm; **B, D, F, H, J, L, N, P**) 40x objective, scale bar= 50µm. Black arrowheads denote tau pathology. **Q**) Quantification of tau pathology, two-way ANOVA with Sidak's post-hoc test. n= 5 for both tau i.c. groups, n= 4 for both vehicle i.c. groups. All data is presented as mean ± SEM. Data is log transformed for analysis. However, most values are <1 therefore the original mean % area is displayed. All data is presented as mean ± SEM.

6.3.6 Tau pathology at the posterior corpus callosum

From examining brain regions at the Bregma AP coordinates of -2.50, analysis was subsequently carried out at Bregma AP coordinates of -3.00. This region is posterior to the injection site. The regions of interest are the corpus callosum, hippocampus, perirhinal cortex and mammillary nuclei. Biotinylated AT8 antibody was used to detect pathological forms of tau.

The initial analysis was the corpus callosum. This white matter tract is found at a large range of Bregma coordinates because the commissure connects the two hemispheres and is essential for integration of signals between hemispheres. There was significant deposition of tau in the corpus callosum at the injection site (**Figure 6-5**), so analysis was carried out to determine whether the pathology has spread to a region 5mm posterior.

Wild type C57BL/6 mice showed no pathology following an i.c. injection of vehicle (**Figure 6-9**). bAT8 immunoreactivity was detected in the ipsilateral hemisphere of mice receiving tau i.c. injections, but no difference in tau pathology after saline i.p. or a systemic bacterial infection (tau i.c./saline i.p.= 0.03% ± 0.01; tau i.c./*S. typhimurium* i.p.= 0.02% ± 0.004, p= 0.79). As a result, there was no significant main effect of *S. typhimurium* i.p. injection ($F(1, 11)= 0.84$, $p= 0.38$). However, there was a significant main effect of hemisphere ($F(1, 11)= 39.09$, $p<0.001$). There is also a significant interaction of hemisphere and i.c. injection ($F(1, 11)= 6.58$, $p<0.05$). There was pathology present in the contralateral hemisphere of the tau i.c./*S. typhimurium* i.p. group. However overall, the contralateral corpus callosum showed minimal AT8 immunoreactivity (tau i.c./saline i.p.= 0.002% ± 0.001; tau i.c./*S. typhimurium* i.p.= 0.01% ± 0.004, p= 0.08).

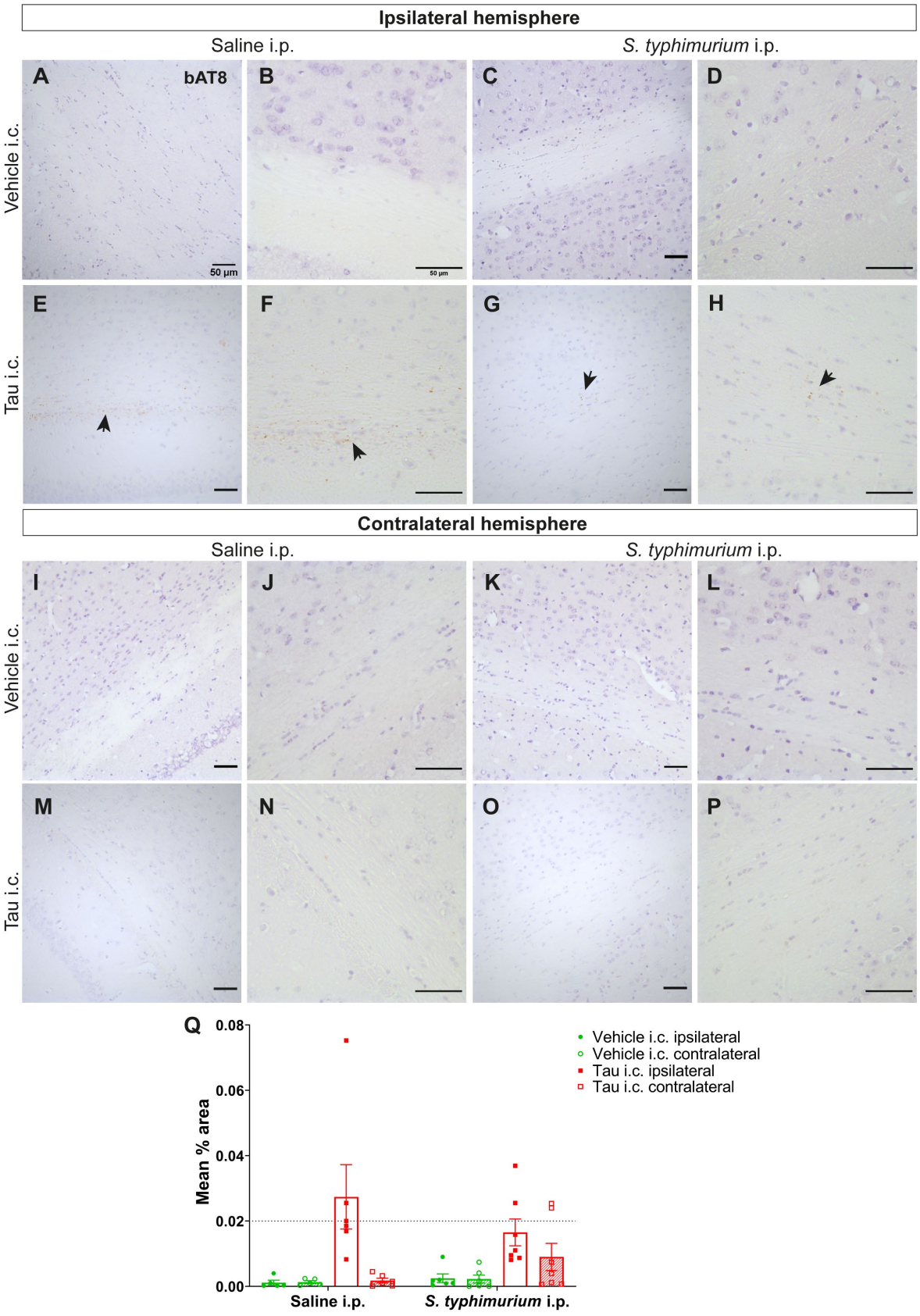
Ipsilateral hemisphere
Saline i.p.
S. typhimurium i.p.
A
bAT8
B
C
D
Vehicle i.c.
50 µm
E
F
G
H
Tau i.c.
Contralateral hemisphere
Saline i.p.
S. typhimurium i.p.
I
J
K
L
Vehicle i.c.
M
N
O
P
Tau i.c.
Q
Mean % area
0.08
0.06
0.04
0.02
0.00
Saline i.p.
S. typhimurium i.p.
Vehicle i.c. ipsilateral
Vehicle i.c. contralateral
Tau i.c. ipsilateral
Tau i.c. contralateral

Figure 6-9: Tau pathology at the corpus callosum posterior to injection site

A, C, I, K) Representative images of vehicle i.c. injected mice and **E, G, M, O**) tau i.c. injected mice; 20x objective, scale bar= 50μm. **B, D, J, L**) High magnification images of tau pathology from vehicle i.c. injected mice and **F, H, N, P**) tau i.c. injected mice; 40x objective, scale bar= 50μm. Black arrowheads denote tau pathology. **Q**) Quantification of tau pathology comparing effect of i.p. injection and hemisphere, two-way ANOVA with Sidak's post-hoc test. n= 6 for tau i.c./saline i.p., n= 7 for tau i.c./*S. typhimurium* i.p., n= 5 for vehicle i.c./saline i.p., n= 6 vehicle i.c./*S. typhimurium* i.p. group. For analysis, data is log transformed. However, because most values are <1, data in the graph is not log transformed to view the mean % area. All data is presented as mean ± SEM.

When examining H1*Mapt-/-* mice, there is minimal pathology at the corpus callosum at Bregma position -3.00. No pathology was observed in any vehicle i.c. group or the contralateral hemisphere of either tau i.c. group. **Figure 6-10** suggests that *S. typhimurium* increased tau pathology two-fold in the ipsilateral hemisphere, when compared to saline control (tau i.c./saline i.p.= 0.01% ± 0.006; tau i.c./*S. typhimurium* i.p.= 0.02% ± 0.01). However, a Student's t-test determined that this was not significantly difference ($t(6.07)= 0.82$, $p= 0.45$), likely due to low levels of pathology and biological variance. Furthermore, the contralateral hemisphere showed no AT8 immunoreactivity in either tau i.c. group (tau i.c./saline i.p.= 0.002% ± 0.001; tau i.c./*S. typhimurium* i.p.= 0.01% ± 0.002). In conclusion, H1*Mapt-/-* mice displayed minimal pathology. By contrast, C57BL/6 mice show tau deposition, yet there is no clear effect of *S. typhimurium* in this ROI.

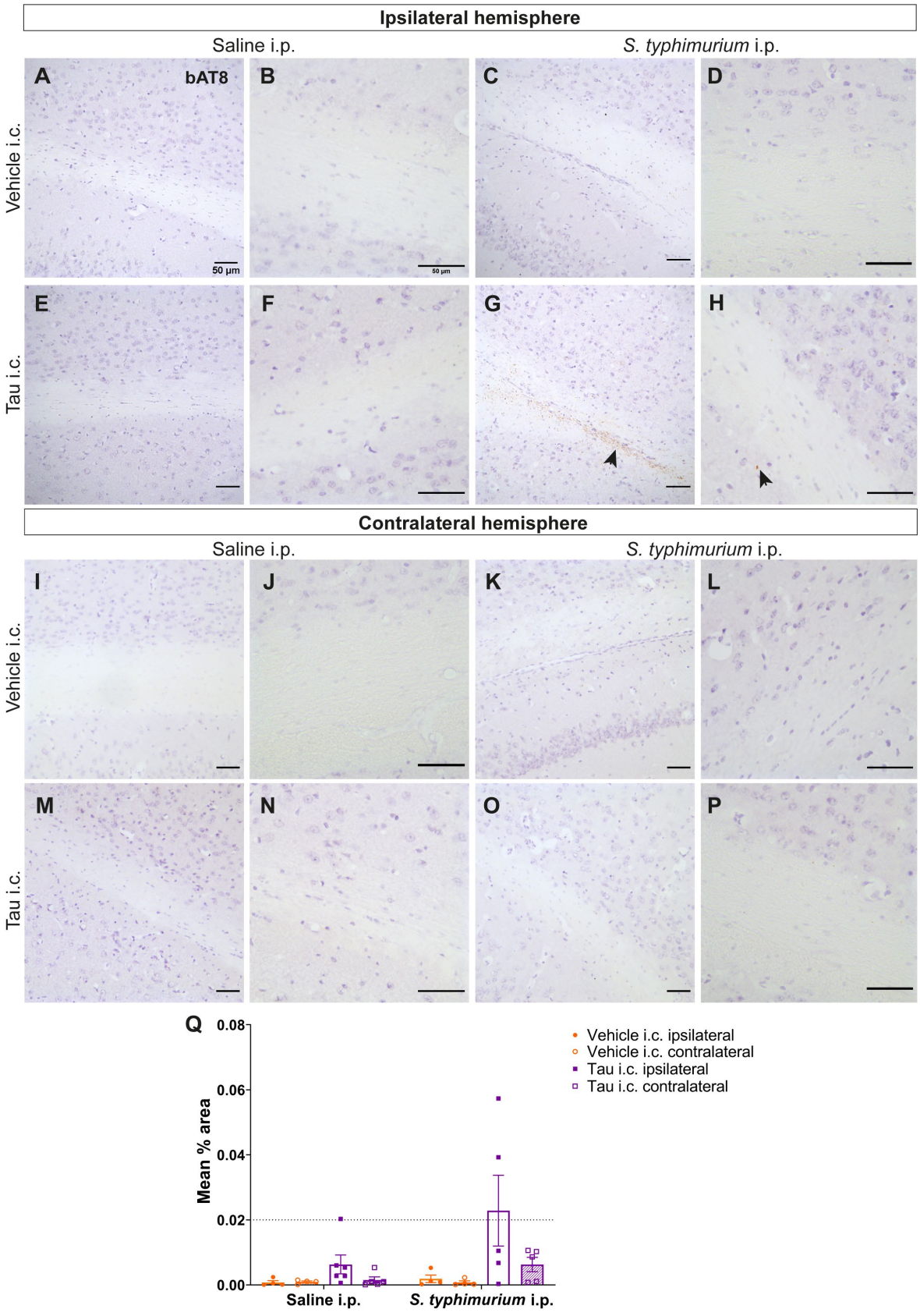
Ipsilateral hemisphere
Saline i.p.
S. typhimurium i.p.
A
bAT8
B
C
D
Vehicle i.c.
50 µm
E
F
G
H
Tau i.c.
Contralateral hemisphere
Saline i.p.
S. typhimurium i.p.
I
J
K
L
Vehicle i.c.
M
N
O
P
Tau i.c.
Q
Mean % area
0.08
0.06
0.04
0.02
0.00
Saline i.p.
S. typhimurium i.p.
Vehicle i.c. ipsilateral
Vehicle i.c. contralateral
Tau i.c. ipsilateral
Tau i.c. contralateral

Figure 6-10: Tau pathology in H1*Mapt-/-* corpus callosum following systemic infection

A, C, I, K) Representative images of vehicle i.c. injected mice and (**E, G, M, O**) tau i.c. injected mice; 20x objective, scale bar= 50μm. High magnification images of tau pathology from (**B, D, J, L**) vehicle i.c. injected mice and (**F, H, N, P**) tau i.c. injected mice; 40x objective, scale bar= 50μm. Black arrowheads denote tau pathology. **Q**) Quantification of tau pathology comparing effect of i.p. injection and hemisphere, unpaired Student's t-test with Welch's correction. n= 5 for both tau i.c. groups, n= 4 for both vehicle i.c. groups. For analysis, data is log transformed. However, because most values are <1, data in the graph is not log transformed to view the mean % area. All data is presented as mean ± SEM

6.3.7 Tau pathology in the ventral hippocampus

The ventral hippocampus was also analysed (Bregma AP= -3.00), again with the dentate gyrus included in analysis (**Figure 6-11**). When examining histology in C57BL/6 mice, the only pathology observed in this ROI was in the tau i.c./*S. typhimurium* i.p. injection group. There was not a significant main effect of i.p. injection ($F(1, 12)= 4.30$, $p= 0.06$), but there was a trend. There was a significant main effect of hemisphere ($F(1, 12)= 8.35$, $p<0.05$). Specific to the ipsilateral hemisphere, the tau i.c./*S. typhimurium* i.p. group showed four-fold increase in AT8 immunoreactivity compared to the tau i.c./saline i.p. group (tau i.c./saline i.p.= 0.01% ± 0.003; tau i.c./*S. typhimurium* i.p.= 0.04% ± 0.02, p= 0.15). Pathology was observed in the contralateral hemisphere of the tau i.c./*S. typhimurium* i.p. group only, but only a select few mice within this group (tau i.c./saline i.p.= 0.004% ± 0.001; tau i.c./*S. typhimurium* i.p.= 0.01% ± 0.004, p= 0.14). AT8 immunoreactivity in the ventral hippocampus only shows positive staining in the tau i.c./*S. typhimurium* i.p. group, however as observed at the hippocampus (Bregma AP= -2.50) in **Figure 6-7**, AT8 staining is not detected in all mice within the group.

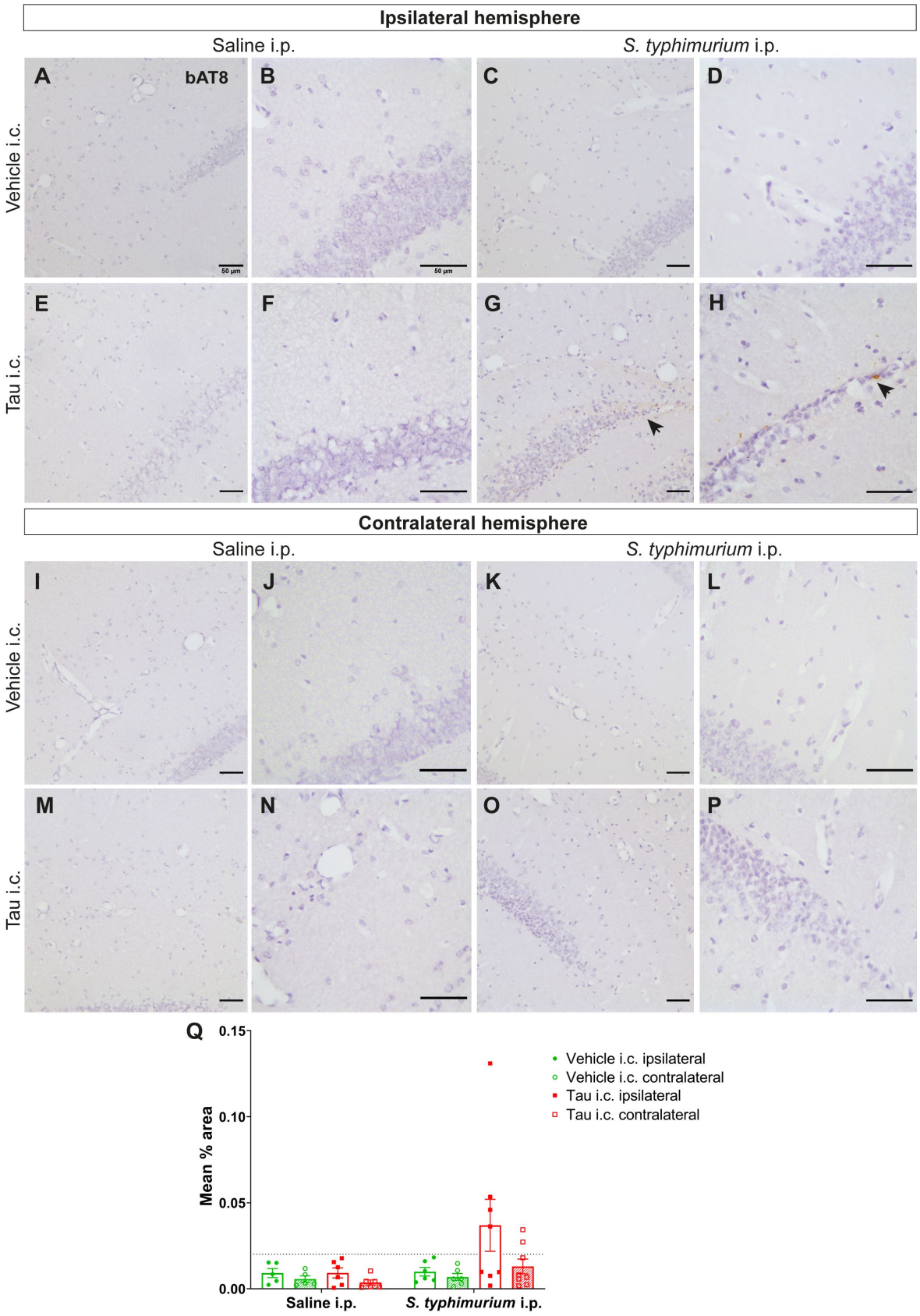
Ipsilateral hemisphere
Saline i.p.
S. typhimurium i.p.
A
bAT8
B
C
D
Vehicle i.c.
E
F
G
H
Tau i.c.
Contralateral hemisphere
Saline i.p.
S. typhimurium i.p.
I
J
K
L
Vehicle i.c.
M
N
O
P
Tau i.c.
Q
Mean % area
0.15
0.10
0.05
0.00
Saline i.p.
S. typhimurium i.p.
Vehicle i.c. ipsilateral
Vehicle i.c. contralateral
Tau i.c. ipsilateral
Tau i.c. contralateral

Figure 6-11: Pathology in the C57BL/6 ventral hippocampus after *S. typhimurium* infection

A, C, I, K) Representative images of vehicle i.c. injected mice and (**E, G, M, O**) tau i.c. injected mice; 20x objective, scale bar= 50µm. High magnification images of tau pathology from (**B, D, J, L**) vehicle i.c. injected mice and (**F, H, N, P**) tau i.c. injected mice; 40x objective, scale bar= 50µm. Black arrowheads denote tau pathology. **Q**) Quantification of tau pathology in C57BL/6 demonstrating the effect of systemic infection, two-way ANOVA with Sidak's post-hoc test. n= 6 for tau i.c./saline i.p., n= 8 for tau i.c./*S. typhimurium* i.p., n= 5 for vehicle i.c./saline i.p., n= 6 vehicle i.c./*S. typhimurium* i.p. injection group. Data is log transformed for analysis, however due to most values <1, the graph is not log transformed to view the data. All data is presented as mean ± SEM.

As before, when examining tau pathology in the dentate gyrus of the H1*Mapt-/-* mice there was no pathology observed in any mouse (**Figure 6-12**). There was no pathology either in the ipsilateral (tau i.c./saline i.p.= 0.01% ± 0.001; tau i.c./*S. typhimurium* i.p.= 0.01% ± 0.001) or contralateral (tau i.c./saline i.p.= 0.01% ± 0.003; tau i.c./*S. typhimurium* i.p.= 0.004% ± 0.001) hemisphere. Subsequently there was no significant main effect of i.p. injection ($F(1, 9)= 4.81$, $p= 0.06$) or hemisphere ($F(1, 9)= 1.61$, $p= 0.24$). This allows me to conclude that AT8 immunoreactivity is only present in the ventral C57BL/6 hippocampus. Furthermore, this is predominantly observed in tau i.c./*S. typhimurium* i.p. group. This highlights how there is a clear effect of systemic infection, yet mouse strains show clear difference. Due to the lack of significance in **Figure 6-11**, this also highlights how AT8-positive staining is not consistent in the hippocampus and biological variability prevents statistical significance despite clear difference

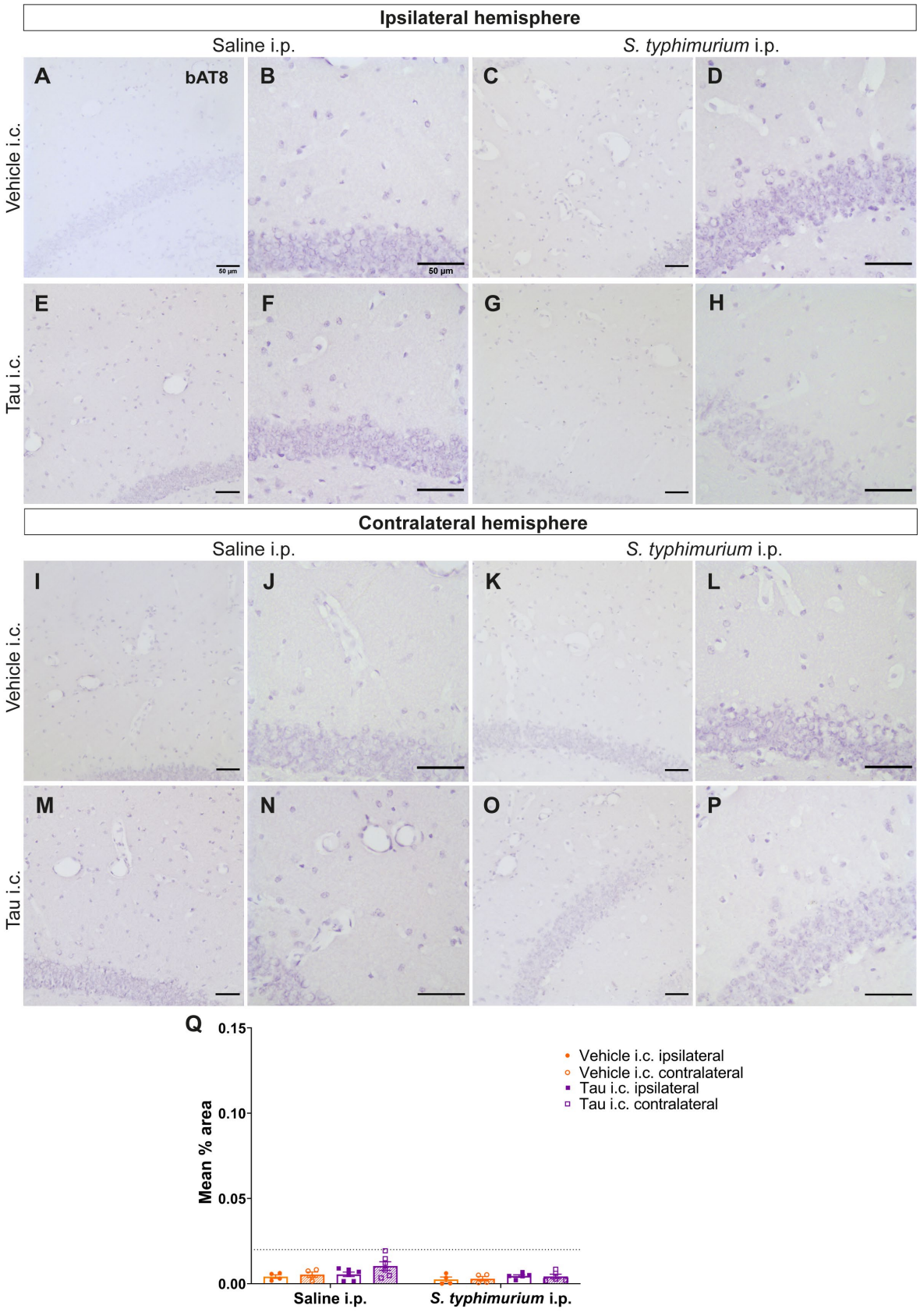
Ipsilateral hemisphere
Saline i.p.
S. typhimurium i.p.
A
bAT8
B
C
D
Vehicle i.c.
50 µm
E
F
G
H
Tau i.c.
Contralateral hemisphere
Saline i.p.
S. typhimurium i.p.
I
J
K
L
Vehicle i.c.
M
N
O
P
Tau i.c.
Q
Mean % area
0.15
0.10
0.05
0.00
Vehicle i.c. ipsilateral
Vehicle i.c. contralateral
Tau i.c. ipsilateral
Tau i.c. contralateral
Saline i.p.
S. typhimurium i.p.

.

Figure 6-12: AT8 staining in the ventral hippocampus of H1*Mapt-/-* mice

Representative images of analysis for (**A, B**) vehicle i.c./saline i.p., (**C, D**) vehicle i.c./*S. typhimurium* i.p., (**E, F**) tau i.c./saline i.p. and (**G, H**) tau i.c./*S. typhimurium* i.p. groups in the ipsilateral hemisphere. **I-P**) Representative images were included from the same groups for the contralateral hemisphere. **A, C, E, G, I, K, M, O**) 20x objective, scale bar= 50μm; **B, D, F, H, J, L, N, P**) 40x objective, scale bar= 50μm. **Q**) Quantification of tau pathology, two-way ANOVA with Sidak's post-hoc test. n= 6 for tau i.c./saline i.p., n= 5 for tau i.c./*S. typhimurium* i.p. injection groups, n= 4 for both vehicle i.c. groups. All data is presented as mean ± SEM.

6.3.8 AT8 immunoreactivity in the perirhinal cortex

The perirhinal cortex is located dorsal to the entorhinal cortex as part of the parahippocampal gyrus. This cortex has significant connections to both the entorhinal cortex and hippocampus (Vismer *et al.*, 2015). In this brain region, tau deposition was observed following i.c. injection of the human tau lysate, specifically in the ipsilateral hemisphere. Moreover, in C57BL/6 mice two-fold higher expression of AT8 was observed following *S. typhimurium* infection in the ipsilateral hemisphere (tau i.c./saline i.p.= 0.02% ± 0.004; tau i.c./*S. typhimurium* i.p.= 0.05% ± 0.01; $p<0.05$) (**Figure 6-13**). There is not a significant main effect of *S. typhimurium* ($F(1, 12)= 3.62$, $p= 0.08$), however because of the post-hoc significance it is also possible to observe a trend with the main effect. There is a significant main effect of hemisphere ($F(1, 12= 15.83$, $p<0.01$), yet no significant main interaction of these two variables ($F(1, 12)= 2.98$, $p= 0.11$). There was pathology observed in the contralateral perirhinal cortex, however this was only consistent in one mouse in the tau i.c./*S. typhimurium* i.p. group (tau i.c./saline i.p.= 0.01% ± 0.002; tau i.c./*S. typhimurium* i.p.= 0.02% ± 0.01, $p= 0.66$). Other mice within the tau i.c. groups did show inclusions in the contralateral hemisphere however this was not consistently observed throughout all slices, as a result the mean percentage area is low (~0.02%). However, this finding is represented in the tau scoring in **Figure 6-25**. From quantification in **Figure 6-13**, it is clear to observe that tau deposition is increased by systemic infection and predominantly observed in the ipsilateral hemisphere at this time point.

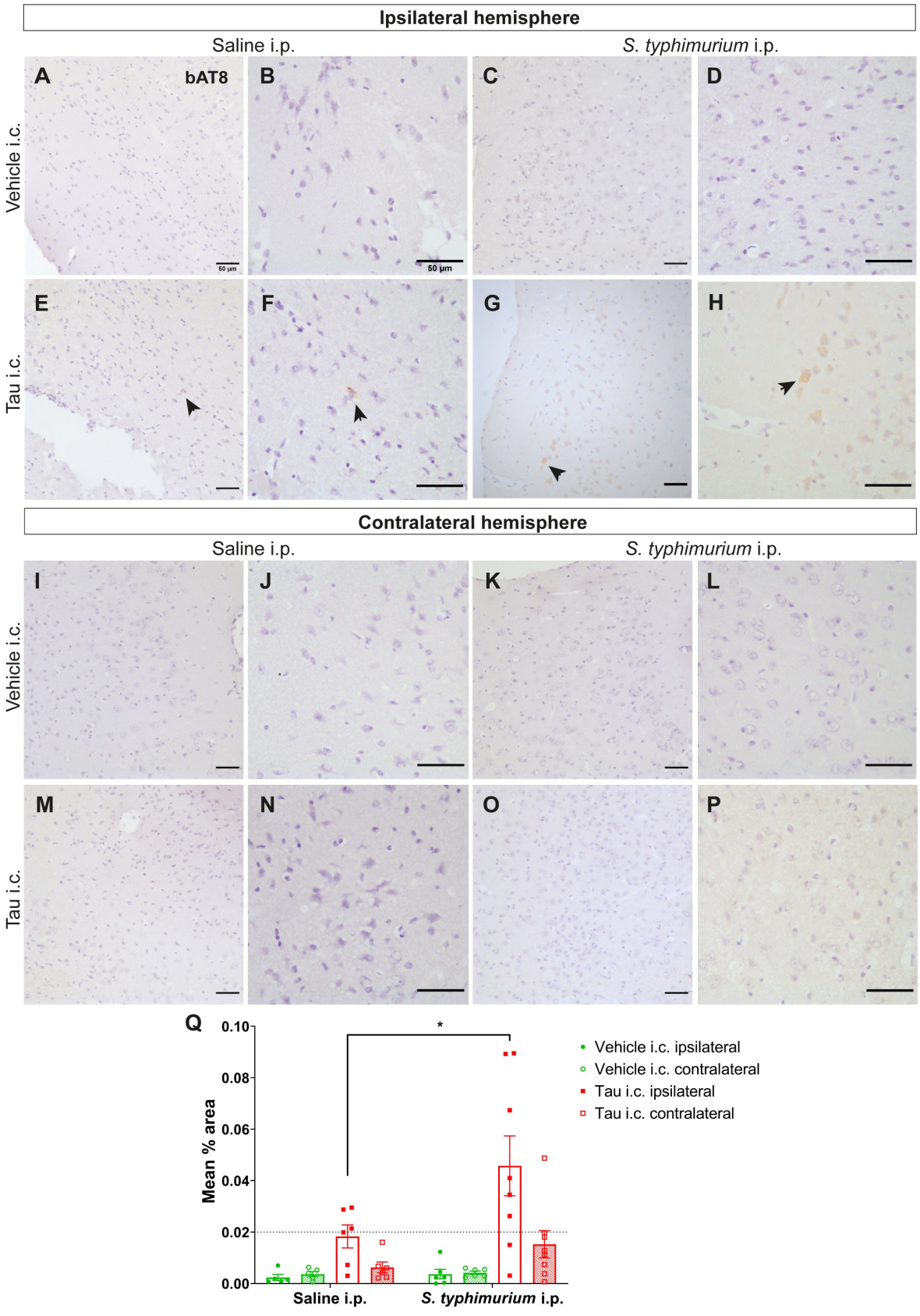
Ipsilateral hemisphere
Saline i.p.
S. typhimurium i.p.
Vehicle i.c.
Tau i.c.
A
bAT8
B
C
D
E
F
G
H
50 µm
Contralateral hemisphere
Saline i.p.
S. typhimurium i.p.
Vehicle i.c.
Tau i.c.
I
J
K
L
M
N
O
P
Q
Mean % area
0.10
0.08
0.06
0.04
0.02
0.00
*
Saline i.p.
S. typhimurium i.p.
Vehicle i.c. ipsilateral
Vehicle i.c. contralateral
Tau i.c. ipsilateral
Tau i.c. contralateral

Figure 6-13: AT8-positive tau in the perirhinal cortex following systemic infection in C57BL/6 mice

A, C, I, K) Representative images of vehicle i.c. injected mice and (**E, G, M, O**) tau i.c. injected mice; 20x objective, scale bar= 50µm. High magnification images of tau pathology from (**B, D, J, L**) vehicle i.c. injected mice and (**F, H, N, P**) tau i.c. injected mice; 40x objective, scale bar= 50µm. Black arrowheads denote tau pathology. **Q**) Quantification of bAT8 expression in C57BL/6 mice, two-way ANOVA with Sidak's post-hoc test (*$p<0.05$). n= 6 for tau i.c./saline i.p., n= 8 for tau i.c./*S. typhimurium* i.p., n= 5 for vehicle i.c./saline i.p., n= 6 vehicle i.c./*S. typhimurium* i.p. injection group. All data is presented as mean ± SEM.

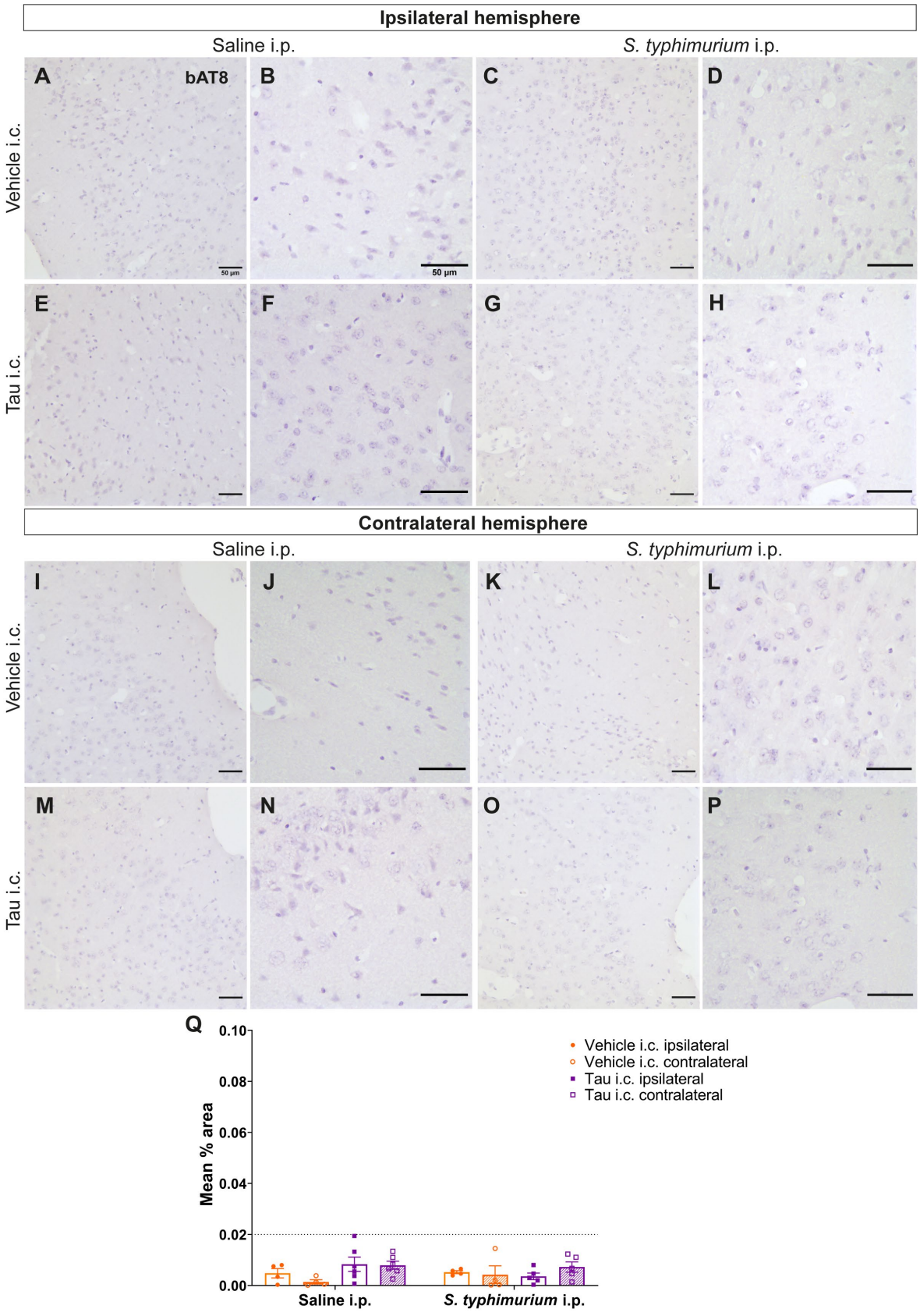
Ipsilateral hemisphere
Saline i.p.
S. typhimurium i.p.
A
bAT8
B
C
D
Vehicle i.c.
50 µm
E
F
G
H
Tau i.c.
Contralateral hemisphere
Saline i.p.
S. typhimurium i.p.
I
J
K
L
Vehicle i.c.
M
N
O
P
Tau i.c.
Q
Mean % area
0.10
0.08
0.06
0.04
0.02
0.00
Saline i.p.
S. typhimurium i.p.
Vehicle i.c. ipsilateral
Vehicle i.c. contralateral
Tau i.c. ipsilateral
Tau i.c. contralateral

Figure 6-14: AT8 immunoreactivity in the perirhinal cortex of H1*Mapt-/-* mice

Representative images of analysis for (**A, B**) vehicle i.c./saline i.p., (**C, D**) vehicle i.c./*S. typhimurium* i.p., (**E, F**) tau i.c./saline i.p. and (**G, H**) tau i.c./*S. typhimurium* i.p. groups in the ipsilateral hemisphere. **I-P**) Representative images were included from the same groups for the contralateral hemisphere. **A, C, E, G, I, K, M, O**) 20x objective, scale bar= 50μm; **B, D, F, H, J, L, N, P**) 40x objective, scale bar= 50μm. **Q**) Quantification of bAT8 expression, two-way ANOVA with Sidak's post-hoc test. n= 6 for tau i.c./saline i.p., n= 5 for tau i.c./*S. typhimurium* i.p., n= 4 for vehicle i.c. injection groups. All data is presented as mean ± SEM.

By contrast, H1*Mapt-/-* mice show no tau pathology in the ipsilateral perirhinal cortex in either tau i.c. group (tau i.c./saline i.p.= 0.01% ± 0.003; tau i.c./*S. typhimurium* i.p.= 0.004% ± 0.001, p= 0.23) (**Figure 6-14**). There was also no AT8 immunoreactivity observed in the contralateral perirhinal cortex (tau i.c./saline i.p.= 0.01% ± 0.002; tau i.c./*S. typhimurium* i.p.= 0.01% ± 0.002, p= 0.97). As a result, there was no significant main effect of i.p. injection ($F(1, 9)= 1.84$, p= 0.21) or hemisphere ($F(1, 9)= 0.56$, p= 0.47). This suggests that H1*Mapt-/-*mice consistently display less pathology than C57BL/6 mice. There is small deposition in a select few of the C57BL/6 tau i.c./saline i.p. mice; this is not observed in the equivalent H1*Mapt-/-* mice and so the baseline spatiotemporal spread is different.

6.3.9 Tau deposition in the mammillary nuclei

The mammillary nuclei are found ventral to the injection site as part of the diencephalon. The mammillary nuclei consist of the lateral and medial nucleus, with the supramammillary nuclei (SuMN) located directly dorsal. Whilst the mammillary nuclei were imaged, there was minimal pathology observed in the lateral mammillary nuclei (LMN), with pathology consistently found in the SuMN. In C57BL/6 mice, pathology is predominantly observed in the tau i.c./*S. typhimurium* i.p. group (**Figure 6-15**). The pathology also appears more like inclusions than the dot-like staining in the white matter. AT8-positive tau is observed in both tau i.c. groups, however there is a ten-fold increase in tau pathology following systemic infection (tau i.c./saline i.p.= 0.01% ± 0.005; tau i.c./*S. typhimurium* i.p.= 0.11% ± 0.04; $p<0.05$). As a result, there is a significant main effect of i.p. injection ($F(1, 12)= 6.12$, $p<0.05$), yet no effect of hemisphere ($F(1, 12)= 3.84$, p= 0.07). Notably, there is consistent pathology in both the ipsilateral and contralateral hemisphere of the tau i.c./*S. typhimurium* i.p. group, yet contralateral pathology is only observed in a couple of mice in the saline i.p. group (tau i.c./saline i.p. = 0.01% ± 0.004; tau i.c./*S. typhimurium* i.p.= 0.05% ± 0.02, p= 0.16). Quantification of AT8 immunoreactivity demonstrates that the mammillary nucleus was

one ROI where the spreading of tau pathology is increased in the tau i.c./*S. typhimurium* i.p. group compared to the saline i.p. group.

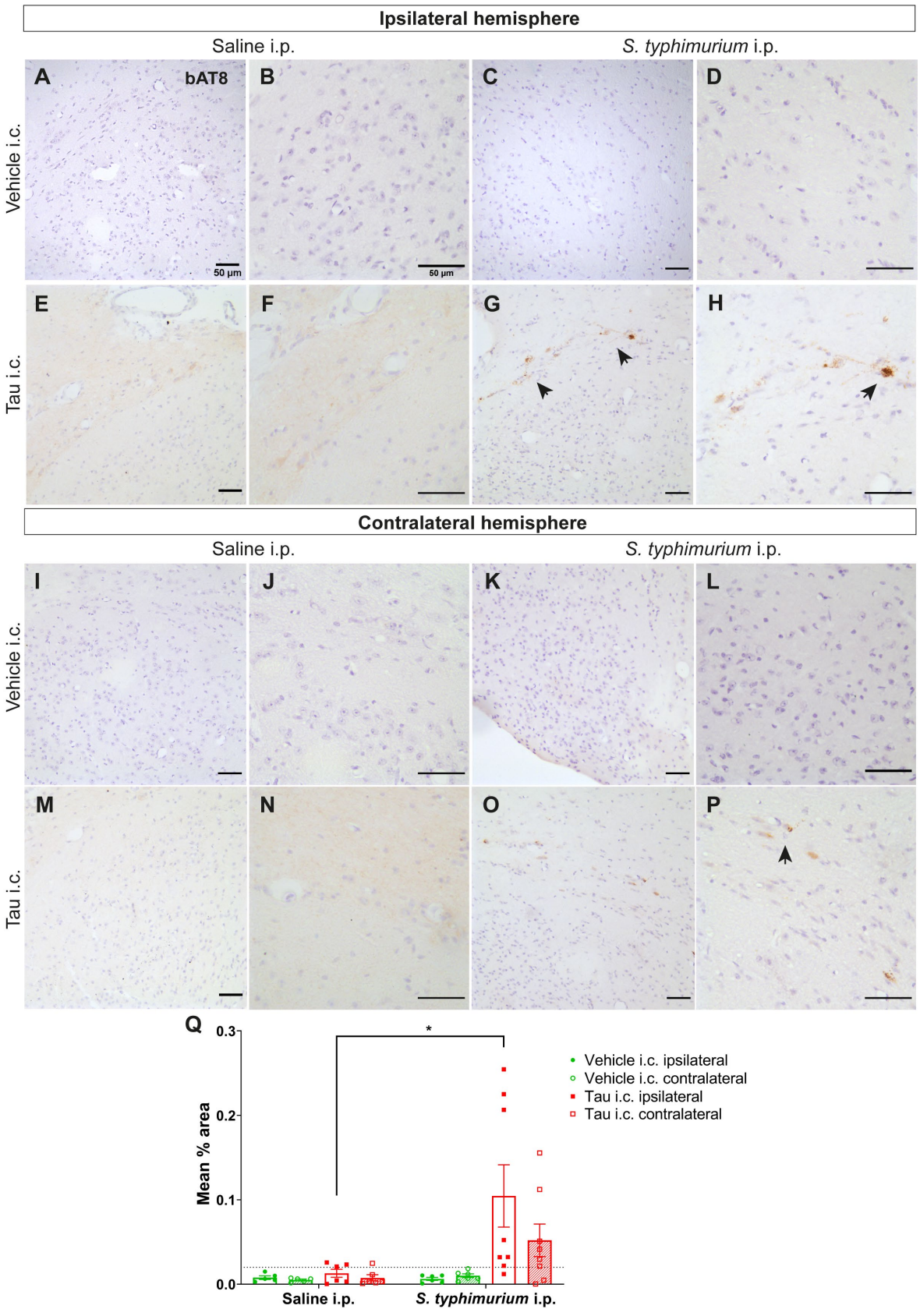

Figure 6-15: Tau pathology in the mammillary nuclei of C57BL/6 mice

A, C, I, K) Representative images of vehicle i.c. injected mice and (**E, G, M, O**) tau i.c. injected mice; 20x objective, scale bar= 50µm. High magnification images of tau pathology from (**B, D, J, L**) vehicle i.c. injected mice and (**F, H, N, P**) tau i.c. injected mice; 40x objective, scale bar= 50µm. Black arrowheads denote tau pathology. **Q**) Immunohistochemical analysis of bAT8 expression in C57BL/6 mice, two-way ANOVA with Sidak's post-hoc test, (*$p<0.05$). n= 6 for tau i.c./saline i.p., n= 8 for tau i.c./*S. typhimurium* i.p., n= 5 for vehicle i.c./saline i.p., n= 6 vehicle i.c./*S. typhimurium* i.p. injection group. Data was log transformed for analysis, due to most values being <1, the data presented in this graph is the original mean % area values. All data is presented as mean ± SEM.

By contrast H1*Mapt-/-* mice showed no pathology in the mammillary nuclei (**Figure 6-16**) either ipsilateral (tau i.c./saline i.p.= 0.01% ± 0.004; tau i.c./*S. typhimurium* i.p.= 0.01% ± 0.002, p= 0.82) or contralateral (tau i.c./saline i.p.= 0.01% ± 0.002; tau i.c./*S. typhimurium* i.p.= 0.01% ± 0.002, p= 0.38). Subsequently there was no significant main effect of i.p. injection ($F(1, 8)= 2.26$, $p=0.17$) or hemisphere ($F(1, 8)= 2.37$, $p= 0.16$). As throughout all analysis, no pathology was observed in mice receiving vehicle i.c. injection. These results all indicate that C57BL/6 mice show more tau pathology than the H1*Mapt-/-*mice. Furthermore, C57BL/6 wild type mice show greater pathology and earlier deposition in regions synaptically connected following systemic infection.

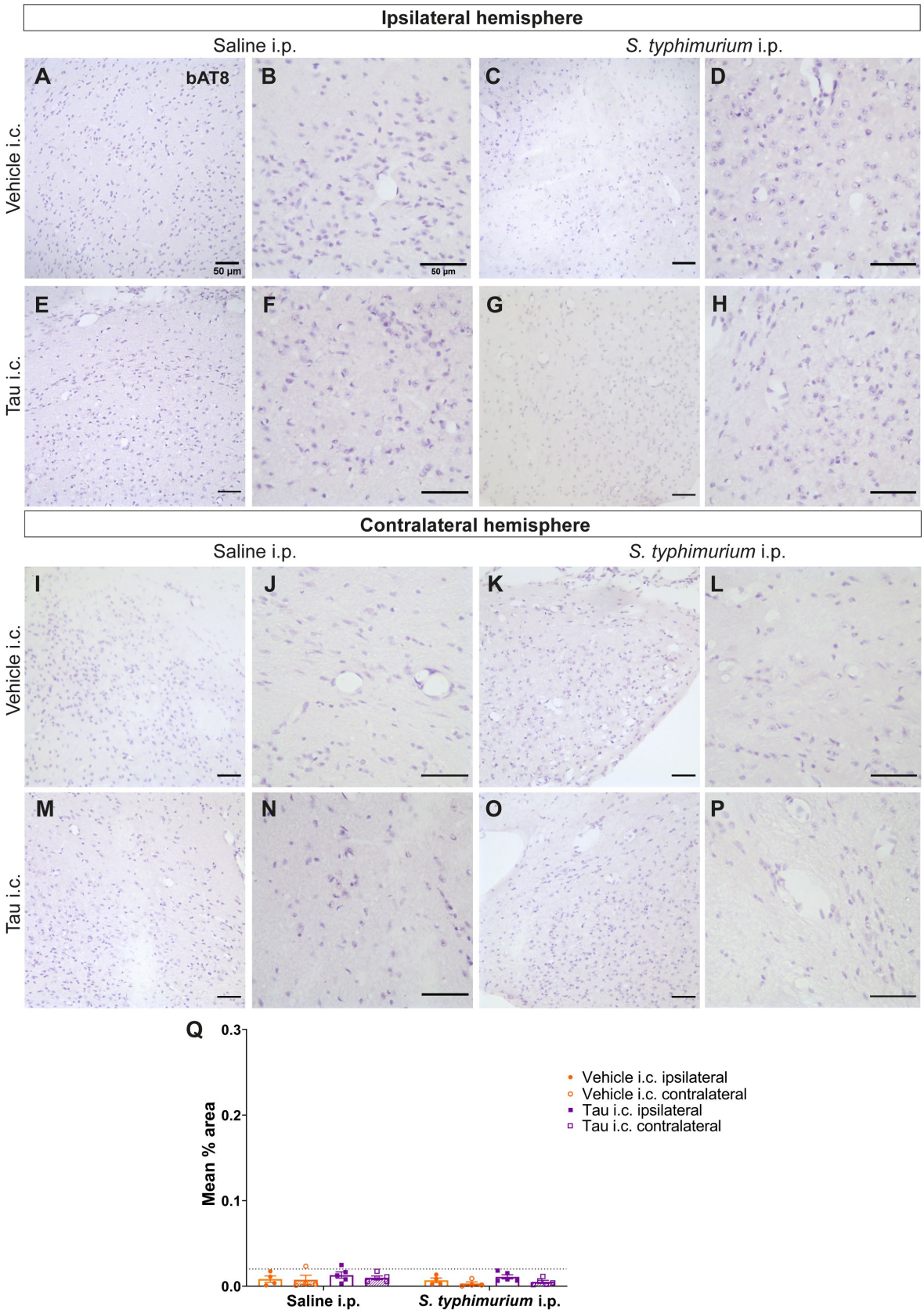
Ipsilateral hemisphere
Saline i.p.
S. typhimurium i.p.
A
bAT8
B
C
D
Vehicle i.c.
50 µm
50 µm
E
F
G
H
Tau i.c.
Contralateral hemisphere
Saline i.p.
S. typhimurium i.p.
I
J
K
L
Vehicle i.c.
M
N
O
P
Tau i.c.
Q
Mean % area
0.3
0.2
0.1
0.0
Saline i.p.
S. typhimurium i.p.
Vehicle i.c. ipsilateral
Vehicle i.c. contralateral
Tau i.c. ipsilateral
Tau i.c. contralateral

Figure 6-16: Tau pathology in the mammillary nuclei of H1*Mapt-/-* mice

A, C, I, K) Representative images of vehicle i.c. injected mice and (**E, G, M, O**) tau i.c. injected mice; 20x objective, scale bar= 50µm. Images of tau pathology at a higher magnification were also included from (**B, D, J, L**) vehicle i.c. injected mice and (**F, H, N, P**) tau i.c. injected mice; 40x objective, scale bar= 50µm. **Q**) Immunohistochemical analysis of bAT8 expression in C57BL/6 mice. Two-way ANOVA with Sidak's post-hoc test; n= 5 for both tau i.c. groups, n= 4 for both vehicle i.c. groups. Data was log transformed for analysis.

6.3.10 Tau pathology at the dorsal fornix

The final brain region examined was dorsal to the injection site (Bregma AP= -1.00). Only the corpus callosum and dorsal fornix ROIs were analysed. The fornix is a white matter tract with synaptic pathways from the hippocampus which connects regions in the limbic system such as the mammillary bodies (Douet and Chang, 2015). After examining the dorsal fornix in C57BL/6 mice, no pathology was observed in mice receiving vehicle i.c. injection (**Figure 6-17**). However, i.c. injection of human tau lysate results in pathology in this region, with the same speckled morphology observed previously in the white matter. Moreover, an eight-fold higher expression of AT8 was observed in mice exposed to systemic infection (tau i.c./saline i.p.= 0.03% ± 0.02; tau i.c./*S. typhimurium* i.p.= 0.25% ± 0.12). A Mann Whitney test determined there was a significant difference between the bAT8 staining in the tau i.c./saline i.p. or tau i.c./*S. typhimurium* i.p. dorsal fornix ($U= 4$, $p<0.01$).

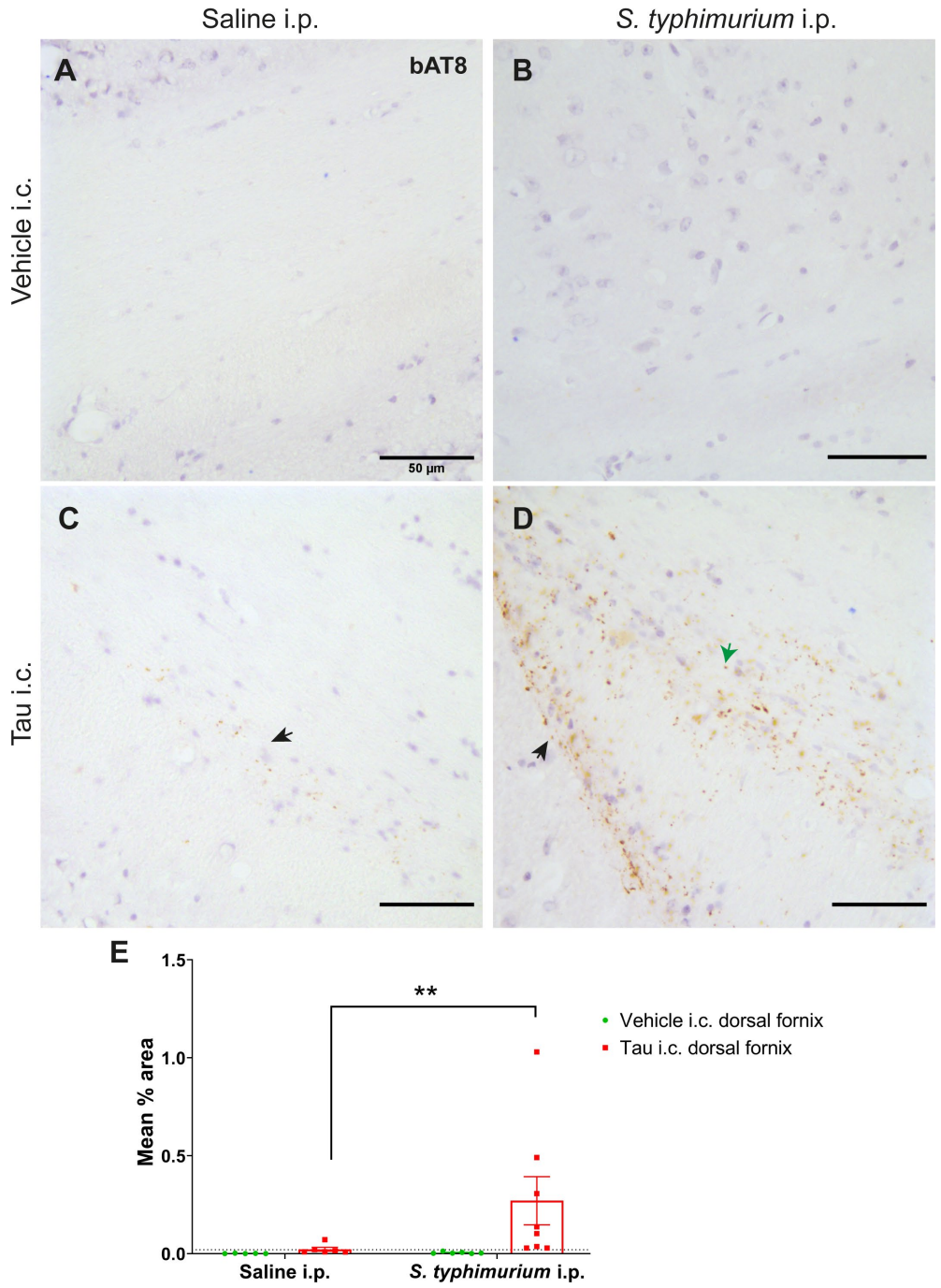

Figure 6-17: AT8-positive tau in the dorsal fornix of C57BL/6 mice

Tau pathology in (**A**) vehicle i.c./saline i.p., (**B**) vehicle i.c./*S. typhimurium* i.p., (**C**) tau i.c./saline i.p. and (**D**) tau i.c./*S. typhimurium* i.p. groups. 40x objective, scale bar= 50µm. Black arrowheads denote tau pathology, green arrowhead denoted corpus callosum which was not included in analysis. **E**) Quantification of bAT8 expression, Mann Whitney U test was used (**p<0.01). n= 6 for tau i.c./saline i.p., n= 8 for tau i.c./*S. typhimurium* i.p., n= 5 for vehicle i.c./saline i.p., n= 6 vehicle i.c./*S. typhimurium* i.p. injection group. All data is presented as mean ± SEM.

In the corpus callosum pathology was observed in both C57BL/6 tau i.c. groups (**Figure 6-18**). However, despite a clear outlier there are similar levels of tau staining between these two groups (tau i.c./saline i.p.= 0.36% ± 0.15; tau i.c./*S. typhimurium* i.p.= 0.59% ± 0.17). As a result, a Mann Whitney U test determined that there was no significant effect of *S. typhimurium* i.p. (U= 21, p= 0.75). This highlights a potential difference between tau pathology observed in the corpus callosum versus the dorsal fornix. In the contralateral hemisphere, the corpus callosum showed low levels of pathology in the tau i.c./*S. typhimurium* i.p. group (tau i.c./saline i.p.= 0.02% ± 0.01; tau i.c./*S. typhimurium* i.p.= 0.09% ± 0.03). These results suggest that there is a trend that mice which underwent a bacterial infection express greater AT8-positive tau pathology at this ROI.

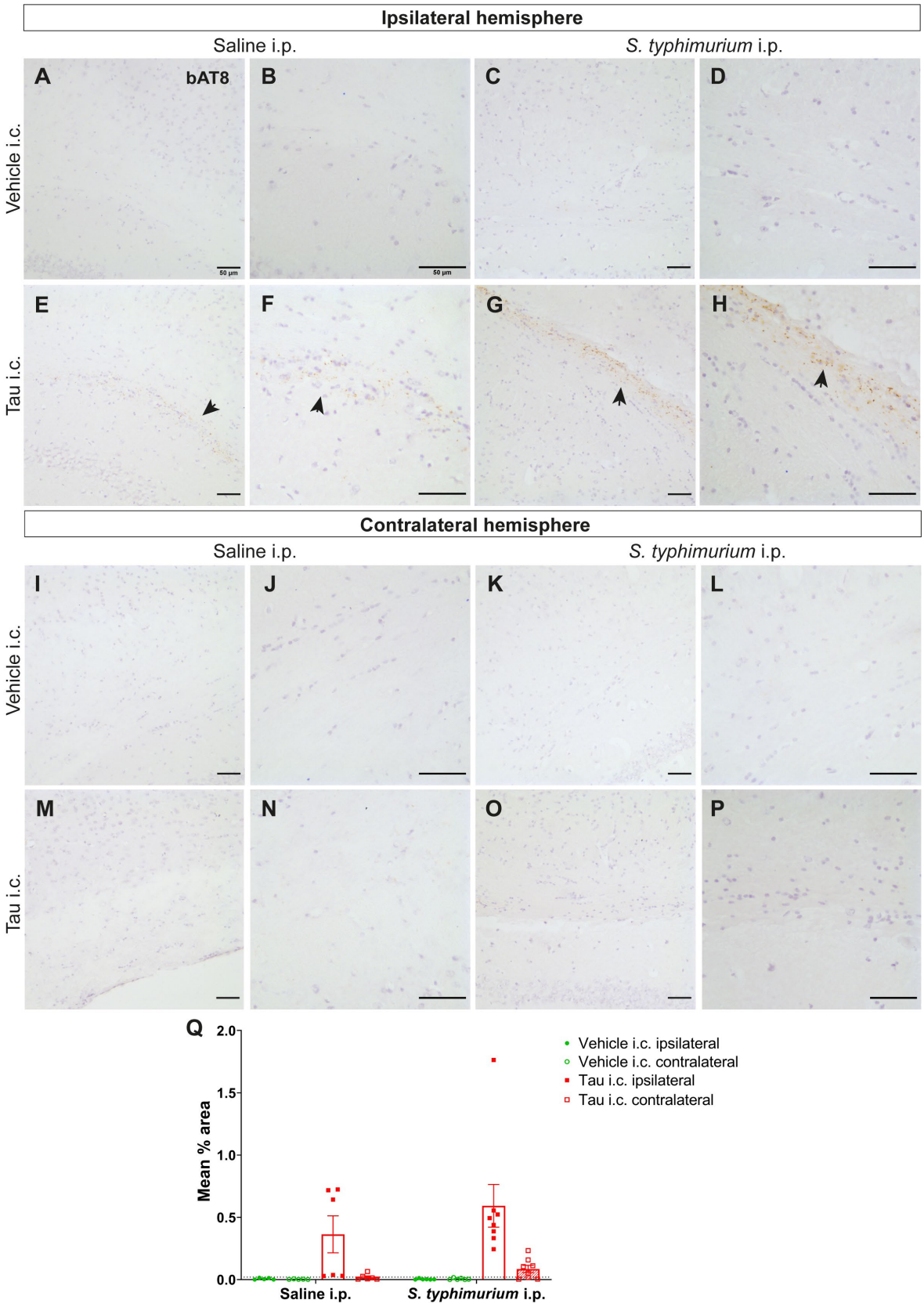
Ipsilateral hemisphere
Saline i.p.
S. typhimurium i.p.
A
bAT8
B
C
D
Vehicle i.c.
E
F
G
H
Tau i.c.
Contralateral hemisphere
Saline i.p.
S. typhimurium i.p.
I
J
K
L
Vehicle i.c.
M
N
O
P
Tau i.c.
Q
Mean % area
2.0
1.5
1.0
0.5
0.0
Saline i.p.
S. typhimurium i.p.
Vehicle i.c. ipsilateral
Vehicle i.c. contralateral
Tau i.c. ipsilateral
Tau i.c. contralateral

Figure 6-18: AT8-positive tau within the corpus callosum of C57BL/6 mice

A, C, I, K) Representative images of vehicle i.c. injected mice and (**E, G, M, O**) tau i.c. injected mice; 20x objective, scale bar= 50µm. Images at a higher magnification were also included from (**B, D, J, L**) vehicle i.c. injected mice and (**F, H, N, P**) tau i.c. injected mice; 40x objective, scale bar= 50µm. Black arrowheads denote tau pathology. **Q**) Quantification of bAT8 expression in C57BL/6 mice, Mann-Whitney U test. n= 6 for tau i.c./saline i.p., n= 8 for tau i.c./*S. typhimurium* i.p., n= 5 for vehicle i.c./saline i.p., n= 6 vehicle i.c./*S. typhimurium* i.p. injection group. All data is presented as mean ± SEM

By contrast, in the H1*Mapt-/-* mice, the dorsal fornix in H1*Mapt-/-* showed no significant effect of *S. typhimurium* i.p. injection (t(8)= 0.05, p= 0.69) (**Figure 6-19**). There was very similar AT8 immunoreactivity within the tau i.c. groups (tau i.c./saline i.p.= 0.05% ± 0.03; tau i.c./*S. typhimurium* i.p.= 0.05% ± 0.03). There is very minimal tau propagation to the dorsal fornix in these mice. This highlights a further difference in the propagation rates of tau pathology in the C57BL/6 and H1*Mapt-/-* mice. The H1*Mapt-/-* mice also showed tau pathology in the corpus callosum (**Figure 6-20**). However, in the ipsilateral hemisphere expression was very similar between the two tau i.c. groups (tau i.c./saline i.p.= 0.07% ± 0.03; tau i.c./*S. typhimurium* i.p.= 0.08% ± 0.05). In the contralateral hemisphere AT8 immunoreactivity was demonstrably lower in both tau i.c. groups (tau i.c./saline i.p.= 0.04% ± 0.02; tau i.c./*S. typhimurium* i.p.= 0.01% ± 0.01). There was no significant main effect of i.p. injection ($F(1, 8)= 0.42$, $p= 0.53$), however there was a significant main effect of hemisphere ($F(1, 8)= 5.34$, $p<0.05$). Therefore, this shows the clear distinction between tau propagation in C57BL/6 and H1*Mapt-/-* mice.

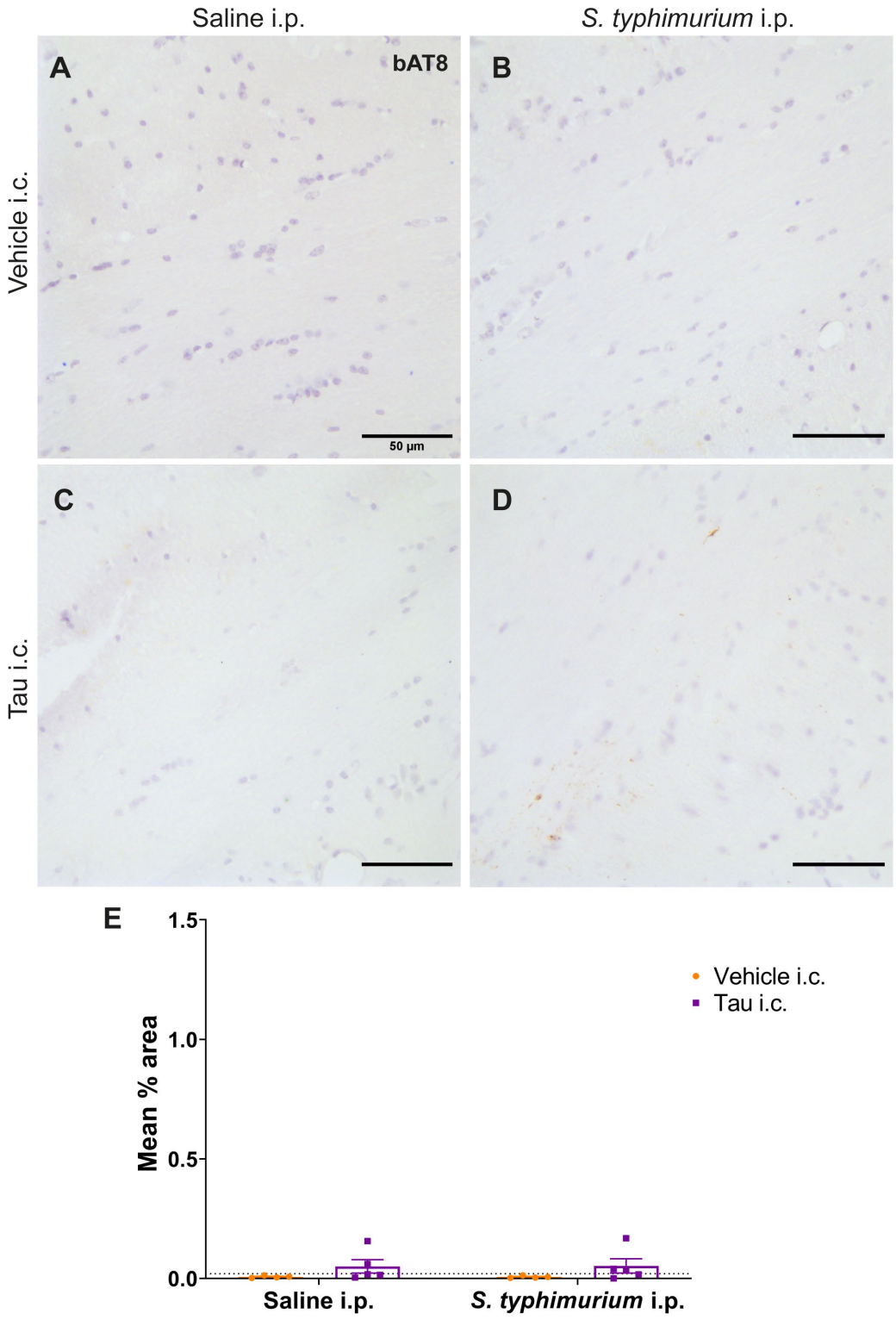

Figure 6-19: Dorsal fornix tau histology in H1*Mapt-/-* mice

Tau pathology in (**A**) vehicle i.c./saline i.p., (**B**) vehicle i.c./*S. typhimurium* i.p., (**C**) tau i.c./saline i.p. and (**D**) tau i.c./*S. typhimurium* i.p. groups. 40x objective, scale bar= 50µm. **E**) Quantification of bAT8 expression, Unpaired Student's t-test. n= 5 for both tau i.c. groups, n= 4 for vehicle i.c. groups. Data was log transformed for analysis. However, most original values are <1, therefore the graph shows the original mean % area results which are not log transformed. All data is presented as mean ± SEM.

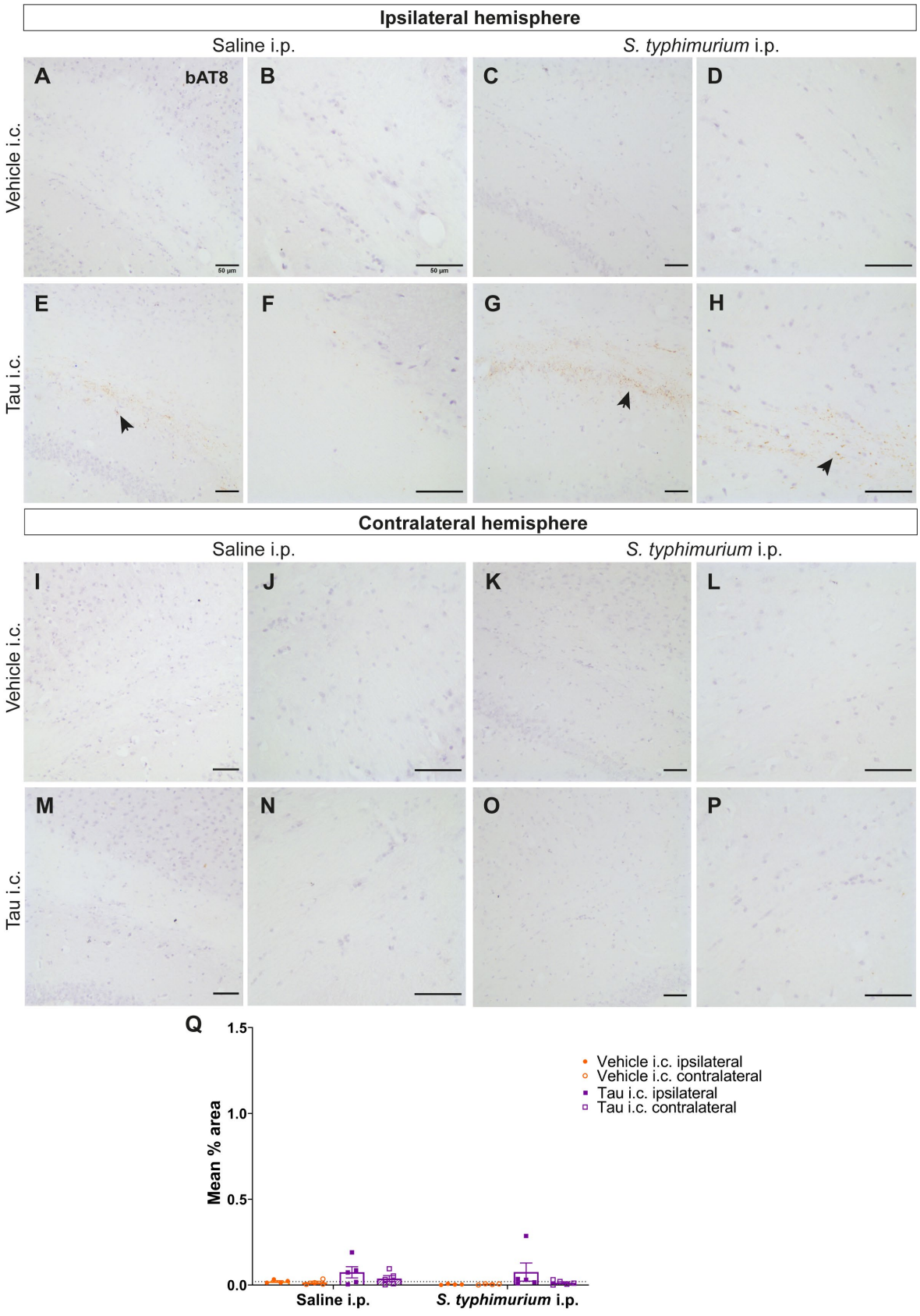
Ipsilateral hemisphere
Saline i.p.
S. typhimurium i.p.
A
bAT8
B
C
D
Vehicle i.c.
E
F
G
H
Tau i.c.
Contralateral hemisphere
Saline i.p.
S. typhimurium i.p.
I
J
K
L
Vehicle i.c.
M
N
O
P
Tau i.c.
Q
Mean % area
1.5
1.0
0.5
0.0
Saline i.p.
S. typhimurium i.p.
Vehicle i.c. ipsilateral
Vehicle i.c. contralateral
Tau i.c. ipsilateral
Tau i.c. contralateral

Figure 6-20: Phosphorylated tau in corpus callosum of H1*Mapt-/-* mice

A, C, I, K) Representative images of vehicle i.c. injected mice and (**E, G, M, O**) tau i.c. injected mice; 20x objective, scale bar= 50µm. Images at a higher magnification were also included from (**B, D, J, L**) vehicle i.c. injected mice and (**F, H, N, P**) tau i.c. injected mice; 40x objective, scale bar= 50µm. Black arrowheads denote tau pathology. **Q**) Quantification of bAT8 expression in C57BL/6 mice, two-way ANOVA with Sidak's post-hoc test. n= 5 for both tau i.c. groups, n= 4 for both vehicle i.c. groups. Data was log transformed for analysis. However, most original values are <1, therefore the graph shows the original mean % area results which are not log transformed. All data is presented as mean ± SEM

6.3.11 Notable pathology outside of ROIs

Whilst ROIs were determined and utilised to analyse the tau pathology, there were several regions where pathology was only observed in one brain out of 44 brains in total which were examined. In this case the region was not analysed throughout the cohort and instead demonstrated here separately. The reasons for this pathology are unclear, yet all regions where pathology was detected were initially scanned for pathology due to strong synaptic connections to the injection site. In **Figure 6-21** three distinct regions are stained for; it is notable that all three images are not from the same brain, yet all mice underwent tau i.c. followed by *S. typhimurium* i.p. injection. Pathology is observed dorsal to the injection site at the ventral fornix (**Figure 6-21**), and at the injection site, pathology was observed in the retrosplenial cortex. Finally, ventral to the injection site pathology is observed in the CA3.

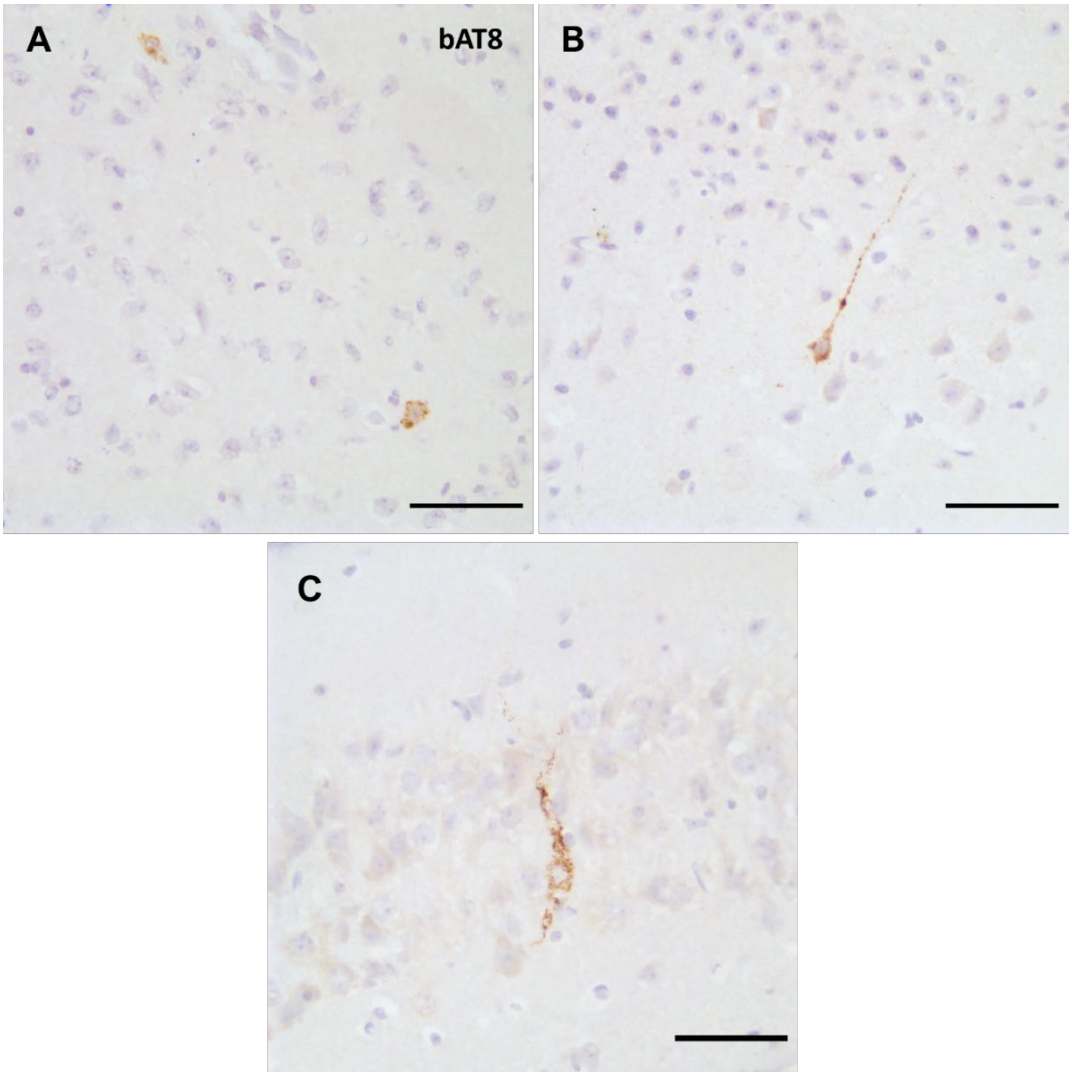

Figure 6-21: Notable regions within the brain that showed additional AT8-positive tau

A) Ventral fornix, **B)** retrosplenial cortex and **C)** hilus region stained for bAT8. All images taken at 40x objective; scale bar= 50µm. All images taken from tau i.c./*S. typhimurium* i.p. group.

In addition, one mouse was excluded from analysis. This mouse underwent tau i.c. injection followed by saline i.p. injection. However, upon perfusion it was discovered that this mouse had a spleen of 180mg, suggesting a possible systemic inflammatory response. This spleen is distinctly larger and outside the range of spleen weights for the saline i.p. group regardless of i.c. injection. It was also noted after analysis that this mouse showed gradual weight loss from baseline over time after the saline i.p. injection; this is in direct contradiction to other mice in the same group. This suggests that this mouse had a procedural issue with the i.p. injection and therefore should be excluded. This is potentially due to injury to the gut during the i.p. injection, however no

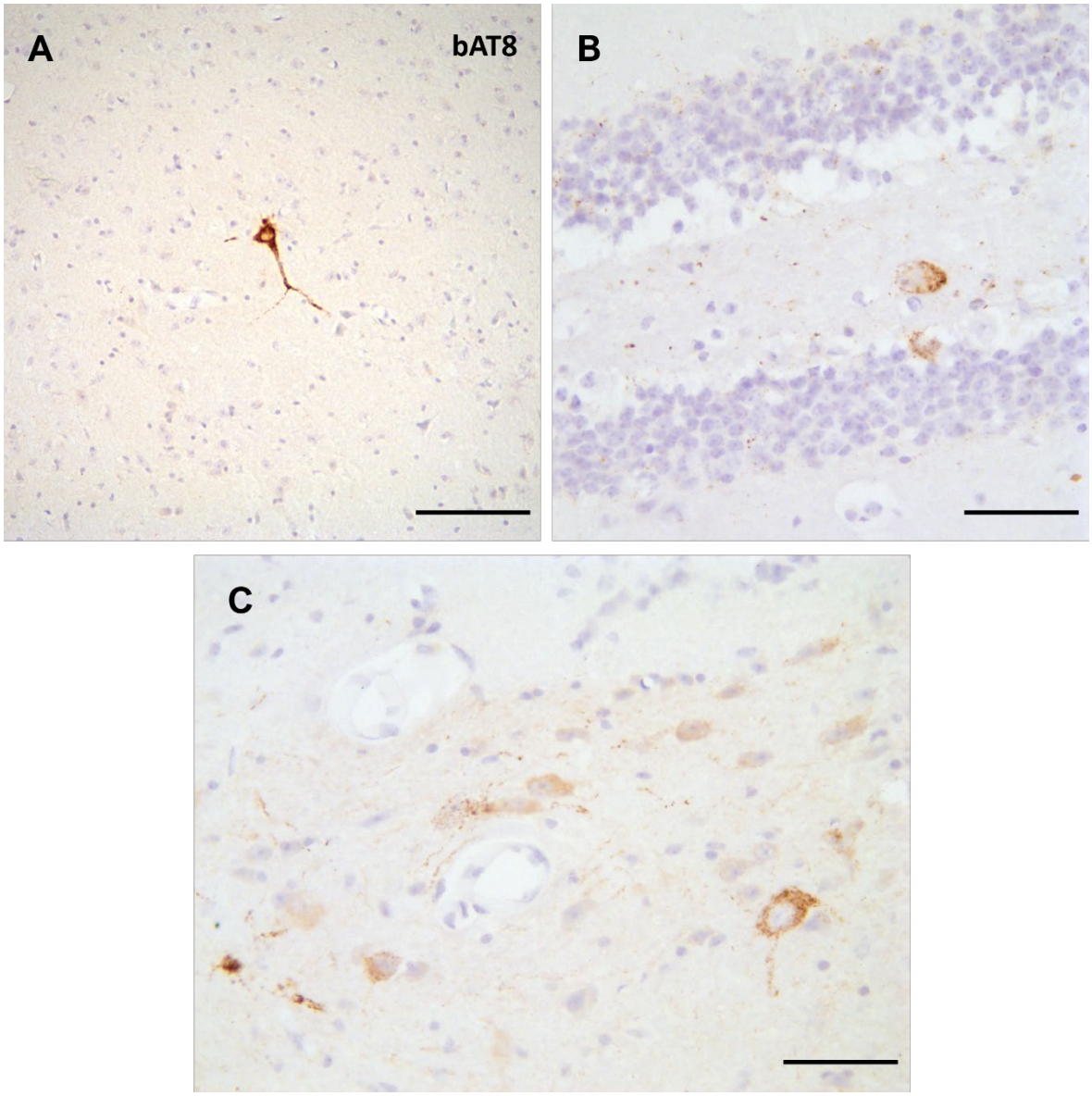

Figure 6-22: Notable AT8-positive tau in mouse excluded for experimental outliers

A) Ventral fornix, **B)** hilus region and **C)** mammillary nuclei stained for bAT8. **A)** Image taken at 20x objective; scale bar= 100µm **B, C)** images taken at 40x objective; scale bar= 50µm. All images taken from tau i.c./*S. typhimurium* i.p. group.

sickness behaviour was noted, and the weight loss was gradual and never within range of concern for welfare. Therefore, it is unlikely to be caused by a full caecal puncture as this would cause sepsis and has a very low survival rate (Dejager *et al.*, 2011).

Whilst this mouse has been excluded from the overall cohort, images of the tau pathology were still recorded (**Figure 6-22**). Interestingly, this mouse displayed significant amounts of pathology, akin to pathology observed in the tau i.c./*S. typhimurium* i.p. group. Pathology from the ventral fornix, CA4 and mammillary nuclei are all recorded.

6.3.12 Detection of amyloidogenic protein

Following on from the previous chapter, it was noted that the human lysate used for the seed prep may contain other Sarkosyl-insoluble proteins, such as aggregated amyloid or α-Synuclein. To investigate this, I also stained sections with Thioflavin S and antibodies to detect the presence of amyloid and α-Synuclein deposition. Thioflavin S is a histological stain which detects β-pleated sheet amyloid deposition (Rajamohamedsait and Sigurdsson, 2012). However, because it detects β-pleated sheet structures this means PHFs and NFTs can also be detected. For Aβ pathology I used the human-amyloid 1-42 specific antibody bapineuzumab, and an antibody that binds to phosphorylated human α-Synuclein was used to analyse α-Synuclein pathology. No immunoreactivity of bapineuzumab was observed, as shown in **Figure 6-23** with the dentate gyrus as an example. Small deposits of thioflavin S staining were detected along the dentate gyrus, coinciding with AT8-positive staining. Given that the post-mortem cases were Braak stage V-VI it is likely that the AD-tau within the lysate is heavily enriched for beta-pleated sheet structures. Therefore, given the morphology of the stain and the location within the brain it is unlikely that there is Aβ deposition in these brains.

For detection of α-Synuclein pathology, brain sections were analysed for presence of phosphorylated epitopes of α-Synuclein at S129 epitope (**Figure 6-23**). This phosphorylated epitope is detected in α-Synuclein pathology in Lewy bodies, and is commonly used as a marker in Parkinson's disease research (Sato, Kato and Arawaka, 2013). No α-Synuclein pathology was observed throughout the brain in mice receiving either saline or *S. typhimurium* i.p. injection. There is non-specific background in mice that were exposed to *S. typhimurium* i.p. As the α-Synuclein antibody is a mouse antibody, this staining is likely due to the presence of mouse IgG as these same results were obtained using an unconjugated mouse anti-AT8 antibody.

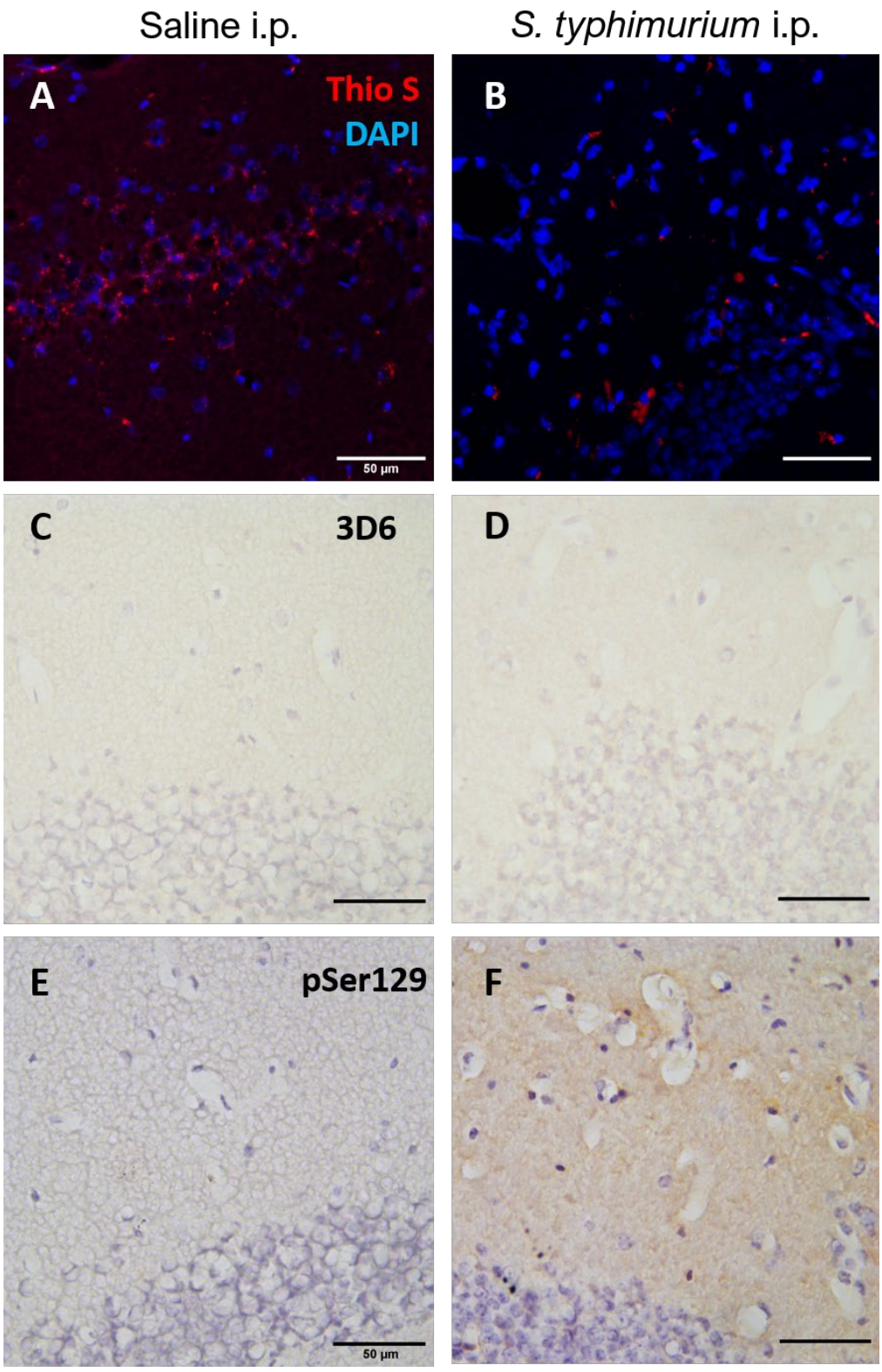

Figure 6-23: Detection of amyloidogenic and α-Synuclein proteins

A, B) Thioflavin S and DAPI staining in the dentate gyrus of mice which receiving tau i.c. injection followed by saline or *S. typhimurium* infection. **C, D)** Bapineuzumab staining in the dentate gyrus. **E, F)** Phosphorylated α-Synuclein in the dentate gyrus, Mike Hurley carried out histology for α-Synuclein. All images taken at 40x objective; scale bar= 50µm. All images taken from mice that received an i.c. injection of human tau-enriched seed prep.

6.3.13 Analysis of tau pathology using western blot

To further investigate if a systemic bacterial infection promotes tau pathology and to confirm histological analysis, a western blot was carried out (**Figure 6-24**). At three months post-injection there is minimal overt pathology observed in histology, yet there may be hyperphosphorylation detectable at the protein level. Hippocampal brain homogenates were prepared from C57BL/6 mice which received vehicle or tau i.c. injection, followed by systemic infection or saline i.p. injection. Each sample was diluted with dH_2O and 4x loading buffer to reach 50µg total protein concentration in each well. Following separation of the sample on SDS-PAGE, proteins were transferred to PVDF membrane and incubated with antibodies against AT8, total tau and beta actin. This allowed expression of AT8 as a ratio of total tau, normalised to beta actin.

There is negligible detection of AT8-positive tau in either the vehicle i.c. or tau i.c. groups which underwent saline i.p. injection. The results showed a twenty-fold increase in AT8/total tau ratio in mice exposed to *S. typhimurium* compared to the tau i.c./saline i.p. group. There was a main effect of *S. typhimurium* ($F(1, 12)= 8.81$, $p<0.05$, with no significant main effect of tau i.c. injection ($F(1, 12)= 3.12$, $p= 0.1$) or interaction ($F(1, 12)= 3.87$, $p= 0.07$). **Figure 6-24** shows a band at ~50 kDa in both groups of mice exposed to *S. typhimurium* i.p. However, there is a four-fold increase in the AT8/total tau ratio in mice which received the tau i.c. injection compared to the vehicle i.c./*S. typhimurium* i.p. group (vehicle i.c./*S. typhimurium* i.p.= 5.42 ±2.23; tau i.c./*S. typhimurium* i.p.= 21.86 ± 17.31, $p= 0.09$). The lack of post-hoc significance is likely due to the variability within the tau i.c. mice. Whilst four mice within each group underwent tissue processing for biochemical analysis, to reduce the variability further repeats of this blot would be carried out given greater time. Heavy chain mouse IgG is detected at approximately 50kDa in SDS-PAGE. Given systemic infection with *S. typhimurium* results in BBB breakdown, it is possible that the band in the vehicle i.c./*S. typhimurium* i.p. group is due to mouse IgG expression. Despite this, the western blot shows clear upregulation of tau specifically in those mice which had an i.c. injection of tau and systemic infection.

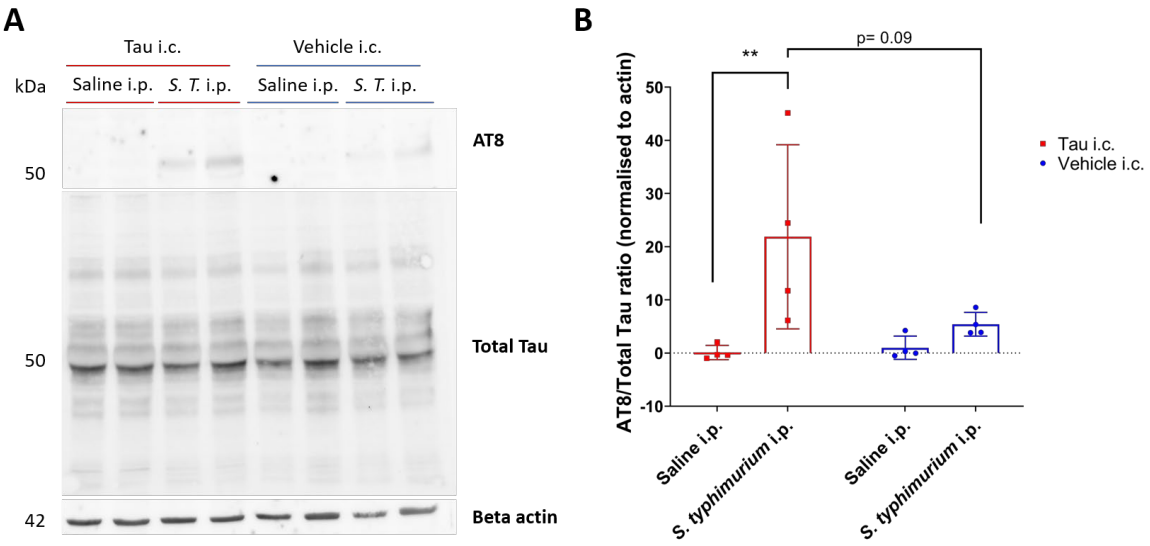

Figure 6-24: Detection of AT8-positive hyperphosphorylation of tau using biochemical analysis

A) Western blot showing expression levels of AT8, total tau and beta actin in the hippocampus of C57BL/6 mice which received either vehicle or tau i.c. injection followed by saline or *S. typhimurium* i.p. injection. n= 4 in all groups. S.T.= *S. typhimurium* **B)** Two-way ANOVA with Tukey's post-hoc test, **($p<0.01$). All data is presented as Mean ± SD.

6.4 Discussion

Comparing tau spreading of human AD-tau lysate in both C57BL/6 and H1*Mapt-/-* mice has resulted in clear differences between the two mouse strains. C57BL/6 mice demonstrate a greater deposition of tau pathology compared to H1Mapt-/- mice. Most AT8-positive tau was observed in brain regions close to the injection site, however significant deposition of tau was observed distant from the injection site, including the mammillary nuclei in C57BL/6 mice (**Figure 6-15**). This indicates that tau is indeed spreading to synaptically connected regions, and this propagation is in part enabled by systemic infection. This propagation to distal regions was not observed to the same extent in H1*Mapt-/-* mice (**Figure 6-16**). However, it is unclear whether this is due to a difference in the native tau protein or a difference in the systemic infection response. All images taken for quantification were also scored blind from a scale of 0-3, with 0 displaying no pathology. This is an accompaniment to the threshold analysis; scoring allows for visualisation of levels of pathology across brain regions and Bregma coordinates (**Figure 6-25**). Scoring data can be found in the Appendix A (Figure S5 and S6). In this chapter it is possible to observe that systemic

infection increased tau pathology both in regions close and distal to the injection site, and in both grey and white matter.

It must be emphasised that the levels of pathology were low overall. This study was carried out at three months after i.c. injection of human tau lysate, which is a very early timepoint considering what has been reported in published studies. One study reported minimal tau pathology in C57BL/6 mice injected with human AD tau lysate at three months post-injection (Narasimhan *et al.*, 2017), with significantly more pathology observed at nine months post-injection. However, Narasimhan *et al.* (2017) reports greater pathology at 3 months than observed in this study with pathology throughout the hilus.

Previous tau propagation studies in P301S mice show propagation of tau pathology after two months (Ahmed *et al.*, 2014). P301S mice overexpress the human 4R0N isoform of tau which has same isotype as the 'seed' lysate. This may explain higher levels of pathology since propagation of tau requires the pathological tau 'seed' to bind to endogenous tau; the higher the levels of recruitable tau, the more spreading can occur. He *et al.* (2020) injected lysate from post-mortem tissue either from four-repeat tau tauopathies (PSP and CBD), three-repeat tau tauopathies (PiD) or AD post-mortem tissue which contains both three-repeat and four-repeat tau pathology. They demonstrated that in WT mice, only the PSP, CBD and AD lysate showed significant tau propagation. By contrast in transgenic T44mTauKO mice which only express three-repeat tau (**Table 1-1**), significant pathology was only observed following i.c. injection of the PiD and AD lysate (He *et al.*, 2020). This suggests that similarities in isoform between the native tau protein expressed in the mouse and the protein within the lysate, determines how successfully tau pathology propagates within the brain. This highlights how unexpected the lack of pathology in H1*Mapt-/-* mice is within this chapter. However, it suggests that the native protein expression or the immune response to systemic infection is a determining factor.

6.4.1 Physiological changes following *S. typhimurium* injection

C57BL/6 and H1*Mapt-/-* mice received an intracerebral injection of tau lysate or vehicle. The small weight change following these injections was recovered by one-week post injection for the majority of the mice, with all mice within 2% of initial baseline weight by two weeks post injection. At 8 weeks post-i.c. injection, mice were administered either single saline or *S. typhimurium* i.p. injection. Weight loss was recorded and four weeks later, the mice were perfused, and the spleens weighed for signs of splenomegaly (**Figure 6-3**). Both the weight change and spleen weights highlight that both C57BL/6 mice and H1*Mapt-/-* mice develop an immune response following the bacterial infection. Mice injected with *S. typhimurium* show an

initial weight loss of approximately 7% for C57BL/6 mice and 5% for H1*Mapt-/-* mice, and all mice recovered after approximately a week post-infection. These results suggest that both C57BL/6 and H1*Mapt-/-* mice exhibit robust weight loss in response to systemic infection. Following perfusion, spleen weight was recorded to determine if splenomegaly had occurred. **Figure 6-3** shows that splenomegaly occurred in the majority of mice, indicating a robust systemic immune response as a result of the bacterial infection. One observation is that H1*Mapt-/-* mice which received tau i.c. injection presented with significantly smaller spleens than C57BL/6 mice which received tau i.c. injection. Spleen weight varies between mice, however this biological variability has a clear range within which to establish whether an infection occurred within the mouse. The only mouse excluded was from the tau i.c./saline i.p. group with the enlarged spleen as aforementioned.

At 5 weeks post-i.c. injection habituation to burrowing activity was carried out (**Figure 6-4**). Ideally by the end of the three habituation sessions (described in full in Chapter 2), mice would burrow all pellets and so establish a baseline of 100%. Only 18% of mice were unable to remove all pellets by the end of the burrowing sessions and these mice were spread over different groups, suggesting that there was no effect of i.c. injection on this behavioural task. After habitation and one week prior to *S. typhimurium* injection, burrowing was recorded to establish a baseline and recorded again at six days post-i.p. injection, to examine the effects of the bacterial infection. Due to missing values analysis is limited, however data presented in **Figure 6-4** suggest that *S. typhimurium* infection changes burrowing regardless of i.c. injection. Mice that received vehicle i.c. injection return to baseline burrowing approximately a week earlier than mice exposed to tau lysate, suggesting that systemic infection and i.c. injection may modulate this hippocampal-dependent task. Similar observations were made in H1*Mapt-/-* mice. However, given the changes made due to Covid-19 restrictions, conclusions regarding burrowing are limited without repetition of this experiment.

Burrowing as a behavioural test has been used to examine effects of neuropathy (Shepherd *et al.*, 2018) and sickness behaviours following injection of viral and bacterial mimics (Cunningham *et al.*, 2007; Püntener *et al.*, 2012). Burrowing deficits have been linked to hippocampal function, through both targeted lesions (Deacon and Rawlins, 2005) and pathology in Tg2576 mice (Deacon *et al.*, 2009), but further study is required to confirm if burrowing findings in this chapter. It is possible that because this study described in this chapter only involves a unilateral injection of tau, it will be unlikely that significant burrowing deficits will occur. Whilst this is a limitation as pertains to burrowing results, the unilateral injection allows the observation of spreading and so is integral to the study.

Burrowing studies highlight a key discrepancy between neurodegenerative and immunology studies. Studies which examine the inflammatory response in mice often use acute models and therefore observations are carried out with days not weeks. By contrast, longer studies examining behavioural deficits in tau models as a result of pathology cannot often elucidate whether deficits are observed due to the neurotoxicity of tau pathology or due to the proinflammatory changes in immune cells caused by accumulating pathology. Extending the experiment to allow greater pathology development would likely incur greater hippocampal dysfunction, amplified by systemic inflammation.

6.4.2 Tau pathology accumulation and spread

This study aimed to examine whether systemic infection increased the deposition of AT8-positive tau within the mouse brain. Lysate enriched for AT8-positive tau was generated from post-mortem AD tissue and injected i.c. into C57BL/6 and H1*Mapt-/-* mice. Mice received either a tau or vehicle i.c. injection and two months later received either a saline or *S. typhimurium* i.p. injection. The primary aim of this study was to examine AT8 immunoreactivity within the brain using histology. Three regions in the brain were examined; the injection site (AP:-2.50), ventral to the injection site (AP:-3.00) and dorsal to the injection site (AP:-1.00). Upon analysis and quantification of the histological findings, the region with pathology consistent across both tau i.c./saline i.p. and tau i.c./*S. typhimurium* i.p. groups was the corpus callosum and the fornix. All regions throughout the brain were also scored on a scale of 0-3 (with 0 representing no pathology). As shown in **Figure 6-25**, the spread throughout the brain dependent on mouse genotype and i.p. injection is clear to observe. The corpus callosum is situated in close proximity to the injection site and this fibre bundle connects the two hemispheres, making the corpus callosum a crucial ROI. The fornix is a bundle of fibres which originate from the hippocampus connecting to the limbic circuit, including the mammillary bodies (Douet and Chang, 2015). The fornix has been highlighted as a region which expresses tau pathology in human brain-derived tau propagation studies (Ahmed *et al.*, 2014; He *et al.*, 2020).

Tau pathology was observed in the corpus callosum at all three Bregma positions (**Figure 6-5**, **Figure 6-9** and **Figure 6-18**). The AT8 immunoreactivity showed dot-like staining throughout these white matter tracts. The corpus callosum is one of the few areas in this study where the tau i.c./saline i.p. groups in both mouse strains display any pathology. Despite AT8 immunoreactivity being detected in both C57BL/6 tau i.c. groups, systemic infection causes a five-fold increase in AT8 quantification in the corpus callosum at the injection site (**Figure 6-5**). In the corpus callosum measured anterior to the injection site (Bregma AP= -1.00) similar levels of AT8 tau were observed in both C57BL/6 tau i.c. groups. **Figure 6-17** shows that in C57BL/6 mice, pathology is observed in

the dorsal fornix (Bregma AP= -1.00), with *S. typhimurium* infected mice demonstrating an eight-fold increase in AT8 immunoreactivity compared to mice receiving a saline injection. H1*Mapt-/-* mice show negligible pathology at this Bregma coordinate, either in the dorsal fornix or the corpus callosum. In the corpus callosum posterior to the injection site (Bregma AP= -3.00), in both C57BL/6 and H1*Mapt-/-* mice AT8 staining is observable but low in both tau i.c. groups.

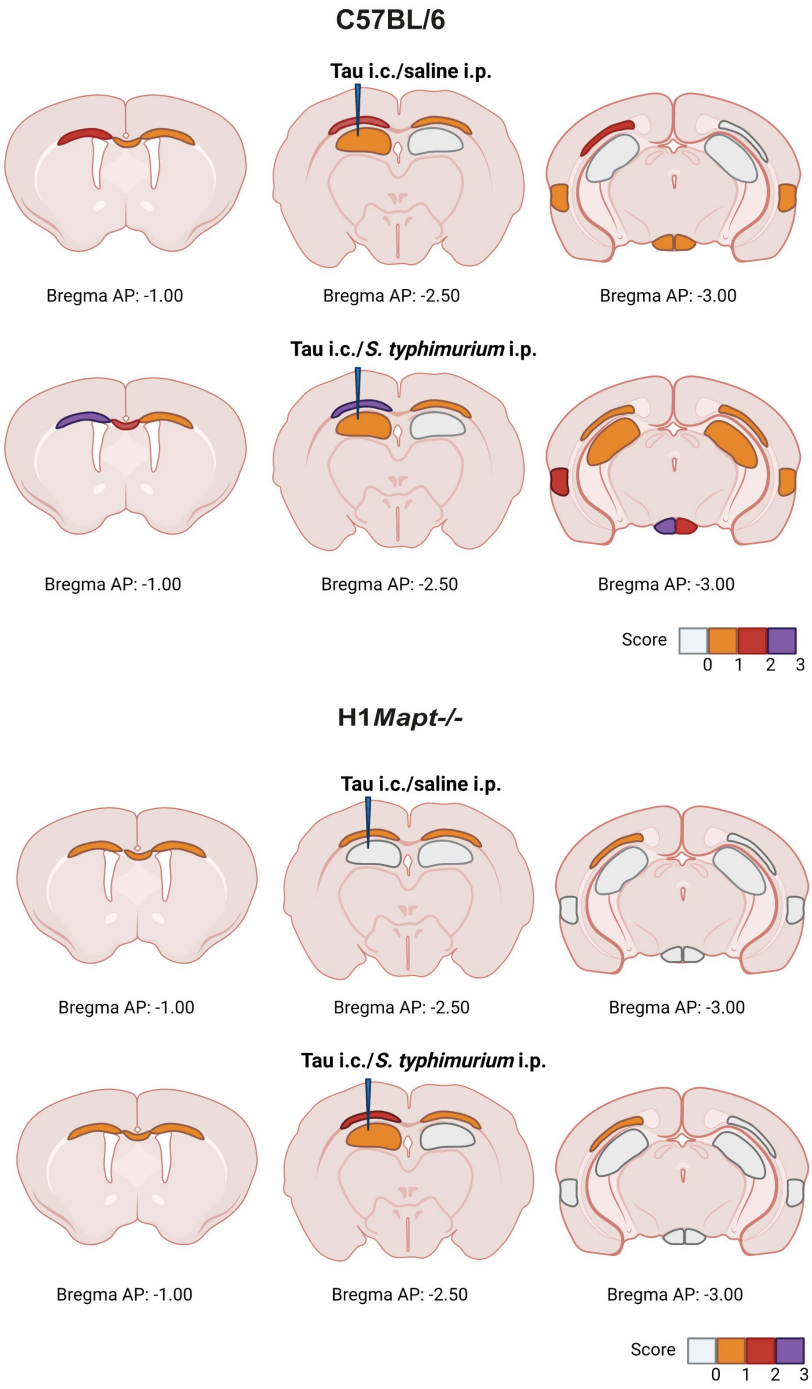

Figure 6-25: Scoring of AT8 immunoreactivity throughout the brain of C57BL/6 and H1*Mapt-/-* mice

All regions of interest quantified were also scored to provide a visual map of the AT8 immunoreactivity. A score of 0, 1, 2 or 3 was assigned with 0 referring to no pathology and 3 the highest level of AT8-positive tau. An average score of 0 was represented in grey, 0-1 represented in orange, 1-2 represented in red and 2-3 represented in purple. Individual scores shown in Appendix A. Created with BioRender.com.

This suggests propagation through these white matter tracts in both ventral and dorsal directions. The exact mechanism of transportation in the white matter tracts is unknown. A reported *in vitro* seeding assays demonstrated that tau derived from white matter possessed seeding capacity (De Vos *et al.*, 2018). Therefore, the white matter clearly plays a role in the degeneration observed in AD and is used to transport pathology throughout the brain along synaptically connected pathways. Previous studies which inject C57BL/6 mice with lysate isolated from AD post-mortem tissue show AT8-positive staining within the white matter tract with similar dot-like immunoreactivity as reported in this chapter (He *et al.*, 2020). Furthermore, in the human brain, diffusion tensor imaging (DTI) has demonstrated that the fornix and corpus callosum are connected (Jang and Kwon, 2014). These results suggest that the corpus callosum and the fornix are two major pathways of tau spreading in C57BL/6 mice. Systemic infection induces greater propagation of tau through the white matter tracts away from the injection site. Therefore, this suggests that in the white matter tract, whether intraneuronal or taken up by microglia, tau burden is increased by systemic infection.

When examining the H1*Mapt-/-* mice, there is less pathology in the corpus callosum at the injection site compared to levels observed in the C57BL/6 mice (**Figure 6-6**). Furthermore, at the posterior corpus callosum there are lower levels of pathology to C57BL/6 mice observed, and still no significant effect of *S. typhimurium* i.p. on tau accumulation (**Figure 6-10**). When examining the anterior corpus callosum (**Figure 6-20**) and the dorsal fornix (**Figure 6-19**), minimal tau pathology is observed, with no evidence of an effect of *S. typhimurium*. This highlights an overarching conclusion of this chapter; H1*Mapt-/-* mice show less propagation of tau pathology.

The hippocampus was a second key region of interest. The dentate gyrus and the CA3-CA4 axis are regions highlighted in many tau spreading studies (Ahmed *et al.*, 2014; Guo *et al.*, 2016; Jackson *et al.*, 2016; Narasimhan *et al.*, 2017; He *et al.*, 2020). Despite this, minimal tau pathology is reported in the dentate gyrus in this chapter, in either C57BL/6 or H1Mapt-/- mice. As anticipated, there is no pathology in the vehicle groups and negligible pathology was found in the dentate gyrus of mice receiving an i.c. injection of the human tau lysate followed by saline i.p. (Figure 1-5). Only one C57BL/6 mouse in the tau i.c./saline i.p. group of either C57BL/6 or H1*Mapt-/-* mice showed hippocampal AT8 immunoreactivity. In contrast, increased AT8-positive tau was observed in the dentate gyrus of C57BL/6 mice in half of the tau i.c./*S. typhimurium* i.p. group (**Figure 6-7**). The tau i.c./*S. typhimurium* i.p. group shows AT8 immunoreactivity in the ipsilateral hippocampus. Only one H1*Mapt-/-* mouse in the tau i.c./*S. typhimurium* i.p. group showed AT8-positive tau (**Figure 6-8**). This highlights how the hippocampus shows low levels of AT8-positive tau, with the H1*Mapt-/-* mice demonstrating lower levels of tau than the C57BL/6

mice. Systemic infection appears to have an effect on tau burden in C57BL/6 mice, however this is not consistent within the tau i.c./*S. typhimurium* i.p. group.

Posterior to the injection site, tau pathology was observed in the ventral hippocampus (**Figure 6-11**). AT8-positive staining in the hippocampus was only observed in the tau i.c./*S. typhimurium* i.p. group. As observed in the hippocampus at the injection site (**Figure 6-7**), pathology was inconsistent within this group and there was biological variability associated with this propagation model. No pathology was observed in the CA1 or CA2, only the dentate gyrus. This highlights the early stage of propagation examined. These results clearly show the effect of *S. typhimurium* on tau propagation. Whilst no significance is observed at the injection site, the ventral hippocampus shows a trend of increased tau pathology after systemic bacterial infection.

Analysis of tissue from H1*Mapt-/-* mice, indicates there is no pathology following i.c. injection of human tau lysate at the ventral hippocampus (**Figure 6-12**: AP= -3.00). Furthermore, systemic bacterial infection failed to promote tau pathology. Considering that only one H1*Mapt-/-* mouse demonstrated AT8-positive tau in the hippocampus at the injection site (**Figure 6-7**: AP= -2.50), this highlights how much lower the tau burden is compared to observations in C57BL/6 mice. This result is seen throughout the brain, whereby the H1*Mapt-/-* mice show less tau pathology than C57BL/6 mice. The likely explanation is low expression of endogenous human tau and lack of mouse tau in these mice. Therefore, expression of all isoforms of human tau in the H1*Mapt-/-* mice does not confer to greater seeding capacity if protein expression is inadequate. In addition, it is also possible that lack of increased tau pathology after systemic infection is due to a reduced immune response to *S. typhimurium* in H1*Mapt-/-* mice compared to C57BL/6 mice.

The perirhinal cortex showed clear AT8-positive inclusions and a significant increase in tau following systemic infection. In comparison to the white matter tracts, the AT8-positive stain in the perirhinal cortex appeared to be intraneuronal. However, this is purely based on the morphology observed, co-staining with neuronal markers such as NeuN in future experiments would be required to confirm this. It has long been associated with recognition memory through lesion studies, highlighting a link with the visual association cortex (Brown and Aggleton, 2001). Pathology was observed in both groups that received an i.c. injection of tau lysate (**Figure 6-13**). However, only half of the mice in the tau i.c./saline i.p. group show pathology in the ipsilateral hemisphere, and there was a two-fold increase in AT8 immunoreactivity when mice underwent systemic infection. Although this pathology is largely restricted to the ipsilateral hemisphere, both tau i.c. groups show pathology in the contralateral hemisphere, but this is highly variable. As aforementioned, all pathology observed is reported in the tau scores in **Figure 6-25**. Because pathology observed in the contralateral perirhinal cortex was so inconsistent, only one mouse in

the tau i.c./*S. typhimurium* i.p. group showed an average percentage of AT8 immunoreactivity above 0.02% (**Figure 6-13**). No tau pathology was observed in any H1*Mapt-/-* mice (**Figure 6-14**). This again supports the hypothesis that systemic infection induces a greater rate of propagation in C57BL/6 mice.

The final region analysed posterior to the injection site was the mammillary nuclei. The predominant projection to the mammillary bodies is the fornix from the hippocampus. The LMN has been associated with episodic memory retrieval (Roy *et al.*, 2017) and spatial navigation (Yoder and Taube, 2011). There is comparatively little research on the SuMN, it is understood to send afferent fibres to the dentate gyrus and the CA2. Following this research, it has since been purported that the SuMN connections to the dentate gyrus are crucial for spatial memory retrieval (Li *et al.*, 2020).

Tau pathology in the mammillary nuclei was exclusively observed in C57BL/6 mice and then predominantly within the group which received an i.c. injection of human tau and subsequent exposure to *S. typhimurium* i.p. injection (**Figure 6-15**). There is minimal pathology in a few mice within the tau i.c./saline i.p. group, but the majority of mice showed no pathology. This is conclusive evidence that systemic bacterial infection induces greater propagation of tau pathology. In H1*Mapt-/-* mice there was no pathology in the mammillary nuclei regardless of the treatment (**Figure 6-16**), highlighting again how differences in genotype have resulted in a different rate of tau spread.

One interesting observation is the presence of pathology in the contralateral SuMN. A study examining rat and macaque projections suggested that at the ventral hippocampus, projections could be made to the contralateral mammillary body through the intersecting fornix (Mathiasen *et al.*, 2019). However, this has not been established fully and so the mechanism behind this remains unclear. However, our collaborators at Eli Lilly also reported ipsilateral and contralateral pathology in the SuMN following the P301S propagation study (Ahmed *et al.*, 2014). A similar propagation study in mice also injected i.c. lysate enriched for tau from AD post-mortem tissue. In this study, pathology in the SuMN was detected from 3 months post-injection and steadily increases throughout the timepoints, with contralateral pathology present (Henderson *et al.*, 2020). The study also reports that the CA1 only demonstrated significant pathology at six months post-injection, whilst the dentate gyrus showed pathology at three months post-injection.

To summarise the findings presented in this chapter, there is a clear effect of *S. typhimurium* on the propagation of tau pathology. There is no tau pathology observed in any of the vehicle i.c. injection groups confirming that injury caused by the Hamilton needle alone cannot perpetuate tau pathology. There is minimal spreading observed in the H1*Mapt-/-* mice,

examining inflammatory markers in Chapter 7 may elucidate the reasoning behind this. There is clear evidence of tau spreading through the fornix and corpus callosum, both anterior and posterior to the injection site. Increased pathology in these connected regions are predominantly found in mice receiving both the i.c. tau injection and *S. typhimurium* infection 2 months later. Pathology at the SuMN is indicative of retrograde spread from the hippocampus, as there are no inputs from the hippocampus to the SuMN (Vann, 2010). Furthermore, pathology is observed in the LMN, but this is minimal and not consistently found in C57BL/6 mice. An example of one brain which does show LMN pathology is demonstrated in **Figure 6-26**. This provides definitive evidence of retrograde spread of tau pathology to the SuMN. However, further research would be required to establish whether there is consistent anterograde spread at this early time point post injection of human tau. At a later timepoint, for example six months post-injection, pathology in these two regions may be more pronounced.

In conclusion, both anterograde and retrograde spread of tau can be observed in this mouse spreading model at this time point in this mouse. However, retrograde spread likely precedes anterograde within the cohort. Especially when compared to the pathology in the hippocampus which is inconsistent, SuMN pathology was observed in all mice that received human tau lysate and *S. typhimurium* infection, with the exception of one mouse. This suggests that retrograde spread is one of the earliest propagation pathways in this model.

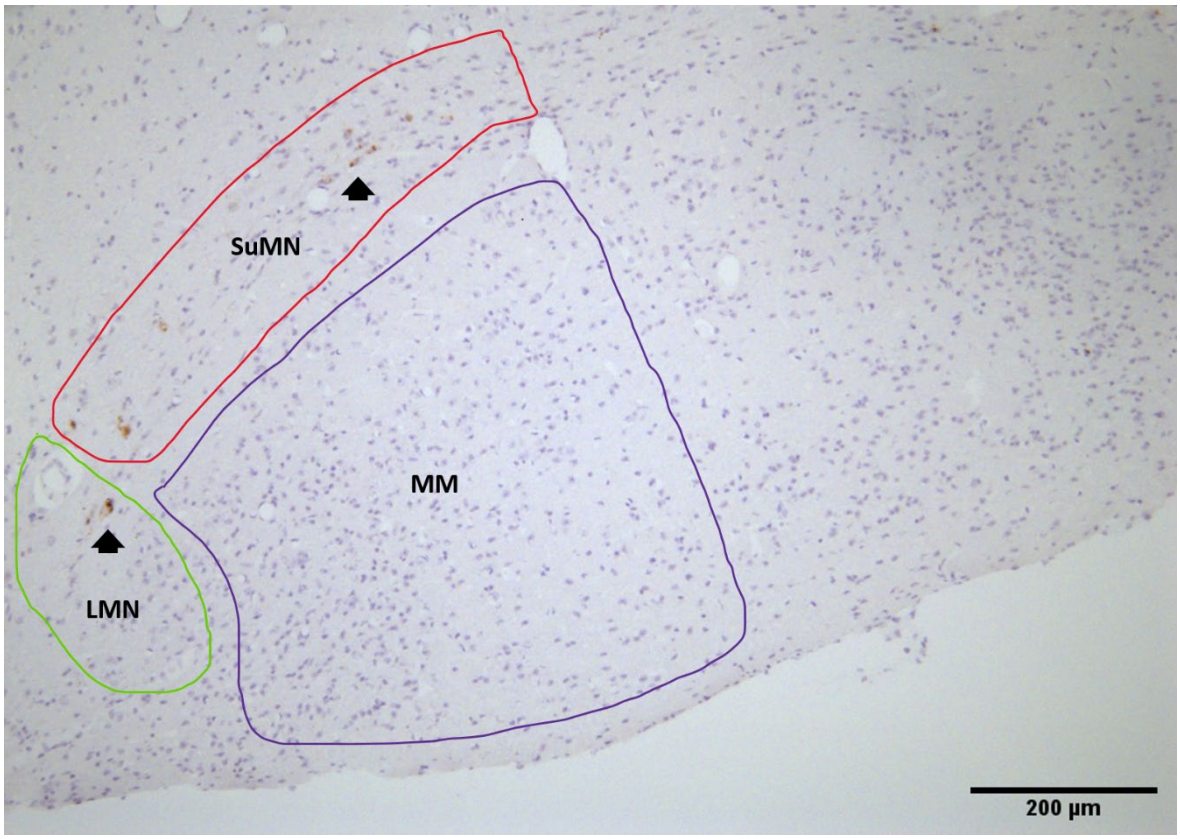

Figure 6-26: Mammillary nuclei pathology

Pathology in the mammillary nuclei of a mouse which underwent tau i.c. followed by *S. typhimurium* i.p. Stained for biotinylated AT8. LMN= lateral mammillary nucleus; MM= medial mammillary nucleus; SuMN= supramammillary nucleus. Image taken at 10x objective, scale bar= 200µm

Furthermore, I have established that there is likely no overt Aβ or α-Synuclein pathology in this tau spreading model. However, the α-Synuclein experiment was very brief with only one brain from each group undergoing histology. By contrast, three brains per group were used to detect Aβ pathology. Therefore, in potential future experiments which may examine the brains at six months post-injection, this should be repeated. Given greater time, an ELISA for both of these pathological forms of the respective proteins would be carried out on the Sarkosyl-insoluble fraction. Now that the effect of systemic infection of tau pathology has been established, it would be advantageous to either use control brain lysate or immunodepleted tau lysate.

When examining the histology data and the western blot data there is a clear effect of systemic infection on tau pathology and phosphorylation. Whilst it was highlighted that the vehicle i.c./*S. typhimurium* i.p. group may express IgG in the western blot, tau phosphorylation at the AT8 epitope Thr205 has been reported in C57BL/6 wild-type mice after i.p. injection of LPS (*Salmonella enterica* serotype abortus equi, 5mg/kg). Therefore, it is possible the result is an

increase in tau phosphorylation due to systemic infection. Nevertheless, any changes in phosphorylation following systemic infection observed in the vehicle i.c. groups, is not equivalent to the deposition of AT8-positive tau observed in histology in the tau i.c. group. Furthermore, AT8/total tau ratio was four-fold increased in the tau i.c. group compared to the vehicle i.c. group following systemic infection. Therefore, whilst systemic infection may induce changes in phosphorylation to the native tau protein, the seeding of human AD-tau is a distinct finding.

6.4.3 Conclusion

This chapter demonstrates that tau pathology is present in the brain of C57BL/6 and H1*Mapt-/-* mice which received an i.c. injection of AD-tau lysate. A key finding is that H1*Mapt-/-* mice consistently show less pathology than C57BL/6 mice, and only minimal effect of *S. typhimurium* on tau propagation. In both H1*Mapt-/-* and C57BL6 mice, there was AT8-positive tau in the corpus callosum and the fornix, this was significantly affected by *S. typhimurium* injection in C57BL/6 mice (**Figure 6-25**). In regions such as the SuMN and the perirhinal cortex in the C57BL/6 mice, there was a significant increase in deposition of tau pathology following *S. typhimurium* i.p. injection. Therefore it is possible to conclude that in C57BL/6 mice, systemic bacterial infection does increase spread of tau pathology and one of the most affected regions is the mammillary nuclei.

Future aims:

- *To determine if systemic infection alters the rate of tau spreading in vivo*

Chapter 7 The effect of tau pathology and systemic infection on microglial markers

7.1 Introduction

The previous chapter established that *S. typhimurium* induced greater tau propagation and early deposition of tau pathology in synaptically connected regions. However, the mechanism through which this occurs is unclear. It is theorised that tau spreading could be facilitated by microglia endocytosis and/or exocytosis function. Using microglial marker Iba1, microglia have been shown to co-localise with tau oligomers in post-mortem AD tissue (Nilson *et al.*, 2017) and depleting microglia, or inhibition of microglial exosome synthesis suppressed the propagation of tau in experimental studies (Asai *et al.*, 2015). However, whether the relationship between tau pathology and microglial activation is beneficial or detrimental in AD is unclear.

In Chapter 3 I established the infection response to *S. typhimurium* in C57BL/6 and H1*Mapt-/-* mice. It was observed that both mouse strains showed weight loss and splenomegaly. However, dampened splenomegaly was observed in the H1*Mapt-/-* mice compared to C57BL/6 mice both in Chapter 3 and Chapter 6. Furthermore, only C57BL/6 mice showed significant upregulation of MHCII and FcγRI in the brain.

Chapter 6 showed minimal tau pathology in H1*Mapt-/-* mice, in the absence or presence of *S. typhimurium* infection, when compared to C57BL/6 mice. In this chapter, I will investigate the link between tau pathology and microglial marker expression. Furthermore, to what extent the presence of tau pathology lowers the threshold for activation in response to a second insult, in this case systemic infection.

Aims addressed in this chapter are as follows:

- *To determine if tau pathology induces an inflammatory response*
- *To determine if S. typhimurium infection exaggerates microglial activation in the presence of tau pathology*
- *To compare the inflammatory response in H1Mapt-/- mice and C57BL/6 mice*

7.2 Methods

7.2.1 *In vivo* experimental data

An initial pilot project was undertaken with a sample size of three C57BL/6 mice in each group (tau i.c./saline i.p. and tau i.c./*S. typhimurium* i.p.). These six mice received intracerebral injections using ketamine-rompun as the surgical anaesthetic (Appendix A, Figure S3). These six mice also underwent perfusion with PFA fixation, however technical issues meant that the hippocampal neurons were destroyed likely due to the osmolarity of the fixative. Therefore, they are excluded from the tau histology. In this chapter, they are included as the parenchyma was intact for staining of inflammatory markers.

7.2.2 Histology

Following Covid-19 restrictions, access to histology facilities was controlled and therefore limited. Tissue from Cohort 3 was stained for tau pathology but there was insufficient time to stain for microglial markers in this particular cohort (**Table 2-9**).

All regions quantified for histology were kept identical to the ROIs described in chapter 6, apart from the corpus callosum. The corpus callosum images were cropped to ensure only white matter was analysed.

7.3 Results

7.3.1 MHCII expression levels in the cortex following systemic infection

The first brain region analysed for expression of MHCII was the injection site (Bregma AP= -2.50), and the cortex above the corpus callosum containing the needle tract. Expression of MHCII was not detected in any mouse receiving saline i.p. injection regardless of i.c. injection (**Figure 7-1**). This suggests that injection of tau lysate into the cortex is not sufficient to cause sustained MHCII activation at the injection site. MHCII expression was observed in all mice infected with *S. typhimurium*, regardless of i.c. injection. Therefore, statistical analysis only compared the *S. typhimurium* i.p. groups. Between mice injected with *S. typhimurium*, the tau i.c. group showed a three-fold increase of MHCII in the ipsilateral cortex compared to the vehicle i.c. group (vehicle i.c./*S. typhimurium* i.p.= 3.31% ± 0.69; tau i.c./*S. typhimurium* i.p.= 12.28% ± 3.50, $p<0.01$). There was a significant main effect of i.c. injection ($F(1, 10)= 5.10$, $p<0.05$). There was no significant main effect of hemisphere ($F(1, 9)= 3.77$, $p= 0.08$) but the p value shows a clear trend. The lack of significance is likely due to biological variability. As a result, no post-hoc significance was observed.

One observation was the presence of microglia amongst cerebral vascular staining. A cell count was also carried out to determine the number of MHCII-positive cells (**Figure 7-1**). Staining that was localised to endothelial cells was excluded, this was possible due to distinct morphology of the cells. A distinct increase in cell count was observed in the tau i.c./*S. typhimurium* i.p. group, with a three-fold increase compared to the vehicle i.c./*S. typhimurium* i.p. group (vehicle i.c./*S. typhimurium* i.p.= 26.46% ± 11.02; tau i.c./*S. typhimurium* i.p.= 95.15% ± 35.31, $p<0.05$). There is a significant main effect of hemisphere ($F(1, 9)= 6.79$, $p<0.05$) with no significant main effect of i.c. injection ($F(1, 10)= 1.44$, $p= 0.26$). However, there was a significant interaction of hemisphere and i.c. injection ($F(1, 9)= 5.57$).

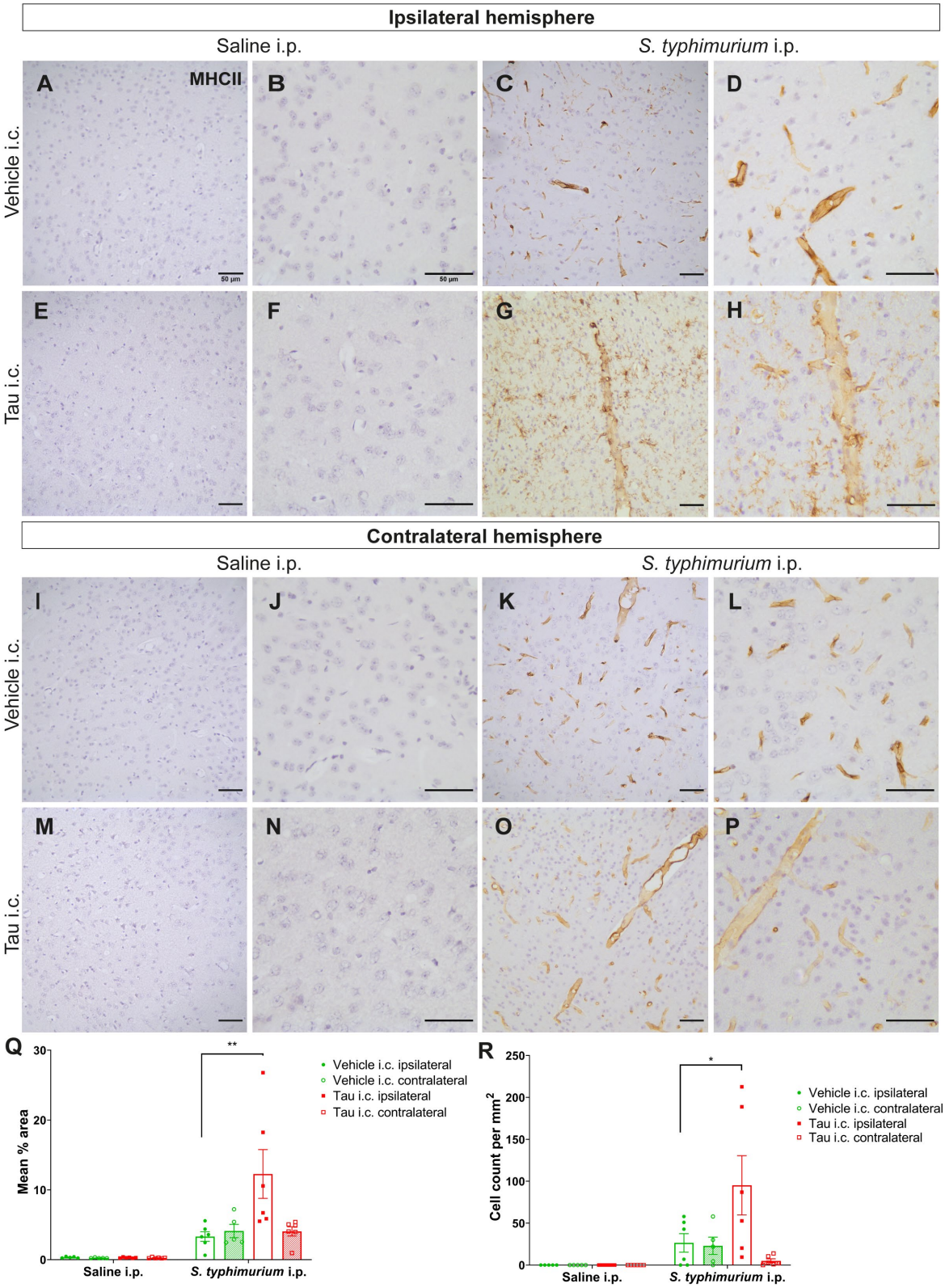
Ipsilateral hemisphere
Saline i.p.
S. typhimurium i.p.
Vehicle i.c.
Tau i.c.
A
MHCII
B
C
D
E
F
G
H
50 µm
Contralateral hemisphere
Saline i.p.
S. typhimurium i.p.
Vehicle i.c.
Tau i.c.
I
J
K
L
M
N
O
P
Q
Mean % area
30
20
10
0
**
Saline i.p.
S. typhimurium i.p.
Vehicle i.c. ipsilateral
Vehicle i.c. contralateral
Tau i.c. ipsilateral
Tau i.c. contralateral
R
Cell count per mm2
250
200
150
100
50
0
*
Saline i.p.
S. typhimurium i.p.
Vehicle i.c. ipsilateral
Vehicle i.c. contralateral
Tau i.c. ipsilateral
Tau i.c. contralateral

Figure 7-1: MHCII expression in the cortical injection site of C57BL/6 mice

A, C) Representative images of MHCII expression in mice which received vehicle i.c. injection followed by saline i.p. or *S. typhimurium* i.p. injection in the ipsilateral and **I, K**) contralateral hemisphere. **E, G. M, O**) Representative images of MHCII expression following tau i.c. injection; 20x objective, scale bar= 50µm. **B, D, F, H, J, L, N, P**) Corresponding images at 40x objective, scale bar= 50µm. **Q**) Quantification of MHCII mean percentage area. Mixed effects analysis with Sidak's post-hoc test, (*p<0.05, **p<0.01); n= 5 for vehicle i.c./saline i.p., n= 6 for tau i.c. groups and vehicle i.c./*S. typhimurium* i.p. **R**) Count of MHCII-positive microglia within the same region of interest, Mixed-effects analysis with Sidak's post-hoc test. All data is presented as mean ± SEM.

Histology from H1*Mapt-/-* mice was also examined for MHCII expression within the cortical injection site (**Figure 7-2**). No MHCII expression was detected in any saline i.p. treated mouse. Total MHCII expression at the ipsilateral hemisphere of the tau i.c./*S. typhimurium* i.p. group was two-fold higher when compared to the vehicle i.c. (vehicle i.c./*S. typhimurium* i.p. = 2.35% ± 0.53; tau i.c./*S. typhimurium* i.p. = 5.15% ± 0.97, p<0.05). This led to post-hoc significance. There was a significant main effect of i.c. injection ($F(1, 7)= 5.62$, $p<0.05$) yet no significant main effect of hemisphere ($F(1, 7)= 3.62$, $p= 0.1$). The MHCII cell count for H1*Mapt-/-* mice in the injection site showed high variability (**Figure 7-2**). Whilst there was an apparent increase in MHCII-positive microglia in the tau i.c./*S. typhimurium* i.p. group, this was likely underpowered and matched by expression of MHCII-positive microglia in the vehicle i.c./*S. typhimurium* i.p. group. Therefore, a Mann-Whitney test determined no significant difference between the ipsilateral hemispheres of the tau i.c./*S. typhimurium* i.p. group and the vehicle i.c./*S. typhimurium* i.p. group ($U= 6$, $p= 0.41$). The H1*Mapt-/-* cell count for MHCII-positive cells was also lower compared to C57BL/6 mice, as visible in **Figure 7-2**.

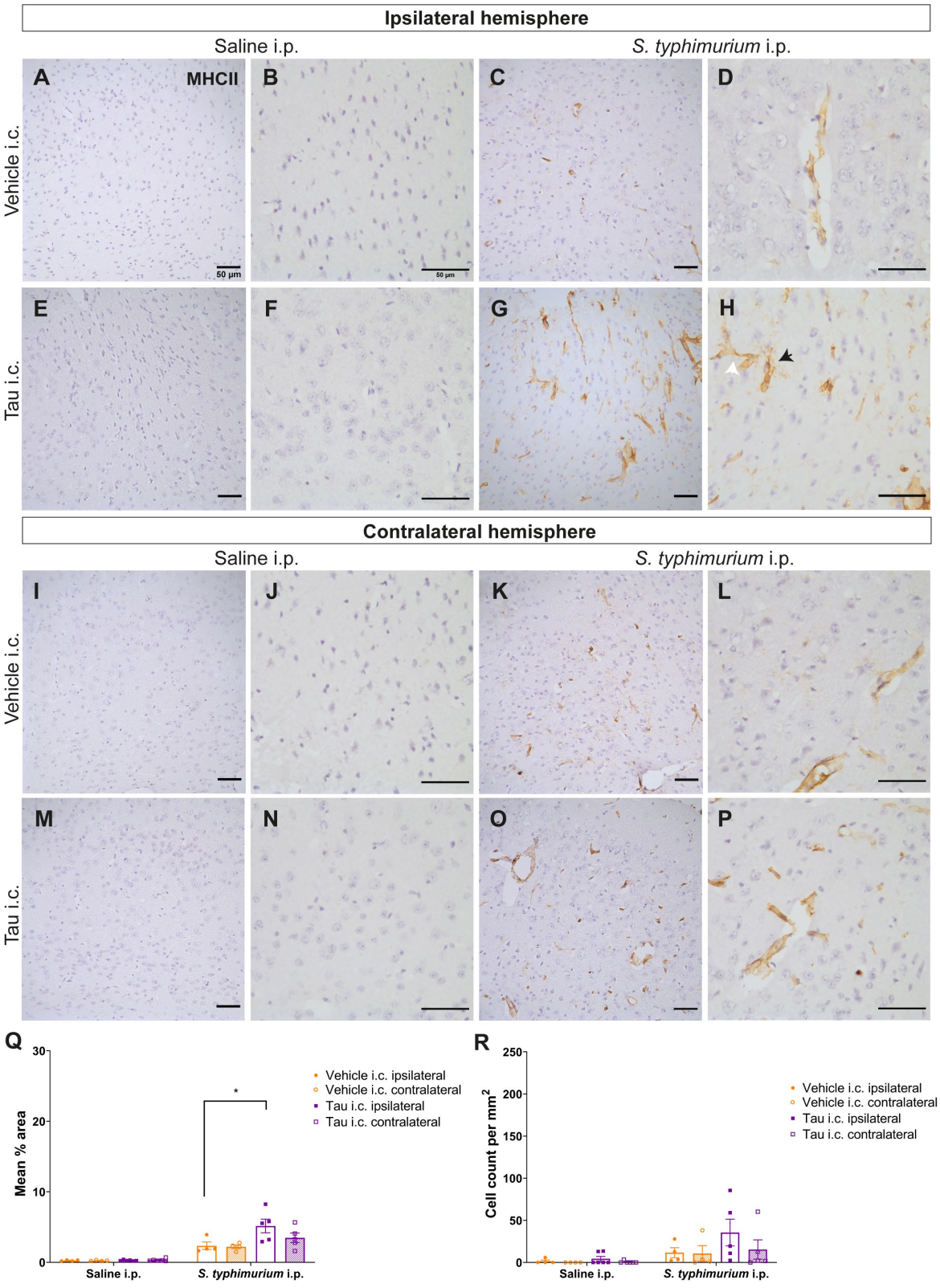
Ipsilateral hemisphere
Saline i.p.
S. typhimurium i.p.
A
MHCII
B
C
D
Vehicle i.c.
50 µm
E
F
G
H
Tau i.c.
Contralateral hemisphere
Saline i.p.
S. typhimurium i.p.
I
J
K
L
Vehicle i.c.
M
N
O
P
Tau i.c.
Q
Mean % area
30
20
10
0
*
Saline i.p.
S. typhimurium i.p.
Vehicle i.c. ipsilateral
Vehicle i.c. contralateral
Tau i.c. ipsilateral
Tau i.c. contralateral
R
Cell count per mm2
250
200
150
100
50
0
Saline i.p.
S. typhimurium i.p.
Vehicle i.c. ipsilateral
Vehicle i.c. contralateral
Tau i.c. ipsilateral
Tau i.c. contralateral

Figure 7-2: MHCII expression in the cortical injection site of H1*Mapt-/-* mice

A, C) Representative images of MHCII expression in mice which received vehicle i.c. injection followed by saline i.p. or *S. typhimurium* i.p. injection in the ipsilateral and **I, K**) contralateral hemisphere. **E, G, M, O**) Representative images of MHCII expression following tau i.c. injection; 20x objective, scale bar= 50µm. **B, D, F, H, J, L, N, P**) Corresponding images at 40x objective, scale bar= 50µm. White arrow denotes vascular endothelial MHCII expression. Black arrow denotes MHCII-positive macrophages. **Q**) Two-way ANOVA with Sidak's post-hoc test (*p<0.05); n= 6 for tau i.c./saline i.p, n= 5 for tau i.c./*S. typhimurium* i.p., n= 4 for vehicle i.c. groups. Data is log transformed for analysis. However, most values are <1 therefore the original mean % area is displayed. **R**) Cell count of MHCII-positive microglia cells, Mann-Whitney test. All data is presented as mean ± SEM.

7.3.2 MHCII expression in the corpus callosum of the C57BL/6 and H1*Mapt-/-* mice

Next, MHCII expression in the corpus callosum was examined (**Figure 7-3**). The black box denotes the white matter tract and the area cropped for analysis. In C57BL/6 mice, there was upregulation of MHCII in the white matter observed in all mice following *S. typhimurium* infection compared to saline i.p. injection. Compared to mice which had undergone vehicle i.c. injection, MHCII showed six-fold higher expression in the ipsilateral white matter tract of tau i.c. mice following *S. typhimurium* (vehicle i.c./*S. typhimurium* i.p.= 2.17% ± 0.53; tau i.c./*S. typhimurium* i.p.= 13.85% ± 4.68, p<0.01). Again, no MHCII expression was observed in the tau i.c./saline i.p. group. There was a significant main effect of hemisphere ($F(1, 10)= 8.61$, $p<0.05$), i.c. injection ($F(1, 10)= 5.29$, $p<0.05$) and interaction ($F(1, 10)= 6.98$, $p<0.05$).

H1*Mapt-/-* also demonstrated upregulation of MHCII in the ipsilateral corpus callosum of the tau i.c./*S. typhimurium* group compared to vehicle i.c. (vehicle i.c./*S. typhimurium* i.p.= 1.86% ± 0.27; tau i.c./*S. typhimurium* i.p.= 5.75% ± 2.87) (**Figure 7-4**). A Mann-Whitney test established there was no effect on i.c. injection between the vehicle i.c./*S. typhimurium* i.p. and tau i.c./*S. typhimurium* i.p. groups ($U= 3$, $p= 0.11$). Overall mean percentage area of MHCII expression appears lower in these mice compared to C57BL/6 mice.

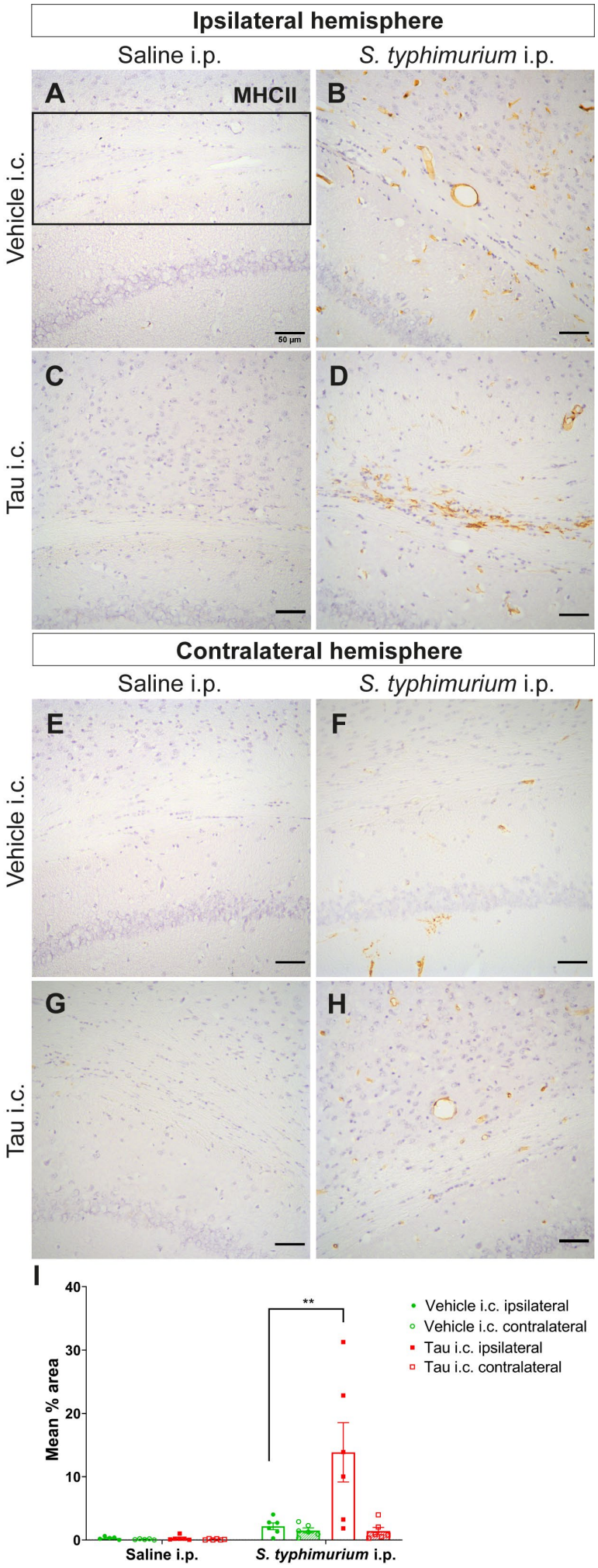
Ipsilateral hemisphere
Saline i.p.
S. typhimurium i.p.
A
MHCII
B
Vehicle i.c.
50 µm
C
D
Tau i.c.
Contralateral hemisphere
Saline i.p.
S. typhimurium i.p.
E
F
Vehicle i.c.
G
H
Tau i.c.
I
Mean % area
40
30
20
10
0
**
Saline i.p.
S. typhimurium i.p.
Vehicle i.c. ipsilateral
Vehicle i.c. contralateral
Tau i.c. ipsilateral
Tau i.c. contralateral

Figure 7-3: MHCII expression in the corpus callosum of C57BL/6 mice

Representative images of MHCII expression in the corpus callosum of mice which received vehicle i.c. injection followed by saline i.p. or *S. typhimurium* i.p. injection, in the **(A, B)** ipsilateral and **(E, F)** contralateral hemisphere. Representative images of MHCII expression in the corpus callosum of mice which received tau i.c. injection followed by saline i.p. or *S. typhimurium* i.p. injection, in the **(C, D)** ipsilateral and **(G, H)** contralateral hemisphere; 20x objective, scale bar= 50µm.. **I**) MHCII expression quantification; two-way ANOVA with Sidak's post-hoc test (**p<0.01). n= 6 for all groups except vehicle i.c./saline i.p. where n= 5. All data is presented as mean ± SEM.

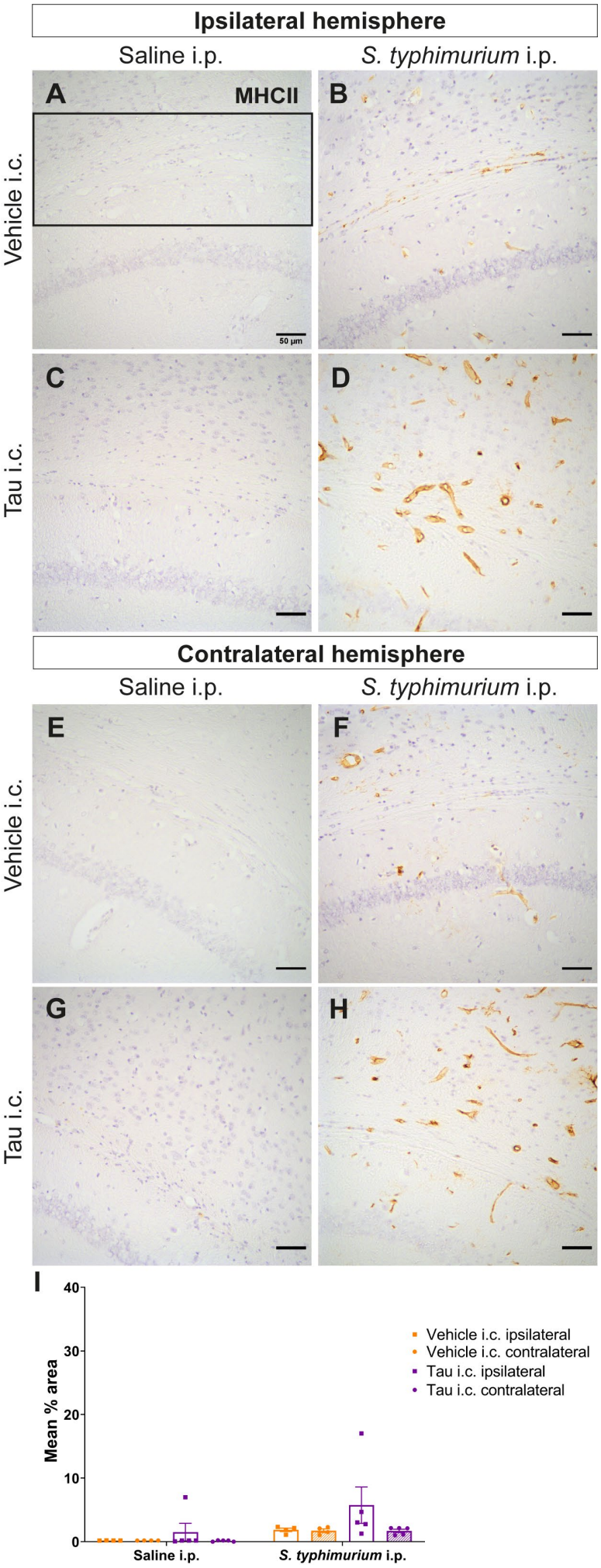
Ipsilateral hemisphere
Saline i.p.
S. typhimurium i.p.
A
MHCII
B
Vehicle i.c.
50 µm
C
D
Tau i.c.
Contralateral hemisphere
Saline i.p.
S. typhimurium i.p.
E
F
Vehicle i.c.
G
H
Tau i.c.
I
Mean % area
40
30
20
10
0
Saline i.p.
S. typhimurium i.p.
Vehicle i.c. ipsilateral
Vehicle i.c. contralateral
Tau i.c. ipsilateral
Tau i.c. contralateral

Figure 7-4: **MHCII expression in the corpus callosum of H1*Mapt-/-* mice**

A, B, C, D) Representative images of MHCII expression in mice which received vehicle or tau i.c. injection followed by saline i.p. or *S. typhimurium* i.p. injection in the ipsilateral hemisphere. **E, F, G, H**) Representative images of MHCII expression in mice which received vehicle or tau i.c. injection followed by saline i.p. or *S. typhimurium* i.p. injection in the contralateral hemisphere; 20x objective, scale bar= 50μm. **I**) Quantification of MHCII expression based on mean percentage area, Mann-Whitney test. n= 4 for vehicle i.c. groups, n= 5 for tau i.c. groups. All data is presented as mean ± SEM.

7.3.3 MHCII expression in the hippocampus following systemic infection

The next ROI analysed was the hippocampus, including the granule cell layer of the dentate gyrus (**Figure 7-5**). The hippocampus showed consistent MHCII expression in all C57BL/6 mice infected with *S. typhimurium*. In the ipsilateral hemisphere, MHCII expression in the tau i.c. group was an almost two-fold increase over the vehicle i.c. group following systemic infection (vehicle i.c./*S. typhimurium* i.p.= 3.41% ± 0.72; tau i.c./*S. typhimurium* i.p.= 6.97% ± 1.96). Contrastingly, no difference in MHCII expression was observed in the contralateral hemisphere (vehicle i.c./*S. typhimurium* i.p.= 3.66% ± 0.39; tau i.c./*S. typhimurium* i.p.= 3.06% ± 0.60). There was no significant main effect of i.c. injection ($F(1, 19)= 1.64$, $p= 0.22$) or hemisphere ($F(1, 19)= 2.51$, $p= 0.13$). However, there was definite biological variability in the ipsilateral hemisphere of the tau i.c./*S. typhimurium* i.p. group. To what extent this is due to variability in tau is unclear.

In the C57BL/6 mice, MHCII-positive cell count was also carried out in the hippocampus (**Figure 7-5**). There was a definite 1.5-fold increase in the tau i.c./*S. typhimurium* i.p. group which reflected the percentage area results (vehicle i.c./*S. typhimurium* i.p.= 53.11 ± 16.54; tau i.c./*S. typhimurium* i.p.= 90.06% ± 34.21, $p= 0.44$). There was a significant main effect of hemisphere ($F(1, 9)= 7.03$, $p<0.05$) yet no significant main effect of i.c. injection ($F(1, 10)= 0.33$, $p= 0.58$). There was also no significant interaction of these two variables ($F(1\ 9)= 2.10$, $p= 0.18$). There was no significant effect of the tau lysate on MHCII-positive microglial expression in the hippocampus, again likely due to biological variability. The cell count and percentage area results are similar and therefore it can be suggested the increase in the tau i.c./*S. typhimurium* i.p. group is derived from the microglial expression of MHCII. Co-staining analysis in fluorescence would be required to confirm this.

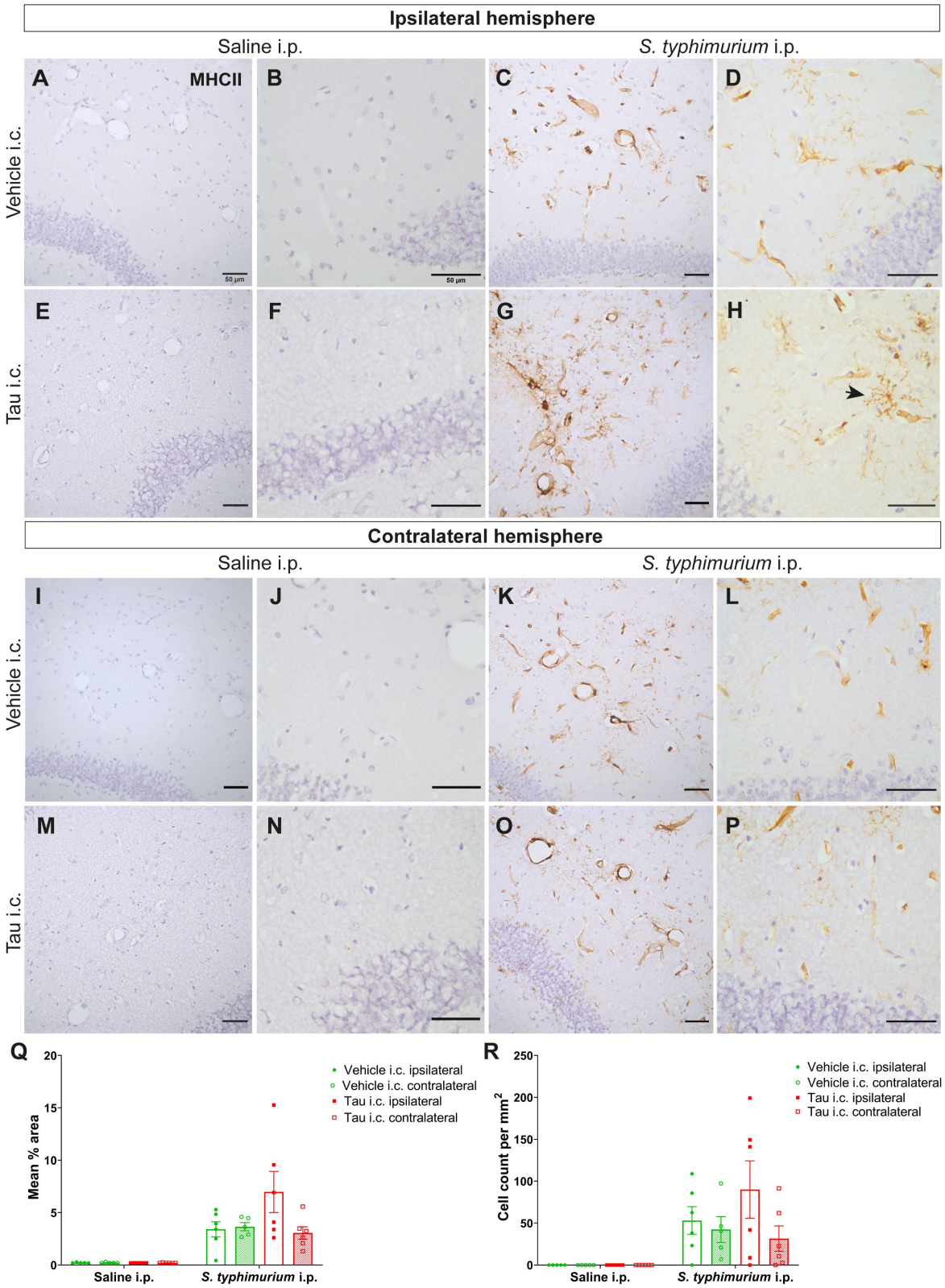
Ipsilateral hemisphere
Saline i.p.
S. typhimurium i.p.
Vehicle i.c.
Tau i.c.
A
MHCII
B
C
D
E
F
G
H
50 µm
Contralateral hemisphere
Saline i.p.
S. typhimurium i.p.
Vehicle i.c.
Tau i.c.
I
J
K
L
M
N
O
P
Q
Mean % area
20
15
10
5
0
Saline i.p.
S. typhimurium i.p.
Vehicle i.c. ipsilateral
Vehicle i.c. contralateral
Tau i.c. ipsilateral
Tau i.c. contralateral
R
Cell count per mm2
250
200
150
100
50
0
Saline i.p.
S. typhimurium i.p.
Vehicle i.c. ipsilateral
Vehicle i.c. contralateral
Tau i.c. ipsilateral
Tau i.c. contralateral

Figure 7-5: MHCII expression in the hippocampus of C57BL/6 mice

A, I) Representative images of MHCII expression in mice which received vehicle i.c. injection followed by saline i.p. in the ipsilateral and contralateral hemisphere. **C, K**) Representative images following vehicle i.c./*S. typhimurium* i.p. injection. **E, G, M, O**) Representative images of MHCII expression following tau i.c. injection; 20x objective, scale bar= 50µm. **B, D, F, H, J, L, N, P**) Corresponding images at 40x objective, scale bar= 50µm. **Q**) Quantification of MHCII expression in the hippocampus, mixed-effects analysis with Sidak's post-hoc test. n= 5 for vehicle i.c./saline i.p., n= 6 for both tau i.c. groups and vehicle i.c./*S. typhimurium* i.p. **R**) Count of MHCII-positive microglia cells, Mixed-effects analysis with Sidak's post-hoc test. All data is presented as mean ± SEM.

The hippocampus of H1*Mapt-/-* mice demonstrated no significant change in MHCII expression as a result of either tau i.c. injection or systemic infection (**Figure 7-6**). There was no significant main effect of i.c. injection ($F(1, 7)= 1.42$, $p= 0.27$) or hemisphere ($F(1, 7)= 3.57$, $p= 0.1$). The tau i.c./*S. typhimurium* i.p. group demonstrated similar expression to the vehicle i.c. group (vehicle i.c./*S. typhimurium* i.p.= 2.48% ± 0.38; tau i.c./*S. typhimurium* i.p.= 3.48% ± 0.37). Therefore, the lack of tau pathology also translated to a lack of MHCII expression change. The MHCII-positive cell count in H1*Mapt-/-* mice (**Figure 7-6**) however did demonstrate a two-fold increase in cell count in the tau i.c. group compared to the vehicle i.c. group when there is systemic infection (vehicle i.c./*S. typhimurium* i.p.= 18.25% ± 3.12; tau i.c./*S. typhimurium* i.p.= 37.28% ± 12.69, $p= 0.84$). There was no significant main effect of i.c. injection ($F(1, 7)= 0.01$, $p= 0.91$), however a significant main effect of hemisphere ($F(1, 7)= 5.91$, $p<0.05$). The effect is small; however, this is also likely due to biological variability and a small sample size. There was no post-hoc significance with the contralateral hemisphere (vehicle i.c./*S. typhimurium* i.p.= 13.33% ± 6.07; tau i.c./*S. typhimurium* i.p.= 14.89% ± 9.59, $p= 0.93$).

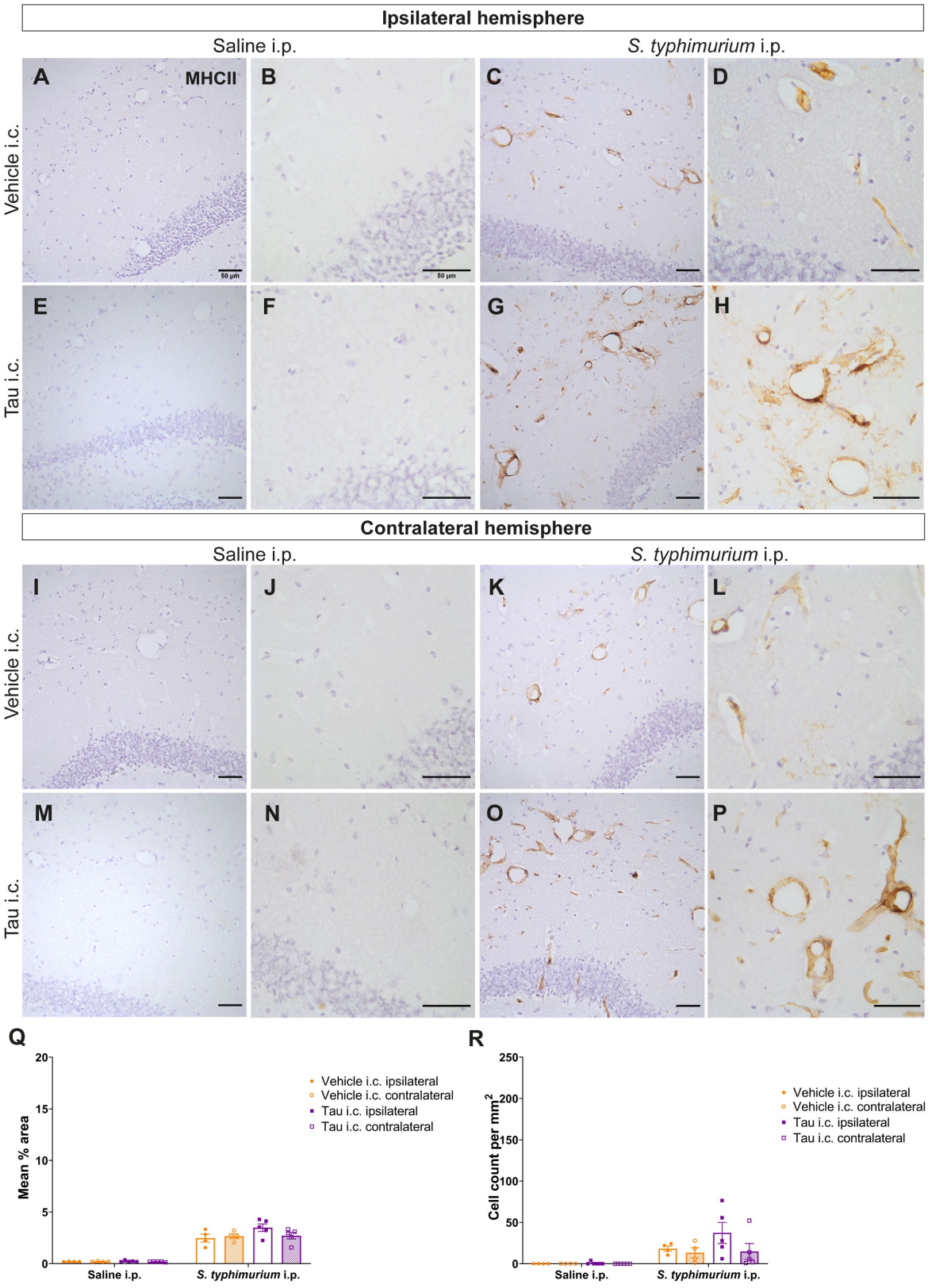
Ipsilateral hemisphere
Saline i.p.
S. typhimurium i.p.
Vehicle i.c.
Tau i.c.
A
MHCII
B
C
D
E
F
G
H
50 µm
Contralateral hemisphere
Saline i.p.
S. typhimurium i.p.
Vehicle i.c.
Tau i.c.
I
J
K
L
M
N
O
P
Q
Mean % area
20
15
10
5
0
Saline i.p.
S. typhimurium i.p.
Vehicle i.c. ipsilateral
Vehicle i.c. contralateral
Tau i.c. ipsilateral
Tau i.c. contralateral
R
Cell count per mm2
250
200
150
100
50
0
Saline i.p.
S. typhimurium i.p.
Vehicle i.c. ipsilateral
Vehicle i.c. contralateral
Tau i.c. ipsilateral
Tau i.c. contralateral

Figure 7-6: MHCII expression in the hippocampus of H1*Mapt-/-* mice

A, C I, K) Representative images of MHCII expression in mice which received vehicle i.c. injection followed by saline i.p. or *S. typhimurium* i.p. injection. **E, G, M, O**) Representative images of MHCII expression in mice which received tau i.c. injection followed by saline i.p. or *S. typhimurium* i.p. injection; 20x objective, scale bar= 50µm. **B, D, F, H, J, L, N, P**) Corresponding images at 40x objective, scale bar= 50µm. **Q**) Quantification of MHCII expression in the hippocampus. Two-way ANOVA with Sidak's post-hoc test; n= 4 for vehicle i.c. groups, n= 5 for tau i.c. groups. **R**) Count of MHCII-positive microglia cells, two-way ANOVA with Sidak's post-hoc test. Data is log transformed for analysis. However, most values are <1 therefore the original mean % area is displayed. All data is presented as mean ± SEM.

7.3.4 MHCII expression in the ventral hippocampus

MHCII expression appears to be exaggerated in the injection site of mice with tau pathology, as compared to *S. typhimurium* infection alone. To examine if these observations are linked to damage associated with tau propagation, I next analysed brain regions which are 5mm dorsal to the injection site.

The initial ROI to be analysed was the hippocampus (Bregma AP= -3.00), focused at the dentate gyrus (**Figure 7-7**). Expression of MHCII in the ipsilateral hemisphere of the tau i.c./*S. typhimurium* i.p. injection group was marginally increased compared to the vehicle i.c. group (vehicle i.c./*S. typhimurium* i.p.= 4.20% ± 0.99; tau i.c./*S. typhimurium* i.p.= 6.52% ± 2.15, p= 0.36). However, this was not statistically significant. No change in MHCII expression was observed in the contralateral hemisphere between these two groups (vehicle i.c./*S. typhimurium* i.p.= 3.38% ± 0.67; tau i.c./*S. typhimurium* i.p.= 2.79% ± 0.28, p= 0.93). There was no significant main effect of i.c. injection ($F(1, 10)= 0.36$, $p= 0.56$), however there was a significant main effect of hemisphere ($F(1, 10)= 5.32$, $p<0.05$). This was also mimicked in the MHCII-positive cell count in the C57BL/6 hippocampus (**Figure 7-7**). There is a non-significant increase in MHCII-positive cells in the tau i.c./*S. typhimurium* i.p. injection group compared to vehicle (vehicle i.c./*S. typhimurium* i.p.= 41.42 ± 14.38; tau i.c./*S. typhimurium* i.p..= 73.77 ± 28.02, p= 0.41). There was a significant main effect of hemisphere ($F(1, 10)= 9.83$, $p<0.05$) yet there was no significant main effect of i.c. injection ($F(1, 10)= 0.70$, $p= 0.42$). MHCII expression on microglia in this distant brain region may suggest that the effects are not due to injection of brain per se, but that it follows the tau spreading. However, co-localisation analysis would be required to confirm this.

The H1*Mapt-/-* mice showed similar MHCII expression to C57BL/6 mice in the ventral hippocampus (**Figure 7-8**). The tau i.c./*S. typhimurium* i.p. injection group showed two-fold

increased MHCII expression in the ipsilateral hemisphere compared to the vehicle i.c./*S. typhimurium* i.p. (vehicle i.c./*S. typhimurium* i.p.= 2.31% ± 0.38; tau i.c./*S. typhimurium* i.p.= 5.89% ± 2.00). However, because of the biological variability this does not confer a significant main effect of i.c. injection ($F(1, 7)= 1.58$, $p= 0.25$) or hemisphere ($F(1, 7)= 4.19$, $p= 0.08$). Furthermore, in the contralateral hemisphere there was no significant difference between i.c. injection groups following systemic infection (vehicle i.c./*S. typhimurium* i.p.= 2.30% ± 0.38; tau i.c./*S. typhimurium* i.p.= 2.61% ± 0.75, $p= 0.98$). MHCII-positive cells were also counted in the ventral hippocampus of H1*Mapt-/-* mice (**Figure 7-8**). There was an over ten-fold increase in cell count in the tau i.c./*S. typhimurium* i.p. group compared to the vehicle i.c. group (vehicle i.c./*S. typhimurium* i.p.= 4.35 ± 2.07; tau i.c./*S. typhimurium* i.p.= 68.48 ± 34.55). The Mann-Whitney test determined that there was no significant difference between the vehicle i.c./*S. typhimurium* i.p. and tau i.c./*S. typhimurium* i.p. injection groups ($U= 4$, $p= 0.19$). This lack of significance is likely due to the biological variability in the tau i.c. group following systemic infection.

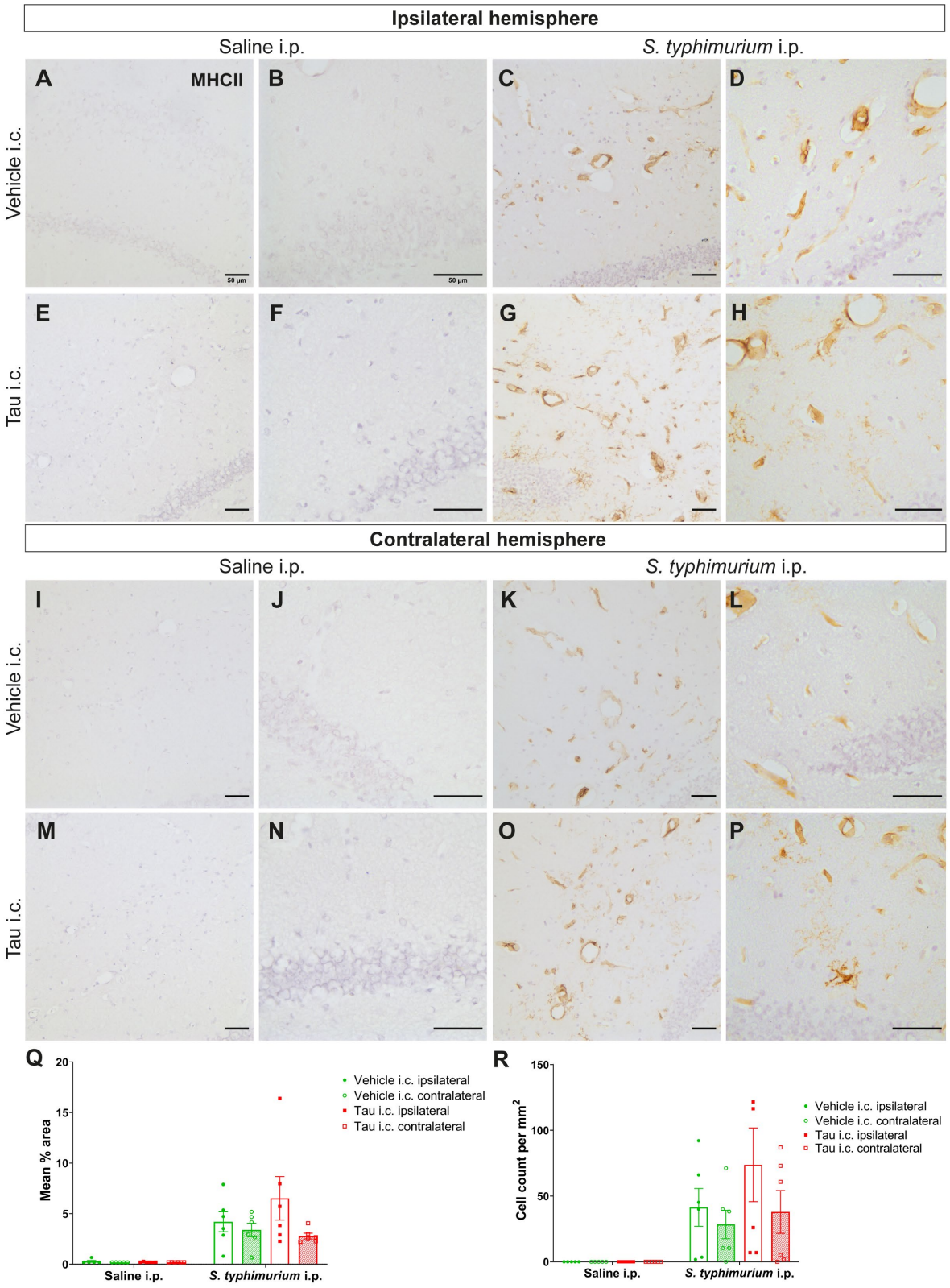
Ipsilateral hemisphere
Saline i.p.
S. typhimurium i.p.
Vehicle i.c.
Tau i.c.
A
MHCII
B
C
D
E
F
G
H
50 µm
Contralateral hemisphere
Saline i.p.
S. typhimurium i.p.
Vehicle i.c.
Tau i.c.
I
J
K
L
M
N
O
P
Q
Mean % area
Vehicle i.c. ipsilateral
Vehicle i.c. contralateral
Tau i.c. ipsilateral
Tau i.c. contralateral
Saline i.p.
S. typhimurium i.p.
R
Cell count per mm2
Vehicle i.c. ipsilateral
Vehicle i.c. contralateral
Tau i.c. ipsilateral
Tau i.c. contralateral
Saline i.p.
S. typhimurium i.p.

Figure 7-7: MHCII expression in the ventral hippocampus of C57BL/6 mice

A, C, I, K) Representative images of MHCII expression in mice which received vehicle i.c. injection followed by saline i.p. or *S. typhimurium* i.p. injection in the ipsilateral and contralateral hemisphere. **E, G, M, O**) Representative images of MHCII expression following tau i.c. injection; 20x objective, scale bar= 50µm. **B, D, F, H, J, L, N, P**) Corresponding images at 40x objective, scale bar= 50µm. **Q**) MHCII expression quantification, two-way ANOVA with Sidak's post-hoc test; n= 6 for tau i.c. groups and vehicle i.c./*S. typhimurium* i.p., n= 5 for vehicle i.c./saline i.p. **R**) Count of MHCII-positive microglia, two-way ANOVA with Sidak's post-hoc test. All data is presented as mean ± SEM.

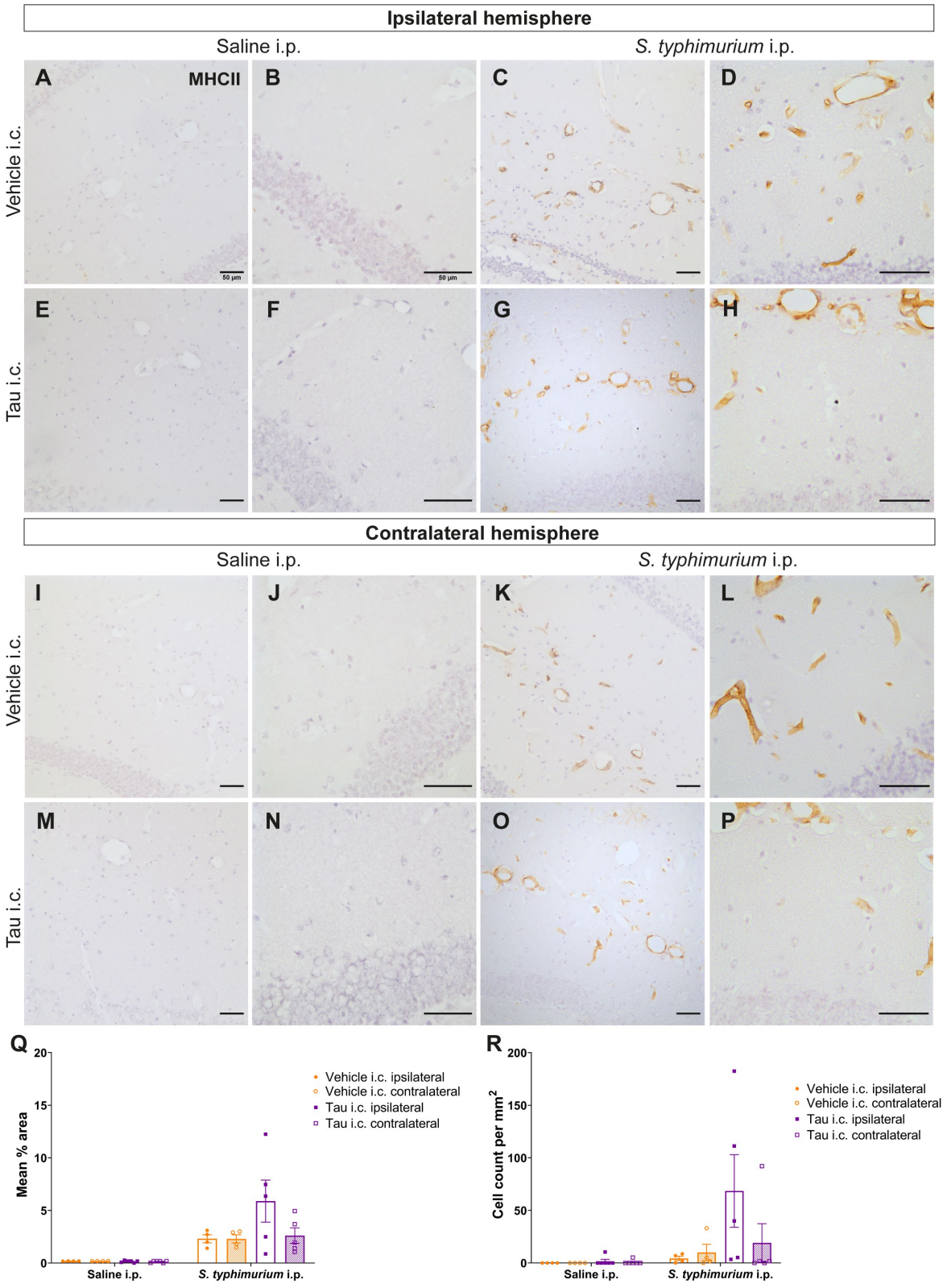
Ipsilateral hemisphere
Saline i.p.
S. typhimurium i.p.
Vehicle i.c.
Tau i.c.
A
MHCII
B
C
D
E
F
G
H
50 µm
Contralateral hemisphere
Saline i.p.
S. typhimurium i.p.
Vehicle i.c.
Tau i.c.
I
J
K
L
M
N
O
P
Q
Mean % area
20
15
10
5
0
Saline i.p.
S. typhimurium i.p.
Vehicle i.c. ipsilateral
Vehicle i.c. contralateral
Tau i.c. ipsilateral
Tau i.c. contralateral
R
Cell count per mm2
200
150
100
50
0
Saline i.p.
S. typhimurium i.p.
Vehicle i.c. ipsilateral
Vehicle i.c. contralateral
Tau i.c. ipsilateral
Tau i.c. contralateral

Figure 7-8: MHCII expression in the ventral hippocampus of H1*Mapt-/-* mice

A, C, I, K) Representative images of MHCII expression in mice which received vehicle i.c. injection followed by saline i.p. or *S. typhimurium* i.p. injection in the ipsilateral and contralateral hemisphere. **E, G, M, O**) Representative images of MHCII expression following tau i.c. injection; 20x objective, scale bar= 50µm. **B, D, F, H, J, L, N, P**) Corresponding images at 40x objective, scale bar= 50µm. **Q**) MHCII expression quantification, two-way ANOVA with Sidak's post-hoc test; n= 6 for tau i.c./saline i.p., n= 5 for tau i.c./*S. typhimurium* i.p., n= 4 for vehicle i.c. groups. **R**) Count of MHCII-positive microglia, Mann-Whitney test. All data is presented as mean ± SEM.

7.3.5 MHCII expression in the perirhinal cortex

The perirhinal cortex was also analysed as a region where tau pathology was observed in C57BL/6 mice (**Figure 7-9**). In the C57BL/6 mice, a minimal increase of MHCII expression was observed in one mouse in the tau i.c./*S. typhimurium* i.p. injection group compared to the vehicle i.c./*S. typhimurium* i.p. injection group (vehicle i.c./*S. typhimurium* i.p.= 3.12% ± 0.80; tau i.c./*S. typhimurium* i.p.= 5.14% ± 1.87). However, this was not significant, therefore there is no effect of tau i.c. injection on MHCII expression in the perirhinal cortex ($F(1, 10)= 0.72$, $p= 0.42$). Furthermore, there was no significant main effect of hemisphere ($F(1, 10)= 1.02$, $p= 0.34$).

The microglial cell count carried out for C57BL/6 mice in the perirhinal cortex was not normally distributed (**Figure 7-9**). Therefore, the analysis compared MHCII-positive microglial cell count between the ipsilateral hemispheres of the tau i.c./*S. typhimurium* i.p. and vehicle i.c./*S. typhimurium* i.p. groups. There was a two-fold increase in MHCII-positive cell count in the tau i.c. group compared to vehicle i.c. (vehicle i.c./*S. typhimurium* i.p.= 17.09 ± 11.73; tau i.c./*S. typhimurium* i.p.= 44.03 ± 22.02), however the variance is very high. A Mann-Whitney test determined that there was no significant difference between these two groups ($U= 11.50$, $p= 0.33$). This data may suggest that tau pathology is not directly linked to MHCII on microglia, but perhaps is linked to the vasculature.

MHCII expression was analysed in the perirhinal cortex of H1*Mapt-/-* mice (**Figure 7-10**). MHCII expression showed no significant main effect of i.c. injection ($F(1, 7)= 0.34$, $p= 0.58$) or hemisphere ($F(1, 7)= 0.14$, $p= 0.72$). As a result, there is no significant difference between the ipsilateral hemispheres of vehicle and tau i.c. groups following systemic infection (vehicle i.c./ *S. typhimurium* i.p.= 1.83% ± 0.39; tau i.c./*S. typhimurium* i.p.= 2.62% ± 0.97). There was also no difference observed in the contralateral hemisphere (vehicle i.c./*S. typhimurium* i.p.= 2.15% ± 0.66; tau i.c./*S. typhimurium* i.p.= 2.45% ± 0.66). This ROI in particular highlights how comparatively low MHCII expression is in the H1*Mapt-/-* mice following systemic infection compared to C57BL/6 mice.

MHCII-positive cell count was recorded for the perirhinal cortex in the H1*Mapt-/-* group (**Figure 7-10**). There was no significant effect of tau i.c. compared to vehicle i.c. groups after systemic infection in the ipsilateral hemisphere (vehicle i.c./*S. typhimurium* i.p.= 4.78 ± 3.28; tau i.c./*S. typhimurium* i.p.= 15.29 ± 14.01). A Mann-Whitney test confirmed that regardless of i.c. injection, microglial cell count following *S. typhimurium* was not significantly different ($U= 10$, $p= 0.5$). This suggests that in the H1*Mapt-/-* mice there does not appear to be any correlation to the tau pathology at this timepoint.

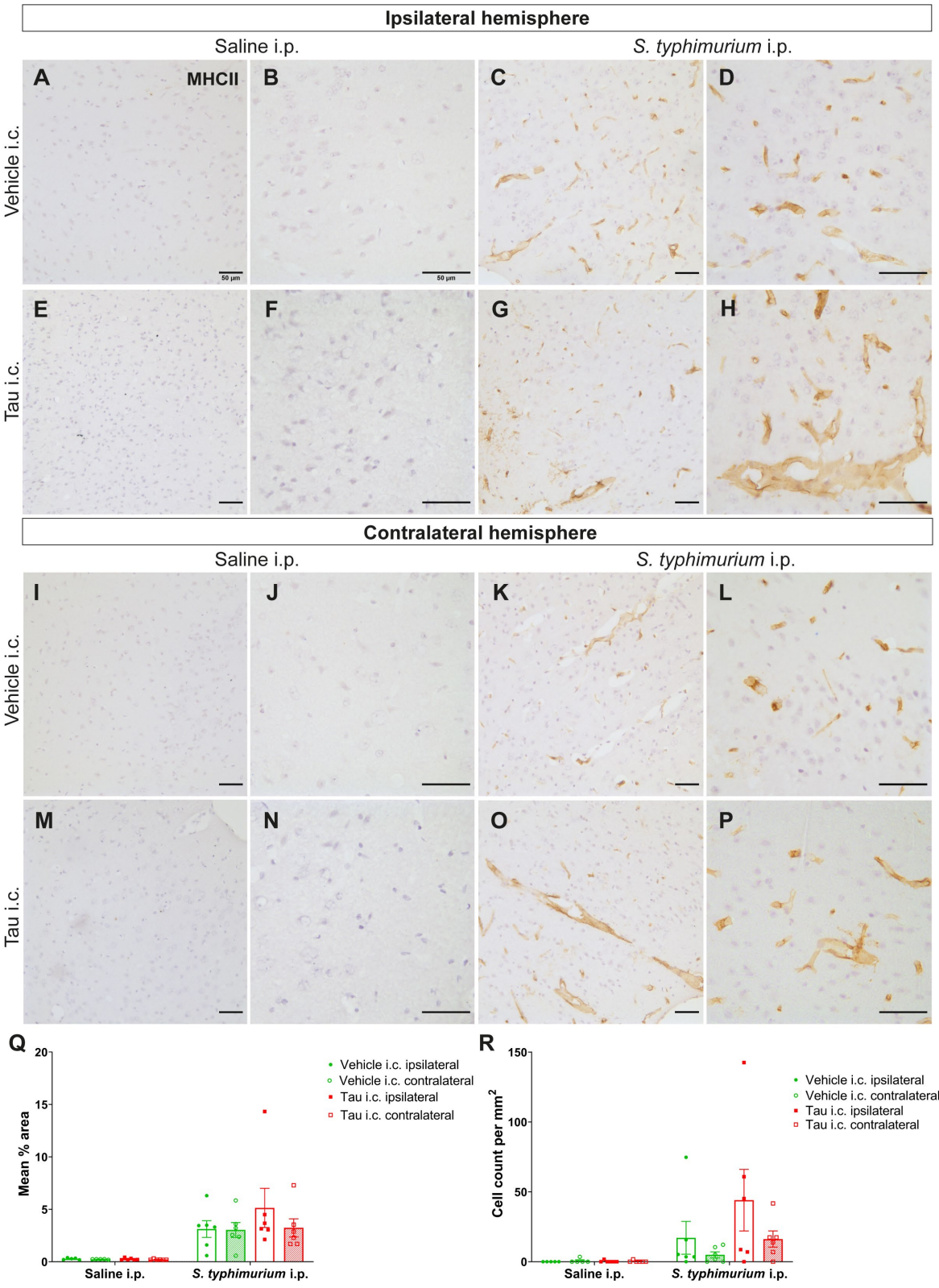
Ipsilateral hemisphere
Saline i.p.
S. typhimurium i.p.
A
MHCII
B
C
D
Vehicle i.c.
E
F
G
H
Tau i.c.
50 µm
Contralateral hemisphere
Saline i.p.
S. typhimurium i.p.
I
J
K
L
Vehicle i.c.
M
N
O
P
Tau i.c.
Q
Mean % area
20
15
10
5
0
Saline i.p.
S. typhimurium i.p.
Vehicle i.c. ipsilateral
Vehicle i.c. contralateral
Tau i.c. ipsilateral
Tau i.c. contralateral
R
Cell count per mm2
150
100
50
0
Saline i.p.
S. typhimurium i.p.
Vehicle i.c. ipsilateral
Vehicle i.c. contralateral
Tau i.c. ipsilateral
Tau i.c. contralateral

Figure 7-9: MHCII expression in the perirhinal cortex of C57BL/6 mice

A, C, I, K) Representative images of MHCII expression in mice which received vehicle i.c. injection followed by saline i.p. or *S. typhimurium* i.p. injection in the ipsilateral and contralateral hemisphere. **E, G, M, O**) Representative images of MHCII expression following tau i.c. injection; 20x objective, scale bar= 50µm. **B, D, F, H, J, L, N, P**) Corresponding images at 40x objective, scale bar= 50µm. **Q**) MHCII expression quantification, two-way ANOVA with Sidak's post-hoc test; n= 6 for tau i.c. groups and vehicle i.c./*S. typhimurium* i.p., n= 5 for vehicle i.c./saline i.p. Data is log transformed for analysis. However, most values are <1 therefore the original mean % area is displayed. **R**) Count of MHCII-positive microglia, Mann-Whitney test. All data is presented as mean ± SEM.

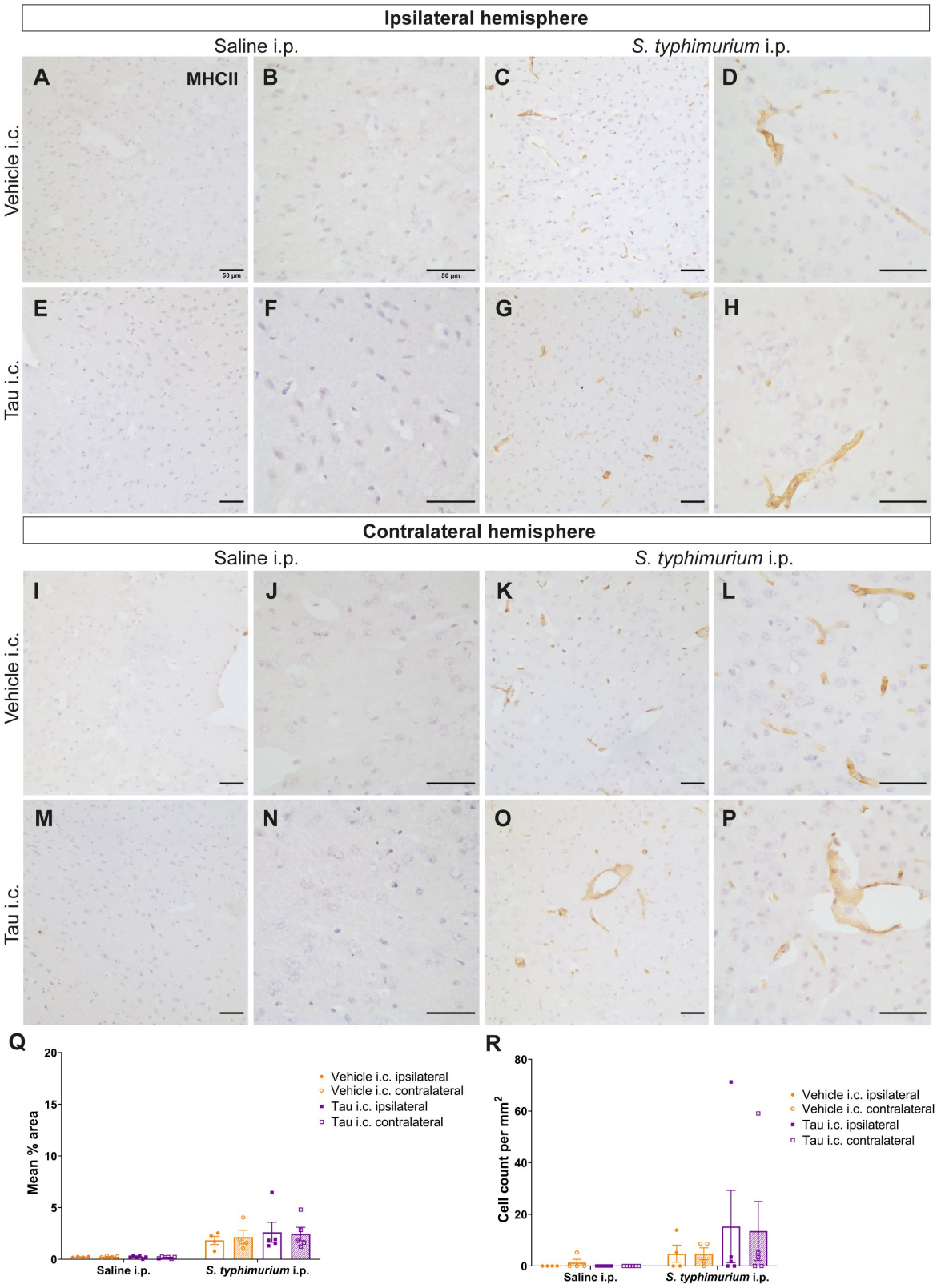
Ipsilateral hemisphere
Saline i.p.
S. typhimurium i.p.
A
MHCII
B
C
D
Vehicle i.c.
50 µm
E
F
G
H
Tau i.c.
Contralateral hemisphere
Saline i.p.
S. typhimurium i.p.
I
J
K
L
Vehicle i.c.
M
N
O
P
Tau i.c.
Q
Mean % area
20
15
10
5
0
Saline i.p.
S. typhimurium i.p.
Vehicle i.c. ipsilateral
Vehicle i.c. contralateral
Tau i.c. ipsilateral
Tau i.c. contralateral
R
Cell count per mm2
80
60
40
20
0
Saline i.p.
S. typhimurium i.p.
Vehicle i.c. ipsilateral
Vehicle i.c. contralateral
Tau i.c. ipsilateral
Tau i.c. contralateral

Figure 7-10: MHCII expression in the perirhinal cortex of H1*Mapt-/-* mice

A, C, I, K) MHCII expression in the perirhinal cortex following vehicle i.c. injection and subsequent saline i.p. or *S. typhimurium* i.p. injection in the ipsilateral and contralateral hemisphere. **E, G, M, O**) Representative images of tau i.c. injection groups in the ipsilateral and contralateral hemispheres; 20x objective, scale bar= 50µm. (**B, D, F, H, J, L, N, P**) Images at 40x objective for each respective group were included for greater observation of MHCII-positive cell morphology; 40x objective, scale bar= 50µm. **Q**) MHCII expression quantification, two-way ANOVA with Sidak's post-hoc test; n= 6 for tau i.c./saline i.p., n= 5 for tau i.c./*S. typhimurium* i.p., n= 4 for vehicle i.c. groups. Data is log transformed for analysis. However, most values are <1 therefore the original mean % area is displayed. **R**) Count of MHCII-positive microglia, Mann-Whitney test. All data is presented as mean ± SEM.

7.3.6 MHCII expression in the mammillary nuclei of C57BL/6 and H1*Mapt-/-* mice

The final region examined in C57BL/6 mice was the mammillary nuclei (**Figure 7-11**). There was no significant main effect of i.c. injection ($F(1, 10)= 0.03$, $p= 0.87$) or hemisphere ($F(1, 10)= 2.43$, $p= 0.15$). As a result, there was no change in MHCII expression in the ipsilateral hemisphere following systemic infection regardless of i.c. injection (vehicle i.c./*S. typhimurium* i.p.= 5.14% ± 1.13; tau i.c./*S. typhimurium* i.p.= 3.98% ± 0.89). There was also no change in MHCII expression in the contralateral hemisphere between the tau and vehicle i.c. groups (vehicle i.c./*S. typhimurium* i.p.= 4.83% ± 1.01; tau i.c./*S. typhimurium* i.p.= 4.79% ± 1.16). This demonstrates that MHCII expression in the mammillary nuclei is very similar following *S. typhimurium* injection regardless of prior i.c. injection. MHCII-positive cell count was carried out in the C57BL/6 mammillary nuclei (**Figure 7-11**). There is a three-fold increase in cell count per mm^2 in the ipsilateral hemisphere of the tau i.c./*S. typhimurium* i.p. group versus the vehicle i.c. group after systemic infection (vehicle i.c./*S. typhimurium* i.p.= 8.11% ± 2.72; tau i.c./*S. typhimurium* i.p.= 27.81 ± 14.25). A Mann-Whitney test demonstrated no significant difference in cell count between the ipsilateral vehicle i.c./ *S. typhimurium* i.p. and tau i.c./ *S. typhimurium* i.p. groups ($U= 14.50$, $p= 0.61$).

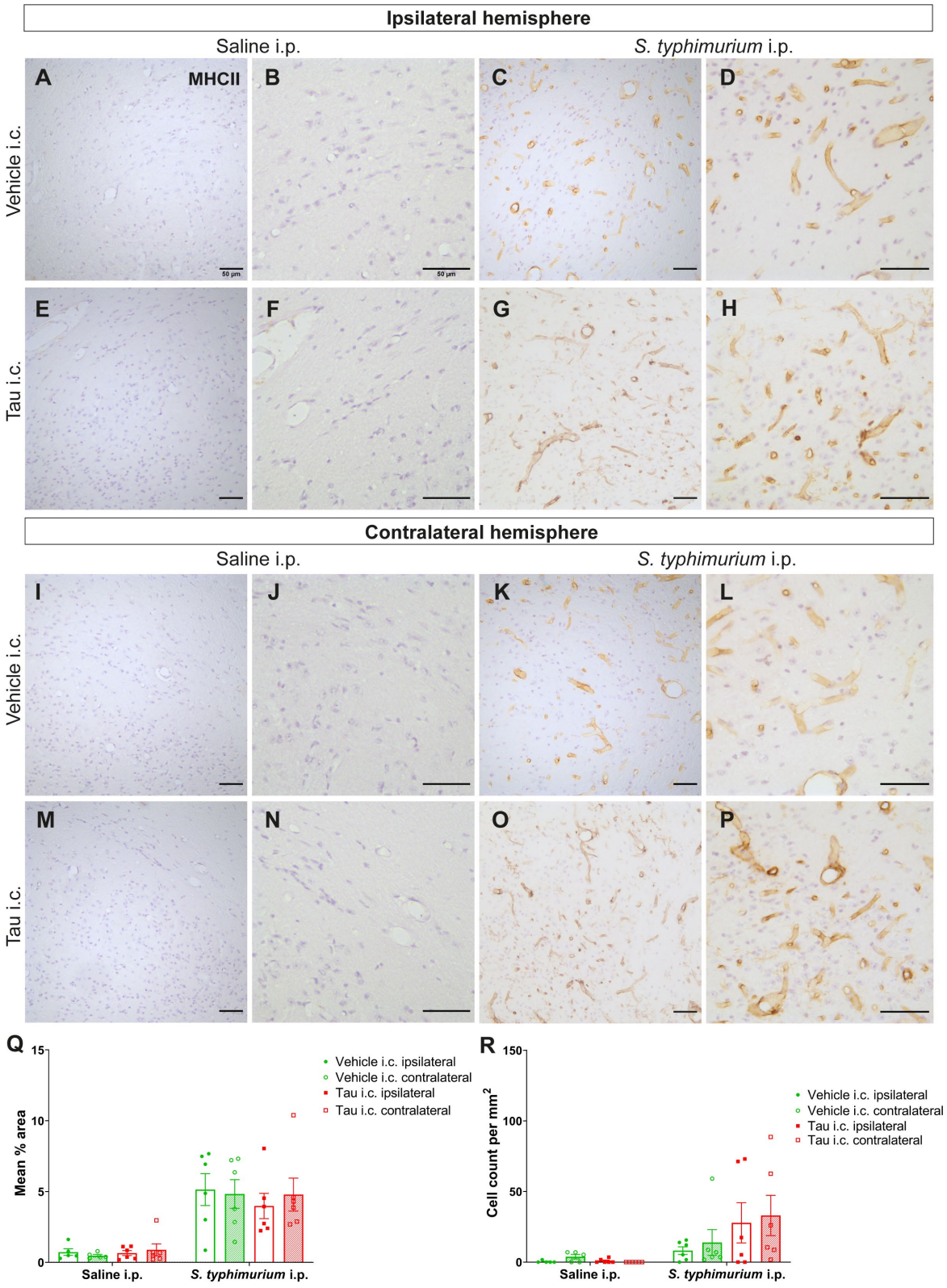
Ipsilateral hemisphere
Saline i.p.
S. typhimurium i.p.
Vehicle i.c.
Tau i.c.
A
MHCII
B
C
D
E
F
G
H
Contralateral hemisphere
Saline i.p.
S. typhimurium i.p.
Vehicle i.c.
Tau i.c.
I
J
K
L
M
N
O
P
Q
Mean % area
Vehicle i.c. ipsilateral
Vehicle i.c. contralateral
Tau i.c. ipsilateral
Tau i.c. contralateral
Saline i.p.
S. typhimurium i.p.
R
Cell count per mm2
Vehicle i.c. ipsilateral
Vehicle i.c. contralateral
Tau i.c. ipsilateral
Tau i.c. contralateral
Saline i.p.
S. typhimurium i.p.

Figure 7-11: MHCII expression in the mammillary nuclei of C57BL/6 mice

A, C, I, K) Representative images of MHCII expression in mice which received vehicle i.c. injection followed by saline i.p. or *S. typhimurium* i.p. injection in the ipsilateral and contralateral hemisphere. **E, G, M, O**) Representative images of tau i.c. injection groups in the ipsilateral and contralateral hemispheres; 20x objective, scale bar= 50μm. (**B, D, F, H, J, L, N, P**) Images at 40x objective for each respective group were included for greater observation of MHCII-positive cell morphology; 40x objective, scale bar= 50μm. **Q**) MHCII expression quantification, two-way ANOVA with Sidak's post-hoc test; n= 6 for tau i.c. groups and vehicle i.c./*S. typhimurium* i.p., n= 5 for vehicle i.c./saline i.p. Data is log transformed for analysis. However, most values are <1 therefore the original mean % area is displayed. **R**) Count of MHCII-positive microglia, Mann-Whitney test. All data is presented as mean ± SEM.

The expression of MHCII in H1*Mapt-/-* mice was consistent across all groups in the mammillary nuclei which underwent systemic infection (**Figure 7-12**). There was no significant main effect of i.c. injection ($F(1, 7)= 0.52$, $p= 0.50$) or hemisphere ($F(1, 7)= 2.98$, $p= 0.13$). Both in the ipsilateral hemisphere (vehicle i.c./*S. typhimurium* i.p.= 4.95% ± 0.91; tau i.c./*S. typhimurium* i.p.= 4.35% ± 1.03,$p= 0.90$) and the contralateral hemisphere (vehicle i.c./*S. typhimurium* i.p.= 4.54% ± 0.76; tau i.c./*S. typhimurium* i.p.= 3.19% ± 1.13, $p= 0.59$). The MHCII-positive cell count in the mammillary nuclei of H1*Mapt-/-* mice (**Figure 7-12**) showed no significant difference in expression between the vehicle i.c./ *S. typhimurium* i.p. and tau i.c./ *S. typhimurium* i.p. groups (vehicle i.c./*S. typhimurium* i.p.= 11.12 ± 4.10; tau i.c./*S. typhimurium* i.p.= 9.56 ± 2.88). A Mann-Whitney U test confirmed there was no statistical significance ($U= 10$, $p>0.99$). Therefore, the H1*Mapt-/-* mice also shows a clear effect of systemic infection but no difference between i.c. injection groups.

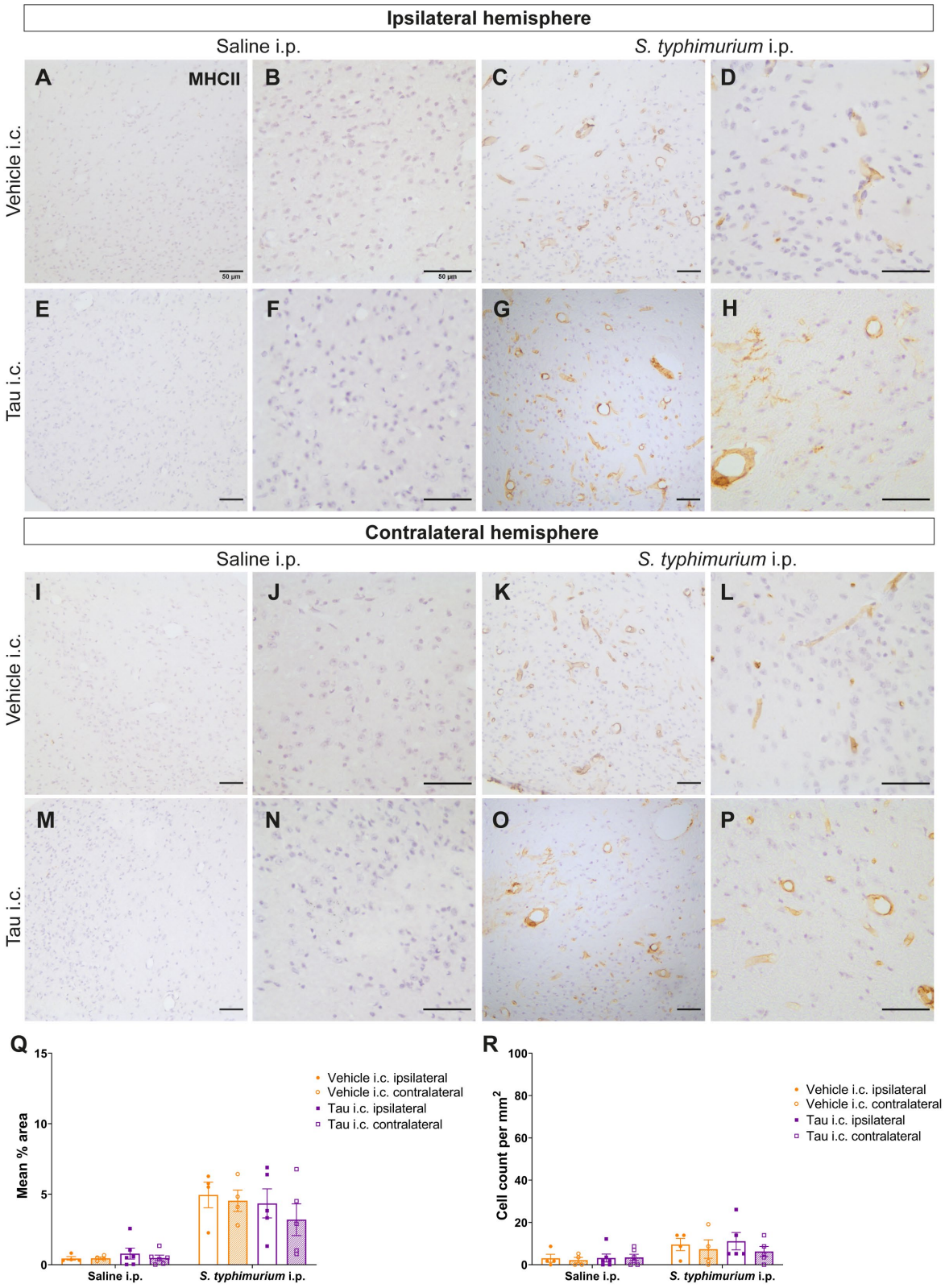
Ipsilateral hemisphere
Saline i.p.
S. typhimurium i.p.
A
MHCII
B
C
D
Vehicle i.c.
50 µm
E
F
G
H
Tau i.c.
Contralateral hemisphere
Saline i.p.
S. typhimurium i.p.
I
J
K
L
Vehicle i.c.
M
N
O
P
Tau i.c.
Q
Mean % area
15
10
5
0
Saline i.p.
S. typhimurium i.p.
Vehicle i.c. ipsilateral
Vehicle i.c. contralateral
Tau i.c. ipsilateral
Tau i.c. contralateral
R
Cell count per mm2
100
80
60
40
20
0
Saline i.p.
S. typhimurium i.p.
Vehicle i.c. ipsilateral
Vehicle i.c. contralateral
Tau i.c. ipsilateral
Tau i.c. contralateral

Figure 7-12: MHCII expression in the mammillary nuclei of H1*Mapt-/-* mice

A, C, I, K) Representative images of MHCII expression in mice which received vehicle i.c. injection followed by saline i.p. or *S. typhimurium* i.p. injection in the ipsilateral and contralateral hemisphere. **E, G, M, O**) Representative images of tau i.c. injection groups in the ipsilateral and contralateral hemispheres; 20x objective, scale bar= 50μm. (**B, D, F, H, J, L, N, P**) Images at 40x objective for each respective group were included for greater observation of MHCII-positive cell morphology; 40x objective, scale bar= 50μm. **Q**) MHCII expression quantification, two-way ANOVA with Sidak's post-hoc test; n= 6 for tau i.c./saline i.p., n= 5 for tau i.c./*S. typhimurium* i.p., n= 4 for vehicle i.c. groups. **R**) Count of MHCII-positive microglia, Mann-Whitney test. All data is presented as mean ± SEM.

7.3.7 FcγRI expression in the cortex following systemic infection

FcγRI is a macrophage/microglial-specific which was used to examine microglial responses to *S. typhimurium* in the presence or absence of tau pathology. The first brain region analysed was the injection site within the cortex in the C57BL/6 mice (**Figure 7-13**). Both groups which received tau i.c. injection showed upregulation of FcγRI expression, however following systemic infection FcγRI expression was increased two-fold (tau i.c./saline i.p.= 7.44% ± 2.35; tau i.c./*S. typhimurium* i.p.= 15.80% ± 4.57). Comparing groups which received systemic infection, mice receiving human tau lysate showed a ten-fold increase in FcγRI expression over the vehicle i.c. group in the ipsilateral hemisphere (vehicle i.c./*S. typhimurium* i.p.= 1.49% ± 0.55; tau i.c./*S. typhimurium* i.p.= 15.80% ± 4.57), suggesting robust microglial activation. A Mann-Whitney test determined that there was a clear trend, but lack of significant difference between the ipsilateral FcγRI expression in vehicle i.c./*S. typhimurium* i.p. and tau i.c./*S. typhimurium* i.p. groups (U= 4, p= 0.052).

FcγRI expression in the injection site was also analysed in the H1*Mapt-/-* mice (**Figure 7-14**). The H1*Mapt-/-* mouse showed no significant main effect of i.c. injection ($F(1, 15)= 1.15$, $p= 0.30$) or i.p. injection ($F(1, 15)= 0.03$, $p= 0.87$), however there was a significant main effect of hemisphere ($F(1, 15)= 17.99$, $p<0.001$). There is no significant difference between both tau i.c. groups, regardless of i.p. injection (tau i.c./saline i.p.= 7.64% ± 4.15; tau i.c./*S. typhimurium* i.p.= 9.95% ± 3.02, p= 0.93). When comparing FcγRI expression across groups which received systemic infection, the ipsilateral hemisphere of the tau i.c. group showed a three-fold increase in expression compared to vehicle i.c. group (vehicle i.c./*S. typhimurium* i.p.= 2.90% ± 2.21; tau i.c./*S. typhimurium* i.p.= 9.95% ± 3.02, p= 0.36). Biological variability is likely to explain for the lack of significance between the systemic infection groups which received vehicle or tau i.c. injection.

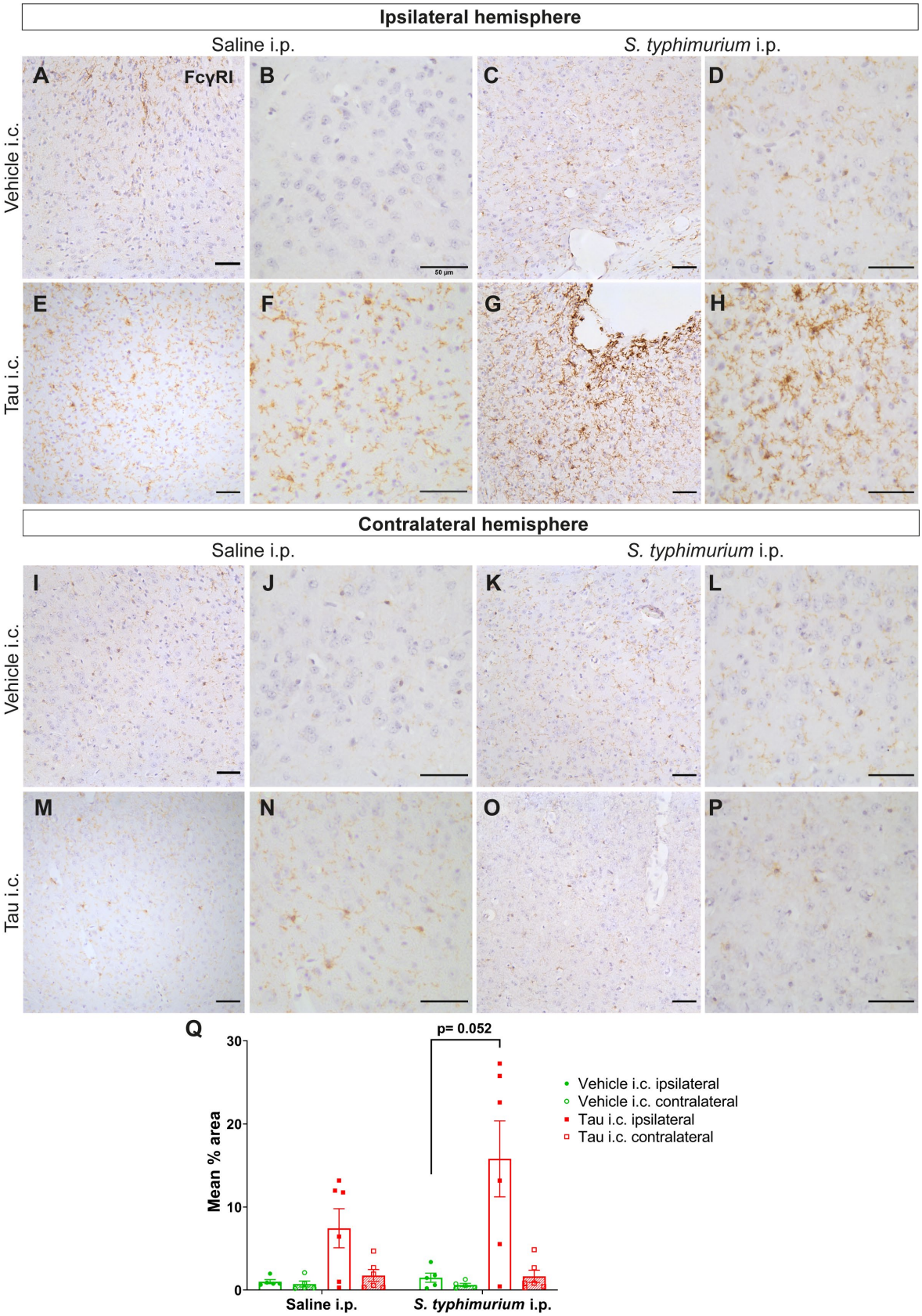
Ipsilateral hemisphere
Saline i.p.
S. typhimurium i.p.
A
FcγRI
B
C
D
Vehicle i.c.
50 µm
E
F
G
H
Tau i.c.
Contralateral hemisphere
Saline i.p.
S. typhimurium i.p.
I
J
K
L
Vehicle i.c.
M
N
O
P
Tau i.c.
Q
p= 0.052
Mean % area
30
20
10
0
Saline i.p.
S. typhimurium i.p.
Vehicle i.c. ipsilateral
Vehicle i.c. contralateral
Tau i.c. ipsilateral
Tau i.c. contralateral

Figure 7-13: FcγRI expression in the injection site of C57BL/6 mice

Representative images of FcγRI histology in the cortical injection site of C57BL/6 mice which received (**A, C, I, K**) vehicle i.c. or (**E, G, M, O**) tau i.c. injection; 20x objective, scale bar= 50μm. expression (**B, D, F, H, J, L, N, P**) Further images at 40x objective were included for greater observation of FcγRI expression; scale bar= 50μm. **Q**) Image quantification of mean percentage area. Mann-Whitney U test; n= 6 for both tau i.c. groups, n= 5 for both vehicle i.c. groups. All data is presented as mean ± SEM.

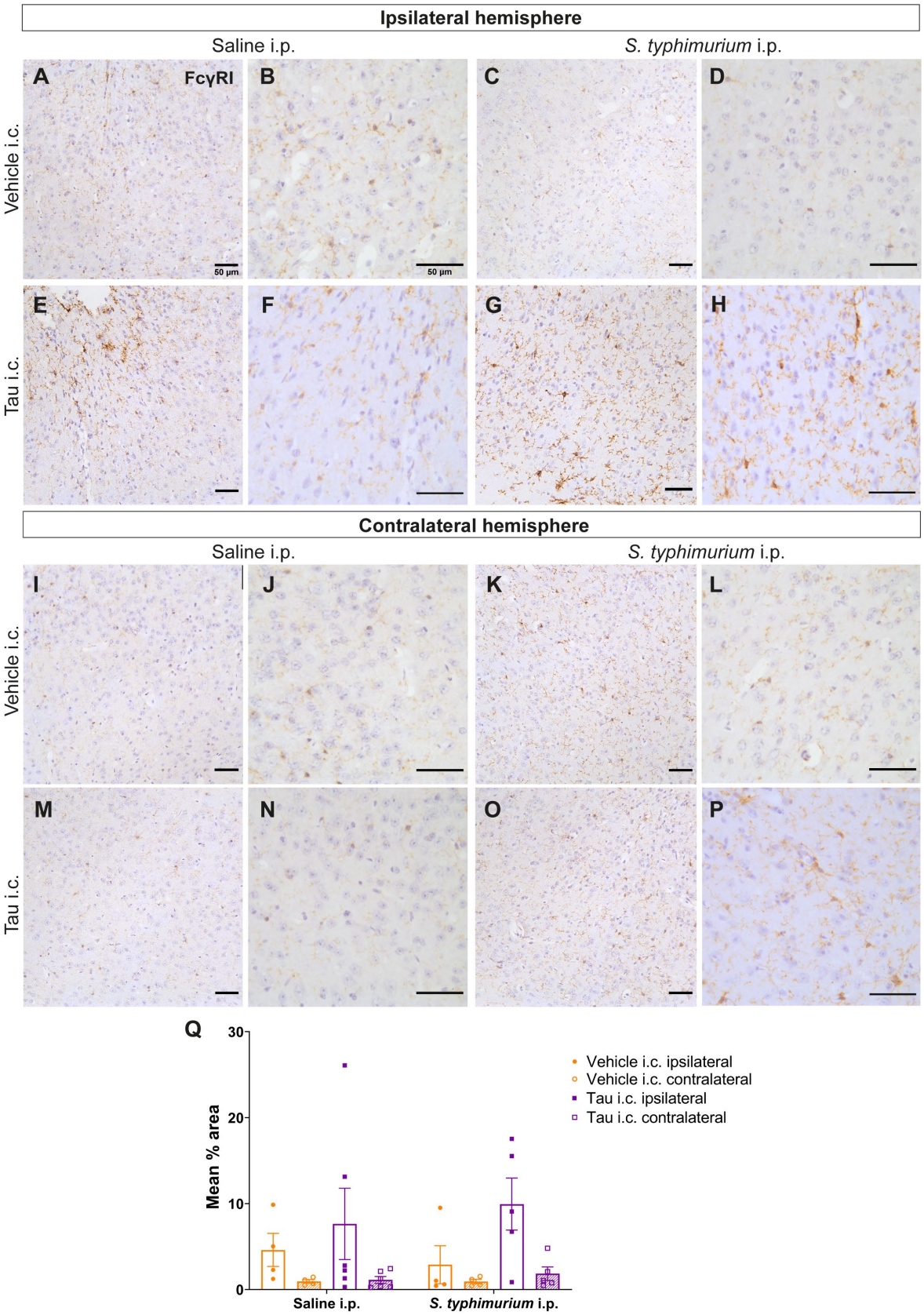
Ipsilateral hemisphere
Saline i.p.
S. typhimurium i.p.
A
FcγRI
B
C
D
Vehicle i.c.
50 µm
50 µm
E
F
G
H
Tau i.c.
Contralateral hemisphere
Saline i.p.
S. typhimurium i.p.
I
J
K
L
Vehicle i.c.
M
N
O
P
Tau i.c.
Q
Mean % area
30
20
10
0
Saline i.p.
S. typhimurium i.p.
Vehicle i.c. ipsilateral
Vehicle i.c. contralateral
Tau i.c. ipsilateral
Tau i.c. contralateral

Figure 7-14: FcγRI expression in the cortical injection site of H1*Mapt-/-* mice

A, C, I, K) FcγRI expression in the cortical injection site following vehicle i.c. injection and either saline i.p. or *S. typhimurium* i.p. injection in the ipsilateral and contralateral hemisphere. **E, G, M, O**) Representative images of tau i.c. injection groups in the ipsilateral and contralateral hemispheres; 20x objective, scale bar= 50µm. (**B, D, F, H, J, L, N, P**) Images at 40x objective for each respective group were included for greater observation of FcγRI-positive cell morphology; 40x objective, scale bar= 50µm. **Q**) Three-way ANOVA with Tukey's post-hoc test; n= 6 for tau i.c./saline i.p., n= 5 for tau i.c./*S. typhimurium* i.p., n= 4 for vehicle i.c. groups. Data is log transformed for analysis. However, most values are <1 therefore the original mean % area is displayed. All data is presented as mean ± SEM.

7.3.8 FcγRI expression in the corpus callosum of C57BL/6 and H1*Mapt-/-* mice

Next the corpus callosum was examined for changes in FcγRI expression in the C57BL/6 mice (**Figure 7-15**). There was a significant main effect of i.c. injection ($F(1, 18)= 15.52$, $p<0.001$), hemisphere ($F(1, 18)= 43.62$, $p<0.001$) and i.p. injection ($F(1, 18)= 4.55$, $p<0.05$). C57BL/6 mice showed small upregulation of FcγRI expression in mice receiving tau lysate and systemic infection compared to the tau i.c./saline i.p. group (tau i.c./saline i.p.= 7.12% ± 6.83; tau i.c./*S. typhimurium* i.p.= 13.53% ± 8.25, p= 0.82). There was a ten-fold increase in FcγRI expression in the ipsilateral hemisphere of the tau i.c./saline i.p. group compared to the vehicle i.c./saline i.p. group (vehicle i.c./saline i.p.= 0.71% ± 1.12; tau i.c./saline i.p.= 7.12% ± 6.83, $p<0.05$). There was an eight-fold increase in FcγRI expression in the tau i.c./*S. typhimurium* group compared to the vehicle i.c./*S. typhimurium* i.p. group (vehicle i.c./*S. typhimurium* i.p.= 1.67% ± 1.45; tau i.c./*S. typhimurium* i.p.= 13.53% ± 8.25, p= 0.08). Having compared ipsilateral hemispheres between groups, there was also differences between hemispheres. For example, FcγRI expression in the ipsilateral hemisphere of the tau i.c./saline i.p. group was four-fold higher compared to contralateral (ipsilateral= 7.12% ± 6.83; contralateral= 1.50% ± 1.32, $p<0.05$) and the tau i.c./*S. typhimurium* i.p. ipsilateral hemisphere showed eight-fold higher FcγRI expression than the contralateral (ipsilateral= 13.53% ± 8.25; contralateral= 1.60% ± 1.35, $p<0.05$). This highlights that FcγRI expression in the white matter is increased specific to regions which show AT8 immunoreactivity.

The corpus callosum was also analysed in the H1*Mapt-/-* mouse for changes in FcγRI expression (**Figure 7-16**). There was a significant main effect of hemisphere ($F(1, 15)= 9.54$, $p<0.01$), yet no significant main effect of i.c. injection ($F(1, 15)= 0.62$, p= 0.44) or i.p. injection ($F(1, 15)= 2.19$, p= 0.16). Notably, there was a seven-fold increase in FcγRI expression in the tau i.c./*S. typhimurium* i.p. group in the ipsilateral hemisphere compared to mice which had saline i.p. (tau i.c./saline= 1.19% ± 0.42; tau i.c./*S. typhimurium* i.p.= 9.56% ± 3.69; $p<0.01$). Notably, significantly upregulated FcγRI expression was observed in the ipsilateral hemisphere versus the contralateral of the tau i.c./*S. typhimurium* i.p. group (ipsilateral= 9.56% ± 3.69; contralateral= 1.59% ± 0.6, $p<0.01$), but not the tau i.c./saline i.p. group (ipsilateral= 1.19% ± 0.42; contralateral= 0.45% ± 0.13, p= 0.99). This result highlights that H1*Mapt-/-* mice in the tau i.c./saline i.p. group do not demonstrate the same response to tau pathology observed in C57BL/6 mice. This suggests that the changes in FcγRI expression in the tau i.c. groups may be dependent on the level of tau pathology.

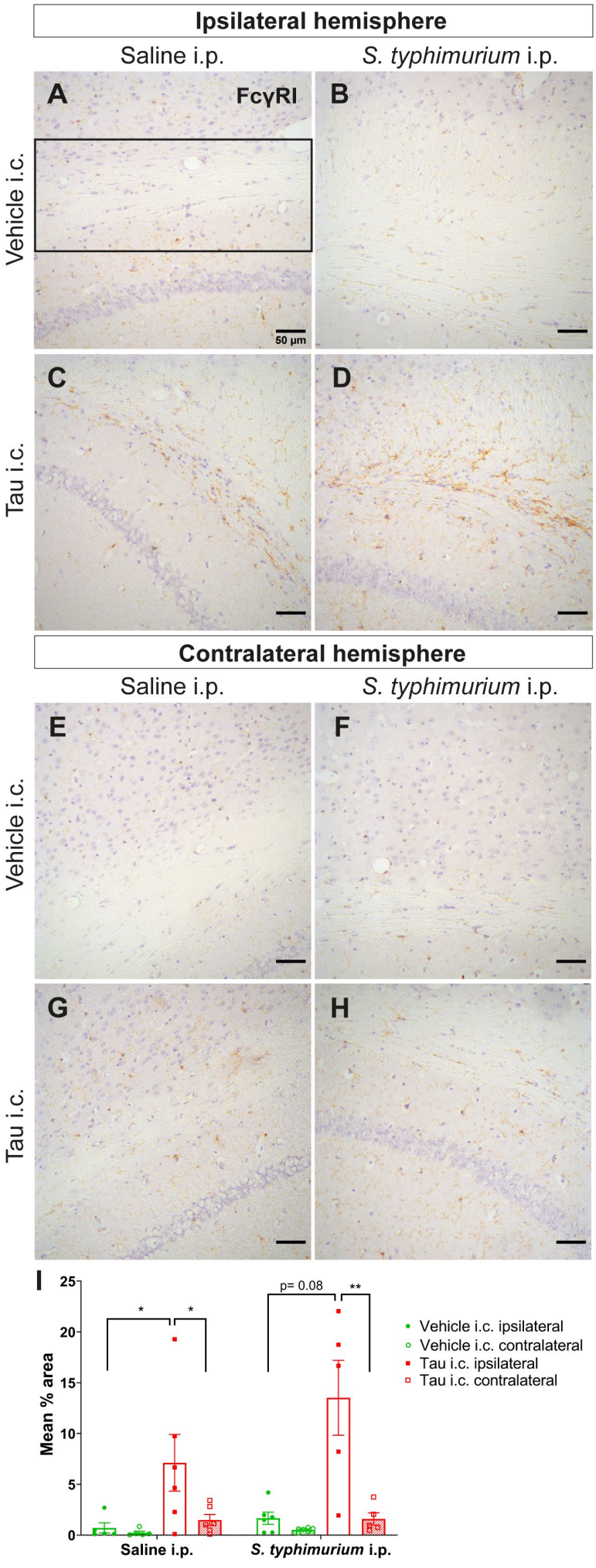
Ipsilateral hemisphere
Saline i.p.
S. typhimurium i.p.
A
FcγRI
B
Vehicle i.c.
50 µm
C
D
Tau i.c.
Contralateral hemisphere
Saline i.p.
S. typhimurium i.p.
E
F
Vehicle i.c.
G
H
Tau i.c.
I
Mean % area
25
20
15
10
5
0
*
*
p= 0.08
**
Vehicle i.c. ipsilateral
Vehicle i.c. contralateral
Tau i.c. ipsilateral
Tau i.c. contralateral
Saline i.p.
S. typhimurium i.p.

Figure 7-15: FcγRI expression in the corpus callosum of C57BL/6 mice

A, B, E, F) Representative images of vehicle i.c. injection both following saline i.p. and *S. typhimurium* i.p. injection in the ipsilateral and contralateral hemisphere. **C, D, G, H**) Representative images of tau i.c. injection in the ipsilateral and contralateral hemispheres; 20x objective, scale bar= 50μm. **I**) Three-way ANOVA with Tukey's post-hoc test (*$p<0.05$, **$p<0.01$); n= 6 for tau i.c./saline i.p. and vehicle i.c./*S. typhimurium* i.p. groups, n= 5 for vehicle i.c./saline i.p. and tau i.c./*S. typhimurium* i.p. groups. Data is log transformed for analysis. However, the original mean % area is displayed. All data is presented as mean ± SEM.

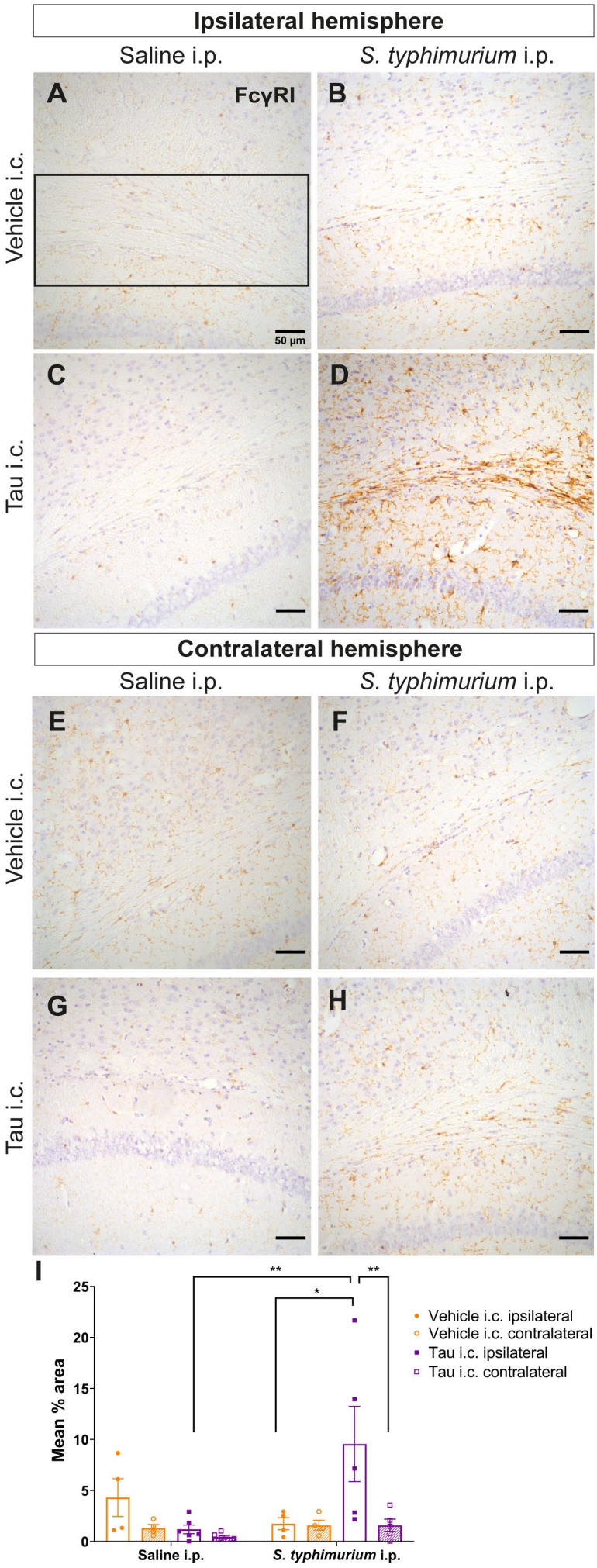
Ipsilateral hemisphere
Saline i.p.
S. typhimurium i.p.
A
FcγRI
B
Vehicle i.c.
50 µm
C
D
Tau i.c.
Contralateral hemisphere
Saline i.p.
S. typhimurium i.p.
E
F
Vehicle i.c.
G
H
Tau i.c.
I
Mean % area
25
20
15
10
5
0
**
*
**
Vehicle i.c. ipsilateral
Vehicle i.c. contralateral
Tau i.c. ipsilateral
Tau i.c. contralateral
Saline i.p.
S. typhimurium i.p.

Figure 7-16: FcγRI expression in corpus callosum following i.c. injection in H1*Mapt-/-* mice

A, B) FcγRI expression in the ipsilateral hemisphere of mice which underwent vehicle i.c. injection followed by saline or *S. typhimurium* i.p. injection. **E. F**) Corresponding contralateral hemisphere. **C, D**) Representative images of FcγRI expression in tau i.c. injection groups in the ipsilateral and **G. H**) contralateral hemispheres; 20x objective, scale bar= 50μm. **I**) Three-way ANOVA with Tukey's post-hoc test (*p<0.05, **p<0.01); n= 6 for tau i.c./saline i.p. n= 5 for tau i.c./*S. typhimurium* i.p., n= 4 for vehicle i.c. groups. All data is presented as mean ± SEM.

7.3.9 FcγRI expression in the hippocampus of C57BL/6 and H1*Mapt-/-* mice

Next, the hippocampus was analysed for FcγRI expression (**Figure 7-17**). In C57BL/6 mice there was no significant main effect of i.c. injection ($F(1, 19)= 3.73$, $p= 0.07$), but there was a significant main effect of i.p. injection ($F(1, 19)= 13.28$, $p<0.01$) and hemisphere ($F(1, 19)= 26.17$, $p<0.001$). In addition, the interaction of hemisphere and i.c. injection was significant ($F(1, 19)= 5.81$, $p<0.05$). There was a notable increase in FcγRI expression when comparing hemispheres between the tau i.c./*S. typhimurium* i.p. group (ipsilateral= 9.92% ± 3.11; contralateral= 5.53% ± 1.53; $p<0.05$) and the tau i.c./saline i.p. group (ipsilateral= 4.48% ± 1.83, contralateral= 2.47% ± 0.99, $p<0.05$). However, there was no significant difference observed between the two tau i.c. groups in the ipsilateral hippocampus ($p= 0.38$). No significance was observed between the two infection groups, regardless of i.c. injection, despite a two-fold increase in expression in the tau i.c. group (vehicle i.c./*S. typhimurium* i.p.= 4.65% ± 1.06; tau i.c./*S. typhimurium* i.p.= 9.92% ± 3.12, $p= 0.91$). This suggests that the presence of tau aggregate may be adequate to induce upregulation of FcγRI expression.

FcγRI expression in the hippocampus was much more sporadic in H1*Mapt-/-* mice than observed in C57BL/6 mice (**Figure 7-18**). In groups which underwent systemic infection there was an almost two-fold upregulation of FcγRI expression in the tau i.c. group (vehicle i.c./*S. typhimurium* i.p.= 6.51% ± 1.84; tau i.c./*S. typhimurium* i.p.= 12.62% ± 1.94). Nonetheless, a Mann-Whitney test demonstrated that the hippocampus in the H1*Mapt-/-* mice only demonstrated a trend when comparing the vehicle i.c./*S. typhimurium* i.p. group to the tau i.c./*S. typhimurium* i.p. group ($U= 2$, $p= 0.06$). Again, the group with greater tau pathology (C57BL/6 mice) demonstrated a larger change in FcγRI expression. It is likely this is in response to the presence of aggregated tau, as both C57BL/6 and H1*Mapt-/-* mice show evidence of priming.

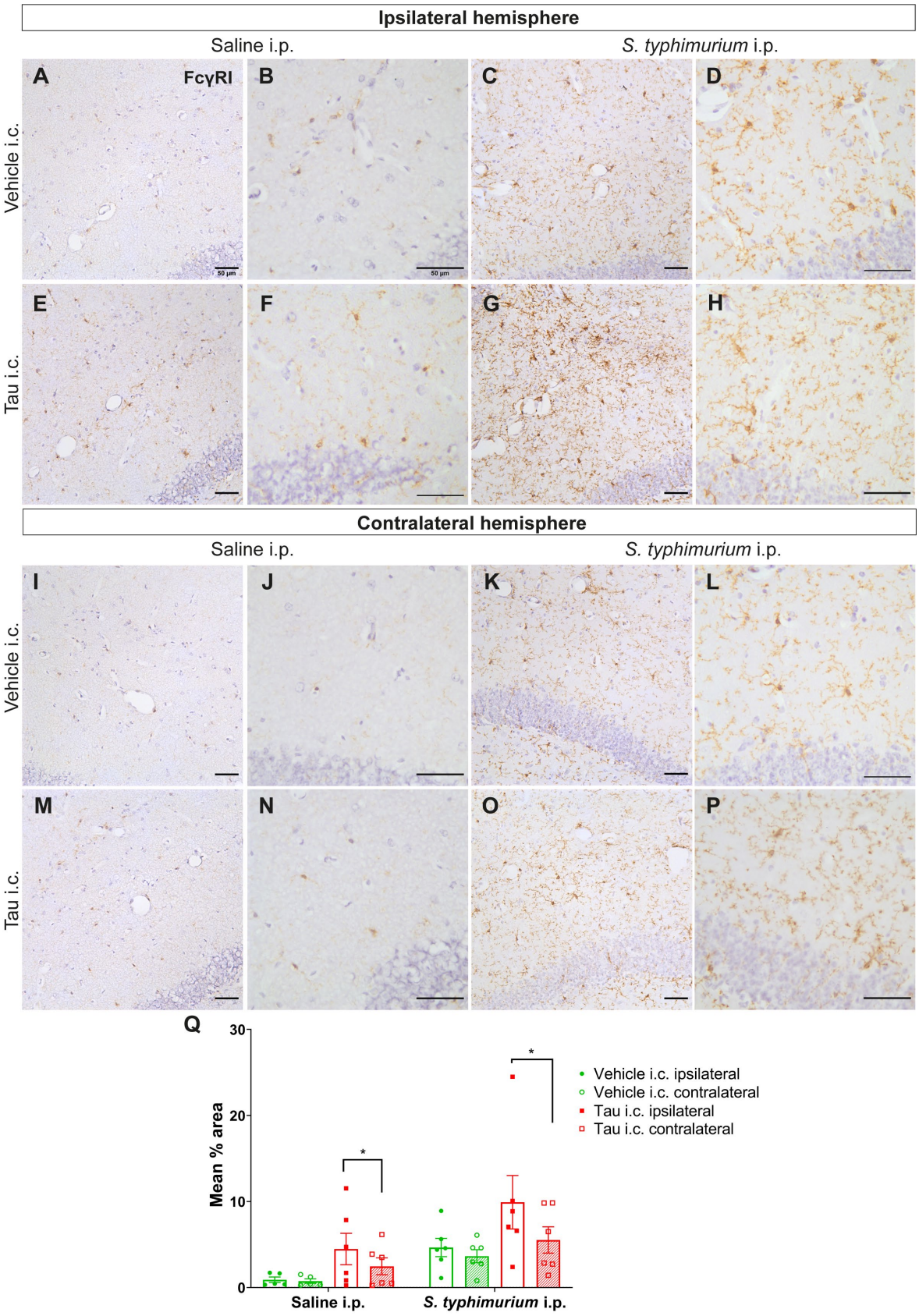
Ipsilateral hemisphere
Saline i.p.
S. typhimurium i.p.
Vehicle i.c.
Tau i.c.
A
FcγRI
B
C
D
E
F
G
H
50 µm
Contralateral hemisphere
Saline i.p.
S. typhimurium i.p.
Vehicle i.c.
Tau i.c.
I
J
K
L
M
N
O
P
Q
Mean % area
30
20
10
0
*
*
Vehicle i.c. ipsilateral
Vehicle i.c. contralateral
Tau i.c. ipsilateral
Tau i.c. contralateral
Saline i.p.
S. typhimurium i.p.

Figure 7-17: FcγRI expression in the hippocampus of C57BL/6 mice

A, C, I, K) Representative images of vehicle i.c. injection both following saline i.p. and *S. typhimurium* i.p. injection in the ipsilateral and contralateral hemisphere. **E, G, M, O**) Representative images of tau i.c. injection groups in the ipsilateral and contralateral hemispheres; 20x objective, scale bar= 50µm. (**B, D, F, H, J, L, N, P**) Images at 40x objective for each respective group were included for greater observation of FcγRI-positive cell morphology; 40x objective, scale bar= 50µm. **Q**) Three-way ANOVA with Tukey's post-hoc test (*$p<0.05$); n= 6 for both tau i.c. groups and vehicle i.c./*S. typhimurium* i.p., n= 5 for vehicle i.c./saline i.p.. Data is log transformed for analysis. However, most values are <1 therefore the original mean % area is displayed. All data is presented as mean ± SEM.

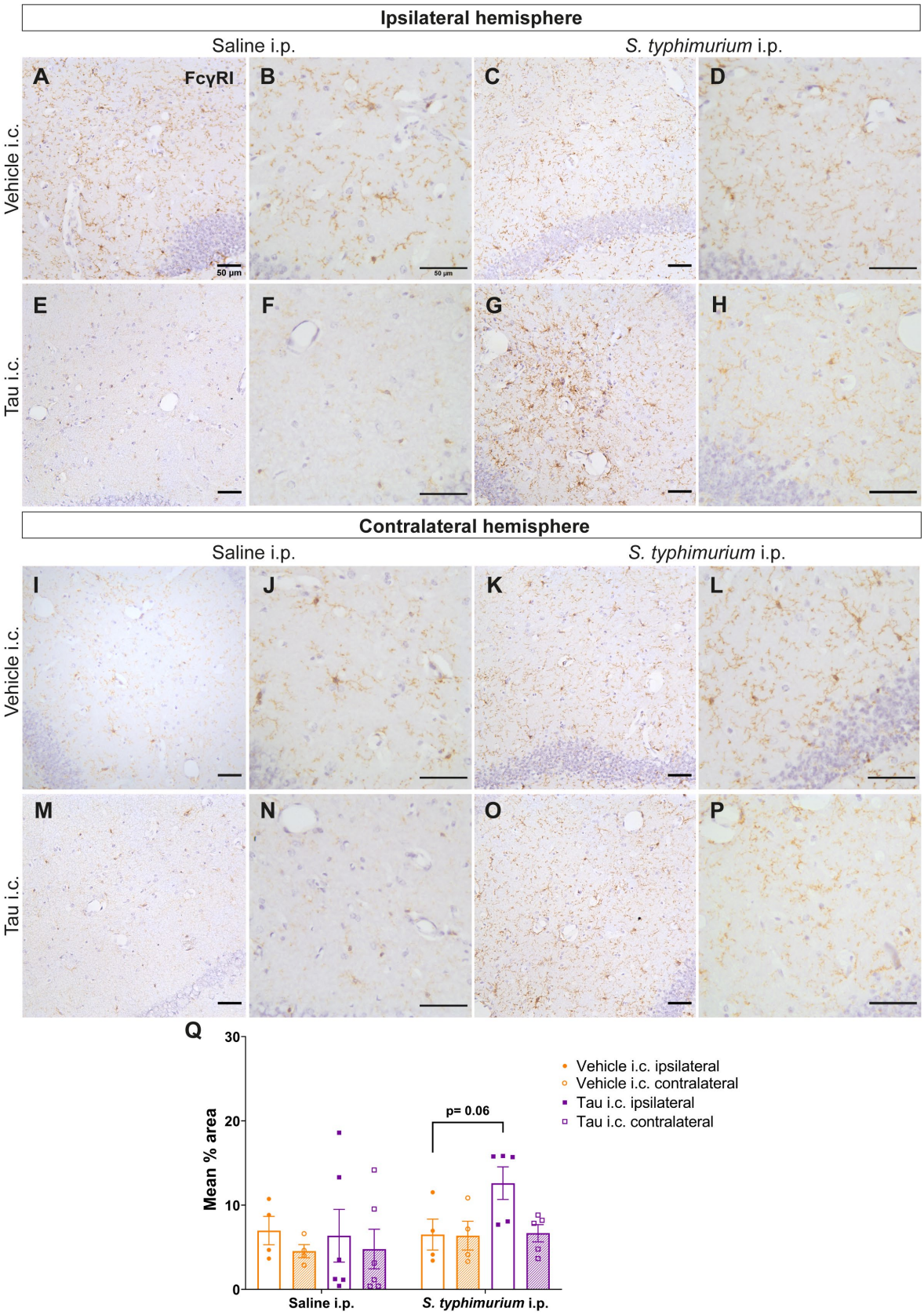
Ipsilateral hemisphere
Saline i.p.
S. typhimurium i.p.
Vehicle i.c.
Tau i.c.
A
FcγRI
B
C
D
E
F
G
H
50 µm
Contralateral hemisphere
Saline i.p.
S. typhimurium i.p.
Vehicle i.c.
Tau i.c.
I
J
K
L
M
N
O
P
Q
Mean % area
30
20
10
0
p= 0.06
Vehicle i.c. ipsilateral
Vehicle i.c. contralateral
Tau i.c. ipsilateral
Tau i.c. contralateral
Saline i.p.
S. typhimurium i.p.

Figure 7-18: FcγRI expression in hippocampus following i.c. injection in H1*Mapt-/-* mice

A, C) FcγRI expression in the ipsilateral hemisphere of mice which underwent vehicle i.c. injection followed by saline or *S. typhimurium* i.p. injection. **I, K**) Corresponding contralateral hemisphere. **E, G**) Representative images of FcγRI expression in tau i.c. injection groups in the ipsilateral and **M, O**) contralateral hemispheres; 20x objective, scale bar= 50μm. **B, D, F, H, J, L, N, P**) Corresponding images to show microglial morphology with greater clarity; 40x objective, scale bar= 50μm. **Q**) Mann-Whitney test; n= 6 for tau i.c./saline i.p. n= 5 for tau i.c./*S. typhimurium* i.p., n= 4 for vehicle i.c. groups. All data is presented as mean ± SEM.

7.3.10 FcγRI expression in the ventral hippocampus post-*S. typhimurium* infection

Following analysis of FcγRI expression at Bregma coordinate -2.50 (AP), the ventral hippocampus (Bregma AP: -3.00) was analysed to determine whether FcγRI expression is upregulated in brain regions distant from the injections site.

In C57BL/6 mice, FcγRI expression was analysed in the dentate gyrus (**Figure 7-19**). FcγRI expression between the vehicle i.c. and tau i.c. groups which underwent systemic infection was similar (vehicle i.c./*S. typhimurium* i.p.= 13.14% ± 1.49; tau i.c./*S. typhimurium* i.p.= 11.33% ± 3.97). However, the tau i.c./*S. typhimurium* i.p. group showed a two-fold increase in FcγRI expression compared to the tau i.c./saline i.p. group (tau i.c./saline i.p.= 4.66% ± 1.19; tau i.c./*S. typhimurium* i.p.= 11.33% ± 3.97). Despite this, due to biological variability a Student's t-test determined there was no significant effect of systemic infection on expression in the ipsilateral hippocampus, when comparing tau i.c. groups ($t(5.90)= 1.61$, $p= 0.16$). There is upregulation of FcγRI expression following *S. typhimurium* in both tau i.c. and vehicle i.c. groups compared to their respective saline i.p. control groups. This is observed both in the ipsilateral and contralateral hemispheres.

FcγRI expression was also analysed in the hippocampus of H1*Mapt-/-* mice (**Figure 7-20**). There was a two-fold increase in FcγRI expression in the tau i.c. injection group which had systemic infection compared to the tau i.c./saline i.p. group (tau i.c./saline i.p.= 8.61% ± 2.81; tau i.c./*S. typhimurium* i.p.= 15.88% ± 3.75). A Student's t-test was carried out, with no significant effect of systemic infection on FcγRI expression in the ipsilateral hippocampus between the tau i.c./saline i.p. and tau i.c./*S. typhimurium* i.p. groups ($t(7.80)= 1.55$, $p= 0.16$). This demonstrates how both C57BL/6 and H1*Mapt-/-* mice do not show significant upregulation of FcγRI expression as a result of priming from tau pathology in this region. However, biological variability is a key issue within this region.

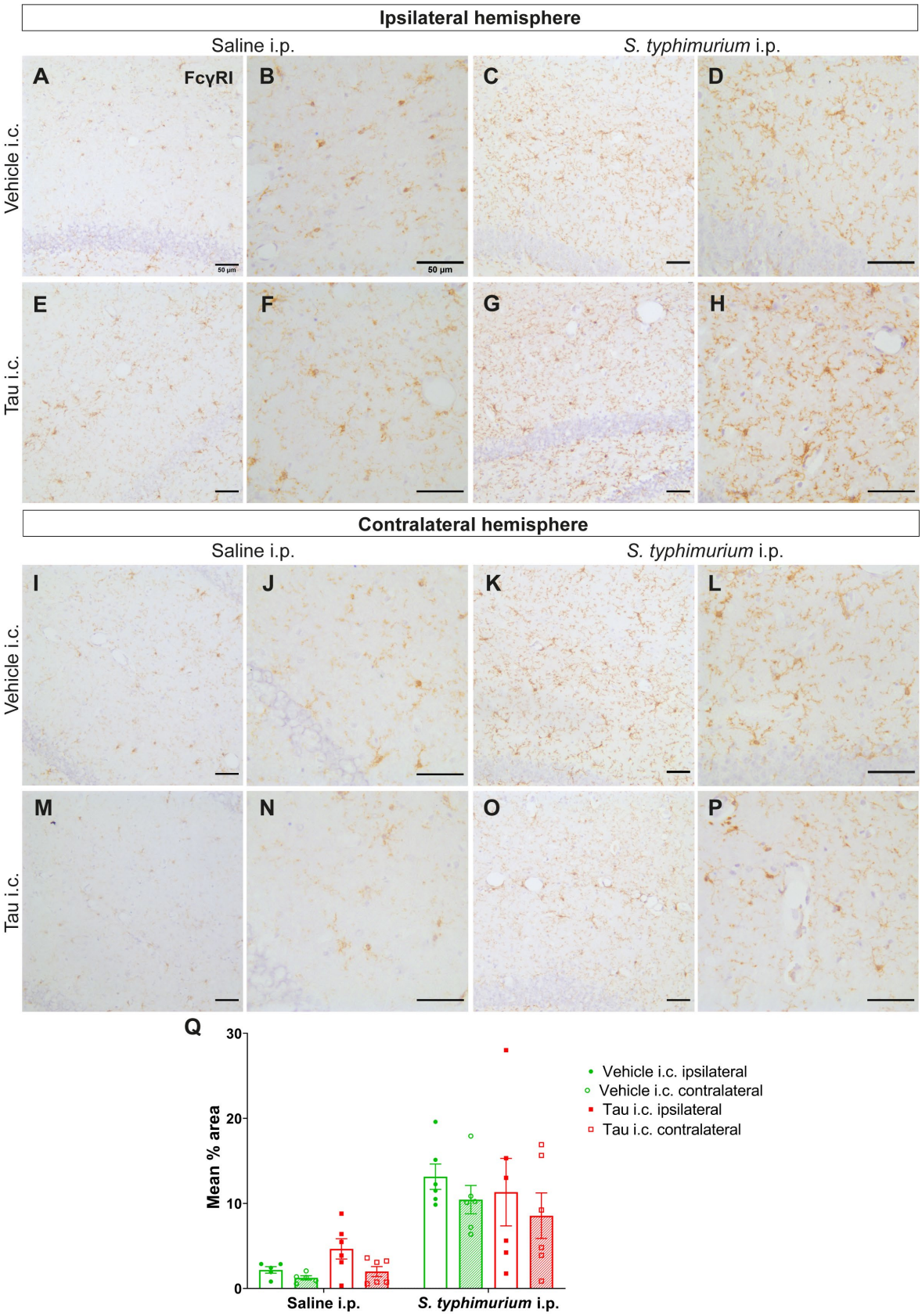
Ipsilateral hemisphere
Saline i.p.
S. typhimurium i.p.
A
FcγRI
B
C
D
Vehicle i.c.
50 µm
E
F
G
H
Tau i.c.
Contralateral hemisphere
Saline i.p.
S. typhimurium i.p.
I
J
K
L
Vehicle i.c.
M
N
O
P
Tau i.c.
Q
Mean % area
30
20
10
0
Saline i.p.
S. typhimurium i.p.
Vehicle i.c. ipsilateral
Vehicle i.c. contralateral
Tau i.c. ipsilateral
Tau i.c. contralateral

Figure 7-19: FcγRI expression in ventral hippocampus following i.c. injection in C57BL/6 mice

A, C) FcγRI expression in the ipsilateral hemisphere of mice which underwent vehicle i.c. injection followed by saline or *S. typhimurium* i.p. injection. **I, K**) Corresponding contralateral hemisphere. **E, G**) Representative images of FcγRI expression in tau i.c. injection groups in the ipsilateral and **M, O**) contralateral hemispheres; 20x objective, scale bar= 50µm. **B, D, F, H, J, L, N, P**) Corresponding images to show microglial morphology with greater clarity; 40x objective, scale bar= 50µm. **Q**) Unpaired Student's t-test with Welch's correction; n= 6 for tau i.c. groups and vehicle i.c./*S. typhimurium* i.p., n= 5 for vehicle i.c./saline i.p. All data is presented as mean ± SEM.

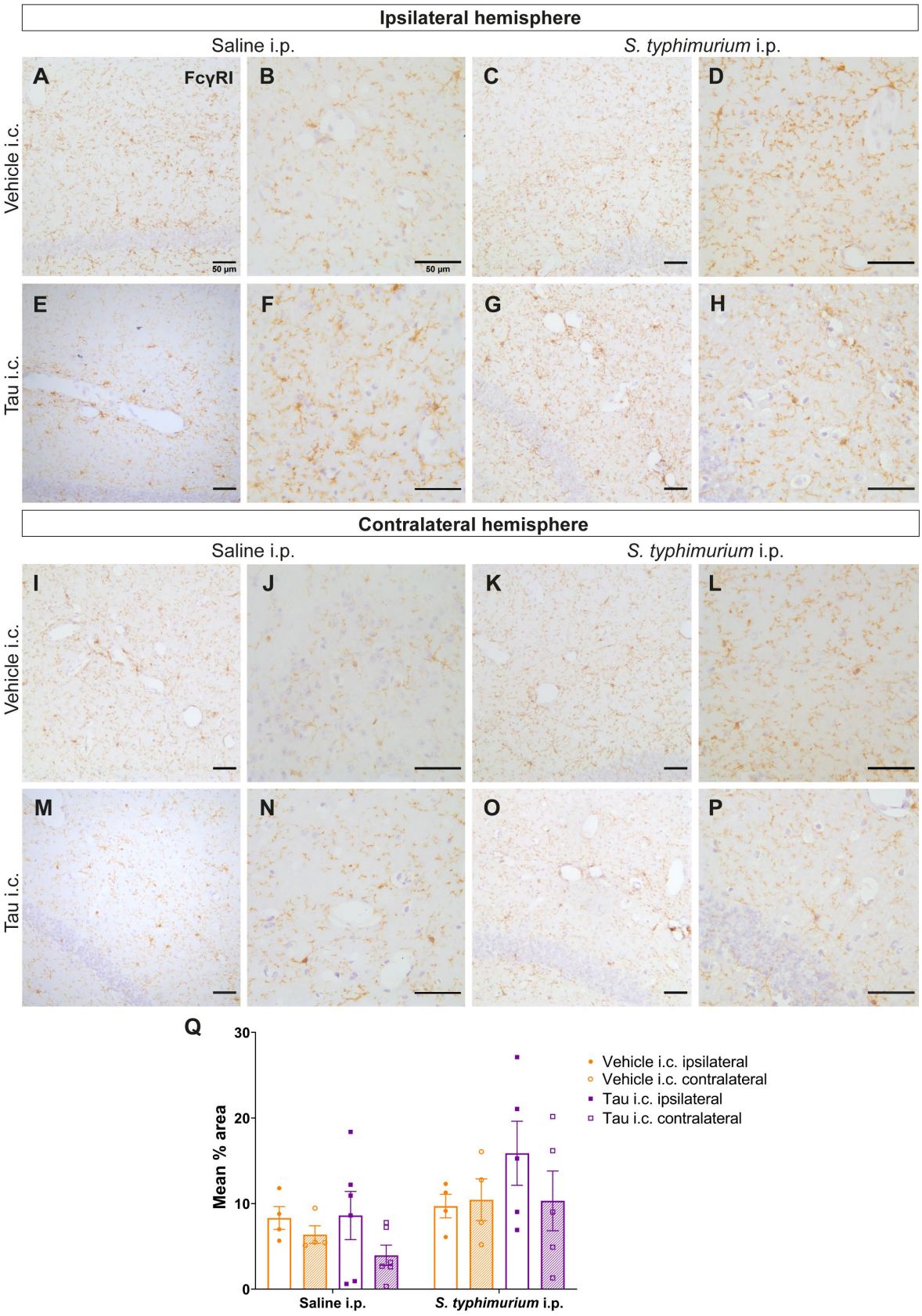
Ipsilateral hemisphere
Saline i.p.
S. typhimurium i.p.
Vehicle i.c.
Tau i.c.
A
FcγRI
B
C
D
E
F
G
H
50 µm
Contralateral hemisphere
Saline i.p.
S. typhimurium i.p.
Vehicle i.c.
Tau i.c.
I
J
K
L
M
N
O
P
Q
Mean % area
30
20
10
0
Saline i.p.
S. typhimurium i.p.
Vehicle i.c. ipsilateral
Vehicle i.c. contralateral
Tau i.c. ipsilateral
Tau i.c. contralateral

Figure 7-20: FcγRI expression in the ventral hippocampus following systemic infection in H1*Mapt-/-* mice

A, C) FcγRI expression in the ipsilateral hemisphere of mice which underwent vehicle i.c. injection followed by saline or *S. typhimurium* i.p. injection. **I, K**) Corresponding contralateral hemisphere. **E, G**) Representative images of FcγRI expression in tau i.c. injection groups in the ipsilateral and **M, O**) contralateral hemispheres; 20x objective, scale bar= 50µm. **B, D, F, H, J, L, N, P**) Corresponding images to show microglial morphology with greater clarity; 40x objective, scale bar= 50µm. **Q**) Unpaired Student's t-test with Welch's correction; n= 6 for tau i.c./saline i.p., n= 5 for tau i.c./*S. typhimurium* i.p., n= 4 for vehicle i.c. groups. All data is presented as mean ± SEM. A batch effect was observed in one of the cohorts which received tau i.c. injection. As a result, this cohort had a separate threshold to all other tau i.c. and vehicle i.c. injection mice.

7.3.11 FcγRI expression in the perirhinal cortex of C57BL/6 and H1*Mapt-/-* mice

The perirhinal cortex of C57BL/6 mice was analysed for FcγRI expression. The graph (**Figure 7-21**) demonstrates a two-fold increase in FcγRI expression in the ipsilateral hemisphere of the tau i.c./*S. typhimurium* i.p. group compared to the tau i.c./saline i.p. group (tau i.c./saline i.p.= 8.97% ± 1.24; tau i.c./*S. typhimurium* i.p.= 18.72% ± 2.33). Given that FcγRI expression was so similar across all groups except for the ipsilateral hemispheres of the mice which received tau i.c. injection and saline i.p. or systemic infection, a t-test was carried out. A Student's t-test showed significant increase in FcγRI expression in in the ipsilateral hemisphere of the tau i.c./*S. typhimurium* i.p. group compared to the tau i.c./saline i.p. group ($t(10)= 3.69$, $p<0.01$). This suggests that the i.c. injection of tau lysate influences the difference in hemisphere specific FcγRI expression.

The perirhinal cortex analysis for FcγRI expression in the H1*Mapt-/-* mice showed different interactions compared to the C57BL/6 analysis for the same ROI (**Figure 7-22**). There was no notable difference in ipsilateral FcγRI expression between both tau i.c. groups (tau i.c./saline i.p.= 14.85% ± 3.52; tau i.c./*S. typhimurium* i.p.= 17.88% ± 3.41, $p>0.99$). There was a significant main effect of hemisphere ($F(1, 15)= 10.54$, $p<0.01$) yet no significant main effect of i.c. injection ($F(1, 15)= 0.47$, $p= 0.50$) yet a significant interaction between these two factors ($F(1, 15)= 6.42$, $p<0.05$). There was also no significant main effect of i.p. injection ($F(1, 15)= 0.87$, $p= 0.36$).

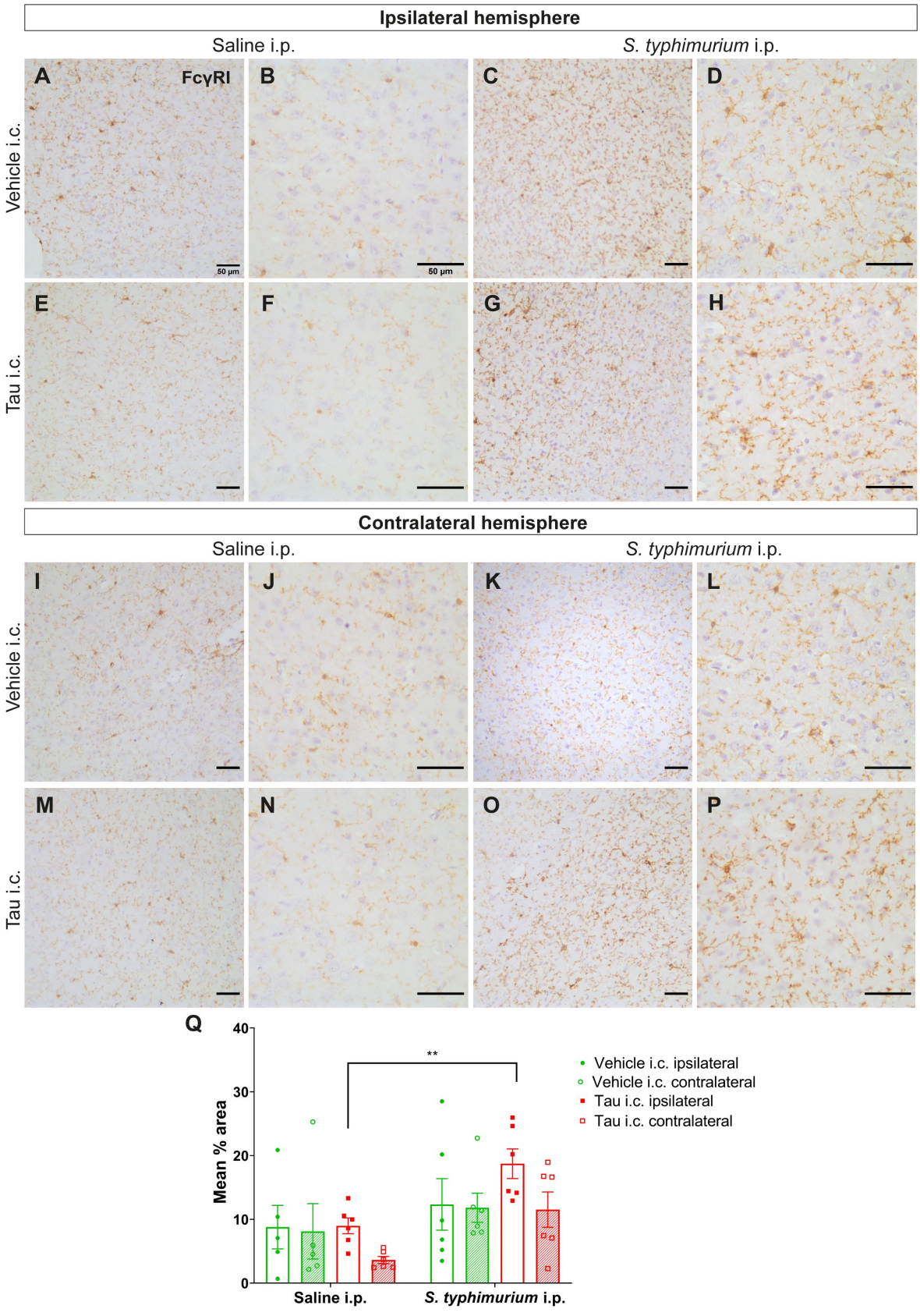
Ipsilateral hemisphere
Saline i.p.
S. typhimurium i.p.
A
FcγRI
B
C
D
Vehicle i.c.
50 µm
50 µm
E
F
G
H
Tau i.c.
Contralateral hemisphere
Saline i.p.
S. typhimurium i.p.
I
J
K
L
Vehicle i.c.
M
N
O
P
Tau i.c.
Q
Mean % area
40
30
20
10
0
**
Saline i.p.
S. typhimurium i.p.
Vehicle i.c. ipsilateral
Vehicle i.c. contralateral
Tau i.c. ipsilateral
Tau i.c. contralateral

Figure 7-21: FcγRI expression following tau or vehicle i.c. injection in the perirhinal cortex of C57BL/6 mice

A, C, I, K) FcγRI expression in the perirhinal cortex following vehicle i.c. injection and either saline i.p. or *S. typhimurium* i.p. injection in the ipsilateral and contralateral hemisphere. **E, G, M, O**) Representative images of tau i.c. injection groups in the ipsilateral and contralateral hemispheres; 20x objective, scale bar= 50µm. **B, D, F, H, J, L, N, P**) Images at 40x objective for each respective group were included for greater observation of FcγRI-positive cell morphology; 40x objective, scale bar= 50µm. **Q**) Unpaired Student's t-test (**$p<0.01$); n= 6 for both tau i.c. groups and vehicle i.c./*S. typhimurium* i.p., n= 5 for vehicle i.c./saline i.p. All data is presented as mean ± SEM.

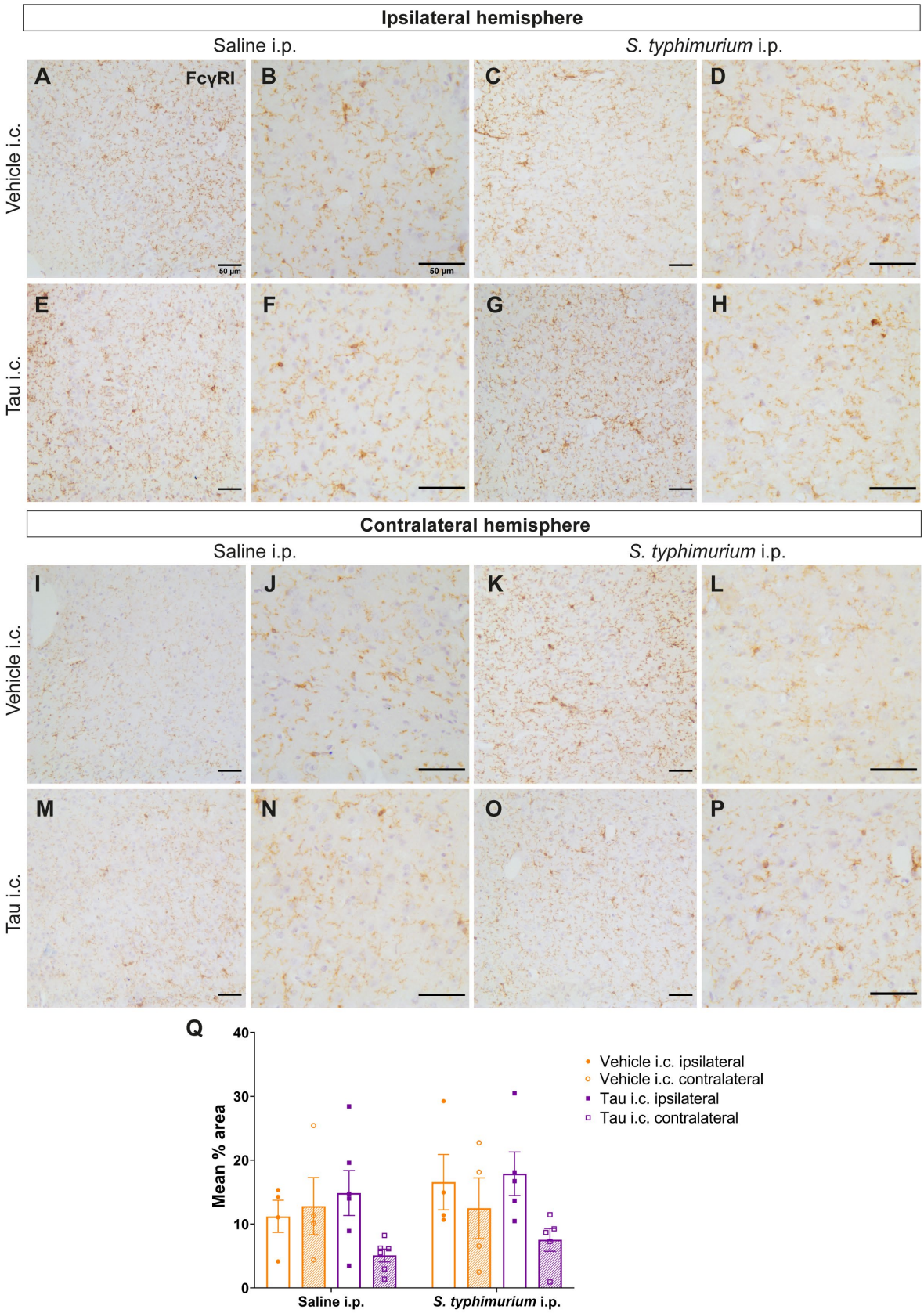
Ipsilateral hemisphere
Saline i.p.
S. typhimurium i.p.
Vehicle i.c.
Tau i.c.
A
FcγRI
B
C
D
E
F
G
H
50 µm
Contralateral hemisphere
Saline i.p.
S. typhimurium i.p.
Vehicle i.c.
Tau i.c.
I
J
K
L
M
N
O
P
Q
Mean % area
40
30
20
10
0
Saline i.p.
S. typhimurium i.p.
Vehicle i.c. ipsilateral
Vehicle i.c. contralateral
Tau i.c. ipsilateral
Tau i.c. contralateral

Figure 7-22: FcγRI expression following systemic infection in the perirhinal cortex of H1*Mapt-/-* mice

A, C, I, K) FcγRI expression in the perirhinal cortex following vehicle i.c. injection and either saline i.p. or *S. typhimurium* i.p. injection in the ipsilateral and contralateral hemisphere. **E, G, M, O**) Representative images of tau i.c. injection groups in the ipsilateral and contralateral hemispheres; 20x objective, scale bar= 50μm. **B, D, F, H, J, L, N, P**) Images at 40x objective for each respective group were included for greater observation of FcγRI-positive cell morphology; 40x objective, scale bar= 50μm. **Q**) Three-way ANOVA with Tukey's post-hoc test; n= 6 for tau i.c./saline i.p. n= 5 for tau i.c./*S. typhimurium* i.p., n= 4 for vehicle i.c. groups. All data is presented as mean ± SEM.

7.3.12 FcγRI expression in the mammillary nuclei of C57BL/6 and H1*Mapt-/-* mice

Finally, the mammillary nuclei were examined to determine the effect of tau pathology on FcγRI expression. In the C57BL/6 mice (**Figure 7-23**), there was a significant main effect of hemisphere ($F(1, 19)= 6.40$, $p<0.05$) and i.p. injection ($F(1, 19)= 6.51$, $p<0.05$). However, there was no significant main effect of i.c. injection ($F(1, 19)= 2.86$, $p= 0.11$). This is likely due to how similar FcγRI expression was between both systemic infection groups in the ipsilateral hemispheres (vehicle i.c./*S. typhimurium* i.p.= 5.21% ± 0.56; tau i.c./*S. typhimurium* i.p.= 6.98% ± 2.03, $p= 0.99$). This suggests that it is predominantly systemic infection which is affecting FcγRI expression in this region.

FcγRI expression in the mammillary nuclei of H1*Mapt-/-* mice appears highly consistent across all groups (**Figure 7-24**). There was no significant main effect of i.c. injection ($F(1, 15)= 2.95$, $p= 0.11$), i.p. injection ($F(1, 15)= 0.37$, $p= 0.55$) or hemisphere ($F(1, 15)= 3.52$, $p= 0.08$). FcγRI expression in the ipsilateral hemispheres of all groups was notably similar across all groups (vehicle i.c./saline i.p.= 4.94% ± 1.04; tau i.c./saline i.p.= 2.87% ± 0.67; vehicle i.c./*S. typhimurium* i.p.= 5.72% ± 2.26; tau i.c./*S. typhimurium* i.p.= 5.14% ± 1.13). This suggests that in this region there isn't even a FcγRI expression response to systemic infection in the H1*Mapt-/-* mice.

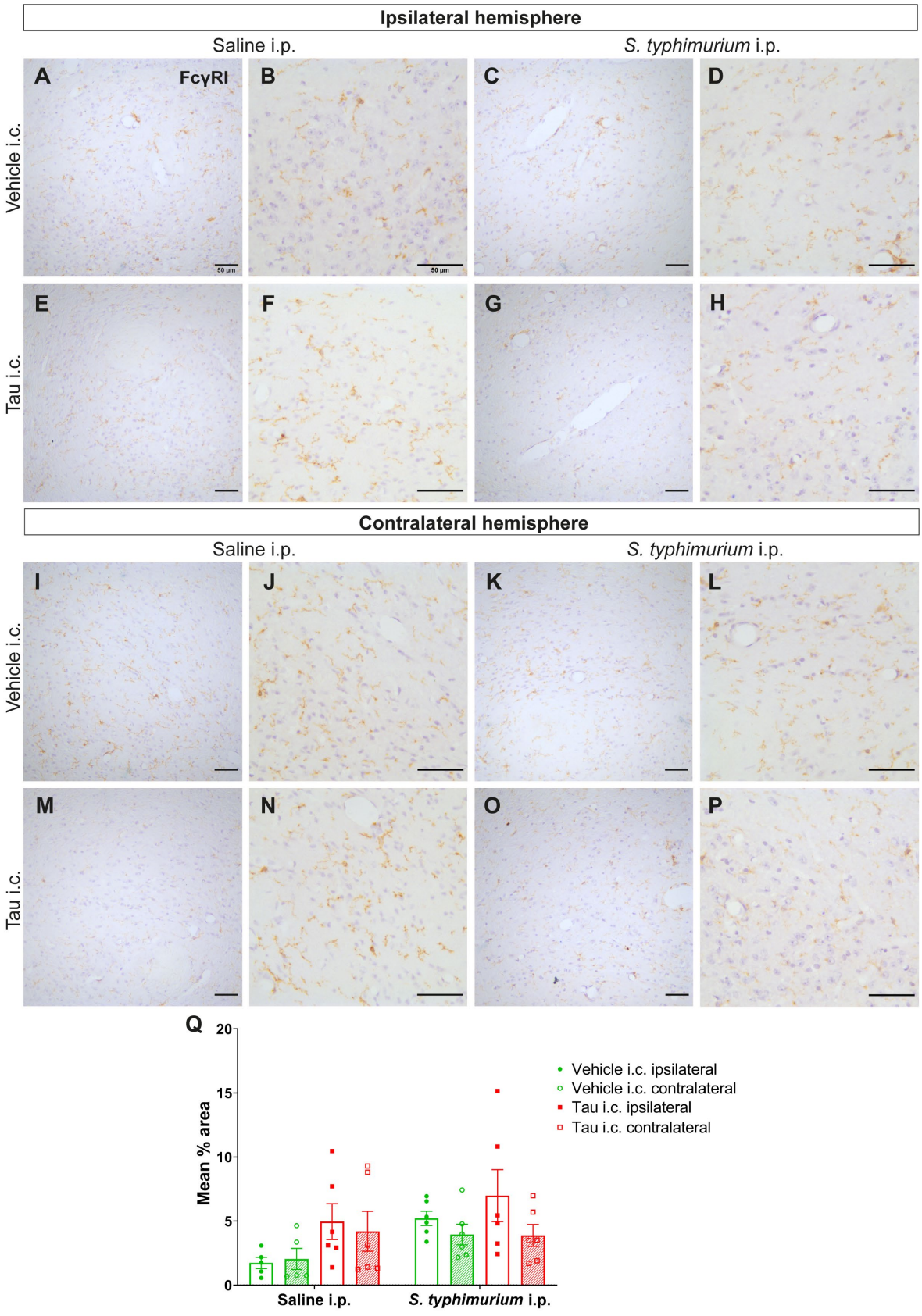
Ipsilateral hemisphere
Saline i.p.
S. typhimurium i.p.
A
FcγRI
B
C
D
Vehicle i.c.
50 µm
E
F
G
H
Tau i.c.
Contralateral hemisphere
Saline i.p.
S. typhimurium i.p.
I
J
K
L
Vehicle i.c.
M
N
O
P
Tau i.c.
Q
Mean % area
20
15
10
5
0
Saline i.p.
S. typhimurium i.p.
Vehicle i.c. ipsilateral
Vehicle i.c. contralateral
Tau i.c. ipsilateral
Tau i.c. contralateral

Figure 7-23: Mammillary nuclei FcγRI expression in C57BL/6 mice

A, C, I, K) FcγRI expression in the mammillary nuclei following vehicle i.c. injection in the ipsilateral and contralateral hemisphere. **E, G, M, O**) Representative images of tau i.c. injection groups in the ipsilateral and contralateral hemispheres; 20x objective, scale bar= 50µm. (**B, D, F, H, J, L, N, P**) Images at 40x objective for each respective group were included for greater observation of FcγRI-positive cell morphology; 40x objective, scale bar= 50µm. **Q**) Three-way ANOVA with Tukey's post-hoc test; n= 6 for both tau i.c. groups and vehicle i.c./*S. typhimurium* i.p., n= 5 for vehicle i.c./saline i.p. Data is log transformed for analysis. However, most values are <1 therefore the original mean % area is displayed. All data is presented as mean ± SEM. A batch effect was observed in one of the cohorts which received tau i.c. injection. As a result, this cohort had a separate threshold to all other tau i.c. and vehicle i.c. injection mice.

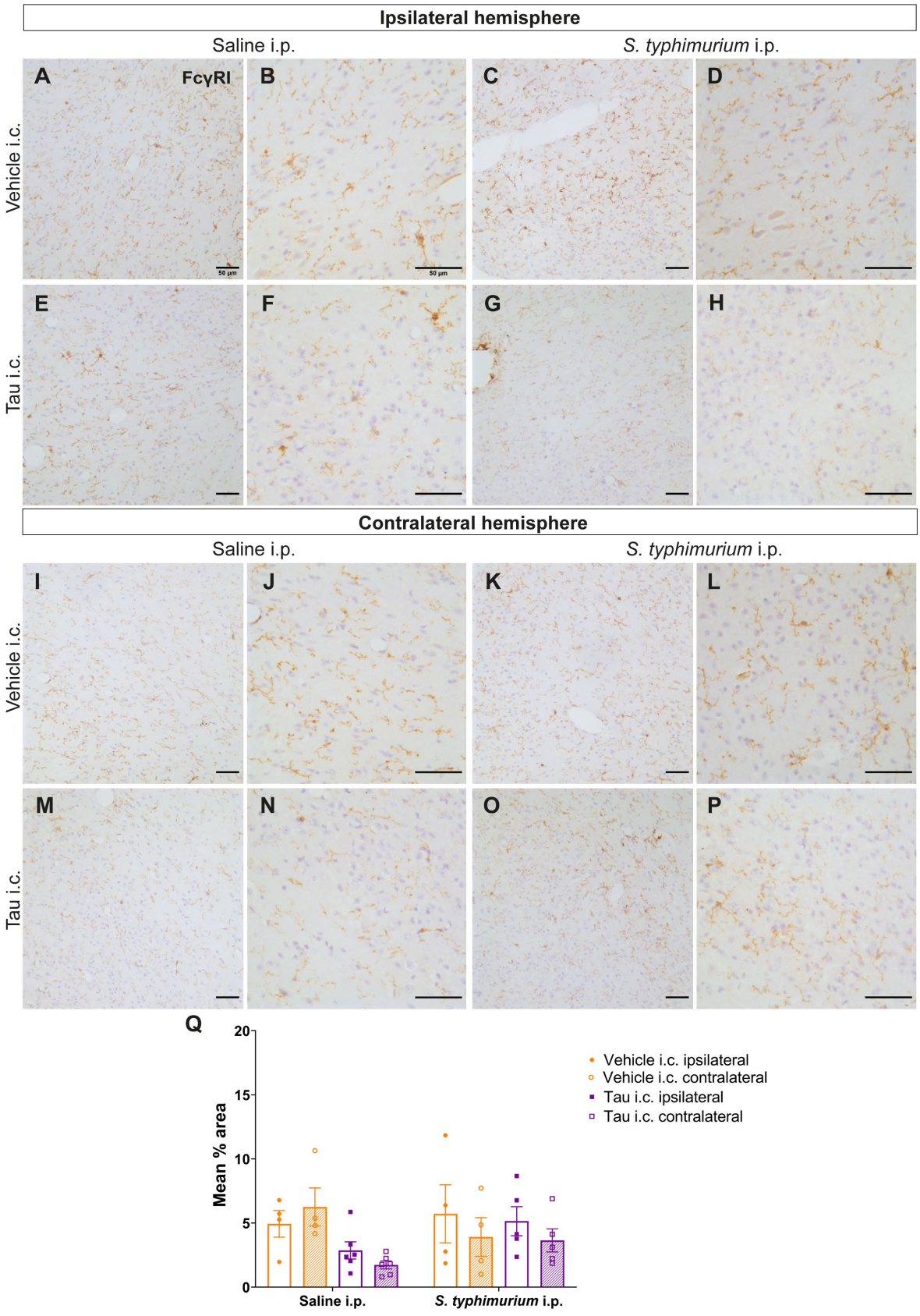
Ipsilateral hemisphere
Saline i.p.
S. typhimurium i.p.
A
FcγRI
B
C
D
Vehicle i.c.
E
F
G
H
Tau i.c.
50 µm
Contralateral hemisphere
Saline i.p.
S. typhimurium i.p.
I
J
K
L
Vehicle i.c.
M
N
O
P
Tau i.c.
Q
Mean % area
20
15
10
5
0
Saline i.p.
S. typhimurium i.p.
Vehicle i.c. ipsilateral
Vehicle i.c. contralateral
Tau i.c. ipsilateral
Tau i.c. contralateral

Figure 7-24: Mammillary nuclei FcγRI expression in H1*Mapt-/-* mice

A, C, I, K) FcγRI expression in the mammillary nuclei following vehicle i.c. injection and subsequent saline or *S. typhimurium* i.p. injection. **E, G, M, O**) Representative images of tau i.c. injection groups following either saline or *S. typhimurium* i.p. injection; 20x objective, scale bar= 50μm. (**B, D, F, H, J, L, N, P**) Images at 40x objective for each respective group were included for greater observation of FcγRI-positive cell morphology; 40x objective, scale bar= 50μm. **Q**) Three-way ANOVA with Tukey's post-hoc test; n= 6 for tau i.c./saline i.p. n= 5 for tau i.c./*S. typhimurium* i.p., n= 4 for both vehicle i.c. groups. All data is presented as mean ± SEM.

7.3.13 Cytokine levels in the brain and spleen following systemic infection

Four weeks post-*S. typhimurium* i.p. injection, cytokine protein levels in the brain and spleen were analysed to determine if there was still an effect of systemic infection. This was only examined in the C57BL/6 mice. In the hippocampus (**Figure 7-25**), cytokines IL-1β ($F(1, 12)= 6.54$, $p<0.05$), TNFα ($F(1, 12)= 14.04$, $p<0.01$), IL-6 ($F(1, 12)= 9.38$, $p<0.001$), Keratinocyte chemoattractant (KC)/human growth-regulated oncogene (GRO) ($F(1, 12)= 8.62$, $p<0.05$) and IL-2 ($F(1, 12)= 9.78$, $p<0.01$) all showed a significant main effect of i.p. injection. However, when examining the effect of hemisphere, only IL-1β ($F(1, 12)= 5.23$, $p<0.05$), IL-10 ($F(1, 12)= 6.55$, $p<0.05$), IL-4 ($F(1, 12)= 9.30$, $p<0.05$) and KC/GRO ($F(1, 12)= 5.17$, $p<0.05$) showed a significant main effect. No cytokine showed a significant main effect of i.c. injection in the brain.

Due to two readings below detection range in the vehicle i.c./*S. typhimurium* i.p. group, only a Student's t-test was carried out for IFNγ between the tau i.c. groups (n= 3 for tau i.c./saline i.p., n= 4 tau i.c./*S. typhimurium* i.p.). Tau i.c./*S. typhimurium* i.p. mice showed a seven-fold fold increase in IFNγ expression compared to mice which received a saline injection (tau i.c./saline i.p.= 0.008pg/mg ± 0.002; tau i.c./*S. typhimurium* i.p.= 0.07pg/mg ± 0.07) and this increase was significant ($t(5)= 3.78$, $p<0.05$). Statistical analysis was not carried out for IL-12p70 in either the brain or the spleen due to readings below detection range.

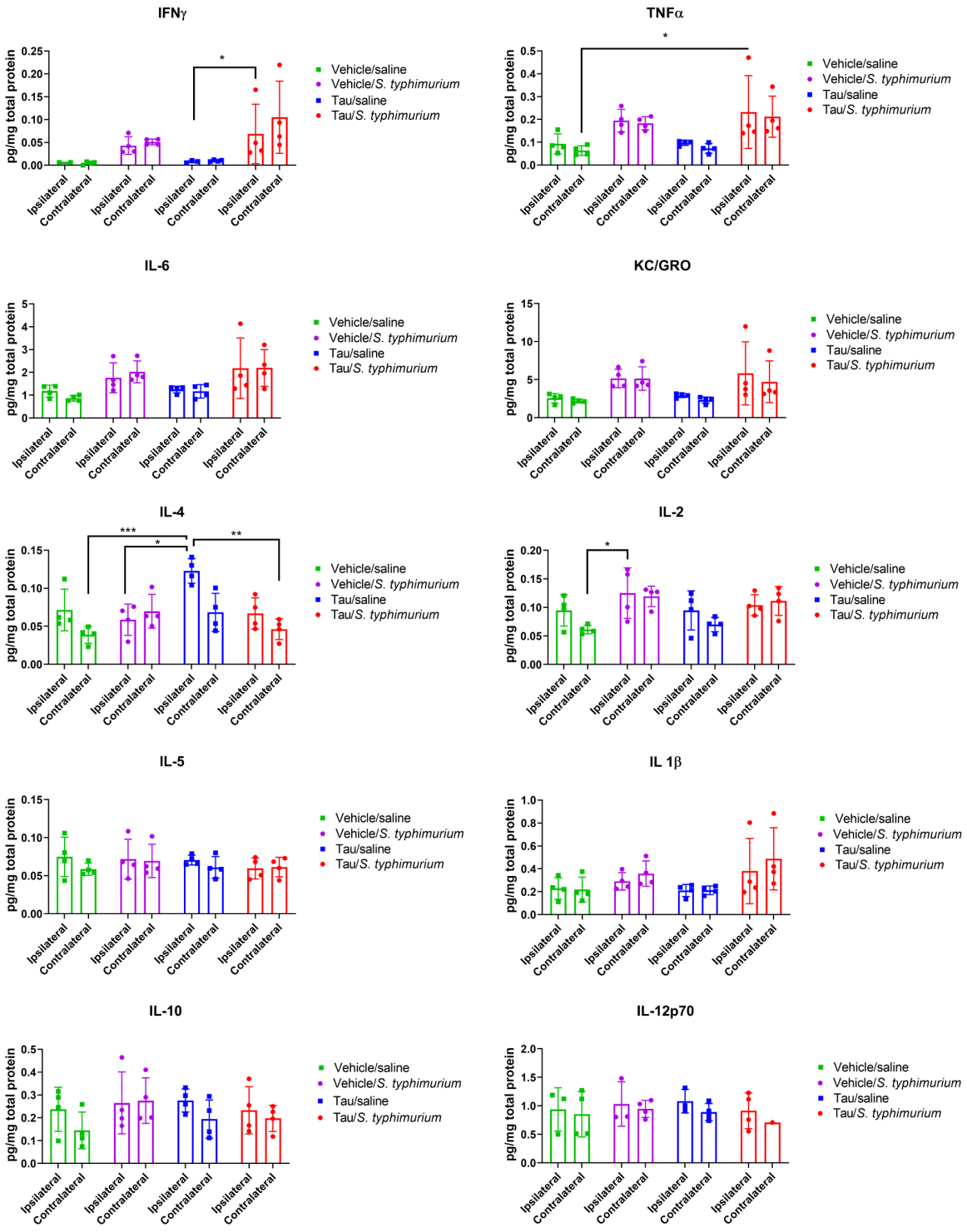

Figure 7-25: Mesoscale results for cytokine expression after systemic infection

Cytokine protein levels were examined in the C57BL/6 mice after vehicle or tau i.c. injection, then saline or *S. typhimurium* i.p. injection. Pg/ml values were normalised to protein concentration (mg/ml) using BCA assay values to reach pg/mg of total protein. n= 4 in all groups, except where noted in text due to detection level issues. Three-way ANOVA with Tukey's post-hoc test, an unpaired Student's t-test was carried out for IFNγ; *p<0.05, **p<0.01, ***p<0.001. All data is presented as mean ± SD.

By contrast in the spleen (**Figure 7-26**), a significant main effect of i.c. injection was observed in cytokines IFNγ ($F(1, 12)= 178.5$, $p<0.001$), TNFα ($F(1, 12)= 14.04$, $p<0.01$), IL-6 ($F(1, 12)= 69.57$, $p<0.001$), IL-1β ($F(1, 12)= 45.03$, $P<0.001$), IL-4 ($F(1, 12)= 14.87$, $p<0.01$), KC/GRO ($F(1, 12)= 28.86$, $p<0.001$) and IL-10 ($F(1, 12)= 50.30$). Again, IL-12p70 was not analysed due to detection threshold issues. In mice that received tau i.c. injection, there was a twenty-fold increase in IFNγ expression in the mice which underwent systemic infection (tau i.c./saline i.p.= 0.75pg/mg ± 0.18; tau i.c./*S. typhimurium* i.p.= 22.29pg/mg ± 2.29, $p<0.001$). Tau i.c./*S. typhimurium* i.p. mice also showed a two-fold increase in TNFα expression in the spleen compared to mice which received saline i.p. injection (tau i.c./saline i.p.= 16.39pg/mg ± 2.50; tau i.c./*S. typhimurium* i.p.= 43.25pg/mg ± 2.48, $p<0.001$). Finally, there was a four-fold increase in IL-1β after systemic infection in mice which received tau i.c. injection (tau i.c./saline i.p.= 170.02pg/mg ± 24.87; tau i.c./*S. typhimurium* i.p.= 811.18pg/mg ± 227.10, $p<0.001$). This confirms that even at four weeks-post injection, the cytokine response is still visible in the brain and spleen.

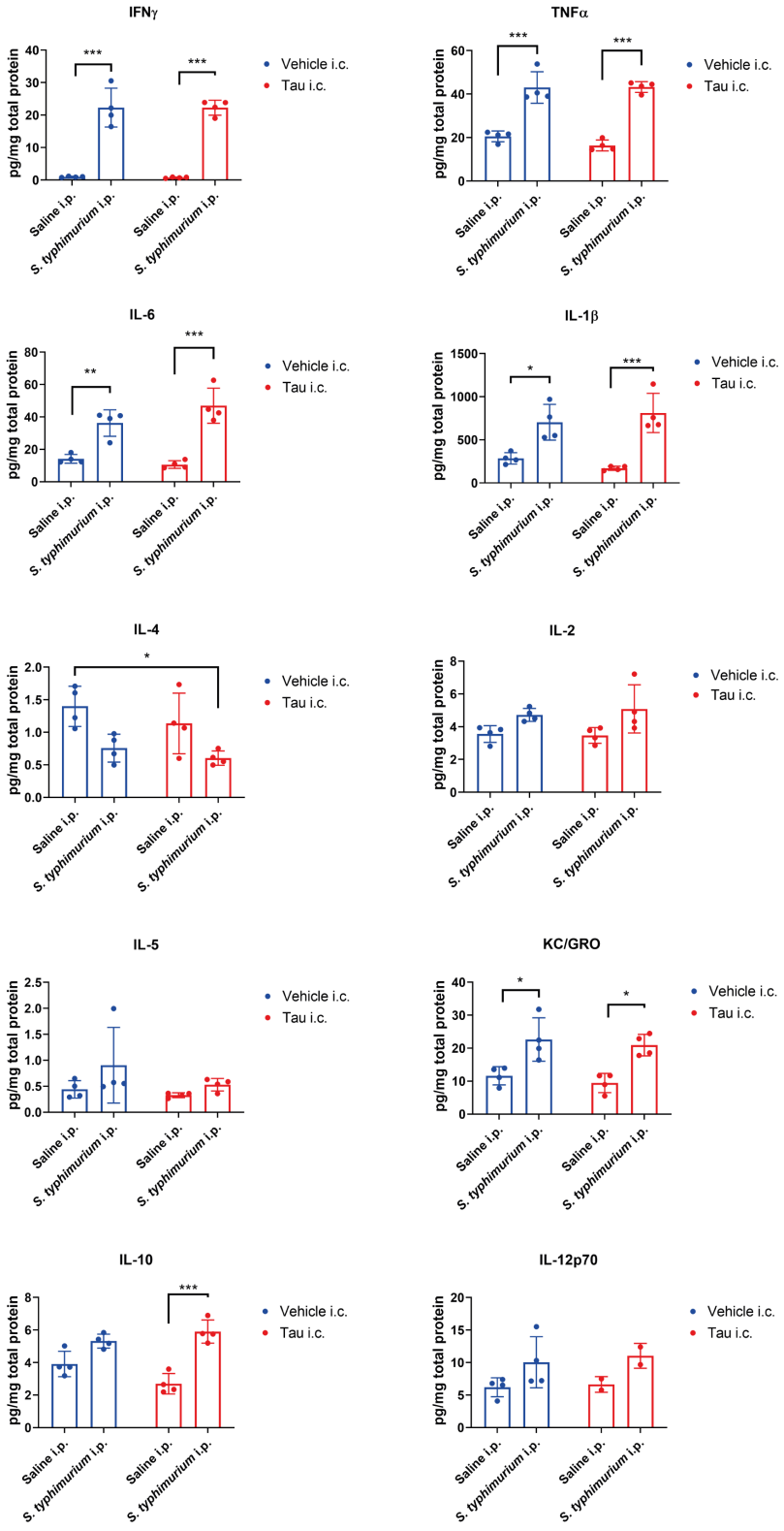

Figure 7-26: Spleen cytokine levels in C57BL/6 mice after systemic infection

Splenic cytokine levels were examined in the C57BL/6 mice after vehicle or tau i.c. injection, then saline or *S. typhimurium* i.p. injection. Mesoscale values (pg/ml) were normalised to protein concentration (mg/ml) using BCA assay values to reach pg/mg of total protein. n= 4 in all groups except for IL-2p70 noted in text. Two-way ANOVA with Sidak's post-hoc test; *p<0.05, **p<0.01, ***p<0.001. All data is presented as mean ± SD.

7.3.14 Microglia and AT8-positive tau at the hippocampus

In order to examine whether microglia were potentially responsible for the spread of tau observed through uptake, immunofluorescence was carried out with both a microglial (MHCII) and tau marker (bAT8). Due to time limitation, quantification could not be carried out utilising these images. One image from the dentate gyrus of a mouse which received a tau i.c. and *S. typhimurium* i.p. injection is included below (**Figure 7-27**). This image demonstrates that MHCII-positive microglia show overlap with the AT8 immunoreactivity. This image is taken along the dentate gyrus where pathology was observed in this group using DAB immunohistochemistry. However, further analysis would be required to conclude the role of microglial cells in the spreading of tau.

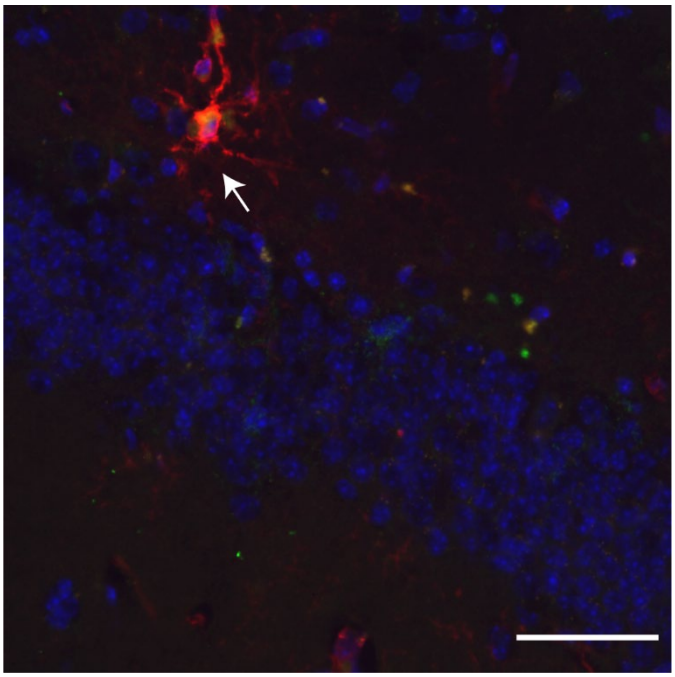

Figure 7-27: MHCII and bAT8 immunofluorescence at the dentate gyrus

Image taken of dentate gyrus stained for MHCII and bAT8. Brain tissue is from a single mouse in the tau i.c/*S. typhimurium* i.p. group. White arrow demarcates microglial cell of interest. Image taken with 40x objective, scale bar= 50µm.

7.4 Discussion

7.4.1 Tau pathology and systemic infection alter MHCII expression

MHCII as a marker of cellular activation plays a crucial initial role in the inflammatory response through antigen presentation to $CD4^+$ T- cells (Holling, Schooten and van Den Elsen, 2004). MHCII has been shown to be upregulated on vascular endothelium and microglia, following *S. typhimurium* i.p. injection in Chapter 3 and Chapter 4. Therefore, it was examined whether this effect caused by systemic infection would be exaggerated by the presence of tau pathology. There is no MHCII expression change in any saline i.p. group. Therefore, comparison of MHCII expression in this chapter was exclusively between vehicle i.c./*S. typhimurium* i.p. mice versus tau i.c./*S. typhimurium* i.p. mice. The increased MHCII expression in the tau i.c./*S. typhimurium* i.p. group is only observed in the injection site and the corpus callosum of the C57BL/6 mice. However, as regions posterior to the injection site are examined, any priming effect appears to be lost.

The first region examined was the cortical injection site. The primary reason to analyse this region is twofold; tau lysate was injected into both the cortex and the hippocampus, and secondly it was of interest to confirm whether *S. typhimurium* caused reactivation of microgliosis from the needle damage. Damage caused by the needle was minimal, with no gross structural changes to the corpus callosum or CA1 structure, classical markers of the needle being removed abruptly from the parenchyma. However, the insertion of the needle would cause an acute microglial response, it was the important to investigate whether a bacterial infection would induce reactivation of this microglia population.

As in all regions examined, in the cortex MHCII expression on vascular endothelial cells was only observed in mice which had received systemic infection, no mice which received saline i.p. injection expressed MHCII. The ipsilateral cortical MHCII expression in the tau i.c./*S. typhimurium* i.p. group is significantly upregulated at the injection site, with significant main effect of i.c. injection and main effect of hemisphere showing a clear trend (p= 0.08) (**Figure 7-1**). An overview of all main effects discussed in this chapter can be referred to in Figure 1-28. The tau i.c./*S. typhimurium* i.p. group showed significantly more MHCII expression in the ipsilateral hemisphere compared to the vehicle i.c./*S. typhimurium* i.p. group in post-hoc tests. Despite the lack of significant main effect of hemisphere, there was no post-hoc significance between the two groups which received systemic infection in the contralateral hemisphere.

Table A: Main effect of tau i.c. injection				
Region (Bregma AP coordinate)	MHCII (C57BL/6)	MHCII (H1*Mapt-/-*)	FcγRI (C57BL/6)	FcγRI (H1*Mapt-/-*)
Injection site (-2.50)				
Corpus callosum (-2.50)				
Hippocampus (-2.50)				
Ventral hippocampus (-3.00)				
Perirhinal cortex (-3.00)				
Mammillary nuclei (-3.00)				

Table B: Main effect of *S. typhimurium* injection		
Region (Bregma AP coordinate)	FcγRI (C57BL/6)	FcγRI (H1*Mapt-/-*)
Injection site (-2.50)		
Corpus callosum (-2.50)		
Hippocampus (-2.50)		
Ventral hippocampus (-3.00)		
Perirhinal cortex (-3.00)		
Mammillary nuclei (-3.00)		

Table C: Main effect of ipsilateral hemisphere				
Region (Bregma AP coordinate)	MHCII (C57BL/6)	MHCII (H1*Mapt-/-*)	FcγRI (C57BL/6)	FcγRI (H1*Mapt-/-*)
Injection site (-2.50)				
Corpus callosum (-2.50)				
Hippocampus (-2.50)				
Ventral hippocampus (-3.00)				
Perirhinal cortex (-3.00)				
Mammillary nuclei (-3.00)				

Figure 7-28: Overview of significant main effects described in this chapter

Table A shows significant main effect of i.c. injection for MHCII and FcγRI expression in C57BL/6 and H1*Mapt-/-* mice. **Table B** shows significant main effect of i.p. injection for FcγRI expression in C57BL/6 and H1*Mapt-/-* mice. Only groups which received *S. typhimurium* i.p. injection were compared for MHCII expression. **Table C** shows significant main effect of hemisphere for FcγRI expression in C57BL/6 and H1*Mapt-/-* mice.

MHCII-positive cell count was also carried out, as microglial-like staining was observed. As with mean percentage analysis, the tau i.c./*S. typhimurium* i.p. group showed significantly more MHCII-positive cells per mm^2 than the vehicle i.c./*S. typhimurium* i.p. group (**Figure 7-1**). This was again restricted to the ipsilateral hemisphere. There was a significant main effect of hemisphere yet no main effect of i.c. injection. Considering the mean percentage area and cell count analysis, it highlights that both vascular endothelial cells and microglial cells are likely to further upregulate MHCII expression when tau pathology is present. Only those mice which received systemic infection show MHCII expression, suggesting that the brain homogenate itself does not induce cell

activation at three months post-injection. The remaining question is whether the changes in MHCII expression is due to injection of brain lysate, or tau and this can only be fully answered by further experiments using normal brain or tau-depleted lysate.

H1*Mapt-/-* mice did show a significant main effect of i.c. injection for MHCII expression in the cortical injection site (**Figure 7-2**). Mice which received tau i.c. injection also showed significantly upregulated MHCII expression compared to the vehicle i.c. injection group. A Mann-Whitney U tests determined there was no significant difference in the MHCII-positive cell count between the vehicle i.c./*S. typhimurium* i.p. and tau i.c./*S. typhimurium* i.p. groups. The microglial cell count suggests that the MHCII expression changes are predominantly due to both vasculature and microglial expression in C57BL/6 mice, and only vascular in the H1*Mapt-/-* mice. The H1*Mapt-/-* mice do consistently show dampened MHCII expression when compared to quantification of MHCII expression in C57BL/6 mice. This suggests that whilst there is a similar relationship between the H1*Mapt-/-* experimental groups, the response to systemic infection is overall reduced.

The corpus callosum was analysed for MHCII expression, with a significant main effect of i.c. injection and hemisphere in C57BL/6 mice (**Figure 7-3**). A significant upregulation of MHCII expression in the ipsilateral hemisphere was observed in the tau i.c./*S. typhimurium* i.p. group compared to the vehicle i.c./*S. typhimurium* i.p. group. This effect was not observed in the contralateral hemispheres of these two groups. This result demonstrated that in C57BL/6 mice, the white matter is one region which shows high levels of tau pathology and associated high levels of MHCII expression. Notably, there is no MHCII expression in the tau i.c./saline i.p. mice suggesting that this degree of tau burden is insufficient to induce MHCII expression and vascular endothelial cell activation. The H1*Mapt-/-* mice do not show a significant difference in MHCII expression within the ipsilateral hemispheres of vehicle i.c./*S. typhimurium* i.p. and tau i.c./*S. typhimurium* i.p. groups (**Figure 7-4**). However, the normality assumption was not met and so the Mann Whitney test only provides a narrow understanding of the interactions between these groups. However, the MHCII expression in H1*Mapt-/-* mice is observably lower than observed in C57BL/6 mice. To what extent this is due to the reduced tau pathology in H1*Mapt-/-* mice, or a reduced systemic infection response is unclear.

In the C57BL/6 hippocampus, MHCII expression showed no significant effect of i.c. injection or hemisphere (**Figure 7-5**). Whilst there are a few mice within the tau i.c./*S. typhimurium* i.p. group which show upregulated MHCII expression, there are as many within this group that show expression akin to the vehicle i.c./*S. typhimurium* i.p. group. However, it must be noted that the mouse which shows the highest MHCII expression is also one of the few mice which exhibited tau

pathology within the hippocampus (**Figure 6-7**), the subject with the highest level of tau pathology in the hippocampus). This suggests that whilst there is biological variability, there is a consistent increase in MHCII expression when comparing the ipsilateral hemisphere of the tau i.c./*S. typhimurium* i.p. group to the vehicle i.c./*S. typhimurium* i.p. group. Furthermore, MHCII and bAT8 co-stains suggest that the MHCII-positive microglia may interact with the AT8-positive tau in the dentate gyrus (**Figure 7-27**). The H1*Mapt-/-* mice do not show any variation in MHCII expression within the hippocampus, which suggests that brain homogenate alone is insufficient to induce both vascular and microglial upregulation of MHCII expression (**Figure 7-6**). Further analysis which could separate the vascular endothelial cell and microglial contribution to MHCII expression would determine whether tau pathology is inducing vascular changes or microglia cells are primed.

7.4.2 MHCII expression posterior to the injection site

MHCII expression at the Bregma AP coordinate of -3.00 was examined in the hippocampus, perirhinal cortex and mammillary nuclei. Whilst there was a significant main effect of hemisphere in the ventral hippocampus of C57BL/6 mice, there was no main effect of i.c. injection (**Figure 7-7**). This was not translated into post-hoc significance in either the ipsilateral or contralateral hemisphere. Furthermore, there was no significant main effect of i.c. injection in either C57BL/6 or H1*Mapt-/-* mice in the hippocampus (C57BL/6: **Figure 7-7**) (H1*Mapt-/-*: **Figure 7-8**), perirhinal cortex (C57BL/6: **Figure 7-9**) (H1*Mapt-/-*: **Figure 7-10**) or the mammillary nuclei (C57BL6: **Figure 7-11**) (H1*Mapt-/-*: **Figure 7-12**). This is also true for observations regarding the MHCII-positive cell count. This suggests that the majority of changes in MHCII expression occur in the white matter and grey matter at the Bregma coordinate of the injection site. The cortical injection site and corpus callosum demonstrate a significant increase in MHCII-positive microglia in the ipsilateral hemisphere of the tau i.c. group compared to the vehicle i.c. group following systemic infection. This suggests that the microglial activation may be responsible for the significance in the mean percentage area analysis, not the vasculature. This is supported by the findings at the mammillary nuclei, where a lack of MHCII-positive microglia is noted and there is no significant effect of tau i.c. injection on overall MHCII mean percentage area.

One clear limitation is that the ventral hippocampus is potentially underpowered in regard to tissue slices. The mammillary nucleus is a small distinct region, slices were selected preferentially for the biotinylated AT8 antibody staining. Therefore, staining using MHCII and FcγRI antibodies was limited to two sections per brain. Furthermore, given the propensity of the mammillary nuclei to fold, there are several brains where only one section per marker was carried out. This likely accounts for the variability within groups, however it must also be considered that

three months post-injection is a very early time point. Perhaps if greater tau accumulation had occurred, MHCII expression in the ventral hippocampus would reflect this. Changes to MHCII expression caused by systemic infection are possible to observe in all regions both proximal and distal to the injection site. However, it will be important to determine in future studies whether activation of the vasculature, microglia or both is linked to tau pathology. MHCII-positive cell count in the ipsilateral hemisphere of tau i.c./*S. typhimurium* i.p. group is three-fold higher in the cortical injection site and hippocampus compared to the mammillary nuclei. This suggests either that tau pathology must be present for longer to induce any priming effect, or the brain homogenate induces this response.

Two of the main aims in this chapter were to establish whether tau pathology induces an inflammatory response, or if there is a priming effect of systemic infection. MHCII expression was not increased purely by the injection of tau lysate without systemic infection. However, following systemic infection a priming effect of tau was observed in the corpus callosum and cortex. However, this was only observed in the ipsilateral hemisphere and in regions of high AT8 immunoreactivity close to the injection site. Finally, MHCII expression is notably dampened in the H1*Mapt-/-* mice compared to C57BL/6 mice. This suggests that the absence of tau pathology appears to diminish any priming effect.

7.4.3 FcγRI expression appears to correlate with tau pathology at the injection site

FcγRI expression was examined in histology because of the role of the Fc receptor binding to IgG and as a marker of microglial activation (Diamond *et al.*, 2009). Given that FcγRI is expressed in the healthy brain, quantification of FcγRI expression examines the effect both of the i.c. and i.p. injection. In C57BL/6 mice which underwent systemic infection, the ipsilateral cortical injection site showed a clear trend of increased FcγRI expression in mice which received tau i.c. injection above what is observed for the vehicle i.c. groups (**Figure 7-13**). Due to the data not meeting normality assumptions only a Mann Whitney test could be carried out comparing the ipsilateral hemispheres. This showed a clear trend ($p= 0.052$) of tau i.c. injection altering FcγRI expression, compared to vehicle. Notably the tau i.c./saline i.p. group also showed an increased percentage area seven-fold higher than FcγRI expression in the vehicle i.c./saline i.p. group (**Figure 7-13**). However biological variability limits statistical analysis to comparison of the *S. typhimurium* i.p. groups. This data shows a clear microglial response to tau pathology in the cortex. Because this is where the needle injected the lysate, this cortical region will have been exposed to the highest levels of tau aggregate. However, whilst systemic infection induces upregulation of FcγRI in all injection groups, it appears that the injection of human tau lysate is also a defining factor regarding FcγRI upregulation in this specific region.

By contrast, H1*Mapt-/-* mice showed highly variable FcγRI expression in the cortical injection site (**Figure 7-14**). As a result, there was only a significant main effect of hemisphere. This analysis did suggest that activation of microglia had occurred at the injection site in the vehicle i.c. groups. However, this was not significant with no clear trend. The increased expression in the vehicle i.c. groups were clear outliers and so this would require further histology to refine the biological variability.

Following analysis of the cortex, the corpus callosum was examined in C57BL/6 mice (**Figure 7-15**). For FcγRI expression there was a significant main effect of i.c. injection in FcγRI within the corpus callosum. FcγRI expression was upregulated ten-fold in the tau i.c./saline i.p. group compared to vehicle i.c./saline i.p. group, whilst expression was upregulated eight-fold in the tau i.c./*S. typhimurium* i.p. group compared to the vehicle i.c./*S. typhimurium* i.p. group. FcγRI expression in the corpus callosum shows a clear effect of tau i.c. injection. In both tau i.c. groups, regardless of i.p. injection there was upregulation compared to the vehicle control and the corresponding contralateral hemisphere. The corpus callosum of the H1*Mapt-/-* mice also showed significant effects of tau i.c. injection, with a seven-fold increase in FcγRI expression in the tau i.c./*S. typhimurium* i.p. group compared to the vehicle i.c./*S. typhimurium* i.p. group (**Figure 7-16**). One notable difference between strains is that the tau i.c./saline i.p. group did not show the same upregulation of FcγRI expression in the H1*Mapt-/-* mice compared to C57BL/6 mice. In the corpus callosum the C57BL/6 mice show greater FcγRI expression than vehicle following both saline and *S. typhimurium* i.p. injection. This suggests that tau pathology alone induces this. This does not happen in the H1*Mapt-/-* mice, as the vehicle i.c./saline i.p. and tau i.c./saline i.p. are not significantly different. Therefore, it is likely not just brain lysate, but maybe FcγRI expression is dependent on a certain level of pathology.

FcγRI expression in the C57BL/6 hippocampus (**Figure 7-17**) had a significant main effect of i.p. injection and hemisphere. Whilst there was not a significant main effect of i.c. injection there was a significant interaction of hemisphere and i.c. injection. Both the tau i.c./saline i.p. and tau i.c./*S. typhimurium* i.p. groups demonstrated significantly higher (1.5-fold higher in both cases) FcγRI expression in the ipsilateral hemisphere compared to the contralateral. Whilst there was no post-hoc significance between the two tau i.c. groups, the above ANOVA results suggest that presence of tau pathology in the ROI is associated with greater FcγRI expression. FcγRI expression in the hippocampus of the H1*Mapt-/-* mice was again highly variable (**Figure 7-18**). Unfortunately, the normality assumption could not be met, therefore it is only possible to comment on the clear increased trend in FcγRI expression following systemic infection in mice which received tau i.c. injection compared to vehicle i.c. injection ($p = 0.06$). FcγRI expression at the injection site, corpus callosum and hippocampus of C57BL/6 mice showed a similar result to

MHCII expression, whereby priming occurred in the ipsilateral hemisphere of the tau i.c./*S. typhimurium* i.p. group. However, one distinct result is that FcγRI expression in the tau i.c./saline i.p. group is higher in the ipsilateral compared to the contralateral hemisphere and also compared to the ipsilateral hemisphere of the vehicle i.c./saline i.p. group. This is observed to some degree in the injection site (**Figure 7-13**), corpus callosum (**Figure 7-15**) and hippocampus (**Figure 7-17**). This finding is notably distinct to the MHCII expression results, where no saline i.p. group demonstrates MHCII expression. This result also points to the human tau lysate alone altering FcγRI expression.

7.4.4 FcγRI expression posterior to the injection site

Analysis of FcγRI expression at the ventral hippocampus was also carried out (Bregma AP -3.00) (**Figure 7-19**). Given the changes in FcγRI expression at the injection site, it was of interest to observe FcγRI expression in regions where tau had propagated. In C57BL/6 mice, FcγRI expression in the hippocampus showed a significant main effect of hemisphere and i.p. injection. FcγRI expression across groups which had received *S. typhimurium* i.p. injection showed similar levels of expression in the hippocampus regardless of i.c. injection or hemisphere. The tau i.c./*S. typhimurium* i.p. group had two-fold higher FcγRI expression compared to the tau i.c./saline i.p. group. Whilst these results showed a clear effect of *S. typhimurium*, there was no significant difference between the tau i.c. groups that received saline or *S. typhimurium* i.p. injection. In the perirhinal cortex, it was observed in mice that received tau lysate there was a two-fold increase in FcγRI expression after systemic infection compared to those which received saline i.p. injection (**Figure 7-21**). Given that this is an exploratory project, and the question raised here related specifically to the analysis within the ipsilateral hemisphere of these two groups, a Student's t-test was carried out and this showed a clear significant difference. Therefore, in the perirhinal cortex, FcγRI expression is significantly upregulated in tau i.c./*S. typhimurium* i.p. mice compared to tau i.c./saline i.p. mice. The mammillary nuclei demonstrated a significant main effect of i.p. injection yet no significant main effect of i.c. injection (**Figure 7-23**). It must be considered that the tau i.c./saline i.p. mice show minimal tau pathology in this region at three months post-i.c. injection. Therefore, it is unsurprising that within this region only the effect of systemic infection is observed.

In the H1*Mapt-/-* mice there was no significant main effect of systemic infection on FcγRI expression in the hippocampus (**Figure 7-20**), perirhinal cortex (**Figure 7-22**) or mammillary nuclei (**Figure 7-24**). However, there was a significant interaction of i.c. injection and hemisphere in the mammillary nuclei and perirhinal cortex. Again, these regions show high variability of FcγRI expression, and no real effect of tau pathology is observed. It must be considered that the

H1*Mapt-/-* mice do not show tau pathology within these regions. At the regions posterior to injection, FcγRI expression do not show a clear effect of tau pathology either in the C57BL/6 and H1*Mapt-/-* mice. It is possible that this is due to the degree of pathology present. Therefore, this suggests that FcγRI expression in the tau i.c./saline i.p. group is not upregulated preceding overt pathology development in regions of interest such as the mammillary nuclei. At three months post-injection, significant pathology is observed in the mammillary nuclei in the tau i.c./*S. typhimurium* i.p. group therefore it is surprising that there is no change in FcγRI expression similar to the observation in the perirhinal cortex. The significance in the C57BL/6 perirhinal cortex between the tau i.c. groups suggests that AT8-positive inclusions and systemic infection combined do alter FcγRI expression. A later time point, six months-post injection for example, may render different results and with greater pathology present elucidate whether FcγRI expression is altered by tau deposition.

The primary limitation for this study is the limited tissue available at the ventral hippocampus. Tissue from the final cohort was processed for tau histological analysis, however given time restrictions microglial markers were not stained for in this tissue. Given greater time tissue from this cohort would be stained for microglial markers so correlation between pathology and MHCII or FcγRI expression could be carried out on a larger sample size. Another limitation is the MHCII-positive cell count; whilst vascular endothelial cells were excluded from the count, it is not conclusive that all cells were microglia and not perivascular macrophages. Therefore, MHCII-positive cell counts in future would benefit from fluorescent co-stain with Iba1 a pan microglial marker. Further analysis could be carried out whereby vascular endothelial cell and macrophage expression of MHCII is separated. This would show the relative importance of the vasculature and resident immune cells in the interaction of tau propagation and systemic infection.

7.4.5 Cytokine production in the brain and spleen

Cytokine levels were detected at four weeks post-infection in the brain and the spleen. Only C57BL/6 mice were included given the low levels of pathology and dampened inflammatory response observed in the H1*Mapt-/-* mice. If time allowed, it would have been very interesting to compare the cytokine expression between genotypes and determine if cytokine levels in the H1*Mapt-/-* mice were also dampened. Cytokine levels in the C57BL/6 brain were still detectable by mesoscale (**Figure 7-25**). IL-1β, TNFα, KC/GRO and IL-2 showed a significant main effect of infection, with both vehicle i.c. and tau i.c. groups showing similar upregulation of pro-inflammatory cytokines after systemic infection. IFNγ showed a significant seven-fold increase in expression after systemic infection in the tau i.c. group compared to tau i.c./saline i.p. mice. IFNγ is essential for clearing *S. typhimurium* infection (Bao *et al.*, 2000), with both $CD4^+$ T cells and

natural killer cells responsible for the majority of the synthesis (Kupz *et al.*, 2013). IFNγ has been shown *in vitro* to induce MHCII expression of cerebral vascular endothelial cells (McCarron *et al.*, 1991). This proposes a potential mechanism behind the observations in this chapter where MHCII is clearly upregulated on vascular endothelial cells within the mouse brain. IL-4 is notable in that brain expression of this cytokine is significantly upregulated in the tau i.c./saline i.p. group. The response generated to *S. typhimurium* infection is predominantly carried out by Type 1 T helper cells (Th1), which confers release of IFNγ and TNFα (O'Donnell and McSorley, 2014) as opposed to Th2 which release IL-4 and IL-5 amongst others. This is clear to observe both in the brain and in the spleen. It has been suggested that IL-4 has a role in cognition *in vivo* and is potentially neuroprotective *in vitro* (Gadani *et al.*, 2013). Therefore, IL-4 may provide a future avenue of investigation. One limitation was that the pg/mg values in the brain were very low overall.

By contrast, in the spleen similar expression of cytokines such as IL-1β was observed in this chapter compared to three weeks post-systemic infection (Püntener *et al.*, 2012). IFNγ, TNFα, IL-6, IL-1β, IL-4, KC/GRO and IL-10 all showed a significant main effect of systemic infection, with no effect of i.c. injection (**Figure 7-26**). Therefore, it is clear to observe that even at four weeks post-infection, cytokine upregulation is still observable in the brain and spleen. This confirms the systemic infection induces a sustained immune response and also supports the findings concerning MHCII expression within the brain. These results highlight the vasculature as a key area of interest.

7.4.6 Conclusions

Examining how the presence of tau pathology alters the expression of microglial markers further demonstrates the separate effects of systemic infection and aggregated protein. There is upregulation of MHCII expression only following systemic infection in both vehicle i.c. and tau i.c. groups. However, MHCII expression in the white matter and injection site particularly is also upregulated by the injection of AD-tau lysate. These results overall demonstrate that there may be an exaggerated response to *S. typhimurium* infection when there is existing pathology. However, when examining regions removed from the injection site there is a loss of effect. Whilst there appears to be biological trends, it is possible this timepoint is too early to observe significant changes. FcγRI expression is upregulated in the injection site and corpus callosum in both tau i.c. groups, specifically within the ipsilateral hemisphere. This highlights that FcγRI expression is upregulated by the injection of AD-tau lysate and a priming effect is clearly observable after systemic infection. The perirhinal cortex is a key area of interest for future experiments, as it is one of the few distal regions where there is a significant increase in FcγRI expression in the tau i.c./*S. typhimurium* i.p. group compared to the tau i.c./saline i.p. group.

This chapter highlights key differences between MHCII and FcγRI expression. The advantage in comparing these two markers is that MHCII is not expressed in the brain without an inflammatory response. Therefore, it is possible to conclude that at this time point, the AD-tau lysate does not induce MHCII expression without systemic infection. However, the potential priming effect on MHCII expression observed in the tau i.c./*S. typhimurium* i.p. group and the upregulation of FcγRI expression in the tau i.c./saline i.p. group suggests the tau lysate does change the profile of brain macrophages. FcγRI expression results suggests that prior to systemic infection microglia within the brain are activated by the injection of tau lysate; so following systemic infection priming occurs both with MHCII and FcγRI expression. It is proposed that at six months post-injection, the increase in tau pathology may in turn cause further changes in these two microglial markers. Further study with greater accumulation of tau pathology and subsequent infection would help greater elucidate the exact relationship between tau pathology and microglial activation.

Chapter 8 Discussion

Although the mechanism of action behind development of AD is unknown, the pathological aggregation of tau has been proposed to correlate with cognitive decline. The spreading model of tau described in this thesis has been well-established in multiple studies of both non-transgenic mice and mice expressing human tau, such as the P301S mouse model of tauopathy (Ahmed *et al.*, 2014; Narasimhan *et al.*, 2017). These studies have shown that tau spreads through synaptically connected networks, rather than those brain regions which are proximal. Furthermore, lysate generated from human post-mortem tissue from different tauopathies has been shown to induce distinctive pathology in the mouse brain following intracerebral injection, suggestive of each specific tauopathy (Narasimhan *et al.*, 2017). This demonstrates the importance of protein conformation in determining how tau pathology propagates through the brain.

The spreading of tau appears to be partially mediated by microglial cells (Asai *et al.*, 2015; Luo *et al.*, 2015). These immune cells have previously been linked to clearance of Aβ (Cho *et al.*, 2014; Srikant Rangaraju *et al.*, 2018) and subsequently glial cell dysfunction in AD has long been hypothesised to play a role in disease progression (Hansen, Hanson and Sheng, 2018). Neuroinflammation and its interaction with pathology appears to correlate with the spreading of tau and also the rate of cognitive decline. The work collated in this thesis aimed to examine to what extent external factors such as systemic bacterial infection may influence disease progression by altering spreading of pathology.

8.1 Establishing the immune response to *S. typhimurium*

In order to accept or reject the main hypothesis of this thesis, that systemic infection alters the spatiotemporal spread of tau, it was crucial to establish an experimental model of a non-neurotrophic *S. typhimurium* infection. The multiple pathways which are activated by the infection of *S. typhimurium* provide a complex model, more akin to human infection. However, as a result this also induces biological variability, as observed in Chapter 3. In this chapter, the immune response to *S. typhimurium* was analysed in C57BL/6, P301S, H1*Mapt-/-* and *Mapt-/-* mice. The response varied, in part due to differences in background strain and also in the expression or lack thereof of the H1 transgene.

The effect of *S. typhimurium* i.p. injection on weight change, splenomegaly and MHCII expression within the brain was further confirmed in Chapter 4. Mice received saline or LPS i.c. injection followed by saline or *S. typhimurium* i.p. injection. This chapter exclusively used C57BL/6 mice, therefore only Chapter 3 deals with variability between genotypes. This chapter examined to what extent an initial acute inflammatory insult alters the response to systemic infection.

However, both Chapter 3 and Chapter 4 help to provide inside into the baseline immune response after *S. typhimurium* infection.

8.2 Peripheral changes in response to systemic infection

The initial readout for all mice after systemic infection was weight loss. This is to examine metabolic changes following bacterial infection. Throughout Chapter 3, C57BL/6 mice showed significant weight loss from 24 hours post-i.p. injection to approximately five days post-infection. This established a baseline as to what extent weight loss occurred after *S. typhimurium* infection and acted as a direct comparison to the P301S and H1*Mapt-/-* mice. P301S, H1*Mapt-/-* and *Mapt-/-* mice all show significant weight loss following *S. typhimurium* injection compared to the respective saline i.p. groups (**Figure 3-2**) (**Figure 3-8**). When comparing weight loss in P301S to C57BL/6 mice, there is a significant main effect of genotype; P301S mice appear to gain weight and return to baseline faster than the C57B/6 mice. By contrast, there was no significant main effect of genotype on the weight change observed in C57BL/6, H1*Mapt-/-* and *Mapt-/-* mice. Differences in baseline weight and the metabolic response suggest that the addition of the H1 haplotype may rescue the effect of the *Mapt* gene deletion. From examining weight change after systemic infection, genotypic differences are highlighted and so were considered when choosing the mouse utilised in the tau spreading model in Chapter 6.

In Chapter 4, the individual effect of LPS i.c. injection and *S. typhimurium* i.p. injection on weight loss was observed. No weight loss is observed after saline i.c. injection, therefore an intracerebral injection does not induce peripheral metabolic changes (**Figure 4-4**). Chapter 4 does not show a significant effect of LPS injection on weight following *S. typhimurium* infection. It must be noted that in Chapter 4, a post-hoc significance was not observed between the saline i.p. and *S. typhimurium* i.p. groups. It was discussed how this experiment was likely underpowered, yet it is possible to observe a biological effect of systemic infection on weight loss.

Following infection, the bacteria colonises the spleen and the erythroid population in the red pulp undergo significant expansion and invade the white pulp, with concurrent expansion of leukocyte and macrophage populations as part of the adaptive immune response (Jackson *et al.*, 2011; Rosche *et al.*, 2015). In Chapter 4, LPS i.c. injection had no effect on spleen size, highlighting the potential difference between routes of administration. In Chapter 3, where only an i.p. injection of *S. typhimurium* was administered, both the H1*Mapt-/-* and *Mapt-/-* mice showed significantly increased spleen size compared to the saline-treated controls. However, both H1*Mapt-/-* and *Mapt-/-* mice showed significantly smaller spleen size than the C57BL/6 mice after systemic infection (**Figure 3-9**). Alternative studies have reported spleen weight differences 7

days post-*S. typhimurium* infection between different genetic strains, however they did not observe this difference weeks after the infection (Kobets, Nesterenko and Balunets, 2013). Therefore, it appears the H1*Mapt-/-* and *Mapt-/-* mice are susceptible to *S. typhimurium*, yet they may undergo a less robust infection than in the C57BL/6 mice. Which biological mechanism explains these reduced effects is unclear. Histological staining or flow cytometry for macrophage (F4/80) or $CD4^+$ T-cell population changes in the spleen and analysis of peripheral cytokine levels, would potentially reveal whether there is specific dampening of pathways such as Th1 response to the salmonella infection.

Metabolic markers of an infection response such as weight loss and splenomegaly denote one main conclusion. That whilst immunological signs of an infection were observed in all mice, there is variance within genotypes in weight loss and splenomegaly observed after *S. typhimurium* infection. Considering that the aim of this thesis is to induce an immune response within the brain, further information is derived from examining markers of activation within the brain parenchyma.

8.3 Markers of cellular and microglial activation within the brain following systemic infection

To determine whether the difference in weight loss is reflected in a dampened immune response within the brain, MHCII expression was examined in the hippocampal fissure. MHCII is a marker of cellular activation expressed on classical and non-classical antigen presenting cells. Quantification of this marker within the brain helps to elucidate whether any immune cell response to the infection has occurred within the brain. Predominantly induced by IFNγ, MHCII can be expressed on cells that are not classical APCs, often in response to inflammation. The function of MHCII is to present antigens to T cells, however without co-stimulation this may in turn lead to tolerance. As a result, MHCII expression in the brain is indicative of cellular activation due to pro-inflammatory cytokine production (Holling, Schooten and van Den Elsen, 2004).

In Chapter 3, MHCII expression was first examined in the hippocampus of saline and *S. typhimurium*-injected C57BL/6 mice and P301S mice. Throughout this chapter C57BL/6 mice show MCHII-positive staining in the cerebral vasculature. Unlike C57BL/6 mice, there is no evidence of MHCII expression on APCs, classical or non-classical in P301S mice following *S. typhimurium* infection (**Figure 3-3**). MHCII was stained for at four weeks post-injection, at this point the average weight of P301S mice had recovered to baseline. This further confirmed that the P301S mouse model of tauopathy is capable of resolving *S. typhimurium* infection. Repeated LPS i.p. injections in a previous study did not induce MHCII expression on the cerebral vasculature of

C57BL/6 mice (Püntener *et al.*, 2012). This same paper reported MHCII expression on vascular endothelial cells in severe combined immunodeficient (SCID) mice following *S. typhimurium* (SL3261) infection; these mice have severely depleted B and T cell populations meaning MHCII expression in the brain is likely induced by macrophage production of IFNγ. Considering that there is no evidence of an immune response in the P301S brain, this suggests that the active production of IFNγ had ceased or was dampened enough that MHCII upregulation in the brain did not occur. Therefore, P301S mice are able to resolve this bacterial infection. The potential mechanism behind this was highlighted by the CBA background of the P301S mouse and its expression of Nramp1. Therefore, the background strain of the mouse model of tauopathy may play a significant role in inflammation commonly studied in the context of AD.

MHCII expression was also examined in the brains of H1*Mapt-/-* mice to observe whether a similar immune response to C57BL/6 mice occurred following *S. typhimurium* infection. Unlike in the P301S mouse, MHCII-positive staining was observed in the cerebral vasculature of the *S. typhimurium*-injected H1*Mapt-/-* mice (**Figure 3-10**). Immunofluorescence co-staining with laminin confirmed that staining is associated with the basement membrane. As discussed in Chapter 3, activation of MHCII is an indicator of peripheral infection and as a marker can be used to compare the strength of infection. MHCII expression in the brain explains differences in spleen size and associated inflammatory markers. Whilst in C57BL/6 mice, post-hoc significance for MHCII expression was observed when comparing the saline i.p. and *S. typhimurium* i.p. group, the H1*Mapt-/-* mice did not show post-hoc significance. Combined with the reduced splenomegaly, this again highlights how different genotypes appear to undergo a dampened immune response. It must be considered that whilst the H1*Mapt-/-* mice show a clear immune response in the brain and periphery, it is dampened compared to observations in C57BL/6 mice. These results support findings in Chapter 6 and 7 where tau spread is lowered in these mice.

In Chapter 4, *S. typhimurium* i.p. injection in C57BL/6 mice induced MHCII expression on vascular endothelial cells whereas LPS i.c. injection did not (**Figure 4-5**). Furthermore, a trend of dampened MHCII expression in the LPS i.c./*S. typhimurium* i.p. group was observed, suggestive of tolerance. Therefore, MHCII upregulation observed on non-classical APCs in this chapter is likely due to the initiation of the adaptive immune response.

Due to the likely involvement of macrophages in the immune response observed in the brain parenchyma, microglial markers of activation were examined. CD11b is included in part due to its upregulation in response to oxidative stress and binding to plasma protein fibrinogen (Petersen, Ryu and Akassoglou, 2018), all of which have linked CD11b to the immune response in AD. At four weeks post-injection in Chapter 3, CD11b expression shows a significant main effect of

infection, yet neither C57BL/6 or H1*Mapt-/-* mice have post-hoc significance between saline and *S. typhimurium* i.p. injection groups (**Figure 3-12**). In Chapter 4, CD11b was highlighted as a marker predominantly affected by LPS i.c. injection rather than systemic infection at one-week post-*S. typhimurium* injection (**Figure 4-7**). A previous study utilising *S. typhimurium* (strain SL3261 used in this thesis) showed expression of CD11b peaks at one-week post-infection (Püntener *et al.*, 2012). Therefore, CD11b as a marker of microglial activation was not included in Chapter 7 as *S. typhimurium* did not induce a clear upregulation at four weeks.

FcγRI binds IgG and works through ITAM signalling to induce downstream cytokine production and phagocytosis. IFNγ has been shown to induce upregulation of FcγRI expression on macrophages (Chenoweth *et al.*, 2015). This suggests that following systemic infection there may be greater infiltration of IgG and pro-inflammatory cytokines into the brain due to increased BBB permeability. This influx of plasma proteins and IFNγ may in turn drive increased levels of FcγRI.

At four weeks post-infection in Chapter 3, C57BL/6 mice showed a qualitative increase in FcγRI expression compared to P301S mice. When analysing FcγRI expression in the H1*Mapt-/-* mice, FcγRI expression was significantly increased in C57BL/6 mice infected with *S. typhimurium* compared to saline (**Figure 3-13**). The H1*Mapt-/-* mice do not show any post-hoc significance. Following systemic infection in Chapter 4, FcγRI expression within the brain is not significantly increased at one week in C57BL/6 mice. Furthermore, LPS induces no early primed response following a secondary insult in the form of systemic infection. Therefore, FcγRI is a clear marker of microglial activation at four weeks post-*S. typhimurium* infection.

The overarching aim in Chapter 3 was to establish whether P301S or H1*Mapt-/-* mice are susceptible to *S. typhimurium* infection. The P301S mouse is not a suitable model for examining the effect of systemic infection on tau spread, as the infection is quickly resolved and there is no observable effect on the immune cells within the brain at four weeks post-infection. This finding is novel in a mouse model of tauopathy as the majority of research into inflammation in these mice utilise LPS given its robustness as a bacterial infection mimetic.

As AD research increasingly focuses on humanised models, the limitations of the P301S mouse model become increasingly prominent. Primarily, AD has no known link to the P301S mutation which has long been reported in primary tauopathies such as FTD and FTDP-17 (Lossos *et al.*, 2003). The P301S mouse model limits study to a single isoform and does not form a complete picture of tau propagation in AD. Given the aforementioned importance assigned to tau conformation (Siddiqua and Margittai, 2010), employing tau derived from post-mortem AD tissue should provide greater recapitulation of the human disease.

An immune response in the periphery and the brain was observed in the H1*Mapt-/-* and C57BL/6 mice. Metabolic changes and splenomegaly were observed in the periphery whilst microglial activation and cellular activation occur in the brain. Whilst genotypic differences are observed, the H1*Mapt-/-* mice definitively show a robust response to the infection. Therefore, these results supported the use of the H1*Mapt-/-* mouse in the tau spreading model discussed in Chapter 6. However, the results in Chapter 6 and 7 highlight that the findings in Chapter 3 after *S. typhimurium* infection may illuminate the reasoning behind reduced tau burden in the H1*Mapt-/-* mice.

In Chapter 4, understanding the effects of an i.c. injection and subsequent inflammatory response is important for the tau propagation model addressed in Chapter 6 and Chapter 7. By confirming that a previous LPS injection has a minimal effect on a subsequent systemic infection, this suggests that the injection itself does not induce long-lasting changes to microglia. Injection of aggregated tau is not easily resolved unlike an LPS injection and therefore may induce a sustained effect on the microglial population. The continued presence of aggregated tau is proposed to induce sustained changes to the microglial population, leading to an increasingly pro-inflammatory profile.

8.4 Generation of AT8-positive seed prep

By establishing that the P301S mouse was unsuitable given its ability to resolve systemic infection, this changed the nature of the methodology. If a mouse model such as P301S or Tg4510 had been utilised, where a single isoform is expressed, then only P301S or Tg4510 brain homogenate containing the same isoform would have been injected into the brains of the respective transgenic mouse models. However, the H1*Mapt-/-* mouse model provided the scope to generate a model of tau propagation that was closer to the human disease and follow on from existing literature examining the spread of human post-mortem AD-tau (Guo *et al.*, 2016; Henderson *et al.*, 2020). By establishing that both H1*Mapt-/-* and C57BL/6 mice are suitable mouse strains for this project, it was then possible to generate the seed prep for stereotaxic injection.

Therefore, in Chapter 5 a lysate enriched for AT8-positive HMW tau was generated from AD post-mortem tissue. Through biochemical analysis it was established which of the 10 frontal cortex samples possessed the highest AT8/total tau ratio (**Figure 5-3**). Following this, a lysate enriched for HMW AT8-positive tau was generated using the three cases with the highest ratio (**Figure 5-6**). The AT8-positive Sarkosyl-insoluble fraction has previously been shown in the P301S mouse model to have the highest seeding capacity by stereotaxic injection of different sucrose

gradient fractions (Jackson *et al.*, 2016). This is why these phosphorylation epitopes were the focus of the AD 'seed prep'.

In Chapter 5, tau yield was prioritised over purity. However, analogous protocols published demonstrated a high percentage of tau through ELISA plates (He *et al.*, 2020). Given greater time it would be imperative to test the human tau lysate used in this thesis for presence of other proteins in the Sarkosyl fractions, such as Aβ or α-Synuclein protein. This is because the cases chosen to be processed for the final AD-tau lysate did also present with co-morbidities such as CAA. Two of the three chosen cases also reported the co-morbidities DLB and LBD as tertiary diagnosis. Therefore, it is possible that in enriching for Sarkosyl-insoluble tau, amyloid protein and aggregated α-Synuclein are also enriched within the same fraction. This is unlikely given the histology results in Chapter 6, however it is essential that this is considered within the scope of this thesis.

Referring to Chapter 4, an initial inflammatory response such as i.c. injection is not sufficient to alter the response to systemic infection. In Chapter 6, no AT8 immunoreactivity was observed in the vehicle i.c. groups; furthermore, expression of activation markers was lower after systemic infection compared to the tau i.c. group. One future direction is the inclusion of a control group injected with lysate immunodepleted for tau. Immunodepleted tau is often included as an internal control to determine the effect of injecting lysate derived from human post-mortem tissue (Guo *et al.*, 2016). However, this was not feasible given both the lysate yield and time available for this project. As discussed in Chapter 5, repetition of this experiment would require further post-mortem tissue to be obtained from SWDBB. Greater tissue could be obtained with the intention of half the lysate to be processed for immunodepletion of tau.

The intention of this thesis is to observe the effect of systemic infection on the spread of tau pathology. If the progression of tau closely mimics the spread observed in the human disease, then a mix of aggregated proteins is not necessarily a limitation. The tau i.c./saline i.p. injection group is a control within itself, as the addition of the systemic infection is the main variable observed within this study. It can be concluded that the lysate was enriched for AT8-positive tau and facilitated the progression of this exploratory study into the effects of systemic infection. Histology in Chapter 6 confirmed that no overt evidence of Aβ or α-Synuclein pathology could be detected in the mouse brain after three months post-i.c. injection. Thus, the model appears to be tau specific and allowed me to test the hypothesis that systemic infection modifies spreading of tau through the brain. The question remains why a systemic infection leads to accelerated spreading – is this mediated by microglia and if so through which downstream pathways?

8.5 Systemic infection increases the rate of spread of tau pathology

The hypothesis of this thesis was that systemic inflammation alters the spatiotemporal propagation of tau pathology. In Chapter 6, I show that stereotaxic injection of AD-tau lysate leads to AT8 immunoreactivity throughout regions of interest in both C57BL/6 and H1*Mapt-/-* mice; and that *S. typhimurium* infection promotes the spread of tau pathology and greater propagation to regions such as mammillary nuclei (**Figure 6-15**). As expected, mice receiving AD-tau i.c. injection followed by saline i.p., showed only small amounts of AT8 positive cells in the perirhinal cortex and mammillary nuclei at 3 months post i.c. injection. In contrast, mice exposed to tau lysate and systemic infection showed significantly higher tau burden in these brain regions, suggesting infection did not appear to change the route of spreading rather increased the rate of spread.

Pathology throughout the brain is low, as a result I also scored the images to generate the representative diagram in Chapter 6 (**Figure 6-25**). If greater pathology was present, a heat map based on percentage area would likely have been beneficial. However, the range of detection at three months post-injection was a limiting factor. The limbic circuit highlights affected regions within this study. Pathology observed in the C57BL/6 hippocampus, perirhinal cortex and mammillary nuclei point to the importance of synaptic connections in determining the spread of tau. Half of the mice exposed to both tau and systemic infection showed AT8 immunoreactivity in the hippocampus, whereas only 1 out of 6 tau i.c./saline i.p. mice showed AT8 immunoreactivity. These results suggest that the hippocampus does not show early deposition of tau pathology, yet systemic infection appears to have a biological effect (**Figure 6-7**). Quantifying AT8 expression in the perirhinal cortex showed a significant effect of systemic infection (**Figure 6-13**). Despite there being tau present regardless of i.p. injection, tau i.c./*S. typhimurium* i.p. mice show significantly greater tau burden than tau i.c./saline i.p. mice.

The results in the mammillary nuclei also showed a significant effect of systemic infection (**Figure 6-15**). AT8-positive tau is detected in 7 out of 8 mice which received tau i.c. and *S. typhimurium* i.p. injections, only half of the tau i.c./saline i.p. group show pathology in the mammillary nuclei and expression is significantly lower. This demonstrates that in mice exposed to infection, regions distal to the injection site develop tau pathology much earlier than mice exposed to human tau lysate only. Furthermore, regions distal to the injection site developed pathology to a higher degree than regions proximal highlighting the importance of synaptic connectivity in the limbic circuit.

The degree of pathology present at three months post-injection has been reported in multiple studies, all of which investigate the propagation of tau (Guo *et al.*, 2016; Narasimhan *et al.*, 2017; He *et al.*, 2020; Henderson *et al.*, 2020). These studies utilised C57BL/6 mice between 3-

5 months of age, akin to this thesis. My findings in the tau i.c./saline i.p. group correlate with what Henderson *et al.* (2020) report at three months post-injection in the mammillary nuclei. However, in all four studies, the hippocampus shows greater AT8 immunoreactivity than the tau i.c./saline i.p. mice in Chapter 6 at three months post-injection. In fact, AT8 immunoreactivity in the hippocampus observed in the tau i.c./*S. typhimurium* i.p. group is closer to observations in these studies. It must be noted that despite similar Bregma coordinates even the papers reported above show variability in tau burden. Narasimhan *et al.* (2017) shows a higher tau burden in the dentate gyrus at three months post-injection than reported in Henderson *et al.* (2020). This highlights how specific AD cases may result in variable tau burden.

In Guo *et al.* (2016), Henderson *et al.* (2020) and Narasimhan *et al.* (2017) negligible pathology is reported at one-month post-injection. This suggests that the subsequent two months are a crucial time point for accumulation of tau pathology. In Chapter 6, systemic infection is administered at two months post-injection. Therefore, it is theoretically possible that the immune response facilitates greater uptake of tau and so increased spreading to the mammillary nuclei. It must also be considered that housing of these mice may in turn affect these results. The outlier reported in Chapter 6 showed significant tau burden despite no *S. typhimurium* injection. An interesting experiment would be to observe whether the brains of specific pathogen free mice show less AT8 immunoreactivity after i.c. injection of AD-tau than observed in these papers and reported in Chapter 6. However, results in Chapter 6 point to a clear role of infection in the spreading of tau.

The most likely conclusion as to the difference in hippocampal pathology is drawn when comparing the Bregma coordinates. In Chapter 6, the Bregma coordinates used (AP= -2.50, ML= -2.00, DV= -1.80 and -0.80) differ in the dorsal-ventral (DV) axis to those reported in Henderson *et al.* (2020) and Guo *et al*. (2016) (AP= -2.50, ML= +2.00, DV= -2.40 and -1.40). The DV hippocampal and cortex injection coordinates of -2.40 and -1.40 respectively are significantly more ventral than the coordinates utilised in Chapter 6 (-1.80 and -0.80). The coordinates I used are based off published data from industrial collaborators (Ahmed *et al.*, 2014). However, the published ventral coordinates (DV= -2.40, -1.40) place the needle injection site at the hilus of the dentate gyrus, whereas the coordinates I used place the needle injection site at the hippocampal fissure. This may have resulted in greater pathology within the corpus callosum. In Guo *et al.* (2016) and Narasimhan *et al.* (2017) similar or lower white matter pathology is reported at three months post-injection compared to results reported in Chapter 6. Both tau i.c./saline i.p. and tau i.c./*S. typhimurium* i.p. mice show high levels of AT8 immunoreactivity in the white matter tracts at three months post-injection. The strong connection of the fornix to the mammillary nuclei would elucidate why the mammillary nuclei is an area of high tau deposition in this thesis.

It would be interesting to analyse tau pathology at later time points, for example six- or nine-months post-injection and explore whether regions such as the thalamus and entorhinal cortex presented with changes in tau pathology after systemic infection. The entorhinal cortex is not included in this analysis as no pathology was observed in this region. In similar studies examining tau pathology at three months post-injection of AD-tau lysate, the entorhinal cortex showed pathology, but at very low levels (Narasimhan *et al.*, 2017). If this experiment was continued and a six-month post-injection time point were to be examined, it is possible that overt entorhinal cortex pathology would be present. This is based both upon existing studies (Guo et al., 2016; Narasimhan et al., 2017) and literature referring to the importance of hippocampal connections to the entorhinal cortex (Brown, Eldridge and Banks, 2016). Henderson reported perirhinal pathology at six months post-injection of human AD-tau lysate in C57BL/6 wild type mice, along with significant entorhinal cortex pathology (Henderson *et al.*, 2020). If greater pathology is observed at six months post-injection this may lead to less variation between mice because there is a longer span of time for pathology to develop. The question arises whether in this future experiment, systemic infection would be induced at the original two months or novel five months post-injection. Chapter 6 establishes that *S. typhimurium* i.p. injection at two months post-i.c. injection does result in a significant effect. However, would that effect be lost at six months post-i.c. injection, or would it reveal greater differences due to an early departure in the rate of spread? The advantage of waiting to administer systemic infection at five months post-injection is that the immune response is still ongoing when tissue is collected. Therefore, it would also examine whether infections at a later stage of pathology still induce a significant increase in tau burden.

Whole brain images would enable greater analysis of separate brain regions. Regions where pathology was observed in a single mouse but not throughout a tau i.c. group are described in Chapter 6 (Figure 6-20). No overt pathology was consistently observed in any regions other than those described in Chapter 6. The figure adapted from Ahmed *et al.* (2014) shown in Chapter 1 is updated in **Figure 8-1** to show the regions where pathology was observed and quantified, and also future regions of interest such as the retrosplenial cortex.

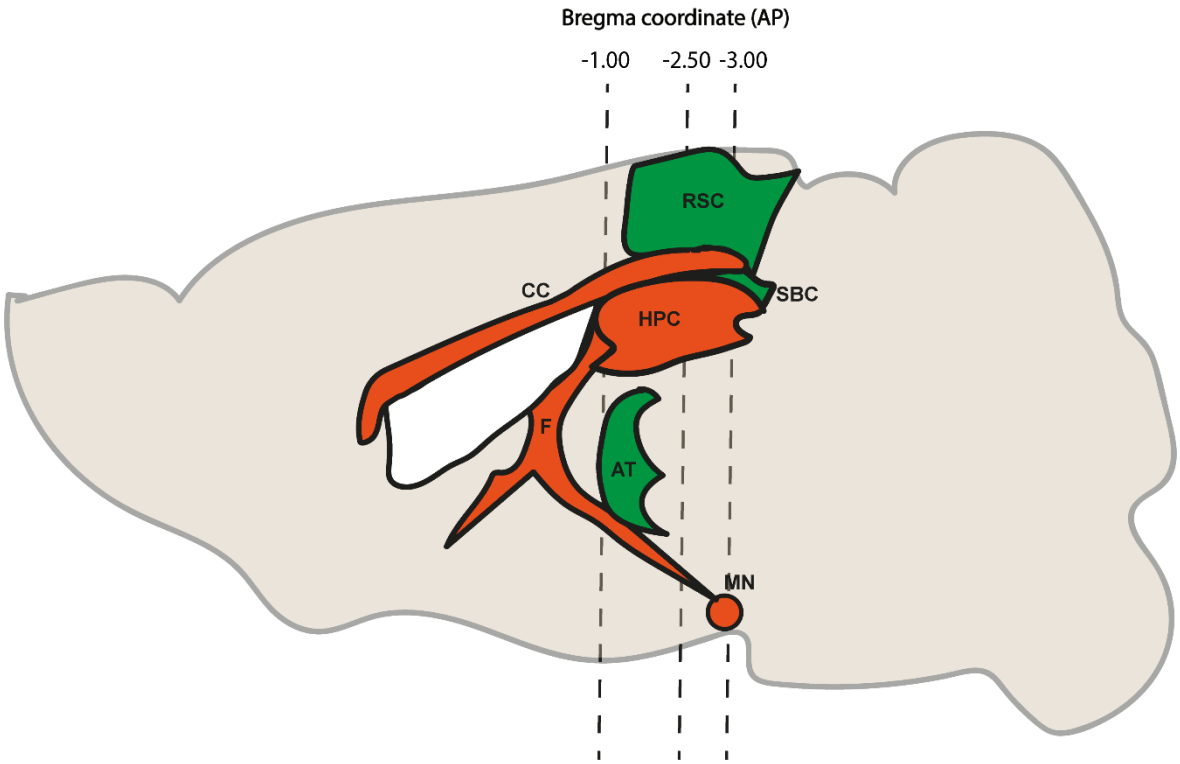

Figure 8-1: Evidence of tau propagation through limbic circuit

Following quantification of AT8 immunoreactivity, regions where pathology is observed are shown in red. These include the corpus callosum (CC), fornix (F), hippocampus (HPC) and mammillary nuclei (MN). Areas of interest in future studies are highlighted in green, including but not limited to the retrosplenial cortex (RSC), the subiculum (SBC) and anterior thalamus (AT). Anterior-posterior Bregma coordinates included. Figure adapted from Ahmed *et al.* (2014).

The primary conclusion of this thesis is that *S. typhimurium* infection drives propagation of tau to the same regions identified in previously published propagation studies. Whilst overall tau burden is low, *S. typhimurium* prompts greater AT8 immunoreactivity than observed in mice which received saline i.p. injection (**Figure 6-13**). These areas are synaptically connected to the hippocampus with major pathways regulating memory and learning. Future directions discussed below evaluate how changes to these pathways may be assessed in behavioural tests.

One key finding from Chapter 6 is the difference in AT8-immunoreactivity between C57BL/6 and H1*Mapt-/-* mice. After saline i.p. injection, both mice show similar AT8 immunoreactivity. By contrast, after systemic infection H1*Mapt-/-* mice consistently show lower levels of tau burden and no AT8 positive staining in the mammillary nuclei or perirhinal cortex and minimal pathology in the ventral hippocampus (**Figure 6-12**, **Figure 6-13**, **Figure 6-16**). The levels of endogenous tau protein in the H1*Mapt-/-* are lower than in C57BL/6 mice. However, it was expected that the AD-tau seed prep would propagate quicker in the H1*Mapt-/-* mice due to these mice expressing

all six isoforms of human tau. Chapter 3 and 7 demonstrate that microglial and vascular activation markers are significantly lower in H1*Mapt-/-* mice compared to C57BL/6 mice after systemic infection. Differences discussed in Chapter 3 were also observed in Chapter 6; following i.p. injection of *S. typhimurium* weight loss and splenomegaly was significantly dampened in H1*Mapt-/-* mice when comparing the tau i.c. groups (**Figure 6-3**) (**Figure 3-9**). Therefore, it is plausible this lack of increased tau burden observed in H1mapt-/- mice is due to reduced inflammatory response. Consistent findings throughout this thesis point to the inflammatory response playing a significant role in the degree of tau burden observed.

A key role of the peripheral immune system driving tau spread was further supported by the observations from a mouse excluded in Chapter 6, a C57BL/6 mouse which received tau i.c. injection followed by saline i.p. injection. This mouse showed strong AT8 immunoreactivity in the hippocampus and mammillary nuclei; an enlarged spleen and gradual weight loss following intraperitoneal injection of saline highlighted this mouse as an outlier within the saline i.p. injection group. Therefore, the inflammatory response in the periphery may in turn affect the spreading of tau through the induction of immune activation in the brain parenchyma.

8.6 Evidence of microglial priming in mice exposed to AD-tau

To explore if microglial activation contributes to tau burden, I quantified expression levels of the cellular activation markers MHCII and FcγRI. MHCII expression was not observed in any saline treated mice (as also reported in Chapters 3 and 4). Systemic infection caused upregulation of MHCII expression, particularly in the corpus callosum. Furthermore, compared to mice exposed to tau only, MHCII expression was six-fold higher in mice exposed to both tau and *S. typhimurium*, suggesting that the presence of tau pathology may 'prime' microglia (**Figure 7-3**). However, as distal regions were examined any potential priming effect was lost. These observations may suggest that it is the injection of brain homogenate not tau specifically which induces this change, however H1*Mapt-/-* mice do not show the same response in the corpus callosum (**Figure 7-4**). Reported studies where lysate from control brains were injected into the brain do not report tau pathology at six months post-injection (Guo *et al.*, 2016). Further study with injection of control brain or immunodepleted tau lysate would further help to confirm this finding in this study specifically.

MHCII-positive microglia were observed in the parenchyma following systemic infection, this was not observed in mice exposed to *S. typhimurium* described in Chapters 3 and 4. This was proposed to be partially due to changes in tissue preparation. Tissue in Chapter 3 and Chapter 4 was perfused with saline only, whereas tissue used in Chapter 7 was perfused and fixed with 4%

PFA. In the ipsilateral cortical injection site, mice within the tau i.c./*S. typhimurium* i.p. group had a three-fold increase in MHCII-positive cell count compared to the mice which received vehicle i.c./*S. typhimurium* i.p. injections (**Figure 7-1**). *S. typhimurium* induces expression of MHCII on microglia as well as the vasculature. However, H1*Mapt-/-* mice overall show lower percentage area for MHCII expression than C57BL/6 mice. In future experiments separating the mean percentage area analysis for the MHCII-positive vasculature and microglia would elucidate which cell type is predominantly responsible for upregulation of MHCII expression. Deciphering the molecular and cellular pathways responsible for microglial priming observed would refine future avenues of research.

FcγRI expression was quantified in Chapter 7 given the effect of systemic infection on expression observed in Chapter 3. Only C57BL/6 mice showed significant upregulation of FcγRI expression in Chapter 3 at four weeks post-*S. typhimurium* infection, the H1*Mapt-/-* mice did not show significant activation of this microglial marker after systemic infection. In Chapter 7, C57BL/6 and H1*Mapt-/-* mice show a similar degree of FcγRI expression at the hippocampus, injection site and cortex after *S. typhimurium* infection (**Figure 7-13**, **Figure 7-17**). The corpus callosum in C57BL/6 and H1*Mapt-/-* mice show a trend and significantly upregulated FcγRI expression respectively in the tau i.c./*S. typhimurium* i.p. group compared to the vehicle i.c./*S. typhimurium* i.p. group (**Figure 7-15**). The ipsilateral FcγRI expression in the corpus callosum of both the C57BL/6 and H1*Mapt-/-* tau i.c./*S. typhimurium* i.p. group is significantly upregulated compared to the contralateral hemisphere. Furthermore, when examining FcγRI expression in the hippocampus of C57BL/6 mice, the both tau i.c. groups show significantly increased expression levels in the ipsilateral versus contralateral hemisphere. This highlights the white matter tract as a potential region of interest to examine microglial activation in response to AT8-positive tau. These results also suggest that FcγRI expression is upregulated and sustained by the injection of AD-tau lysate.

When examining FcγRI expression posterior to the injection site, a loss of significant effect is observed. *S. typhimurium* infection did not alter expression levels of FcγRI in the ventral hippocampus and mammillary nuclei of C57BL/6 or H1*Mapt-/-* mice (**Figure 7-20**, **Figure 7-23**). In the perirhinal cortex, C57BL/6 mice showed significantly upregulated FcγRI expression in the ipsilateral hemisphere of the tau i.c./*S. typhimurium* i.p. group versus the tau i.c./saline i.p. group (**Figure 7-21**). There is also significantly more tau pathology reported in the perirhinal cortex in the tau i.c./*S. typhimurium* i.p. group compared to the tau i.c./saline i.p. group in this region. This strongly suggests that greater propagation of tau induced by systemic infection also leads to greater FcγRI expression. The presence of tau pathology in the brain may induce microglial activation and prime these immune cells. IgG expression was observed in the brain at one-month

post-i.c. injection of AD-tau (Appendix A, Figure S4). Future experiments with a co-stain of FcγRI, IgG and laminin would highlight whether FcγRI expression is localised around blood vessels. This would help determine whether changes in BBB permeability changes lead to upregulation of FcγRI expression. This is likely a combined effect of the AT8-tau deposition and the systemic infection where both insults lead to an increasingly pro-inflammatory microglial population.

These results overall suggest that MHCII upregulation occurs on microglia and vascular cells, particularly after systemic infection. Microglia in mice exposed to tau and *S. typhimurium* show increased levels of MHCII, possibly due to a priming effect of the tau-containing brain lysate. By contrast, FcγRI expression showed significant upregulation following injection of only tau lysate. Significant upregulation of FcγRI expression was also detected in regions distant from the injection site, but only in mice exposed to both tau and systemic infection. This suggests that microglia are activated in response to the injection of AD-tau lysate and these cells show exaggerated upregulation of activation markers following systemic infection. To what extent this finding facilitates tau propagation is still unclear. MHCII is observably lower in the H1*Mapt-/-* mice in these regions (**Figure 7-6**). Therefore, this suggests that the H1*Mapt-/-* mice are undergoing a dampened immune response and this in turn leads to reduced propagation of tau.

Tau propagation to regions such as the mammillary nuclei in C57BL/6 mice poses questions regarding the mechanism of spread. When comparing the AT8, MHCII and FcγRI staining in the corpus callosum it appears as though microglia may be responsible for transporting tau pathology to the mammillary nuclei. The AT8-positive staining is more dot-like in the white matter tract than the inclusion staining in the SuMN. This suggests that the tau in the white matter tract is either synaptic or found in glial cells. Tau has been reported in the white matter tract of post-mortem AD tissue. Devos *et al.* (2018) extracted the frontal white matter tracts from human Braak stage V/VI post-mortem tissue and significant propagation of tau was observed (De Vos *et al.*, 2018). The authors also reported that tau was upregulated in the synaptosome compared to the cytosol. This supports the long-held hypothesis that in AD there is progression of tau pathology along synaptic pathways, however uptake by microglia may be the primary method of spread in this *in vivo* study.

Whilst the synaptic connections between these regions is discussed in Chapter 6, the results from Chapter 7 provide an indication as to a potential mechanism. A small experiment was carried out to examine bAT8 and MHCII staining at Bregma AP= -2.50. It is possible to observe in **Figure 7-27**, that in a mouse which has received tau i.c./*S. typhimurium* i.p. injections there is distinct overlap of AT8-positive staining and MHCII-positive microglia. This is captured at the dentate gyrus where tau pathology has been shown in this group with DAB

immunohistochemistry. The AT8 staining is clearly focused within the soma, although a small AT8-positive signal is observed in the microglial processes. Analysis of this data set would determine if there is microglial uptake of tau and facilitation of spread, however greater time would be required to carry out analysis of the full cohort.

In Chapter 7, cytokine expression in the brain and spleen of C57BL/6 mice after systemic infection was examined (**Figure 7-25**, **Figure 7-26**). Given the low levels of pathology, this study was not carried out on the H1*Mapt-/-* mice, however given more time it would be interesting to observe the differences in cytokine levels between the C57BL/6 and H1*Mapt-/-* mice. IFNγ, IL-1β and TNFα levels confirmed that systemic infection affects immune pathways in both the brain and spleen, even after four weeks post-injection. Furthermore, the detection of IFNγ supported the findings of MHCII on the cerebral vasculature as discussed in Chapter 7. Interestingly, no effect of tau i.c. injection was observed on cytokine expression, suggesting microglial and cerebral vasculature activation may play a prominent role in tau spread. Furthermore, that the injection of human lysate did not induce a pro-inflammatory response in the brain at four weeks post-injection. IL-4 was significantly increased in the brain in tau i.c./saline i.p. mice, but levels were not increased after infection. Stereotaxic injections of IL-4 in the 3xTgAD mouse showed improved novel object recognition and significantly decreased pThr205 (AT8) and PHF-1 (Dionisio-Santos *et al.*, 2020). These results highlight a potential detrimental role of Th1 cytokines in the progression of tau spread but requires further study.

When comparing the findings of Chapter 6 and Chapter 7, several questions arise. Does systemic infection induce changes in the microglial population which then uptake tau at an increased rate? Or does systemic infection induce changes in the conformation or hyperphosphorylation of tau both native and injected, which in turn caused greater propagation and subsequent microglial activation? Both MHCII and FcγRI show a clear effect of microglial activation in response to systemic infection and FcγRI expression increase shows association with tau pathology; an overview of these findings is described in **Figure 8-2**. However, there is no significant effect of i.c. injection on FcγRI expression observed at the mammillary nuclei, the area of highest AT8-positive tau burden. This suggests that whilst microglia may facilitate the spread of tau, activation of microglia does not precede the deposition of tau.

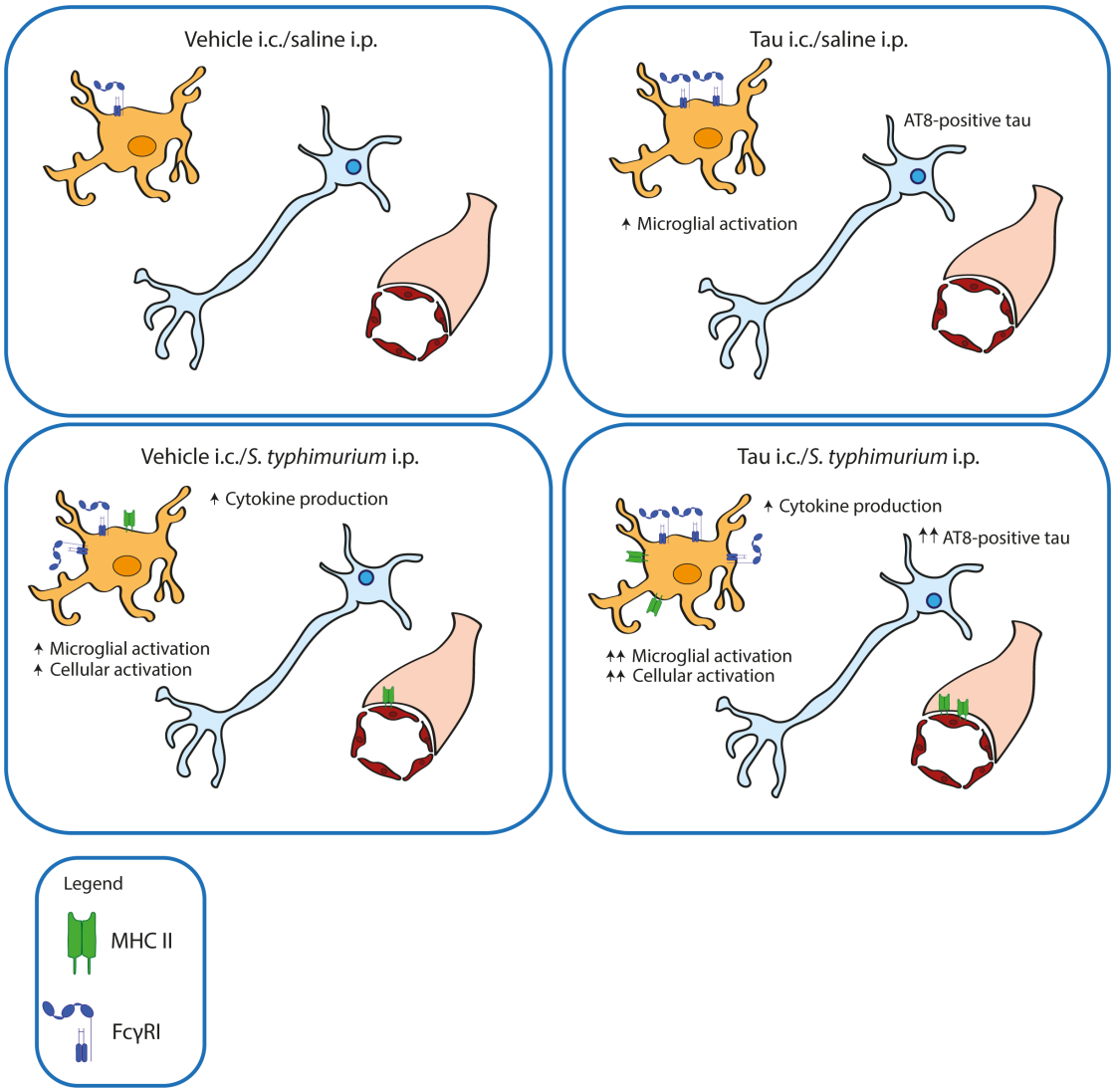

Figure 8-2: Overview of findings in Chapter 6 and Chapter 7 at the corpus callosum

These two results chapters show a clear effect of systemic infection on the spreading of tau. Systemic infection was also related to an increase of cytokine production, regardless of i.c. injection. MHCII was only expressed in the mice which received *S. typhimurium* i.p. injection and showed a main effect of i.c. injection in the corpus callosum and cortex. FcγRI also showed a main effect of infection and tau i.c. injection in the corpus callosum. However, FcγRI expression was also significantly upregulated in tau i.c./saline i.p. mice compared to vehicle i.c./saline i.p. mice.

8.7 Future directions

Whilst this thesis has addressed the main objective regarding whether systemic infection would cause increased propagation of tau pathology, many questions regarding the exact mechanism are left unsolved. One key limitation of this thesis is the low levels of AT8-positive tau detected within the brain at 3 months post-injection. Longer incubation of the tau pathology would potentially provide stronger association with the effects of systemic infection. Histology at six months or nine months post-injection would likely show greater AT8-positive tau inclusions

within the brain. *S. typhimurium* injection could be administered at three months post-injection and then three months later the tissue could be collected for analysis. This would show whether there are long-term effects of systemic infection and whether this would lead to greater differences in pathology between tau i.c./saline i.p. and tau i.c./*S. typhimurium* i.p. groups. This would also provide the opportunity to examine multiple timepoints and demonstrate the progressive change caused by systemic infection.

Based on existing publications, greater time for the propagation of tau should allow for inclusions to form in the hippocampus and the cortex (Henderson *et al.*, 2020). Examining whether pro-inflammatory cytokine expression such as IL-1β change with the increasing build of tau pathology would help to detect potential pathways responsible for priming. LTP has been shown to be reduced by the presence of tau both *in vivo* and *in vitro* (Balschun and Rowan, 2018; Acquarone *et al.*, 2019), therefore electrophysiology throughout this longer experiment would help to identify whether synaptic plasticity changes as a result of AT8-positive tau accumulation. By combining these two readouts it would provide a wealth of data regarding functional changes in the brain, particularly when combined with behavioural tests. However, it must be considered that synapse or neuronal loss is often not reported in these models (Guo *et al.*, 2016), and with only a unilateral injection the contralateral hippocampus may adequately compensate in behavioural tasks to mask any synaptic changes. Most studies exclusively examine the effects of pathology and so a second insult may result in synaptic changes and subsequent behavioural deficits.

There is definite biological variability in Chapter 6 observed in AT8 immunoreactivity in groups which received tau i.c. injection. However, a power calculation based on the AT8 analysis in the hippocampus suggests that the group sizes included in Chapter 6 are adequately powered ($n= 6$, $\alpha= 0.05$, Power= 90%). Results such as AT8 quantification in the hippocampus is indicative of histology at three months post-injection, whereby there is minimal pathology. Therefore, at six- or nine-months post-injection, it is likely that a larger proportion of the tau i.c./*S. typhimurium* i.p. group will present with AT8 immunoreactivity. In my current analysis, brains can be categorised by their absence or presence of pathology rather than degree of tau burden. Furthermore, given that statistical significance is observed, increasing group sizes may not be deemed appropriate within the scope of the 3R's (Prescott and Lidster, 2017). However, mimicking cognitive decline in the AD patient *in vivo* is a translational readout, behavioural experiments often require a large group size to detect potential subtle changes in memory. If it is possible to determine effects on cognition, a robust behavioural test such as the MWM must be utilised, which tests the ability to learn and memorise spatial information (Vorhees and Williams, 2006).

Behavioural tests are unfortunately limited due to working within the CL2 facility. The behavioural tests that would provide the greatest information regarding pathology within the confines of the CL2 facility are the object location and recognition tests (Vogel-Ciernia, 2015). Lesioning the perirhinal cortex and hippocampus leads to significant deficits in both these tests in rats (Barker and Warburton, 2011) and mice (Cinalli *et al.*, 2020). Given that these two regions show pathology deposition in Chapter 6 and have been implicated in other tau propagation studies (Henderson *et al.*, 2020), it would be interesting to observe the effect of systemic infection when greater pathology has developed within the mouse brain. The radial arm maze is also a test of spatial memory feasible within the confines of the CL2 facility. This test is hippocampal-dependent and would assess the key regions of interest and the capacity of each group to retain spatial information (Mohseni, Behnam and Rafaiee, 2020).

In this longer experiment, the use of antibodies such as HT7 and MC1 (Guo *et al.*, 2016) would provide further information regarding the tau aggregates present within the brain. HT7, as discussed in Chapter 6 is an antibody which detects human tau but has no reactivity with murine tau, unlike AT8 which has immunoreactivity both with human and mouse tau. Testing both AT8 and HT7 on brain slices which are only 10 microns apart would determine whether the results in Chapter 6 simply show spreading of the human tau through neurons or seeding of the native murine tau. Comparing these two antibodies both at the injection site and the mammillary nuclei would allow greater understanding of the results observed in Chapter 6. For example, does systemic infection induce greater propagation of the aggregated human tau or greater recruitment of the unfolded mouse tau? MC1 and Thioflavin S would then provide any insight about progressive changes in tau conformation.

This thesis demonstrates that after tau i.c. and *S. typhimurium* i.p. injections, the spread of AT8-positive tau from the injection site results in AT8-positive tau within the mammillary nuclei. However, it is unclear whether this transportation of tau occurs through glial uptake or synaptic uptake. Isolating synaptosome fractions from the white matter tracts and utilising the AT8 HTRF assay (Chapter 5) would demonstrate whether AT8-positive tau is propagating through the white matter pathway itself. Determining if microglial uptake is occurring in the white matter tract could be carried out with the use of *MacGreen* mice (Sasmono and Williams, 2012), which express green fluorescent protein under the Csf1r promoter, or pharmacological inhibition of microglial exosomes which have previously been shown to cease tau propagation (Asai *et al.*, 2015). However, these interventions have wide-reaching consequences and may not answer the specific research question or encourage translational research to understand human AD pathogenesis.

In vitro experiments utilising microfluidic chambers may allow closer analysis of the mechanism behind these findings (Hallinan *et al.*, 2019). By exposing primary neurons with pro-inflammatory mediators such as IFNγ and TNFα and specific kinase inhibitors, it will be possible to examine effects on posttranslational modifications, such as phosphorylation. The advantage of microfluidic chambers is the physical separation of synaptic connections, allowing analysis of individual single synaptic connections rather than the web of connections formed in a well. Simultaneously, culturing primary neurons with conditioned media from microglia and/or macrophages after exposure to *S. typhimurium* would allow us to examine pathways in microglia that are activated following the bacterial infection and how this affects neuronal activity. Furthermore, identification of potential kinases involved may help to further elucidate the mechanism behind how the response to *S. typhimurium* may alter tau phosphorylation. For example, *S. typhimurium* infection has been proposed to mediate MAPK signalling pathways, pathways which have been repeatedly highlighted for excessive activation in AD patients (Uchiya and Nikai, 2008). However, it must be considered that there is no evidence that the *aroA* mutant *S. typhimurium* strain used in this thesis (SL3261) reaches the brain. Therefore, the response microglia would have *in vitro* to the bacterium itself is likely different to the microglial response *in vivo* from potential infiltration of peripheral immune cells or cytokines. This could be mitigated by the addition of cytokines instead of the bacteria itself to the microglial culture such as IFNγ and TNFα. However, this raises the same concern as with using LPS *in vivo*, by painting an incomplete picture the effect of the cytokines may not elicit an accurate physiological response. Therefore, *in vivo* is likely to remain the most viable method of studying infection response for the research questions.

The potential role of the BBB on tau propagation in Chapter 6 remains to be fully investigated. This thesis highlights the activation of cerebral vasculature through MHCII staining in Chapters 3, 4 and 7. The role of the BBB in AD is described in part in Chapter 1. One such study examined tight junction proteins such as Occludin and Claudin-5 (Yamazaki *et al.*, 2019). The authors reported a significant decrease in these proteins in AD post-mortem tissue versus post-mortem tissue from control subjects both with and without amyloid plaque deposition. This is one paper amongst a body of research highlighting how disruption in the BBB and cerebral vasculature either precedes or is associated with pathological hallmarks of tauopathies (Michalicova, Majerova and Kovac, 2020). Therefore, this work could also be combined with staining for tight junction proteins or vascular cell adhesion protein 1 (VCAM1) and intercellular Adhesion Molecule 1 (ICAM1). Both of these markers are upregulated in AD patients (Janelidze *et al.*, 2018) and in response to *S. typhimurium in vivo* (Püntener *et al.*, 2012). Human AD post-mortem tissue has been shown to contain fibrinogen and IgG within the parenchyma, both classical signs of BBB

breakdown (Ryu and McLarnon, 2009). Furthermore, histology carried out at one-month post-injection in this thesis show distinct IgG staining in macrophages by the dentate gyrus (Appendix A, Figure S4). By staining for fibrinogen, IgG, VCAM1 and ICAM1 including other markers of BBB breakdown this may help to understand to what extent the observations are due to increased infiltration of peripheral immune cells and plasma proteins (Majerova *et al.*, 2019).

A tau propagation study injected lysate enriched for AD-tau from human post-mortem tissue into 8 month-old 5XFAD mouse model (**Table 1-1**) (He *et al.*, 2018). This study demonstrated significant tau observed around plaques within the hippocampus and cortex and greater AT8-positive tau compared to the wild-type controls. Notably this tau was localised around plaques. This study confirms that amyloid plaque deposition likely plays a role in the propagation of tau. A tau propagation study could be designed where an amyloid model such as the APP/PS1 or 5XFAD mouse was injected with the AD-tau seed and then injected i.p. with *S. typhimurium*. When including the WT littermates, this would allow comparison of tau spread in the presence of amyloid plaques versus a naïve brain. However, given our understanding of how amyloid and now tau pathology is affected by *S. typhimurium*, it is to be expected that combining the pathology would lead to greater tau deposition and propagation. It may in fact be more novel to target factors with greater involvement in the immune response.

One such pathway of interest is the complement pathway. It has been established both in the P301S mouse model and post-mortem AD brain tissue that complement 1q (C1q) will demarcate post-synaptic densities for microglial phagocytosis through activation of complement 3 (C3) receptor (Dejanovic *et al.*, 2018). Furthermore, C3a receptor (C3aR) expression correlates to Braak stages in AD post-mortem tissue, and when deleted in PS19 mice reduced PHF1-positive tau pathology and pro-inflammatory cytokines (Litvinchuk *et al.*, 2018). Establishing tau spread in a C3aR-/- mouse with and without systemic infection would investigate whether this receptor plays a role in the results observed in Chapter 6. This would also elucidate to what extent the uptake of tau by microglia through this mechanism facilitates spread.

One alternative avenue is to target microglial populations through membrane proteins such as colony stimulating factor 1 receptor (CSF1R). CSF1R is expressed on microglia and involved in the response to infection or injury through promoting proliferation and cytokine production (Mitrasinovic *et al.*, 2005). A recent paper showed that P301S mice given CSF1R inhibitor (JNJ527) for 8 weeks within their diet showed decreased AT8 to total tau ratio and significantly improved performance in the rotarod test. However, these mice still performed significantly worse than wild-type controls (Mancuso *et al.*, 2019). Whether CSF1R inhibitor administered throughout systemic infection would in turn reduce the propagation of tau is unclear. CSF1R does not simply

deplete microglial populations, it also depletes peripheral macrophage populations (Lei *et al.*, 2020). Furthermore, depletion of CSF1R signalling reduces tight junction proteins *in vitro*, suggesting a potential role in maintaining the BBB (Delaney *et al.*, 2021). Therefore, CSF1R may be preferable to examine as a marker of microglial activation given that studying the effect of systemic infection is an overarching aim of this thesis.

Findings in this thesis suggest that FcγRI expression is upregulated in the presence of tau pathology. Furthermore, the FcγRI results in Chapter 7 highlight a potential role for effector function on microglial activity (Lee *et al.*, 2016). One potential avenue is to examine the role of FcγRII and FcγRIII. These two Fc receptors have been shown in multiple studies to facilitate antibody-mediated uptake of fibrillar tau *in vitro* (Congdon *et al.*, 2013; Funk *et al.*, 2015). With Aβ immunotherapies, a role of Fc receptors has also been suggested. Microglia from Tg2576 mice bred with FcRγ$^{-/-}$ mice demonstrated significantly reduced uptake of the immune complexes (Das *et al.*, 2003). However, knockout of the FcRγ chain causes loss of FcγRIII expression and also loss of FcγRI effector function. Inducing tau propagation in the FcRγ$^{-/-}$ mice would potentially slow the spread of tau following systemic infection. FcRγ$^{-/-}$ mice show reduced splenomegaly and lower serum concentrations of TNFα and IL-6 following *E. coli* infection through i.p. injection (Wei *et al.*, 2019).

In turn, Chapter 7 demonstrated that FcγRI expression was significantly upregulated after systemic infection. A study looked at FcγRI$^{-/-}$ mice after they received an i.v. injection of the same *aroA* mutant strain of *S. typhimurium* (SL3261) used in this thesis but with a lower dose of cfu administered (5 x10^5 cfu versus 10^6 cfu in this thesis). There was higher initial cfu in the spleen and liver of FcγRI$^{-/-}$ mice compared to wild-type mice which suggests that clearance of the bacteria is slower without this Fc receptor (Menager *et al.*, 2007). Therefore, establishing the same tau propagation study in the FcγRI$^{-/-}$ mouse may highlight the importance of this Fc receptor in tau propagation through microglial uptake and downstream ITAM signalling pathways. In a separate study, deletion of the fractalkine receptor and downstream ITIM signalling increases tau propagation in the murine brain (Maphis *et al.*, 2015). Therefore, reduction of ITAM signalling associated with FcγRI may similarly reduce the propagation of tau through amelioration of microglial activation. However, it must be considered that there is a clear balance between peripheral clearance of bacterial infection and microglia responding to aggregated protein. Therefore, a mouse with reduced Fc receptor function may in turn show less microglial activation and tau propagation, but reduced ability to clear pathogens may lead to greater release of pro-inflammatory cytokines through other compensatory mechanisms.

8.8 Summary

Targeting the propagation of tau is an important avenue for halting or slowing the cognitive decline of AD. Understanding the link between systemic infection and tau propagation should lead to greater recognition of how therapeutic intervention may be achieved. This thesis highlights a clear need for bridging the gap between immunology research and dementia research. This work demonstrates *in vivo* that human AD tau pathology propagates to distinct brain regions at a greater rate under the presence of a bacterial infection. This propagation is sustained and does not merely reflect acute hyperphosphorylation, rather the premature formation of pathology. The importance of the white matter tract cannot be understated, and human studies highlight the association between white matter disruption and greater tau pathology deposition

Microglia appear to play a role with both MHCII and FcγRI expression altered by the presence of tau pathology and systemic infection. This thesis does pose many unanswered questions regarding the exact mechanism behind the change in spatiotemporal spread of tau. Future investigation into which pathways facilitate this may help to understand why tau propagation and systemic infection have such a profound effect on cognitive decline in AD, and potential therapeutic avenues.

Appendix A

A.1 Sex-dependent weight change following *S. typhimurium* infection in H1*Mapt-/-* mice and *Mapt-/-* mice

We find no significant main effect of sex on weight change in the H1*Mapt-/-* mice ($F(1,16)= 0.002$, $p= 0.97$). H1*Mapt-/-* male and female mice exhibit very similar weight loss 24 hours post-*S. typhimurium* injection (Male= -6.3% ± 1.71; Female= -5.83% ± 2.68). No statistical analysis was carried out for the *Mapt-/-* cohort due to the reduced sample size of the male group but weight change is notably similar in the initial 24 hours post-infection (Male= 7.81% ± 0.14; Female= -7.36% ± 4.19).

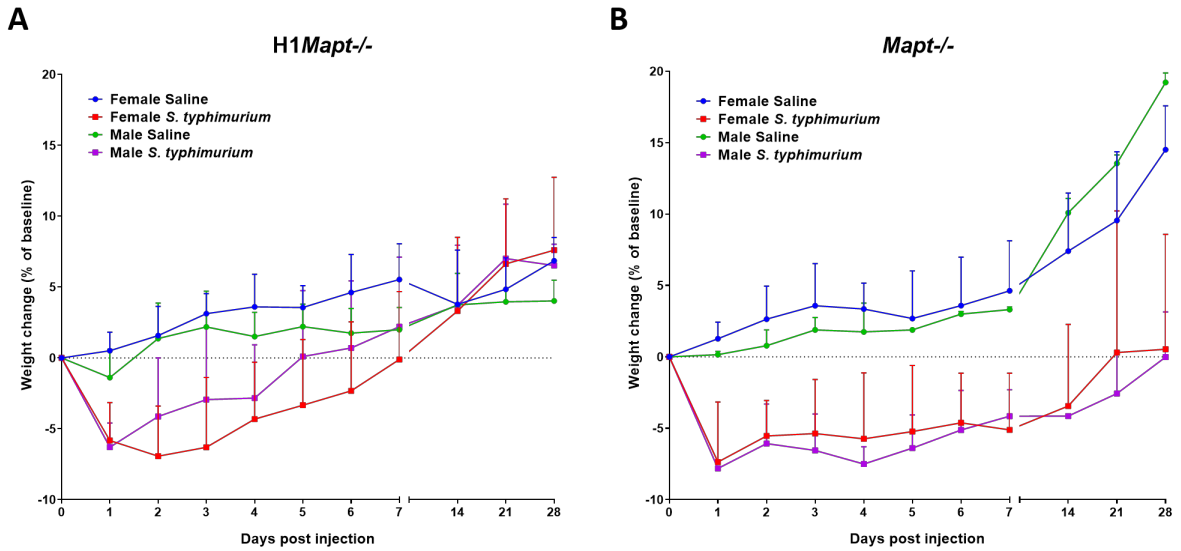

Figure S1. Sex-dependent differences in weight change following *S. typhimurium* infection.

A) H1*Mapt-/-* mice weight change following IP injection of saline or *S. typhimurium*. n= 5 for all groups. Repeated measures ANOVA with Huynh-Feldt correction and Tukey's post-hoc test **B)** *Mapt-/-* mice weight change following IP injection of saline or *S. typhimurium*. n= 4 for both female groups, n= 2 for both male groups. All data is presented as mean ± standard deviation (SD).

A.2 Linear regression of spleen weight compared to weight change 24 hours post-infection

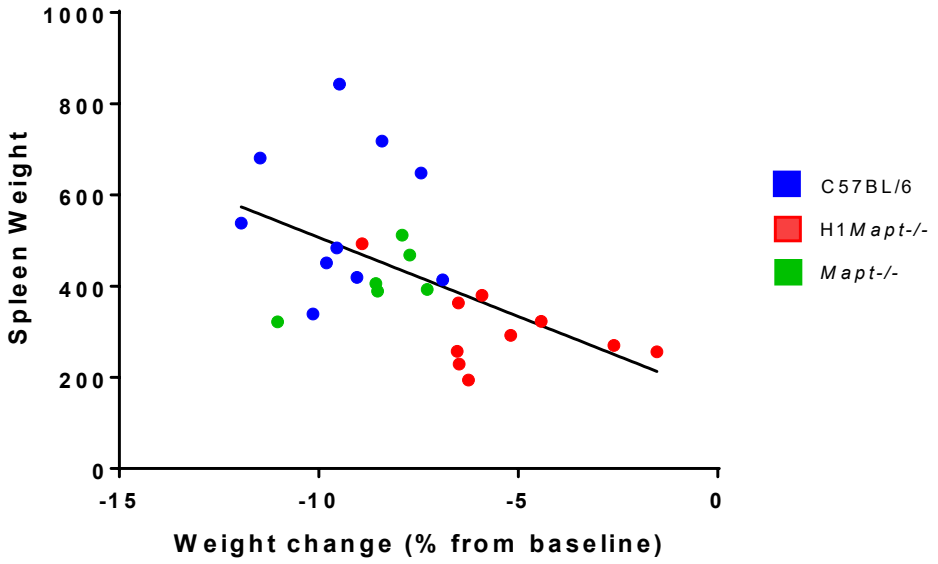

Figure S2: Weight change and spleen weight in the C57BL/6, H1*Mapt-/-* and *Mapt-/-* mice.

Spleen weight was plotted in a linear regression model against weight change recorded one day post-infection in *S. typhimurium*-treated groups of C57BL/6, H1*Mapt-/-* and *Mapt-/-* mice. The slope is significant at $p<0.01$. However the R^2 value is 0.3, meaning that 70% of the variance isn't accounted for by this regression.

A.3 Weight change post-intracerebral injection

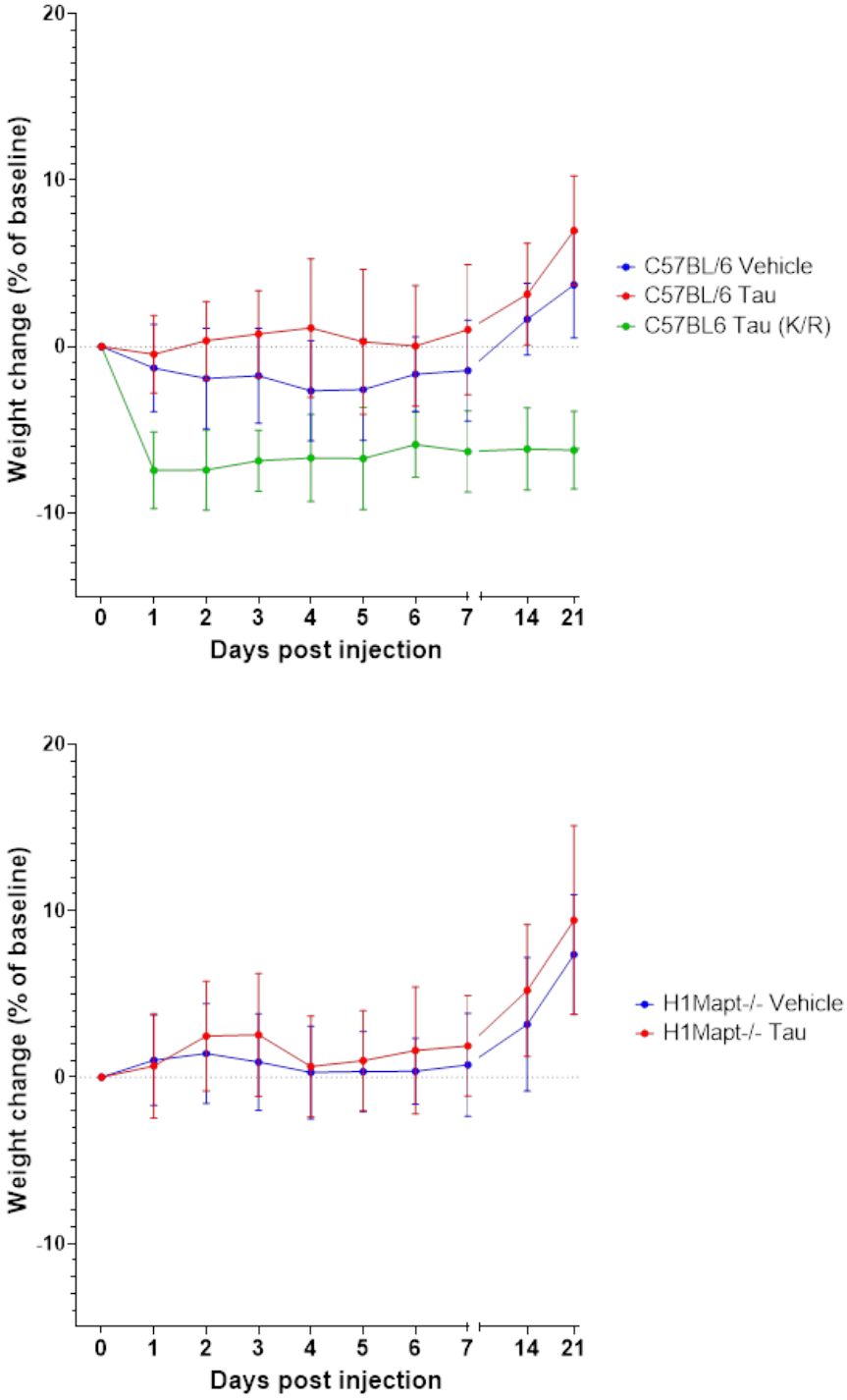

Figure S3: Weight change following i.c. injection

Weight change following i.c. injection in C57BL/6 and H1*Mapt-/-* mice. All mice underwent stereotaxic surgery through isofluorane inhalation anaesthetic. C57BL/6 (KR) denotes mice in initial cohort which received ketamine rompun as the surgical anaesthesia.

A.4 BCA values for 0.5g prep of 10 AD post-mortem cases

Table S1: BCA values for AD post-mortem cases

Sample	minus blank	mg/ml (diluted 1:10 in assay)	mg/ml
859	0.496933331	0.261191593	2.611916
903	0.421533326	0.187385793	1.873858
912	0.466600001	0.231499609	2.314996
935	0.382750005	0.149422479	1.494225
959	0.434800009	0.200371974	2.00372
962	0.432666669	0.19828374	1.982837
966	0.405866673	0.172050384	1.720504
982	0.421900004	0.187744718	1.877447
1027	0.3706	0.137529366	1.375294
1033	0.465433329	0.230357605	2.303576

A.5 IgG staining in the dentate gyrus one-month post-injection of AD-seed prep

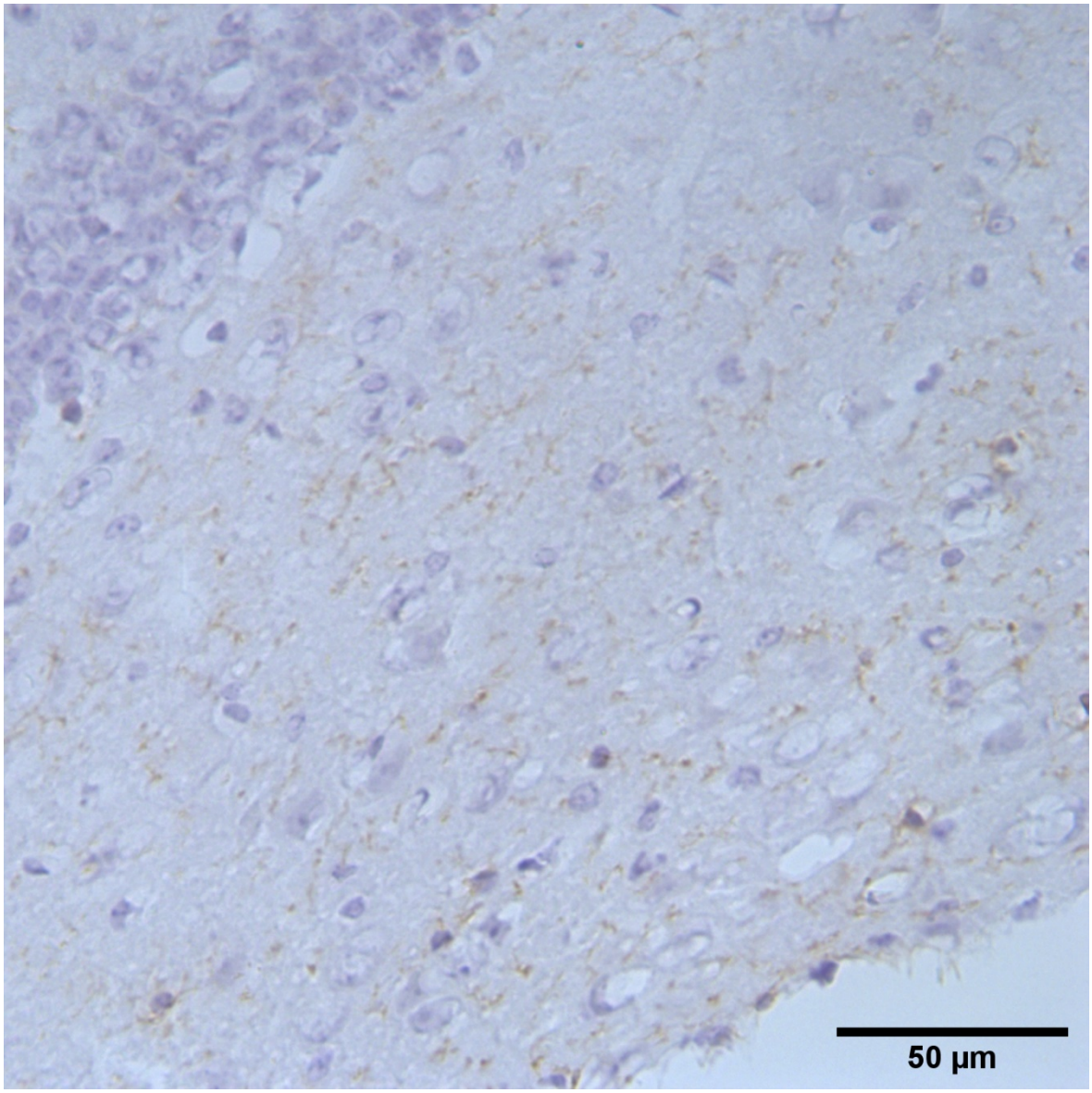

Figure S4: IgG positive staining

IgG staining using biotinylated anti-Mouse secondary antibody. Mouse received tau i.c. injection and was perfused two months post-injection.

A.6 Tau scoring data

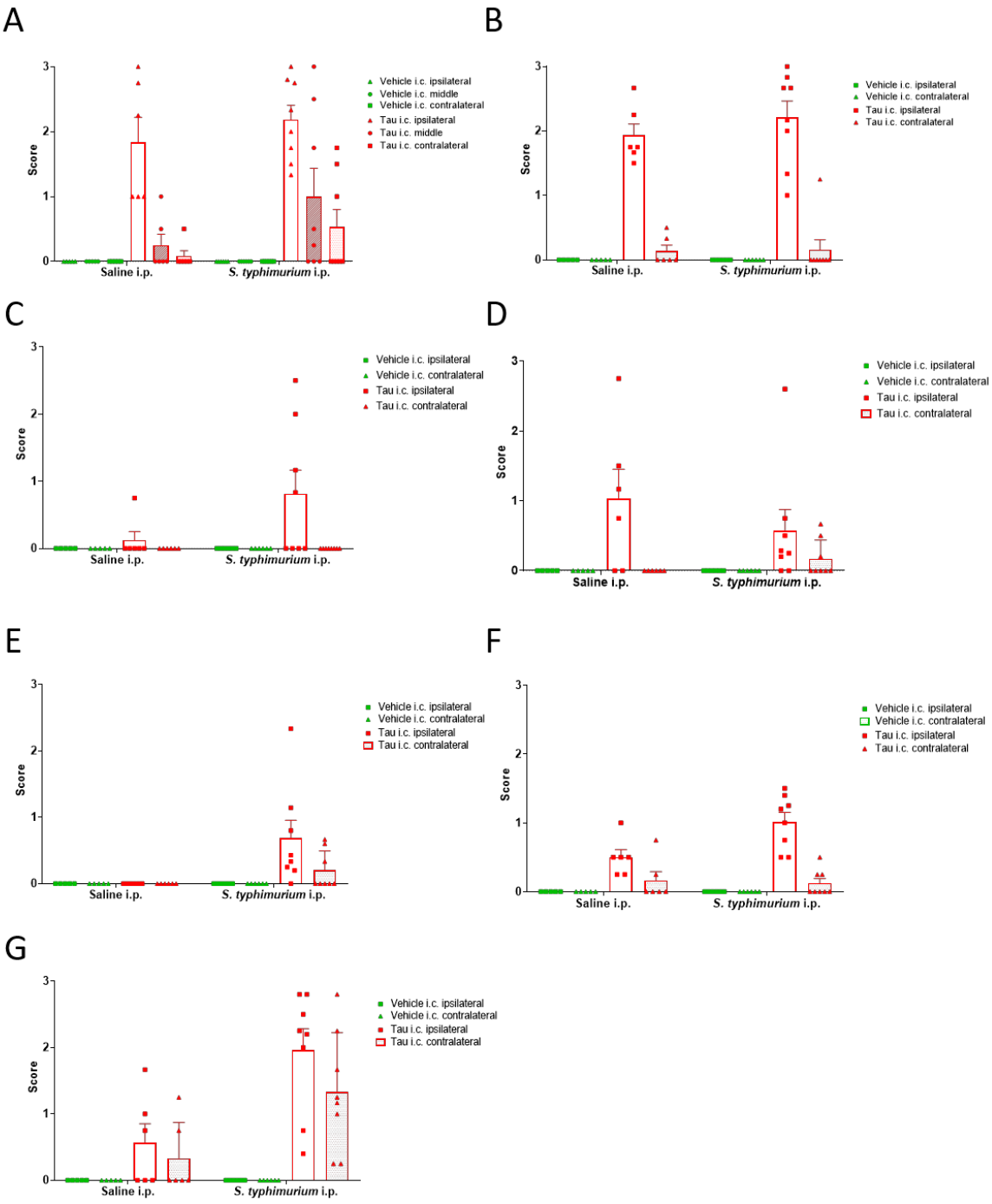

Figure S5: Tau scoring in the C57BL/6 mice

Tau scoring from 0-3 in **A)** dorsal fornix and corpus callosum (CC) at AP= -1.00. At AP= -2.50 tau is scored at the **B)** corpus callosum and **C)** hippocampus. At Bregma AP= -3.00, tau is scored at the **D)** corpus callosum, **E)** hippocampus, **F)** perirhinal cortex and **G)** mammillary nuclei.

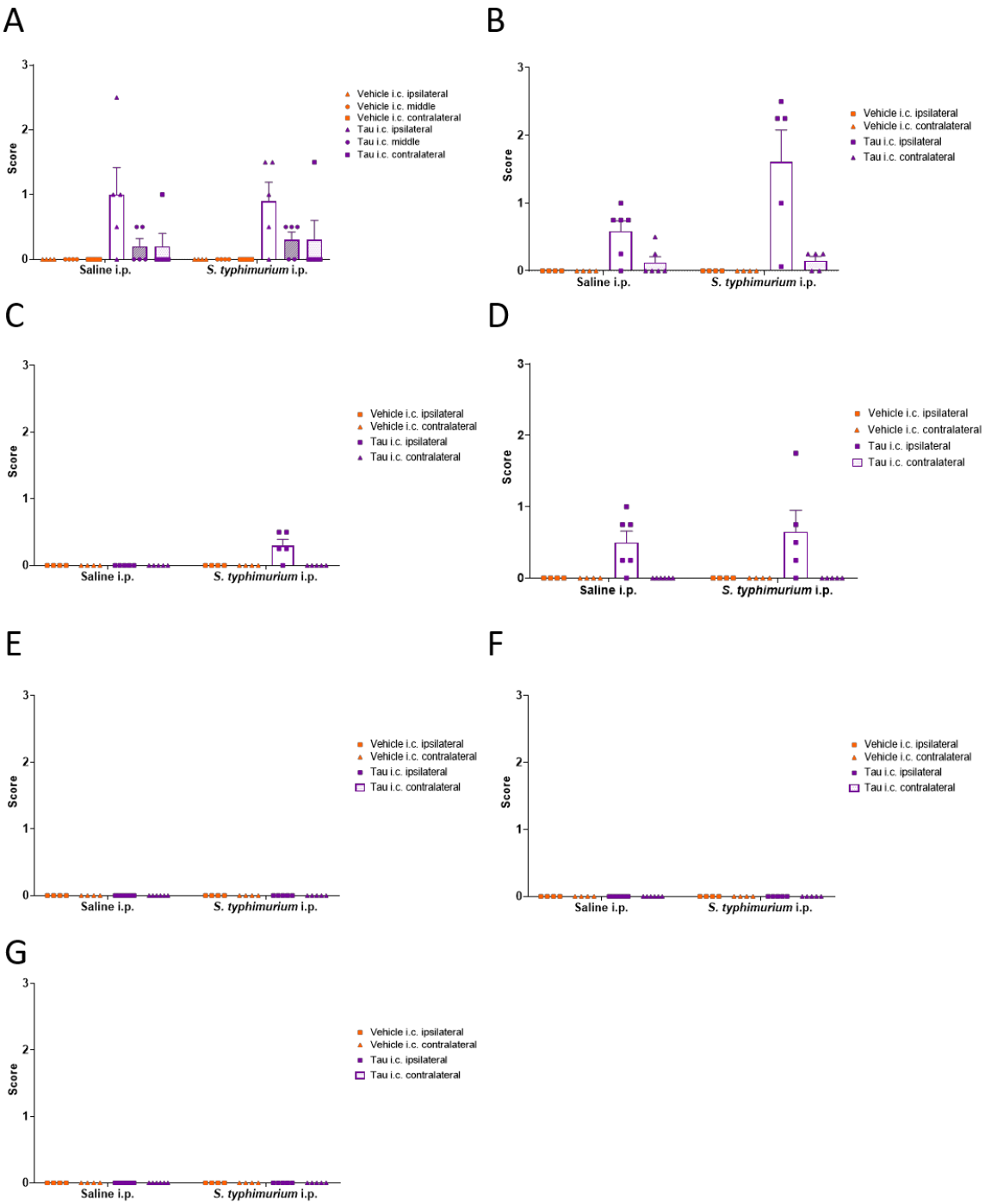

Figure S6: Tau scoring in the H1*Mapt-/-* mice

Tau scoring from 0-3 in **A)** dorsal fornix and corpus callosum (CC) at AP= -1.00. At AP= -2.50 tau is scored at the **B)** corpus callosum and **C)** hippocampus. At Bregma AP= -3.00, tau is scored at the **D)** corpus callosum, **E)** hippocampus, **F)** perirhinal cortex and **G)** mammillary nuclei.

Appendix B

Table 1- DNA Lysis Buffer for genotyping the H1*Mapt-/-* (for 25 samples)

Starting concentration	**Volume (final concentration)**
1M TRIS (Fisher Scientific)	25µl (10mM)
500mM EDTA (Fisher Scientific)	50µl (10mM)
3M NaCl (Acros Organics)	83.3µl (100mM)
20% SDS (Sigma)	125µl
100 mg/ml Proteinase K (Sigma)	10µl (0.4 mg/ml)
Make up to 2.5ml with DNase-free water	

Table 2- Line 102 PCR master mix (Genotyping)

Reagent	**Volume**
REDTaq Master Mix	12.5µl
PrP-S-J primer	1µl
PrP-As-J primer	1µl
Tn10 primer	2µl
VP16 primer	2µl
S36 primer	1µl
DNA sample	1µl
Make up to 25µl with DNase-free water	

Table 3- *Mapt* PCR master mix (Genotyping)

Reagent	**Volume**
Go Taq Master Mix	12.5µl
MAPT WT forward primer	1µl
MAPT WT reverse primer	1µl
MAPT KO forward primer	1µl
MAPT KO reverse primer	1µl
DNA sample	1µl
Make up to 25µl with DNase-free water	

Table 4- Line 102 PCR cycle conditions (Genotyping)

Step	**Time**	**Temperature**
1 cycle	5 minutes	94°C
37 cycles	30 seconds	94°C
	1 minute	64°C
	1 minute	72°C
1 cycle	10 minutes	72°C
1 cycle	Forever	4°C

Table 5- *Mapt* PCR cycle conditions (Genotyping)

Step	**Time**	**Temperature**
1 cycle	5 minutes	94°C
36 cycles	30 seconds	94°C
	30 seconds	53°C
	2 minutes	72°C
1 cycle	10 minutes	72°C
1 cycle	Forever	4°C

Table 6- Standard dilutions for *Gapdh* and H1 qPCR (Genotyping)

Standard	**DNA concentration (ng/µl)**
1	100
1/2	50
1/4	25
1/8	12.5
1/16	6.25

Table 7- *Gapdh* and H1 qPCR master mix (Genotyping)

Reagent	**Volume**
SYBR Green	10µl
Forward primer	0.8µl
Reverse primer	0.8µl
DNase-free water	7.6µl
DNA sample	0.8µl

Table 8- H1 qPCR cycle conditions (Genotyping)

Step		**Time**	**Temperature**
Holding: 1 cycle		15 minutes	95°C
33 cycles	Denaturing	30 seconds	95°C
	Annealing	30 seconds	63°C
	Extension	90 seconds	72°C
Melt Curve: 1 cycle		10 minutes	72°C
		10 minutes	35°C
		1 minute	95°C
1 cycle		Forever	4°C

Table 9- *Gapdh* qPCR cycle conditions (Genotyping)

Step		**Time**	**Temperature**
Holding: 1 cycle		2 minutes	94°C
30 cycles	Denaturing	1 minute	94°C
	Annealing	30 seconds	58°C
	Extension	30 seconds	72°C
Melt Curve: 1 cycle		10 minutes	72°C
		10 minutes	35°C
		1 minute	95°C
1 cycle		Forever	4°C

Table 10- *Slc11a1* PCR mix

Component	**Amount (µl per sample)**
DNA-free water	21.6
Slc11a1 primer (forward)	0.6
Slc11a1 primer (reverse)	0.6
Gapdh primer (forward)	0.6
Gapdh primer (reverse)	0.6
DNA	1

Table 11- *Slc11a1* PCR cycle conditions

Step	**Time**	**Temperature**
1 cycle	3 minutes	94°C
35 cycles	30 seconds	94°C
	1 minute	55°C
	1 minute	72°C
1 cycle	2 minutes	72°C
1 cycle	Forever	4°C

Appendix B

Table 12- Lysis buffer for tissue homogenisation

Reagent	**Stock concentration**	**Final concentration**	**Volume**
Tris-HCL (Fisher Scientific)	1M	25mM	1000µl
NaCl (Fisher Scientific)	3M	150mM	2000µl
Triton 100X (Fisher Scientific)	100%	1%	400µl
dH20	-	-	33ml
Filter for 30ml			
PhosSTOP (Roche, UK)			3 tablets (1 per 10ml)
cOmplete Protease Inhibitor (Roche)			3 tablets (1 per 10ml)

Table 13- Migration and stacking gel recipe

Reagent	**10% Migration Gel**	**Stacking Gel**
Acrylamide 30% (Sigma)	4.0ml	0.52ml
TRIS 1.5M pH 8.8 (Fisher Scientific)	3.0ml	-
TRIS 0.5M pH 6.8 (Fisher Scientific)	-	1.0ml
APS (ammonium persulfate) 10% (Sigma)	120µl	40µl
SDS (sodium dodecyl sulfate) 10% (Sigma)	120µl	40µl
ddH_2O	5.0ml	2.5ml
TEMED (tetramethylethylenediamine) (Sigma)	12µl	4µl

5X TBE (Tris/Borate/EDTA) buffer (1L)

- 54g Tris Base
- 27.5g Boric acid
- 3.72g EDTA

0.9% Saline (1L)

- 9g sodium chloride
- 1000ml dH_2O

Salmonella *typhimurium* (SL3261)

- 200µl aliquot of *S. typhimurium* (8e9) diluted in 1400µl 0.9% saline (Fannin, UK) = 1:8 dilution
- 100µl of the 1:8 dilution diluted with 900µl of saline = 1:80 dilution
- 100µl of the 1:80 dilution diluted with 9,900µl of saline = 1:8000 dilution (10^6 cfu)

Avertin (2, 2, 2-Tribromoethanol)

Avertin concentrate (mix well):

- 25g 2,2,2,Tribromothanol crystals
- 15.5ml Tertiary amyl alcohol

Anaesthetic solution:

- 250ml 0.9% saline (Autoclaved)
- 20ml Analytical absolute alcohol
- 5ml of Rat Avertin Concentrate

Mix covered in foil, stirring constantly for at least 6 hours. Filter and store at 4°C

4% Paraformaldehyde

- 40g Paraformaldehyde
- 500ml dH_2O
- 500ml 0.2M phosphate buffer

Store at -20°C

30% sucrose

- 3g sucrose
- 10m 1X phosphate buffered saline

10X Phosphate buffered saline

- 8g NaCl
- 0.2g KCl
- 0.24g KH_2PO_4
- 1.44g NA_2PO_4

Make up to a litre in dH_2O and adjust pH to 7.4

0.2M Phosphate buffer

- 85.8g NA_2HPO_4
- 12.5g NAH_2PO_4

Make up to 2 litres in dH_2O and adjust pH to 7.4

3,3 Di-aminobenzidine (DAB) substrate solution (25mg/ml)

- 250ml 0.1M Phosphate buffer
- 125µl 30% H_2O_2
- 5ml DAB

Mowiol-DABCO mounting media

- 4.8g Mowiol 4-88
- 12ml Glycerol
- 12ml dH_2O

Mix for 1 hour

- 24ml 0.2M Tris-Cl (pH 8.5)

Mix at 50°C until dissolved. Centrifuge at 5,000 rcf for 15 minutes at room temperature. Remove supernatant.

- 2.5% DABCO (Merck, Germany)

Store at -20°C

50X TAE (Tris/Acetate/EDTA) buffer

- 242g Tris Base
- 57.1ml Acetic acid
- 100ml 0.5M EDTA

Make to a litre with dH_2O

4X Sample buffer

- 4% SDS
- 10% 2-mercaptoethanol
- 20% Glycerol
- 0.004% Bromophenol Blue
- 0.125M Tris-HCl

Store at -20°C

10X Laemmli buffer

- 30g Tris Base
- 144g Glycine

- 10g SDS
- 1L dH_2O

Store at 4°C

Transfer buffer

- 1400ml dH_2O
- 200ml 10X laemmli buffer
- 400ml Methanol

Store at 4°C

10X Tris buffered saline

- 60.6g Tris Base
- 87.6g NaCl
- 1M HCl

Dissolve Tris Base and NaCl in 800ml dH_2O and adjust pH to 7.6 with HCl. Make up to a litre with dH_2O, filter and store at 4°C.

Gelatinised slide coating

- 5g gelatine
- 0.5g chromium potassium sulphate dodecahydrate
- 1L dH_20

Filter the solution and coat the slides in solution, dry at room temperature for 48 hours.

APS slide coating

- 5% APS in methanol solution
- 100% methanol

Coat slides in the 5% APS solution followed by 100% methanol, rinse slides and dry overnight at 37°C overnight

.

Bibliography

Acquarone, E. *et al.* (2019) 'Synaptic and memory dysfunction induced by tau oligomers is rescued by up-regulation of the nitric oxide cascade', *Molecular Neurodegeneration*, 14(1), pp. 1–19. doi: 10.1186/s13024-019-0326-4.

Adams, S. J. *et al.* (2010) 'Three Repeat Isoforms of Tau Inhibit Assembly of Four Repeat Tau Filaments', *PLoS ONE*, 5(5), pp. 1–9. doi: 10.1371/journal.pone.0010810.

Ahmed, Z. *et al.* (2014) 'A novel in vivo model of tau propagation with rapid and progressive neurofibrillary tangle pathology: The pattern of spread is determined by connectivity, not proximity', *Acta Neuropathologica*, 127(5), pp. 667–683. doi: 10.1007/s00401-014-1254-6.

Alberici, A. *et al.* (2004) 'Frontotemporal dementia: impact of P301L tau mutation on a healthy carrier.', *Journal of Neurology, Neurosurgery and Psychiatry*, 75(11), pp. 1607–10. doi: 10.1136/jnnp.2003.021295.

Allen, B. *et al.* (2002) 'Abundant Tau Filaments and Nonapoptotic Neurodegeneration in Transgenic Mice Expressing Human P301S Tau Protein', *The Journal of Neuroscience*, 22(21), pp. 9340–9351. doi: 22/21/9340 [pii].

Amadoro, G. *et al.* (2020) 'N-terminal tau truncation in the pathogenesis of Alzheimer's disease (AD): Developing a novel diagnostic and therapeutic approach', *Biochimica et Biophysica Acta - Molecular Basis of Disease*. Elsevier, 1866(3), p. 165584. doi: 10.1016/j.bbadis.2019.165584.

Anand, K. S. and Dhikav, V. (2012) 'Hippocampus in health and disease: An overview', *Annals of Indian Academy of Neurology*. Medknow Publications & Media Pvt Ltd, 15(4), pp. 239–246. doi: 10.4103/0972-2327.104323.

Andorfer, C. *et al.* (2003) 'Hyperphosphorylation and aggregation of tau in mice expressing normal human tau isoforms', *Journal of Neurochemistry*, 86(3), pp. 582–590. doi: 10.1046/j.1471-4159.2003.01879.x.

Asai, H. *et al.* (2015) 'Depletion of microglia and inhibition of exosome synthesis halt tau propagation', *Nature Neuroscience*, 18(11), pp. 1584–1593. doi: 10.1038/nn.4132.

Asby, D. *et al.* (2021) 'Systemic infection exacerbates cerebrovascular dysfunction in Alzheimer's disease', *Brain*, 144(6), pp. 1869–1883. doi: 10.1093/brain/awab094.

Askew, K. and Gomez-Nicola, D. (2018) 'A story of birth and death: Insights into the formation and

dynamics of the microglial population', *Brain, Behavior, and Immunity*, 69, pp. 9–17. doi: 10.1016/j.bbi.2017.03.009.

Augustinack, J. C. *et al.* (2002) 'Specific tau phosphorylation sites correlate with severity of neuronal cytopathology in Alzheimer's disease', *Acta Neuropathologica*, 103(1), pp. 26–35. doi: 10.1007/s004010100423.

Aujla, S. J., Dubin, P. J. and Kolls, J. K. (2007) 'Th17 cells and Mucosal Host Defense', *Seminars in Immunology*, 19(6), pp. 377–382. doi: 10.1016/j.smim.2007.10.009.

Babcock, A. a. *et al.* (2003) 'Chemokine Expression by Glial Cells Directs Leukocytes to Sites of Axonal Injury in the CNS', *The Journal of Neuroscience*, 23(21), pp. 7922–7930. doi: 23/21/7922 [pii].

Balschun, D. and Rowan, M. J. (2018) 'Hippocampal synaptic plasticity in neurodegenerative diseases: Aß, tau and beyond', *Neuroforum*, 24(3), pp. A133–A141. doi: doi:10.1515/nf-2017-A063.

Bao, S. *et al.* (2000) 'Interferon-γ plays a critical role in intestinal immunity against Salmonella typhimurium infection', *Immunology*, 99(3), pp. 464–472. doi: 10.1046/j.1365-2567.2000.00955.x.

Barker, G. R. I. and Warburton, E. C. (2011) 'When Is the Hippocampus Involved in Recognition Memory?', *The Journal of Neuroscience*, 31(29), pp. 10721–10731. doi: 10.1523/JNEUROSCI.6413-10.2011.

Barron, M. *et al.* (2017) 'A state of delirium: Deciphering the effect of inflammation on tau pathology in Alzheimer's disease', *Experimental Gerontology*, 94, pp. 103–107. doi: 10.1016/j.exger.2016.12.006.

Becker, T. C. *et al.* (2005) 'Bone Marrow Is a Preferred Site for Homeostatic Proliferation of Memory CD8 T Cells', *The Journal of Immunology*, 174(3), pp. 1269–1273. doi: 10.4049/jimmunol.174.3.1269.

Bemiller, S. M. *et al.* (2017) 'TREM2 deficiency exacerbates tau pathology through dysregulated kinase signaling in a mouse model of tauopathy', *Molecular Neurodegeneration*, 12(74), pp. 1–12. doi: 10.1186/s13024-017-0216-6.

Benilova, I., Karran, E. and De Strooper, B. (2012) 'The toxic Aβ oligomer and Alzheimer's disease: an emperor in need of clothes.', *Nature Neuroscience*, 15(3), pp. 349–357. doi: 10.1038/nn.3028.

Bertolotti, A. (2018) 'Importance of the subcellular location of protein deposits in

neurodegenerative diseases', *Current Opinion in Neurobiology*, 51, pp. 127–133. doi: 10.1016/j.conb.2018.03.004.

Betz, K. J. *et al.* (2018) 'Enhanced survival following oral and systemic Salmonella enterica serovar Typhimurium infection in polymeric immunoglobulin receptor knockout mice', *PLoS ONE*, 13(6), pp. 1–16. doi: 10.1371/journal.pone.0198434.

Bhaskar, K. *et al.* (2010) 'Regulation of Tau Pathology by the Microglial Fractalkine Receptor', *Neuron*, 68(1), pp. 19–31. doi: 10.1016/j.neuron.2010.08.023.

Biber, K., Vinet, J. and Boddeke, H. W. G. M. (2008) 'Neuronal Chemokines: Versatile Messengers In Central Nervous System Cell Interaction', *Journal of Neuroimmunology*, 198(1–2), pp. 69–74. doi: 10.1016/j.jneuroim.2008.04.012.

Blackmore, T. *et al.* (2017) 'Tracking progressive pathological and functional decline in the rTg4510 mouse model of tauopathy', *Alzheimer's Research & Therapy*, 9(1), p. 77. doi: 10.1186/s13195-017-0306-2.

Bolós, M. *et al.* (2015) 'Direct Evidence of Internalization of Tau by Microglia in Vitro and in Vivo', *Journal of Alzheimer's Disease*, 50(1), pp. 77–87. doi: 10.3233/JAD-150704.

Bolós, M. *et al.* (2017) 'Absence of CX3CR1 impairs the internalization of Tau by microglia', *Molecular Neurodegeneration*, 12(59), pp. 1–14. doi: 10.1186/s13024-017-0200-1.

Bonilla, F. A. and Oettgen, H. C. (2010) 'Adaptive Immunity', *Journal of Allergy and Clinical Immunology*, 125(2), pp. S33-40. doi: 10.1016/j.jaci.2009.09.017.

Boulangé, C. L. *et al.* (2016) 'Impact of the gut microbiota on inflammation, obesity, and metabolic disease', *Genome Medicine*, 8(42), pp. 1–12. doi: 10.1186/s13073-016-0303-2.

Braak, H. *et al.* (2006) 'Staging of Alzheimer disease-associated neurofibrillary pathology using paraffin sections and immunocytochemistry', *Acta Neuropathologica*, 112(4), pp. 389–404. doi: 10.1007/s00401-006-0127-z.

Braak, H. and Braak, E. (1991) 'Neuropathological stageing of Alzheimer-related changes', *Acta Neuropathologica*, 82(4), pp. 239–259. doi: 10.1109/ICINIS.2015.10.

Brier, M. R. *et al.* (2016) 'Tau and Aβ imaging, CSF measures, and cognition in Alzheimer's disease', *Science Translational Medicine*, 8(338), pp. 1–19. doi: 10.1126/scitranslmed.aaf2362.Tau.

Brown, D. E. *et al.* (2013) 'Salmonella enterica Causes More Severe Inflammatory Disease in

C57/BL6 Nramp1G169 Mice Than Sv129S6 Mice', 50(5), pp. 867–876. doi: 10.1177/0300985813478213.Salmonella.

Brown, M. W. and Aggleton, J. P. (2001) 'Recognition memory: What are the roles of the perirhinal cortex and hippocampus?', *Nature Reviews Neuroscience*, 2(1), pp. 51–61. doi: 10.1038/35049064.

Brown, M. W., Eldridge, M. A. and Banks, P. J. (2016) 'Perirhinal cortex: Neural representations', in *The Curated Reference Collection in Neuroscience and Biobehavioral Psychology*. doi: 10.1016/B978-0-12-809324-5.21078-X.

Broz, P. *et al.* (2010) 'Redundant roles for inflammasome receptors NLRP3 and NLRC4 in host defense against Salmonella', *The Journal of Experimental Medicine*, 207(8), pp. 1745–1755. doi: 10.1084/jem.20100257.

Broz, P., Ohlson, M. B. and Monack, D. M. (2012) 'Innate immune response to Salmonella typhimurium, a model enteric pathogen', *Gut Microbes*, 3(2), pp. 62–70. doi: 10.4161/gmic.19141.

Bubb, E. J., Kinnavane, L. and Aggleton, J. P. (2017) 'Hippocampal–diencephalic–cingulate networks for memory and emotion: An anatomical guide', *Brain and Neuroscience Advances*, 1(1), pp. 1–20. doi: 10.1177/2398212817723443.

Buckle, G. C., Walker, C. L. F. and Black, R. E. (2012) 'Typhoid fever and paratyphoid fever: Systematic review to estimate global morbidity and mortality for 2010.', *Journal of Global Health*, 2(1), pp. 1–9. doi: 10.7189/jogh.02.010401.

Bugiani, O. *et al.* (1999) 'Frontotemporal Dementia and Corticobasal Degeneration in a Family with a P301S Mutation in Tau', *Journal of Neuropathology and Experimental Neurology*, 58(6), pp. 667–677. doi: 10.1097/00005072-199906000-00011.

Burton, M. D., Sparkman, N. L. and Johnson, R. W. (2011) 'Inhibition of interleukin-6 trans-signaling in the brain facilitates recovery from lipopolysaccharide-induced sickness behavior', *Journal of Neuroinflammation*, 8(54), pp. 1–13. doi: 10.1186/1742-2094-8-54.

Butterfield, A., Di Domenico, F. and Barone, E. (2015) 'Elevated Risk of Type 2 Diabetes for Development of Alzheimer Disease: a Key Role for Oxidative Stress in Brain', *Biochimica et Biophysica Acta*, 1842(9), pp. 1693–1706. doi: 10.1016/j.bbadis.2014.06.010.Elevated.

Cai, Z., Hussain, M. D. and Yan, L.-J. (2014) 'Microglia, neuroinflammation, and beta-amyloid protein in Alzheimer's disease', *International Journal of Neuroscience*, 124(5), pp. 307–21. doi: 10.3109/00207454.2013.833510.

Campsall, K. D. *et al.* (2002) 'Characterization of transgene expression and Cre recombinase activity in a panel of Thy-1 promoter-Cre transgenic mice', *Developmental Dynamics*, 224(2), pp. 135–143. doi: 10.1002/dvdy.10092.

Cardona, A. E. *et al.* (2006) 'Control of microglial neurotoxicity by the fractalkine receptor', *Nature Neuroscience*, 9(7), pp. 917–924. doi: 10.1038/nn1715.

Carson, M. J. *et al.* (2006) 'CNS immune privilege: hiding in plain sight', *Immunological reviews*, 213, pp. 48–65. doi: 10.1111/j.1600-065X.2006.00441.x.

Casati, M. *et al.* (2018) 'Increased expression of TREM2 in peripheral cells from mild cognitive impairment patients who progress into Alzheimer's disease', *European Journal of Neurology*, 25(6), pp. 805–810. doi: 10.1111/ene.13583.

Castanho, I. *et al.* (2020) 'Transcriptional Signatures of Tau and Amyloid Neuropathology', *Cell Reports*. ElsevierCompany., 30(6), pp. 2040–2054. doi: 10.1016/j.celrep.2020.01.063.

Cavazzoni, P. (2021) *FDA's Decision to Approve New Treatment for Alzheimer's Disease*, *FDA.gov*. Available at: https://www.fda.gov/drugs/news-events-human-drugs/fdas-decision-approve-new-treatment-alzheimers-disease.

Chambers, C. B. *et al.* (1999) 'Overexpression of Four-Repeat Tau mRNA Isoforms in Progressive Supranuclear Palsy but Not in Alzheimer's Disease', *Annals of Neurology*, 46(3), pp. 325–332. doi: 10.1002/1531-8249(199909)46:3<325::AID-ANA8>3.0.CO;2-V.

Chang, L. Y. L. *et al.* (2014) 'Alzheimer's disease in the human eye. Clinical tests that identify ocular and visual information processing deficit as biomarkers', *Alzheimer's and Dementia*, 10(2), pp. 251–261. doi: 10.1016/j.jalz.2013.06.004.

Chapman, P. F. *et al.* (1999) 'Impaired synaptic plasticity and learning in aged amyloid precursor protein transgenic mice.', *Nature Neuroscience*, 2(3), pp. 271–276. doi: 10.1038/6374.

Chen, J. *et al.* (1992) 'Projection domains of MAP2 and tau determine spacings between microtubules in dendrites and axons', *Nature*, 360, pp. 674–677. doi: 10.1038/360674a0.

Chenoweth, A. M. *et al.* (2015) 'The high-affinity receptor for IgG, FcγRI, of humans and non-human primates', *Immunological Reviews*, 268(1), pp. 175–191. doi: https://doi.org/10.1111/imr.12366.

Cherry, J. D. *et al.* (2014) 'Neuroinflammation and M2 microglia: the good, the bad, and the inflamed', *Journal of Neuroinflammation*, 11(98), pp. 1–15. doi: 10.1186/1742-2094-11-98.

Chesselet, M.-F. and Richter, F. (2011) 'Modelling of Parkinson's disease in mice', *The Lancet Neurology*, 10(12), pp. 1108–1118. doi: 10.1016/S1474-4422(11)70227-7.

Chidambaram, H., Das, R. and Chinnathambi, S. (2020) 'Interaction of Tau with the chemokine receptor, CX3CR1 and its effect on microglial activation, migration and proliferation', *Cell & Bioscience*, 10(109). doi: 10.1186/s13578-020-00474-4.

Cho, H. *et al.* (2016) 'In Vivo Cortical Spreading Pattern of Tau and Amyloid in the Alzheimer Disease Spectrum', *Annals of Neurology*, 80(2), pp. 247–258. doi: 10.1002/ana.24711.

Cho, M. H. *et al.* (2014) 'Autophagy in microglia degrades extracellular β-amyloid fibrils and regulates the NLRP3 inflammasome', *Autophagy*, 10(10), pp. 1761–1775. doi: 10.4161/auto.29647.

Cho, Y. E., Lee, M. H. and Song, B. J. (2017) 'Neuronal Cell Death and Degeneration through Increased Nitroxidative Stress and Tau Phosphorylation in HIV-1 Transgenic Rats', *PLoS ONE*, 12(1), p. e0169945. doi: 10.1371/journal.pone.0169945.

Chou, R. C. *et al.* (2016) 'Treatment for Rheumatoid Arthritis and Risk of Alzheimer's Disease: A Nested Case-Control Analysis', *CNS Drugs*, 30(11), pp. 1111–1120. doi: 10.1007/s40263-016-0374-z.

Chu, V. T. and Berek, C. (2013) 'The establishment of the plasma cell survival niche in the bone marrow', *Immunological Reviews*, 251(1), pp. 177–188. doi: 10.1111/imr.12011.

Chukwu, J. E. *et al.* (2018) 'Tau Antibody Structure Reveals a Molecular Switch Defining a Pathological Conformation of the Tau Protein', *Scientific Reports*, 8(6209), pp. 1–11. doi: 10.1038/s41598-018-24276-4.

Ciechanover, A. and Kwon, Y. T. a. (2015) 'Degradation of misfolded proteins in neurodegenerative diseases: therapeutic targets and strategies', *Experimental & Molecular Medicine*, 47(3), p. e147. doi: 10.1038/emm.2014.117.

Cinalli, D. A. *et al.* (2020) 'Object Recognition Memory: Distinct Yet Complementary Roles of the Mouse CA1 and Perirhinal Cortex', *Frontiers in Molecular Neuroscience*, 13(527543), pp. 1–16. doi: 10.3389/fnmol.2020.527543.

Clavaguera, F. *et al.* (2013) 'Brain homogenates from human tauopathies induce tau inclusions in mouse brain', *Proceedings of the National Academy of Sciences*, 110(23), pp. 9535–9540. doi: 10.1073/pnas.1301175110.

Colbran, R. J. (2004) ‘Targeting of calcium/calmodulin-dependent protein kinase II’, *Biochemical Journal*, 378(1), pp. 1–16. doi: 10.1042/BJ20031547.

Collcutt, Alex (2017), "The impact of systemic inflammation on neuroinflammation and tau phosphorylation in healthy ageing and pathology", University of Southampton, School of Biological Sciences, PhD thesis

Congdon, E. E. *et al.* (2013) ‘Antibody Uptake into Neurons Occurs Primarily via Clathrin-dependent FcγReceptor Endocytosis and Is a Prerequisite for Acute Tau Protein Clearance’, *The Journal of Biological Chemistry*, 288(49), pp. 35452–35465. doi: 10.1074/jbc.M113.491001.

Conlan, J. W. and North, R. J. (1992) ‘Early pathogenesis of infection in the liver with the facultative intracellular bacteria Listeria monocytogenes, Francisella tularensis, and Salmonella typhimurium involves lysis of infected hepatocytes by leukocytes’, *Infection and Immunity*, 60(12), pp. 5164–5171. doi: 10.1128/iai.60.12.5164-5171.1992.

Cooper, M. D. and Alder, M. N. (2006) ‘The Evolution of Adaptive Immune Systems’, *Cell*, 124(4), pp. 815–822. doi: 10.1016/j.cell.2006.02.001.

Costa, M. J. F. *et al.* (2021) ‘Relationship of Porphyromonas gingivalis and Alzheimer’s disease: a systematic review of pre-clinical studies’, *Clinical Oral Investigations*, 25(3), pp. 797–806. doi: 10.1007/s00784-020-03764-w.

Coughlan, G. *et al.* (2018) ‘Spatial navigation deficits — Overlooked cognitive marker for preclinical Alzheimer disease?’, *Nature Reviews Neurology*, 14(8), pp. 496–506. doi: 10.1038/s41582-018-0031-x.

Cruts, M., Theuns, J. and Van Broeckhoven, C. (2012) ‘Locus-Specific Mutation Databases for Neurodegenerative Brain Diseases’, *Human Mutation*, 33(9), pp. 1340–1344. doi: 10.1002/humu.22117.

Cullen, K. M., Kócsi, Z. and Stone, J. (2005) ‘Pericapillary Haem-Rich Deposits: Evidence for Microhaemorrhages in Aging Human Cerebral Cortex’, *Journal of Cerebral Blood Flow and Metabolism*, 25(12), pp. 1656–1667. doi: 10.1038/sj.jcbfm.9600155.

Cunningham, C. *et al.* (2007) ‘The sickness behaviour and CNS inflammatory mediator profile induced by systemic challenge of mice with synthetic double-stranded RNA (poly I:C)’, *Brain, Behavior, and Immunity*, 21(4), pp. 490–502. doi: 10.1016/j.bbi.2006.12.007.

Cunningham, C. L., Martinez-Cerdeno, V. and Noctor, S. C. (2013) ‘Microglia Regulate the Number of Neural Precursor Cells in the Developing Cerebral Cortex’, *The Journal of Neuroscience*, 33(10),

pp. 4216–4233. doi: 10.1523/JNEUROSCI.3441-12.2013.

Das, P. *et al.* (2003) 'Amyloid-β Immunization Effectively Reduces Amyloid Deposition in FcRγ-/- Knock-Out Mice', *The Journal of Neuroscience*, 23(24), pp. 8532–8538. doi: 10.1523/jneurosci.23-24-08532.2003.

Davalos, D. *et al.* (2012) 'Fibrinogen-induced perivascular microglial clustering is required for the development of axonal damage in neuroinflammation', *Nature Communications*, 3(1227), pp. 1–15. doi: 10.1038/ncomms2230.

Davies, C. and Spires-Jones, T. L. (2018) 'Complementing Tau: New Data Show that the Complement System Is Involved in Degeneration in Tauopathies', *Neuron*, 100(6), pp. 1267–1269. doi: 10.1016/j.neuron.2018.12.003.

Davies, D. S. *et al.* (2017) 'Microglia show altered morphology and reduced arborization in human brain during aging and Alzheimer's disease', *Brain Pathology*, 27(6), pp. 795–808. doi: 10.1111/bpa.12456.

Dawson, H. N. *et al.* (2001) 'Inhibition of neuronal maturation in primary hippocampal neurons from tau deficient mice', *Journal of Cell Science*, 114(6), pp. 1179–1187. doi: 10.1242/jcs.114.6.1179.

Deacon, R. M. J. *et al.* (2009) 'Aged Tg2576 mice are impaired on social memory and open field habituation tests', *Behavioural Brain Research*, 197(2), pp. 466–468. doi: 10.1016/j.bbr.2008.09.042.

Deacon, R. M. J. (2009) 'Burrowing: A sensitive behavioural assay, tested in five species of laboratory rodents', *Behavioural Brain Research*, 200(1), pp. 128–133. doi: 10.1016/j.bbr.2009.01.007.

Deacon, R. M. J. and Rawlins, J. N. P. (2005) 'Hippocampal lesions, species-typical behaviours and anxiety in mice', *Behavioural Brain Research*, 156(2), pp. 241–249. doi: 10.1016/j.bbr.2004.05.027.

Dejager, L. *et al.* (2011) 'Cecal ligation and puncture: The gold standard model for polymicrobial sepsis?', *Trends in Microbiology*, 19(4), pp. 198–208. doi: 10.1016/j.tim.2011.01.001.

Dejanovic, B. *et al.* (2018) 'Changes in the Synaptic Proteome in Tauopathy and Rescue of Tau-Induced Synapse Loss by C1q Antibodies', *Neuron*, 100(6), pp. 1322-1336.e7. doi: 10.1016/j.neuron.2018.10.014.

Delaney, C. *et al.* (2021) 'Attenuated CSF-1R signalling drives cerebrovascular pathology', *EMBO Molecular Medicine*, 13(2), p. e12889. doi: 10.15252/emmm.202012889.

Dempsey, P. W., Vaidya, S. A. and Cheng, G. (2003) 'The Art of War: Innate and adaptive immune responses', *Cellular and Molecular Life Sciences*, 60(12), pp. 2604–2621. doi: 10.1007/s00018-003-3180-y.

Denes, A., Lopez-Castejon, G. and Brough, D. (2012) 'Caspase-1: Is IL-1 just the tip of the ICEberg?', *Cell Death and Disease*, 3(7), p. e338. doi: 10.1038/cddis.2012.86.

Dhavan, R. and Tsai, L.-H. (2001) 'A decade of CDK5', *Nature Reviews Molecular Cell Biology*, 2(10), pp. 749–759. doi: 10.1038/35096019.

Diamond, B. *et al.* (2009) 'Losing your nerves? Maybe it's the antibodies', *Nat Rev Immunol*, 9(6), pp. 449–456. doi: 10.1038/nri2529.

Diner, I., Nguyen, T. and Seyfried, N. T. (2017) 'Enrichment of Detergent-insoluble Protein Aggregates from Human Postmortem Brain', *Journal of Visualized Experiments*, 128(55835), pp. 1–8. doi: 10.3791/55835.

Dionisio-Santos, D. A. *et al.* (2020) 'Evaluating the Effect of Interleukin-4 in the 3xTg Mouse Model of Alzheimer's Disease', *Frontiers in Neuroscience*, 14(441), pp. 1–10. doi: 10.3389/fnins.2020.00441.

Dixit, R. *et al.* (2008) 'Differential Regulation of Dynein and Kinesin Motor Proteins by Tau', *Science*, 319(5866), pp. 1086–1089. doi: 10.1126/science.1152993.

Douet, V. and Chang, L. (2015) 'Fornix as an imaging marker for episodic memory deficits in healthy aging and in various neurological disorders', *Frontiers in Aging Neuroscience*, 6(343), pp. 1–19. doi: 10.3389/fnagi.2014.00343.

Duff, K. *et al.* (2000) 'Characterization of Pathology in Transgenic Mice Over-Expressing Human Genomic and cDNA Tau Transgenes', *Neurobiology of Disease*, 7(2), pp. 87–98. doi: 10.1006/nbdi.1999.0279.

Eidenmüller, J. *et al.* (2000) 'Structural and Functional Implications of Tau Hyperphosphorylation: Information from Phosphorylation-Mimicking Mutated Tau Proteins', *Biochemistry*, 39(43), pp. 13166–13175. doi: 10.1021/bi001290z.

Eikelenboom, P. *et al.* (2012) 'Whether, when and how chronic inflammation increases the risk of developing late-onset Alzheimer's disease', *Alzheimer's Research & Therapy*, 4(3), pp. 1–9. doi:

10.1186/alzrt118.

Engelhardt, B. *et al.* (2016) 'Vascular, glial, and lymphatic immune gateways of the central nervous system', *Acta Neuropathologica*, 132(3), pp. 317–338. doi: 10.1007/s00401-016-1606-5.

Epelman, S., Lavine, K. J. and Randolph, G. J. (2014) 'Origin and Functions of Tissue Macrophages', *Immunity*, 41(1), pp. 21–35. doi: 10.1016/j.immuni.2014.06.013.

Fan, Y., Xie, L. and Chung, C. Y. (2017) 'Signaling Pathways Controlling Microglia Chemotaxis', *Molecules and Cells*, 40(3), pp. 163–168. doi: 10.14348/molcells.2017.0011.

Felgner, S. *et al.* (2016) 'aroA -Deficient Salmonella enterica Serovar Typhimurium Is More Than a Metabolically Attenuated Mutant', *mBio*, 7(5), pp. e01220-16. doi: 10.1128/mBio.01220-16.

Fiandaca, M. S. *et al.* (2015) 'Identification of preclinical Alzheimer's disease by a profile of pathogenic proteins in neurally derived blood exosomes: A case-control study', *Alzheimer's and Dementia*, 11(6), pp. 600–607. doi: 10.1016/j.jalz.2014.06.008.

van der Flier, W. M. *et al.* (2011) 'Early-onset versus late-onset Alzheimer's disease: The case of the missing APOE e4 allele', *The Lancet Neurology*, 10(3), pp. 280–288. doi: 10.1016/S1474-4422(10)70306-9.

Fogg, D. K. *et al.* (2006) 'A Clonogenic Bone Marrow Progenitor Specific for Macrophages and Dendritic Cells', *Science*, 311(5757), pp. 83–87. doi: 10.1126/science.1117729.

Friebel, A. *et al.* (2001) 'SopE and SopE2 from Salmonella typhimurium Activate Different Sets of RhoGTPases of the Host Cell', *The Journal of Biological Chemistry*, 276(36), pp. 34035–34040. doi: 10.1074/jbc.M100609200.

Friedhoff, P. *et al.* (1998) 'A nucleated assembly mechanism of Alzheimer paired helical filaments', *Proceedings of the National Academy of Sciences of the United States of America*, 95(26), pp. 15712–15717. doi: 10.1073/pnas.95.26.15712.

Fritsche, G. *et al.* (2012) 'Slc11a1 (Nramp1) impairs growth of Salmonella enterica serovar Typhimurium in macrophages via stimulation of lipocalin-2 expression.', *Journal of Leukocyte Biology*, 92(2), pp. 353–359. doi: 10.1189/jlb.1111554.

Fu, B. and Wright, N. (2018) 'Transport Across the Blood-Brain Barrier', in *Molecular, Cellular, and Tissue Engineering of the Vascular System. Advances in Experimental Medicine and Biology*, pp. 235–259.

Funk, K. E. *et al.* (2015) 'Distinct Therapeutic Mechanisms of Tau Antibodies: Promoting Microglial

Clearance Versus Blocking Neuronal Uptake', *The Journal of Biological Chemistry*, 290(35), pp. 21652–21662. doi: 10.1074/jbc.M115.657924.

Gadani, S. P. *et al.* (2013) 'Interleukin-4: A Cytokine to Remember', *The Journal of Immunology*, 189(9), pp. 4213–4219. doi: 10.4049/jimmunol.1202246.Interleukin-4.

Gart, E. V. *et al.* (2016) 'Salmonella Typhimurium and Multidirectional Communication in the Gut', *Frontiers in Microbiology*, 7(1827), pp. 1–18. doi: 10.3389/fmicb.2016.01827.

Gaskill, B. N. and Pritchett-Corning, K. R. (2016) 'Nest building as an indicator of illness in laboratory mice', *Applied Animal Behaviour Science*, 82(51012), pp. 140–146. doi: 10.1016/j.applanim.2016.04.008.

Gasparotto, J. *et al.* (2015) 'Increased tau phosphorylation and receptor for advanced glycation endproducts (RAGE) in the brain of mice infected with Leishmania amazonensis', *Brain, Behavior, and Immunity*, 43, pp. 37–45. doi: 10.1016/j.bbi.2014.06.204.

Gebert, a, Rothkötter, H. J. and Pabst, R. (1996) 'M Cells in Peyer's Patches of the Intestine', *International Review of Cytology*, 167, pp. 91–159. doi: http://dx.doi.org/10.1016/S0074-7696(08)61346-7.

Geissmann, F., Jung, S. and Littman, D. R. (2003) 'Blood Monocytes Consist of Two Principal Subsets with Distinct Migratory Properties', *Immunity*, 19(1), pp. 71–82. doi: 10.1016/S1074-7613(03)00174-2.

Geiszler, P. C., Barron, M. R. and Pardon, M. C. (2016) 'Impaired burrowing is the most prominent behavioral deficit of aging htau mice', *Neuroscience*, 329, pp. 98–111. doi: 10.1016/j.neuroscience.2016.05.004.

Geppert, T. D. and Lipsky, P. E. (1985) 'Antigen presentation by interferon-gamma-treated endothelial cells and fibroblasts: differential ability to function as antigen-presenting cells despite comparable Ia expression.', *The Journal of Immunology*, 135(6), pp. 3750–62.

Gerson, J. *et al.* (2016) 'Tau Oligomers Derived from Traumatic Brain Injury Cause Cognitive Impairment and Accelerate Onset of Pathology in Htau Mice', *Journal of Neurotrauma*, 33(22), pp. 2034–2043. doi: 10.1089/neu.2015.4262.

Ghoshal, N. *et al.* (2002) 'Tau Conformational Changes Correspond to Impairments of Episodic Memory in Mild Cognitive Impairment and Alzheimer's Disease', *Experimental Neurology*, 177(2), pp. 475–493. doi: 10.1006/exnr.2002.8014.

Giacobini, E. and Gold, G. (2013) 'Alzheimer disease therapy—moving from amyloid-β to tau', *Nature Reviews Neurology*, 9(12), pp. 677–686. doi: 10.1038/nrneurol.2013.223.

Gibson, Y. *et al.* (2013) 'A driver or a passenger? D421-caspase cleaved tau is associated with aggregated and insoluble tau', in *Molecular Neurodegeneration*, p. 47. doi: 10.1186/1750-1326-8-s1-p47.

Ginhoux, F. *et al.* (2010) 'Fate Mapping Analysis Reveals That Adult Microglia Derive from Primitive Macrophages', *Science*, 330(6005), pp. 841–845. doi: 10.1126/science.1194637.

Ginsberg, S. D. *et al.* (2006) 'Shift in the ratio of three-repeat tau and four-repeat tau mRNAs in individual cholinergic basal forebrain neurons in mild cognitive impairment and Alzheimer's disease', *Journal of Neurochemistry*, 96(5), pp. 1401–1408. doi: 10.1111/j.1471-4159.2005.03641.x.

Giridharan, V. V. *et al.* (2019) 'Infection-Induced Systemic Inflammation Is a Potential Driver of Alzheimer's Disease Progression', *Frontiers in Aging Neuroscience*, 11(122), pp. 1–5. doi: 10.3389/fnagi.2019.00122.

Goedert, M. *et al.* (1989) 'Multiple isoforms of human microtubule-associated protein tau: sequences and localization in neurofibrillary tangles of Alzheimer's disease', *Neuron*, 3(4), pp. 519–526. doi: 10.1016/0896-6273(89)90210-9.

Goedert, M., Jakes, R. and Vanmechelen, E. (1995) 'Monoclonal antibody AT8 recognises tau protein phosphorylated at both serine 202 and threonine 205', *Neuroscience Letters*, 189(3), pp. 167–169. doi: 10.1016/0304-3940(95)11484-E.

Goldmann, T. *et al.* (2016) 'Origin, fate and dynamics of macrophages at central nervous system interfaces', *Nature Immunology*, 17(7), pp. 797–805. doi: 10.1038/ni.3423.

Gomez-Isla, T. *et al.* (1997) 'Neuronal Loss Correlates with but Exceeds Neurofibrillary Tangles in Alzheimer 's Disease', *Annals of Neurology*, 41(1), pp. 17–24. doi: 10.1002/ana.410410106.

Gonçalves, R. A. *et al.* (2020) 'Behavioral Abnormalities in Knockout and Humanized Tau Mice', *Frontiers in Endocrinology*, 11(124), pp. 1–13. doi: 10.3389/fendo.2020.00124.

Gong, C.-X. and Iqbal, K. (2008) 'Hyperphosphorylation of Microtubule-Associated Protein Tau: A Promising Therapeutic Target for Alzheimer Disease', *Current Medicinal Chemistry*, 15(23), pp. 2321–2328. doi: 10.2174/092986708785909111.

Gottfried-Blackmore, A. *et al.* (2009) 'Acute in vivo exposure to interferon-gamma enables

resident brain dendritic cells to become effective antigen presenting cells.', *Proceedings of the National Academy of Sciences of the United States of America*, 106(49), pp. 20918–20923. doi: 10.1073/pnas.0911509106.

Götz, J. *et al.* (1995) 'Somatodendritic localization and hyperphosphorylation of tau protein in transgenic mice expressing the longest human brain tau isoform', *The EMBO Journal*, 14(7), pp. 1304–1313. doi: 10.1002/j.1460-2075.1995.tb07116.x.

Grammas, P. and Ovase, R. (2001) 'Inflammatory factors are elevated in brain microvessels in Alzheimer's disease', *Neurobiology of Aging*, 22(6), pp. 837–842. doi: 10.1016/S0197-4580(01)00276-7.

Griffin, W. S. *et al.* (1989) 'Brain interleukin 1 and S-100 immunoreactivity are elevated in Down syndrome and Alzheimer disease.', *Proceedings of the National Academy of Sciences of the United States of America*, 86(19), pp. 7611–7615. doi: 10.1073/pnas.86.19.7611.

Griffith, H. R. *et al.* (2006) 'Amnestic mild cognitive impairment: Diagnostic outcomes and clinical prediction over a two-year time period', *Journal of the International Neuropsychological Society*, 12(2), pp. 166–175. doi: 10.1017/S1355617706060267.

Guadagno, J. *et al.* (2013) 'Microglia-derived TNFα induces apoptosis in neural precursor cells via transcriptional activation of the Bcl-2 family member Puma', *Cell Death and Disease*, 4(3), p. e358. doi: 10.1038/cddis.2013.59.

Guerreiro, R. J., Gustafson, D. R. and Hardy, J. (2012) 'The genetic architecture of Alzheimer's disease: Beyond APP, PSENS and APOE', *Neurobiology of Aging*, 33(3), pp. 437–456. doi: 10.1016/j.neurobiolaging.2010.03.025.

Guo, H., Callaway, J. B. and Ting, J. P. Y. (2015) 'Inflammasomes: Mechanism of action, role in disease, and therapeutics', *Nature Medicine*, 21(7), pp. 677–687. doi: 10.1038/nm.3893.

Guo, J. L. *et al.* (2016) 'Unique pathological tau conformers from Alzheimer's brains transmit tau pathology in nontransgenic mice', *The Journal of Experimental Medicine*, 213(12), pp. 2635–2654. doi: 10.1084/jem.20160833.

den Haan, J. M. M., Arens, R. and van Zelm, M. C. (2014) 'The activation of the adaptive immune system: Cross-talk between antigen-presenting cells, T cells and B cells', *Immunology Letters*, 162(2), pp. 103–112. doi: 10.1016/j.imlet.2014.10.011.

Halliday, M. R. *et al.* (2016) 'Accelerated pericyte degeneration and blood-brain barrier breakdown in apolipoprotein E4 carriers with Alzheimer's disease', *Journal of Cerebral Blood Flow*

and Metabolism, 36(1), pp. 216–227. doi: 10.1038/jcbfm.2015.44.

Hallinan, G. I. *et al.* (2019) 'Tau Misfolding Efficiently Propagates between Individual Intact Hippocampal Neurons', *The Journal of Neuroscience*, 39(48), pp. 9623–9632. doi: 10.1523/JNEUROSCI.1590-19.2019 Copyright.

Hanel, R. A. *et al.* (2000) 'Multiple brain abscesses caused by Salmonella typhi: case report', *Surgical Neurology*, 53(1), pp. 86–90. doi: 10.1016/S0090-3019%2899%2900161-5.

Hansen-Wester, I. and Hensel, M. (2001) 'Salmonella pathogenicity islands encoding type III secretion systems', *Microbes and Infection*, 3(7), pp. 549–559. doi: 10.1016/S1286-4579(01)01411-3.

Hansen, D. V., Hanson, J. E. and Sheng, M. (2018) 'Microglia in Alzheimer's disease', *Journal of Cell Biology*, 217(2), pp. 459–472. doi: 10.1083/jcb.201709069.

Haraga, A., Ohlson, M. B. and Miller, S. I. (2008) 'Salmonellae interplay with host cells', *Nature Reviews Microbiology*, 6(1), pp. 53–66. doi: 10.1038/nrmicro1788.

Hardy, J. and Selkoe, D. J. (2002) 'The Amyloid Hypothesis of Alzheimer's Disease: Progress and Problems on the Road to Therapeutics', *Science*, 297(5580), pp. 353–356. doi: 10.1126/science.1072994.

Hart, A. D. *et al.* (2012) 'Age related changes in microglial phenotype vary between CNS regions: Grey versus white matter differences', *Brain, Behavior, and Immunity*, 26(5), pp. 754–765. doi: 10.1016/j.bbi.2011.11.006.

Hartlage-Rübsamen, M., Lemke, R. and Schliebs, R. (1999) 'Interleukin-1β, Inducible Nitric Oxide Synthase, and Nuclear Factor-κB Are Induced in Morphologically Distinct Microglia After Rat Hippocampal Lipopolysaccharide/Interferon-γ Injection', *Journal of Neuroscience Research*, 57(3), pp. 388–398. doi: 10.1002/(SICI)1097-4547(19990801)57:3<388::AID-JNR11>3.0.CO;2-2.

Hashimoto, D. *et al.* (2013) 'Tissue-Resident Macrophages Self-Maintain Locally throughout Adult Life with Minimal Contribution from Circulating Monocytes', *Immunity*, 38(4), pp. 792–804. doi: 10.1016/j.immuni.2013.04.004.

Haslund-Vinding, J. *et al.* (2017) 'NADPH oxidases in oxidant production by microglia: Activating Receptors, Pharmacology, and Association with Disease', *British Journal of Pharmacology*, 174(12), pp. 1733–1749. doi: 10.1111/bph.13425.

Haynes, S. E. *et al.* (2006) 'The P2Y12 receptor regulates microglial activation by extracellular

nucleotides.', *Nature Neuroscience*, 9(12), pp. 1512–1519. doi: 10.1038/nn1805.

He, Z. *et al.* (2018) 'Amyloid-β plaques enhance Alzheimer's brain tau-seeded pathologies by facilitating neuritic plaque tau aggregation', *Nature Medicine*. Nature Publishing Group, 24(1), pp. 29–38. doi: 10.1038/nm.4443.

He, Z. *et al.* (2020) 'Transmission of tauopathy strains is independent of their isoform composition', *Nature Communications*, 11(7), pp. 1–18. doi: 10.1038/s41467-019-13787-x.

Henderson, M. X. *et al.* (2020) 'Tau pathology spreads between anatomically-connected regions of the brain and is modulated by a LRRK2 mutation', *bioRxiv*. doi: 10.1101/2020.10.13.337857.

Heneka, M. T. *et al.* (2013) 'NLRP3 is activated in Alzheimer's disease and contributes to pathology in APP/PS1 mice', *Nature*, 493(7434), pp. 674–678. doi: 10.1038/nature11729.

Henry, C. J. *et al.* (2009) 'Peripheral lipopolysaccharide (LPS) challenge promotes microglial hyperactivity in aged mice that is associated with exaggerated induction of both pro-inflammatory IL-1β and anti-inflammatory IL-10 cytokines', *Brain, Behavior, and Immunity*, 23(3), pp. 309–317. doi: 10.1016/j.bbi.2008.09.002.

Heun, R. *et al.* (2013) 'Alzheimer's disease and co-morbidity: Increased prevalence and possible risk factors of excess mortality in a naturalistic 7-year follow-up', *European Psychiatry*, 28(1), pp. 40–48. doi: 10.1016/j.eurpsy.2011.06.001.

Hoeijmakers, L. *et al.* (2016) 'Microglial Priming and Alzheimer's Disease: A Possible Role for (Early) Immune Challenges and Epigenetics?', *Frontiers in Human Neuroscience*, 10(398), pp. 1–15. doi: 10.3389/fnhum.2016.00398.

Hoffmann, N. A. *et al.* (2014) 'Impaired plasticity of cortical dendritic spines in P301S tau transgenic mice', *Acta Neuropathologica Communications*, 1(82), pp. 1–11. doi: 10.1186/2051-5960-1-82.

Hoiseth, S. K. and Stocker, B. A. D. (1981) 'Aromatic-dependent Salmonella typhimurium are non-virulent and effective as live vaccines', *Nature*, 291(5812), pp. 238–239. doi: 10.1038/291238a0.

Holling, T. M., Schooten, E. and van Den Elsen, P. J. (2004) 'Function and Regulation of MHC Class II Molecules in T-Lymphocytes: Of Mice and Men', *Human Immunology*, 65(4), pp. 282–290. doi: 10.1016/j.humimm.2004.01.005.

Holmes, B. B. *et al.* (2013) 'Heparan sulfate proteoglycans mediate internalization and propagation of specific proteopathic seeds', *Proceedings of the National Academy of Sciences of*

the United States of America, 110(33), pp. E3138-3147. doi: 10.1073/pnas.1301440110.

Holmes, C. *et al.* (2008) 'Long-term Effects of Aβ42 Immunisation in Alzheimer's disease: Follow-up of a Randomised, Placebo-controlled Phase I Trial', *The Lancet*, 372(9634), pp. 216–223. doi: 10.1016/S0140-6736(08)61075-2.

Holmes, C. *et al.* (2009) 'Systemic inflammation and disease progression in Alzheimer disease', *Neurology*, 73(10), pp. 768–774. doi: 10.1212/WNL.0b013e3181b6bb95.

Holmes, C. *et al.* (2011) 'Proinflammatory cytokines, sickness behavior, and Alzheimer disease', *Neurology*, 77(3), pp. 212–218. doi: 10.1212/WNL.0b013e318225ae07.

Hopperton, K. E. *et al.* (2018) 'Markers of microglia in post-mortem brain samples from patients with Alzheimer's disease: A systematic review', *Molecular Psychiatry*, 23(2), pp. 177–198. doi: 10.1038/mp.2017.246.

Hsiao, K. *et al.* (1996) 'Correlative Memory Deficits, Aβ Elevation, and Amyloid Plaques in Transgenic Mice', *Science*, 274(5284), pp. 99–102. doi: 10.1126/science.274.5284.99.

Hu, Y. *et al.* (2021) 'Replicative senescence dictates the emergence of disease-associated microglia and contributes to Ab pathology', *bioRxiv*, 35(10), p. 109228. doi: 10.1101/2021.03.22.436174.

Huang, C.-C. *et al.* (2014) 'Diabetes Mellitus and the Risk of Alzheimer's Disease: A Nationwide Population-Based Study', *PLoS ONE*, 9(1), p. e87095. doi: 10.1371/journal.pone.0087095.

Husain, M. A., Laurent, B. and Plourde, M. (2021) 'APOE and Alzheimer's Disease: From Lipid Transport to Physiopathology and Therapeutics', *Frontiers in Neuroscience*, 15(630502), pp. 1–15. doi: 10.3389/fnins.2021.630502.

Hyman, B. T. *et al.* (1984) 'Alzheimer's Disease: Cell-Specific Pathology Isolates the Hippocampal Formation', *Science*, 225(4667), pp. 1168–1170. doi: 10.1126/science.6474172.

Ide, M. *et al.* (2016) 'Periodontitis and Cognitive Decline in Alzheimer's Disease', *PLoS ONE*, 11(3), pp. 1–9. doi: 10.1371/journal.pone.0151081.

Ikegami, S., Harada, A. and Hirokawa, N. (2000) 'Muscle weakness, hyperactivity, and impairment in fear conditioning in tau-deficient mice', *Neuroscience Letters*, 279(3), pp. 129–132. doi: 10.1016/S0304-3940(99)00964-7.

Ingelsson, M. *et al.* (2004) 'Early Aβ accumulation and progressive synaptic loss, gliosis, and tangle formation in AD brain', *Neurology*, 62(6), pp. 925–931. doi: 10.1212/01.WNL.0000115115.98960.37.

Ingelsson, M. *et al.* (2007) 'Increase in the relative expression of tau with four microtubule binding repeat regions in frontotemporal lobar degeneration and progressive supranuclear palsy brains', *Acta Neuropathologica*, 114(5), pp. 471–479. doi: 10.1007/s00401-007-0280-z.

Iqbal, K. *et al.* (1998) 'Mechanisms of neurofibrillary degeneration and the formation of neurofibrillary tangles', *Journal of Neural Transmission*, 53, pp. 169–180. doi: 10.1007/978-3-7091-6467-9_15.

Iqbal, K. *et al.* (2010) 'Tau in Alzheimer Disease and Related Tauopathies', *Current Alzheimer Research*, 7(8), pp. 656–664. doi: 10.2174/156720510793611592.

Ishihara, T. *et al.* (1999) 'Age-Dependent Emergence and Progression of a Tauopathy in Transgenic Mice Overexpressing the Shortest Human Tau Isoform', *Neuron*, 24(3), pp. 751–762. doi: 10.1016/S0896-6273(00)81127-7.

Ising, C. *et al.* (2019) 'NLRP3 inflammasome activation drives tau pathology', *Nature*, 575(7784), pp. 669–673. doi: 10.1038/s41586-019-1769-z.

Ittner, L. M. and Götz, J. (2007) 'Pronuclear injection for the production of transgenic mice', *Nature Protocols*, 2(5), pp. 1206–1215. doi: 10.1038/nprot.2007.145.

Jackson, A. *et al.* (2011) 'Innate Immune Activation during Salmonella Infection Initiates Extramedullary Erythropoiesis and Splenomegaly', *The Journal of Immunology*, 185(10), pp. 6198–6204. doi: 10.4049/jimmunol.1001198.Innate.

Jackson, G. R. *et al.* (2002) 'Human Wild-Type Tau Interacts with wingless Pathway Components and Produces Neurofibrillary Pathology in Drosophila', *Neuron*, 34(4), pp. 509–519. doi: 10.1016/S0896-6273(02)00706-7.

Jackson, S. J. *et al.* (2016) 'Short Fibrils Constitute the Major Species of Seed-Competent Tau in the Brains of Mice Transgenic for Human P301S Tau.', *The Journal of Neuroscience*, 36(3), pp. 762–772. doi: 10.1523/JNEUROSCI.3542-15.2016.

Jacobsen, J. S. *et al.* (2006) 'Early-onset behavioral and synaptic deficits in a mouse model of Alzheimer's disease', *Proceedings of the National Academy of Sciences of the United States of America*, 103(13), pp. 5161–5166. doi: 10.1073/pnas.0600948103.

Janelidze, S. *et al.* (2018) 'CSF biomarkers of neuroinflammation and cerebrovascular dysfunction in early Alzheimer disease', *Neurology*, 91(9), pp. e867–e877. doi: 10.1212/WNL.0000000000006082.

Janelsins, M. C. *et al.* (2005) 'Early correlation of microglial activation with enhanced tumor necrosis factor-alpha and monocyte chemoattractant protein-1 expression specifically within the entorhinal cortex of triple transgenic Alzheimer's disease mice', *Journal of Neuroinflammation*, 2(23). doi: 10.1186/1742-2094-2-23.

Jang, S. H. and Kwon, H. G. (2014) 'Perspectives on the neural connectivity of the fornix in the human brain', *Neural Regeneration Research*, 9(15), pp. 1434–1436. doi: 10.4103/1673-5374.139459.

Jansen, A. H. P., Reits, E. A. J. and Hol, E. M. (2014) 'The ubiquitin proteasome system in glia and its role in neurodegenerative diseases', *Frontiers in Molecular Neuroscience*, 7(73). doi: 10.3389/fnmol.2014.00073.

Jepson, M. A. and Clark, M. A. (2001) 'The role of M cells in Salmonella infection', *Microbes and Infection*, 3(14–15), pp. 1183–1190. doi: 10.1016/S1286-4579(01)01478-2.

Jicha, G. A. *et al.* (1999) 'cAMP-Dependent Protein Kinase Phosphorylations on Tau in Alzheimer's Disease', *The Journal of Neuroscience*, 19(17), pp. 7486–7494. doi: 10.1523/jneurosci.19-17-07486.1999.

Jirkof, P. (2014) 'Burrowing and nest building behavior as indicators of well-being in mice', *Journal of Neuroscience Methods*, 234, pp. 139–146. doi: 10.1016/j.jneumeth.2014.02.001.

Joie, R. La *et al.* (2020) 'Prospective longitudinal atrophy in Alzheimer's disease correlates with the intensity and topography of baseline tau-PET', *Science Translational Medicine*, 12(524), pp. 1–25. doi: 10.1126/scitranslmed.aau5732.Prospective.

Jones, B. D., Ghori, N. and Falkow, S. (1994) 'Salmonella typhimurium initiates murine infection by penetrating and destroying the specialized epithelial M cells of the Peyer's patches.', *The Journal of Experimental Medicine*, 180(1), pp. 15–23. doi: 10.1084/jem.180.1.15.

Jul, P. *et al.* (2016) 'Hyperactivity with Agitative-Like Behavior in a Mouse Tauopathy Model', *Journal of Alzheimer's Disease*, 49(3), pp. 783–795. doi: 10.3233/JAD-150292.

Jurga, A. M., Paleczna, M. and Kuter, K. Z. (2020) 'Overview of General and Discriminating Markers of Differential Microglia Phenotypes', *Frontiers in Cellular Neuroscience*, 14(198), pp. 1–18. doi: 10.3389/fncel.2020.00198.

Kamer, A. *et al.* (2015) 'Periodontal disease associates with higher brain amyloid load in normal elderly', *Neurobiology of Aging*, 36(2), pp. 627–633. doi: 10.1016/j.neurobiolaging.2014.10.038. Periodontal.

Kamer, A. R. *et al.* (2009) 'TNF-α and antibodies to periodontal bacteria discriminate between Alzheimer's disease patients and normal subjects', *Journal of Neuroimmunology*, 216(1), pp. 92–97. doi: 10.1016/j.jneuroim.2009.08.013.

Kametani, F. and Hasegawa, M. (2018) 'Reconsideration of Amyloid Hypothesis and Tau Hypothesis in Alzheimer's Disease', *Frontiers in Neuroscience*, 12(25), pp. 1–11. doi: 10.3389/fnins.2018.00025.

Kao, L.-T. *et al.* (2016) 'Rheumatoid Arthritis Was Negatively Associated with Alzheimer's Disease: A Population-Based Case-Control Study.', *PLoS ONE*, 11(12), pp. 1–9. doi: 10.1371/journal.pone.0168106.

Keren-Shaul, H. *et al.* (2017) 'A Unique Microglia Type Associated with Restricting Development of Alzheimer's Disease', *Cell*, 169(7), pp. 1276–1290. doi: 10.1016/j.cell.2017.05.018.

Kim, K.-A. *et al.* (2002) 'IFNγ/TNFα synergism in MHC class II induction: effect of nicotinamide on MHC class II expression but not on islet-cell apoptosis', *Diabetologia*, 45(3), pp. 385–393. doi: 10.1007/s00125-001-0755-8.

Kimura, T., Ishiguro, K. and Hisanaga, S.-I. (2014) 'Physiological and pathological phosphorylation of tau by Cdk5.', *Frontiers in Molecular Neuroscience*, 7(65), pp. 1–10. doi: 10.3389/fnmol.2014.00065.

Kirby, A. C., Yrlid, U. and Wick, M. J. (2002) 'The Innate Immune Response Differs in Primary and Secondary Salmonella Infection', *The Journal of Immunology*, 169(8), pp. 4450–4459. doi: 10.4049/jimmunol.169.8.4450.

Kitazawa, M. (2005) 'Lipopolysaccharide-Induced Inflammation Exacerbates Tau Pathology by a Cy clin-Dependent Kinase 5-Mediated Pathway in a Transgenic Model of Alzheimer's Disease', *The Journal of Neuroscience*, 25(39), pp. 8843–8853. doi: 10.1523/JNEUROSCI.2868-05.2005.

Kitazawa, M. *et al.* (2011) 'Blocking IL-1 Signaling Rescues Cognition, Attenuates Tau Pathology, and Restores Neuronal-Catenin Pathway Function in an Alzheimer's Disease Model', *The Journal of Immunology*, 187(12), pp. 6539–6549. doi: 10.4049/jimmunol.1100620.

Kobets, N. V, Nesterenko, L. N. and Balunets, D. V (2013) 'Local and Systemic Immune Responses to Salmonella in Genetically Susceptible I/St Mice after Mucosal Challenge', *ISRN Immunology*, 2013(865671). doi: 10.1155/2013/865671.

Koellhoffer, E. C., McCullough, L. D. and Ritzel, R. M. (2017) 'Old Maids: Aging and Its Impact on Microglia Function', *International Journal of Molecular Sciences*, 18(4), p. 769. doi:

10.3390/ijms18040769.

Kumar, D. K. V. *et al.* (2016) 'Amyloid-β peptide protects against microbial infection in mouse and worm models of Alzheimer's disease.', *Science Translational Medicine*, 8(340), pp. 340–372. doi: 10.1126/scitranslmed.aaf1059.

Kumar, H., Kawai, T. and Akira, S. (2011) 'Pathogen Recognition by the Innate Immune System', *International Reviews of Immunology*, 30(1), pp. 16–34. doi: 10.3109/08830185.2010.529976.

Kupz, A. *et al.* (2013) 'Contribution of Thy1+ NK cells to protective IFN- γ production during Salmonella Typhimurium infections', *Proceedings of the National Academy of Sciences of the United States of America*, 110(6), pp. 2252–2257. doi: 10.1073/pnas.1222047110.

Lacovich, V. *et al.* (2017) 'Tau Isoforms Imbalance Impairs the Axonal Transport of the Amyloid Precursor Protein in Human Neurons', *The Journal of Neuroscience*, 37(1), pp. 58–69. doi: 10.1523/JNEUROSCI.2305-16.2016.

Lai, K. S. P. *et al.* (2017) 'Peripheral inflammatory markers in Alzheimer's disease: A systematic review and meta-analysis of 175 studies', *Journal of Neurology, Neurosurgery and Psychiatry*, 88(10), pp. 876–882. doi: 10.1136/jnnp-2017-316201.

Lauro, C. *et al.* (2015) 'Fractalkine in the nervous system: Neuroprotective or neurotoxic molecule?', *Annals of the New York Academy of Sciences*, 1351(1), pp. 141–148. doi: 10.1111/nyas.12805.

Lavin, Y. *et al.* (2015) 'Regulation of macrophage development and function in peripheral tissues', *Nature Reviews Immunology*, 15(12), pp. 731–744. doi: 10.1038/nri3920.

Lawrence, C. B., Brough, D. and Knight, E. M. (2012) 'Obese mice exhibit an altered behavioural and inflammatory response to lipopolysaccharide', *Disease Models & Mechanisms*, 5(5), pp. 649–659. doi: 10.1242/dmm.009068.

Lawson, L. J. *et al.* (1990) 'Heterogeneity in the distribution and morphology of microglia in the normal adult mouse brain', *Neuroscience*, 39(1), pp. 151–170. doi: 10.1016/0306-4522(90)90229-W.

Lee, D. C. *et al.* (2010) 'LPS- induced inflammation exacerbates phospho-tau pathology in rTg4510 mice.', *Journal of Neuroinflammation*, 7(56), pp. 1–16. doi: 10.1186/1742-2094-7-56.

Lee, S. *et al.* (2012) 'Accumulation of Vesicle-Associated Human Tau in Distal Dendrites Drives Degeneration and Tau Secretion in an In Situ Cellular Tauopathy Model', *International Journal of*

Alzheimer's Disease, 2012(172837). doi: 10.1155/2012/172837.

Lee, S. H. *et al.* (2016) 'Antibody-Mediated Targeting of Tau In Vivo Does Not Require Effector Function and Microglial Engagement', *Cell Reports*, 16(6), pp. 1690–1700. doi: 10.1016/j.celrep.2016.06.099.

Lehnardt, S. *et al.* (2003) 'Activation of innate immunity in the CNS triggers neurodegeneration through a Toll-like receptor 4-dependent pathway', *Proceedings of the National Academy of Sciences of the United States of America*, 100(14), pp. 8514–8519. doi: 10.1073/pnas.1432609100.

Lehner, M. D. *et al.* (2001) 'Improved Innate Immunity of Endotoxin-Tolerant Mice Increases Resistance to Salmonella enterica Serovar Typhimurium Infection despite Attenuated Cytokine Response', *Infection and Immunity*, 69(1), pp. 463–471. doi: 10.1128/IAI.69.1.463-471.2001.

Lei, F. *et al.* (2020) 'CSF1R inhibition by a small-molecule inhibitor is not microglia specific; Affecting hematopoiesis and the function of macrophages', *Proceedings of the National Academy of Sciences of the United States of America*, 117(38), pp. 23336–23338. doi: 10.1073/pnas.1922788117.

Lei, L. *et al.* (2016) 'Salmonella Virulence Factor SsrAB Regulated Factor Modulates Inflammatory Responses by Enhancing the Activation of NF-κB Signaling Pathway', *Journal of Immunology*, 196(2), pp. 792–802. doi: 10.4049/jimmunol.1500679.

Lemstra, A. W. *et al.* (2007) 'Microglia activation in sepsis: A case-control study', *Journal of Neuroinflammation*, 4(4). doi: 10.1186/1742-2094-4-4.

Lewis, J. *et al.* (2001) 'Enhanced Neurofibrillary Degeneration in Transgenic Mice Expressing Mutant Tau and APP', *Science*, 293(5534), pp. 1487–1491. doi: 10.1126/science.1058189.

Li, J.-W. *et al.* (2018) 'Microglial priming in Alzheimer's disease', *Annals of Translational Medicine*, 6(10), pp. 176–176. doi: 10.21037/atm.2018.04.22.

Li, Y. *et al.* (2020) 'Supramammillary nucleus synchronizes with dentate gyrus to regulate spatial memory retrieval through glutamate release', *eLife*, 9(e53129), pp. 1–23. doi: 10.7554/eLife.53129.

Licastro, F. *et al.* (2000) 'Increased plasma levels of interleukin-1, interleukin-6 and antichymotrypsin in patients with Alzheimer's disease: Peripheral inflammation or signals from the brain?', *Journal of Neuroimmunology*, 103(1), pp. 97–102. doi: 10.1016/S0165-5728(99)00226-X.

Lim, S. C., Mamun, K. and Lim, J. K. H. (2014) 'Comparison between elderly inpatient fallers with and without dementia', *Singapore Medical Journal*, 55(2), pp. 67–71. doi: 10.11622/smedj.2014017.

Ling, G. S. *et al.* (2014) 'Integrin CD11b positively regulates TLR4-induced signalling pathways in dendritic cells but not in macrophages', *Nature Communications*, 5(3039), pp. 1–12. doi: 10.1038/ncomms4039.

Linkenhoker, J. R. and Linton, C. G. (2013) 'Effect of Nesting Material on Body Weights of Mice Infected with Toxoplasma gondii', *Journal of the American Association for Laboratory Animal Science : JAALAS*, 52(5), pp. 531–533.

Litvinchuk, A. *et al.* (2018) 'Complement C3aR inactivation attenuates tau pathology and reverses an immune network deregulated in tauopathy models and Alzheimer's disease', *Neuron*, 100(6), pp. 1337–1353. doi: 10.1016/j.neuron.2018.10.031.Complement.

Liu, C. C. *et al.* (2020) 'Tau and apolipoprotein E modulate cerebrovascular tight junction integrity independent of cerebral amyloid angiopathy in Alzheimer's disease', *Alzheimer's and Dementia*, 16(10), pp. 1372–1383. doi: 10.1002/alz.12104.

Liu, D. *et al.* (2019) 'Recent advances in endotoxin tolerance', *Journal of Cellular Biochemistry*, 120(1), pp. 56–70. doi: 10.1002/jcb.27547.

Liu, L. and Chan, C. (2014) 'The role of inflammasome in Alzheimer's disease', *Ageing Research Reviews*, 15(1), pp. 6–15. doi: 10.1016/j.arr.2013.12.007.

Loomis, W. P. *et al.* (2014) 'Temporal and Anatomical Host Resistance to Chronic Salmonella Infection Is Quantitatively Dictated by Nramp1 and Influenced by Host Genetic Background', *PLoS ONE*, 9(10), p. e111763. doi: 10.1371/journal.pone.0111763.

Lossos, A. *et al.* (2003) 'Frontotemporal dementia and parkinsonism with the P301S tau gene mutation in a Jewish family', *Journal of Neurology*, 250(6), pp. 733–740. doi: 10.1007/s00415-003-1074-4.

Lu, Y. C., Yeh, W. C. and Ohashi, P. S. (2008) 'LPS/TLR4 signal transduction pathway', *Cytokine*, 42(2), pp. 145–151. doi: 10.1016/j.cyto.2008.01.006.

Luders, E., Thompson, P. M. and Toga, A. W. (2010) 'The Development ofthe Corpus Callosum in the Healthy Human Brain', *The Journal of Neuroscience*, 30(33), pp. 10985–10990. doi: 10.1523/JNEUROSCI.5122-09.2010.

Lukas, G., Brindle, S. D. and Greengard, P. (1971) 'The route of absorption of intraperitoneally administered compounds.', *The Journal of Pharmacology and Experimental Therapeutics*, 178(3), pp. 562–564. doi: 10.2307/1572220.

Lull, M. E. and Block, M. L. (2010) 'Microglial Activation and Chronic Neurodegeneration', *Neurotherapeutics*, 7(4), pp. 354–365. doi: 10.1016/j.nurt.2010.05.014.

Luo, W. *et al.* (2015) 'Microglial internalization and degradation of pathological tau is enhanced by an anti-tau monoclonal antibody.', *Scientific Reports*, 5(11161), pp. 1–12. doi: 10.1038/srep11161.

Luo, X.-G., Ding, J.-Q. and Chen, S.-D. (2010) 'Microglia in the aging brain: relevance to neurodegeneration', *Molecular Neurodegeneration*, 5(12), pp. 1–9. doi: 10.1186/1750-1326-5-12.

Madry, C. and Attwell, D. (2015) 'Receptors, Ion Channels and Signaling Mechanisms Underlying Microglial Dynamics', *The Journal of Biological Chemistry*, 290(20), pp. 12443–12450. doi: 10.1074/jbc.R115.637157.

Majerova, P. *et al.* (2019) 'Trafficking of immune cells across the bloodbrain barrier is modulated by neurofibrillary pathology in tauopathies', *PLoS ONE*, 14(5), pp. 1–27. doi: 10.1371/journal.pone.0217216.

Malpetti, M. *et al.* (2020) 'Microglial activation and tau burden predict cognitive decline in Alzheimer's disease', *Brain*, 143(5), pp. 1588–1602. doi: 10.1093/brain/awaa088.

Mancuso, R. *et al.* (2019) 'CSF1R inhibitor JNJ-40346527 attenuates microglial proliferation and neurodegeneration in P301S mice', *Brain*, 142(10), pp. 3243–3264. doi: 10.1093/brain/awz241.

Maphis, N. *et al.* (2015) 'Loss of tau rescues inflammation-mediated neurodegeneration', *Frontiers in Neuroscience*, 9(196), pp. 1–12. doi: 10.3389/fnins.2015.00196.

Marciniak, E. *et al.* (2017) 'Tau deletion promotes brain insulin resistance', *The Journal of Experimental Medicine*, 214(8), pp. 2257–2269. doi: 10.1084/jem.20161731.

Marlovits, T. C. *et al.* (2004) 'Structural Insights into the Assembly of the Type III Secretion Needle Complex', *Science*, 306(5698), pp. 1040–1042. doi: 10.1126/science.1102610.

Martin, L., Latypova, X. and Terro, F. (2011) 'Post-translational modifications of tau protein: Implications for Alzheimer's disease', *Neurochemistry International*, 58(4), pp. 458–471. doi: 10.1016/j.neuint.2010.12.023.

Mass, E. *et al.* (2016) 'Specification of tissue-resident macrophages during organogenesis', *Science*, 353(6304), pp. 1114–1127. doi: 10.1126/science.aaf4238.

Mathiasen, M. L. *et al.* (2019) 'Trajectory of hippocampal fibres to the contralateral anterior thalamus and mammillary bodies in rats, mice, and macaque monkeys', *Brain and Neuroscience Advances*, 3(2398212819871205), pp. 1–18. doi: 10.1177/2398212819871205.

Mathys, H. *et al.* (2019) 'Single-cell transcriptomic analysis of Alzheimer's disease', *Nature*, 570(7761), pp. 332–337. doi: 10.1038/s41586-019-1195-2.Single-cell.

McCarron, R. M. *et al.* (1991) 'Class II MHC antigen expression by cultured human cerebral vascular endothelial cells', *Brain Research*, 566(1–2), pp. 325–328. doi: https://doi.org/10.1016/0006-8993(91)91718-G.

McLaughlin, P. A. and van der Velden, A. W. M. (2016) 'Salmonella Gives MARCH(ing) Orders to MHC-II', *Cell Host and Microbe*, 20(5), pp. 551–552. doi: 10.1016/j.chom.2016.10.019.

Menager, N. *et al.* (2007) 'Fcγ receptors are crucial for the expression of acquired resistance to virulent Salmonella enterica serovar Typhimurium in vivo but are not required for the induction of humoral or T-cell-mediated immunity', *Immunology*, 120(3), pp. 424–432. doi: 10.1111/j.1365-2567.2006.02527.x.

Mendez, M. F. (2019) 'Early-onset Alzheimer Disease and Its Variants', *Continuum*, 25(1), pp. 34–51. doi: 10.1212/CON.0000000000000687.Early-onset.

Merlini, M., Wanner, D. and Nitsch, R. M. (2016) 'Tau pathology-dependent remodelling of cerebral arteries precedes Alzheimer's disease-related microvascular cerebral amyloid angiopathy', *Acta Neuropathologica*, 131(5), pp. 737–752. doi: 10.1007/s00401-016-1560-2.

Michalicova, A., Majerova, P. and Kovac, A. (2020) 'Tau Protein and Its Role in Blood–Brain Barrier Dysfunction', *Frontiers in Molecular Neuroscience*, 13(570045), pp. 1–13. doi: 10.3389/fnmol.2020.570045.

Miklossy, J. *et al.* (2006) 'Beta-amyloid deposition and Alzheimer's type changes induced by Borrelia spirochetes', *Neurobiology of Aging*, 27(2), pp. 228–236. doi: 10.1016/j.neurobiolaging.2005.01.018.

Miklossy, J. (2015) 'Historic evidence to support a causal relationship between spirochetal infections and Alzheimer's disease', *Frontiers in Aging Neuroscience*, 7(46), pp. 1–12. doi: 10.3389/fnagi.2015.00046.

Mitrasinovic, O. M. *et al.* (2005) 'Microglia Overexpressing the Macrophage Colony-Stimulating Factor Receptor Are Neuroprotective in a Microglial-Hippocampal Organotypic Coculture System', *The Journal of Neuroscience*, 25(17), pp. 4442–4451. doi: 10.1523/JNEUROSCI.0514-05.2005.

Mittrücker, H., Köhler, A. and Kaufmann, S. H. E. (2002) 'Characterization of the Murine T-Lymphocyte Response to Salmonella enterica Serovar Typhimurium Infection', *Infection and immunity*, 70(1), pp. 199–203. doi: 10.1128/IAI.70.1.199.

Miyoshi, K. (2009) 'What is "early onset dementia"?', *Psychogeriatrics*, 9(2), pp. 67–72. doi: 10.1111/j.1479-8301.2009.00274.x.

Mizuguchi, H. and Hayakawa, T. (2002) 'The tet-off system is more effective than the tet-on system for regulating transgene expression in a single adenovirus vector', *The Journal of Gene Medicine*, 4(3), pp. 240–247. doi: 10.1002/jgm.261.

Mkaddem, S. B., Benhamou, M. and Monteiro, R. C. (2019) 'Understanding Fc Receptor Involvement in Inflammatory Diseases: From Mechanisms to New Therapeutic Tools', *Frontiers in Immunology*, 10(811), pp. 1–12. doi: 10.3389/fimmu.2019.00811.

Mogasale, V. *et al.* (2014) 'Burden of typhoid fever in low-income and middle-income countries: A systematic, literature-based update with risk-factor adjustment', *The Lancet Global Health*, 2(10), pp. 570–580. doi: 10.1016/S2214-109X(14)70301-8.

Mohseni, F., Behnam, S. G. and Rafaiee, R. (2020) 'A Review of the Historical Evolutionary Process of Dry and Water Maze Tests in Rodents', *Basic and Clinical Neuroscience*, 11(4), pp. 389–401. doi: 10.32598/bcn.11.4.1425.1.

Monack, D. M., Bouley, D. M. and Falkow, S. (2004) 'Salmonella typhimurium Persists within Macrophages in the Mesenteric Lymph Nodes of Chronically Infected Nramp1 +/+ Mice and Can Be Reactivated by IFNγ Neutralization', *The Journal of Experimental Medicine*, 199(2), pp. 231–241. doi: 10.1084/jem.20031319.

Montagne, A. *et al.* (2015) 'Blood-Brain Barrier Breakdown in the Aging Human Hippocampus', *Neuron*, 85(2), pp. 296–302. doi: 10.1016/j.neuron.2014.12.032.

Moon, J. J. and McSorley, S. J. (2009) 'Tracking the Dynamics of Salmonella specific T cell responses', *Current Topics in Microbiology and Immunology*, 334, pp. 179–198. doi: 10.1007/978-3-540-93864-4-8.

Morganti, J. M., Riparip, L. K. and Rosi, S. (2016) 'Call Off the Dog(ma): M1/M2 Polarization Is Concurrent following Traumatic Brain Injury', *PLoS ONE*, 11(1), p. e0148001. doi: 10.1371/journal.pone.0148001.

Mrdjen, D. *et al.* (2018) 'High-Dimensional Single-Cell Mapping of Central Nervous System Immune Cells Reveals Distinct Myeloid Subsets in Health, Aging, and Disease', *Immunity*, 48(2),

pp. 380–395. doi: 10.1016/j.immuni.2018.01.011.

Mroczek, K. H., Annesley, S. J. and Fisher, P. R. (2020) *Tau and its interactions with other proteins in neurodegenerative diseases*, *The Neuroscience of Parkinson's, Volume 2*. doi: 10.1016/b978-0-12-815950-7.00028-x.

Mroczko, B., Groblewska, M. and Litman-Zawadzka, A. (2019) 'The Role of Protein Misfolding and Tau Oligomers (TauOs) in Alzheimer's Disease (AD)', *International Journal of Molecular Sciences*, 20(19), p. 4661. doi: 10.3390/ijms20194661.

Narasimhan, S. *et al.* (2017) 'Pathological Tau Strains from Human Brains Recapitulate the Diversity of Tauopathies in Nontransgenic Mouse Brain', *The Journal of Neuroscience*, 37(47), pp. 11406–11423. doi: 10.1523/JNEUROSCI.1230-17.2017.

Nauciel, C. and Espinasse-Maes, F. (1992) 'Role of gamma interferon and tumor necrosis factor alpha in resistance to Salmonella typhimurium infection.', *Infection and immunity*, 60(2), pp. 450–454. doi: 10.1128/iai.60.2.450-454.1992.

Negus, S. S. *et al.* (2015) 'Effects of Ketoprofen, Morphine, and Kappa Opioids On Pain-Related Depression of Nesting in Mice', *Pain*, 156(6), pp. 1153–1160. doi: 10.1097/j.pain.0000000000000171.

Neher, J. J. and Cunningham, C. (2019) 'Priming Microglia for Innate Immune Memory in the Brain', *Trends in Immunology*, 40(4), pp. 358–374. doi: 10.1016/j.it.2019.02.001.

Neil, K. P. *et al.* (2012) 'A Large Outbreak of Typhoid Fever Associated With a High Rate of Intestinal Perforation in Kasese District, Uganda, 2008–2009', *Clinical Infectious Diseases*, 54(8), pp. 1091–1099. doi: 10.1093/cid/cis025.

Nelson, A. J. D., Perry, J. C. and Vann, S. D. (2018) 'Chapter 15 - The Papez Circuit and Recognition Memory: Contributions of the Medial Diencephalon and Retrosplenial Cortex to What, Where and When Aspects of Object Recognition Memory', in *Handbook of Object Novelty Recognition*, pp. 217–226. doi: https://doi.org/10.1016/B978-0-12-812012-5.00015-X.

Nemzek, J. A., Hugunin, K. M. S. and Opp, M. R. (2008) 'Modeling sepsis in the laboratory: Merging sound science with animal well-being', *Comparative Medicine*, 58(2), pp. 120–128.

Newcombe, E. A. *et al.* (2018) 'Inflammation: the link between comorbidities, genetics, and Alzheimer's disease', *Journal of Neuroinflammation*, 15(276), pp. 1–26. doi: 10.1186/s12974-018-1313-3.

Niess, J. H. *et al.* (2005) 'CX3CR1-Mediated Dendritic Cell Access to the Intestinal Lumen and Bacterial Clearance', *Science*, 307(5707), pp. 254–258. doi: 10.1126/science.1102901.

Nilson, A. N. *et al.* (2017) 'Tau Oligomers Associate with Inflammation in the Brain and Retina of Tauopathy Mice and in Neurodegenerative Diseases', *Journal of Alzheimer's Disease*, 55(3), pp. 1083–1099. doi: 10.3233/JAD-160912.

Nimmerjahn, F. and Ravetch, J. (2007) 'Fc-Receptors as Regulators of Immunity', in *Advances in Immunology*, pp. 179–204. doi: https://doi.org/10.1016/S0065-2776(07)96005-8.

O'Donnell, H. and McSorley, S. (2014) 'Salmonella as a Model for Non-Cognate Th1 Cell Stimulation', *Frontiers in Immunology*, 5(621), pp. 1–13. doi: 10.3389/fimmu.2014.00621.

Oakley, H. *et al.* (2006) 'Intraneuronal β-Amyloid Aggregates, Neurodegeneration, and Neuron Loss in Transgenic Mice with Five Familial Alzheimer's Disease Mutations: Potential Factors in Amyloid Plaque Formation', *The Journal of Neuroscience*, 26(40), pp. 10129–10140. doi: 10.1523/JNEUROSCI.1202-06.2006.

Oddo, S. *et al.* (2003) 'Triple-Transgenic Model of Alzheimer's Disease with Plaques and Tangles: Intracellular Aβ and Synaptic Dysfunction', *Neuron*, 39(3), pp. 409–421. doi: 10.1016/S0896-6273(03)00434-3.

Ojala, J. *et al.* (2009) 'Expression of interleukin-18 is increased in the brains of Alzheimer's disease patients', *Neurobiology of Aging*, 30(2), pp. 198–209. doi: 10.1016/j.neurobiolaging.2007.06.006.

Olah, M. *et al.* (2018) 'A transcriptomic atlas of aged human microglia', *Nature Communications*, 9(539), pp. 1–8. doi: 10.1038/s41467-018-02926-5.

Pan, K. M. *et al.* (1993) 'Conversion of alpha-helices into beta-sheets features in the formation of the scrapie prion proteins.', *Proceedings of the National Academy of Sciences of the United States of America*, 90(23), pp. 10962–10966. doi: 10.1073/pnas.90.23.10962.

Panegyres, P. K. and Chen, H.-Y. (2013) 'Differences between early and late onset Alzheimer's disease.', *American Journal of Neurodegenerative Disease*, 2(4), pp. 300–306. doi: 10.1176/appi.neuropsych.12100240.

Paolicelli, R. C. *et al.* (2011) 'Synaptic Pruning by Microglia Is Necessary for Normal Brain Development', *Science*, 333(6048), pp. 1456–1458. doi: 10.1126/science.1202529.

Parachikova, A. *et al.* (2007) 'Inflammatory changes parallel the early stages of Alzheimer disease', *Neurobiology of Aging*, 28(12), pp. 1821–1833. doi: 10.1016/j.neurobiolaging.2006.08.014.

Pastor, P. *et al.* (2016) 'MAPT H1 Haplotype is Associated with Late-Onset Alzheimer's Disease Risk in APOEε4 Noncarriers: Results from the Dementia Genetics Spanish Consortium', *Journal of Alzheimer's Disease*, 49(2), pp. 343–352. doi: 10.3233/JAD-150555.

Patrick, G. N. *et al.* (1999) 'Conversion of p35 to p25 deregulates Cdk5 activity and promotes neurodegeneration', *Nature*, 402(6762), pp. 615–622. doi: 10.1038/45159.

Paul, J., Strickland, S. and Melchor, J. P. (2007) 'Fibrin deposition accelerates neurovascular damage and neuroinflammation in mouse models of Alzheimer's disease', *The Journal of Experimental Medicine*, 204(8), pp. 1999–2008. doi: 10.1084/jem.20070304.

Peavy, G. M. *et al.* (2013) 'Neuropsychiatric Features of Frontal Lobe Dysfunction in Autopsy-Confirmed Patients with Lewy Bodies and "Pure" Alzheimer Disease', *American Journal of Geriatric Psychiatry*, 21(6), pp. 509–519. doi: 10.1016/j.jagp.2012.10.022.

Peeraer, E. *et al.* (2015) 'Intracerebral injection of preformed synthetic tau fibrils initiates widespread tauopathy and neuronal loss in the brains of tau transgenic mice', *Neurobiology of Disease*, 73, pp. 83–95. doi: 10.1038/jid.2014.371.

Perlmutter, L. S. *et al.* (1992) 'MHC class II-positive microglia in human brain: Association with alzheimer lesions', *Journal of Neuroscience Research*, 33(4), pp. 549–558. doi: 10.1002/jnr.490330407.

Perry, V. H. (2004) 'The influence of systemic inflammation on inflammation in the brain: Implications for chronic neurodegenerative disease', *Brain, Behavior, and Immunity*, 18(5), pp. 407–413. doi: 10.1016/j.bbi.2004.01.004.

Perry, V. H. and Holmes, C. (2014) 'Microglial priming in neurodegenerative disease', *Nature Reviews Neurology*, 10(4), pp. 217–224. doi: 10.1038/nrneurol.2014.38.

Perry, V. H. and Teeling, J. (2013) 'Microglia and macrophages of the central nervous system: The contribution of microglia priming and systemic inflammation to chronic neurodegeneration', *Seminars in Immunopathology*, 35(5), pp. 601–612. doi: 10.1007/s00281-013-0382-8.

Peruzzi, P. P. *et al.* (2009) 'Physiological Transgene Regulation and Functional Complementation of a Neurological Disease Gene Deficiency in Neurons', *Molecular Therapy*, 17(9), pp. 1517–1526. doi: 10.1038/mt.2009.64.

Peters, A., Josephson, K. and Vincent, S. L. (1991) 'Effects of aging on the neuroglial cells and pericytes within area 17 of the rhesus monkey cerebral cortex', *The Anatomical Record*, 229(3), pp. 384–398. doi: 10.1002/ar.1092290311.

Petersen, M. A., Ryu, J. K. and Akassoglou, K. (2018) 'Fibrinogen in neurological diseases: mechanisms, imaging and therapeutics', *Nature Reviews Neuroscience*, 19(5), pp. 283–301. doi: 10.1038/nrn.2018.13.

Petry, F. R. *et al.* (2014) 'Specificity of Anti-Tau Antibodies when Analyzing Mice Models of Alzheimer's Disease: Problems and Solutions', *PLoS ONE*, 9(5). doi: 10.1371/journal.pone.0094251.

Pober, J. S. *et al.* (2017) 'Antigen Presentation by Vascular Cells', *Frontiers in Immunology*, 8(1907), pp. 1–7. doi: 10.3389/fimmu.2017.01907.

Polanco, J. C. *et al.* (2016) 'Extracellular Vesicles Isolated from the Brains of rTg4510 Mice Seed Tau Protein Aggregation in a Threshold-dependent Manner', *The Journal of Biological Chemistry*, 291(24), pp. 12445–12466. doi: 10.1074/jbc.M115.709485.

Polydoro, M. *et al.* (2009) 'Age-Dependent Impairment of Cognitive and Synaptic Function in the htau Mouse Model of Tau Pathology', *The Journal of Neuroscience*, 29(34), pp. 10741–10749. doi: 10.1523/JNEUROSCI.1065-09.2009.

Pooler, A. M. *et al.* (2013) 'Physiological release of endogenous tau is stimulated by neuronal activity', *EMBO Reports*, 14(4), pp. 389–394. doi: 10.1038/embor.2013.15.

Porrini, V. *et al.* (2015) 'CHF5074 (CSP-1103) induces microglia alternative activation in plaque-free Tg2576 mice and primary glial cultures exposed to beta-amyloid', *Neuroscience*, 302, pp. 112–120. doi: 10.1016/j.neuroscience.2014.10.029.

Potkins, D. *et al.* (2003) 'Language impairment in dementia: Impact on symptoms and care needs in residential homes', *International Journal of Geriatric Psychiatry*, 18(11), pp. 1002–1006. doi: 10.1002/gps.1002.

Prescott, M. J. and Lidster, K. (2017) 'Improving quality of science through better animal welfare: The NC3Rs strategy', *Lab Animal*, 46(4), pp. 152–156. doi: 10.1038/laban.1217.

Prince, M. *et al.* (2014) 'Dementia UK: Second Edition', *Alzheimer's Society*. doi: 10.1037/023990.

Prusiner, S. B. (1982) 'Novel Proteinaceous Infectious Particles Cause Scrapie', *Science*, 216(4542), pp. 136–144. doi: 10.1126/science.6801762.

Püntener, U. *et al.* (2012) 'Long-term impact of systemic bacterial infection on the cerebral vasculature and microglia.', *Journal of Neuroinflammation*, 9(146), pp. 1–13. doi: 10.1186/1742-2094-9-146.

Qin, Y. *et al.* (2016) 'Stimulation of TLR4 Attenuates Alzheimer's Disease–Related Symptoms and Pathology in Tau-Transgenic Mice', *The Journal of Immunology*, 197(8), pp. 3281–3292. doi: 10.4049/jimmunol.1600873.

Qiu, C., Kivipelto, M. and Von Strauss, E. (2009) 'Epidemiology of Alzheimer's disease: occurrence, determinants, and strategies toward intervention', *Dialogues in Clinical Neuroscience*, 11(2), pp. 111–128. doi: 10.1097/ALN.0b013e318212ba87.

Qu, Y. *et al.* (2016) 'NLRP3 recruitment by NLRC4 during Salmonella infection', *The Journal of Experimental Medicine*, 213(6), pp. 877–885. doi: 10.1084/jem.20132234.

Rajamohamedsait, H. B. and Sigurdsson, E. M. (2012) 'Histological staining of amyloid and pre-amyloid peptides and proteins in mouse tissue', in *Methods in Molecular Biology*, pp. 411–424. doi: 10.1007/978-1-61779-551-0_28.

Rakic, S. *et al.* (2018) 'Systemic infection modifies the neuroinflammatory response in late stage Alzheimer's disease', *Acta Neuropathologica Communications*, 6(88). doi: 10.1186/s40478-018-0592-3.

Ralay Ranaivo, H. and Wainwright, M. S. (2010) 'Albumin activates astrocytes and microglia through mitogen-activated protein kinase pathways', *Brain Research*, 1313, pp. 222–231. doi: 10.1016/j.brainres.2009.11.063.

Rangaraju, S. *et al.* (2018) 'Identification and therapeutic modulation of a pro-inflammatory subset of disease-associated-microglia in Alzheimer's disease', *Molecular Neurodegeneration*, 13(24). doi: 10.1186/s13024-018-0254-8.

Rangaraju, Srikant *et al.* (2018) 'Quantitative proteomics of acutely-isolated mouse microglia identifies novel immune Alzheimer's disease-related proteins', *Molecular Neurodegeneration*, 13(34). doi: 10.1186/s13024-018-0266-4.

Ravindran, R. *et al.* (2005) 'Expression of T-bet by CD4 T Cells Is Essential for Resistance to Salmonella Infection', *The Journal of Immunology*, 175(7), pp. 4603–4610. doi: 10.4049/jimmunol.175.7.4603.

Ravindran, R. and McSorley, S. J. (2005) 'Tracking the dynamics of T-cell activation in response to Salmonella infection', *Immunology*, 114(4), pp. 450–458. doi: 10.1111/j.1365-2567.2005.02140.x.

Reitz, C., Brayne, C. and Mayeux, R. (2011) 'Epidemiology of Alzheimer disease', *Nature Reviews Neurology*, 7, pp. 137–152. doi: 10.1038/nrneurol.2011.2.

Ren, Z. *et al.* (2009) 'Effect of age on susceptibility to Salmonella Typhimurium infection in C57BL/6 mice', *Journal of Medical Microbiology*, 58(12), pp. 1559–1567. doi: 10.1099/jmm.0.013250-0.

Rodríguez-Martín, T. *et al.* (2013) 'Tau phosphorylation affects its axonal transport and degradation', *Neurobiology of Aging*, 34(9), pp. 2146–2157. doi: 10.1016/j.neurobiolaging.2013.03.015.

Roher, A. E. *et al.* (2013) 'Bapineuzumab Alters Aβ Composition: Implications for the Amyloid Cascade Hypothesis and Anti-Amyloid Immunotherapy', *PLoS ONE*, 8(3), p. e59735. doi: 10.1371/journal.pone.0059735.

Rolls, E. T. (2015) 'Limbic systems for emotion and for memory, but no single limbic system', *Cortex*, 62, pp. 119–157. doi: 10.1016/j.cortex.2013.12.005.

Rosche, K. L. *et al.* (2015) 'Infection with Salmonella enterica Serovar Typhimurium Leads to Increased Proportions of F4/80+ Red Pulp Macrophages and Decreased Proportions of B and T Lymphocytes in the Spleen', *PLoS ONE*, 10(6), p. e0130092. doi: 10.1371/journal.pone.0130092.

Rösler, T. W. *et al.* (2019) 'Four-repeat tauopathies', *Progress in Neurobiology*, 180, p. 101644. doi: 10.1016/j.pneurobio.2019.101644.

Roy, A. *et al.* (2006) 'Up-regulation of Microglial CD11b Expression by Nitric Oxide', *The Journal of Biological Chemistry*, 281(21), pp. 14971–14980. doi: 10.1074/jbc.M600236200.

Roy, D. S. *et al.* (2017) 'Distinct Neural Circuits for the Formation and Retrieval of Episodic Memories', *Cell*, 170(5), pp. 1000–1012. doi: 10.1016/j.cell.2017.07.013.

Ryu, J. K. and McLarnon, J. G. (2009) 'A leaky blood-brain barrier, fibrinogen infiltration and microglial reactivity in inflamed Alzheimer's disease brain', *Journal of Cellular and Molecular Medicine*, 13(9A), pp. 2911–2925. doi: 10.1111/j.1582-4934.2008.00434.x.

Saito, T. *et al.* (2011) 'Potent amyloidogenicity and pathogenicity of Aβ43', *Nature Neuroscience*, 14(8), pp. 1023–1032. doi: 10.1038/nn.2858.

Salazar-Gonzalez, R. M. *et al.* (2006) 'CCR6-Mediated Dendritic Cell Activation of Pathogen-Specific T Cells in Peyer's Patches', *Immunity*, 24(5), pp. 623–632. doi: 10.1016/j.immuni.2006.02.015.

Saman, S. *et al.* (2012) 'Exosome-associated Tau Is Secreted in Tauopathy Models and Is Selectively Phosphorylated in Cerebrospinal Fluid in Early Alzheimer Disease', *The Journal of*

Biological Chemistry, 287(6), pp. 3842–3849. doi: 10.1074/jbc.M111.277061.

Sanchez-Mejias, E. *et al.* (2016) 'Soluble phospho-tau from Alzheimer's disease hippocampus drives microglial degeneration', *Acta Neuropathologica*, 132(6), pp. 897–916. doi: 10.1007/s00401-016-1630-5.

Sankowski, R., Mader, S. and Valdés-Ferrer, S. I. (2015) 'Systemic inflammation and the brain: novel roles of genetic, molecular, and environmental cues as drivers of neurodegeneration.', *Frontiers in Cellular Neuroscience*, 9(28), pp. 1–20. doi: 10.3389/fncel.2015.00028.

SantaCruz, K. *et al.* (2005) 'Tau Suppression in a Neurodegenerative Mouse Model Improves Memory Function', *Science*, 309(5733), pp. 476–481. doi: 10.3816/CLM.2009.n.003.Novel.

Santos, R. L. *et al.* (2001) 'Animal models of Salmonella infections: enteritis versus typhoid fever', *Microbes and Infection*, 3(14–15), pp. 1335–1344. doi: 10.1016/S1286-4579(01)01495-2.

Sasmono, R. T. and Williams, E. (2012) 'Generation and Characterization of MacGreen Mice, the Cfs1r-EGFP Transgenic Mice', in *Leukocytes*, pp. 157–176. doi: 10.1007/978-1-61779-527-5_11.

Sato, H., Kato, T. and Arawaka, S. (2013) 'The role of Ser129 phosphorylation of α-synuclein in neurodegeneration of Parkinson's disease: A review of in vivo models', *Reviews in the Neurosciences*, 24(2), pp. 115–123. doi: 10.1515/revneuro-2012-0071.

Scattoni, M. L. *et al.* (2010) 'Early behavioural markers of disease in P301S tau transgenic mice', *Behavioural Brain Research*, 208(1), pp. 250–257. doi: 10.1016/j.bbr.2009.12.002.

Schaafsma, W. *et al.* (2015) 'Long-lasting pro-inflammatory suppression of microglia by LPS-preconditioning is mediated by RelB-dependent epigenetic silencing', *Brain, Behavior, and Immunity*, 48, pp. 205–221. doi: 10.1016/j.bbi.2015.03.013.

Schindowski, K. *et al.* (2006) 'Alzheimer's Disease-Like Tau Neuropathology Leads to Memory Deficits and Loss of Functional Synapses in a Novel Mutated Tau Transgenic Mouse without Any Motor Deficits', *The American Journal of Pathology*, 169(2), pp. 599–616. doi: 10.2353/ajpath.2006.060002.

Schoemaker, D. *et al.* (2020) 'Memory impairment is a clinical marker of tau pathology in cerebral amyloid angiopathy', *Alzheimer's & Dementia*, 16(S4), p. e037524. doi: 10.1002/alz.037524.

Schultz, C., Del Tredici, K. and Braak, H. (2010) 'Neuropathology of Alzheimer's Disease', in *Alzheimer's Disease: A Physician's Guide to Practical Management*, pp. 21–31. doi: 10.1002/msj.20157.Neuropathology.

Serino, S. *et al.* (2015) 'Detecting early egocentric and allocentric impairments deficits in Alzheimer's disease: An experimental study with virtual reality', *Frontiers in Aging Neuroscience*, 7(88), pp. 1–10. doi: 10.3389/fnagi.2015.00088.

Serlin, Y. *et al.* (2015) 'Anatomy and Physiology of the Blood-Brain Barrier', *Seminars in Cell & Developmental Biology*, 38, pp. 2–6. doi: 10.1016/j.semcdb.2015.01.002.

Shafiei, S. S., Guerrero-Muñoz, M. J. and Castillo-Carranza, D. L. (2017) 'Tau Oligomers: Cytotoxicity, Propagation, and Mitochondrial Damage', *Frontiers in Aging Neuroscience*, 9(83), pp. 1–9. doi: 10.3389/fnagi.2017.00083.

Sharif, Y. *et al.* (2018) 'The Blood Brain Barrier: A Review of its Anatomy and Physiology in Health and Disease', *Clinical Anatomy*, 31(6), pp. 812–823. doi: 10.1111/joms.

Shea, J. E. *et al.* (1999) 'Influence of the Salmonella typhimurium Pathogenicity Island 2 Type III Secretion System on Bacterial Growth in the Mouse', *Infect Immun*, 67(1), pp. 213–219. doi: 10.1128/IAI.67.1.213-219.1999.

Shepherd, A. J. *et al.* (2018) 'Deficits in Burrowing Behaviors Are Associated With Mouse Models of Neuropathic but Not Inflammatory Pain or Migraine', *Frontiers in Behavioral Neuroscience*, 12(124), pp. 1–11. doi: 10.3389/fnbeh.2018.00124.

Shi, Y. and Holtzman, D. M. (2018) 'Interplay between innate immunity and Alzheimer disease: APOE and TREM2 in the spotlight', *Nature Reviews Immunology*, 18(12), pp. 759–772. doi: 10.1038/s41577-018-0051-1.

Shin, J. *et al.* (2021) 'Thioflavin-positive tau aggregates complicating quantification of amyloid plaques in the brain of 5XFAD transgenic mouse model.', *Scientific Reports*, 11(1617). doi: 10.1038/s41598-021-81304-6.

Siddiqua, A. and Margittai, M. (2010) 'Three- and Four-repeat Tau Coassemble into Heterogeneous Filaments', *The Journal of Biological Chemistry*, 285(48), pp. 37920–37926. doi: 10.1074/jbc.M110.185728.

Šimić, G. *et al.* (2016) 'Tau Protein Hyperphosphorylation and Aggregation in Alzheimer's Disease and Other Tauopathies, and Possible Neuroprotective Strategies', *Biomolecules*, 6(1), p. 6. doi: 10.3390/biom6010006.

Singhrao, S. K. *et al.* (2015) 'Porphyromonas gingivalis Periodontal Infection and Its Putative Links with Alzheimer's Disease', *Mediators of Inflammation*, 2015(137357). doi: 10.1155/2015/137357.

Smits, L. L. *et al.* (2015) 'Early onset APOE E4-negative Alzheimer's disease patients show faster cognitive decline on non-memory domains', *European Neuropsychopharmacology*, 25(7), pp. 1010–1017. doi: 10.1016/j.euroneuro.2015.03.014.

Spires-Jones, T. L. and Hyman, B. T. (2014) 'The Intersection of Amyloid Beta and Tau at Synapses in Alzheimer's Disease', *Neuron*, 82(4), pp. 756–771. doi: 10.1016/j.neuron.2014.05.004.

Srinivasan, A. *et al.* (2007) 'Innate Immune Activation of CD4 T Cells in Salmonella-Infected Mice Is Dependent on IL-18', *The Journal of Immunology*, 178(10), pp. 6342–6349. doi: 10.4049/jimmunol.178.10.6342.

Srinivasan, K. *et al.* (2020) 'Alzheimer's Patient Microglia Exhibit Enhanced Aging and Unique Transcriptional Activation', *Cell Reports*, 31(13), p. 107843. doi: 10.1016/j.celrep.2020.107843.

Steinman, R. (1983) 'Dendritic cells are the principal stimulators of the primary mixed leukocyte reaction in mice', *The Journal of Experimental Medicine*, 157(2), pp. 613–627. doi: 10.1084/jem.157.2.613.

Stoothoff, W. H. and Johnson, G. V. W. (2005) 'Tau phosphorylation: Physiological and pathological consequences', *Biochimica et Biophysica Acta - Molecular Basis of Disease*, 1739(2), pp. 280–297. doi: 10.1016/j.bbadis.2004.06.017.

Stover, K. R. *et al.* (2015) 'Analysis of motor function in 6-month-old male and female 3xTg-AD mice.', *Behavioural Brain Research*, 281, pp. 16–23. doi: 10.1016/j.bbr.2014.11.046.

Streit, W. J. *et al.* (2004) 'Dystrophic Microglia in the Aging Human Brain', *GLIA*, 45(2), pp. 208–212. doi: 10.1002/glia.10319.

Streit, W. J. *et al.* (2009) 'Dystrophic (senescent) rather than activated microglial cells are associated with tau pathology and likely precede neurodegeneration in Alzheimer's disease', *Acta Neuropathologica*, 118(4), pp. 475–485. doi: 10.1007/s00401-009-0556-6.

Sun, Y. *et al.* (2020) 'The behavioural and neuropathologic sexual dimorphism and absence of MIP-3α in tau P301S mouse model of Alzheimer's disease', *Journal of Neuroinflammation*, 17(72). doi: 10.1186/s12974-020-01749-w.

Swart, A. L. and Hensel, M. (2012) 'Interactions of Salmonella enterica with dendritic cells.', *Virulence*, 3(7), pp. 660–667. doi: 10.4161/viru.22761.

Sweeney, M. D., Sagare, A. P. and Zlokovic, B. V. (2018) 'Blood-brain barrier breakdown in Alzheimer disease and other neurodegenerative disorders', *Nature Reviews Neurology*, 14(3), pp.

133–150. doi: 10.1038/nrneurol.2017.188.

Sweeney, M. D., Sagare, A. P. and Zlokovic, B. V (2015) 'Cerebrospinal Fluid Biomarkers of Neurovascular Dysfunction in Mild Dementia and Alzheimer's Disease', *Journal of Cerebral Blood Flow & Metabolism*, 35(7), pp. 1055–1068. doi: 10.1038/jcbfm.2015.76.

Sy, M. *et al.* (2011) 'Inflammation Induced by Infection Potentiates Tau Pathological Features in Transgenic Mice', *American Journal of Pathology*, 178(6), pp. 2811–2822. doi: 10.1016/j.ajpath.2011.02.012.

Tai, H. C. *et al.* (2012) 'The Synaptic Accumulation of Hyperphosphorylated Tau Oligomers in Alzheimer Disease Is Associated With Dysfunction of the Ubiquitin-Proteasome System', *American Journal of Pathology*, 181(4), pp. 1426–1435. doi: 10.1016/j.ajpath.2012.06.033.

Takahashi, S. *et al.* (2003) 'Tau Phosphorylation by Cyclin-dependent Kinase 5/p39 during Brain Development Reduces Its Affinity for Microtubules', *The Journal of Biological Chemistry*, 278(12), pp. 10506–10515. doi: 10.1074/jbc.M211964200.

Takeuchi, H. *et al.* (2011) 'P301S Mutant Human Tau Transgenic Mice Manifest Early Symptoms of Human Tauopathies with Dementia and Altered Sensorimotor Gating', *PLoS ONE*, 6(6), p. e21050. doi: 10.1371/journal.pone.0021050.

Tam, J. W. *et al.* (2014) 'CD11b+ Ly6Chi Ly6G− Immature Myeloid Cells Recruited in Response to Salmonella enterica Serovar Typhimurium Infection Exhibit Protective and Immunosuppressive Properties', *Infection and Immunity*, 82(6), pp. 2606–2614. doi: 10.1128/IAI.01590-13.

Tam, M. A. *et al.* (2008) 'Early cellular responses to Salmonella infection: dendritic cells, monocytes, and more', *Immunological Reviews*, 225(1), pp. 140–162. doi: 10.1111/j.1600-065X.2008.00679.x.

Tang, X. *et al.* (2016) 'Spatial learning and memory impairments are associated with increased neuronal activity in 5XFAD mouse as measured by manganese-enhanced magnetic resonance imaging', *Oncotarget*, 7(36), pp. 57556–57570. doi: 10.18632/oncotarget.11353.

Tenner, A. J. (2020) 'Complement-Mediated Events in Alzheimer's Disease: Mechanisms and Potential Therapeutic Targets', *The Journal of Immunology*, 204(2), pp. 306–315. doi: 10.4049/jimmunol.1901068.

Thompson, A., Fulde, M. and Tedin, K. (2018) 'The metabolic pathways utilized by Salmonella Typhimurium during infection of host cells', *Environmental Microbiology Reports*, 10(2), pp. 140–154. doi: 10.1111/1758-2229.12628.

Togo, T. *et al.* (2002) 'Occurrence of T cells in the brain of Alzheimer's disease and other neurological diseases', *Journal of Neuroimmunology*, 124(1–2), pp. 83–92. doi: 10.1016/S0165-5728(01)00496-9.

Tokoyoda, K. *et al.* (2009) 'Professional Memory CD4+ T Lymphocytes Preferentially Reside and Rest in the Bone Marrow', *Immunity*, 30(5), pp. 721–730. doi: 10.1016/j.immuni.2009.03.015.

Toledo, J. B. *et al.* (2013) 'Contribution of cerebrovascular disease in autopsy confirmed neurodegenerative disease cases in the National Alzheimer's Coordinating Centre', *Brain*, 136(9), pp. 2697–2706. doi: 10.1093/brain/awt188.

Torres-Lista, V. and Giménez-Llort, L. (2013) 'Impairment of nesting behaviour in 3xTg-AD mice', *Behavioural Brain Research*, 247, pp. 153–157. doi: 10.1016/j.bbr.2013.03.021.

Tremblay, M.-È. *et al.* (2011) 'The Role of Microglia in the Healthy Brain', *The Journal of Neuroscience*, 31(45), pp. 16064–9. doi: 10.1523/JNEUROSCI.4158-11.2011.

Uchiya, K. I. and Nikai, T. (2008) 'Salmonella virulence factor SpiC is involved in expression of flagellin protein and mediates activation of the signal transduction pathways in macrophages', *Microbiology*, 154(11), pp. 3491–3502. doi: 10.1099/mic.0.2008/021667-0.

Uppington, H. *et al.* (2006) 'Effect of immune serum and role of individual Fcγ receptors on the intracellular distribution and survival of Salmonella enterica serovar Typhimurium in murine macrophages', *Immunology*, 119(2), pp. 147–158. doi: 10.1111/j.1365-2567.2006.02416.x.

Valdez, Y. *et al.* (2008) 'Nramp1 Expression by Dendritic Cells Modulates Inflammatory Responses During Salmonella Typhimurium Infection', *Cellular Microbiology*, 10(8), pp. 1646–1661. doi: 10.1111/j.1462-5822.2008.01155.x.

Vann, S. D. (2010) 'Re-evaluating the role of the mammillary bodies in memory', *Neuropsychologia*, 48(8), pp. 2316–2327. doi: 10.1016/j.neuropsychologia.2009.10.019.

Varatharaj, A. and Galea, I. (2017) 'The blood-brain barrier in systemic inflammation', *Brain, Behavior, and Immunity*, 60, pp. 1–12. doi: 10.1016/j.bbi.2016.03.010.

Vargas-Caballero, M. *et al.* (2017) 'Wild-Type, but Not Mutant N296H, Human Tau Restores Aβ-Mediated Inhibition of LTP in Tau-/- mice', *Frontiers in Neuroscience*, 11(201), pp. 1–8. doi: 10.3389/fnins.2017.00201.

Vazquez-Terres, A. *et al.* (1999) 'Extraintestinal dissemination of Salmonella by CD18-expressing phagocytes', *Nature*, 401(6755), pp. 804–808. doi: 10.1038/44593.

Vismer, M. S. *et al.* (2015) 'The piriform, perirhinal, and entorhinal cortex in seizure generation', *Frontiers in Neural Circuits*, 9(27), pp. 1–14. doi: 10.3389/fncir.2015.00027.

Voedisch, S. *et al.* (2009) 'Mesenteric Lymph Nodes Confine Dendritic Cell-Mediated Dissemination of Salmonella enterica Serovar Typhimurium and Limit Systemic Disease in Mice', *Infection and Immunity*, 77(8), pp. 3170–3180. doi: 10.1128/IAI.00272-09.

Vogel-Ciernia, A. and M. A. W. (2015) 'Examining Object Location and Object Recognition Memory in Mice', *Current Protocols in Neuroscience*, 72(2), pp. 181–204. doi: 10.1002/0471142301.ns0831s69.Examining.

Vogel, J. W. *et al.* (2020) 'Spread of pathological tau proteins through communicating neurons in human Alzheimer's disease', *Nature Communications*, 11(2612), pp. 1–15. doi: 10.1038/s41467-020-15701-2.

Vorhees, C. and Williams, M. (2006) 'Morris water maze: procedures for assessing spatial and related forms of learning and memory', *Nature Protocols*, 1(2), pp. 848–858. doi: 10.1038/nprot.2006.116.Morris.

De Vos, S. L. *et al.* (2018) 'Synaptic Tau Seeding Precedes Tau Pathology in Human Alzheimer's Disease Brain', *Frontiers in Neuroscience*, 12(267), pp. 1–15. doi: 10.3389/fnins.2018.00267.

Wagner, C. and Hensel, M. (2011) 'Adhesive Mechanisms of Salmonella enterica', in *Advances in Experimental Medicine and Biology*, pp. 17–34. doi: 10.1007/978-94-007-0940-9_2.

Walker, L. C. *et al.* (2013) 'Mechanisms of Protein Seeding in Neurodegenerative Diseases', *JAMA Neurology*, 70(3), pp. 304–310. doi: 10.1001/jamaneurol.2013.1453.

Wang, R. and Reddy, P. H. (2017) 'Role of Glutamate and NMDA Receptors in Alzheimer's Disease', *Journal of Alzheimer's Disease*, 57(4), pp. 1041–1048. doi: 10.3233/JAD-160763.

Wang, X. *et al.* (2018) 'Early intervention of tau pathology prevents behavioral changes in the rTg4510 mouse model of tauopathy', *PLoS ONE*, 13(4), pp. 1–15. doi: 10.1371/journal.pone.0195486.

Wang, Y. *et al.* (2015) 'TREM2 Lipid Sensing Sustains the Microglial Response in an Alzheimer's Disease Model', *Cell*, 160(6), pp. 1061–1071. doi: 10.1016/j.cell.2015.01.049.

Wang, Y. and Mandelkow, E. (2016) 'Tau in physiology and pathology', *Nature Reviews Neuroscience*, 17(1), pp. 22–35. doi: 10.1038/nrn.2015.1.

Wegmann, S. *et al.* (2015) 'Removing endogenous tau does not prevent tau propagation yet

reduces its neurotoxicity.', *The EMBO Journal*, 34(24), pp. 3028–3041. doi: 10.15252/embj.201592748.

Wei, Z. M. *et al.* (2019) 'FcRγ deficiency improves survival in experimental sepsis by down-regulating TLR4 signaling pathway', *Immunologic Research*, 67(1), pp. 77–83. doi: 10.1007/s12026-018-9039-y.

Weller, R. O. *et al.* (2018) 'The meninges as barriers and facilitators for the movement of fluid, cells and pathogens related to the rodent and human CNS', *Acta Neuropathologica*, 135(3), pp. 363–385. doi: 10.1007/s00401-018-1809-z.

Wendeln, A. C. *et al.* (2018) 'Innate immune memory in the brain shapes neurological disease hallmarks', *Nature*, 556(7701), pp. 332–338. doi: 10.1038/s41586-018-0023-4.

Weng, N. P. (2006) 'Aging of the Immune System: How Much Can the Adaptive Immune System Adapt?', *Immunity*, 24(5), pp. 495–499. doi: 10.1016/j.immuni.2006.05.001.

Wes, P. D. *et al.* (2014) 'Tau Overexpression Impacts a Neuroinflammation Gene Expression Network Perturbed in Alzheimer's Disease', *PLoS ONE*, 9(8), pp. 24–31. doi: 10.1371/journal.pone.0106050.

Wesson, D. and Wilson, D. (2011) 'Age and gene overexpression interact to abolish nesting behavior in Tg2576 amyloid precursor protein (APP) mice', *Behavioural Brain Research*, 216(1), pp. 408–413. doi: 10.1111/j.1743-6109.2008.01122.x.Endothelial.

Westerman, M. A. *et al.* (2002) 'The Relationship between Aβ and Memory in the Tg2576 Mouse Model of Alzheimer's Disease', *The Journal of Neuroscience*, 22(5), pp. 1858–1867. doi: 10.1523/JNEUROSCI.22-05-01858.2002.

Wickham, M. E. *et al.* (2007) 'Oral infection of mice with Salmonella enterica serovar Typhimurium causes meningitis and infection of the brain', *BMC Infectious Diseases*, 7(65). doi: 10.1186/1471-2334-7-65.

Wlodarczyk, A. *et al.* (2014) 'Comparison of microglia and infiltrating CD11c+ cells as antigen presenting cells for T cell proliferation and cytokine response', *Journal of Neuroinflammation*, 11(57). doi: 10.1186/1742-2094-11-57.

Wobst, H. J. *et al.* (2017) 'Increased 4R tau expression and behavioural changes in a novel MAPT-N296H genomic mouse model of tauopathy', *Scientific Reports*, 7(43198), pp. 1–14. doi: 10.1038/srep43198.

Woywodt, A. *et al.* (2002) 'Circulating endothelial cells: Life, death, detachment and repair of the endothelial cell layer', *Nephrology Dialysis Transplantation*, 17(10), pp. 1728–1730. doi: 10.1093/ndt/17.10.1728.

Wray, C. and Sojka, W. J. (1978) 'Experimental Salmonella typhimurium infection in calves.', *Research in Veterinary Science*, 25(2), pp. 139–143. doi: 10.1016/s0034-5288(18)32968-0.

Wszolek, Z. K. *et al.* (2006) 'Frontotemporal dementia and parkinsonism linked to chromosome 17 (FTDP-17)', *Orphanet Journal of Rare Diseases*, 1(30). doi: 10.1186/1750-1172-1-30.

Xie, J. *et al.* (2017) 'Microglia-Synapse Pathways: Promising Therapeutic Strategy for Alzheimer's Disease', *BioMed Research International*, 2017(2986460). doi: 10.1155/2017/2986460.

Xu, H. *et al.* (2014) 'Memory deficits correlate with tau and spine pathology in P301S MAPT transgenic mice', *Neuropathology and Applied Neurobiology*, 40(7), pp. 833–843. doi: 10.1111/nan.12160.

Yamada, K. (2017) 'Extracellular Tau and Its Potential Role in the Propagation of Tau Pathology', *Frontiers in Neuroscience*, 11(667). doi: 10.3389/fnins.2017.00667.

Yamazaki, Y. *et al.* (2019) 'Selective loss of cortical endothelial tight junction proteins during Alzheimer's disease progression', *Brain*, 142(4), pp. 1077–1092. doi: 10.1093/brain/awz011.

Yang, N. *et al.* (2011) 'Attenuated Salmonella typhimurium carrying shRNA-expressing vectors elicit RNA interference in murine bladder tumors', *Acta Pharmacologica Sinica*, 32(3), pp. 368–374. doi: 10.1038/aps.2010.224.

Yasojima, K. *et al.* (1999) 'Up-Regulated Production and Activation of the Complement System in Alzheimer's Disease Brain', *American Journal of Pathology*, 154(3), pp. 927–936. doi: 10.1016/S0002-9440(10)65340-0.

Ye, L. *et al.* (2013) 'IL-1β and TNF-α induce neurotoxicity through glutamate production: A potential role for neuronal glutaminase', *Journal of Neurochemistry*, 125(6), pp. 897–908. doi: 10.1111/jnc.12263.

Yoder, R. M. and Taube, J. S. (2011) 'Projections to the anterodorsal thalamus and lateral mammillary nuclei arise from different cell populations within the postsubiculum: implications for the control of head direction cells', *Hippocampus*, 21(10), pp. 1062–1073. doi: 10.1002/hipo.20820.

Yoshiyama, Y. *et al.* (2007) 'Synapse Loss and Microglial Activation Precede Tangles in a P301S

Tauopathy Mouse Model', *Neuron*, 53(3), pp. 337–351. doi: 10.1016/j.neuron.2007.01.010.

Zhang, B. *et al.* (2005) 'Microtubule-binding drugs offset tau sequestration by stabilizing microtubules and reversing fast axonal transport deficits in a tauopathy model', *Proceedings of the National Academy of Sciences of the United States of America*, 102(1), pp. 227–231. doi: 10.1073/pnas.0406361102.

Zhang, Y. *et al.* (2011) 'APP processing in Alzheimer's disease.', *Molecular Brain*, 4(3). doi: 10.1186/1756-6606-4-3.

Zheng, Q. *et al.* (2016) 'Dysregulation of Ubiquitin-Proteasome System in Neurodegenerative Diseases', *Frontiers in Aging Neuroscience*, 8(303), pp. 1–10. doi: 10.3389/fnagi.2016.00303.

Zhou, D. *et al.* (2001) 'A Salmonella inositol polyphosphatase acts in conjunction with other bacterial effectors to promote host cell actin cytoskeleton rearrangements and bacterial internalization', *Molecular Microbiology*, 39(2), pp. 248–259. doi: 10.1046/j.1365-2958.2001.02230.x.

Zhou, Q. *et al.* (2007) 'Protection from direct cerebral cryptococcus infection by interferon-gamma-dependent activation of microglial cells.', *The Journal of Immunology*, 178(9), pp. 5753–5761. doi: 178/9/5753 [pii].

Zhou, X. *et al.* (2005) 'LPS activation of Toll-like receptor 4 signals CD11b/CD18 expression in neutrophils', *American Journal of Physiology-Lung Cellular and Molecular Physiology*, 288(4), pp. L655–L662. doi: 10.1152/ajplung.00327.2004.

Zhou, Y. *et al.* (2018) 'Relevance of Phosphorylation and Truncation of Tau to the Etiopathogenesis of Alzheimer's Disease', *Frontiers in Aging Neuroscience*, 10(27). doi: 10.3389/fnagi.2018.00027.

Zhou, Y. and Bai, B. (2017) 'Tau and Pet/Mri Imaging Biomarkers for Detecting and Diagnosing Early Dementia', *Jacobs Journal of Medical Diagnosis and Medical Imaging*, 2(1), p. 17. doi: 10.1146/annurev-immunol-032713-120240.Microglia.

Zhu, K. *et al.* (2020) 'Absence of microglia or presence of peripherally-derived macrophages does not affect tau pathology in young or old hTau mice', *Glia*, 68(7), pp. 1466–1478. doi: 10.1002/glia.23794.

Zilkova, M. *et al.* (2020) 'Humanized tau antibodies promote tau uptake by human microglia without any increase of inflammation', *Acta Neuropathologica Communications*, 8(74), pp. 1–19. doi: 10.1186/s40478-020-00948-z.